Kenji Kashiwaya · Ji Shen
Ju Yong Kim *Editors*

Earth Surface Processes and Environmental Changes in East Asia

Records From Lake-catchment Systems

Springer

Earth Surface Processes and Environmental Changes in East Asia

Kenji Kashiwaya • Ji Shen • Ju Yong Kim
Editors

Earth Surface Processes and Environmental Changes in East Asia

Records From Lake-catchment Systems

Springer

Editors
Kenji Kashiwaya
Kanazawa University
Kanazawa, Japan

Ju Yong Kim
Korea Institute of Geoscience
and Mineral Resources (KIGAM)
Daejeon, Korea

Ji Shen
Nanjing Institute of Geography
and Limnology
Nanjing, China

ISBN 978-4-431-55539-1 ISBN 978-4-431-55540-7 (eBook)
DOI 10.1007/978-4-431-55540-7

Library of Congress Control Number: 2015941285

Springer Tokyo Heidelberg New York Dordrecht London

Printed on acid-free paper

Springer Japan KK is part of Springer Science+Business Media (www.springer.com)

Preface

We may be faced with natural and anthropogenic environmental changes never found in instrumental observation records, not only locally but also globally. Generally, it is comparatively easy to find the cause and effect of local and short-term changes, whereas it is difficult to establish causal relationships for global and long-term environmental issues. One of the most significant issues in environmental changes to be discussed is knowing how earth surface environments responded to the changes in the past, because that knowledge is required in order to estimate future environmental responses to changes. We have only limited short-term observational data in the instrumental observation period to provide some clues to find causal relations for the estimation. Most areas lack past quantitative records, especially data available for quantitative discussion, although data on earth surface responses to large and long-term global changes are included in past proxy records.

One of the attempts to overcome this situation is to establish studies on lake-catchment systems (e.g., limno-geomorphology). The systems may provide a key to understanding cause and effect in past environments, because current sediment information can be compared with present observations in the systems (process understanding); environmental information, especially having to do with catchments, may be causally connected with observational data. Lacustrine sediments of the systems are recording media, and phenomena that occurred in the systems are recorded in the media. Comparatively short-term lake-catchment processes and process-recording mechanisms are clarified mainly with instrumental observation. The time interval and precision of recorded data depend on the length of the recording media (thickness of sediments) and resolution (sedimentation rate). These instrumental observation and high-resolution records fundamentally provide clues to clarify past processes and reconstruct past changes, and they will furnish ideas for predicting future changes according to the data length and precision.

A goal of this book is to make clear the relations among climato-hydrological changes, land use, natural disasters, and so on during the recent (geological) past, especially in the periods of rapid environmental shifts (rapid global warming, rapid global cooling, rapid tectonic movement, and others), by using lake-catchment systems in northeast Asia from Mongolia to Taiwan. Northeast Asian districts,

located in the middle latitudinal zone, are not only affected by westerly circulation but also controlled by East Asian monsoons. In winter, the cold surge, which sweeps eastern Asia, usually breaks out around Siberia and Mongolian areas. In summer, the Asian summer monsoon flowing through Japan and Korea can reach northeast China as well. In spring, large amounts of aeolian dust (loess) due to the westerlies are transported to northeast China, Korea, and Japan from central Asia and west China. Therefore, climates and environments of these districts are closely related to one another. The districts are under similar climatic conditions with some systematic differences in climatic factors (temperature, precipitation, etc.), tectonic factors, and anthropogenic factors. This means that both proxy and observation data may be available for the East Asian countries in view of their own unique provision as well as common data associated with disasters and climato-hydrological events.

The systems discussed are of various origin: lava-flow dammed lakes, e.g., Terhin Tsagaan Lake (Mongolia) and Jingpo Lake (northeast China); a volcanic debris-flow dammed lake, e.g., Lake Onuma (Japan); tectonic lakes, e.g., Xinkai Lake (northeast China), Lake Biwa (Japan), Lake Yogo (Japan), Qilu Lake (south China), and Ri-yue-tan ("Sun-Moon Lake") (Taiwan); coastal lagoons, e.g., Hwajinpo (Korea), Songjiho (Korea), Bongpo (Korea), Cheonjinho (Korea), Ssangho (Korea), and Soonpogaeho (Korea); artificial reservoirs, e.g., Eurimji (Korea) and Kobe Kawauso-ike (Japan). Especially Xinkai Lake, Jingpo Lake, Eurimji, and Lake Onuma are common targets of joint research among Kanazawa University, the Nanjing Institute of Geography and Limnology, and the Korea Institute of Geoscience and Mineral Resources.

All the systems selected here have varying timescales of information on climatic changes and environmental changes in the recent geological past, including tectonic and anthropogenic activities in the area. We hope that the results contained here along with further information on the systems will provide valuable knowledge of past environments and significant clues for future prediction and provision.

All manuscripts were peer-reviewed by many devoted reviewers. In addition, the editors were assisted in a variety of ways by many individuals and organizations during the editorial process. They especially wish to thank K.N. Cho, R. Chen, J.A. Dearing, N. Endo, H. Ganzawa, Y. Ge, N. Hasebe, T. Iida, M. Ji, K. Katsuki, C. Li, H. Long, J. Lim, W.K. Nahm, H.S. Park, H. Shimazu, W. Sun, H. Takahara, Y. Tanaka, K. Tanaka, Y. Tani, Y. Wang, J. Wu, X. Yang, M. Yoshimoto, and E. Zhang. The patience and assistance of the editorial staff of Springer Japan are highly appreciated. The financial support for research works from the Strategic International Research Cooperative Program of the Japan Science and Technology Agency (JST) and from the Japan Society for the Promotion of Science (Grants-in-Aid for Scientific Research) are gratefully acknowledged. These research works were also supported by the National Basic Research Program of China (973 Program, 2012CB956100) and the CAS/SAFEA international partnership program for creative research teams (No. KZZD-EW-TZ-08). Funds from the National Research Foundation of Korea and the financial support of both the Basic Research Project of the Korea Institute of Geoscience and Mineral Resources (KIGAM-15-3113) and the Radioactive Waste Management of the Korea Institute of Energy Technology

Evaluation and Planning (KETEP-20121710200001B) were invaluable for successful performance of the Japan–China–Korea joint research project (2011–2013) and this publication.

Kanazawa, Japan — Kenji Kashiwaya
Nanjing, China — Ji Shen
Daejeon, Korea — Ju Yong Kim
February 2015

Contents

Chapter 1
Present Earth-Surface Processes and Historical Environmental Changes Inferred from Lake-Catchment Systems

K. Kashiwaya, T. Okimura, T. Itono, K. Ishikawa, and T. Kusumoto

Abstract Environmental changes in lake-catchment systems due to climatic, tectonic, and anthropogenic activities (processes) have been imprinted on lacustrine sediments. Long continuous observation in a small pond-catchment system at Kobe, Japan following the 1995 Kobe earthquake provides good data on environmental changes. These records are available for establishing a mathematical model in which the rate of sedimentation varies in two stages before arriving at the pre-earthquake stage. The model's calculations are fairly consistent with observational results, indicating that the model is acceptable. The 1995 earthquake is faintly recorded in the physical properties of sediments obtained in the system (increase in density and

K. Kashiwaya (✉)
Institute of Nature and Environmental Technology, Kanazawa University, Kakuma, Kanazawa 920-1192, Japan

Department of Geography, National Taiwan University, Daan District, Taipei 10617, Taiwan
e-mail: kashiwaya@staff.kanazawa-u.ac.jp

T. Okimura
Research Center for Urban Safety and Security, Kobe University, Rokkodai, Nada, Kobe 657-0017, Japan

T. Itono
Institute of Nature and Environmental Technology, Kanazawa University, Kakuma, Kanazawa 920-1192, Japan

K. Ishikawa
Department of Earth Sciences, Kanazawa University, Kakuma, Kanazawa 920-1192, Japan

Present Address: Japan Pile Co., 2-1-1, Nihonbashi-Hamacho, Chuo-ku, Tokyo 103-0007, Japan

T. Kusumoto
Department of Earth Sciences, Kanazawa University, Kakuma, Kanazawa 920-1192, Japan

Present Address: Kyowa Hakko Kirin Co., Ltd, 1-6-1, Ootemachi, Chiyoda-ku, Tokyo 100-8185, Japan

K. Kashiwaya et al. (eds.), *Earth Surface Processes and Environmental Changes in East Asia*, DOI 10.1007/978-4-431-55540-7_1

slight change in grain size). A combination of grain density (or mineral content) and grain size may be useful as an indicator for the occurrence of comparatively large earthquakes in tectonically active and climatically humid areas. The Tong-hai earthquake of 1970 in Yunnan, China was detected in the combination (density increase and grain size decrease) for the core sediments obtained from Qilu-he. The Kanbun earthquake of 1662 in Lake Biwa catchment was also detected in the corresponding data from some cores obtained from Lake Biwa, Japan.

Keywords Lake-catchment system • Lacustrine sediment • Physical properties

1.1 Introduction

It is difficult to establish the causes of global environmental issues, especially past issues. However, lake-catchment systems may provide a key to understanding cause and effect in past physical environments, because current sediment information can be correlated with present observation in the system (mechanical understanding). Environmental information, especially as recorded in catchments, may be causally connected with observed events, which means that past information recorded in sediments may be useful for reconstructing past environmental changes and for predicting future changes.

Some research in geomorphology aims to combine "present" science, mainly based on instrumental observation, with "historical" science, based on field observation, but most areas lack past records, especially quantitative data available for quantitative discussion. One of the attempts to overcome this situation is to establish geomorphology of lake-catchment systems (or "limno-geomorphology"). In these systems, lacustrine sediments are a form of recording media and phenomena in the systems are recorded in the media. Comparatively short-term lake-catchment processes and process-recording mechanisms are assayed mainly by instrumental observation. The time interval and precision of recorded data depends on the length of recording media (thickness of sediments) and resolution (sedimentation rate). These instrumental observations and high-resolution records provide clues to elucidate past processes and postdict past changes, and they facilitate the prediction of future trends, depending on the quantity and precision of data.

Sedimentary records include much environmental information in addition to hydrological and geomorphological one. However, it is difficult to obtain useful information because observations must be filtered in specific ways for each discipline, such as hydro-geomorphology. Three processes are important for identifying observational results: climatic, tectonic, and anthropogenic activities (processes). In this paper, several processes and environmental changes related to these three activities will be analyzed for the two time windows (present and historical).

1.2 Typical Lake-Catchment Systems for Present Climatic, Tectonic, and Anthropogenic Processes – Observation and Modeling

Most modern lake-catchment systems have been influenced by climatic, tectonic, and anthropogenic processes and their lacustrine sediments record information related to the three processes. Furthermore, the processes have exerted their mutual effects for an extended interval. Dominant processes (events) are comparatively easily detected in sediment records over long intervals, whereas a multiplicity of processes may be identified for recent short intervals. Here we will consider some lake-catchment systems for discussion about the processes and sediment information.

1.2.1 Observation for Kawauso-ike System in Kobe

In Kobe district, several natural disasters caused by heavy rainfall and earthquake have occurred over the past instrumental observation period, in addition to large-scale artificial land transformation, including the development of artificial islands in the 1960s–1990s. The Kawauso-ike pond-catchment system is located in the Rokko Mountains of Kobe City (Fig. 1.1), which is known for its heavy rainfall (Kashiwaya et al. 1984, 1987, 1988, 1990, 1995, 1997) and earthquake records (Kashiwaya et al. 2004, 2012). In this system, several core samples were obtained before and after the 1995 Kobe earthquake. After the earthquake, two sediment traps were set on the bottom surface for nearly 15 years (two circles in Fig. 1.2).

Figure 1.3 shows grain size (solid line) and density (dotted line) fluctuations of core sediments obtained after the 1995 Kobe earthquake, and rainfall intensity measured at Kobe Marine Observatory. Blanc arrows in Fig. 1.3a show the 1938 and 1967 heavy rainfall events in addition to the 1995 Kobe earthquake; 100 mm excess rainfall (solid line; annual summation of excess amount of 100 mm daily rainfall) corresponds to increase in grain size while annual rainfall (dotted line) was not correlated to the grain size fluctuation. The earthquake did not appear to have direct influence on sediment grain size variation, although the sedimentation rate following the earthquake rapidly increased (Fig. 1.4; Kashiwaya et al. 2004).

Events after 1967 constituted comparatively heavy rainfall in 1983 and check (sabo) dam construction in the west tributary in 1984–1985 (a check dam in the east tributary was constructed in 1989–1990) (see Fig. 1.2). Slight increase in grain size between the 1967 heavy rainfall and 1986 sampling may be related to the comparatively large rainfall around 1983. The subsequent decrease in grain density corresponds to the years of 1984–1985, when the check dam in the west tributary was constructed. Materials in the west tributary flowed into Kawauso-ike directly, suggesting that the check dam might play an important role in trapping mineral materials produced in the catchment, while materials in the east tributary, by contrast, flowed into the pond via a delta at the mouth of the river, where some materials might have contributed to delta formation (Fig. 1.2). Potential volume

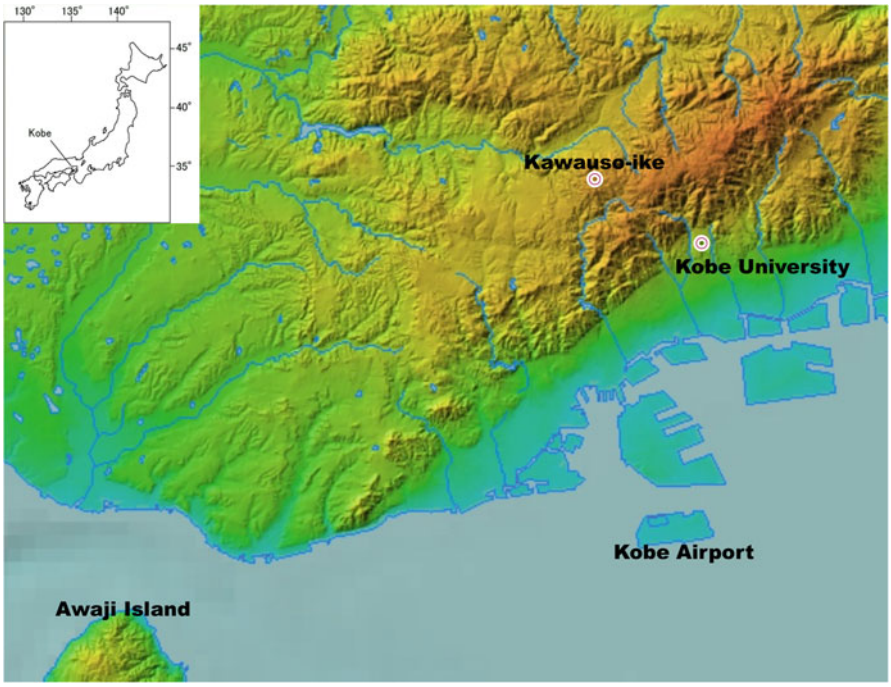

Fig. 1.1 Location map of studied area in Kobe, Japan (original map by Geospatial Information Authority of Japan)

of dam-induced deposition was 540 m^3 for the west tributary and 5,561 m^3 for the east tributary when the check dams were constructed (Kobe City Government). Generally, check dams prevent materials, especially coarse particles, from flowing into reservoirs. This may have been related to the lack of increase in grain size during the 1995 earthquake, although mineral materials increased.

As shown above, climatic (heavy rainfall), tectonic (seismic) and anthropogenic impacts affected the pond-catchment system, and their impacts were surely recorded in lacustrine sediments, suggesting that modern lacustrine sediments may provide clues for evaluating past environmental changes on the basis of understanding of processes.

1.2.2 Modeling Erosion-Sedimentation Processes in a Lake-Catchment System – A Phenomenological Model After the Earthquake

It is necessary to quantitatively express temporal changes in physical phenomena for appropriate understanding of lake-catchment processes, which in turn allows

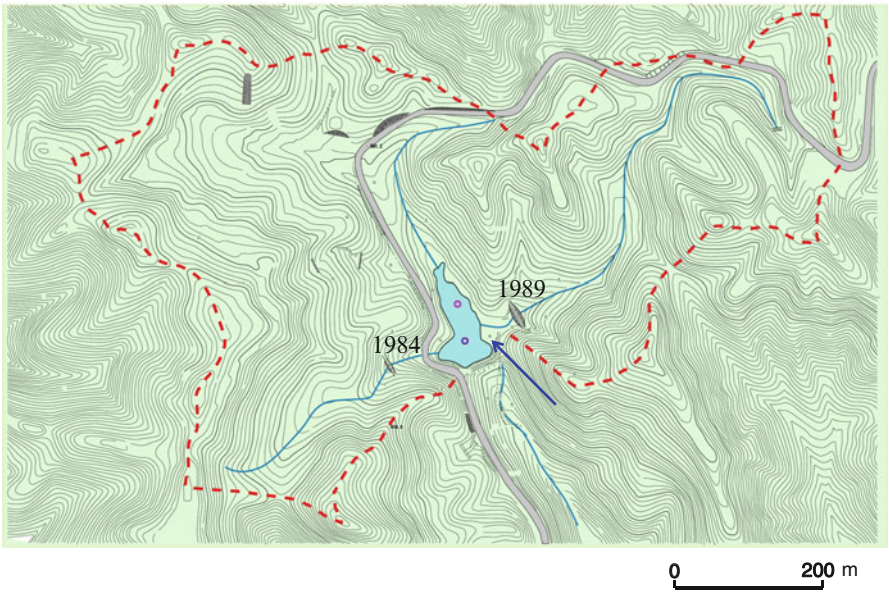

Fig. 1.2 Kawauso-ike pond–catchment system. Figures mean the construction years of the check dams. An arrow indicates a small delta. (original map by Geospatial Information Authority of Japan)

provision and prediction. Hence, temporal observation for the Kawauso-ike system after the earthquake was begun in May 1995. Two sediment traps were emplaced on the pond bed in May 1995 (two circles in Fig. 1.2). Sediments were removed from the traps once or twice a month, so that their physical properties could be measured and analyzed. Meteorological data from the Kobe Marine Observatory were also incorporated into this study.

While a limited study based on the observational results obtained before 2000 was performed by Kashiwaya et al. (2004), we introduce here a mathematical model for temporal changes in the system based on over 10 years of observations.

Figure 1.4a shows temporal changes in the median grain size of sediments collected in traps during the past five years (first stage). This figure also shows little overall difference in the samples, despite small increase and decrease parts for recent years. This may reflect the fact that there was little severe rainfall and few rapid mass movements during this interval.

The annual sedimentation rate inferred from the two sediment traps is shown in Fig. 1.4b. The rate was high just after the earthquake and then gradually decreased (first stage, 1995–1999; Fig. 1.5). Seasonal changes in the sedimentation rate are generally controlled by seasonal rainfall, but no large fluctuation in seasonal rainfall was observed, despite a temporal decrease in the sedimentation rate (1995–1999; Fig. 1.5b). It seems that significant earthquake influence on sedimentation rate

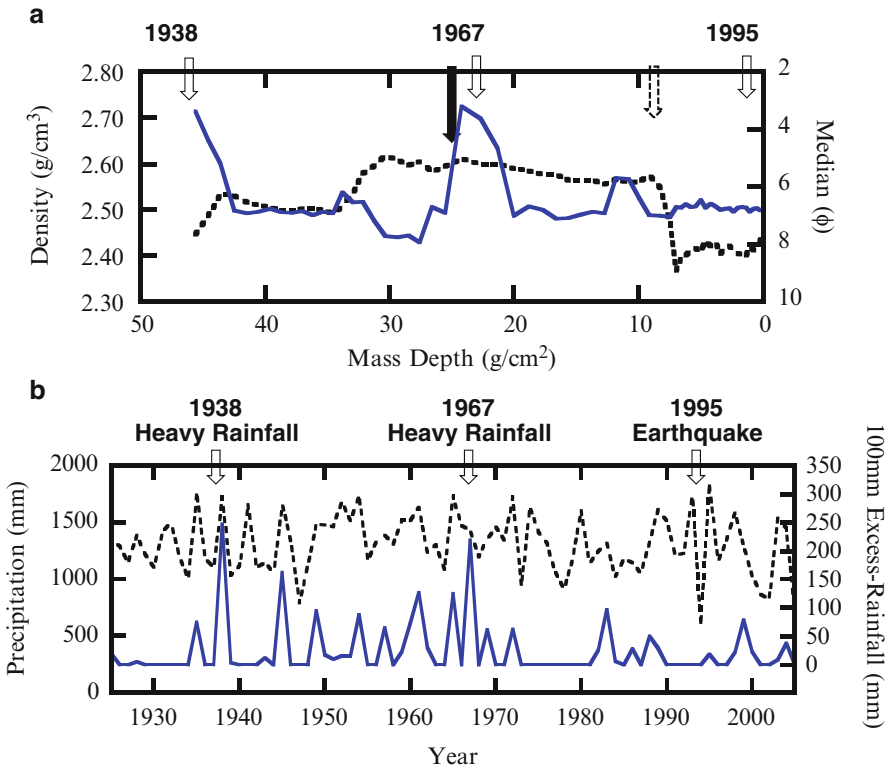

Fig. 1.3 (**a**) Grain size (ϕ) fluctuation. A *solid arrow* indicates the peak of Cs-137 concentration (1963) and a *dotted arrow* means the year of 1984. (**b**) Annual precipitation (mm) and annual excess rainfall (mm) in Kobe

disappeared during the second stage (2002–2007) although the sedimentation rate was larger than before the 1995 earthquake despite some no-observation periods (Fig. 1.5).

Following an investigation based on field observation in the Rokko Mountains and laboratory experiments, Torii et al. (2007) postulated that the increase in material erodibility after the earthquake was related to the destruction of the skeletal structure of weathered materials (granites) by the earthquake. This result suggests that there may be three stages of evolution of the (lake-catchment) system environments after the earthquake: (1) rapid increase and gradual decrease in sedimentation rate, (2) stationary stage; more erodible materials than before the earthquake, and (3) new weathering-limited stage, similar to that before the earthquake. The three stages must be taken into account to establish models (Fig. 1.6).

Conditions after the earthquake may be assumed as shown in Fig. 1.7. A basic model for the system is introduced here (Kashiwaya et al. 2004). First, it is assumed that for the basic model, the sedimentation rate in the lake ($SR(t)$) is proportional to the erosion rate in its catchment ($dE(t)/dt$), which yields

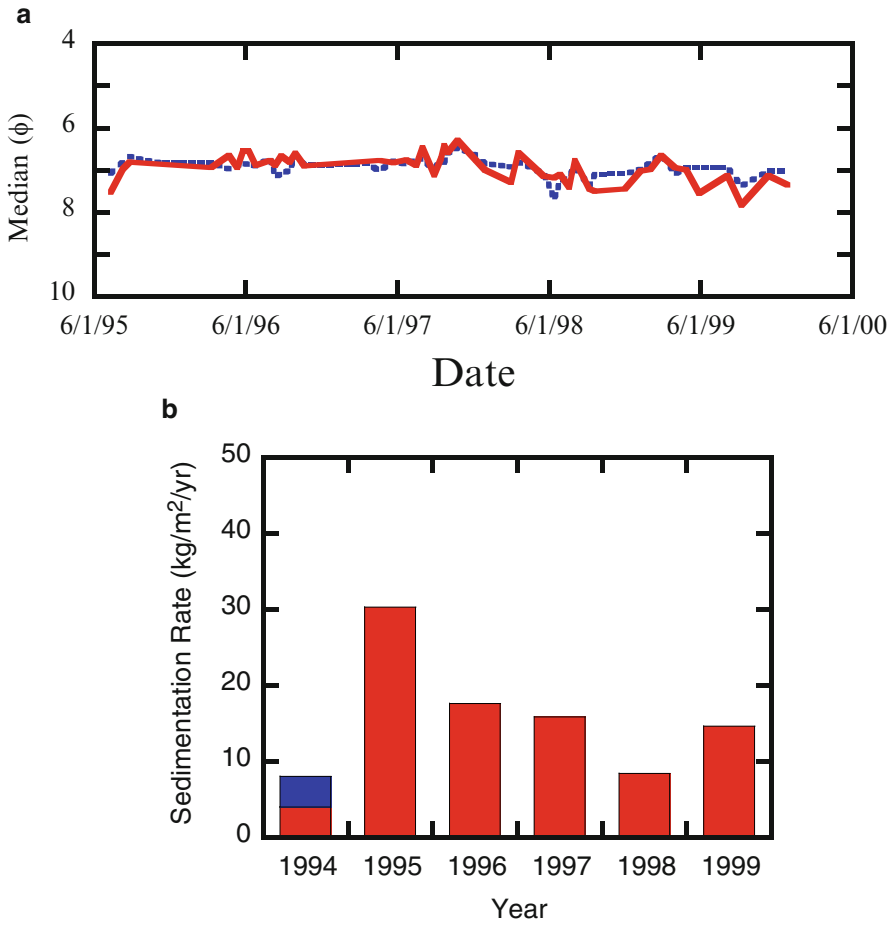

Fig. 1.4 (**a**) Monthly grain size fluctuation in two sediment traps since the 1995 (*solid line*; front trap, *dotted line*; back trap). (**b**) Annual sedimentation rate (kg/m^2/year) (averaged) in the traps and estimated one before 1995 (*blue part*; maximum one)

$$SR(t) = \alpha \frac{dE(t)}{dt}, \tag{1.1}$$

where $E(t)$ is the volume of material moved at time t and α is a proportionality factor (sediment delivery factor related to material conditions) in the catchment. The erosion rate in the catchment is proportional to the volume of material to be eroded at t ($V(t)$):

$$\frac{dE(t)}{dt} = \lambda(t)V(t), \tag{1.2}$$

with $\lambda(t)$, erosion factor related to external forces (e.g., rainfall).

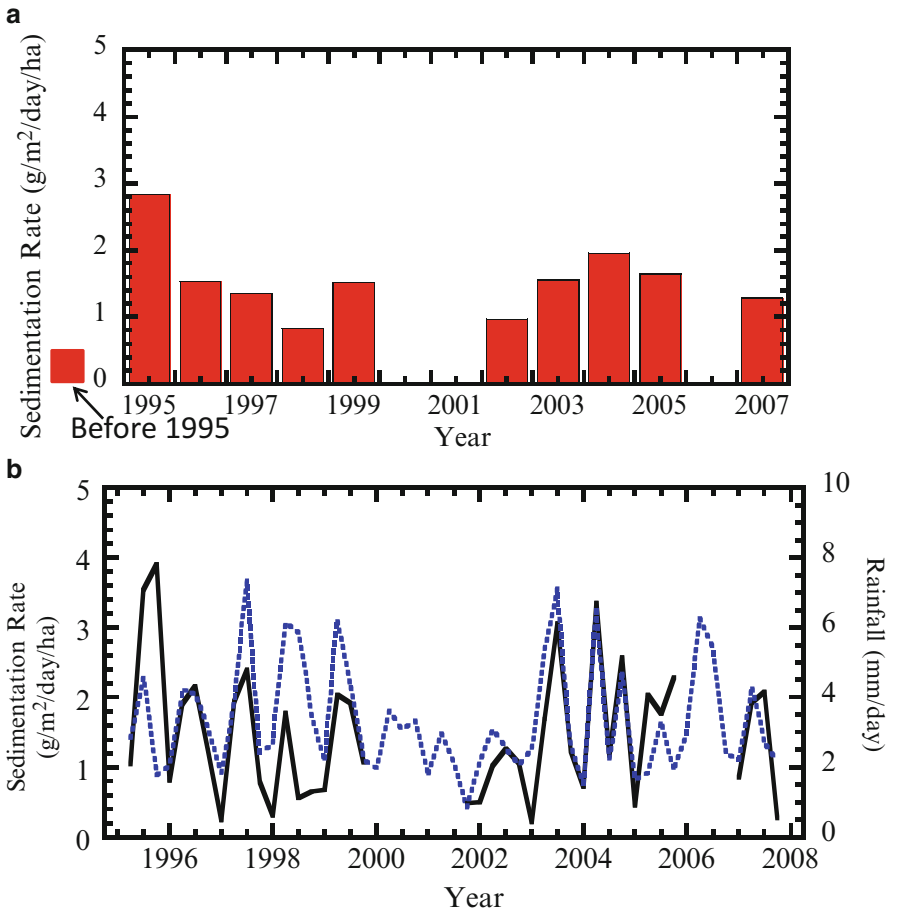

Fig. 1.5 (**a**) Annual sedimentation rate (g/m^2/day/ha) and (**b**) seasonal sedimentation rate (*solid line*; g/m^2/day/ha) and seasonal rainfall (*dotted line*; mm/day) for Kawauso-ike system

Let us consider the first stage for the model. Volume of fine material produced by the earthquake ($V(t)$) to be eroded is expressed as

$$V(t) = V_T - \{V_{DW} + V_W(t) + V_U(t)\} - E(t), \tag{1.3}$$

where V_T is the total volume of material in a catchment area at the initial stage, V_{DW} is the destroyed weathered part of the material, $V_W(t)$ is the weathering part of the material, and $V_U(t)$ is the non-erodible part of the material at time t. Then, we obtain

$$\frac{dV(t)}{dt} = -\frac{d\{V_W(t) + V_U(t) + E(t)\}}{dt} \tag{1.4}$$

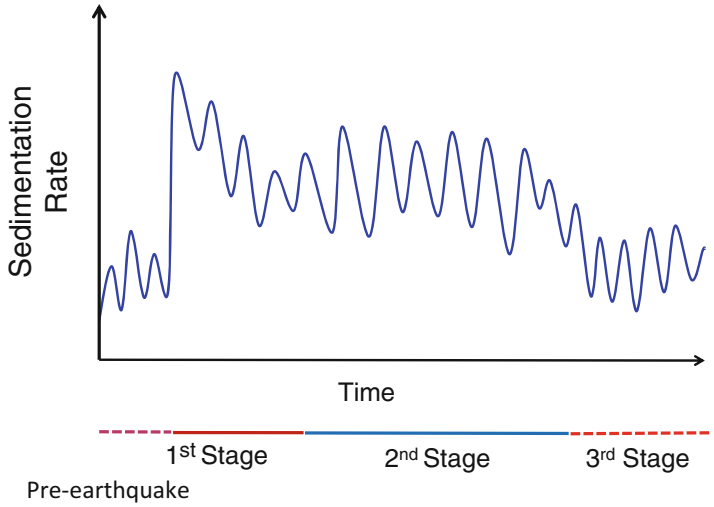

Fig. 1.6 Idealized stages for sedimentational condition in a lake-catchment system after earthquake

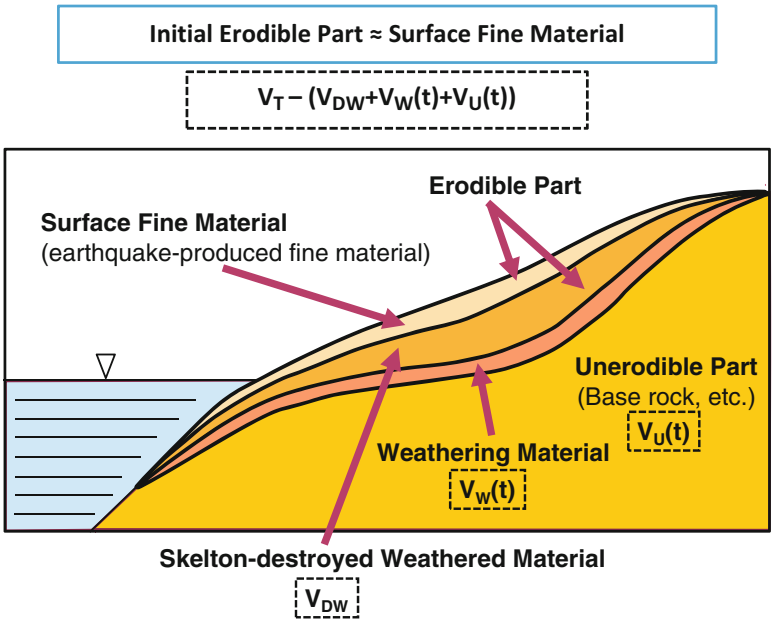

Fig. 1.7 An idealized model for erosion-sedimentation process in a lake-catchment system after earthquake-influence

This leads to

$$-\frac{dV(t)}{dt} = \lambda(t)V(t) + \frac{d\{V_W(t) + V_U(t)\}}{dt} \tag{1.5}$$

It is assumed that

$$\frac{d\{V_W(t) + V_U(t)\}}{dt} = f_{WU}(t), \tag{1.6}$$

we have

$$V(t) = e^{-\int^t \lambda(\tau)\,d\tau} \left\{ -\int^t f_{WU}(t) e^{-\int^t \lambda(\tau)\,d\tau} dt + V_0 \right\}, \tag{1.7}$$

assuming $V(0) = V_0$.

Therefore, the sedimentation rate is expressed as follows

$$SR(t) = \alpha\lambda(t) \left[e^{-\int^t \lambda(\tau)\,d\tau} \left\{ -\int^t f_{WU}(t) e^{-\int^t \lambda(\tau)\,d\tau} dt + V_0 \right\} \right]. \tag{1.8}$$

In the first stage, it is assumed that only the fine surface materials produced in the earthquake are eroded because no extremely heavy rainfall has occurred since the 1995 Kobe earthquake. Moreover, in the first stage, erodible materials seem to be limited to earthquake-produced fine materials. Then, it may be assumed that

$$V_T - \{V_{DW} + V_W(t) + V_U(t)\} = \text{const.},\ f_{WU}(t) = 0.$$

Eq. (1.8) becomes

$$SR(t) = \alpha_1 \lambda_1(t) V_{01} e^{-\int^t \lambda_1(\tau)\,d\tau}, \tag{1.9}$$

where α_1 is a proportionality factor related to the fine materials, $\lambda_1(t)$, an erosion factor related to rainfall intensity in the first stage, and V_{01} is the initial volume of material before the first step of erosion. The model is checked in the first stage using the data. Then, an erosion factor $\lambda_1(t)$ is assumed to be a temporal function of seasonal rainfall:

$$\lambda_1(t) = \sum_i p_{1i} \sin q_{1i}(t - t_{1i}) + r_{1i}. \tag{1.10}$$

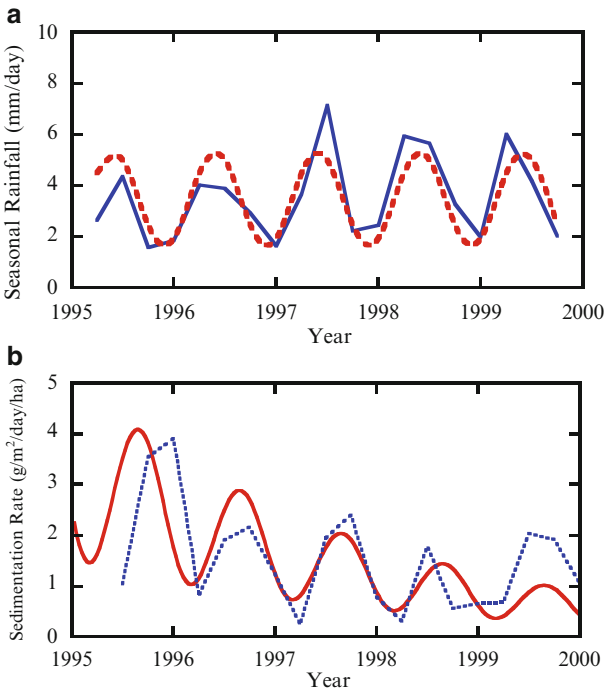

Fig. 1.8 (**a**) Changes in seasonal rainfall (mm/day) for the first stage. *Solid line* is original and *dotted line* is synthesized. (**b**) Changes in seasonal sedimentation rate (g/cm^2/day/ha) in the lake-catchment system. *Solid line* is calculated and *dotted line* is observational

The equation has been introduced with Fourier approximation by using a harmonic analysis (Fig. 1.8a) for the seasonal rainfall data represented by a dotted line. Theoretical sedimentation rate calculated on the basis of Eq. (1.9) (dotted line) and observations (solid line) are shown in Fig. 1.8b, indicating that the erosion factor is expressed as a function of seasonal rainfall and the sedimentation rate is approximately expressed here by eq. (1.5). Therefore, this model is valid for the erosion-related sedimentation processes in the first stage after the earthquake. However, recent (second stage) sedimentation rate seems to be a little higher than before the earthquake, possibly because of the skeleton-destroyed weathered materials (Torii et al. 2007). Therefore, the earthquake evidently continues to influence the earth surface environment. While the direct influence of the 1995 Kobe earthquake rapidly diminished (most earthquake-produced fine materials were transported), the earthquake can also influence physical conditions of the earth surface for a comparatively long time (corresponding to the second stage).

Let us now consider the second stage where most materials to be eroded are the skeleton-destroyed weathered granite (V_{DW} in Fig. 1.7; probably one whose

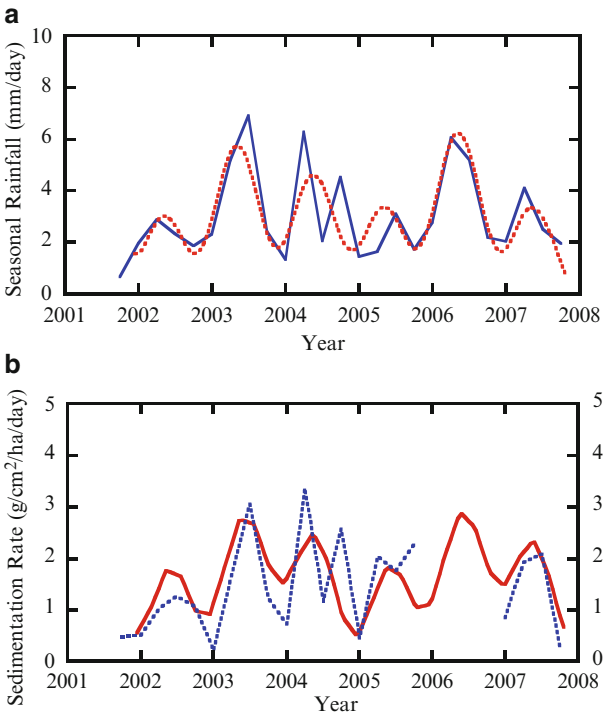

Fig. 1.9 (**a**) Changes in seasonal rainfall (mm/day) for the second stage. *Solid line* is original and dotted line is synthesized. (**b**) Changes in seasonal sedimentation rate (g/cm^2/day/ha) in the lake-catchment system. *Solid line* is calculated and dotted line is observational

structure has been weakened by the earthquake), after the majority of fine materials are removed. In the case of a short interval such as the second stage (2002–2008), the term for weathering and uplifting, $f_{\mathrm{WU}}(t)$ in Eq. (1.7) may be disregarded. Then,

$$SR(t) = \alpha_2 \lambda_2(t) V_{02} e^{-\int^t \lambda_2(\tau)\, d\tau}, \tag{1.11}$$

where α_2 is a proportionality factor related to the skeleton-destroyed materials, $\lambda_2(t)$, an erosion factor related to rainfall intensity in the 2nd stage, and V_{02} is initial volume of material in the second step of erosion. The model is checked using the data in the second stage. Then, the erosion factor $\lambda_2(t)$ is assumed to be a temporal function of seasonal rainfall;

$$\lambda_2(t) = \sum_i p_{2\mathrm{i}} \sin q_{2\mathrm{i}} (t - t_{2\mathrm{i}}) + r_{2\mathrm{i}}. \tag{1.12}$$

The equation has been developed using a harmonic analysis (Fig. 1.9a) for the seasonal rainfall data shown as a dotted line in the figure. Theoretical sedimentation

rate calculated on the basis of Eq. (1.11) (solid line) and observations (dotted line) are shown in Fig. 1.9b, indicating that the model is also valid for the second stage with enough skeleton-destroyed materials. These results suggest that the model introduced here is basically acceptable for the earthquake-influencing interval (first and second stages) after the earthquake.

It is clear that earthquakes generally produce abundant fine materials in addition to various coarse types (rocks). Fine materials are easily moved by relatively light rainfall. The models introduced here are based on simplified assumptions. However, to adequately discuss erosional environments in the catchments after the earthquakes, it is necessary to check thoroughly changes in surface conditions. Additionally, these phenomenological equations will be available for quantitative prediction of surface environments in the near future (10^1-10^2 years), if physical properties for α_1 and α_2 are discussed in detail in relation with material conditions, and if exact values of V_{DW}, V_{01}, V_{02}, etc., are established quantitatively.

1.3 Beyond Observation

Observational data in the recent past may be of great use not only for understanding processes but also for near future prediction in lake-catchment systems. Subsequently, it is necessary for further future discussion to consider the recent past data in areas without instrumental observation system and comparatively long-term data in periods without observation system.

1.3.1 Sediment Information in the Instrumental Observation Period

As shown in the previous section, climatic, tectonic, and anthropogenic activities have been recorded in lacustrine sediments during the instrumental observation period. In the case of the Kawauso-ike pond-catchment system, the 1995 earthquake was identified in observed sedimentation rate, estimated using sediments collected in sediment traps, while heavy rainfall and anthropogenic events were recorded in the physical properties of sediments (Fig. 1.3; discussed below). Generally, it is difficult to obtain flux data such as sedimentation rate without instrumental observation. Therefore, non-flux physical (chemical) properties, which are common in periods both with and without instrumental observation, must be considered for a comparatively long term.

Let us now consider cores obtained before and after the 1995 Kobe earthquake to investigate the earthquake and material physical properties. Figure 1.10 shows the analytical results for the two cores obtained before the earthquake (a) and after the earthquake (b). Two heavy rainfall events (1937 and 1967) and a comparatively

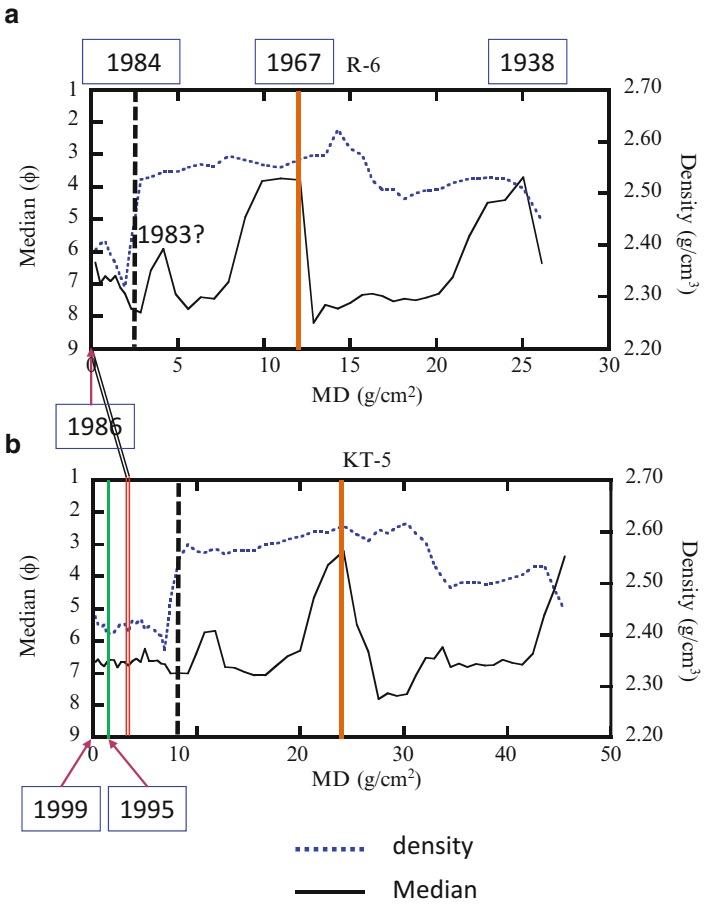

Fig. 1.10 Changes in mineral grain size and grain density of the core obtained in 1986 (R-6) (**a**) and in 1999 (KT-5) (**b**), before and after the 1995 Kobe Earthquake. *Solid lines* mean the year of 1967 heavy rainfall time and *dotted lines* the year of the 1984 check dam construction. A *double line* means the year of R-6 obtained

heavier rainfall event (1983) are detected in the grain size variation (solid line) of both cores. The construction of a check dam in 1984–1985 is also detected in the rapid decrease of grain density in both cores (dotted lines). After the 1986 sampling, although no large change occurred in grain size and grain density variation (Fig. 1.10b), we observe that grain density increased slightly in the core obtained in 1999, compared with that obtained in 1986, which is supported by data from other cores obtained during the same period (Fig. 1.11). Probably, this kind of analytical observation is available in tectonically sensitive zone, such as Japan, Yunnan (China), Taiwan, etc. Sampling sites for the cores are shown in Fig. 1.12. Grain density variations shown in these figures may provide different information.

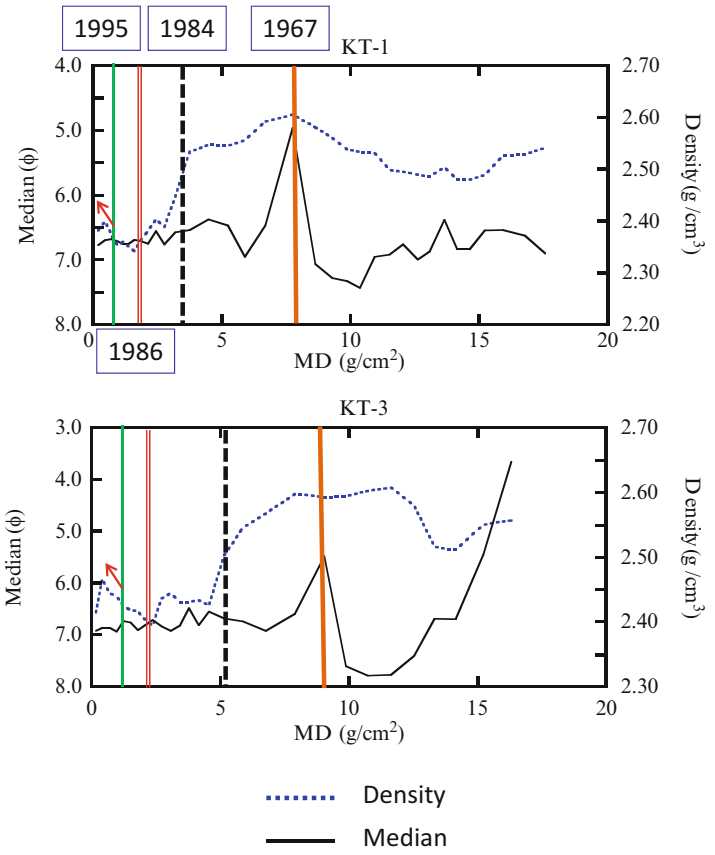

Fig. 1.11 Changes in mineral grain size and grain density in two cores obtained in 1999 (KT-1 and KT-3). *Solid lines* mean the year of 1967 heavy rainfall time and *dotted lines* the year of the 1984 check dam construction. *Double lines* mean the year of R-6 obtained in 1984. Fine *dotted lines* mean 1995 (estimated)

After the 1967 period of heavy rainfall and just before 1986 (the first sampling time), abrupt decrease in grain size density (check dam construction) was detected in all cores. Large sediment accumulation in the check dam may be related not only to a decrease in density, but also to a decrease in mineral content and/or increase in organic content (and bi-SiO_2 content).

1.3.2 Qilu-he System in Yunnan, China

The Yunnan Province is located in the eastern margin of the Tibetan Plateau and has experienced strong tectonic movements related to the collision between the Indian

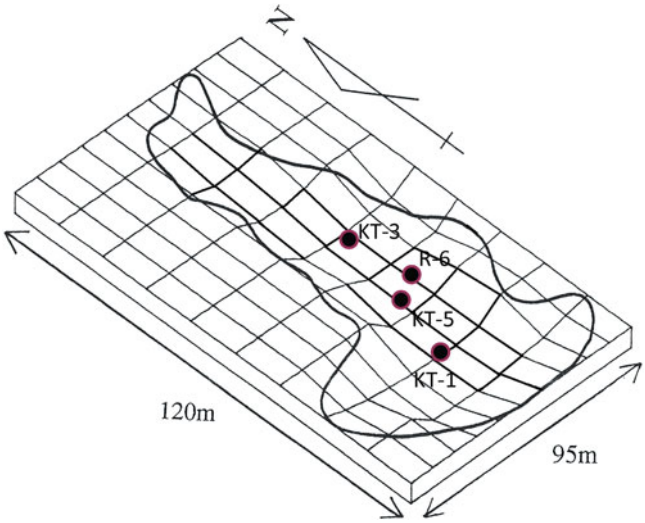

Fig. 1.12 A location map for the cores obtained in 1999

and Eurasian plates. Many earthquakes have occurred in this area. The most recent disastrous earthquake in Northern Yunnan (Zhaotong earthquake; M 6.5), during which more than 600 people were killed, occurred on August 3, 2014. The Lijiang earthquake (M 7.0), which occurred in 1996, also killed more than 300 people. One of the most disastrous earthquakes (M 7.7) in Eastern Yunnan, which was called the Tong-hai earthquake, occurred in 1970. The earthquake killed more than 15,000 people, and also left signs in lacustrine records. It occurred during the period of the Cultural Revolution in China (1966–1976) and, at first, was mistaken for a nuclear attack by the former Soviet Union, which the Chinese central government feared at the time. The occurrence of this earthquake remained a secret until 2000.

Several core samples were obtained in Qilu-he (otherwise, Tong-hai) in 2002 (Fig. 1.13) (Kashiwaya et al. 2006). The epicenter of the Tong-hai earthquake is located at Tong-hai Prefecture in the south of Qilu-he. Age models for the cores are estimated with Cs-137 (Fig. 1.14a). The earthquake effects were detected in Pb-210 concentration and in some physical properties of lacustrine sediments (Figs. 1.14 and 1.15). Water level had often been lowered in this lake since the late 1960s by drought conditions (p.c., information gathered from local fishermen). Increases in HCl-soluble material (open square) and grain size, and decreases in mineral content and grain density since ca. 1963 may be related to the drought conditions (Figs 1.14 and 1.15). However, at about 2.5–4 g/cm^2 part (dotted bars in Fig. 1.14), grain size abruptly decreased, while mineral content and grain density increased. Furthermore, the change in Pb-210 concentration does not show a gradual decrease, which indicates the disturbance of the then bottom surface layer (Fig. 1.14a). Just after the earthquake, increase in grain density (mineral content increase) and decrease in mineral grain size (suggesting no increase in discharge) are often detected in sedi-

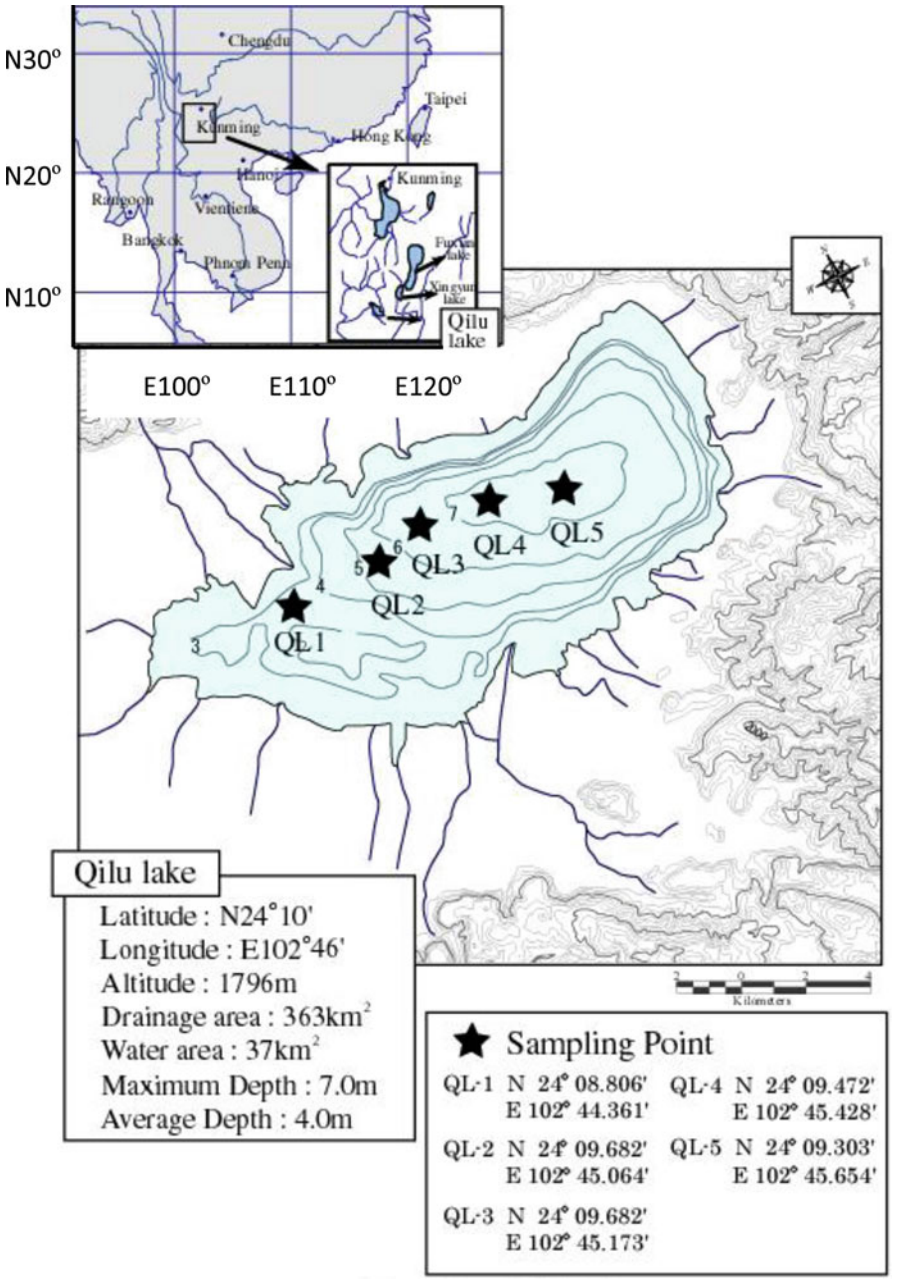

Fig. 1.13 Sampling sites in Qilu-he, Yunnan, China

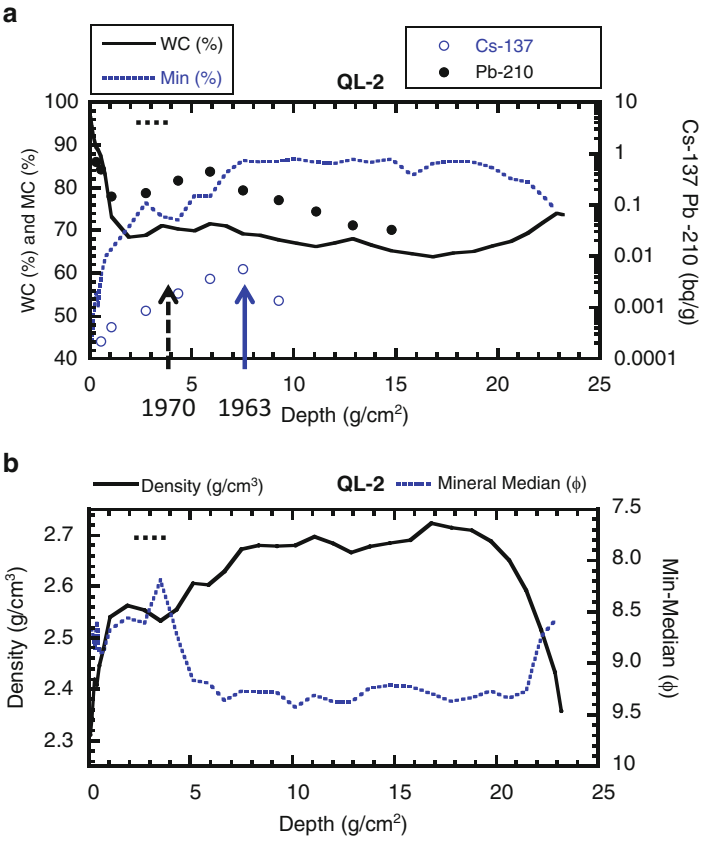

Fig. 1.14 (**a**) Changes in water content (*solid line*) and mineral content (*dotted line*) (*left axis*) and changes in Cs-137 content (*open circle*) and Pb-210 content (*solid circle*) (*right axis*), and (**b**) changes in mineral density (g/cm^3; left axis) (*solid line*) and mineral median (ϕ; *right axis*) (*dotted line*)

ments, as shown by data related to earthquakes mentioned above and below. Hence, the 2.5–4.0 g/cm^2 portion may correspond to the interval around the 1970 Tong-hai earthquake. The results obtained here suggest that finer mineral materials were also accumulated, as shown by the case of the Kobe earthquake (Kashiwaya et al. 2004).

1.4 Long-Term Environmental Changes, and Climatic and Tectonic Activity

In this section, comparatively long-term environmental changes resulting from climatic- and tectonic-related processes will be discussed using the Lake Biwa system.

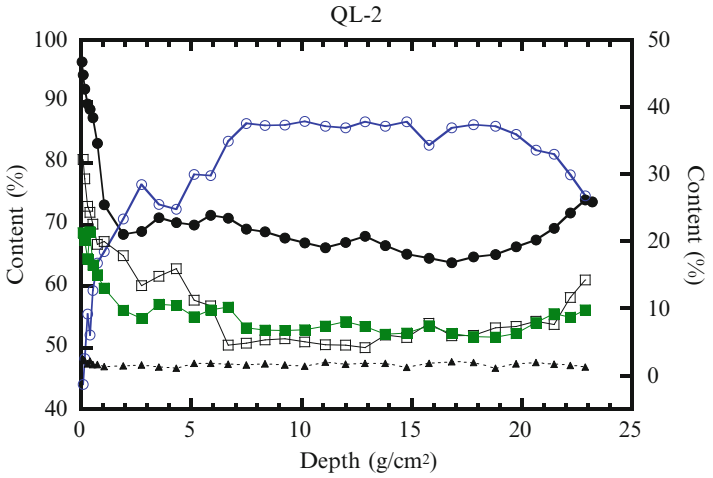

Fig. 1.15 Changes in water content (*solid circle*) and mineral content (*open circle*) (*left axis*), and changes in bi-SiO_2 content (*solid triangle*), Hcl soluble content (*open square*) and organic content (*solid square*) (*right axis*)

Lake Biwa, located in central Japan, is one of the oldest lakes in the world and its lacustrine sediments contain lengthy continuous information on environmental changes in the past 400 kyr (e.g., Kashiwaya et al. 1991). Lake Biwa is a tectonic lake and many active faults are found in its surroundings. Much information on tectonic activity (seismic activity) is also recorded in lacustrine sediments of historical and geological periods, in addition to information on climatic activity (Yamamoto et al. 1985; Kashiwaya et al. 1991; Taishi et al. 1991; Itono et al. 2012). Although some approaches have been attempted (e.g., Inouchi et al. 1996; Simonneau et al. 2013), it is generally difficult to distinguish tectonic events from climatic events in lacustrine sediments of tectonically active and climatically humid areas, especially in the remote past. One reason is that frequency of heavy rainfall occurrence is much greater than that of large earthquakes in the areas. Earthquake-induced phenomena are interspersed with heavy-rainfall-induced ones, and the former are not distinguished from the latter.

The Kanbun earthquake (1662) around Lake Biwa is considered to be one of the most disastrous earthquakes that ever happened in recorded history. The earthquake source fault is estimated to be located in the central western region of the Lake Biwa catchment (Fig. 1.16) (Komatsubara 2006). It killed about 900 people around Lake Biwa and Kyoto (then, the capital of Japan) (Nishiyama and Komatsubara 2006). In the catchment of Lake Biwa many landslides occurred. In particular, a large landslide in the western catchment (Fig. 1.16, Machii-kuzure; kuzure means landslide in Japanese) killed about 560 people and dammed a river called Katsura-gawa (Iwamura et al. 2002). Two weeks later, the dammed lake burst out. Abundant sediment materials then probably flowed into Lake Biwa through the river. It is

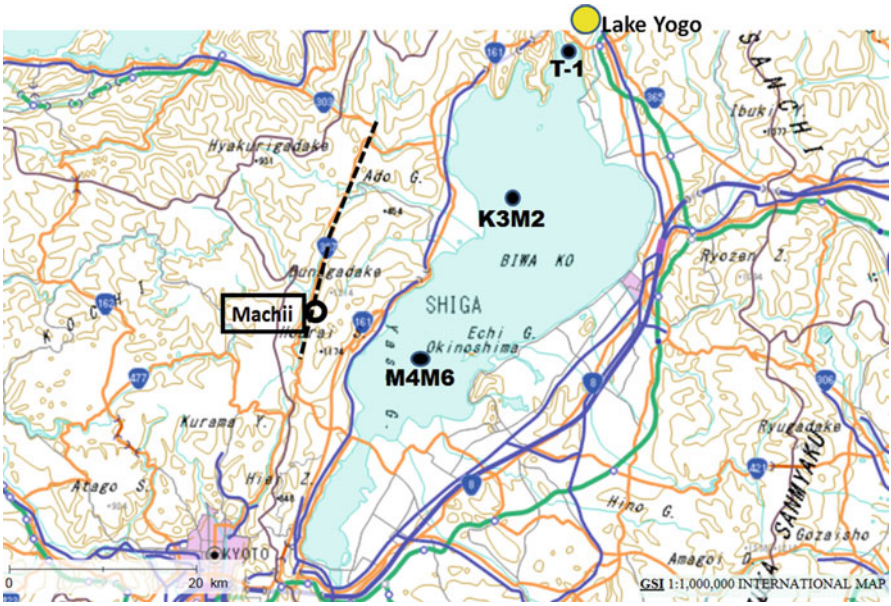

Fig. 1.16 Lake Biwa and its surroundings. *Dotted line*; source fault for Kanbun Earthquake, *open circle*; Machii kuzure, and *solid circles*; sampling points (Based on GIS MAPS; Geospatial Information Authority of Japan)

estimated that most areas around Lake Biwa experienced an earthquake intensity exceeding level 5 on the JMA intensity scale, indicating extremely severe shaking. Documented records report that many houses located around the lake were damaged (Komatsubara 2006).

In Lake Biwa, as mentioned before, various core samples were obtained in many locations also by the Kanazawa University team. Analytical results for the core sediments obtained in the three locations (Fig. 1.16) of the lake are shown in Fig. 1.17. These results display similar variation of mineral content in the common upper parts. They also show that mineral grain size decreased in all of the sampling points and mineral content increased around 1662, assuming that the age model proposed for the T1 core is acceptable (Fig. 1.18, Table 1.1) and that the age at the depth of 52 cm (mass depth of 21.0–21.5 g/cm^2) is correctly assayed by the ^{137}Cs-induced sedimentation rate (0.066 g/cm^2/year). Statistical results for the longest core T1 (Fig. 1.19) also show that some statistical factors begin to fluctuate widely at around 1662 in addition to a decrease in mineral grain size. These may not always be directly related to the earthquake. They may also be related to some large rainfalls after the earthquake. The earthquake may have prepared a large amount of materials to be easily transported. Generally, the rainfalls have occurred relatively shortly after the earthquake according to Japanese climatic characteristics.

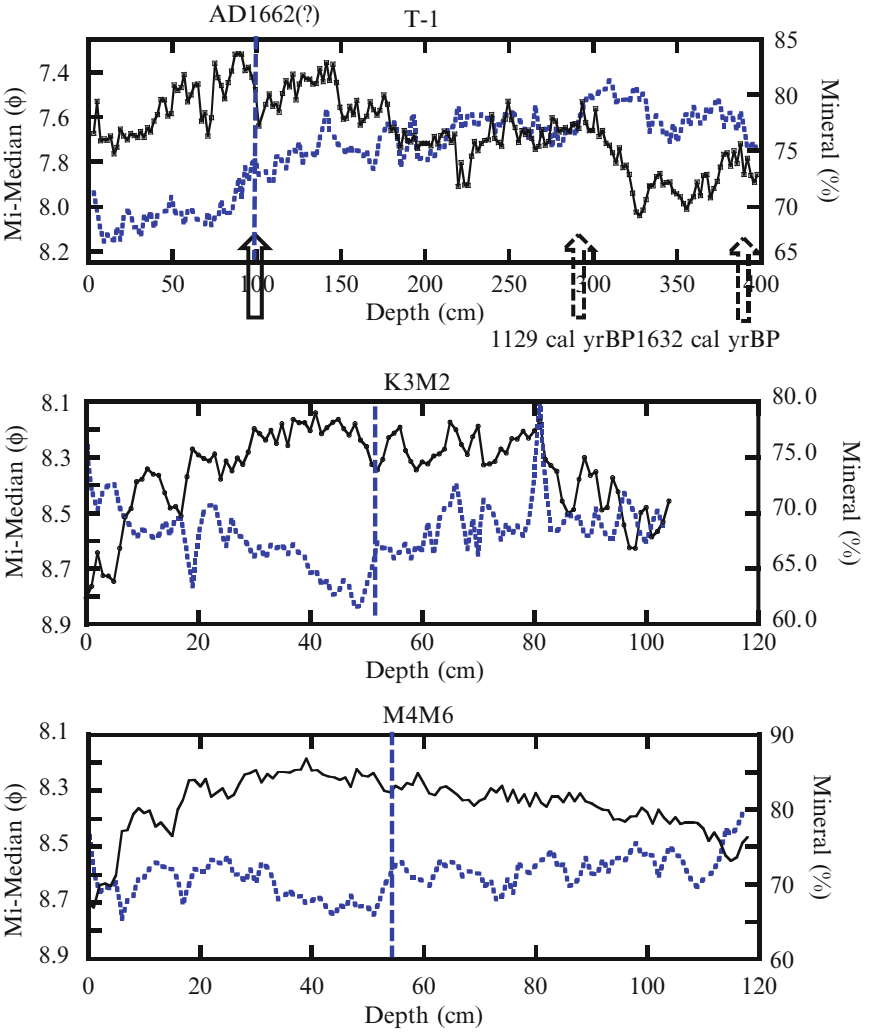

Fig. 1.17 Changes in mineral median (ϕ; *dotted line*) and mineral content (%; *solid line*) of T1 (*upper*), K3M2 (*middle*) and M4M6 (*lower*). *Solid arrow*; C-14 estimated date, *dotted arrow*; C-14 date, and *dotted vertical line*; 1662 (estimated)

1.5 Concluding Remarks

Physical environmental changes in lake-catchment systems due to climatic, tectonic, and anthropogenic activities (processes) have been imprinted on lacustrine sediments. Some physical properties of the sediments provide valuable information on past environmental changes and clues for establishing models.

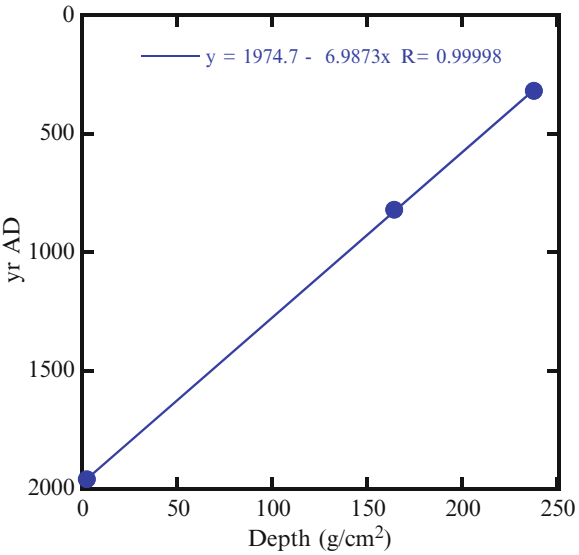

Fig. 1.18 Age model for T1 core; two C-14 dates and one estimated from physical properties

Table 1.1 Dates given with C-14 concentration for T-1 (Lake Biwa)

	Depth (cm)	Material	C-14 Age (year BP)	Calibrated Age (cal. year BP)
IAAA-70659 (BW05T1-4-139)	282 (164.3 g/cm^2)	Wood	1,230 ± 30	1,129 ± 30
IAAA-51425 (BW05T1-4-197)	398 (237.7 g/cm^2)	Wood	1,730 ± 40	1,632 ± 47

Long continuous observation in a small pond-catchment system called Kawausoike following the 1995 Kobe earthquake provides good data on environmental changes. These records are available for establishing a mathematical model for the two stages of evolution of the (lake-catchment) system environments after the earthquake before arriving at the pre-earthquake stage (third stage). Results calculated using the model are fairly consistent with observational ones, indicating that the model is acceptable. Sedimentation rate is a good indicator of erodible conditions in the catchment, which responds to most climatic, tectonic, and anthropogenic activities. However, it is difficult to obtain appropriate estimates of this rate without continuous observation and/or a detailed age model. The 1995 earthquake is faintly recorded in the cores obtained in the same pond. An increase in grain density and slight change in grain size are observed during the earthquake, while a large increase in grain size occurs during the heavy rainfall times. A combination of grain density (or mineral content) and grain size may be useful as an indicator for the occurrence of a comparatively large earthquake in tectonically active and climatically humid areas. The Tong-hai earthquake of 1970 in Yunnan, China was detected in the combination (density increase and grain size decrease) for core sediments obtained from Qilu-he. The Kanbun earthquake of 1662 in the Lake Biwa catchment was also

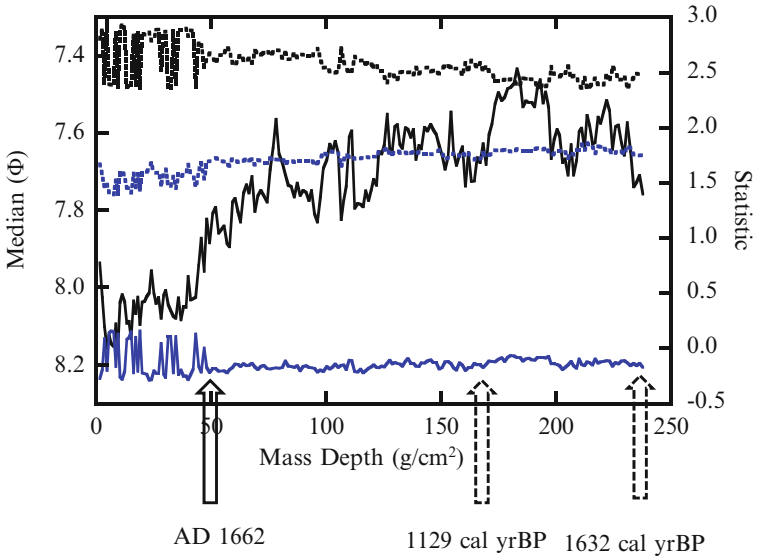

Fig. 1.19 Changes in statistical values for T1: *black line*; median, *dotted blue line*; standard deviation, *solid blue line*; skewness, and *dotted black line*; kurtosis

detected in the corresponding data for some cores obtained from Lake Biwa. The combination of density (mineral content) increase and grain size decrease may be related to erodibility and transportability of surface fine materials produced by the earthquakes.

Acknowledgements We would like to express our heartfelt thanks to all colleagues who worked together at the Limno-geomorphology Laboratory, Institute of Nature and Environmental Technology and Department of Earth Sciences, Kanazawa University, Research Center for Urban Safety, Kobe University, Lake Biwa Research Institute (Dr. M. Kumagai and his colleagues) and Yunnan Institute of Geography, China (Prof. Tang Chuan and his colleagues) for their cooperation in the field and laboratory. Public Construction Bureau of Kobe City Government offered some documents on Kawauso-ike. We (Kashiwaya) also thank Prof. Lin Jiun-Chuan and colleagues of Department of Geography, National Taiwan University for the opportunity to stay at National Taiwan University and to discuss lake-catchment systems in the eastern Asia.

References

Inouchi Y, Kinugasa Y, Kumon F, Yasumatsu S, Nakano S, Shiki T (1996) Turbidites as records of intense paleoearthquakes in Lake Biwa. Jpn Sediment Geol 104:117–125

Itono T, Kashiwaya K, Sakaguchi A (2012) Disastrous flood events found in lacustrine sediments from Lake Biwa. Trans Jpn Geomorphol Union 33:453–468

Iwamura T, Inoue K, Nishiyama A (2002) Biwako-seigan Earthquake (1662) and Machii Landslide Dam. Hist Earthq 18:52–58 (in Japanese)

Kashiwaya K, Okimura T, Hirano M, Okuda S (1984) Geomorphological aspect of landslide and time change of rainfall character in the south-west part of the Rokko-san Mountains. Annuals, Disaster Prevention Research Institute Kyoto University No. 27 B-1:397–408 (in Japanese with English abstract)

Kashiwaya K, Okimura T, Kawatani T (1987) Critical precipitation conditions for landslide and tree ring response in the Rokko Mountains, Kobe, Japan. Inter Assoc Hydr Sci 168:191–197

Kashiwaya K, Taishi H, Kawatani T, Okimura T (1988) Grain size variation of pond sediments and landslide environment in the Rokko Mountains. Trans Jpn Geomorphol Union 9:69–77 (in Japanese with English abstract)

Kashiwaya K, Okimura T, Kawatani T (1990) Reconstruction of past erosional force from tree ring information around the Rokko Mountains, Japan. Quat Res 34:240–248

Kashiwaya K, Yamamoto A, Fukuyama K (1991) Time variation of in coarse materials from lake bottom sediments and secular paleoclimatic change. Geophys Res Lett 18:1245–1248

Kashiwaya K, Okimura T, Kawatani T, Aoki T, Isozumi Y (1995) Landslide environment and pond sediment information. In: Slaymaker O (ed) Steepland geomorphology. Wiley, Chichester

Kashiwaya K, Okimura T, Yatsufuji H (1997) Changes in erosional environment and pond sedimentation in the Rokko Mountains, Kobe, Japan – a preliminary discussion on environmental change due to the Kobe Earthquake, 1995. Trans Jpn Geomorphol Union 18:263–275 (in Japanese with English abstract)

Kashiwaya K, Tsuya Y, Okimura T (2004) Earthquake-related geomorphic environment and pond sediment information. Earth Surf Process Landf 29:785–793

Kashiwaya K, Kusumoto T, Tang C (2006) Lacustrine sediment information in several lakes in Yunnan. In: Kumagai M, Sakamoto T (eds) Lakes and catchments in East Asia monsoonal zone. Nagoya University Press, Nagoya (in Japanese)

Kashiwaya K, Ochiai S, Okimura T, Nahm WH, Yang DY, Kim JY (2012) Erosion and sedimentation in lake-catchment systems in Japan and Korea on the basis of an elementary process model. Trans Jpn Geomorphol Union 33:219–236

Komatsubara T (2006) Historical geographic studies on the disaster areas due to Kanbun (1962) Earthquake. Hist Disaster Stud Kyoto 5:21–38 (in Japanese)

Nishiyama A, Komatsubara T (2006) The damage in the Kyoto-basin due to the 1662 Kanbun Ohmi-Wakasa Earthquake. Hist Earthq 21:165–171 (in Japanese)

Simonneau A, Chapron E, Vannière B, Wirth SB, Gilli A, Di Giovanni C, Anselmetti FS, Desmet M, Magny M (2013) Mass-movement and flood-induced deposits in Lake Ledro, southern Alps, Italy: implications for Holocene palaeohydrology and natural hazards. Clim Past 9:825–840

Taishi H, Okuda S, Shiki T, Kashiwaya K (1991) A sedimentary anomaly and the related sedimentation process in Lake Biwa, Japan. Z Geomorph NF 83:241–249

Torii N, Okimura T, Kato S (2007) Experimental study on slope failure mechanism induced by rainfall after earthquake. J JSCE (C) 63–1:140–149 (in Japanese with English abstract)

Yamamoto A, Kashiwaya K, Fukuyama K (1985) Periodic variations of grain size in Pleistocene sediments in Lake Biwa and earth-orbital cycles. Geophys Res Lett 12:585–588

Chapter 2
Centennial-Scale Environmental Changes in Terhiin Tsagaan Lake, Mongolia Inferred from Lacustrine Sediment: Preliminary Results

Keisuke Fukushi, Nagayoshi Katsuta, Robert G. Jenkins, Kosuke Matsubara, Bunta Takayama, Yukiya Tanaka, Davaadorj Davaasuren, Ochirbat Batkhishig, Noriko Hasebe, and Kenji Kashiwaya

Abstract Terhiin Tsagaan Lake in central Mongolia is a dammed lake formed by the eruption of a volcano at ca 7,000 year BP. Eight short sediment cores, lake water samples and inlet and outlet samples were collected. The concentrations of major

K. Fukushi (✉)
Institute of Nature and Environmental Technology, Kanazawa University, Kakuma, Kanazawa 920-1192, Japan
e-mail: fukushi@staff.kanazawa-u.ac.jp

N. Katsuta • B. Takayama
Faculty of Education, Gifu University, Yanagido 1-1, Gifu 510-1193, Japan

R.G. Jenkins
Faculty of Natural System, Kanazawa University, Kakuma, Kanazawa 920-1192, Japan

K. Matsubara
Faculty of Health sciences, Kanazawa University, Kodatsuno 5-11-80, Kanazawa 920-0942, Japan

Y. Tanaka
Department of Geography, Kyung Hee University, 26, Kyungheedae-ro, Dongdaemun-gu, Seoul 130-701, South Korea

D. Davaasuren
Department of Geography, National University of Mongolia, Ikh surguuliin gudamj – 1, Baga toiruu, Sukhbaatar District, Ulaanbaatar 210646, Mongolia

O. Batkhishig
Institute of Geography, Mongolian Academy of Science, Erkhuu Street, Sukhbaatar District, Ulaanbaatar 14192, Mongolia

N. Hasebe
Institute of Nature and Environmental Technology, Kanazawa University, Kakuma, Kanazawa 920-1192, Japan

Korea Institute of Geoscience and Mineral Resources, 124 Gwahang-no, Yuseong-gu Deajeon 305-350, South Korea

K. Kashiwaya
Institute of Nature and Environmental Technology, Kanazawa University, Kakuma, Kanazawa 920-1192, Japan

Department of Geography, National Taiwan University, Daan District, Taipei 10617, Taiwan

K. Kashiwaya et al. (eds.), *Earth Surface Processes and Environmental Changes in East Asia*, DOI 10.1007/978-4-431-55540-7_2

dissolved species in the samples revealed that the lake water is Ca^{2+}-HCO_3^- type, but that the Ca^{2+} and HCO_3^- levels are relatively low. The water has high dissolved SiO_2 concentrations, which suggests favorable conditions for formation of biogenic silica depending on the surrounding environment. Analyses of the X-ray CT images of the cores showed that the average brightness over the horizontal direction, which represents averaged density of each layer, exhibited pulsed-like peaks as well as gradual fluctuations. The pulsed-like peaks in the pattern were probably resulted from the density currents including clasitic materials from the catchment area, therefore, can be used for the indicator for some hydro-climatic events and/or lake level changes. The gradual fluctuation of the averaged brightness was well correlated with the contents of biogenic silica plus organic matter. The profiles of the brightness can provide high resolution information regarding the biological activities in lake. The patterns of averaged brightness of five cores, obtained from deeper parts of the lake, exhibited similar patterns, with a positive peak in upper part of the sediments, and the minimum brightness just below the positive peak. The comparison of the core obtained from the previous study (Sevastyanov et al. 1989) showed that the short cores obtained from the deeper parts of the lake in present study can provide a record back to 1,000 year B.P. The minimum brightness indicates that the higher biogenic response at 200 years ago. The presence of a positive peak above the minima indicates that the condition became lower biogenic response at 100 years ago and then gradual increase in response as time progressed toward the present.

Keywords Terhiin Tsagaan Lake • Lacustrine sediment • Biogenic silica • Organic matter • X-ray CT

2.1 Introduction

It is essential to understand the environmental changes during the past centuries to millennium to predict future environmental changes, because the period covers both naturally-derived and human-derived environmental changes (Buttler et al. 1996; Tian et al. 2013). Terhiin Tsagaan Lake is located in the Khangai Mountains in central Mongolia (N48°10′15″, E99°43′20″, 2,060 m a.s.l.: Fig. 2.1). The Horgo volcano, which is located 1.5 km NE from the lake, was formed by eruption of a volcano ca 7,000 year B.P. Upon formation of the volcano, the valley of the Terhiin-Gol River was dammed by lava flows (Hunt et al. 2012; Sevastyanov et al. 1989). The area of the lake is 60 km^2, with a length of 16 km, a maximum width of 4.5 km, an average depth of about 6 m and a maximum depth of 20 m (Fig. 2.2). The catchment area of the lake is 7,100 km^2. The lake water outflows via the Sumein-Gol, Orkhon and Selenga rivers to Baikal Lake.

The basin is filled with approximately 4–6 m of lacustrine sediment (Sevastyanov et al. 1989). A thin gravel-sand layer separates these deposits from the underlying basalt lava bedrock. The lacustrine sediments provide a record back to ca 7,000 year B.P. (Sevastyanov et al. 1989). During the1980s, Russian scientists

Fig. 2.1 Location of Terhiin Tsagaan Lake in Mongolia

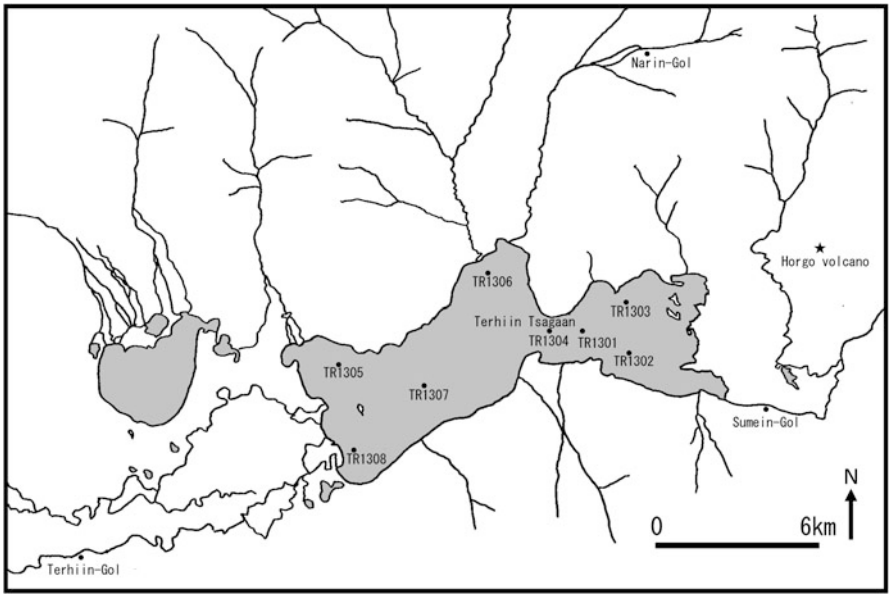

Fig. 2.2 Map showing sampling locations in Terhiin Tsagaan Lake

obtained a 6.1 m sediment core at a water depth of 8.9 m in the northern part of the lake (Sevastyanov et al. 1989), which was used to reconstruct changes in lake level based on the lithology, sedimentation rate and diatom assemblages from lacustrine sediments at a resolution of several hundred years.

The sediments from Terhiin Tsagaan Lake are promising media for environmental records. In this study, eight short sediment cores (70–90 cm) were obtained from the lake in September 2013. We expected to the cores to reflect the environmental record of the past few centuries to millennium. We performed X-ray computed tomography and measured the water contents of the cores and the contents of biogenic silica and organic matter in the dried sample. During the excursion, water samples from the lake, inflows and outflows were corrected and measured for major dissolved species. The purposes of the study were (1) to identify promising environmental proxy in the sediment and (2) to try to preliminarily reconstruct recent environmental changes in Terhiin Tsagaan Lake.

2.2 Materials and Methods

2.2.1 Coring, X-Ray Computed Tomography, Water Contents, H_2O_2 and HCl Soluble Fractions, and Biogenic Silica Contents

Eight short cores were collected from Terhiin Tsagaan Lake in September 2013 (Fig. 2.2). Table 2.1 lists the locations, water depths and lengths of the cores. The core samples were obtained with a gravity core sampler using PVC tubes with an internal diameter of 5.4 cm. Cores were transported to Kanazawa University, Japan in October 2013 and refrigerated at 4 °C. All core samples were investigated by X-ray computed tomography (CT) using a 16-channel multi detector CT scanner, SOMATOM Emotion (Siemens Healthcare), at the School of Health Science, College of Medical, Pharmaceutical and Health Sciences, Kanazawa University. Obtained DICOM images were then used to make cross-sections of each core sample using a zioTerm2009 (Ziosoft, Inc.). The average density of each layer throughout the core samples was calculated from the brightness of the cross-sections made by DICOM image, which is reflected by the X-ray absorption coefficient. During calculations, we only used data from areas in which sediments were present (i.e., we excluded pore space data). After scanning by X-ray CT, four cores (TR1304, 1305, 1307 and 1308) were cut into slices approximately 0.5 cm thick,

Table 2.1 List of core samples collected from Terhiin Tsagaan Lake

	Location		Water depth	Core length
Core	N	E	(m)	(cm)
TR-1301	48°09′59.327″	99°44′41.640″	12.9	73
TR-1302	48°09′28.404″	99°46′07.284″	6.8	75
TR-1303	48°10′29.207″	99°46′00.587″	8.3	86
TR-1304	48°09′59.976″	99°43′42.779″	19.7	80
TR-1305	48°09′23.796″	99°37′07.571″	6.6	72
TR-1306	48°11′08.484″	99°42′01.476″	8.3	83
TR-1307	48°08′49.812″	99°39′56.951″	14.2	76
TR-1308	48°07′39.647″	99°37′29.064″	7.9	68

after which the cut samples were freeze-dried in the laboratory. The water contents of each sample were calculated from the difference in the weights before and after freeze-drying.

The amounts of H_2O_2 and HCl soluble fractions and biogenic silica contents of the dried samples from the TR1304 were measured using the sequential dissolution procedure based on the method by Mortlock and Froelich (1989). For the first step of this procedure, 50 mg portions of dried sample were mixed with 1 ml of 10 % H_2O_2 solution and heated in a water bath for 1 h at 60 °C. After heating, the samples were left at room temperature for 24 h, and then washed in ion-exchanged water, dried for 48 h at 77 °C, and weighed. The amount of H_2O_2 soluble fraction was determined as the mass loss from the original samples. In the second step, the remaining solids after step one were mixed with 1 ml of 1 M HCl solution at room temperature for 20 min, washed in ion-exchanged water, dried for 48 h at 77 °C, and weighed. The amount of HCl soluble fraction was determined as the mass loss from the input samples. In the third step, the remaining solids after step two were mixed with 10 ml of 2 M Na_2CO_3 solution and heated in a water bath for 7 h at 85 °C. After reaction, the reacted supernatants were adequately diluted by pure water. The Si concentration of the solution was then measured using an Inductive Coupled Plasma Optical Emission Spectrometry (ICP-OES) (Ultima2; HORIBA at Gifu University). Amounts of biogenic silica were calculated from the dissolved Si concentration of the samples.

2.2.2 Sampling and Analyses of Lake and River Water

Water samples from Terhiin Tsagaan Lake, two inlets (Terhiin-Gol River and Narin-Gol River) and an outlet (Smein-Gol River) of the lake were collected in September 2013 (Fig. 2.2). Samples were also collected from Lake Hovsgol (N48°38′ E100°10′) and Ugii Lake (N47°45′ E102°46′) for comparison. Samples were collected from the center of Terhiin Tsagaan Lake, which is the deepest part (TR1304 in Fig. 2.2), at varying depths. In addition, pH, electric conductivity (EC), dissolved oxygen (DO) and temperature were measured by a portable pH meter (HM-21P; DKK-TOA Corp.) and a glass multiple electrode (GST-5741C; DKK-TOA Corp.), a portable EC meter (CM-21P; DKK-TOA Corp.) and a portable DO meter (DO-24P; DKK-TOA Corp.). The water samples were filtered through 0.2 or 0.45 μm membranes and stored in three 50 or 100 ml polyethylene bottles separately. One sample was acidified with HNO_3 (trace analysis grade) to give approximately 0.6 % HNO_3 solution for measurement of the major cations and silica concentrations by ICP-OES, while the other two were left unacidified to measure alkalinity and major anion analysis by ion chromatography. The alkalinity was measured within 24 h of sampling. The flow rates of the inlet and outlet were measured by the float method. They were measured by multiplying a cross sectional area of the stream by the velocity of the water obtained from the time required to shift a float a given distance.

The major cations and silica concentrations were measured by ICP-OES (Ultima2; HORIBA at Gifu University for Terhiin Tsagaan Lake and the inlets and outlet; 710-ES; Varian Inc. at Kanazawa University for Lake Hovsgol). The major anion concentrations were measured by ion-chromatography at Gifu University (ICS-1100; Dionex at Gifu University) for samples from Terhiin Tsagaan Lake and its inlet and outlet and high performance liquid chromatography at Kanazawa University (8020 series; TOSOH at Kanazawa University) for the sample from Lake Hovsgol. Speciation calculations were conducted using REACT of The Geochemist's Workbench (Bethke 1998) with the thermodynamics database, "thermo.com.v8.r6 + .dat".

2.3 Results

2.3.1 Water Chemistry

Figure 2.3 shows the temperature, pH, EC and DO with depth at the deepest part of Terhiin Tsagaan Lake measured during daylights hours in September 2013. The temperature of the surface water was 15 °C, while it decreased slightly with depth to 8 m. From 8 m to the bottom (19 m), the water temperature was 13–14 °C. The pH of the surface water was 8.3, and was nearly the same to 16 m, below which it decreased, reaching 7.7 at the bottom. The EC ranged from 14.5 to 15.0 mS/m from the surface to the bottom. The DO of the surface water was 8 mg/L, while this value decreased slightly with depth to 6 mg/L at the bottom.

Table 2.2 shows the water chemistry of lake water samples from the surface, 10 m and the bottom sampled in the morning on the same sampling day. The alkalinity of the surface water was clearly lower than that at 10 m and the bottom, while the dissolved SiO_2 concentration was slightly higher at the bottom than at the surface and 10 m. The concentrations of other components were similar among depths. The water chemistry of Terhiin Tsagaan Lake is characterized by high Ca and alkalinity. The water type of Lake Hovsgol was also Ca-HCO_3 with a slightly alkaline pH. Conversely, the concentrations of the Ca and bicarbonate were almost twice those of Terhiin Tsagaan. The EC of Terhiin Tsagaan Lake is two-thirds that of Lake Hovsgol and one-third that of Ugii Lake.

The water chemistry of Sumein-Gol River (outflow of the lake) was almost the same as that of the lake water. The pH of Sumein-Gol River was slightly higher than that of the lake. That of Terhiin-Gol River was also similar to that of the lake water, although the Ca concentration of Terhiin-Gol River was significantly lower than that of the lake. On the other hand, that of Narin-Gol River was significantly different from that of the lake water. Although the water type of the river was the same as that of the lake (Ca-HCO_3 type), the EC was significantly lower than that of the lake. The flow rate of Terhiin-Gol is significantly higher than that of Narin-gol.

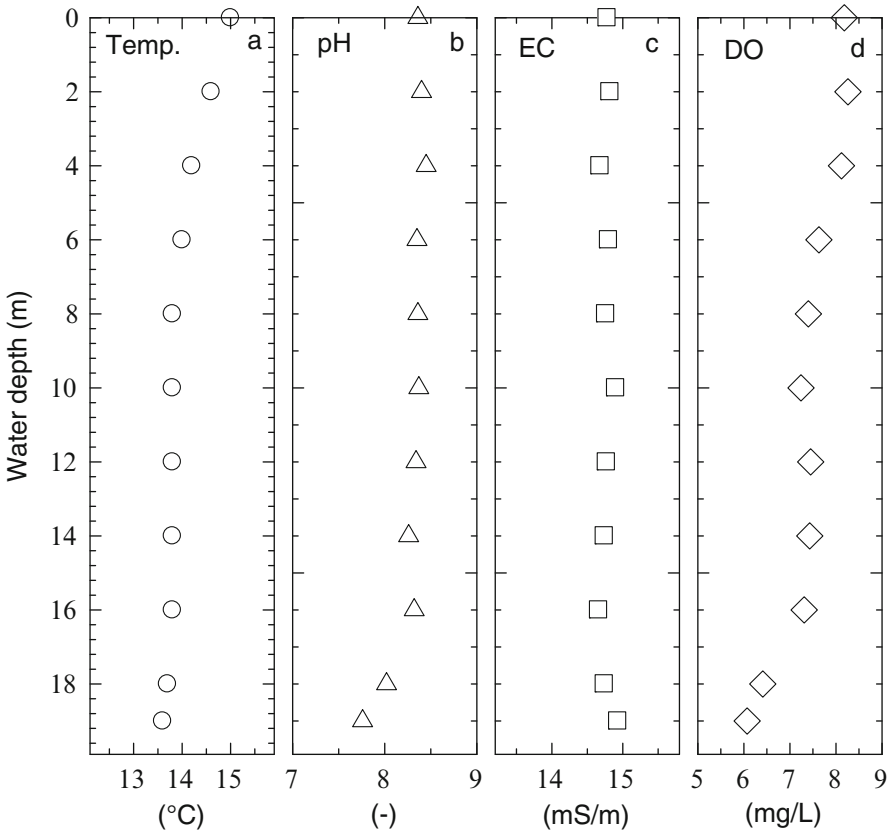

Fig. 2.3 Temperature (**a**), pH (**b**), electrical conductivity (**c**) and dissolved oxygen (**d**) with water depth in Terhiin Tsagaan Lake in September 2014

2.3.2 Short Cores

Figures 2.4, 2.5, and 2.6 show the X-ray CT image and corresponding averaged brightness with depth. In addition to the information from the X-ray CT data, the water contents, H_2O_2 and HCl soluble fractions and biogenic silica contents with depth are given for the selected cores. The cores obtained from shallower parts of the lake (TR1305, TR1302 and TR1308: <8 m) were given in Fig. 2.4. Those obtained from moderate depth parts of the lake (TR1306, TR1303, TR1301 and TR1307: 8–15 m) were given in Fig. 2.5. That from deepest part (TR1304: 19.7 m) was given in Fig. 2.6.

Table 2.2 Water chemistry of Terhiin Tsagaan Lake, its inflows and outflow as well as Lake Hovsgol, Ugii Lake and Lake Baikal

				Coordinates		Flow rate	pH	Temp	EC	DO	Alkalinity	Fe	Ca^{2+}	Mg^{2+}	Na^{+}	K^{+}	SiO_2	Cl^{-}	NO_3^{-}	SO_4^{2-}		Saturation index				
		Sampling date	Source	N	E	(cm^3/s)		°C	mS/m	mg/L	meq/L	mg/L	mg/L	mg/L	mg/L	mg/L	mg/L	mg/L	mg/L	mg/L	Water-type	Calcite	Aragonite	MHC	Quartz	am. SiO_2
Terhiin Tsagan Lake	Surface water	5-Sep-13	This study	48° 10′ 01.76″	99° 43′ 46.27″	–	8.33	13.2	14.81	7.64	0.8	00.32	17.19	3.98	3.99	1.04	3.10	01.40	<0.1	6.66	Ca-HCO_3	−0.15	−0.32	−1.12	−0.07	−1.46
Terhiin Tsagan Lake	10 m depth	5-Sep-13	This study	48° 10′ 01.76″	99° 43′ 46.27″	–	8.36	13.9	15.24	7.41	1.3	00.32	17.43	4.02	3.93	1.02	3.31	01.40	00.25	6.64	Ca-HCO_3	00.09	−0.07	−0.88	−0.06	−1.43
Terhiin Tsagan Lake	19 m depth	5-Sep-13	This study	48° 10′ 01.76″	99° 43′ 46.27″	–	7.55	13.2	15.53	3.48	1.3	00.34	16.80	3.97	3.92	1.07	5.92	01.39	00.45	6.19	Ca-HCO_3	−0.75	−0.92	−1.72	00.22	−1.17
Sumein-Gol River	Outflow	4-Sep-13	This study	48° 08′ 18.11″	99° 49′ 59.82″	28.2	8.79	16.0	14.52	7.66	1.2	00.32	17.14	4.12	4.03	1.15	3.06	01.43	00.27	6.58	Ca-HCO_3	00.51	00.34	−0.47	−0.15	−1.51
Narin-Gol River	Inflow	5-Sep-13	This study	48° 15′ 22.59″	99° 45′ 57.75″	0.08	8.03	10.2	4.62	8.52	0.15	00.32	05.16	0.83	1.91	0.44	2.95	00.41	01.69	7.26	Ca-HCO_3	−1.70	−1.86	−2.66	−0.03	−1.44
Terhiin-Gol River	Inflow	6-Sep-13	This study	48° 05′ 46.18″	99° 29′ 19.36″	18.1	8.24	14.0	13.91	7.84	1.2	00.34	13.04	3.06	3.40	0.75	3.64	01.03	00.68	6.02	Ca-HCO_3	−0.17	−0.33	−1.13	−0.02	−1.40
Lake Hovs-gol	Surface water	4-Aug-11	This study	49° 38′	100° 10′	–	8.31	13.9	25.90	–	2.5	<0.1	35.10	9.64	3.27	1.44	1.64	<0.1	<0.1	7.31	Ca-HCO_3	00.59	00.42	−0.38	−0.35	−1.73
Ugii Lake	Surface water	17-Aug-11	This study	47° 45′	102° 46′	–	9.09	26.0	54.20	–	4.9	–	–	–	–	–	–	–	–	–	–	–	–	–	–	–
Lake Baikal	Average	July-1988	Falkner et al. (1991, 1997)	53°	108°	–	7.2	–	–	–	1.1	–	16.1	3.1	3.6	0.9	1.5–4.5	00.4	–	5.5	Ca-HCO_3	−1.35	−1.52	−2.31	max 0.28	max −1.18

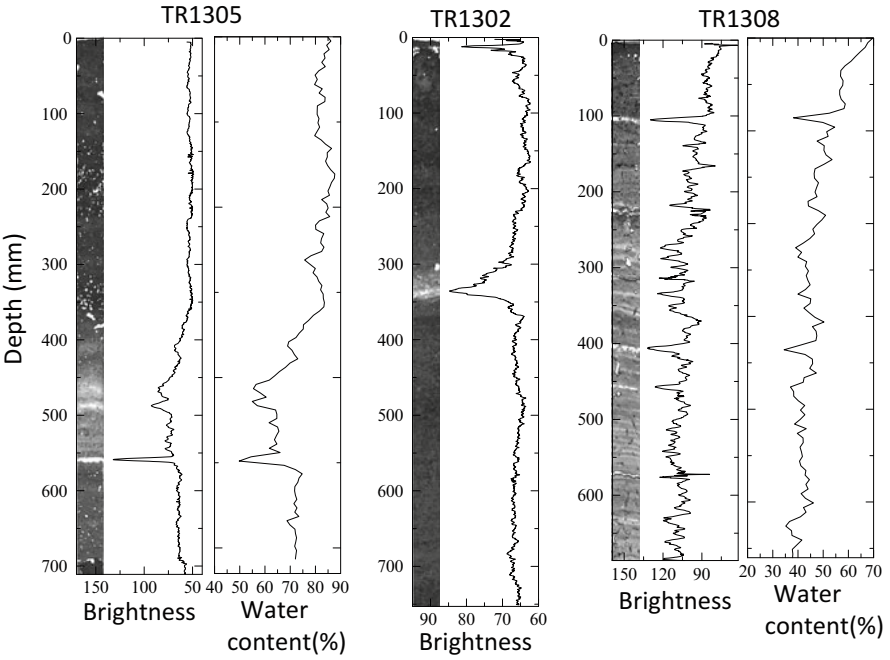

Fig. 2.4 X-ray CT image and corresponding averaged brightness, as well as the water content with depth of the cores taken from shallower parts of the lake (TR1305, TR1302 and TR1308)

2.3.2.1 TR1305

Core TR1305 was obtained from the west side of the lake, where the depth was 6.6 m (Fig. 2.2). The brightness of the CT image represents the density, with brighter areas indicating higher density. The brightest small ellipsoids scattered in the image represent voids filled with gases (bubbles). Few bubbles were observed from the surface to 100 mm and from 470 to 570 mm. However, many bubbles were observed at the other intervals. The contrast of the CT image was low above 400 mm and below 570 mm. Banded layers were observed from 570 to 400 mm. The chart next to the image shows the averaged brightness over horizontal direction with depth. The contributions of the bubble were excluded from the chart. The averaged brightness (hereafter AB) remained nearly constant from the bottom (700 mm) to 580 mm. At 560 mm, a sharp positive peak appeared, while several small peaks were observed between 550 and 500 mm. At 490 mm and 470 mm, relatively large peaks appeared. The AB decreased gradually from 470 to 350 mm, although there were peaks at 410. The minimum AB was observed at 350 mm. Little change in CT was observed at above 350 mm. The water content with depth was similar to that of the AB, and higher AB were associated with lower water contents.

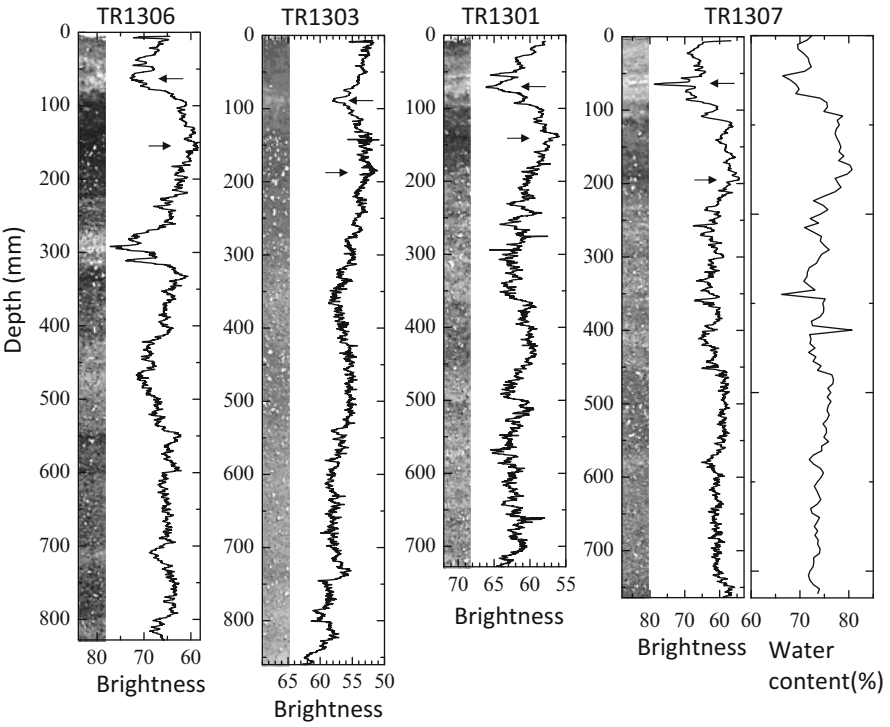

Fig. 2.5 X-ray CT image and corresponding averaged brightness, as well as the water content with depth of the cores taken from moderate depth parts of the lake (TR1306, TR1303, TR1301 and TR1307). The *arrows* (←) indicate positive peak in the *upper* part of the sediments commonly observed in the four cores. The *arrows* (→) indicate the minimum brightness *below* the peak

2.3.2.2 TR1302

Core TR1302 was obtained from the east part of the lake, where the depth was 6.8 m (Fig. 2.2). The core contained few voids with gases and the highest ABs were observed at around 340 and 20 mm.

2.3.2.3 TR1308

Core TR1308 was obtained from the west side of the lake near the mouth of Terhiin-Gol River, where the depth was 7.9 m (Fig. 2.2). There were few bubbles in the core, although relatively large voids were observed at depths of 220, 300, 310, 430 and 580 mm. Banded structures with high and low brightness were observed from the bottom to the top of the CT image of the core. From the bottom to 470 mm, there were many small peaks corresponding to the rhythmic banded structure in the CT image. From 470 to 260 mm, the larger fluctuation of AB was observed, with

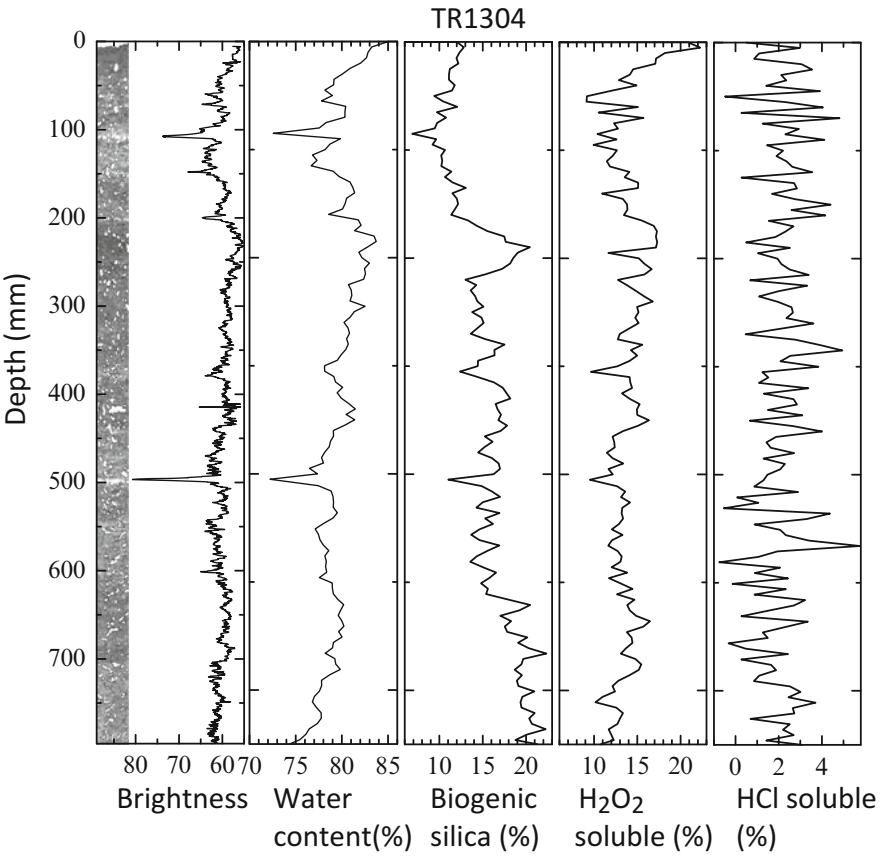

Fig. 2.6 X-ray CT image and corresponding averaged brightness, the water content, the biogenic silica contents and H_2O_2 and HCl soluble fractions with depth of the cores taken from deepest part of the lake (TR1304)

especially strong peaks at 460, 400, 350, 330, 310, 300, 280 and 270 mm. The AB decreased gradually from 260 to 220 mm, then increased rapidly at 220 mm, where a strong peak was observed. The AB remained almost constant from 210 to 170 mm, at which the minimum value was observed. In addition, almost constant AB were observed from 130 to 20 mm, although a strong peak appeared at 100 mm. The pattern of the water content with depth was similar to that of the AB profile.

2.3.2.4 TR1306

Core TR1306 was obtained from the north part of the lake at a depth of 8.3 m (Fig. 2.2). The sampling point was presumably close to that of a previous study conducted by Sevastyanov et al. (1989). Few bubbles were observed from the

surface to 150 mm, while many bubbles were observed below 150 mm. The AB remained almost constant from the bottom (830 mm) to 550 mm, although a broad peak was observed at 700 mm and small negative peaks at 590 and 550 mm. The AB gradually increased from 550 to 460 mm, then slightly decreased at 450 mm, after which it remained almost constant to 420 mm, then decreased again at 410 mm. The AB remained constant from 400 to 340 mm, while a broad but large peak centered at 280 mm with two sharp sub-peaks at 310 and 290 mm was observed from 340 to 250 mm. The AB then gradually decreased from 250 to 150 mm, although several small peaks were observed in this interval. The minimum AB was observed at 150 mm, after which it increased gradually from 150 to 100 mm. There was a large peak from 100 to 20 mm.

2.3.2.5 TR1303

Core TR1303 was obtained from the northeast part of the lake, where the depth was 8.3 m (Fig. 2.2). Bubbles were scarce from 10 to 120 mm, while many bubbles were observed at below 120 mm. The CT image of the core was visually homogeneous. Despite the relatively low signal-to-noise (SN) ratio especially below 120 mm, systematic variations in the AB were observed with depth. The AB was highest at the bottom of the core (850 mm), and gradually decreased to 820 mm. From 800 mm, it increased and then remained constant from 800 to 740 mm, although a small peak appeared at 780 mm. The AB then rapidly decreased at 740 mm and gradually increased to 680 mm, after which it remained almost constant to 600 mm. From 600 to 500 mm, the AB gradually decreased, with two detectable peaks observed at 580 and 540 mm. From 500 to 360 mm, the AB value again gradually increased, then decreased gradually to 190 mm. During the intervals, there were five small peaks at 370, 320, 280, 260 and 220 mm. The minimum AB was observed at 190 mm, and this value remained almost constant from 190 to 130 mm. The SN ratio generally increased from 120 to 10 mm, where the number of bubbles was low. There was a peak centered at 90 mm within the interval.

2.3.2.6 TR1301

Core TR1301 was obtained from the east part of the lake, where the depth was 12.9 m (Fig. 2.2). Few bubbles were observed from the surface to 160 mm, while many bubbles were observed below 160 mm. Even though the pattern showed a relatively low SN ratio, systematic variations in the AB were observed. The AB remained almost constant from the bottom to 520 mm, although several small peaks appeared at the interval. The AB abruptly increased from 500 mm, then decreased gradually to 440 mm, after which it remained almost constant to 370 mm. The AB then rapidly increased at 370 mm, after which it gradually decreased to 140 mm, and there were two detectable peaks at 230 and 260 mm in this region. The minimum

AB appeared at 140 mm. Above 140 mm, the SN ratio increased, and there was a large peak from 140 mm to the surface. In the large peak, there were five small detectable sub-peaks at 100, 50, 30, 20 and 10 mm. The maximum AB value in the peak appeared at 70 mm.

2.3.2.7 TR1307

Core TR1307 was obtained from the west part of the lake, where the depth was 14.2 m (Fig. 2.2). Bubbles were scarce from the surface to 200 mm, while many bubbles were observed below 200 mm. The AB remained almost constant from the bottom of the core (750 mm) to 460 mm, although a small peak appeared at 580 mm. A relatively large fluctuation in the AB occurred from 450 to 220 mm, and there were many small peaks during the interval. The AB gradually decreased from 220 to 200 mm, with the minimum occurring at 200 mm. The AB then gradually increased from 200 to 70 mm. Within this interval, peaks were observed at 120, 90 and 70 mm. The AB remained almost constant from 50 to 10 mm. The variations in water content with depth were similar to those of the AB.

2.3.2.8 TR1304

Core TR1304 was obtained from the central part of the lake, where the depth was 19.7 m (Fig. 2.2). Many bubbles were distributed from the top to the bottom of the core. The AB remained almost constant from the bottom (800 mm) to 700 mm, after which it decreased and then gradually increased to 550 mm. The AB decreased at 540 mm, then rapidly increased at 500 mm, where the highest sharp peak occurred. The AB value then gradually decreased to 430 mm, after which it remained generally constant to 260 mm. The AB then slightly decreased at 220 mm, where the minimum value was observed. Next, the AB increased and formed a peak centered at 200 mm. The AB value was generally similar from 190 to 50 mm, although there were two dominant peaks at 150 and 110 mm. The AB gradually decreased from 50 mm to the surface. The variations in water content with depth were similar to the AB.

The biogenic silica contents ranged from 5 to 23 %. At the bottom, the biogenic silica contents was maximum, then gradually decrease with decrease of the depth. The most of large negative and positive peaks (500, 380 and 110 mm) from the pattern of the biogenic silica contents coincided with the averaged brightness from the CT image. The H_2O_2 soluble fraction presumably represent the organic matter content of the dried sample (Mortlock and Froelich 1989). The H_2O_2 soluble fraction ranged from 9 to 22 %. Except for the top part of the sediments (<50 mm), the H_2O_2 soluble fraction were almost constant at 10 to 15 %. The negative peaks were observed at 70, 500, 380, 250, 170 and 70 mm. Among them, the peaks at 500 and 380 mm coincided with the biogenic silica contents. The HCl soluble fraction

presumably represent the carbonate content (Mortlock and Froelich 1989). The HCl soluble fraction ranged from almost 0 to 6 %. The data was significantly scattered, which represent the analytical uncertainty within the measured ranges. It can be considered that the HCl soluble fraction was negligible in this sample.

2.4 Discussion

2.4.1 Solution Chemistry of Lake Water Relative to Authigenic Mineral Formation

The chemical composition of the Terhiin-Gol River was found to be nearly the same as the lake water (Table 2.2); however, that of Narin-Gol, which is also the inlet of the lake, was very different from the lake water. With the exception of SO_4^{2-} and NO_3^-, the concentrations of dissolved species in Narin-Gol River were significantly lower than those in the lake (Table 2.2). These findings are consistent with Terhiin-Gol River being the primary inflow of the lake, as indicated by the highest flow rates. The concentration of Ca in Terhiin Tsagaan Lake was significantly higher than that of Terhiin-Gol River. One possible explanation for this difference is that Ca is added to the water from lacustrine sediments present in the lake.

The water type of Terhiin Tsagaan Lake is Ca^{2+}-HCO_3^-. Formations of authigenic calcium carbonate have been observed in sediment cores from other Mongolian lakes such as Lake Hovsgol (Hovsgol Drilling Project Members 2009) and Lake Ugii (Schwanghart et al. 2009). The formation of calcium carbonates in Mongolian inland lakes may be a good proxy of environmental climate changes (Fukushi et al. 2006; Kashiwaya et al. 2010; Nishiyama et al. 2013). Table 2.2 lists the saturation indices of calcium carbonates. The lake surface water was found to be nearly in equilibrium with calcite and highly undersaturated with monohydrocalcite (MHC). The saturation index of the minerals in Lake Hovsgol was clearly higher than that in Terhiin Tsagaan Lake, which indicates that the formation of authigenic calcium carbonate is a less suitable proxy of environmental changes in Terhiin Tsagaan Lake than in Lake Hovsgol. This was likely because the geology of the catchment area in which Terhiin Tsagaan is located is dominated by granitic rock, while that in the Hovsgol catchment area is dominated by limestone (MRAM and MAS 1998).

The concentration of dissolved SiO_2 in Terhiin Tsagaan Lake was higher than that in Lake Hovsgol. Accordingly, the saturation indices of silica phases (quartz and amorphous silica) of Terhiin Tsagaan Lake are higher than those of Lake Hovsgol. This can also be attributed to the geological characteristics of the catchment area. The amount of biologically formed authigenic silica minerals (biogenic silica) has been used as the proxy of paleoenvironment in Lake Baikal sediments (Colman et al. 1995; Kashiwaya et al. 1999), and the dissolved SiO_2 concentrations of Terhiin Tsagaan Lake were comparable to in Lake Baikal. The relatively high SiO_2

concentration of the lake water indicates that authigenic silica could readily form within the lake. Therefore, the amount of authigenic silica would be a promising environmental proxy for lake sediments in Terhiin Tsagaan Lake.

2.4.2 Characteristics of Core Sediments in Relation to Environmental Proxies

The sediment in Terhiin Tsagaan Lake is black and rich in organic matter. In sulfate free fresh water, the organic materials are easily decomposed to CO_2 and methane by microbiological activities under anoxic conditions (Batviken et al. 2004); accordingly, the bubbles observed in the sediment core may be gases generated by decomposition of the organic materials under such conditions. The SN ratio of the AB in the layers with bubbles were generally lower than those without bubbles (Fig. 2.4), which was likely due to the millimeter-scale disturbances of the sediment because of the formation of gases following sedimentation. There were clear boundaries between the surface bubble free part and bubble rich part in the TR1301, TR1303, TR1306 and TR1307 cores (Fig. 2.4), representing the boundary between the oxic and anoxic sediments. Conversely, the bubbles were distributed from bottom to top in core TR1304 (Fig. 2.4), which was obtained at the deepest part (19.7 m) of the lake, where the anoxic conditions likely started from the surface of the sediment.

The CT image of TR1308 core exhibits the higher brightness except for the top surface region (<100 mm) than other samples (Fig. 2.4). Because the brightness in CT image represent the bulk density, TR1308 is considered to be mainly composed of relatively dense materials. The core TR1308 was obtained near the mouth of Terhiin-Gol River (Fig. 2.2), which is the important inflow to the lake. The sediment in TR1308 must be dominated by the terrigenious clastic material delivered by the inflow. The pulsed-like sharp peaks in the AB profile were frequently observed from the core TR1308. The pulsed-like peaks are resulted from the predominant delivery and deposition of the dense minerals, most likely due to some hydro-climatic events and/or lake level changes. The pulsed like peaks are also observed at 560 mm depth from TR1305, 340 mm depth from TR1302, 60 mm depth from TR1307, 100 and 500 mm depth from TR1304 cores. These peaks from other samples may also represent the delivery and deposition of the dense clastic materials.

In addition to the pulsed-like peaks, the gradual increases and decreases at low brightness ranges were detected especially from the cores obtained from higher water depth (Fig. 2.5). The gradual fluctuation in CT brightness should represent the gradual changes of the compositions of the sediments. The analytical results of TR1304 (Fig. 2.6) shows that the sediments contain high amount of biogenic silica (5–23 %) and organic matter (9–22 %). The sediments obtained from the deeper part of the lake and/or the far from the inflow are expected to be mainly composed of the fine clastic minerals such as clay minerals, organic matters and biogenic

silica. Among them, the biogenic silica and organic matter possess the lower density than the clastic minerals. Therefore, the gradual fluctuation can be considered to represent the gradual changes of the organic matters and/or biogenic silica contents relative to the terrestrial fine minerals. Figure 2.8 shows the comparison of the AB from CT image and changes of the contents of biogenic silica plus organic matter (H_2O_2 soluble fraction) with depth. The comparison shows the good correlation between them. The changes of AB above 80 mm depth are resulted from changes of organic matter content, while the changes of AB below 80 mm depth are mainly attributable to the changes of biogenic silica content (Fig. 2.6). Because the amount of HCl soluble fraction is negligible, the pattern of residue contents is almost a mirror image of the biogenic silica plus organic matter (Fig. 2.7). The residue after H_2O_2, HCl and Na_2CO_3 extraction most likely represent the clastic silicate minerals. Therefore, the AB from CT image can be also used for the indicator of the amount of the clastic silicate minerals.

Russian scientists obtained a 6.1 m core from a water depth of 8.9 m in the northern part of the lake (Sevastyanov et al. 1989). Based on the water depth distribution in Terhiin Tsagaan Lake, the location of the core taken by the Russian group is expected to correspond to core TR1306 (Fig. 2.2). According to investigations by the Russian group, the unit at 0.60–1.00 m in the core was characterized by relatively high diatom abundance (14×10^6 diatoms per gram). The overlying unit at 0.40–0.60 m was characterized by moderate diatom abundance (10×10^6 /gram). The overlying unit at 0.10–0.40 m was characterized by an increase in diatom abundance (12×10^6 /gram), while the surface layer at 0.00–0.10 m showed a sharp decrease in diatom abundance (7×10^6 /gram). The AB of core TR1306 were generally low from the bottom (80 cm) to 60 cm, indicating high biogenic contents. It increased from 60 to 40 cm, indicating moderate biogenic contents. It value generally decreased from 40 to 10 cm, although there was a large peak at around 30 cm. The AB abruptly increased at 10 cm, then took similar value. The changes in the AB from core TR1306 were consistent with the amounts of diatom abundance reported by Savastyanov et al. (1989). This suggests that the TR1306 can be comparable to the core obtained by the Russian group. The plots in Fig. 2.8 shows the ^{14}C ages of bulk organic gyttja of the 6.1 m core obtained by Russian group with depth. There is clear linear correlation between the ages and the depths. The linear correlation indicates the constant sedimentation rate. On the other hand, the extrapolation of the linear relationship to the surface (0 m depth) indicates the systematic ca 500 years shift in the estimated ages. A shift in age to older values is commonly occurred for some Mongolian lakes (Watanabe et al. 2009; Orkhonselenge et al. 2013). The older ages of the surface sediments were resulted from the input of terrestrial organics and were considered as a lake reservoir effect (Watanabe et al. 2009; Orkhonselenge et al. 2013). The dotted line in Fig. 2.8 shows the corrected the age model assuming the age of the surface sediment is present. The age model indicates that 80 cm short core obtained from the deeper parts of the lake in present study provide a record back to 1,000 year B.P.

The biogenic silica and organic matter contents are considered to be the indicators of some biological responses to the surrounding environments in lake.

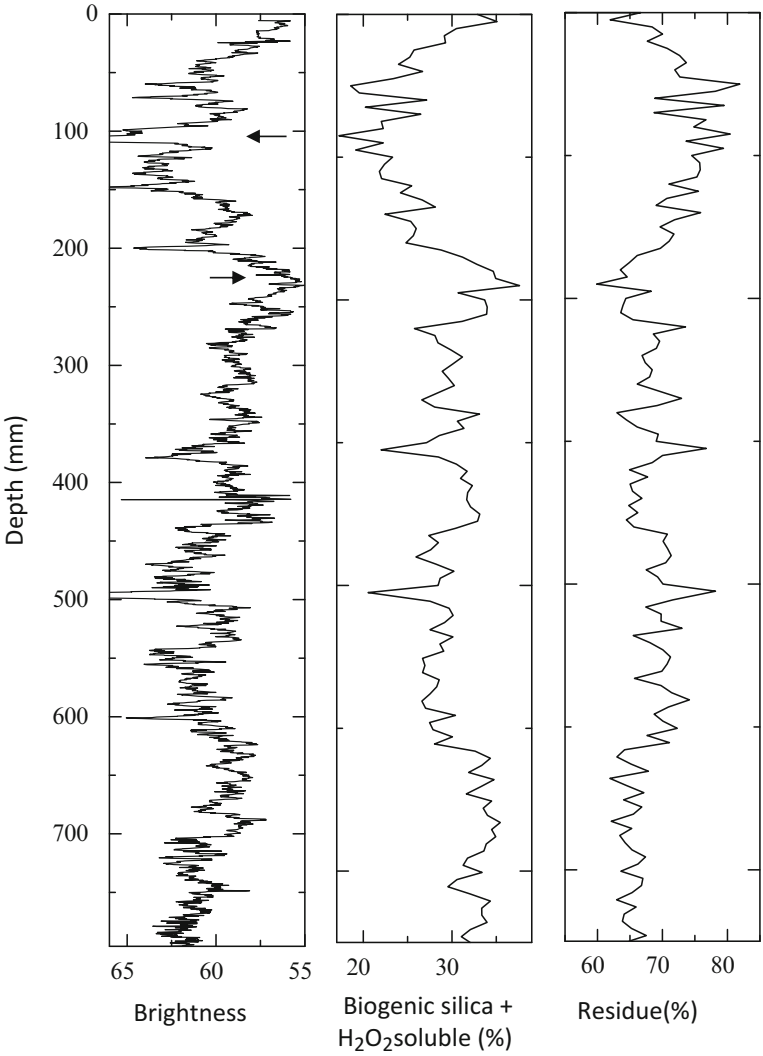

Fig. 2.7 Comparison of the averaged brightness from X-ray CT image, the biogenic silica plus H_2O_2 soluble fraction and the residue after H_2O_2, HCl and Na_2CO_3 extractions of core TR1304

Both detrended curves of TR1306 are similar to the AB curve. Hence, the profiles of the brightness can likely be used to provide high resolution information regarding environmental changes in Terhiin Tsagaan Lake. The patterns of the brightness with depth from TR1301, TR1303, TR1304, TR1306 and TR1307, which are obtained from deeper water depths (>8 m), were similar each other, especially for the upper part of the core. A positive peak was observed in the upper part of the sediments (arrows (←) in Figs. 2.5 and 2.7), while the minimum brightness were observed

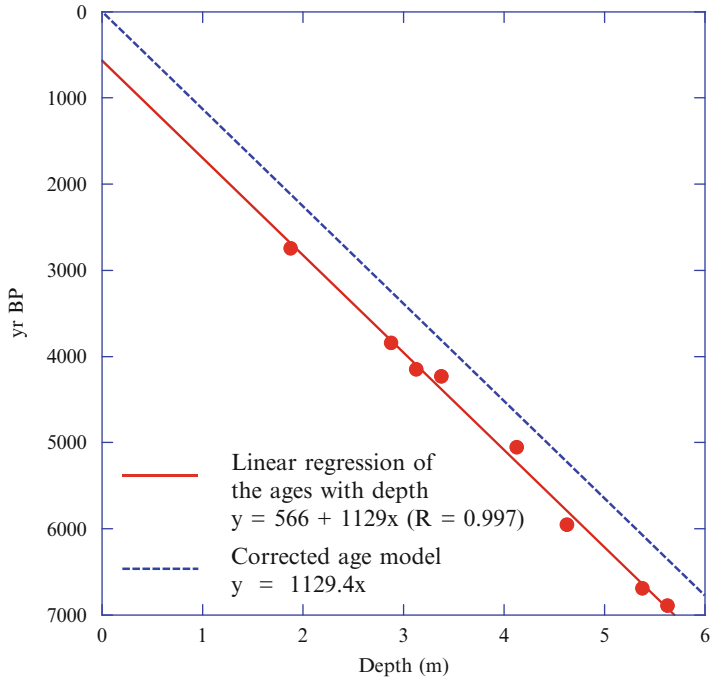

Fig. 2.8 Relationship between the ages and depths of the core obtained and analyzed by Russian group (Sevastyanov et al. 1989). The *line* shows the linear regression of the relationship. The *dotted line* shows the corrected age model

below the positive peaks (arrows (→) in Figs. 2.5 and 2.7). Based on the age model proposed here, the minimum brightness (arrows (←) in Figs. 2.5 and 2.7) and a positive peak above (arrows (→) in Figs. 2.5 and 2.7) correspond to around 200 and around 100 years ago, respectively. Low brightness indicate the high biogenic response in lake at around 200 years ago. The presence of a positive peak above the minima indicates that the conditions became lower biogenic response at around 100 years ago and then gradual increase in response with time toward the present conditions.

2.5 Conclusions

The water chemistry of Terhiin Tsagaan Lake is similar to that of Terhiin-Gol River, which had the highest flow rate and was therefore the predominant inflow into the lake. Stratification of the water body was not observed in the Terhiin Tsagaan Lake during summer. The water type of Terhiin Tsagaan Lake was found to be Ca^{2+}-HCO_3^-, and the concentrations of the calcium and bicarbonate in the

lake were significantly lower than in Lake Hovsgol, where the carbonate mineral contents in the sediments have been used as an environmental proxy. Rather, the water chemistry was characterized by high SiO_2 concentrations, suggesting favorable formation of biogenic silica from the lake water that was dependent on the surrounding environment.

The patterns of the averaged brightness from CT image of the cores exhibited pulsed-like peaks as well as gradual fluctuations. The pulsed-like peaks in the pattern are most likely resulted from the delivery and deposition of the dense clasitic materials from the catchment area. Therefore, the pulsed-like peaks can be used for the indicator for the climatic events and/or the lake level change. The gradual fluctuation of the averaged brightness was well correlated with the contents of both biogenic silica and organic matter of samples. The profiles of the brightness can provide high resolution information regarding the biological response to surrounding environments in lake. The patterns of the brightness with depth from TR1301, TR1303, TR1304, TR1306 and TR1307, which are obtained from deeper water depths (>8 m), were similar each other, especially for the upper part of the core. A positive peak was observed in the upper part of the sediments, while the minimum brightness were observed below the positive peaks. Low brightness indicate the high biogenic response in lake at 200 years ago. The presence of a positive peak above the minima indicates that the conditions became lower biogenic response at 100 years ago and then gradual increase in response with time toward the present conditions.

References

Batviken DJ, Cole M, Pace M, Tranvik L (2004) Methane emissions from lakes: dependence of lake characteristics, two regional assessments, and a global estimate. Global Biogeochem Cycles 18, GB4009. doi:10.1029/2004GB002238

Bethke CM (1998) The geochemist's workbench users guide. University of Illinois, Illinois

Buttler A, Warner BG, Grosvernier P, Yvan M (1996) Vertical patterns of testate amoebae (Protozoa: Rhizopoda) and peat–forming vegetation on cutover bogs in the Jura, Switzerland. New Phytol 134:371–382

Colman SM, Peck JA, Karabanov EB, Carter SJ, Bradbury JP, King JW, Williams DF (1995) Continental climate response to orbital forcing from biogenic silica records in Lake Baikal. Nature 378:769–771

Falkner KK, Measures CI, Herbelin SE, Edmond JM, Weiss RF (1991) The major and minor element geochemistry of Lake Baikal. Limnol Oceanogr 36:413–423

Falkner KK, Church M, Measures CI, Lebaron G, Thouron D, Jeandel C, Stordal MC, Gill GA, Mortlock R, Froelich P, Chan L-H (1997) Minor and trace element chemistry of Lake Baikal, its tributaries, and surrounding hot springs. Limnol Oceanogr 42:329–345

Fukushi K, Fukumoto H, Munemoto T, Nagata T, Kashiwaya K (2006) Carbonate mineralogy in sediment from Lake Hovsgol and its implications for environmental and geochemical changes of lake water. Abstract volume in the 5th international symposium on terrestrial environmental changes in East Eurasia and Adjacent Areas, 12–13

Hovsgol Drilling Project Members (2009) Sedimentary record from Lake Hovsgol, NW Mongolia: results from HDP-04 and HDP-06 drill cores. Quat Int 205:21–37

Hunt AC, Parkinson IJ, Harris NBW, Barry TL, Rogers NW, Yondon M (2012) Cenozoic volcanism on the Hangai Dome, Central Mongolia: geochemical evidence for changing melt sources and implications for mechanisms of melting. J Petrol 53:1913–1942

Kashiwaya K, Ryugo M, Horii M, Sakai H, Nakamura T, Kawai T (1999) Climato-limnological signals during the past 260,000 years in physical properties of bottom sediments from Lake Baikal. J Paleolimnol 21:143–150

Kashiwaya K, Ochiai S, Sumino G, Tsukamoto T, Szyniszewska A, Yamamoto M, Sakaguchi A, Hasebe N, Sakai H, Watanabe T, Kawai T (2010) Climato-hydrological fluctuations printed in long lacustrine records in Lake Hövsgöl, Mongolia. Quat Int 219:178–187

Mortlock RA, Froelich PN (1989) A simple method for the rapid determination of biogenic opal in pelagic marine sediments. Deep-Sea Res 36:1415–1426

MRAM and MAS (Mineral Resources Authority of Mongolia and Mongolian Academy of Sciences) (1998) Geological Map of Mongolia Ulaanbaatar

Nishiyama R, Munemoto T, Fukushi K (2013) Formation condition of monohydrocalcite from $CaCl_2$-$MgCl_2$-Na_2CO_3 solutions. Geochim Cosmochim Acta 100:217–231

Orkhonselenge A, Krivonogov SK, Mino K, Kashiwaya K, Safonova IY, Yamamoto M, Kashima K, Nakamura T, Kim JY (2013) Holocene sedimentary records from Lake Borsog, eastern shore of Lake Khuvsgul, Mongolia, and their paleoenvironmental implications. Quart Int 290–291:95–109

Schwanghart W, Frechen M, Kuhn NJ, Schütt B (2009) Holocene environmental changes in the Ugii Nuur Basin, Mongolia. Palaeogeogr Palaeoclimatol Palaeoecol 279:160–171

Sevastyanov DV, Dorofeyuk NI, Liiva AA (1989) The origin and evolution of the volcanic Terkhiin-Tsagan-Nur Lake in Central Hangai (MPR). Izv Vses Geogr Obshch 121:223–227 (in Russian)

Tian F, Herzschuh U, Dallmeyer A, Xu Q, Mischke S, Biskaborn BK (2013) Environmental variability in the monsoon–westerlies transition zone during the last 1200 years: lake sediment analyses from central Mongolia and supra–regional synthesis. Quat Sci Rev 73:31–47

Watanabe T, Nakamura T, Nara FW, Kakegawa T, Horiuchi K, Senda R, Oda T, Nishimura M, Matsumoto GI (2009) High-time resolution AMS ^{14}C data sets for Lake Baikal and Lake Hovsgol sediment cores: changes in radiocarbon age and sedimentation rates during the transition from the last glacial to the Holocene. Quat Int 205:12–20

Chapter 3
OSL Chronology of the Sand Hills of Xingkai Lake, Northeast China and Its Implication for Environmental Changes Since 200 kyr BP

Ji Shen, Yong Wang, and Yun Zhu

Abstract Xingkai (Khanka) Lake, on the Sino-Russian boundary, is the largest freshwater lake in northeast Asia. It features multiple sand hills to its northern bank formed since the late Pleistocene when the lake surface was larger. High-accuracy chronology is needed to constrain the age of different historical high water level (big-lake) periods, in order to understand the relationship between climate and environmental change. We first tried to use the optically stimulated luminescence (OSL) dating method to date 18 quartz samples from the four sand hills of Xingkai Lake. The analysis of grain-size and magnetic susceptibility (MS) for the nearest two sections were also undertaken to understand the formation mechanism of the sand hills. The OSL chronology indicates that there had been four big-lake periods at 193–183, 136–130, 24–15 and 3–0 kyr BP, respectively. From regional comparisons, we found that these big-lake periods were associated with relatively colder climates, broadly corresponding to the Marine Isotope Stage (MIS) 6, MIS 2 and the late Holocene. This hypothesis is supported by further high resolution OSL chronology for a sediment core XK from Xingkai Lake. OSL chronology for this core reveals contrasting higher sedimentation rates in MIS 6, MIS 4, MIS 2 and late Holocene, compared to other periods. The higher sedimentation rates associated with the cold periods may be related to the rapid accumulation of the <16 μm fraction sediment (comprising more than 80–90 % sediment of core XK) under relatively static water conditions.

Keywords Xingkai (Khanka) Lake • Sand hills • OSL dating • 200 kyr BP • Big-lake periods

J. Shen (✉) • Y. Wang • Y. Zhu
State Key Laboratory of Lake Science and Environment, Nanjing Institute of Geography and Limnology, Chinese Academy of Sciences, 73 East Beijing Road, Nanjing 210008, P.R. China
e-mail: jishen@niglas.ac.cn

K. Kashiwaya et al. (eds.), *Earth Surface Processes and Environmental Changes in East Asia*, DOI 10.1007/978-4-431-55540-7_3

3.1 Introduction

Xingkai Lake (Khanka Lake in Russian), on the border of China and Russia (Fig. 3.1a, b), is the largest freshwater lake in northeast Asia. Northeast Asia, which includes northeast China, is very sensitive to climatic changes, being influenced by the mid- and high-latitude climatic systems. Hence records from this area provide archives for changes in the summer and the winter monsoons of East Asia (An et al. 2000; Li 1998; Fig. 3.1a). Xingkai Lake is the only site in northeast Asia that has been chosen as a drilling point in the PAGES Pole-Equator-Pole Program (Williams et al. 2001).

Despite its significance, there have only been a few paleoclimatic studies on Xingkai Lake (Qiu et al. 1981; Xia and Wang 2000; Yang and Wang 2003; Zhang et al. 2004). The subject of these works was the catchment to the north (the Sanjiang Plain and Muling-Xingkai Plain) and mainly focused on peat bog studies. The peat bog record only covers the time interval since the late Holocene. We carried out research on Xingkai Lake commencing in 2007 and have acquired multi-proxy records for sediment cores (3–4 m in length) from the lake basin (Wu and Shen 2009, 2010). Core drilling is difficult, usually hampered by harsh conditions (strong winds and waves) and high degrees of sediment compaction.

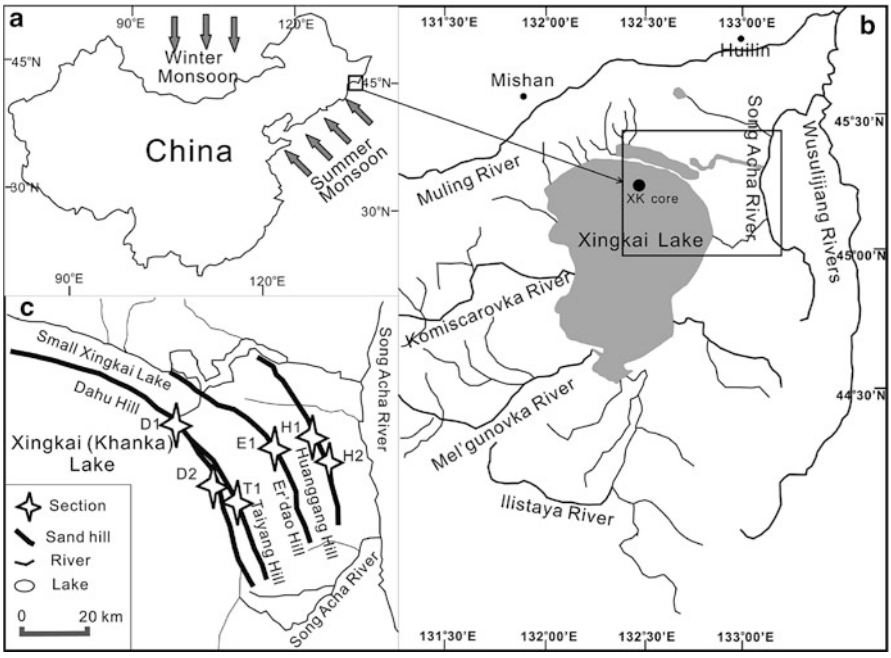

Fig. 3.1 (**a**) Climate of northeast China and the location of Xingkai Lake, (**b**) Hydrological map of Xingkai Lake with *black square* denoting the study area (four sand hills) and (**c**) Map of the sand hills in the northern Xingkai Lake and position of the study sections

In contrast, the sand hills to the northern bank of Xingkai Lake are more accessible, and these are one of the most striking features of the lake (Fig. 3.1c). There are four sand hills to the north of the lake that were formed as the lake retreated since the Late-Pleistocene (Qiu et al. 1988, 2007). Information about the lake's evolution can be inferred from studying the formation and preservation of these sand hills. We can further validate this information by considering the data from the sediment cores. Chronological studies are vital for reconstructing environmental fluctuations. However, only a few dates for the sand hills had been obtained by thermoluminescence (TL) dating in the last century (Qiu et al. 1988). Hence, more detailed and accurate chronological studies are needed.

The optically stimulated luminescence (OSL) dating technique has become a useful tool for dating of late Quaternary sediments (Wintle 1997; Prescott and Robertson 1997; Zhao et al. 2000), and its reliability has been validated by independent methods such as ^{14}C dating (Huntley et al. 1993; Zhao et al. 2007) in not only aeolian deposits (Lu et al. 2006; Yang et al. 2010) but also marine and lacustrine sediments (Long et al. 2011, 2012; Kortekaas et al. 2007; Zhang et al. 2014). Therefore the OSL technique is suitable for dating the sand hills. In addition, the OSL method can normally be used to constrain samples of <200 kyr BP (Murray and Olley 2002). This is another advantage to the ^{14}C dating, the ultimate limit of which is normally <50 kyr BP (Björck and Wohlfarth 2001).

In this article, we show how we use the OSL technique to conduct a systematic chronological study of the sand hills. Our aim is to find the age of formation and mechanism of these preserved sand hills, and their relationship with lake evolution and climatic change. This result has also been compared with the OSL dating results of a sediment core (XK, Fig. 3.1b) from the northern part of Xingkai Lake, in order to validate our inferences.

3.2 Study Area, Section and Samples

Xingkai Lake (N44°32′–N45°21′, E131°58′–E132°51′, 69 m a.s.l.), a trough-fault lake, is located in the Ussuri-Khanka Depression (Fig. 3.1a, b). The lake has a surface area of ~4,380 km^2, with an average water depth of 4–5 m and a maximum water depth of ~10 m. The catchment of the lake is mainly covered by Quaternary sediments, up to 300 m thick, derived from diluvial and alluvial sources. The major inflows include the Komissarovka, Mel'gunovka, Ilistaya and Spasovka rivers in Russia and the Baileng River in China (Fig. 3.1b). Xingkai Lake has a sub-humid continental monsoon climate. The mean annual temperature is 2.9–3.1 °C, with the highest in July (~21 °C) and the lowest in January (approximately −18 °C). The annual precipitation is 554–690 mm and the annual evaporation is about ~490 mm. Southwest winds prevail in spring and summer, while northwest winds prevail in autumn and winter. There are now four sand hills to the north of Xingkai Lake named the Dahu, Taiyang, Er'dao and Huang-Nan sand hills, which are arc shaped and parallel to each other and the lakeshore (Fig. 3.1c). The width of the sand hills ranges from 30 to 200 m, the lengths range from 20 to 80 km, and the heights are between 3 and 10 m (Wang and Chen 2005).

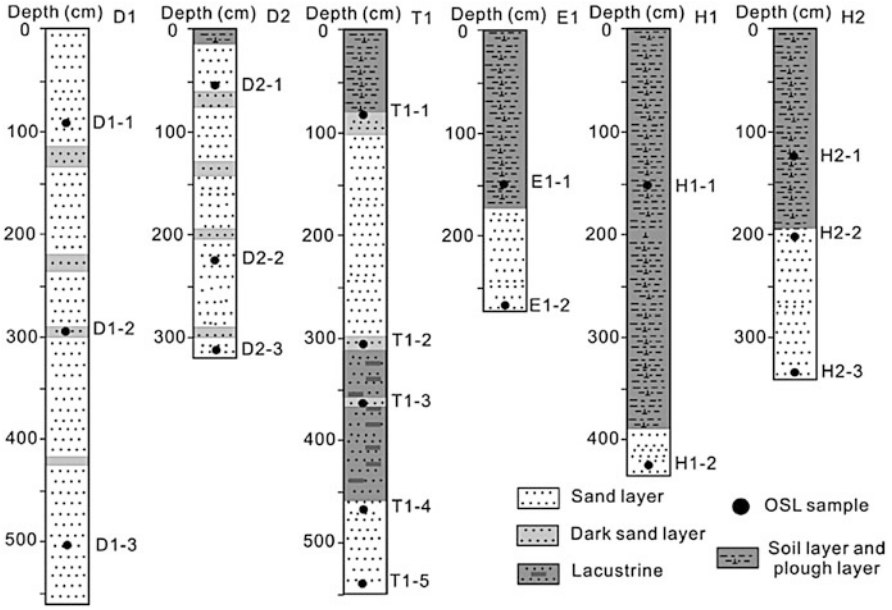

Fig. 3.2 Sections from the sand hills north of Xingkai Lake, showing the lithology and the position of OSL samples

In October 2009, we investigated six sections from the four sand hills: D1 and D2 sections from the Dahu Sand hill, T1 section from the Taiyang Sand hill, E1 section from the Er'dao Sand hill and H1 and H2 sections from the Huang-Nan Sand hill (Fig. 3.1c). From in-situ investigations, each of these sections is composed of two parts: a lower, continuous sand layer without obvious interruption and an upper eroded layer with a developed soil (Fig. 3.2). The Dahu Sand hill is an exception, as it is still growing at the present day. This observation is consistent with previous studies (Qiu et al. 1988, 2007).

Eighteen OSL samples were collected from these six sections (Fig. 3.2). All OSL samples were obtained by hammering steel tubes (20 cm long cylinders with a diameter of 5 cm) into freshly dug vertical sections. The tubes were covered with aluminium foil, and wrapped with black bags and tape to avoid light exposure and moisture loss. Meanwhile, samples at intervals of 5–20 cm were also taken from all the sections for analysis of grain-size and magnetic susceptibility (MS).

3.3 Methods

In the laboratory, under subdued amber light ($\lambda = 640 \pm 10$ nm), the sediment at each end of the tube was scraped for determination of dose rate and water content. The non-light exposed sediment in the middle part of the tube was used for OSL dating.

For each sample, two grain-size fractions, fine-grained quartz (FG, 4–11 μm) and coarse-grained quartz (CG, 90–125 μm) were extracted for equivalent dose (D_e) measurements. The raw samples were pre-treated with HCl (40 %) and H_2O_2 (30 %) to remove carbonates and organic matter. The CG grains were separated by wet sieving, and treated with 30 % H_2SiF_6 for 3 days to corrode feldspars in order to avoid age underestimation (Roberts 2007). Thereafter, 10 % HCl was used to remove fluoride precipitates. Next the FG quartz grains were obtained by treating samples in Atterberg cylinders using Stoke's Law. Finally, the FG quartz grains were dried and placed on stainless steel disks (diameter = 10 mm) using pure water with pipette for D_e measurements. For the CG grains, an electronic magnet was used to remove magnetic minerals. Subsequently, the CG grains were treated with 40 % HF for 1 h to remove feldspars and the alpha-irradiated outer layer of quartz grains, followed by several distilled-water washes. The CG quartz grains obtained were then dried at a temperature of <50 °C and were placed on stainless steel disks using silicone oil for D_e measurements. The purity of the isolated quartz was checked by infrared light stimulation (830 mm) and no obvious infrared stimulated luminescence (IRSL) was observed in any of the samples.

OSL measurements were conducted at the Luminescence Dating Laboratory of the Groundwater Mineral Water and Environmental Supervising and Testing Center (Heibei, China), using a Daybreak 2200 automated OSL reader equipped with a combined blue (470 ± 5 nm) and infrared (880 ± 80 nm) LED unit. Samples were pre-treated by heating at 260 °C for 10 s with a cutheat of 220 °C for 10 s. Irradiation was carried out using a beta source (801 E) built into the reader. The estimated dose rate for artificial irradiation was 0.104 Gy/s. For D_e determination, the simplified multiple aliquot regenerative-dose (SMAR) protocol (Wang et al. 2005) was used for the FG quartz samples while the single aliquot regenerative-dose (SAR) protocol (Murray and Wintle 2000) was used for the CG quartz samples. The U and Th contents were measured by neutron activation analysis, while the K content was measured by atomic absorption spectrophotometry. The cosmic ray dose rate was estimated as a function of depth, altitude and geomagnetic latitude (Prescott and Robertson 1997).

For the grain-size analysis, carbonate and organic carbon were removed by treating the samples with excessive HCl (1 M) and H_2O_2 (30 %). Afterwards, 10 ml of a 10 % solution of $(NaPO_3)_6$ was added to the samples, which were subsequently dispersed through an ultrasonic bath. The grain-size distributions were determined with a Malvern 2000 laser instrument, with a measurement range of 0.02–2,000 μm. Repeated measurements indicated that the analytical error was less than 2 %. The MS analysis was implemented with a Bartington MS 2B (both 4.7 kH and 0.47 kHz) sample sensor. These two sets of experiments were conducted at Nanjing Institute of Geography and Limnology, Chinese Academy of Sciences.

3.4 Results

3.4.1 OSL Data

The OSL signal for FG quartz decreases very quickly in the first few seconds as showed by the shine-down curves, indicating that the OSL signal is dominated by a fast component (Fig. 3.3). The OSL signals from the first 0.64 s stimulation were integrated for growth curve construction after background subtraction. Growth

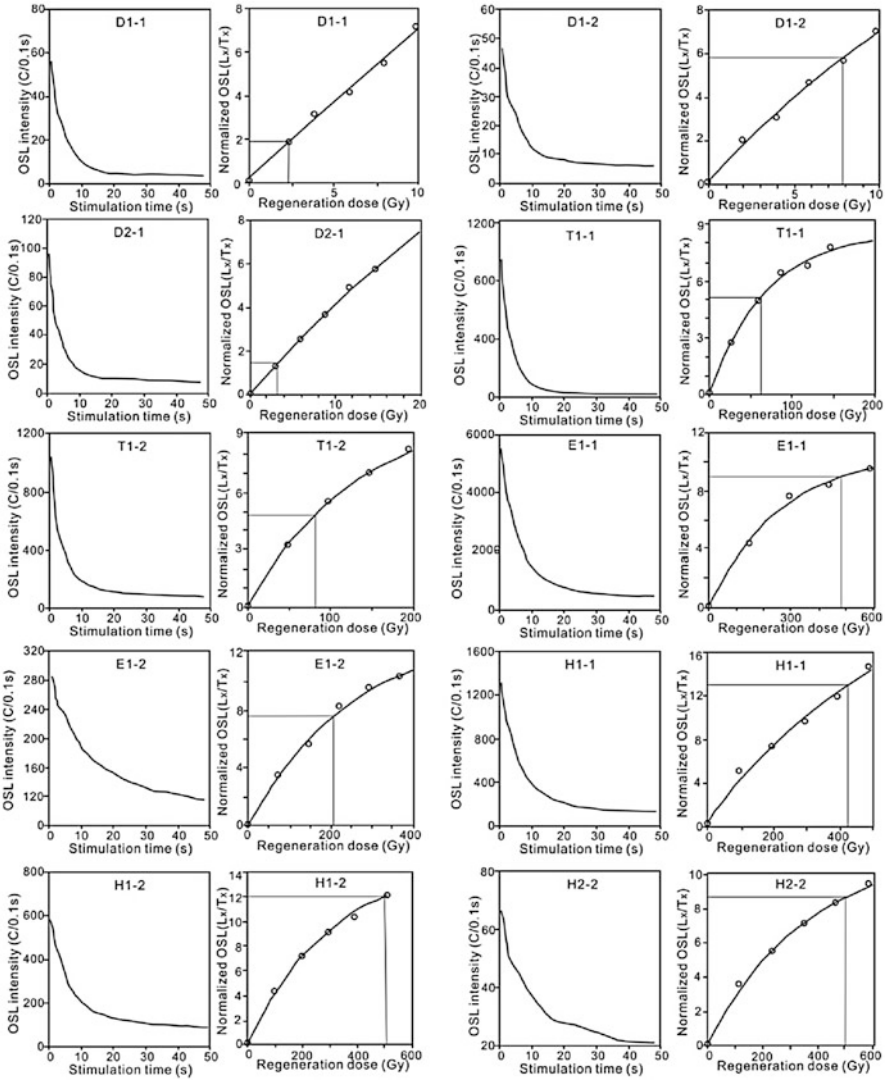

Fig. 3.3 OSL shine-down curves and growth curve for samples from the sand hills of Xingkai Lake

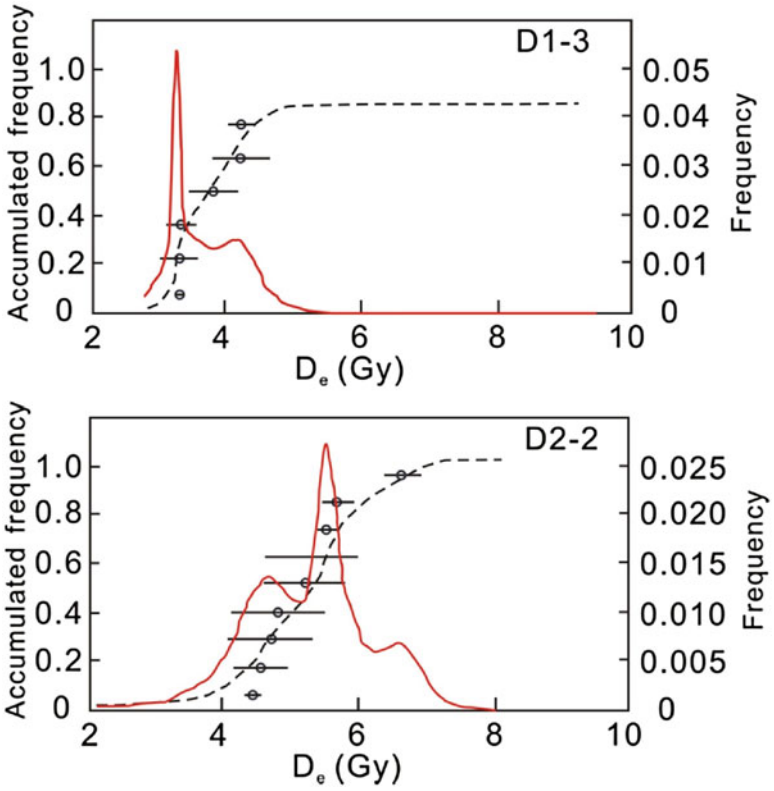

Fig. 3.4 Histograms of D_e distribution for two representative samples (D1-3 and D2-2) from the sand hills of Xingkai Lake

curves (Fig. 3.3) were well constructed by single exponential function, with six regeneration dose points, including a zero-dose for the measurement of recuperation for assessing the sensitivity change correction. Hence the using of the SMAR protocol is appropriate (Roberts and Duller 2004). For most CG quartz samples, the D_e distributions measured by the SAR protocol show a narrow and normal distribution, as shown in Fig. 3.4. This suggests well-bleached sediment prior to deposition (Olley et al. 1999). Based on the averaged D_es, the obtained OSL ages for the sand hills were calculated and they are in stratigraphic order (Table 3.1). These dated range from ~200 ka to ~0.7 ka.

3.4.2 Grain-Size and MS Data

From the grain-size data, the sand hills are primarily composed of fine sand fractions with average median diameter (Md) ranging from 1.8 Φ to 2.4 Φ where the

Table 3.1 OSL dating results for the sand hills of Xingkai Lake

Sample	Depth (cm)	Water content (%)	U (ppm)	Th (ppm)	K (%)	Dose rate (Gy/Ka) s	D_e (Gy)	OSL Age (Ka)
D1-1	85	1.98	0.4	2.08	2.89	3.79	2.32 ± 0.22	0.7 ± 0.1
D1-2	295	4.74	0.4	1.79	2.97	3.42	7.82 ± 0.19	2.3 ± 0.1
D1-3	495	5.69	0.39	1.72	2.88	3.19	9.24 ± 0.44	2.9 ± 0.1
D2-1	57	2.65	0.41	1.87	2.96	3.42	3.23 ± 0.12	0.9 ± 0
D2-2	227	5.41	0.38	1.69	2.88	3.24	5.2 ± 0.42	1.6 ± 0.1
D2-3	317	3.50	0.34	1.21	2.48	2.80	5.72 ± 0.48	2.0 ± 0.2
T1-1	97	3.07	0.38	1.68	3.34	3.85	62.49 ± 3.63	16.2 ± 1.1
T1-2	307	6.44	0.82	3.07	2.71	3.40	82.49 ± 2.63	24.2 ± 1.2
T1-3	370	2.01	0.4	2.25	3.04	3.59	100.41 ± 1.73	28.0 ± 1.2
T1-4	462	3.06	0.75	2.74	3.13	3.81	143.1 ± 3.01	37.6 ± 1.3
T1-5	547	4.40	0.43	1.74	3.08	3.43	163.75 ± 3.6	47.7 ± 2.2
E1-1	152	9.23	1.31	6.62	2.07	3.21	412.69 ± 15.16	128.4 ± 7
E1-2	257	5.11	1.26	5.96	2.45	3.58	483.18 ± 20.25	135.0 ± 7.8
H1-1	152	11.10	1.6	4.66	2.06	3.12	424.14 ± 16.08	135.9 ± 9.1
H1-2	425	19.43	0.68	4.25	2.2	2.59	509.57 ± 17.29	183.8 ± 9.6
H2-1	127	9.37	0.86	4	2.16	2.95	479.48 ± 13.6	162.7 ± 7.7
H2-2	182	20.57	0.77	3.43	2.22	2.73	501.9 ± 13.06	183.8 ± 8.8
H2-3	312	4.52	0.66	2.18	2.39	2.96	568.55 ± 4.45	191.9 ± 7.8

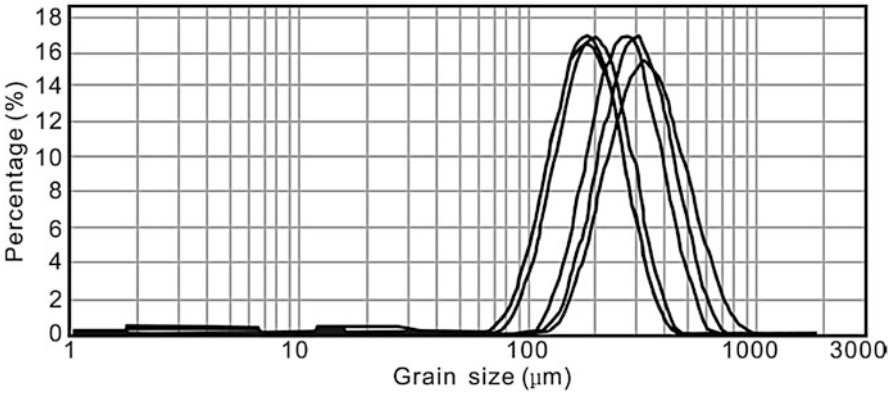

Fig. 3.5 Grain-size distributions for typical samples from the sand hills of Xingkai Lake

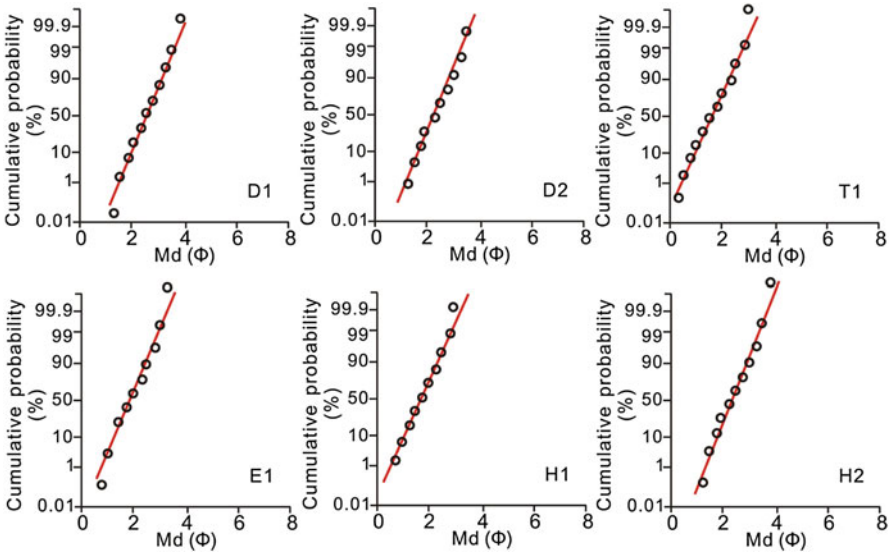

Fig. 3.6 Probability-cumulative curves for all the six sections from the sand hills of Xingkai Lake

contents of silty sand and clay are less than 5 %. The frequency curves of typical samples indicate a unimodal distribution (Fig. 3.5). The probability-cumulative curves (Fig. 3.6) indicate grain size primarily ranging from 0.5 Φ to 4 Φ, with a high content of the saltation-load fraction (>98 %) as compared to the bed-load and suspended-load fractions (STCGC 1976). The C-M plot (C and M denote the maximum and the average kinetic energies respectively) indicates that most samples are confined in the range from 300–1,000 μm C to 200–500 μm M (Fig. 3.7).

The Md and MS results of the soil layer (on top of the sand layer, Fig. 3.2) are quite different from those of the underlying sand layers. The Md and MS of the

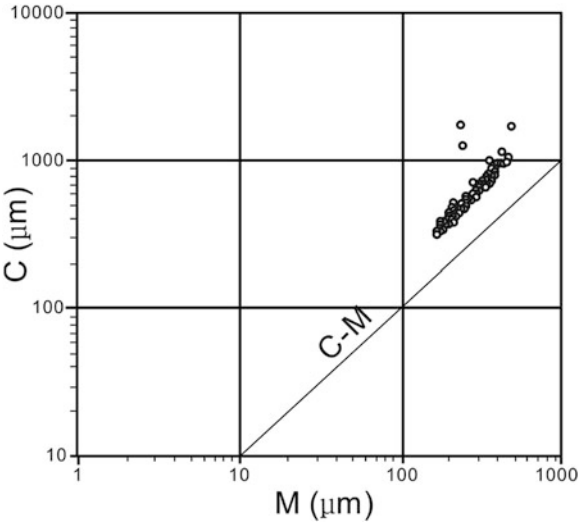

Fig. 3.7 The C-M plot of all samples from the six sections from the sand hills of Xingkai Lake. The *C* and *M* denote the maximum and the average kinetic energy respectively

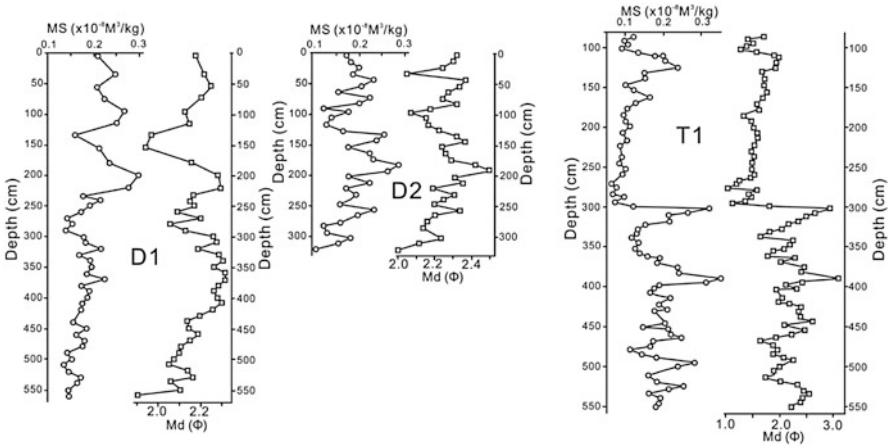

Fig. 3.8 MS and Md results of D1, D2 and T1 sections

sand hill samples are 2.1Φ and 0.5×10^{-8} m^3/kg respectively; while those of the soil-forming layer or plough layer are 5.2Φ and 2.9×10^{-8} m^3/kg respectively. In addition, the results for D1, D2 and T1 sections reveal co-varying changes in the Md and MS data (Fig. 3.8).

3.5 Discussion

3.5.1 Forming and Preservation of the Sand Hills

The sediment of the sand hills is well-sorted, as can be seen from the unimodal distribution of the grain-size data (Fig. 3.5). This is also indicated by the high percentages of the saltation-load fraction, accounting to >98 % (Fig. 3.6). So, the transportation of the sand hill sediment is characterized by a single yet relatively strong dynamic process (Fig. 3.7), typical aeolian processes (STCGC 1976). Nowadays, the development of the Dahu Sand hill can clearly be seen as sands are transported by winds from the beach northwards to an area normally 200–300 m further offshore. These sands show smooth surfaces and high degrees of rounding, proving that they are derived from wave action in the lake. Previous studies also suggest that the arc-shaped sand hills to the northern bank of Xingkai Lake are typical for off-shore landforms, formed by aeolian deposition of beach sand (Hu 2001).

When the lake expands, previously formed sand hills can be eroded or totally destroyed by waves, if near to the lake, or even completely covered by a lake transgression. Erosion by waves can be observed in the case of the present day Dahu Sand hill. Therefore, the relatively stable location of the lake surface is one of the vital factors allowing for formation of sand hills offshore. This not only avoids erosion but also provides sufficient source material for aeolian transportation and deposition. No major transgression following the sand hill formation has allowed the preservation of them until today.

When the lake level is lower, the sand hill development will stop due to increased distance from the material source. In that case, another sand hill will be formed offshore in the inner part of the older arc-shaped sand hill. So regression of the lake surface will give rise to newly-formed sand hills and preservation of the older ones.

Our grain-size and MS data for Taiyang and Dahu sand hills provide proof for the above hypothesis. The coeval changes in the Md and MS values (Fig. 3.8) show that the development of soil layers (higher MS values) was associated with smaller grain-sizes, while the developing of the sand hills was associated with relatively coarser grain-size. As mentioned above, soil development indicates lake regression and cessation of sand hill development. While this is happening, there is likely to be an increasing distance from the forming sand hill to its material source. This leads to the result that only finer grains can be transported and deposited on the sand hill.

3.5.2 Big-Lake Periods

The OSL ages increase with depth in a stratigraphical order (Fig. 3.2; Table 3.1) for all the sections, giving a high degree of confidence that they can represent an acceptable chronology. For the Dahu and Taiyang sand hills, we have also

obtained ^{14}C dates on charcoal (our unpublished data) to validate the OSL ages. This stratification order in OSL dates agrees with the observation in situ that the sand layers of all the sections were continuous, with no obvious hiatus or erosion. If this indicates relatively stable sedimentation, then the methods of interpolation and extrapolation can be used to constructed rough age-depth models for all the sections. In this way, it is clear that there were at least four big-lake periods in the past, i.e., larger lake surfaces (compared with that of today) with lakeshores along the Huang-Nan, Er'dao, Taiyang and Dahu sand hills respectively: this was revealed by our data to be during the periods 193–183, 136–130, 24–15 and 3–0 kyr BP, respectively. This finding has analogues in related studies for the lake and its catchment.

Geological data from the catchment show that a lake body existed during the period 193–183 kyr BP in the downstream reach of the Ilistaya and Mel'gunovka Rivers (discharging into the present day Xingkai Lake from the south Fig. 3.1b) (Korotkii et al. 1980). A lake transgression occurred at about 136 kaBP in the Ussuri-Khanka Depression (Korotkii et al. 1975). Afterwards, the lake probably began to retreat, as indicated by the palynomorphs of shallow water at the base of the Nakhodka Horizon in Russia (Korotkii et al. 2007). During 130–25 kyr BP, there is some evidence for lake transgressions in the catchment of Xingkai Lake (Korotkii et al. 1980; Korotkii 2000). However, this is not supported by our data. Possible reasons might be that the sand hills formed but were destroyed by later lake transgressions. A remarkable transgression of Xingkai Lake at 24 kyr BP has been reported and it shows that its water level probably rose to 1.5–4.0 m above the present level (Korotkii et al. 2007). At that time, the Belaya and Muling rivers (Fig. 3.1b) were flowing into the lake at the east and west sides respectively (Korotkii et al. 1981). From 15 kyr BP, the lake-level started to fall, accompanied by an accumulation of coarse-grained quartz-feldspar beach sands enriched with gravelly material (Bazarova et al. 2008), until about 3 kyr BP. At this time, the emergence of swamps at the modern northern bank suggests a lake-level rise (Bazarova et al. 2008).

3.5.3 Climatic Implication and Possible Mechanism

The timing of the big-lake periods of Xingkai Lake largely coincide with the MIS6, MIS2 and late Holocene (Fig. 3.9). Geological records indicated that these three periods were relatively colder stage (Liu et al. 2009; Xiao et al. 2004). This suggests that a relatively cooler climate allows for the stable, large surface of Xingkai Lake. This explanation is supported by the event that happened on the southern part of the Ussuri–Khanka depression in the Mid- Pleistocene (Bersenev and Sokhin 1969). This also shows that a lake transgression happened in the Shmakovka time when the climate was relatively cool, while water level decreased in the following warm period (the Sungach time) (Korotkii et al. 1980; Pavlyutkin and Khanchuk 2002).

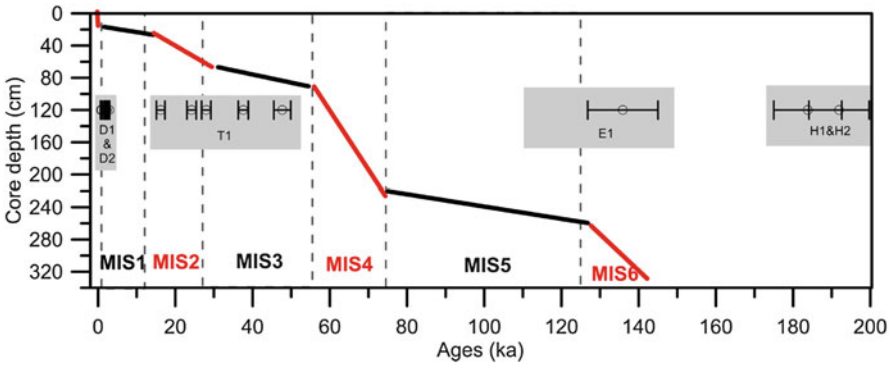

Fig. 3.9 OSL ages of all the sections from the sand hills of Xingkai Lake and its comparison with the curve of OSL ages against depth for core XK (unpublished data)

Interestingly, the links to alternating glacial and interglacial periods is also indicated by the high-resolution OSL chronology for core XK from Xingkai Lake (49 OSL dates for the 310 cm core, Fig. 3.9). The chronology displays abrupt transitions in sedimentation rates in the past 160 kyr BP, with higher sedimentation rates during MIS6, MIS4, MIS2 and the late Holocene, and lower sedimentation rates for MIS5, MIS3 and MIS1 (Fig. 3.9). Moreover, the OSL dates above 1 m of these 49 dates have been validated by six ^{14}C dates, including one on land-derived plant fossils which could avoid old carbon contamination (Björck and Wohlfarth 2001).

Xingkai Lake occupies a present day surface area of as much as 4,380 km^2 with an average water depth of only 4–5 m across a relatively flat basin. Throughout geological history, the formation and development of the lake has been greatly influenced by subsidence of the lake basin (belonging to the Ussuri–Khanka depression). Yet there is no clear evidence for this since the Mid-Pleistocene (Korotkii et al. 1975). Therefore, over the timescales studied here the evolution of Xingkai Lake and its sand hills is mainly related to climatic changes. During warm periods (and likely humid periods as well according to the monsoonal climate), increased precipitation and river discharge led to river-entrenching and headward erosion with no stable and large lake surfaces (Korotkii et al. 2007; Korotkii 1979). In contrast, during cool periods, lower air temperatures and consequent lower lake-water evaporation possibly allowed for increased local humidity and elevated lake-levels. Moreover, the lake can normally drain excess water from melting in this permafrost or snowfield zone (Korotkii 2000). The sediment of Xingkai Lake mainly comprises clay fractions <4 μm and 4–16 μm grains, whereas >16 μm grains amount to only 10–20 % (Wu and Shen 2010). This means precipitation and settlement of these grains to the lake bottom demands relatively static lake water and weak in-lake currents. This condition most likely occurred during cold or cool periods rather than warm periods.

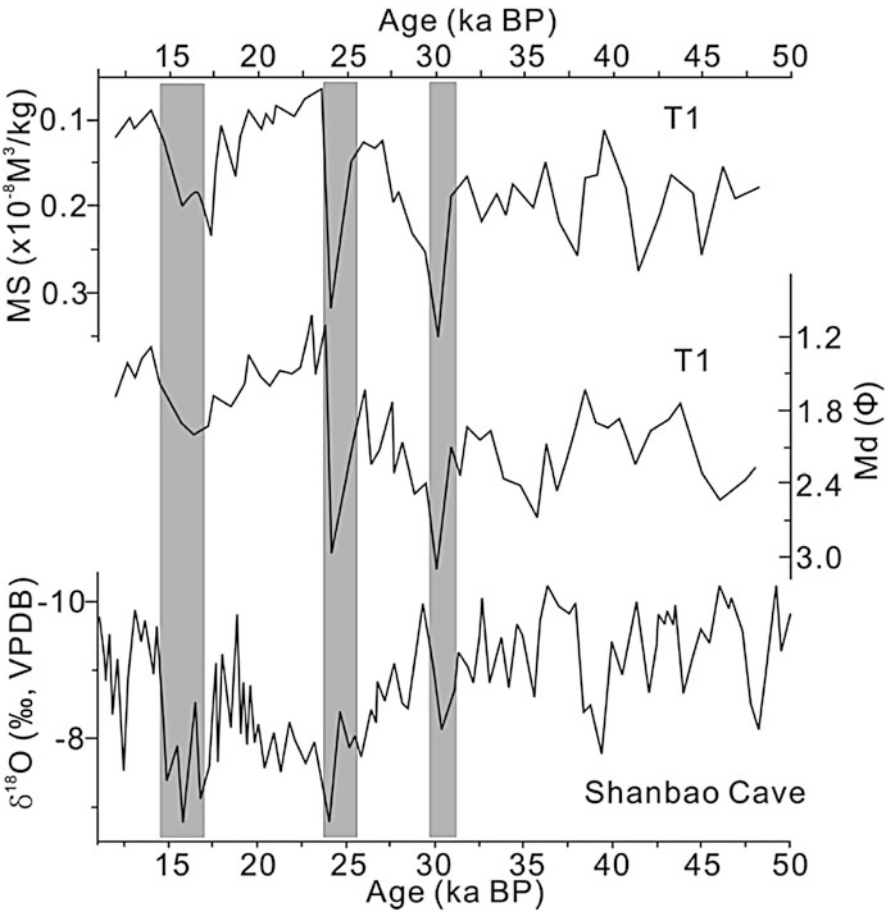

Fig. 3.10 MS and Md results of T1 section along ages and its comparison with records of Shanbao Cave (Shao et al. 2006)

Additionally, the Md and MS records of the T1 section show synchronous changes at ~30, ~25 and ~15 kyr BP, coeval with the cold and dry periods revealed by the stalagmite record from the Shanbao Cave (Fig. 3.10; Shao et al. 2006). That is to say coarser grain-sizes of the sand hills (at a shortened distance from the material source) were most likely associated with cold and dry climatic conditions. If this leads to the development of sand hills (instead of palaeo-soil development, as indicated by the lower MS values), then this provides further evidence for the above hypothesis.

3.6 Conclusion

One of the most striking features of Xingkai Lake is the sand hill formation to its northern bank related to historical big-lake surfaces. For the first time, the OSL method is used to constrain this history of lake regression since the late Pleistocene. The climatic and environmental implications of the results are validated by sedimentary archives from the lake sediments. The four lines of sand hills stretching parallel to the lake shore were found to be formed by aeolian quartz derived grains from the sand beach. Hence the sand hill formation requires relatively stable lake surfaces and shoreline locations. Lake transgression will erode or totally destroy the sand hills, while lake regression will cause termination of the sand hill formation, allowing for preservation of the sand hills if not followed by lake transgression up to the present. Big-lake periods during the periods 193–183, 136–130, 24–15 and 3–0 kyr BP were revealed by our results, which coincide with relatively cold periods and a higher sedimentation rate in core XK recovered from the lake basin. Possible mechanisms for this are suggested, but a deeper understanding requires further work of high-resolution OSL chronology.

Funding This study is supported by National Natural Science Foundation of China (41430530), The CAS/SAFEA International Partnership Program for Creative Research Teams (KZZD - EW-TZ- 08) and National Basic Research Program of China (2012CB956100)

References

An ZS, Porter SC, Kutzbach JE et al (2000) Asynchronous Holocene optimum of the East Asian monsoon. Quat Sci Rev 19:743–762

Bazarova VB, Mokhova LM, Orlova LA et al (2008) Variation of the lake Khanka level in the late Holocene. Russian J Pacific Geol 23:272–276

Bersenev II, Sokhin VK (1969) Quaternary deposits (in Russian). Geol USSR 32:373–389

Björck S, Wohlfarth B (2001) ^{14}C chronostratigraphic techniques in paleolimnology. In: Last WM, Smol JP (eds) Tracking environmental change using lake sediments. Volume 1: basin analysis, coring, and chronological techniques. Kluwer, New York, pp 205–245

Hu JS (2001) Sand hills and its cause of Xingkai Lake (in Chinese). Heilongjiang Geol 12:89–95

Huntley DJ, Hutton HT, Prescott JR (1993) The standed beach-dune sequence of south-east South Australia: a test of thermoluminescence dating, 0-800 ka. Quat Sci Rev 12:1–20

Korotkii AM (1979) Relationship between tectonic and climatic factors during the late Cenozoic evolution of river valleys in the Sikhote Alin and southwestern Primorye (in Russian). Evol River Valleys Lands Reclam:29–35

Korotkii AM (2000) Lake types and Quaternary limnogenesis in the southern far east. Paleoclimatol Paleolimnol Paleoecol 4:106–125

Korotkii AM, Kitaev IV, Mikhailove NA et al (1975) Lithological characteristics of modern sediments in lake Khanka (in Russian). Sed Form Petrol-Bearing Areas Far East:78–96

Korotkii AM, Karaulova LP, Romashkova NI (1980) Lacustrine transgressions and late Cenozoic sedimentation in Ussuri-Khanka depression (in Russian). Geol-Geomor Conf Compl Far East:162–181

Korotkii AM, Karaulova LP, Alekseeva EV et al (1981) On finding the Khorol'sky mammoth (Primorye) (in Russian). Evol Environ:29–50

Korotkii AM, Grebennikova TA et al (2007) Lacustrine transgressions in the late Cenozoic Ussuri-Khanka depression (Primor'e). Russian J Pacific Geol 1:53–68

Kortekaas M, Murray AS, Sandgren P et al (2007) OSL chronology for a sediment core from the southern Baltic Sea: a continuous sedimentation record since deglaciation. Quat Geochronol 2:95–101

Li WY (1998) Quaternary vegetation and environment of China (in Chinese). Science Press, Beijing

Liu XQ, Dong HL, Yang XD et al (2009) Late Holocene forcing of the Asian winter and summer monsoon as evidenced by proxy records from the northern Qinghai–Tibetan Plateau. Earth Planet Sci Lett 280:276–284

Long H, Lai ZP, Wang NL et al (2011) A combined luminescence and radiocarbon dating study of Holocene lacustrine sediments from arid northern China. Quat Geochronol 6:1–9

Long H, Lai ZP, Frenzel P et al (2012) Holocene moist period recorded by the chronostratigraphy of a lake sedimentary sequence from Lake Tangra Yumco on the south Tibetan Plateau. Quat Geochronol 10:136–142

Lu HY, Thomas S, Yi SW et al (2006) An erosional hiatus in Chinese loess sequences revealed by closely spaced optical dating (in Chinese). Chin Sci Bull 51:2767–2772

Murray AS, Olley JM (2002) Precision and accuracy in the optically stimulated luminescence dating of sedimentary quartz: a status review. Geochronometria 21:1–16

Murray AS, Wintle AG (2000) Luminescence dating of quartz using an improved single-aliquot regenerative-dose protocol. Radiat Meas 32:57–73

Olley JM, Caitcheon GG, Roberts RG (1999) The origin of dose distributions in fluvial sediments, and the prospect of dating single grains from fluvial deposits using optically stimulated luminescence. Radiat Meas 30:207–217

Pavlyutkin BI, Khanchuk AI (2002) New data on the age of lake Khanka, the Russian far east. Earth Sci 383:187–189

Prescott JR, Robertson GB (1997) Sediment dating by luminescence: a review. Radiat Meas 27:893–922

Qiu SW, Jiang P, Li FH et al (1981) Preliminary study on the environmental evolution in eastern China since the late Ice Age (in Chinese). Acta Geogr Sin 36:315–327

Qiu SW, Wan EP, Wang PF (1988) Coastline changes of the Xingkai Lake and discovery of ancient source of Song'acha river (in Chinese). Chin Sci Bull 12:937–940

Qiu SW, Wan EP, Li FH et al (2007) Development of the plain in the north of the Xingkai Lake and formation of its wetlands (in Chinese). Wetland Sci 5:153–158

Roberts RM (2007) Assessing the effectiveness of the double-SAR protocol in isolating a luminescence signal dominated by quartz. Radiat Meas 42:1627–1636

Roberts HM, Duller GAT (2004) Standardised growth curves for optical dating of sediment using multiple-grain aliquots. Radiat Meas 38:241–252

Shanbei Team of Chengdu Geological College (1976) Grain-size analysis and its applications of sedimentary rocks (in Chinese). Geological Publishing House, Beijing

Shao XH, Wang YJ, Cheng H et al (2006) Long-term trend and abrupt events of the Holocene Asian monsoon inferred from a stalagmite $\delta^{18}O$ record from Shennongjia in Central China. Chin Sci Bull 51:221–228

Wang KC, Chen GM (2005) On the formation of Xingkai Lake (in Chinese). Heilongjiang SciTech Water Conserv 4:52–53

Wang XL, Lu YC, Li XN (2005) Progress in luminescence dating of Chinese loess by Single-aliquot Regenerative-dose (SAR) protocol (in Chinese). Nucl Tech 28:383–387

Williams DF, Kuzmin MI, Prokopenko AA et al (2001) The lake Baikal drilling project in the context of a global lake drilling initiative. Quat Int 80–81:3–18

Wintle AG (1997) Luminescence dating: laboratory procedures and protocols. Radiat Meas 27:769–817

Wu J, Shen J (2009) Paleoenvieonmental and paleocimatic changes reflected by diffuse reflectance spectroscopy and magnetic susceptibility from Xingka lake sediments (in Chinese). Mar Geol Quat Geol 29:123–130

Wu J, Shen J (2010) Paleoclimate evolution since 27.7 kyr BP reflected by grain size variation of a sediment core from Lake Xingkai, northeastern Asia (in Chinese). J Lake Sci 22:110–118

Xia YM, Wang PF (2000) Peat record of climate change since 3000 years in Yangmu, Mishan region (in Chinese). Geogr Res 19:53–59

Xiao JL, Xu QH, Nakamura T et al (2004) Holocene vegetation variation in the Daihai Lake region of north-central China- a direct indication of the Asian monsoon climatic history. Quat Sci Rev 23:1669–1679

Yang YX, Wang SY (2003) Study on mire development and paleoenvironment change since 8. 0 kyr BP in the northern part of the Sanjiang plain (in Chinese). Sci Geogr Sin 23:32–38

Yang LH, Zhou J, Lai ZP et al (2010) Lateglacial and Holocene dune evolution in the Horqin dunefield of northeastern China based on luminescence dating. Palaeogeogr Palaeoclimatol Palaeoecol 296:44–51

Zhang SQ, Deng W, Yan MH et al (2004) Pollen record and forming process of the peatland in Late Holocene in the north bank of the Xingkai Lake, China (in Chinese). Wetland Sci 2:110–115

Zhang JR, Tsukamoto S, Grube A et al (2014) OSL and ^{14}C chronologies of a Holocene sedimentary record (Garding-2 core) from the German North Sea coast. Boreas 43:1–13

Zhao H, Lu YC, Chen J et al (2000) IRSL and GLSL dating of fine grain from late quaternary sediments in North China (in Chinese). Chin Sci Bull 45:2332–2337

Zhao H, Lu YC, Wang CM et al (2007) Optical dating of Holocene water-laid sediments recorded hydrological environmental changes in the Oasis of Shulehe river alluvial fan in Gansu Province (in Chinese). Nucl Tech 30:893–898

Chapter 4
Palaeoenvironment and Palaeoclimate Evolution of Northeast China: Based on Multi-proxy Analysis of Sediment from Lake Xingkai

Ji Shen, Ming Ji, Jian Wu, and Yong Wang

Abstract A multi-proxy analysis that included magnetic susceptibility, grain size, organic carbon isotope composition ($\delta^{13}C_{org}$), organic nitrogen isotope composition ($\delta^{15}N_{org}$), total organic carbon (TOC), total nitrogen (TN), carbon-to-nitrogen ratio (C/N) and redness analyses was conducted on a 269-cm long sediment core collected from Lake Xingkai to reconstruct the palaeoclimate and palaeoenvironment evolution of Northeast China since 28 ka BP. The analysis results showed that during the period between 27,740 and 25,540 cal a BP, the lake was at a low level and in a cold and dry climate period. During the period between 25,540 and 23,650 cal a BP, precipitation increased compared to the previous period, but the lake level was still relatively low, and the lake region was in a cold and wet climate period. During the period between 23,650 and 19,940 cal a BP, the climate in the lake region was cold and dry, and this period corresponded to the LGM (Last Glacial Maximum). During the period between 19,940 and 14,510 cal a BP, the precipitation increased compared to the previous period and temperature also increased to some extent. During the period between 14,510 and 11,500 cal a BP, the late glacial period, the climate changed from warm and wet to cold and dry, and the lake region was in a Bølling/Older Dryas/Allerød/Younger Dryas climate fluctuation period. During the period between 11,500 and 2,800 cal a BP, the Holocene warm period, and between approximately 8,000 and 5,000 cal a BP, the study region entered the Holocene climate optimum period. After 2,800 cal a BP, the lake level decreased significantly and the climate turned cool and dry. After 1,000 cal a BP, change of sediment grain size composition and magnetic susceptibility, increasing of secondary arborescent pollen in pollen assemblages, which reflects the influence of human activity.

J. Shen (✉) • M. Ji • Y. Wang
State Key Laboratory of Lake Science and Environment, Nanjing Institute of Geography and Limnology, Chinese Academy of Sciences, 73 East Beijing Road, Nanjing 210008, P. R. China
e-mail: jishen@niglas.ac.cn

J. Wu
Neijiang Normal University, 705 Dongtong Road, Neijiang 641112, P. R. China

K. Kashiwaya et al. (eds.), *Earth Surface Processes and Environmental Changes in East Asia*, DOI 10.1007/978-4-431-55540-7_4

Keywords Northeast China • Lake Xingkai • Palaeoclimate and palaeoenvironment evolution • Multi-proxy analysis • 28 ka BP

The high-latitude region in Northeast China is affected by both the East Asian monsoon and polar ice sheet, and it is a sensitive region to global change (An et al. 2000; Li 1998). Since the LGM, warm periods have generally started earlier and also lasted longer in this region than in the low-latitude region, which shows the unique monsoon climate mechanism of this region (Xue and Yu 2005). As the largest fresh water lake in Northeast Asia, Lake Xingkai is the only recommended lake in Northeast China among the global lake drilling sites in the Past Global Changes (PAGES) project, Pole-Equator-Pole, which were proposed based on sensitivity and regional significance of climate change (Williams et al. 2001). Current research on Lake Xingkai focuses on the evolution of the shoreline (Williams et al. 2001; Qiu et al. 1988, 2007) and palaeoclimate and palaeoenvironment change since the Holocene (Zhu et al. 2011; Xia and Wang 2000; Zhang et al. 2004, 2007; Bazarovaa et al. 2008; Korotkii et al. 2007). However, there is little understanding of the palaeoclimate and palaeoenvironment evolution history since the LGM. Therefore, we conducted multi-proxy analysis (magnetic susceptibility, grain size, organic carbon isotope composition ($\delta^{13}C_{org}$), organic nitrogen isotope composition ($\delta^{15}N_{org}$), total organic carbon (TOC), total nitrogen (TN), carbon-to-nitrogen ratio (C/N) and redness) on a 269-cm long sediment core collected from Lake Xingkai to discuss the palaeoclimate and palaeoenvironment changes in the region since approximately 28 ka BP and characteristics of region's response to global change, which provided a scientific basis for an improved understanding the characteristics of the palaeoclimate and palaeoenvironment evolution in high-latitude regions, such as Northeast Asia, since the LGM.

4.1 General Regional Geography

Located in Jixi, Heilongjiang Province, Lake Xingkai is a tectonic lake formed from depression of the Dunhua-Mishan fault zone during the late Tertiary (Wan and Zhong 1997). Lake Xingkai consists of Lake Xingkai and small Lake Xingkai, which are separated by an east-west trending sand mound; in addition, there is a newly opened river channel Xinkailiu flowing into Lake Xingkai. Lake Xingkai is located at 44°32′ ~ 45°21′N, 131°58′ ~ 132°51′E, and the mean altitude of the water level is 69 m. Lake Xingkai is 91.3 km long from south to north, and its maximum east-west width is 62.5 km. The maximum water depth is 10 m, and the mean water depth is 4 ~ 5 m. Lake Xingkai has an area of 4,380 km^2 and is divided by the Sino-Russian border, which runs between the Songacha River estuary and Baileng River estuary. The area of Lake Xingkai within the Chinese territory is 1,080 km^2. The drainage basin area of the entire Lake Xingkai was 22,400 km^2 in 1942; however, construction of the Muxing flood-diversion channel began in 1942,

with one river stream emptying into small Lake Xingkai along the Muxing waterway (flood-diversion channel) and another river stream continuing to flow eastwardly along the original Muling River waterway. The current drainage basin area of the entire Lake Xingkai is 36,400 km^2, and the Songacha River estuary east of the river is the only outlet river (Fig. 4.1).

In the Lake Xingkai water system, the main river within the Chinese territory that flow into Lake Xingkai is the Baileng River, whereas in Russia, the Bolshie Usachi River, Komissarovka River, Melgunovka River, Illistaya River and Spasovka River are the main water sources of Lake Xingkai. Because of the influence of the temperate humid continental monsoon climate, the annual mean temperature of the lake region is 2.9–3.1 °C. The mean temperature of the coldest month, January, is approximately −18 °C, and the mean temperature of the hottest month, July, is 21 °C. The annual precipitation of the lake region is 554–690 mm, and the annual evaporation is approximately 490 mm. The frostless period lasts for 149 d, and the frozen period lasts for 135 d. South-westerly winds prevail in the spring and summer seasons, whereas north-westerly winds prevail in the fall and winter seasons (Zhu et al. 2011; Zhang et al. 2004).

Since the late Pleistocene, lake regression has occurred numerous times in Lake Xingkai, controlled by the geological and geomorphological conditions around the lakeshores as well as the monsoon climate. There are four rows of sand mounds with similar morphology but of various sizes that are arranged in parallel concentric arcs from the lakeshore towards the inland along the northern and eastern lakeshores, and they are followed by the Dahugang, Taiyanggang, Erdaogang hillock and Huanggang-Nangang, which are sandy ridges with narrow widths (30–200 m) and different lengths (20–80 km) and heights (3–10 m) that are parallel or nearly parallel to the lake shorelines.

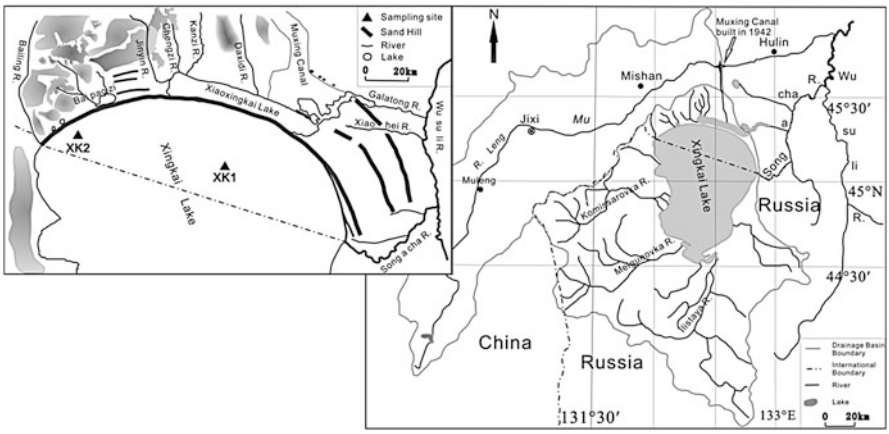

Fig. 4.1 Map of the Lake Xingkai basin, relief map of northern Lake Xingkai and location of drilling

4.2 Sampling and Analysis Methods

In July 2007, we used an Austrian-made UWITEC drilling platform and piston corer to obtain two parallel sediment cores in Lake Xingkai approximately 18 km (45°12′21.7″N, 132°30′33.3″E) from the north lakeshore where the water depth was 6.6 m. One of the sediment cores, XK1, was 269-cm long, and it was used as the study object. Lithology of XK1 was greyish-black, fine-silty mud. There were two sand layers at depths of 80–83 cm and 227–233 cm. After the sediment core was brought to the laboratory, it was subsampled at 1-cm interval.

An MS2 magnetic susceptibility instrument with an MS2B double frequency probe (high and low frequencies of 4.7 KHZ and 0.47 KHZ, respectively) (Bartington; Witney, Oxon, UK) was used to determine the magnetic susceptibilities of the samples. The samples were freeze-dried and grinded (without damaging the natural granules) and then placed into 1-cm^3 cubic sample measurement boxes. After the samples were slightly compacted, they were weighed, and the mass magnetic susceptibilities of the samples were then obtained.

Hydrogen peroxide (H_2O_2) was added to the freeze-dried samples (approximately 0.3 g per sample), which were maintained overnight to allow the H_2O_2 to remove organic matter. Afterwards, hydrochloride acid was added to the samples, which were maintained overnight to allow hydrochloride acid to remove carbonates. Sodium hexametaphosphate was added to disperse the samples, which then underwent ultrasonic vibration. Subsequently, Mastersizer 2000 (Malvern; Malvern, UK) laser grain-size analyser with a measurement range of 0.02–2,000 μm was used to measure the grain sizes. The repeated measurement error was less than 1 %.

Freeze-dried samples were grinded to 100 mesh and then soaked in 5 % hydrochloride acid for over 12 h to remove carbonates. Afterwards, the samples were rinsed with distilled (DI) water and then vacuum freeze-dried again and grinded to 150 mesh. Subsequently, the samples were dried in an bake oven (drying temperature 45 °C), and 20–30 mg of each sample was collected, tightly covered with tin foil and then compacted. A Finnigan Delta^{plus} mass spectrometer was used to determine the concentrations of TOC, TN, $\delta^{13}C_{org}$ and $\delta^{15}N_{org}$ (δ^{13}Corg was expressed relative to the Pee Dee Belemnite (PDB) standard, and $\delta^{15}N_{org}$ was expressed relative to the atmospheric air standard; standard error $\leq \pm 0.1$ ‰).

The measurement of the redness of the samples was completed at the Supergene Geochemistry Laboratory of the School of Earth Sciences and Engineering of Nanjing University. The pretreatment and test analysis steps were as follows (Balsam and Deaton 1991): the samples were grinded to 200 mesh or finer, and a portion of each powered sample was mixed with DI water and smeared on a thin slide, which was dried at a low temperature (<40 °C); afterwards, the thin slide was loaded into a Perkin-Elmer Lambda 900 diffuse reflectance spectrophotometer for measurement. The measurement range of this spectrophotometer was 250–850 nm, the visible band (VIS) was 400–700 nm, and the measured data interval of the sample was 1 nm. According to the standard colour bands, VIS can be divided into 6 bands: purple (400–450 nm), blue (450–490 nm), green (490–560 nm), yellow

(560–590 nm), orange (590–630 nm) and red (630–700 nm). Redness represents the percentage of the ratio of the reflectivity in the wavelength range of 630–700 nm to the total VIS reflectivity of the sample (the sum of the reflectivities in the wavelength range of 400–700 nm).

4.3 Results and Discussion

4.3.1 Establishing the Chronological Sequence

Three pure organic samples from the XK1 core were collected at depths of 10 cm, 223 cm, 258 cm and sent to the University of Tokyo in Japan for accelerator mass spectrometry (AMS) ^{14}C dating. The three ^{14}C ages were 4,410 ± 40 a BP, 25,080 ± 110 a BP and 26,700 ± 130 a BP (Table 4.1). In August 2008, we recovered a short core (XK2) of 71 cm length and another core of approximately 3 m at a position 2.5 km from the southeastern shore of Lotus Lake. The location of the sampling site was 45 °16′2.2″N, 132 °4′5″ E (Fig. 4.1). The lithological features included sands at depths of 64 cm or less, followed by a long portion of silty sands, which suggested that the 64 cm thick sand layer in the core XK-2 corresponded to the 31 cm thick silty sand layer in the core XK1. Core XK2 was divided at an interval of 0.5 cm at the sampling site and sent to the Nanjing Institute of Geography & Limnology, Chinese Academy of Sciences, for ^{137}Cs and ^{210}Pb dating. A γ spectrum analysis system was used that consisted of a high-purity germanium well detector (Ortec HPGe GWL), an Ortec 919 spectrum master (EG&G Ortec Inc., US) and an IBM computer-based 16 k channel analyzer. The results are shown in Fig. 4.2 and include the following: an evident peak of ^{137}Cs accumulation in the core at a depth of 6.75 cm, which is believed to correspond to the year 1963 in Northeast China, when the deposition of ^{137}Cs in the Northern Hemisphere was at its peak (Chu et al. 2005); and the presence of ^{137}Cs beginning at a depth of 8.75 cm, which corresponds to the year 1954, in which global nuclear testing began. The chronology of the 0 ~ 21 cm segment was established with the age calculated by the corrected ^{210}Pb CRS model using the 1963 and 1954 dates as benchmarks (Last and Smol 2004). Observations on the segmented samples indicated that at 16 cm, the sediment became significantly harder, which suggested that the sediment were compacted over a long period of time, and the age was linearly related to the depth, which resulted in a lithologically uniform segment from 16 to 64 cm. Therefore, the age at the bottom (64 cm) was linearly extrapolated to 1,050 a BP (Li et al. 2004; Gao et al. 2007) based on the

Table 4.1 The determined and calibrated ^{14}C ages of the core from Lake Xingkai

Depth (cm)	10	223	258
^{14}C age (a BP)	4,410 ± 40	25,080 ± 110	26,700 ± 130
Old carbon-free ^{14}C age (a BP)	/	20,775 ± 110	22,395 ± 130
Calibrated age (cal a BP)	105	24,760 ± 230	27,030 ± 529

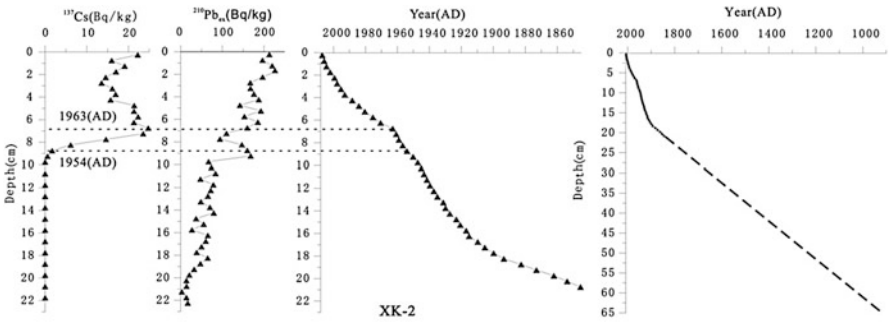

Fig. 4.2 Age dating results of ^{210}Pb and ^{137}Cs

average sedimentation rate of 1.67 mm/a in the 16 ~ 21 cm segment. The age of the bottom of the sand layer in XK1 (31 cm) should also be approximately 1,050 a BP. The ratio between the thicknesses of the upper sand layers of XK1 and XK2 indicated that the ratio between the sedimentation rates of these two cores was approximately 1:2; therefore, the calculated ^{210}Pb age of XK2 at 21 cm was 105 a BP, the age of XK1 at 10 cm should also be approximately 105 a BP, and the ^{14}C age at 10 cm (approximately 4305a) appeared to be older as a result of the "reservoir effect" Because of the extremely low percentage of organic carbon in Lake Xingkai, an average of approximately 0.5 % of the "old carbon" or "dead carbon" resulted from the erosion of older strata in the lake basin, which caused the age to appear older. Assuming that the apparent ages of the upper and lower segment of the core that appeared to be older as a result of the "reservoir effect" were approximately the same, 4305 a were subtracted from both ^{14}C ages (at 223 cm and 258 cm), which resulted in "old carbon"-free ^{14}C ages of 20,775 ± 110 a BP and 22,395 ± 130 a BP, respectively. The two "old carbon"-free ^{14}C ages were then calibrated online with CalPal-online according to the Hughen K calibration curve (Hughen et al. 2004). The two calibrated ages were 24,763 ± 230 cal a BP and 27,032 ± 529 cal a BP. The ages of sediment in various segments of the core were determined by interpolation using the average sedimentation rate or extrapolation based on the age of the bottom (Table 4.1).

4.3.2 Variation Characteristics and Palaeoclimate Significance of the Magnetic Susceptibility, Grain Size, Redness, $\delta^{13}C_{org}$, $\delta^{15}N_{org}$ and C/N of the Lake Xingkai Sediment

Among the paleoenvironment proxies for lake sediment, magnetic susceptibility and grain size are the proxies that reflect the environmental information of a basin, whereas TOC, TN, $\delta^{13}C_{org}$ and $\delta^{15}N_{org}$ record the information of mixed sources and comprehensively reflect change of the lake and basin environments

(Shen 2013). Because these proxies are affected by such factors as the basin and lake environments, they have different indicative significance for different lakes in different regions; therefore, there is a multiplicity of solutions for these proxies. Before using these proxies to reconstruct the palaeoclimate and palaeoenvironment, we must first interpret the indicative significance of the paleoenvironmental proxies for Lake Xingkai.

Magnetic susceptibility (low frequency mass magnetic susceptibility, χ_{Lf}) is an environmental proxy that reflects the content of magnetic minerals in a sample. Previous studies have shown that the main minerals that control the magnetic susceptibility of clastic sediment are magnetites and maghemites (Zhou et al. 1990; Thompson and Oldfield 1986; Wang et al. 1996), and the magnetic susceptibility of clastic sediment is mainly related to the hydrodynamic intensity at the time of sedimentation and provenance of sediment, meaning that the magnetic susceptibility of clastic sediment is related to the grain size composition that reflects the hydrodynamic intensity (Thompson and Oldfield 1986; Wang et al. 1996). Figure 4.3 shows that the magnetic susceptibility of the sediment core collected from Lake Xingkai was generally controlled by variations in the clay (grain size <4 μm) content, with the magnetic susceptibility often relatively high in stratigraphic horizons that had a high clay content, and vice versa. This phenomenon occurred because the mode of occurrence of the magnetic materials changed during the transportation and sedimentation separation process, which resulted in the enrichment of denser ferromagnetic minerals in sediment with smaller grain sizes and is consistent with the modes of occurrence of the magnetic materials in Lake Taihu, Lake Dianchi and Lake Chaohu sediment (Wang et al. 1996, 2008; Yu et al. 1990). Therefore, sediment cores with higher magnetic susceptibility indicate that the sedimentary hydrodynamics were weaker, and vice versa.

A previous study on lake sediment records has shown that the grain size composition and characteristics of sediment can indirectly reflect the influence of precipitation, hydrodynamic conditions, landform and provenance conditions and even human activities at the time of sedimentation (Chen et al. 2000). Generally, fine and coarse sediment represent a decrease and increase, respectively, in the hydrodynamic conditions during the sedimentation process. Normally, sampling sites in deeper lake water or further away from the lakeshore will reflect weaker

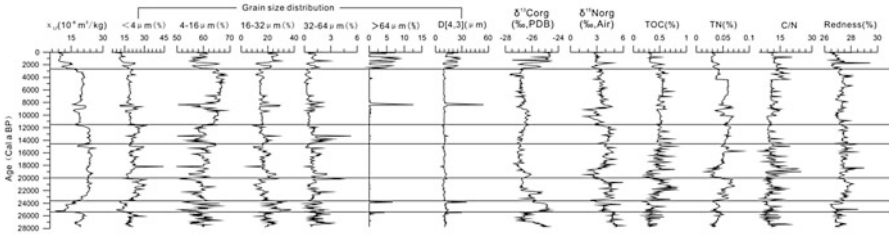

Fig. 4.3 Multi-proxy analysis results of the Lake Xingkai sediment core

sedimentary hydrodynamic intensities, and vice versa. For large lakes, the grain size gradually decreases from the lakeshore to the center of the lake (Yin et al. 2008). Therefore, in large shallow lakes with relatively large water level fluctuations over time, fine and coarse sediment represent the lake expansion period and lake contraction period over a long-term climatic period and at different stages of the same point on a sediment core, respectively (Chen et al. 2000, 2003). During such periods, the lake water level is the primary factor that determines the sediment grain size. However, during a specific climate period when the variation of the lake water level is insignificant, precipitation in the drainage basin of the lake is the key factor. During wet periods when precipitation is high, the sediment grain size will be relatively coarser, whereas during dry periods when precipitation is low, the sediment grain size will be relatively finer. According to the two rows of Shagang hillocks formed from the lowered lake levels near the Komissarovka River estuary, which is west of Lake Xingkai, since 1,000 cal a BP (Bazarovaa et al. 2008), the grain size data indicate that the corresponding coarse silt from 31 cm to the top of the XK1 sediment core increased significantly since 1,050 cal a BP (Fig. 4.3). Additionally, according to the geological section traces, which are located 4.3 m above the lake surface and on the lakeshore 30 m east of the first release sluice of the Dahugang hillock (Table 4.2), there is a 1.45-m thick yellow medium/coarse sand layer beneath an approximately 30-cm thick celadon-grey lacustrine silty sand layer. According to our optically stimulated luminescence dating data, the age of the top section of the silty sand layer at a depth of 10–40 cm was formed 7.1 cal ka BP, and the yellow sand layer at the bottom at a depth of 210–245 cm was formed approximately 14.0 cal ka BP. The Xinkailiu archaeological tomb excavated from the middle silt horizon was buried at approximately 6,100 cal a BP (Qiu et al. 2007), proving that the silt was formed between 14.0 and 7.1 cal ka BP; during this time period, a large lake transgression occurred, and the corresponding grain size of the XK1 sediment core was significantly finer (Fig. 4.3). By selecting a sampling site in the center of the lake that was relatively far from the major Russian inflow rivers, we could show that for a large shallow lake such as Lake Xingkai, whose water level fluctuation amplitude reached more than 2 m within the last 100 years (Liu et al. 2008), an increase in coarse sediment grains over different paleoclimate periods on a long-term time scale generally reflects a decrease in the lake level and

Table 4.2 Sediment grain size of the sand mounds in the Dahugang hillock

Depth (cm)	0–10	10–40	40–70	70–90	90–100	100–130	130–210	210–245
Lithology	Yellow sand Containing fine gravels	Fine gravels Containing a small amount of sand	Celadon-grey mud containing sand	Coarse yellow silt	Celadon-grey Containing large amount of coarse gravels	Celadon-grey Silt	Yellow Medium sand	Yellow Coarse silt

indicates a low precipitation period; conversely, a decrease in coarse sediment grains generally reflects an increase in the lake level, indicating a high precipitation period. According to the Udden-Wentworth grain size classification scheme, the grain size composition of the XK1 sediment core collected from Lake Xingkai was classified into clay (<4 μm), fine silt (4–16 μm), medium silt (16–32 μm), coarse silt (32–64 μm) and sand (>64 μm).

The organic matter in the lake sediment is mainly from terrestrial plants and aquatic plants in the lakes. The TOC and TN contents reflect variation in the primary productivity of a lake region. Indexes, $\delta^{13}C_{org}$, $\delta^{15}N_{org}$ and C/N are often used to indicate the sources of organic matter and factors that affect the sources, such as temperature, humidity and nutrient levels. Therefore, a comprehensive analysis of the $\delta^{13}C_{org}$, $\delta^{15}N_{org}$ and C/N values can relatively accurately determine the aquatic or terrestrial sources of sedimentary organic matter and evolution of their regional environment (Brahney et al. 2008). The general pattern of the organic matter analysis as follows: the measured value of C/N ranges from 4 to 10 in aquatic plants with a high protein content, such as algae, whereas the measured value of C/N is greater than 20 in vascular plants with a high cellulose content; the $\delta^{15}N_{org}$ value of nitrates in lakes ranges from 7 ‰ to 10 ‰, but the $\delta^{15}N_{org}$ value increases to approximately 8 ‰ because of the adsorption of nitrates in lakes by phytoplankton; and the $\delta^{15}N_{org}$ value of atmospheric nitrogen is approximately 0 ‰, but terrestrial C_3 plants primarily use atmospheric nitrogen, which causes the $\delta^{15}N_{org}$ value to increase to approximately 1 ‰ (Watanabe et al. 2004; Meyers and Lallier 1999). The general situations in lakes are as follows: the relative increase in the input of terrestrial organic matter in lake sediment in warm and wet periods reduces the $\delta^{15}N_{org}$ value, whereas the relative increase in the components of sediment originating from phytoplankton in cold and dry periods causes the $\delta^{15}N_{org}$ value to increase; the $\delta^{15}N_{org}$ value of sediment is also affected by increases in the concentration of nitrates, which are caused by surface runoff; and wet climate environments contribute more nitrates to the basin soil, which also slightly increases the $\delta^{15}N_{org}$ value (Watanabe et al. 2004; Meyers and Lallier 1999). According to different photosynthetic pathways, plants can be classified into C3 and C_4 plants. C_3 plants are the most widely distributed, and the $\delta^{13}C_{org}$ of terrestrial C_3 plants is relatively low and ranges from −21 ‰ to −35 ‰, with a mean value of −28 ‰. The $\delta^{13}C_{org}$ of C_4 plants ranges from −9 ‰ to −20 ‰, and the approximate mean $\delta^{13}C_{org}$ is −14 ‰ (Wu et al. 1992; O Leary 1988). Emerged plants generally use atmospheric CO_2 directly for photosynthesis, and their $\delta^{13}C_{org}$ is similar to the $\delta^{13}C_{org}$ of terrestrial C_3 plants. Submerged plants mainly absorb the CO_2 released from the dissolution of bicarbonates in the water instead of absorbing atmospheric CO_2. However, under normal conditions, the $\delta^{13}C$ of HCO_3- ions is 7 ‰ ~ 11 ‰ higher than that of atmospheric CO_2 dissolved in the water. If phytoplankton absorb atmospheric CO_2, then their $\delta^{13}C_{org}$ will be similar to the $\delta^{13}C_{org}$ of C_3 plants. If phytoplankton absorb the CO_2 released from the dissolution of bicarbonates in the water, then their $\delta^{13}C_{org}$ will be relatively high. C_3 plants generally grow in cool and wet environments, whereas C_4 plants generally grow in dry and warm environments,

and significant climate and environmental variations often result in variations of the relative ratio of C_3 plants to C_4 plants (Watanabe et al. 2004; Meyers and Lallier 1999).

Lake Xingkai is a large shallow lake, and there is relatively large wind-wave disturbance that results in an oxygen-rich environment in the water. Therefore, both the TOC and TN contents are relatively low, and their mean values are only 0.455 % and 0.0475 %, respectively. There are very few C_4 plants in temperate areas with an annual mean temperature of less than 10 °C (Watanabe et al. 2004). According to the research conducted by Wu et al., C_3 plants represent more than 80 % of the total plants in Northeast China, and there are higher percentages of C_3 plants further north (Wu et al. 1992). The variation amplitude of the $\delta^{13}C_{org}$ composition of Lake Xingkai sediment is not large (range of $-24.56\,‰ \sim 27.67\,‰$; mean of $-26.34\,‰$), which is within the distribution area of the $\delta^{13}C_{org}$ of C_3 plants. Therefore, the variation of the δ^{13}Corg composition does not represent an alternation between C_3 and C_4 plants; however, it is mainly affected by variations of climatic and environmental factors. Studies have shown that the $\delta^{13}C_{org}$ of C_3 plants exhibited an increasing trend with decreases of annual mean temperature (Wang et al. 2002) and decreases of annual precipitation (Wang and Han 2001; Wang et al. 2003). Therefore, variation of the $\delta^{13}C_{org}$ value of the Lake Xingkai sediment is mainly controlled by the temperature and precipitation of the basin. In addition, according to the results from studies conducted by other international researchers, the ^{13}C enrichment of cyanobacteria also causes the $\delta^{13}C_{org}$ value to increase (Guy et al. 1993; Sakata et al. 1997). The $\delta^{15}N_{org}$ value of the XK1 sediment core ranged from 1.61 ‰ to 5.96 ‰, and its mean value was 3.97 ‰; thus, approximately 40 % of the sedimentary organic matter originated from phytoplankton. The C/N value of XK1 ranged from 5.72 to 25.03, and its mean value was 11.4, indicating that the majority of sedimentary organic matter originated from aquatic plants. There was a relatively strong negative correlation between the $\delta^{13}C_{org}$ and TOC of the Lake Xingkai sediment (correlation coefficient $= -0.457$; significance level $= 0.01$), and there was a relatively strong positive correlation between the C/N value and TOC (correlation coefficient $= 0.508$; significance level $= 0.01$). These correlations also proved that when the $\delta^{13}C_{org}$ value was relatively low, the climate was warm or wet, primary productivity of the basin increased, and contributions from terrestrial organic matter increased, whereas when the climate was cold and dry, the $\delta^{13}C_{org}$ value was high and contributions from the endogenous algae in the lake were dominant. The expressive characteristics of these environmental proxies were also consistent with the degree of palaeoclimate and palaeoenvironment significance indicated by the environmental proxies of Lake Baikal (Watanabe et al. 2004).

Diffuse reflectance spectra are particularly sensitive to iron oxides and hydroxides in soil and sediment, and they have been widely used in studies on the palaeoclimate of oceans, loess and lake sediment (Balsam et al. 2004; Vodyanitskii et al. 2007; Yang et al. 2001; Yin et al. 2002). Redness and lightness are the most commonly used proxies, and the magnitude of the redness of Lake Xingkai sediment cores is primarily controlled by the magnetite and goethite contents. Generally, high redness reflects warm and wet climatic conditions, and low redness reflects cold

and dry climatic conditions. The study conducted by Yang et al. showed that in wet and dry and wet and cold climate environments, the magnetic susceptibility of soil could only partially express the climatic significance because the sources and sedimentation of the main contributors to magnetic susceptibility, magnetite and maghemite, were unstable or there were excessive hydrothermal conditions and high relative humidity that oxidised these magnetic minerals to low magnetic hematites or reduced them to low magnetic goethites (Yang et al. 1999). Hematites and goethites are the most important colouring minerals in nature. Therefore, the colours of the Lake Xingkai sediment in a wet climate region are better indicators of climate change (Yang et al. 2001; Wang 1987).

4.4 Palaeoclimate and Palaeoenvironment Variations in the Lake Xingkai Region Recorded by the Magnetic Susceptibility, Grain Size, $\delta^{13}C_{org}$, $\delta^{15}N_{org}$, TOC, TN, C/N and Redness of Lake Xingkai Sediment

The χ_{Lf} of the Lake Xingkai sediment core XK1 was relatively low, and its mean value was 19.4×10^{-8} m^3/kg, which might be related to the flat marsh wetlands around the lake (Xia and Wang 2000). The mean redness was 27.3 %, which was mainly controlled by the magnetite and goethite contents. High redness reflects warm and wet climatic conditions, whereas low redness reflects cold and dry climatic conditions. The correlation among the clay content, TOC, magnetic susceptibility and redness in XK1 (Table 4.3) showed that there was a strong positive correlation between magnetic susceptibility and clay content and a relatively strong positive correlation between magnetic susceptibility and redness. The vertical variation characteristics of grain size showed that between 27.7 and 2.7 ka BP, the medium silt and clay contents decreased but the fine silt content increased, which reflects the overall trend during this period of increasing precipitation and rising lake levels. The periods between 11.5 and 9.1 ka BP and between 8 and 2.9 ka BP recorded the lowest number of coxarse grains and variation of the mean grain size was also insignificant, thus indicating relatively stable hydrodynamic conditions of abundant precipitation and a relatively stable deep-water sedimentary

Table 4.3 Correlation coefficients of clay, magnetic susceptibility, TOC and redness for the Lake Xingkai sediment (*n = 269; significantly correlation indicated (Pearson's test) at a significance level greater than 0.01)

	Clay content	TOC	Magnetic susceptibility	Redness
Clay content	1			
TOC	0.34	1		
Magnetic susceptibility	0.68	0.38	1	
Redness	0.36	0.33	0.45	1

environment. Since 2.9 ka BP, the grain size coarsened, indicating that the lake level decreased. Based on the proxies magnetic susceptibility, grain size, $\delta^{13}C_{org}$, $\delta^{15}N_{org}$, TOC, TN, C/N and redness (Fig. 4.3), the climatic and environmental variations of Lake Xingkai since 27.7 ka BP are classified into seven periods. The variation characteristics of the climate and environment of each stage are discussed below in detail

1. During the period between 27,740 and 25,540 cal a BP, the mean values of TOC, C/N and redness were all low, mean clay content was relatively low, and the medium silt content was relatively high, indicating that the Lake Xingkai region during this period was at a low lake level and in a cold and dry period. During this period, there was relatively more sand, and the clay content was the lowest in the entire sediment core. The mean magnetic susceptibility was relatively low, which reflects the low magnetic mineral content and indicates that the sampling site during this period was a lakeside sedimentary environment with relatively strong hydrodynamic conditions. The magnetic minerals were washed and separated by strong wind waves, leaving many nonmagnetic feldspars and quartz. In addition, according to the pollen analysis data of the studied sediment core, Poaceae, Chenopodiaceae and *Artemisia* were the main terrestrial plants during this period, and the percentage of *Picea* was the highest in the entire sediment core (publish in Chap. 5), which corresponded to the Ashibing River stadial of the Guxiangtun Formation in the regions of Northeast China, such as the Sanjiang Plain (Wang 1987; Sun et al. 1985), as well as to the high *Picea* content at the Mohe River estuary in Russia (Korotkii et al. 2007). This pollen data were also relatively consistent with the analysis results of the pollen records in the Yangguo Town section of Weinan, Shaanxi and the pollen records in other northeastern regions (Sun et al. 1996; Liu et al. 2008), indicating the universality of cold climates during this period. The $\delta^{15}N_{org}$ value reached its highest mean value in the entire sediment core, and the TOC was also relatively low during this period, indicating that the organic matter in the sediment originated mainly from endogenous algae (Sakata et al. 1997; Balsam et al. 1999). In addition, the primary productivity was also very low, indicating that the lake region was generally in a cold and dry climate environment. The overall $\delta^{13}C_{org}$ exhibited a decreasing trend during this period, and relatively strong fluctuations indicated that the overall fluctuations of temperature and humidity exhibited an increasing trend.
2. During the period between 25,540 and 23,650 cal a BP, the χ_{Lf} and clay content decreased rapidly to the lowest values in the entire sediment core. $\delta^{15}N_{org}$ also exhibited a decreasing trend. However, the medium silt (16–32 μm) content increased to the highest content in the entire sediment core, and $\delta^{13}C_{org}$ increased rapidly to the second highest content in the entire sediment core. The decrease in $\delta^{15}N_{org}$ and high $\delta^{13}C_{org}$ values indicated that the content of terrestrial organic matter increased and the contribution from endogenous algae in the lake gradually decreased. The pollen analysis showed a significant decrease in the amount of Chenopodiaceae, decrease in the number of *Picea*, significant increase

in the number of *Betula*, and increase in the onshore aquatic sedge content. The vegetation type was savannah, which reflects the characteristics of a cold and wet climate. When compared to the previous period, the amount of precipitation increased, but the lake level was still relatively low. Lake Xingkai is a lake with an outlet; therefore, shallow water washing might enable the clay to flow out of the lake through the outlet with the lake current before settling (Williams et al. 2001). Such a situation would result in concentrated silt and a decrease in the clay content, and might cause the χ_{Lf} that is positively correlated to the clay content to decrease to its lowest value in the entire sediment core.

3. The period between 23,650 and 19,940 cal a BP corresponds to the last glacial maximum. During this period, the amount of coarse silt decreased, but the clay content increased rapidly to reach the highest content in the entire sediment core. The χ_{Lf} exhibited a rapid increasing trend with the increasing clay content. The pollen analysis results indicated that the *Betula* content decreased and Chenopodiaceae content reached the mean highest value. During this period, $\delta^{13}C_{org}$ exhibited an overall decreasing trend, whereas $\delta^{15}N_{org}$ exhibited an increasing trend, which indicates that additional organic matter originated from phytoplankton during the last glacial maximum. In addition, because of the relatively long lake-freezing time during the last glacial maximum, organic matter were easily conserved, resulting in a relatively high TOC value during this period.
4. During the period between 19,940 and 14,510 cal a BP, although the clay content fluctuated and rose multiple times, its mean value was below the value recorded for the period between 23,650 and 19,940 cal a BP. The magnetic susceptibility during this period was also slightly lower than that during the previous period. In the sediment grain size composition, the fine silt content exhibited an increasing trend, whereas the medium and coarse silt contents gradually decreased. The $\delta^{13}C_{org}$ content was significantly lower than that during the previous period, whereas the $\delta^{15}N_{org}$ content gradually increased. The pollen analysis results showed that the Chenopodiaceae percentage decreased significantly, Cyperaceae and *Artemisia* percents were still relatively high, and large amounts of *Pediastrum* emerged, which indicates that during this period, the lake level increased, and precipitation also increased compared with that of the previous period. In addition, *Picea* generally disappeared, but the *Betula* content increased, indicating that temperatures increased to some extent.
5. During the period between 14,510 and 11,500 cal a BP, the clay content gradually increased in the sediment grain size composition, whereas the fine silt content significantly decreased and medium silt content increased. The $\delta^{13}C_{org}$ and $\delta^{15}N_{org}$ contents gradually increased, and the C/N value significantly decreased. The pollen analysis results indicated that the *Betula*, *Alnus* and *Myriophyllum* contents initially increased rapidly but subsequently decreased significantly. Correspondingly, the Poaceae, *Artemisia* and Chenopodiaceae contents decreased rapidly, but *Artemisia* subsequently increased and *Betula* decreased, indicating that the climate warmed rapidly at the beginning of this period but experienced a rapid cold and dry trend during the middle and late stages of this period.

Overall, this period corresponded to the Bølling/Older Dryas/Allerød/Younger Dryas climate fluctuation period during the climate warming process in the late glacial period.

6. During the period between 11,500 and 2,800 cal a BP, the magnetic susceptibility decreased significantly with the decreasing clay content. In the sample grain size composition, the clay content decreased significantly, whereas the fine silt content increased significantly to the highest value of the entire sequence and medium silt content decreased significantly. The TN content and redness gradually increased, and the $\delta^{13}C_{org}$ value was low. The TOC content was relatively high, and the $\delta^{15}N_{org}$ value was relatively low and gradually decreasing. The pollen analysis results showed that the *Betula* content reached the highest value of the entire sequence during this period, indicating that this period was a high lake level period during which precipitation was gradually increasing. The increase in the runoff volume increased the current force, resulting in a decrease in the clay content and gradual increase in the fine silt content; therefore, the magnetic susceptibility decreased to some extent. During this period, the vegetation in the basin was luxuriant, and the amount of nutrients contributed by weak surface erosion to the lake decreased, resulting in a relatively low $\delta^{15}N_{org}$ value. This period corresponded to the Holocene warm period. Between 8,000 and 5,000 cal a BP, the stable high values of fine coarse silt, TOC and redness indicated that the climate of the study region during this period was in the Holocene optimum period. At approximately 8,200 cal a BP, the sudden increase in the clay content, χ_{Lf}, medium silt content, sand content and TN concentration and sudden decrease in the fine silt content along with an increase in the Artemisia pollen in sporo-pollen assemblages and rapid decrease in the arborescent pollen content indicated that this was a cold and dry period during which the lake levels decreased rapidly. This period corresponded to the 8.2 cal ka BP cold event that occurred generally in the Northern Hemisphere.
7. Since 2,800 cal a BP, although the clay content had relatively strong fluctuations, it exhibited a decreasing trend overall. In the sediment grain size composition, the clay and fine silt contents decreased, whereas the medium silt content increased and sand content reached the highest value of the entire sequence. The $\delta^{13}C_{org}$ content increased significantly, and the TOC and TN contents gradually decreased. These phenomena indicated that the lake level decreased significantly during this period and the climate was cool and dry. Since approximately 1,000 cal a BP, large amounts of *Quercus*, *Ulmus*, *Salix* and broad-leaved tree pollen emerged, which might indicates the human activity of slashing or burning primary forests, and resulted in the growth of secondary forests that mainly included *Quercus* and *Salix*. Increases in the magnetic susceptibility, clay and fine and medium silt contents also reflected aggravated soil erosion and soil and water loss caused by increasing human activities, resulting in large amounts of fine particles in the topsoil to flow into lakes, which in turn increased the magnetic susceptibility.

4.5 Conclusions

The comprehensive research results of the proxies (magnetic susceptibility, grain size, $\delta^{13}C_{org}$, $\delta^{15}N_{org}$, TOC, TN, C/N and redness) of Lake Xingkai sediment core XK1 reconstructed the palaeoclimate and palaeoenvironment evolution in the Lake Xingkai region since 27.7 ka BP. The grain size composition sensitively recorded the water level fluctuations of the outflowing Lake Xingkai. On thousand-year scale, increases in the medium silt and sand component contents corresponded to a low lake level and low precipitation climatic environment; increases in the fine silt content corresponded to a high lake level and high precipitation climatic environment; and increases in the clay content corresponded to weak sedimentary hydrodynamics and extremely dry climatic environment. There was a strong positive correlation between the magnetic susceptibility and clay content of the XK1, which has been affected by human activities since the late Holocene. The comprehensive proxy research results showed the following: during the period between 27,740 and 25,540 cal a BP, the lake region was at a low lake level in a cold and dry climate period; during the period between 25,540 and 23,650 cal a BP, the precipitation increased compared with the previous period, but the lake level was still relatively low and the lake region was in a cold and wet climate period; during the period between 23,650 and 19,940 cal a BP, which corresponds to the last glacial maximum (LGM), climate of the lake region was cold and dry; during the period between 19,940 and 14,510 cal a BP, the precipitation increased compared with the previous period and the temperature also increased to some extent; during the period between 14,510 and 11,500 cal a BP, the late glacial period began, the climate turned from warm and wet to cold and dry, and the Bølling/Older Dryas/Allerød/Younger Dryas climate fluctuation period occurred; during the period between 11,500 and 2,800 cal a BP, the Holocene warm period began; during the period between approximately 8,000 and 5,000 cal a BP, the climate entered the Holocene optimum period; since 2,800 cal a BP, the lake level has decreased significantly and the climate turned cool and dry; and since approximately 1,000 cal a BP, there has been a significant increase in the sediment coarse grain size composition, magnetic susceptibility and secondary arborescent pollen in the pollen assemblages, which reflects the increase in human activities.

Funding This study is supported by National Natural Science Foundation of China (41430530), The CAS/SAFEA International Partnership Program for Creative Research Teams (KZZD - EW-TZ- 08) and National Basic Research Program of China (2012CB956100)

References

An ZS, Porter SC, Kutzbach JE et al (2000) Asynchronous Holocene optimum of the East Asian monsoon. Quat Sci Rev 19:743–762

Balsam WL, Deaton BC (1991) Sediment dispersal in the Atlantic Ocean: evaluation by visible light spectra. Rev Aqua Sci 4:411–447

Balsam WL, Deaton BC, Damusth JE (1999) Evaluating the optical lightness as a proxy for carbonate content in marine sediment cores: implication for marine sedimentation. Mar Geol 161:141–153

Balsam WL, Ji JF, Chen J (2004) Climatic interpretation of the Luochuan and Lintai loess sections, China, based on changing iron oxide mineralogy and magnetic susceptibility. Earth Planet Sci Lett 223:335–348

Bazarovaa VB, Mokhova LM, Orlova LA et al (2008) Variation of the Lake Khanka level in the Late Holocene, Primorye. Russ J Pac Geol 2(3):272–276

Brahney J, Clague JJ, Menounos B et al (2008) Timing and cause of water level fluctuations in Kluane Lake, Yukon Territory, over the past 5000 years. Quatern Res 70:213–227

Chen JA, Wan GJ, Tang DG et al (2000) The sediment grain size and isotope record of recent climate change of Er Hai. Prog Nat Sci 10(3):252–259

Chen JA, Wan GJ, Zhang F et al (2003) Environment record of lake sediment in different time scales—illustrated by the case of sediment grain size. Sci China (Series D) 33(6):563–568

Chu GQ, Gu ZY, Xu B et al (2005) Varvechronology and radiometric dating (^{137}Cs, ^{210}Pb) from the Sihailongwan Maar, Northeastern China. Quat Sci 25(2):202–207

Gao J, Zhang JW, Zhang CJ et al (2007) Environmental changes during the past 800 years recorded in lake sediments from Hala Lake on the Northern Tibetan Plateau. Quat Sci 27(1):100–107

Guy RD, Fogel ML, Berry JA (1993) Photosynthetic fractionation of the stable isotope of oxygen and carbon. Plant Physiol 101:37–47

Hughen K, Lehm AS, Southon J et al (2004) ^{14}C activity and global carbon cycle changes over the past 50,000 years. Science 303(9):202–207

Ji JF, Shen J, William B et al (2005) Asian monsoon oscillations in the northeastern Qinghai-Tibet Plateau since the late glacial as interpreted from visible reflectance of Qinghai Lake Sediment. Earth Planet Sci Lett 233:61–70

Korotkii AM, Grebennikova TA, Karaulova LP et al (2007) Lacustrine transgressions in the Late Cenozoic Ussuri-Khanka depression (Primor'e). Russ J Pac Geol 1(4):352–365

Li SJ, Wang XT, Xia WL et al (2004) The Little Ice Age climate fluctuations derived from lake sediment of Goulucuo, Qinghai-Xizang Plateau. Quat Sci 24(5):578–584

Li WY (1998) Quaternary vegetation and environment. Science Press, Beijing

Liu YY, Zhang SQ, Liu JQ et al (2008) Vegetation and environment history of Erlongwan Maar Lake during the Late Pleistocene on pollen record. Acta Micropalaeontol Sin 25(3):274–280

Liu ZM, Lv XG, Wu HT et al (2008) Study on lowest water level of Xingkai Lake for ecological safety. Water Resour Hydropower Eng 39(2):8–10

Meyers PA, Lallier VE (1999) Lacustrine sedimentary organic matter records of Late Quaternary paleoclimates. J Paleolimnol 21:345–372

O Leary MH (1988) Carbon isotope in photosynthesis. Bioscience 38(5):328–336

Qiu SW, Wan EP, Wang PF (1988) Lake shoreline changes of the Xingkai Lake and discovery of paleo – riverhead of Songacha River. Chin Sci Bull 33(12):937–940

Qiu SW, Wan EP, Li FH et al (2007) Development of the plain in the north of the Xingkai Lake and formation of its wet lands. Wetl Sci 5(2):153–158

Sakata S, Hayes JM, McTaggart AR et al (1997) Carbon isotope fractionation associated with lipid biosynthesis by a cyanobacterium: relevance for interpretation of biomarker records. Geochin Cosmochin Acta 61:5379–5389

Shen J (2013) Spatiotemporal variations of Chinese lakes and their driving mechanisms since the Last Glacial Maximum: a review and synthesis of lacustrine sediment archives. China Sci Bull 58(1):17–31

Sun JZ, Wang SY, Wang YZ et al (1985) Paleoenvironment of the Last Glacial stage in Northeast China. China Quatern Res 6(1):82–89

Sun XJ, Song CQ, Wang FY (1996) Vegetation history of the southern Loess Plateau of China during the last 100,000 years based on pollen data. Acta Bot Sin 38(12):982–988

Thompson R, Oldfield F (1986) Environmental magnetism. Allen and Unwzn, London, pp 11–18

Vodyanitskii YN, Vasilev AA, Kozheva AV et al (2007) Influence of iron containing pigments on the color of soils on alluvium of the middle Kama Plain. Eurass Soil Sci 40(3):289–301

Wan B, Zhong YL (1997) Features analysis and divisions of new tectonic movement in Northeast China. Seismol Res Northeast China 13(4):64–75

Wang MH (1987) Preliminary study of palaeovegetation and palaeoclimatic index in the late period of late Pleistocene in Northeast Plain of China. J Glaciol Geocryol 9(3):229–238

Wang GA, Han JM (2001) $\delta^{13}C$ variations of C_3 plants in dry and rainy seasons. Mar Geol Quat Geol 21(4):43–47

Wang J, Liu ZC, Jiang WY et al (1996) A relationship between susceptibility and grain size and minerals, and their paleoenvironmental implication. Acta Geogr Sin 51(2):155–163

Wang GA, Han JM, Zhou LP (2002) Relationships between $\delta^{13}C$ values of C_3 plants and the annual average temperature in northern China. Geol China 29(1):55–57

Wang GA, Han JM, Liu DS (2003) The carbon isotope composition of C3 herbaceous plants in loess area of northern China. Sci China (Series D) 46(10):1069–1076

Wang XY, Wu L, Zhang GS et al (2008) Characteristics and environmental significance of magnetic susceptibility and grain size of lake sediment since Holocene in Chaohu Lake, Anhui Province. Acta Geogr Sin 4:549–553

Watanabe T, Naraokaa H, Nishimura M et al (2004) Biological and environmental changes in Lake Baikal during the late Quaternary inferred from carbon, nitrogen and sulfur isotopes. Earth Planet Sci Lett 222:285–299

Williams DF, Kuzmin MI, Prokopenko AA et al (2001) The lake Baikal drilling project in the context of a global lake drilling initiative. Quat Int 80–81:3–18

Wu NQ, Lv HY, Nie GZ et al (1992) The study of phytolith in C_3 and C_4 grass and its paleoecological significance. Quat Sci 12(3):241–251

Xia YM, Wang PF (2000) Peat record of climate change since 3000 years in Yangmu, Mishan region. Geophys Res 19(1):53–59

Xue B, Yu G (2005) Variation mechanism of Chinese lake water quantity and paleoclimate since the last glacial maximum. J Lake Sci 17(1):35–40

Yang SL, Chen SY, Yan MD et al (1999) Soil color: a new sensitive indicator for climatic change. Chin Sci Bull 44(S1):282–285

Yang SL, Fang XM, Li JJ et al (2001) Transformation functions of soil color and climate. Sci China (Series D) 44(S1):218–226

Yin Y, Fang NQ, Hu CY et al (2002) Relative brightness index and its climatic significance from lacustrine sediment of Napahai lake, Northwestern Yunnan Plateau, China. Chin Geogr Sci 12(3):249–253

Yin ZQ, Qin XG, Wu JS et al (2008) Multimodal grain size distribution characteristics and formation mechanism of lake sediment. Quatern Res 28(2):345–353

Yu LZ, Oldfield F, Wu YS et al (1990) Paleoenvironmental implications of magnetic measurements on sediment core from Kunming Basin, Southwest China. J Paleolimnol 3:95–111

Zhang SQ, Deng W, Yan MH et al (2004) Pollen records and forming process of the peatland in Late Holocene in the Xingkai Lake, China. Wetl Sci 2(2):110–115

Zhang XR, Hu K, Hu YF et al (2007) Holocene environmental and climatic changes from the information of peat bog sediment in Northeastern China. Geol Surv Res 30(1):39–45

Zhou LP, Oldfield F, Wintle AG et al (1990) Partly pedogenic origin of magnetic variations in Chinese Loess. Nature 346:737–739

Zhu Y, Shen J, Lei GL et al (2011) Environmental evolution of Xingkai (Khanka) Lake since 200 ka by OSL dating of sand hills. Chin Sci Bull 56(24):2017–2025

Chapter 5
Paleovegetation and Paleoclimate Evolution of Past 27.7 cal ka BP Recorded by Pollen and Charcoal of Lake Xingkai, Northeastern China

Ming Ji, Ji Shen, Jian Wu, and Yong Wang

Abstract Lake Xingkai, a transboundary lake by China and Russia, is the largest freshwater lake in Northeast Asia. An 269 cm long continuous sediment core from Lake Xingkai, has been analyzed firstly in China for pollen and charcoal, in order to study the paleovegetation and paleoclimate evolution in the area. Vegetation and climate change history of Lake Xingkai have been reconstructed since the 27.7 cal ka BP. During 27.7 ~ 25.5 cal ka BP, the study region was occupied by forest steppe dominated by Poaceae, *Artemisia*, Chenopodiaceae and *Picea* that reflected a cold and slightly dry climate. Later, between 25.5 ~ 23.7 cal ka BP, the study region was occupied by coniferous and broad-leaved mixed forest steppe which reflected a relatively cold-wet climate. During 23.7 ~ 19.9 cal ka BP, which corresponded to LGM (Last Glacial Maximum), the study region developed broad-leaved forest steppe indicated cold and dry climate condition. From 19.9 to 14.5 cal ka BP, there was broad-leaved forest steppe with *Betula* and *Artemisia* as the main component when *Pediastrum* and Ferns increased greatly, which suggested a cold-wet climatic trend. During 14.5 ~ 10.8 cal ka BP, the study region was occupied by sparse forest grassland with *Picea*, *Betula*, *Artemisia* and Poaceae as the main components. This stage that corresponds to Bølling/Older Dryas/Allerød/Younger Dryas, was a climatic transition period from warm-wet to cold-dry. From 10.8 to 1.0 cal ka BP, the study region was occupied by broad-leaved forest steppe, which indicated climate changed from temperate and moist to warm and slightly dry in Holocene. After 1.0 cal ka BP, coniferous forest developed with *Pinus* as the main component, indicated climate changed to cool and dry again and human slash activity influence.

M. Ji • J. Shen (✉) • Y. Wang
State Key Laboratory of Lake Science and Environment, Nanjing Institute of Geography and Limnology, Chinese Academy of Sciences, 73 East Beijing Road, Nanjing 210008, P. R. China
e-mail: jishen@niglas.ac.cn

J. Wu
Neijiang Normal University, 705 Dongtong Road, Neijiang 641112, P. R. China

K. Kashiwaya et al. (eds.), *Earth Surface Processes and Environmental Changes in East Asia*, DOI 10.1007/978-4-431-55540-7_5

Keywords Northeast China • Lake Xingkai • Pollen and charcoal • Paleovegetation and paleoclimate evolution • Lake sediment

5.1 Introduction

Lake Xingkai, which located at the eastern border of Heilongjiang Province of China, is on the southern Sanjiang Plain along the Sino-Russian border. Lake Xingkai is the largest freshwater lake in Northeast Asia, and its basin is located in a typical temperate East Asian monsoon region at mid/high latitude. This region is controlled by the Mongolian cold high pressure in the winter with the cold and dry climate characteristics; in the summer, this region is affected by the hot and humid marine airwith the hot and rainy climate characteristics. Therefore, there are distinct seasons year round. Similar to other high-latitude regions in China, the warm period in this region begins earlier and lasts longer than in the low altitude regions since the Last Glacial Maximum (Li 1998; Wang 1998; An et al. 2000). Lake Xingkai is also one of the key lakes in the lake drilling program of the PAGES-PEP (PAGES pole-equator-pole) transect project (Chen and Ni 2008), so it has become a sensitive area for global change research (Williams et al. 2001). Vegetation is a sensitive indicator of climate change and can largely reflect the prevailing climatic conditions. Therefore, the study of pollen records is one of the most important methods of paleoclimate and paleoenvironment changes, and such records cannot be substituted with other materials (Wang 1987; Qiu et al. 2008; Ye et al. 1983; Xia and Wang 2000; Zhang et al. 2004). Because of the lack of long-term and continuous sedimentary records, regional or worldwide comparisons of these studies are subject to significant constraints. Our study is the first in China to use pollen and charcoal records of Lake Xingkai to reconstruct the evolution of vegetation in the basin and evaluate the paleoclimate change in the Lake Xingkai area since the late stage of the last glacial period.

5.2 Regional Geographical Profile

Lake Xingkai is a tectonic lake created by the subsidence of the Dunhua-Mishan fault zone. The paleoclimate fluctuations caused several retreats of Lake Xingkai since the late Pleistocene and left behind four sand mounds distributed in an arc along the northern shore of the lake. After the last lake retreat, a large sand mound divided the lake into Lake Xingkai and xiao Lake Xingkai. Lake Xingkai is in the south, located at 44 °32′ ~ 45 °21′N and 131 °58′ ~ 132 °51′E, and it has an average elevation of approximately 69.0 m. Its maximum length is 91.3 km (north to south), and its maximum width is 62.5 km (east to west) with an average of 48.0 km. The area of the lake is approximately 4,380 km^2, and the boundary of the lake surface is the line connecting the estuaries of the Song acha River and Bailing River. The

area of the lake in Chinese territory is approximately 1,080 km^2. The maximum depth of the water is approximately 10 m, with an average depth of 4 ~ 5 m. The Lake Xingkai Plain is located in the Southern Sanjiang Plain, also known as the Muling-Xingkai Plain, which has high terrain in the northwest and low terrain in the southeast and consists of two levels of lacustrine terraces. The relative height of the first level lacustrine terrace is 3 ~ 5 m, and the relative height of level two lacustrine terrace is 10 ~ 15 m. The southeastern lakeshore is flat with continuous wetlands, and the ground elevation above sea level is approximately 69.5 ~ 71.0 m (Qiu et al. 2007). The lake basin has high peaks with heights above sea level of approximately 1,000 m, and it is adjacent to the Japan Sea in the south and east. Southwest winds prevail in the area in the spring and summer, whereas northwest winds dominate in the autumn and winter. The annual average temperature is 2.9 ~ 3.1 °C; annual average precipitation on the lake surface is 530–600 mm and mean annual evaporation is 636–755 mm (Piao and Wang 2010). The Lake Xingkai Plain has temperate mixed forests, meadows and marsh areas. The zonal vegetation in this area is Pinus koraiensis mixed forest, with Quercus mongolica dominating in the deciduous broadleaved forests (Zhang et al. 2004; Yang and Wang 2003).

The total area of the lake basin was 22,400 km^2 before 1942. In 1942, flood diversion channels were constructed, with a portion of the water fed into the small Lake Xingkai through the Muxing waterway (floodway), and the rest of the water flowed eastward along the original channel of the Muling River. Currently, the total area of the Lake Xingkai basin is 36,400 km^2, and the Song acha River in the northeast is the only outlet with deep water and swift flow, so it is ice-free almost year round (Piao and Wang 2010) (Fig. 5.1). The river in Chinese territory that belongs to the Lake Xingkai water system and flows directly into the Lake Xingkai is Bailing River, whereas the rivers in the Russian territory are Kommissarovka

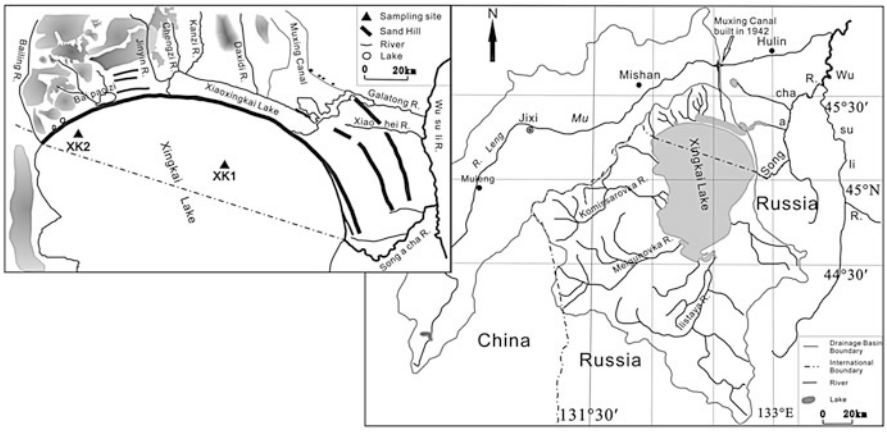

Fig. 5.1 Map of the Lake Xingkai basin, relief map of northern Lake Xingkai and the location of drilling

River, Melgunovka River, Ilistaya River, which are the main water sources of Lake Xingkai. The lake water is high in sediment concentration and has a transparency of approximately 0.15 m (Wang and Dou 1998).

5.3 Sample Collection and Analysis Method

In July 2007, we used an Austrian-manufactured floating platform (UWITEC) and piston corer to drill approximately 18 km away from the northern shore of Lake Xingkai (45 °12′21.7″N, 132 °30′33.3″E) (Fig. 5.1) at a depth of 6.6 m under water and obtained two parallel cores; the 269 cm long complete core (XK1) was used as the study object. The cores were brought to the lab and divided at an interval of 1 cm to generate 269 samples. Materials at 3 ~ 14 g were collected from each wet sample and sent for pollen identification to the pollen lab at the Institute of Hydrogeology and Environmental Geology, Chinese Academy of Geological Sciences. The samples were treated using hydrochloric acid-sodium hydroxide-hydrofluoric acid-hydrochloric acid, the pollen grains were subsequently concentrated with the screening-washing method, and Lycopodium spores were added to calculate the concentrations of pollen and charcoal fragments. The charcoal fragment concentration was calculated as follows: $W = A/B \times C/G$, where W is the charcoal fragment concentration (grains • g^{-1}), A is the mass of charcoal fragments (grain) counted, B is the counted amount of added Lycopodium spores (grains), C is the total number of added Lycopodium spores grains, and G is the mass of the selected wet sample (g).

5.4 Establishing the Core Chronology

Three samples from the XK1 core that collected at depths of 10 cm, 223 cm, 258 cm were sent to the University of Tokyo in Japan for accelerator mass spectrometry (AMS) ^{14}C dating. The three ^{14}C ages were 4,410 ± 40 a BP, 25,080 ± 110 a BP and 26,700 ± 130 a BP (Table 5.1). In August 2008, we retrieved a short core (XK2) of 71 cm length at position of 2.5 km from the southeastern shore of Lotus Lake. The location of the sampling site (XK2) was 45 °16′2.2″N, 132 °4′5″E (Fig. 5.1). The lithological features included sands above depths of 64 cm, followed by silty mud, which suggested that the 64 cm thick sand layer in the core XK2 corresponded to the 31 cm thick sand layer in the core XK1 (Fig. 5.4). Core XK2 was divided in 0.5 cm interval and sent to the Nanjing Institute of Geography and Limnology, Chinese Academy of Sciences, for ^{137}Cs and ^{210}Pb dating. A γ spectrum analysis system was used that consisted of a high-purity germanium well detector (Ortec HPGe GWL), an Ortec 919 spectrum master (EG&G Ortec Inc., US) and an IBM computer-based

Table 5.1 The determined and calibrated ^{14}C ages of the core from Lake Xingkai

Depth (cm)	10	223	258
^{14}C age (yr BP)	4,410 ± 40	25,080 ± 110	26,700 ± 130
Old carbon-free ^{14}C age (yr BP)	/	20,775 ± 110	22,395 ± 130
Calibrated age (cal yr BP)	105	24,760 ± 230	27,030 ± 529

16 k channel analyzer. The results are shown in Fig. 5.2 and include the following: an evident peak of ^{137}Cs accumulation in the core at a depth of 6.75 cm, which is believed to correspond to the year 1963 in Northeast China, when the deposition of ^{137}Cs in the Northern Hemisphere was at its peak (Chu et al. 2005); and the presence of ^{137}Cs beginning at a depth of 8.75 cm, which corresponds to the year 1954, in which global nuclear testing began. The chronology of the 0 ~ 21 cm sediment was established with the age calculated by the corrected ^{210}Pb CRS model using the 1963 and 1954 dates as benchmarks (Last and Smol 2004). Observations on the segmented samples indicated that at 16 cm, the sediments became significantly harder, which suggested that the sediments were compacted over a long period of time, and the age was linearly related to the depth, which resulted in a lithologically uniform segment from 16 to 64 cm. Therefore, the age at the bottom (64 cm) was linearly extrapolated to 1,050 a BP (Li et al. 2004; Gao et al. 2007) based on the average sedimentation rate of 1.67 mm/a in the 16 ~ 21 cm segment. The age of the bottom of the sand layer in XK1 (31 cm) should also be approximately 1,050 a BP. The ratio between the thicknesses of the upper sand layers of XK1 and XK2 indicated that the ratio between the sedimentation rates of these two cores was approximately 1:2; therefore, the calculated ^{210}Pb age of XK2 at 21 cm was 105 a BP, the age of XK1 at 10 cm should also be approximately 105 a BP, and the ^{14}C age at 10 cm (approximately 4305a) appeared to be older as a result of the "reservoir effect" Because of the extremely low percentage of organic carbon in Lake Xingkai, an average of approximately 0.5 % of the "old carbon" or "dead carbon" resulted from the erosion of older strata in the lake basin, which caused the age to appear older. Assuming that the apparent ages of the upper and lower segment of the core that appeared to be older as a result of the "reservoir effect" were approximately the same, 4305 a were subtracted from both ^{14}C ages (at 223 cm and 258 cm) (Wu et al. 2006), which resulted in "old carbon"-free ^{14}C ages of 20,775 ± 110 a BP and 22,395 ± 130 a BP, respectively. The two "old carbon"-free ^{14}C ages were then calibrated online with CalPal-online according to the Hughen K calibration curve (Hughen et al. 2004). The two calibrated ages were 24,763 ± 230 cal a BP and 27,032 ± 529 cal a BP. The ages of sediments in various segments of the core were determined by interpolation using the average sedimentation rate or extrapolation based on the age of the bottom (Table 5.1).

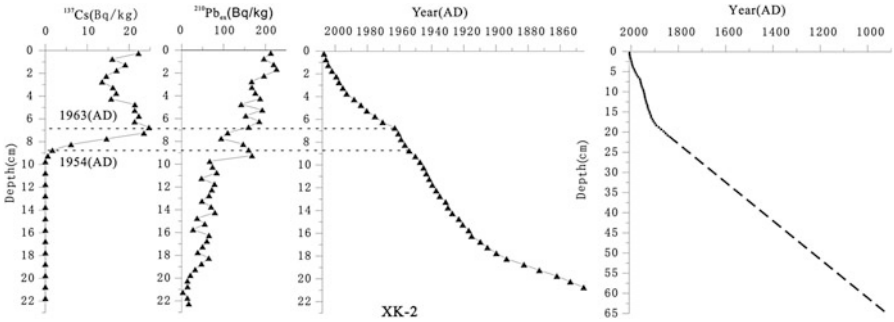

Fig. 5.2 ^{210}Pb and ^{137}Cs specific activity and age with respect to depth

5.5 Characteristics of Pollen and Charcoal Fragment Assemblage

5.5.1 Analysis of Pollen and Charcoal

A total of 134 taxa of pollen and spores were identified in the 269 pollen samples from XK1, including 18 taxa of arbor pollen, 25 taxa of shrub pollen, 65 taxa of xerophytic herb pollen, 7 taxa of aquatic (including hygrophytic) herb pollen and 16 taxa of fern spores. In addition, there were three algal taxa. The terrestrial pollen assemblage was dominated by arbor pollen above depths of 110 cm and dominated by herb pollen below 110 cm; there were few shrub pollen grains, with mostly arbor, herb pollen and fern spores in the entire core. Among the arbor pollen, *Pinus* was the genus with the highest concentration in the upper part of the core, *Betula* was the most abundant genus in the mid part and *Picea* was the dominant genus in the lower part. *Quercus*, *Alnus*, *Ulmus*, *Juglans* and Taxodiaceae pollen presented certain contents. *Larix*, Cupressaceae, *Carpinus*, *Acer* and *Tilia* presented sporadically. Pollen of shrub taxa were mainly represented by *Corylus*, Oleaceae, *Fraxinus*, *Salix*, *Sambucus*, *Myricaria*, *Spiraea*, *Ephedra* and *Tamarix*. Xerophytic herb pollens were dominated by Poaceae, *Artemisia* and Chenopodiaceae, and there were small amounts of Asteraceae, Rosaceae, Ranunculaceae, Cruciferae, Labiatae, Liliaceae, Caryophyllaceae, Solanaceae, *Thalictrum*, *Viola* and *Sanguisorba*, as well as sporadically presented Umbelliferae, Scrophulariaceae, *Polygonum*, *Potentilla*, and *Cuscuta*. Aquatic herbs (including hygrophytic herbs) were mainly of Cyperaceae, *Myriophyllum* and *Nymphoides*, and there was also a small amount of *Potamogeton*. Fern spores were dominated by Filicale, *Lycopodium*, *Selaginella* and *Adiantum*, while *Osmunda*, Polypodiaceae, and *Athyrium* were sporadically represented. In addition, three algal taxa were found at a depth of approximately 150–180 cm that included abundant *Pediastrum* and small amounts of *Zygnema* and *Concentricystes*.

5.5.2 *Pollen Assemblage Characteristics and Pollen Zonation*

The pollen percentage diagram and concentration diagram of the cross section were drafted based on 17 genera of pollens that accounted for more than 5 % of the pollen assemblage and were ecologically representative. From the bottom to top, the pollen diagram was divided into 7 pollen assemblage zones according to the characteristics of the pollen assemblages over time (Figs. 5.3 and 5.4).

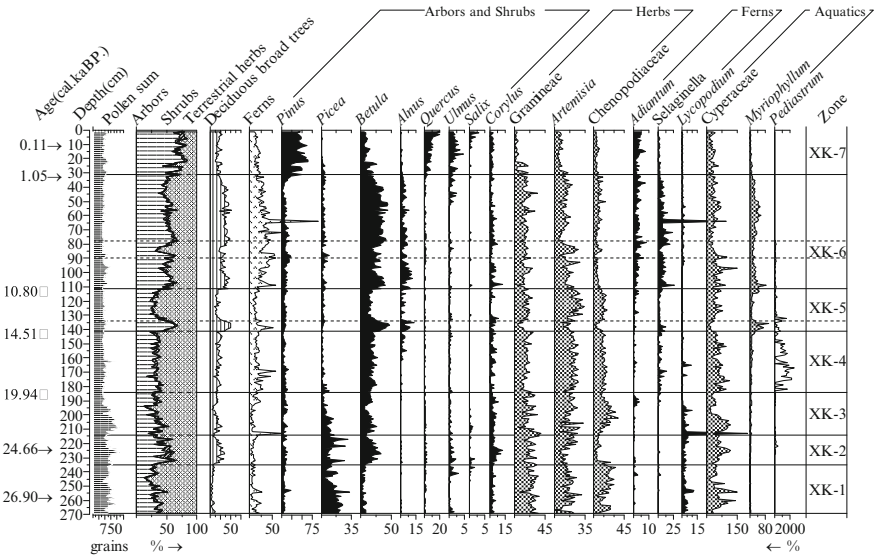

Fig. 5.3 Percentage diagram of major sedimentary pollen taxa in the XK1 core from Lake Xingkai

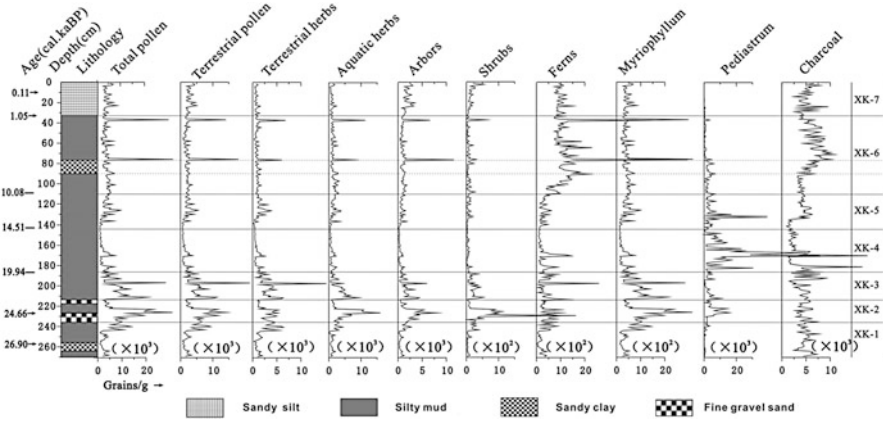

Fig. 5.4 Major sporo-pollen taxa, charcoal fragment concentration and lithology of the XK-1 sediment core recovered from Lake Xingkai

XK-1 assemblage zone (269 ~ 235 cm, approximately 27,740 ~ 25,540 cal a BP): This zone was dominated by terrestrial herb pollens, which accounted for an average of 67.8 % of the total terrestrial pollens; the average percentages of arbor, herb and aquatic fern spores/pollens were 29, 57 and 10 %, respectively. The contents of *Picea* and Poaceae pollen in this zone were the highest in XK1, with averages of 15.5 and 25.7 %, respectively; the percentages of *Artemisia*, Chenopodiaceae and Cyperaceae pollen were relatively high, with averages of 16.2, 18.9 and 56.1 %, respectively. The average concentration of charcoal fragments was 4,906 grains/g.

XK-2 assemblage zone (235 ~ 214 cm, approximately 25,540 ~ 23,650 cal a BP): Arbor pollens were the dominant type, accounting for an average of 67.8 % of the total terrestrial pollens. The average percentages of terrestrial herb pollens, aquatic herb pollens and fern spores were 50, 68 and 8.7 %, respectively. The *Betula* percentage of this segment increased significantly with an average of 19.5 %, and the percentage of *Artemisia*, Chenopodiaceae and Cyperaceae were still relatively high, with averages of 22.8, 14.5 and 65.3 %, respectively. The content of Chenopodiaceae pollen decreased significantly to an average of 6.6 %, and the percentage of *Picea* pollen decreased to an average of 12.9 %, which was still relatively high. The 232 ~ 223 cm segment in this zone had the highest concentration of sporo-pollen over the entire cross section, with an average concentration of 13,116 grains/g. The charcoal fragment concentration somewhat decreased in this zone, with an average of 4,607 grains/g.

XK-3 assemblage zone (214 ~ 184 cm, 23,650 ~ 19,940 cal a BP): Herb pollen still dominated the terrestrial pollen with an average of 65 %, and the average percentages of arbor, aquatic herb and ferns spores/pollen were 28.5, 60.7 and 9.7 %, respectively. In this segment, the percentage of Chenopodiaceae pollen was high with an average of 18.3 %, the content of *Artemisia* pollen increased, and the content of Cyperaceae pollen remained high with an average of 56 %. The content of Poaceae pollen decreased to an average of 19.6 %, the content of *Picea* pollen continue to decline to an average of 6 %, and the content of *Betula* pollen also dropped to an average of 14.7 %. The average total pollen concentration was still high but gradually decreased to an average of 7,909 grains/g. The concentration of charcoal fragments showed little change compared to the previous zone and had an average of 4,566 grains/g.

Lycopodium spores were concentrated in the above three pollen zones with an average high percentage of 3.6 %.

XK-4 assemblage zone (184 ~ 140 cm, 19,940 ~ 14,510 cal a BP): Terrestrial herb pollens continued to dominate, with an average percentage of 64.4 %, and the average percentages of arbor, aquatic herbs and ferns spores/pollen were 32.2, 68 and 19.9 %, respectively. The percentage of *Artemisia* and *Betula* pollens continued to increase, with averages of 21.7 and 20 %, respectively, and the content of Cyperaceae pollen remained high with an average of 58 %. The percentage of Chenopodiaceae pollen further dropped to an average of 14.2 %, and the percentage of Poaceae pollen also decreased to an average of 16.8 %. The presence of a

large number of *Pediastrum* was a distinctive feature of this zone, and it had an average percentage of 907 %. The total pollen concentration of this zone dropped sharply to the core-wide minimum value, which averaged 2,278 grains/g. The charcoal fragment concentration of this zone further decreased to an average of 3,182 grains/g.

XK-5 assemblage zone (140 ~ 110 cm, 14,510 ~ 10,800 cal a BP): In the 140 ~ 132 cm segment of this zone, the percentage of arbor pollen exceeded that of herb pollen for the first time, and it had an average of 53.5 %; in particular, the percentage of *Betula* increased rapidly to an average of 35 %, and more *Alnus* pollen presented for the first time, with an average of 6 %. *Myriophyllum* also presented at high levels for the first time, with an average of 43.7 %. The percentages of Poaceae, *Artemisia* and Chenopodiaceae dropped to low levels. In the subsequent 132 ~ 110 cm segment, the percent of arbor pollen dropped drastically to an average content of 31.6 %, and the average percent of *Betula* dropped to 16.6 %. The percent of *Artemisia* rose to the highest levels over the entire core with an average of 24.7 %, and the percentages of Poaceae and Chenopodiaceae pollens differed little from those in the XK-4 assemblage zone with average of 17.5 and 13 %, respectively. The percent of *Myriophyllum* decreased to a very low level, and the pollen concentration in this zone increased to an average of 4,425 grains/g. The concentration of charcoal fragments showed some increase compared with that of the previous zone, with an average of 3,954 grains/g.

XK-6 assemblage zone (110 ~ 31 cm, 10,800 ~ 1,050 cal a BP): The percentages of arbor pollen and herb pollen were nearly the same at an average of 50.6 %, and the average percent of *Betula* increased to 29.9 %. The percent of *Alnus* was high, with an average of 9.7 %, the percent of *Selaginella* reached a high level for the first time with an average of 21.6 %, and the percent of *Myriophyllum* also reached a relatively high level with an average of 27.4 %. However, at a depth of 90 ~ 78 cm, which represented the period from 8,340 to 6,850 cal a BP, the percent of *Artemisia* increased rapidly, while the percent of arbor pollen and spores decreased rapidly. There was no significant increase in the pollen concentration, and the average concentration was 4,677 grains/g. The concentration of charcoal fragments increased to the highest level observed among the cross sections, with an average of 5,896 grains/g.

XK-7 assemblage zone (31 ~ 0 cm, 1,050 cal a BP to present): Arbor pollen dominated, with an average of 68 %, and the percent of *Pinus* showed a significant increase for the first time with an average of 45 %. *Quercus* and *Ulmus* also presented at high levels for the first time with average percent of 7.7 % and 1.7 %, respectively, and the percent of *Betula* decreased significantly to an average of 10 %. The charcoal fragment concentration of this zone decreased compared to the previous zone to an average of 5,061 grains/g, and the pollen concentration changed little, with an average of 4,229 grains/g.

5.5.3 Evolution of the Climatic Environment and Vegetation, as Reflected by the Characteristics of Sporo-Pollen and Charcoal Fragments

At 269 ~ 235 cm, approximately 27,740 ~ 25,540 cal a BP: The pollen concentration of the XK-1 assemblage zone was relatively low, and the analysis clearly showed that the terrestrial herbs Poaceae, drought-resistant *Artemisia* and Chenopodiaceae were the dominant taxa. The percents of Poaceae and Chenopodiaceae pollen were the highest in the entire cross section. *Picea* was the major taxon among the arbor pollens and was at the highest level of the entire cross section. *Artemisia* and Chenopodiaceae pollen were produced in large quantities and had the greatest ability to spread. *Artemisia* plants are widely distributed in temperate regions of the Northern Hemisphere and mostly in grasslands and develop especially well in the sandy area of grasslands, with many Chenopodiaceae species widely distributed in the desert. During this period, the vegetation around the lake consisted of *Picea* forest and grassland, and a conifer specie that prefers to grow in a cold and wet environment, *Picea*, may have grown in the valleys of a lake basin or low-lying areas around a lake. This analysis might suggest a cold and dry climate, and the high concentration of charcoal fragments also suggested a dry climate. The relatively large proportion of Cyperaceae at the early stage also suggested a large area of lake shore marsh. In the 269 ~ 235 cm segment, the layer that had highest percentage of *Picea* corresponded to the Ashi River stadial of the mid Guxiangtun Formation in the northern suburb of Harbin (Wang 1987; Sun et al. 1985), which also corresponded to the high percentage of *Picea* profile in the Mohe River estuary in the Russian Lake Xingkai during the same period (Korotkii et al. 2007). There was a cold period approximately 28,000 cal a BP, and the Shaanxi Weihe Nanyang Guozhen cross section was also affected by the East Asian summer monsoon and consisted mainly of xerophytic *Artemisia*, and coniferous forest of mainly *Picea*, *Abies* and *Larix* (Korotkii et al. 2007; Sun et al. 1996; Liu et al. 2008) were widely distributed in Northeast China and North China.

At 235 ~ 214 cm, approximately 25,540 ~ 23,650 cal a BP: The pollen concentration of the XK-2 assemblage zone was the highest of the entire cross section. Compared with the previous stage, the proportion of arbor pollens increased and dominated the terrestrial pollen, with the greatest increase found in the *Betula* percentage. Compared with the previous segment, the concentrations of Poaceae pollen, *Artemisia* and charcoal fragments decreased, and the concentration of Chenopodiaceae was drastically reduced. There were numerous fine gravels at 2 cm from the top and 4 cm from the bottom of the core, indicating that the lake surface was low at the beginning and end of this segment. The high pollen concentration during this period may have been a result of the terrestrial pollen that was brought to the near-shore sampling sites by the streams flowing into the lake (Xu et al. 1995; Zhao et al. 2001). The pollen analysis showed that a small amount of *Picea* remained, indicating coniferous forest and conifer-*Betula* mixed forest landscapes,

which suggests a cold and wet climate corresponding to the Shangentun interstadial in the mid Guxiangtun Formation located under the Luohuang Mountain of Harbin (Wang 1987; Sun et al. 1985) and the *Betula*, *Salix* and *Picea* assemblages of the same stage in the Mo River Estuary in Russian Lake Xingkai. The presence of a new shallow-water sedimentary facies in the cross section also confirmed the sedimentary environment with an elevated lake surface (Korotkii et al. 2007) that represented the widely spread warming fluctuations in the Northern Hemisphere before the Last Glacial Maximum (Liu et al. 2008).

At 214 ~ 184 cm, approximately 23,650 ~ 19,940 cal a BP: The pollen concentration in the XK-3 assemblage zone was still high but decreased gradually. The percents of *Betula* and Poaceae decreased, while the *Artemisia* percent increased somewhat, and the Chenopodiaceae percent increased significantly. The percent of *Lycopodium* remained at high levels at the early stage and disappeared at the mid-late stage, whereas the Cyperaceae pollen percent was high at the early stage and low at the late stage. *Picea* and *Betula* percents continued to decline but remained at low levels. *Lycopodium* and Cyperaceae prefer wet environments and usually grow in valleys and swamps. Based on the above analysis, the lake surface was assumed to have been low at the early stage with a large area of swamps surrounding the lake, and the landscapes in plains and hills was assumed to have been conifer-Broadleaved mixed forest and grasslands. The climate was cold and dry, which corresponds to the Last Glacial Maximum.

At 184 ~ 140 cm, approximately 19,940 ~ 14,510 cal a BP: The pollen concentration of the XK-4 assemblage zone decreased sharply to the lowest value of the section. The percentages of Poaceae and Chenopodiaceae decreased, the percentages of *Artemisia* and *Betula* increased, and the number of ferns in the forest and valleys began to increase significantly. The most notable change was the presence of a large number of *Pediastrum. Pediastrum* tend to grow in slow-flowing fresh water (Xu et al. 2004). This change reflected a temperature change and lake surface increase and indicated that the environment of the lake basin was cold and wet, with broadleaved forests and grasslands.

At 140 ~ 110 cm, approximately 14,510 ~ 10,800 cal a BP: The pollen concentration of the XK-5 assemblage zone increased. At the beginning, the percents of *Betula*, *Alnus*, *Myriophyllum* and fern spores increased rapidly and then dropped drastically. Correspondingly, the Poaceae, *Artemisia* and Chenopodiaceae percentages dropped rapidly at the beginning, which was followed by an increase of the percentage of *Artemisia* and decrease of *Betula* percentage at the mid-late stage compared to the previous assemblage zone. The concentration of charcoal fragments also changed from a low level to high level. These combined changes indicated that the climate warmed rapidly at the early stage and then became cold and dry at the mid-late stage. Overall, this period corresponded to the Bølling/Older Dryas/Allerød/Younger Dryas climatic fluctuation period during the temperature rise of the Late Glacial Maximum.

At 110 ~ 31 cm, approximately 10,800 ~ 1,050 cal a BP: The pollen concentration of the XK-5 assemblage zone showed little change and had virtually the same percentages of arbor pollen and herb pollen. The percents of *Betula*, fern spores,

Alnus and *Myriophyllum* remained at high levels, the percents of Poaceae, *Artemisia* and Chenopodiaceae remained at low levels, and the percents of Cyperaceae decreased. *Adiantum* and *Selaginella* presented in large numbers for the first time and remained at relatively high levels. The landscape was *Betula*-dominated deciduous forest with an abundant understory of *Adiantum* and *Selaginella*, which prefer a wet environment and grow vigorously below the lake surface. This change reflected a climate that was warm and humid and a greatly increased lake surface, which corresponded to the Holocene warm period. As a result of the greatly expanded lake surface, the pollen carried by water had to travel a long distance, which resulted in a low sporo-pollen concentration. However, the *Alnus* content remained high, and the charcoal fragment concentration reached the minimum value in the 110 ~ 78 cm segment that represented the early stage, which suggests that the climate was warm and humid. In the later 78 ~ 31 cm (approximately 7,000 ~ 1,050 cal a BP) segment, *Alnus* percent was relatively low, and the charcoal fragment concentration reached its maximum value in the profile, suggesting that the climate was warm and dry. In particular, *Artemisia* percent increased and the arbor pollen percent rapidly decreased in the 90 ~ 78 cm segment (approximately 8,330 ~ 7,000 cal a BP), indicating a cold and dry period during which the lake surface declined rapidly and corresponded to the cold event at 8.2 cal a BP that was widespread in the Northern Hemisphere (Thomas et al. 2007; Wang 2008; Jin et al. 2007).

At 31 ~ 0 cm, approximately 1,050 cal a BP to present: The pollen concentration of the XK-5 assemblage zone showed little change compared to the previous period. The concentration of charcoal fragments was lower than that of the previous period but remained at a high level. The percentage of *Pinus* showed the first sharp increase of the profile, which was consistent with the presence of a large number of pine in the sporo-pollen assemblage of the same period in Sanjiang Plain to the north of Lake Xingkai (Yang and Wang 2003). The percent of the understory *Adiantum*, which prefers a shady and humid environment, reached the profile maximum, and *Quercus* and *Ulmus*, which prefer dry environments, were found in the hills and uplands of the lake basin and presented a mixed forest landscape. The zonal vegetation in this area was broadleaved and *Pinus koraiensis* mixed forest that was mostly distributed in high-altitude mountains such as Changbai Mountain, Xiaoxinganling Mountain and Wanda Mountain (Xu et al. 1995). The pollen assemblage in this segment reflects a cool and dry climatic environment. In addition, the presence of a large number of *Quercus* and *Ulmus* broad-leaved species may reflect the destruction caused by human activities in the environment, with the harvesting or burning of *Pinus koraiensis* forest by humans destroying the primeval forest and resulting in a large number of secondary broadleaved forests, such as *Quercus mongolica* and *Ulmus* forests (Zhou and Shen 2003).

5.6 Conclusions

The pollen record in the sediment cores from Lake Xingkai revealed the following evolution of vegetation and climate in this area since 27.7 cal ka BP: from 27.7 to 25.5 cal ka BP, the study region was occupied by forest steppe dominated by Poaceae, *Artemisia*, Chenopodiaceae and *Picea*. This reflected cold and slightly dry climate. From 25.5 to 23.7 cal ka BP, there developed coniferous and broad-leaved mixed forest steppe dominated by *Betula*, *Picea*, Poaceae and *Artemisia*, which reflected a relatively cold-wet climate. From 23.7 to 19.9 cal Ka BP, the study region developed broad-leaved forest steppe with *Betula*, Poaceae, *Artemisia* and Chenopodiaceae as the main components, indicated cold and dry climate condition. From 19.9 to 14.5 cal ka BP, there was broad-leaved forest steppe with *Betula* and *Artemisia* as the main components when *Pediastrum* and Ferns increased greatly, which suggested a cold-wet climatic trend. From 14.5 to 10.8 cal ka BP, the study region was occupied by sparse forest grassland with *Picea*, *Betula*, *Artemisia* and Poaceae as the main components. This stage that corresponds to Bølling/Older Dryas/Allerød/Younger Dryas, was a climatic transition period from warm-wet to cold-dry. From 10.8 to 1.0 cal ka BP, the study region was occupied by broad-leaved forest steppe dominated by *Betula*, Poaceae, *Artemisia* and *Alnus*, indicated climate changed from temperate and moist to warm and slightly dry in Holocene. After 1.0 ka BP, the vegetation in the lake basin was mainly coniferous broadleaved mixed forest, and the climate turned dry and cool and human slash activity influence.

Funding This study is supported by National Natural Science Foundation of China (41430530), The CAS/SAFEA International Partnership Program for Creative Research Teams (KZZD - EW-TZ- 08) and National Basic Research Program of China (2012CB956100)

References

An ZS, Porter SC, Kutzbash JE et al (2000) Asynchronous Holocene optimum of the East Asian monsoon. Quat Sci Rev 19:743–762

Chen Y, Ni J (2008) Quantitative paleovegetation reconstruction at large scale based on pollen records. J Plant Ecol 32(5):1201–1212

Chu GQ, Gu ZY, Xu B et al (2005) Varvechronology and radiometric dating (^{137}Cs, ^{210}Pb) from the Sihailongwan Maar, Northeastern China. Quat Sci 25(2):202–207

Gao J, Zhang JW, Zhang CJ et al (2007) Environmental changes during the past 800 years recorded in lake sediments from Hala Lake on the Northern Tibetan Plateau. Quat Sci 27(1):100–107

Hughen K, Lehman S, Southon J et al (2004) ^{14}C activity and global carbon cycle changes over the past 50,000 years. Science 303(9):202–207

Jin ZD, Yu J, Wu YH et al (2007) Was there an 8.2 ka BP cooling event in China? Geol Rev 53(5):616–623

Korotkii AM, Grebennikova TA, Karaulova LP et al (2007) Lacustrine transgressions in the late Cenozoic Ussuri-Khanka depression (Primor'e). Russ J Pac Geol 1(4):53–68

Last WM, Smol JP (2004) Tracking environmental change using Lake sediments, vol 1, Basin analysis, coring and chronological techniques. Kluwer, New York/Boston/Dordrecht/London/Moscow, pp 171–196

Li WY (1998) Quaternary vegetation and environment of China. Science Press, Beijing, p 230
Li SJ, Wang XT, Xia WL et al (2004) The Little Ice Age climate fluctuations derived from lake sediments of Goulucuo, Qinghai-Xizang Plateau. Quat Sci 24(5):578–584
Liu YY, Zhang SQ, Liu JQ et al (2008) Vegetation and environment history of Erlongwaan Maar Lake during the Late Pleistocene on pollen record. Acta Micropaleontol Sin 25(3):274–280
Piao DX, Wang FK (2010) Environmental conditions and the protection counter measures for waters of Lake Xingkai. J Lake Sci 23(2):196–202
Qiu SW, Wan EP, Li FH et al (2007) Development of the Plain in the North of the Lake Xingkai and formation of its wetlands. Wetl Sci 5(2):153–158
Qiu SW, Sun GY, Xia YM (2008) Formation and evolution of marshes in the middle-east of the Sanjiang Plain. Wetl Sci 6(2):148–159
Sun JZ, Wang SY, Wang YZ et al (1985) Paleoenvironment of the last glacial stage in Northeast China. Quat Res China 6(1):82–89
Sun XJ, Song CQ, Wang FY et al (1996) Vegetation history of the southern Loess Plateau of China during the Last 100000 years based on pollen data. Acta Bot Sin 38(12):982–988
Thomas ER, Wolff EW, Mulvaney R et al (2007) The 8.2 ka event from Greenland ice cores. Quat Sci Rev 26:70–81
Wang MH (1987) Preliminary study of paleovegetation and paleoclimatic index in the later period of the Late Pleistocene in Northeast Plain of China. J Glaciol Geocryol 9(3):229–238
Wang ZG (1998) Reconstruction of past 5000-year humidity changes of Northeast China using δ13C values of peat cellulose in Jinchuan Region, Jilin Province. Acta Metallurgica Sin 17(1):52–54
Wang SW (2008) 8.2 ka cold event. Adv Clim Change Res 4(3):193–194
Wang SM, Dou HS (1998) Lakes in China. Science Press, Beijing, p 503
Williams DF, Kuzmin MI, Prokopenko AA et al (2001) The Lake Baikal drilling project in the context of a global lake drilling initiative. Quat Int 80–81:3–18
Wu YH, Wang SM, Hou XH (2006) Lake sediment chronology research of Cuo e in Central Qingzang Plateau. Sci China Earth Sci D Ser 36(8):713–722
Xia YM, Wang PF (2000) Peat record of climate change since 3000 years in Yangmu, Mishan region. Geogr Res 19(1):53–59
Xu QH, Yang XL, Wang ZH et al (1995) Study on pollen transportation by rivers. Acta Bot Sin 37(10):829–832
Xu ZL, Li CY, Kong ZC (2004) On the Fossil Pediastrum from the Gaoximage section, Hunshandak sandy land and its ecological significance since 5000 a BP. Acta Bot Sin 46(10):1141–1149
Yang YX, Wang SY (2003) Study on mire development and paleoenvironment change since 8 ka BP in the Northern part of the Sanjiang Plain. Sci Geogr Sin 23(1):32–38
Ye YY, Yan FH, Mai XS (1983) The sporo-pollen assemblages in three well logs from three-river Plain, Northeast China and their geological significance. Sci Geol Sin 3:259–267
Zhang SQ, Deng W, Yan MH et al (2004) Pollen record and forming process of the peatland in Late Holocene in the North bank of the Lake Xingkai, China. Wetl Sci 2(2):110–115
Zhao Y, Chen FH, Zhang JW et al (2001) Effects of depositional environment on pollen assemblages – a case study in the Shiyang River Basin. Acta Sediment Sin 19(2):186–191
Zhou DY, Shen G (2003) Characters and distribution regulations of Korean pine – broad leaf mixed forest in the Northeast of China. Territory Nat Resour Study 2:91–92

Chapter 6
Reconstructing Mid- to Late Holocene East Asian Monsoon Variability in the Jingpo Lake, Northeastern China

Rong Chen and Ji Shen

Abstract The Northeastern China involves complex interactions between the East Asian monsoon (EAM) circulation and the polar climate system, and plays a significant role as the bridge communicating low and high latitude climatic processes. High-resolution multi-proxy analysis of a robust AMS ^{14}C dated lacustrine sediment core recovered from Jingpo Lake in northeastern China provides a detailed history of East Asian monsoon (EAM) variability and vegetation changes during the Mid- to Late Holocene. The multi-proxy results show that the climate was relatively warm and humid during the period from ~5100 to 3600 cal. yr BP, cool and dry between 3600 and 2100 cal. yr BP, and a strengthening of the EAM intensity during the period of 2100 to 150 cal. yr BP. After 150 cal. yr BP, the multi-proxy results reflecting the Jingpo Lake region is affected by intensive human activities. Our findings indicate that variability of the EAM during the Mid- to Late Holocene on multi-decadal to centennial scale are forced by changes in both solar output and oceanic–atmospheric circulations. Furthermore, we have found the evidence that abrupt climate changes coincides with the collapse or the beginning and the chaotically divided of some Chinese dynasties, which will need further research on the relationship between climate and human cultural changes.

Keywords Multi-proxy analyses • Climatic change • East Asian monsoon • Mid- to Late Holocene • Jingpo Lake

R. Chen
State Key Laboratory of Lake and Environment, Nanjing Institute of Geography and Limnology, Chinese Academy of Sciences, 73 East Beijing Road, Nanjing 210008, P. R. China

University of Chinese Academy of Sciences, Beijing 100049, P. R. China

J. Shen (✉)
State Key Laboratory of Lake Science and Environment, Nanjing Institute of Geography and Limnology, Chinese Academy of Sciences, 73 East Beijing Road, Nanjing 210008, P. R. China
e-mail: jishen@niglas.ac.cn

K. Kashiwaya et al. (eds.), *Earth Surface Processes and Environmental Changes in East Asia*, DOI 10.1007/978-4-431-55540-7_6

6.1 Introduction

The Asian monsoon (AM) system consists of two important subsystems, i.e., the East Asian monsoon (EAM) and the Indian monsoon (IM), is an integral part of the global climatic system and plays a significant role in the global hydrological and energy cycles (Wang 2006). Understanding the nature of Asian monsoon variability during the Holocene is essential to understand the present climatic conditions, provide insights into the potential climate forcing mechanisms, and to predict future climatic processes (Long et al. 2012). During the last two decades, there have been numerous studies on Holocene monsoon climate changes in the EAM regions, mostly coming from loess records (Huang et al. 2004; Maher et al. 2003; Porter and An 1995), tree rings (Shao et al. 2010; Zhang et al. 2003), ice cores (Thompson et al. 1989, 1997, 2000), speleothem records (Cosford et al. 2008; Dykoski et al. 2005; Wang et al. 2001, 2005), peat sediment records (Hong et al. 2001, 2003, 2005; Zhou et al. 2004, 2005), and lacustrine sediment records (Ji et al. 2005; Shen et al. 2005, 2013; Wang et al. 2012a, b; Yancheva et al. 2007). These records exhibit a strengthened East Asian summer monsoon (EASM) during the early and mid-Holocene intervals (~10500–4500 cal. yr BP) and a relatively weakened EASM during the late Holocene (since ~4500 cal. yr BP), which corresponds with orbital induced lowering of Northern Hemisphere summer solar insolation during this interval. However, there have still been some controversial issues about specific details of the Holocene monsoon climate changes (Long et al. 2010; Zhang et al. 2011). In addition, most of these investigations have been restricted to low and mid-latitude monsoon regions, there are no substantial high-quality and high-resolution palaeoclimatic records of Holocene climate changes from the mid- and high-latitude monsoon margin region (Chen et al. 2008; Herzschuh 2006; Wang et al. 2010; Zhang et al. 2011).

Compared with the larger glacial–interglacial changes or at the beginning of the Holocene, the Mid- to Late Holocene (since ~5000 cal. yr BP) was particular interest to the understanding of the EASM because the boundary conditions of the climate driving forces at this interval did not change dramatically (Wanner et al. 2008). It is well known that global climate changes during the Mid- to Late Holocene show large oscillations, such as the Current Warm Period (CWP) after 1850 AD, the Little Ice Age (LIA) between 1350 to 1850 AD, the Medieval Warm Period (MWP) between 700 to 1350 AD, the dark ages cold period (DACP), the Roman Warm Period (Ge et al. 2010; Lamb 1985; Mann and Jones 2003; Mann et al. 2009) and the Holocene Event 3 (An et al. 2005; Bond et al. 2001; Wang et al. 2005; Wu and Liu 2004). However, the timing and duration of such abrupt climatic events are different among various areas in the Northern Hemisphere. Furthermore, the knowledge regarding Mid- to Late Holocene climate changes and warm/cold oscillation events is still rather poorly understood in the continental EAM region. Thus, in order to understand temporal and spatial variability of EAM during Mid- to Late Holocene and its forcing mechanisms, more high-resolution regional palaeoclimatic records are needed.

The Northeastern (NE) China located in mid- to high latitudes of the Asian continent, are influenced by the tropical and the polar climate systems. The palaeoclimatic development of NE China has been of considerable interest because of the region's sensitivity to climate fluctuations driven by the EAM and associated shifts in precipitation (Shen 2012). Therefore, the NE China is likely to be a key region for studying the Holocene EAM variability. Recently, a variety of proxy records has been reported to document climate change in NE China (Chu et al. 2009; Hong et al. 2005, 2009; Li et al. 2011; Parplies et al. 2007; Stebich et al. 2009; Wang et al. 2012b; You and Liu 2012). These studies mainly focused on the last deglaciation period (Parplies et al. 2007; Stebich et al. 2009) and the past millennium (Chu et al. 2009; Sun et al. 2013; Wang et al. 2012b), but there are a limited number of Holocene palaeoclimatic records from the NE China (Hong et al. 2005, 2009; Li et al. 2011; You and Liu 2012) that can provide insight into climate change and potential forcing mechanisms. Furthermore, these Holocene palaeoclimatic records display different patterns could be attributed to dating uncertainties, low-resolution and/or climate proxy implications remains uncertain. In order to improve our understanding of the EAM variability and possible climate forcing mechanisms, thus, further well-dated, and high-resolution multi-proxy palaeoclimatic records are necessary.

Lacustrine sediments have widely been used in palaeoclimatic and palaeoenvironmental reconstructions, because it provides abundant information regarding lacustrine evolutional processes (geological, physical, chemical and biological processes) and regional environmental and climatic variations (Shen 2012). In this study, we present the results of high-resolution multi-proxy (sedimentological, magnetic, geochemical and isotopic proxies) of the well-dated lacustrine sediment core from the Jingpo Lake in Heilongjiang Province, NE China, which is utilized to reconstruct the EAM variation during the Mid- to Late Holocene. Furthermore, we combined with the pollen analyses data of same sediment core from Jingpo Lake (Chen et al. 2014) and compared to other palaeoclimate records from EAM region and other region, aim to better understanding the history of variations in the EAM intensity during the Mid- to Late Holocene and the possible climatic forcing mechanisms.

6.2 Study Region

The Jingpo Lake (43°46′ to 44°03′N, 128°27′ to 129°03′E, and ~350 m above sea level) is located in Jingpo Volcanic Field on Ning'an County, Southeastern Heilongjiang Province, NE China (Fig. 6.1). It is the China's largest lava-blocked lake and formed by lava damming of the Mudaniiang River. The Jingpo volcanoes are located in the upper Mudanjiang River, and are around 40 km northwest to Jingpo Lake, they have been active intermittently during the Holocene (Chen et al. 2005; Fan et al. 2003). The length of the Jingpo Lake from north to south is ~45 km and the widest distance between east and west is only ~6 km. The surface

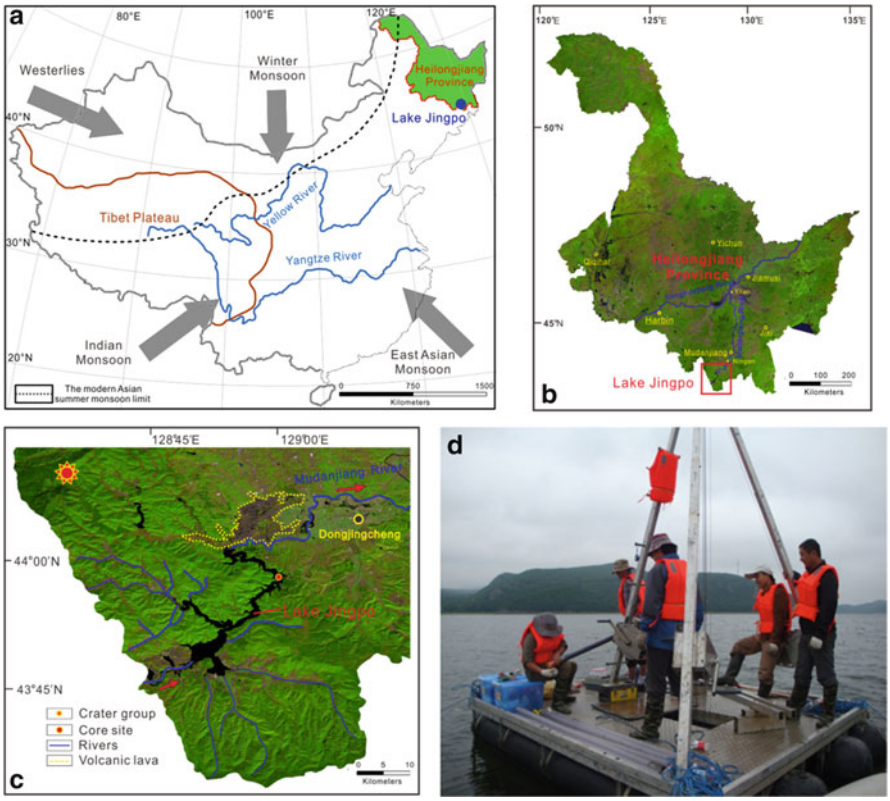

Fig. 6.1 (**a**) The atmospheric circulation systems in China, and the *black dash line* shows the modern Asian summer monsoon limit (Modified from Gao 1962). (**b**) Map showing the location of the Jingpo Lake (*red square*), Heilongjiang Province. (**c**) Topographic map of Jingpo Lake catchment and the coring site; the *red arrow* indicates the water flowing direction of the Mudanjiang River. (**d**) A photo of taking coring in Jingpo Lake

area of the lake is ~92 km^2 and its catchment area is ~11,820 km^2 (Wang and Dou 1998). Jingpo Lake is mainly fed by surface run-off and precipitation (maximum water depth: ~48.0 m; mean water depth: ~12.9 m). There are around 30 rivers flowing into the Jingpo Lake; most of these rivers drain into the south part of lake, and the lake water outflows from the northwest to the Mudanjiang River (Fig. 6.1c). Therefore, the south part of the lake is shallow and the deepest part in the northern part of the lake. The lake is surrounded by the hills and low mountains, with bedrock mainly composed by granite, perlite and basalt (Li et al. 2011).

The Jingpo Lake catchment is climatically controlled by the EAM system, causing distinct seasonal variation in regional heat-mositure (Fig. 6.2). In the summer, the warm and humid air masses are transported by southeasterly winds from the western tropical Pacific; whereas in the winter, the climate is affected by the very dry and cold northwesterly winter monsoon caused by Mongolia–Siberian

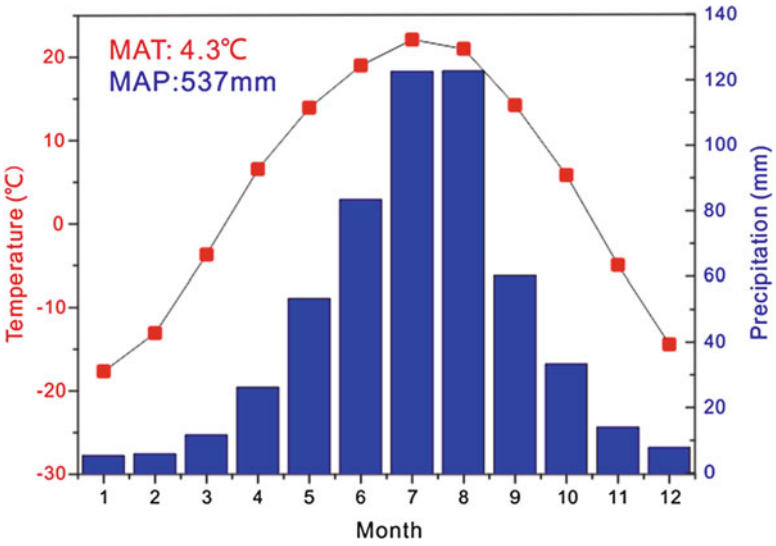

Fig. 6.2 Climate diagram from Ning'an county meteorological station near Jingpo Lake showing monthly temperature and precipitation. All data were from 62-year climate averages for the period 1951–2012 AD. *MAP* mean annual precipitation, *MAT* mean annual temperature

high pressure system (Gao 1962; Wang 2006). The 62-year (1951–2012 AD) meteorological records available from the Ning'an county meteorological station (~40 km north of the Jingpo Lake) indicate a mean annual temperature is 4.3 °C with a maximum monthly mean of 22.1 °C in July and a minimum of −17.7 °C in January (Fig. 6.2). The study area has a mean annual precipitation (including snowfall) is ~545 mm, about 81 % of the annual precipitation falling between May and September in association with the EASM, and with the peak precipitation of ~123 mm in August (Fig. 6.2). The Jingpo Lake is covered with ~70 cm of ice in winter season from December to March.

The modern natural vegetation of the study area belongs to the temperate mixed-forest flora of Changbai Mountain (Qian et al. 2003). The native vegetation is characterized by a *Pinus koraieusis* mixed conifer and broadleaved forest zone. The coniferous trees are dominated by *P. koraieusis*, and also include *Picea jezoensis*, *Picea koriensis* and *Abies mephrolepis*. The deciduous trees mainly consist of *Betula costata*, *Betula platyphylla*, *Fraxinus mandschurica*, *Quercus mongolica*, *Phellodendron amurense*, *Juglans mandshurica*, *Ulmus propinqua*, *Carpinus cordata*, *Tilia amurensis*, *Tilia mandshurica*, *Populus ussuriensis*, *Acer mono* and *Acer mandshurica* (Li et al. 2011; Qian et al. 2003). The shrub layer includes species such as *Corylopsis*, *Corylus*, *Philadelphus*, *Spiraea*, *Lonicera* and *Rhododendron*. Herbaceous species include *Artemisia*, *Chenopodiaceae*, *Gramineae* and *Cyperaceae* (Li et al. 2011; Zhou 1997).

6.3 Materials and Methods

6.3.1 Materials

In August 2012, three parallel sediment cores (JP-A, JP-B and JP-C, 43°59′N, 129°02′E) were collected from a water depth of 30.9 m in the northeastern part of Jingpo Lake (Fig. 6.1c, d), using Austria UWITEC^{TM} piston coring system with PVC tubes in 2.0 m length and 60 mm diameter. The sediment cores were placed in PVC tubes and transported to the Nanjing Institute of Geography and Limnology, Chinese Academy of Sciences. All sediment cores were stored at 4 °C until analyzed.

The overlap between the core segments are identified using magnetic susceptibility data scanned at 1-cm intervals with a Bartington Magnetic Susceptibility meter connected to a 12 cm diameter loop. Comparison of the three sediment cores shows good agreement of magnetic data, and the adjustment of sediment depth was undertaken using magnetic susceptibility profiles. In this study, the longest sediment core JP-C (1272 cm) was selected for further analyses. The core JP-C was split in half, photographed, and visual stratigraphy was recorded. The core JP-C mainly composed of black brown silty clay, dark brown clayey silt and gray brown sand, except for the core base part (1,232–1,272 cm) that mainly consists of coarse sands and gravels. Sediments were sampled at 2 cm interval, all subsamples were dried with a vacuum freeze dryer. This study will focus on the upper sediment (0–1,154 cm) of core JP-C to study the palaeoenvironmental and palaeoclimatic changes.

6.3.2 Methods

In this study, a total of 13 from the JP-C core were collected for accelerator mass spectrometry (AMS) ^{14}C dating at Beta Analytic Inc., Miami, USA. Nine from terrestrial plant fragments (leaves) and four from bulk organic matter samples. Samples for AMS ^{14}C dating were initially rinsed in deionized water, then dried at 40 °C and weighed before submission for dating. The resultant AMS ^{14}C dates were calibrated into calendar years (cal. yr BP) using Calib 6.0 (Stuiver and Reimer 1993) with IntCal 09 calibration dataset (Reimer et al. 2009).

Sub-samples for total organic carbon content (%TOC), total nitrogen content (%TN), carbon isotopes values of total organic matter ($\delta^{13}C_{org}$), grain size and magnetic susceptibility analyses were taken continuously from the sediments sequence at 4-cm intervals. A total of 288 sediment subsamples were collected for laboratory analyses. All these analyses were performed in the State Key Laboratory of Lake Science and Environment, Nanjing Institute of Geography and Limnology, Chinese Academy of Sciences.

Samples for %TOC and %TN were homogenized by grinding in an agate mortar and pretreated with 5 % HCl to remove possible trace amounts of carbonate, then rinsed repeatedly with deionized water and freeze dried prior to analyses. The dried sample was weighed and analyzed using a CE Model 440 Elemental Analyzer. Replicate analyses of well-mixed samples indicates a precision of $\pm$<0.1 % (1 SD). TOC and TN mass accumulation rates (TOC-MAR and TN-MAR) are better measures of delivery and preservation of organic matter than %TOC content (Lücke et al. 2003; Meyers and Lallier-Vergès 1999; Wang et al. 2013b), and expressed as mass of TOC and TN per unit of lake bottoms area per unit of time, typically mg cm $^{-2}$ years $^{-1}$. %TOC and %TN was calibrated to TOC-MAR and TN-MAR calculated by multiplying the TOC content (mg C/g dry sediment) by the dry bulk density (g/cm^3) and sedimentation rate (cm/year). Carbon/nitrogen (C/N) in our study refers to the atomic ratio of %TOC to %TN for each sample. Weight percentages can be multiplied by 1.167 (the ratio of atomic weights of nitrogen and carbon) to yield C/N atomic ratios.

The pretreated samples for %TOC and %TN analyses were also used for $\delta^{13}C_{org}$ determination. Isotope ratios were determined using a Thermo Finnigan Delta^{plus} Isotope Ratio Mass Spectrometer. All isotopic values are presented in standard δ-notation in per mil (‰) relative to the Vienna Pee Dee Belemnite (VPDB) (Craig 1957). The calibration and assessment of the reproducibility and accuracy of the isotopic analyses were based on replicate analyses of laboratory standard materials and international reference materials. Replicate analyses of well-mixed samples indicated a precision of $\pm$<0.1 ‰ (1 SD).

For grain size analyses, the sediment samples of 0.5 g were pretreated with 10–20 ml of 30 % H_2O_2 to remove organic matter and subsequently with 10 ml of 10 % HCl to remove carbonates. About 1,000 ml of deionized water were added, and then the sample solution was kept for 24 h to rinse acidic ions. Biogenic silica was removed with a 20 mL 1M NaOH digestion (8 h at 60°C) and then treated with 20 ml of 0.05 M Na-hexametaphosphate on an ultrasonic oscillator for 15 min to facilitate dispersion aggregates before grain size analyses. Grain size distributions between 0.02 and 2,000 μm were determined using a Malvern Mastersizer-2000 analyzer, and then yields the percentages of the related size fractions of a sample with a relative error of less than 1 %. The median grain size (Md) of a sample is the diameter at the 50th percentile of the distribution.

Mass specific low frequency magnetic susceptibility values (χ_{lf}) was measured on freeze dried and homogenized samples using a Bartington Ltd MS2 Magnetic Susceptibility System coupled to a Dual Frequency Sensor (Dearing 1994). χ_{lf} was measured four times, with air correction measurements made twice in order to normalize each sample against background, and then each pair of sample measurements was averaged, and the results readings are expressed as $\times 10^{-8}$ m^3 kg^{-1}.

6.4 Results

6.4.1 Lithology and Chronology

The lithological change of the core JP-C generally coincides with median grain size (Md) and color variation throughout the core JP-C (Fig. 6.3). The lacustrine sediment of the upper 1,154 cm can be divided into three lithological units: (1) 0–490 cm: black brown silty clay with Md values around 5 μm, (2) 490–850 cm: dark brown clayey silt with Md with values close to 8 μm, (3) 850–1,154 cm: black brown silty clay with Md values around 6 μm (Fig. 6.3).

Reliable and robust chronology for lacustrine sediment cores is of crucial importance for the palaeoclimate and palaeoenvironment reconstructions (He et al. 2013). A number of previous studies suggested that the ^{14}C dating of bulk organic matter samples often suffer from contamination from sources of hard-water effect (or carbon reservoir effect). For instance, in northwestern China (Huang et al. 2009; Liu et al. 2008; Wang et al. 2013a), in Northern China (Guo et al. 2007; Xiao et al. 2004; Zhai et al. 2011) and in Tibetan Plateau (Herzschuh et al. 2006; Hou et al. 2012; Shen et al. 2005; Wischnewski et al. 2011; Zhu et al. 2009). One way can solve this problem is to use terrestrial plant fragments (such as leaves, twigs and fruits) from lake sediments for AMS ^{14}C dating, because these will not be influenced by the hard-water effect (Walker 2005) and thus they can yield reliable radiocarbon dates.

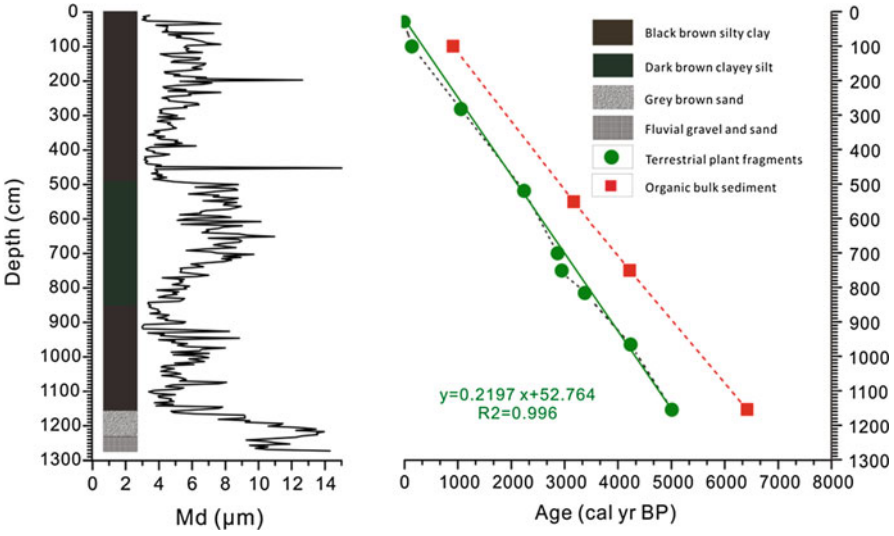

Fig. 6.3 Lithology, median grain sizes and age–depth model of the sediment core JP-C. *Green circles* and *red squares* represent the ages derived from terrestrial plant fragments and bulk organic matter, respectively. The *red squares* are dates that were not used in the age–depth model

AMS ^{14}C dating results for JP-C core are presented in Table 6.1 and Fig. 6.3. According to the results of four bulk organic matter samples indicated that the hard-water effect could be 740–1380 year (Table. 6.1; Fig. 6.3). Therefore, the chronological sequence for the core JP-C was established based on the two adjacent terrestrial plant fragments the mid-points of the 2-sigma calibrated age range using linear interpolation. The upper 1,154 cm lacustrine sediments sequence basal age is ~5100 cal. yr BP, and the age-depth model shows a linear relation ($R^2 = 0.996$; Fig. 6.3). Sedimentation rates were calculated based on linear interpolation between the terrestrial plant fragments radiocarbon dates. The sediment deposition rate of the upper 11.54 m varied from ~0.169 to 0.495 cm year $^{-1}$, which had a nearly constant sedimentation rate of ~0.228 cm year $^{-1}$. In present study, the 4-cm interval analyses results corresponds to ~18-year-resolution.

6.4.2 *Multi-proxy Records*

Grain size (GS), χ_{lf}, TOC-MAR, TN-MAR, C/N and $\delta^{13}C_{org}$ analyses results of the sediment core JP-C are compiled in Fig. 6.4. The JP-C record is divided into four obviously zones based on geochemical and physical values using CONISS cluster analyses (Grimm 1987). These proxies results fluctuation in the sediment core JP-C exhibited stratigraphic changes that generally corresponded to changes in the pollen assemblage zones (Fig. 6.5) (Chen et al. 2014) from the same sediment core, namely, the divided four zones of this study show a clear correlation with the pollen assemblage zones. The characteristics of these zones are described from bottom to top as follows.

Zone A (1,154–852 cm; ~5100–3600 cal. yr BP). The core JP-C is mainly composed of clay and silt, and sand content is generally <10 % (Fig. 6.4). In this zone, the fractions of clay, silt, and sand fluctuate between 21.0 % and 62.1 %, 37.1 % and 77.3 %, and 0.4 % and 18.8 %, averaging 43.8 %, 53.4 %, and 2.8 %, respectively (n = 76). The Md values range from 3.0 to 8.9 μm with a mean value of 5.1 μm (n = 76). The χ_{lf} values are relatively low, and they range from 17.7 to 35.2×10^{-8} m^3 kg^{-1}, with an average value of 23.7×10^{-8} m^3 kg^{-1} (n = 76). The zone A is characterized by the relatively high TOC-MAR and TN-MAR values, TOC-MAR ranged from 2.08 to 4.24 mg C cm $^{-2}$ years $^{-1}$ with an average value of 2.83 mg C cm $^{-2}$ years $^{-1}$ and TN ranged from 0.20 to 0.37 mg C cm $^{-2}$ years $^{-1}$ with an average value of 0.27 mg C cm $^{-2}$ years $^{-1}$ (n = 76) (Fig. 6.4). C/N ratios and $\delta^{13}C_{org}$ values are highest for the entire core (mean of 12.2 and −26.4 ‰, ranging from 11.3 to 14.3 and −27.4 ‰ to −25.9 ‰, respectively. n = 76) (Fig. 6.4). In this zone, pollen percentages of conifer trees and broadleaf trees and shrubs are highest (means of 14.3 % and 74.1 % respectively) (Fig. 6.5), and the highest pollen percentages of *Pinus*, *Quercus*, *Ulmus*, *Carpinus*, *Juglans* and *Corylopsis* for the entire core. On the contrary, the pollen percentages of herbs are lowest (means of 11.7 %) for the entire core, and dominated by *Artemisia* and *Chenopodiaceae* (Fig. 6.5).

Table 6.1 AMS ^{14}C dates for JP-C core together with sampling location and dating materials. All ages were calibrated using Calib 6.0 (Stuiver and Reimer 1993) with IntCal 09 dataset (Reimer et al. 2009)

Lab number	Sample name	Core depth (cm)	Dating material	Age (^{14}C year BP ± 1σ)	$^{13}C/^{12}C$ ‰	Calibrated age (cal year BP) 2σ ranges	Median age (cal year BP)
Beta-330281	JPP-1	28.5	Leaf fragment	Modern carbon	NA	Modern carbon	Modern
Beta-330291	JPP-11	100	Leaf fragment	110 ± 30	−29.8	10–270	140
Beta-330292[a]	JPPS-1	100	Bulk organic matter	1000 ± 30	−27.0	800–960	880
Beta-330282	JPP-2	282	Leaf fragment	1150 ± 30	−26.8	980–1170	1075
Beta-330283	JPP-3	519	Leaf fragment	2210 ± 30	−27.0	2140–2330	2235
Beta-330293[a]	JPPS-2	551	Bulk organic matter	2980 ± 30	−27.2	3070–3260	3165
Beta-330285	JPP-5	700	Leaf fragment	2790 ± 30	−25.4	2800–2960	2880
Beta-330286	JPP-6	750	Leaf fragment	2830 ± 30	−27.2	2860–3040	2950
Beta-330294[a]	JPPS-3	750	Bulk organic matter	3840 ± 30	−26.5	4150–4410	4280
Beta-330287	JPP-7	815	Leaf fragment	3160 ± 30	−27.6	3350–3440	3395
Beta-330289	JPP-9	965	Leaf fragment	3850 ± 30	−27.1	4150–4410	4280
Beta-330290	JPP-10	1154	Leaf fragment	4420 ± 30	−28.0	4870–5260	5065
Beta-330295[a]	JPPS-4	1154	Bulk organic matter	5670 ± 40	−26.3	6350–6540	6445

[a]The dates were not used for building up the age framework of JP-C core

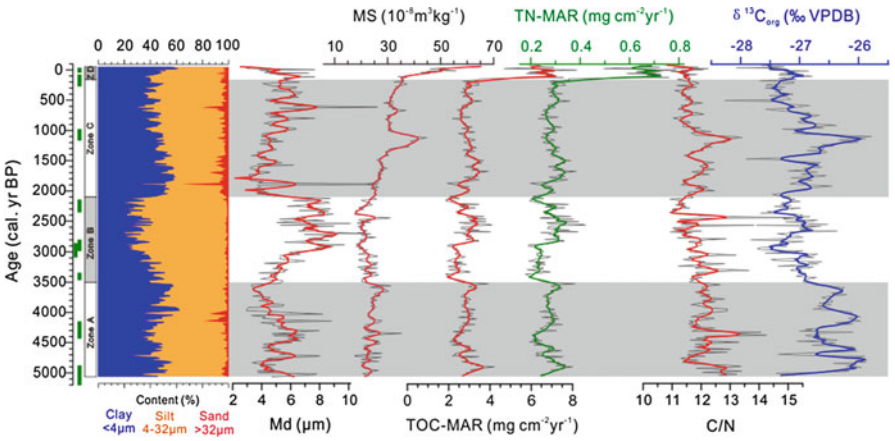

Fig. 6.4 Variations in TOC-MAR, TN-MAR, C/N, $\delta^{13}C$ of total organic matter, grain size proxies including the sand, clay, silt fractions and median grain size values, and magnetic susceptibility values of core JP-C in Jingpo Lake. The *thick lines* indicate 10-points smoothing results. *Green bars* indicate terrestrial plant fragments AMS ^{14}C dates of core JP-C with 2σ error

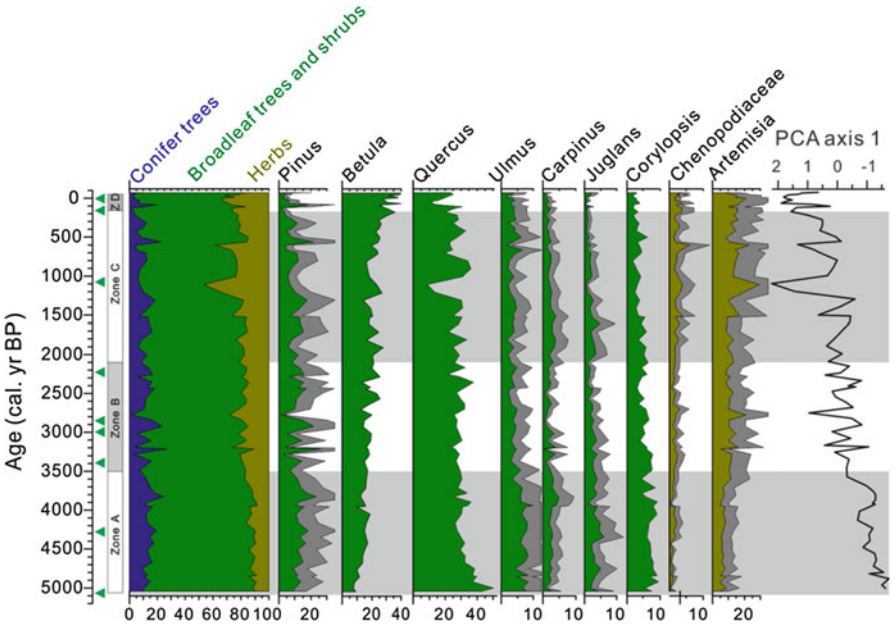

Fig. 6.5 Simplified pollen percentage diagram and PCA sample axis 1 scores of core JP-C from Jingpo Lake. Exaggeration (×2) is indicated by *grey* shading. *Green bars* indicate terrestrial plant fragments AMS ^{14}C dates of core JP-C with 2σ error

Zone B (852–492 cm; ~3600–2100 cal. yr BP). This zone is characterized by the lowest clay fraction content (mean of 32.2 %, ranging from 15.2 to 57.4 %, n = 90) and χ_{lf} values (mean of 21.8×10^{-8} m^3 kg^{-1}, ranging from 17.5 to 31.2×10^{-8} m^3 kg^{-1}, n = 90) (Fig. 6.4). The Md values range from 3.3 to 11 μm with a mean value of 6.8 μm (n = 90). TOC-MAR and TN-MAR values are lowest for the entire core (mean of 2.7 and 0.26 mg C cm^{-2} $years^{-1}$, ranging from 1.8 to 4.1 mg C cm^{-2} $years^{-1}$ and 0.18 to 0.42 mg C cm^{-2} $years^{-1}$, respectively. n = 90) (Fig. 6.4). C/N ratios (mean of 11.8, ranging from 10.9 to 15.3. n = 90) and $\delta^{13}C_{org}$ values (mean of −27.1 ‰, ranging from −27.8 ‰ to −26.4‰. n = 90) decrease slightly (Fig. 6.4). In addition, this zone is noticeable for obviously decrease in pollen percentages of conifer trees, broadleaf trees and shrubs (means of 12.6 % and 68.9 % respectively) (Fig. 6.5), and increase in pollen percentages of herbs (means of 18.5 %) caused mainly by the increase in *Artemisia* (Fig. 6.5).

Zone C (492–104 cm; ~2100–150 cal. yr BP). In the zone, the Md values (mean of 5.0 μm, ranging from 3.1 to 16.0 μm, n = 97) and silt fractions content (mean of 50.1 %, ranging from 37.6 to 62.0 %, n = 97) decrease obviously. Notably is the significantly increased of clay fraction content (mean of 45.0 %, ranging from 17.1 to 58.6 %, n = 97), sand fraction content (mean of 5.0 %, ranging from 0.7 to 36.1 %, n = 97) and χ_{lf} values (mean of 30.9×10^{-8} m^3 kg^{-1}, ranging from 22.0 to 44.9×10^{-8} m^3 kg^{-1}, n = 97). The TOC-MAR, TN-MAR, C/N ratios and $\delta^{13}C_{org}$ values increase slightly. TOC-MAR ranged from 1.94 to 3.92 mg C cm^{-2} $years^{-1}$ with an average value of 2.96 mg C cm^{-2} $years^{-1}$ and TN ranged from 0.20 to 0.38 mg C cm^{-2} $years^{-1}$ with an average value of 0.29 mg C cm^{-2} $years^{-1}$ (n = 97) (Fig. 6.4). C/N ratios are ranging from 11.0 to 13.4 with an average value of 11.8 and $\delta^{13}C_{org}$ values ranging from −28.3 ‰ to −25.8 ‰ with a mean of −27.0 ‰ (n = 97) (Fig. 6.4). The pollen percentages of *Pinus*, *Ulmus*, *Carpinus*, *Juglans* and *Corylopsis* at the beginning of Zone C relatively high, then gradually decreased. Pollen percentages of herbs (mean of 23.0 %) (Fig. 6.5) increased significantly, caused mainly by the increase in *Artemisia* and *Chenopodiaceae*. Notably, a sharp fluctuation in many proxies is recorded at 268–328 cm interval (~1250–1050 cal. yr BP or ~700–900 AD), in addition, the pollen percentages of conifer trees, broadleaf trees and shrubs and herbs has significantly fluctuation too (Fig. 6.5).

Zone D (104–0 cm; ~150 cal. yr BP–present). The most striking feature of this zone is sharp increase in TOC-MAR and TN-MAR values (mean of 6.6 and 0.67 mg C cm^{-2} $years^{-1}$, ranging from 4.7 to 8.2 mg C cm^{-2} $years^{-1}$ and 0.50 to 0.80 mg C cm^{-2} $years^{-1}$, respectively. n = 25), and the χ_{lf} values (mean of 46.5×10^{-8} m^3 kg^{-1}, ranging from 34.0 to 65.1×10^{-8} m^3 kg^{-1}, n = 25) are also increasing rapidly. The Md values drops to an average of 6.8 μm (range from 3.0 to 7.7 μm. n = 25) (Fig. 6.4). C/N ratios (mean of 11.4, ranging from 10.8 to 12.3. n = 25) and $\delta^{13}C_{org}$ values (mean of −27.3 ‰, ranging from −28.1 ‰ to −26.8 ‰. n = 25) decrease slightly (Fig. 6.4). The pollen percentages of *Pinus* and *Quercus* decrease slightly, and the pollen percentages of herbs increase slightly (means of 25.8 %) (Fig. 6.5).

6.4.3 Proxy Interpretations

6.4.3.1 TOC-MAR, TN-MAR, C\N and $\delta^{13}C_{org}$ of Organic Matter

The type and amount of lacustrine sedimentary organic matter (OM) can be used to reflect past fluctuations in lake productivity and terrestrial inputs linked to climate-induced environmental changes, catchment-related processes and lake-internal changes (Leng et al. 2006; Meyers 1997). Variations in TOC-MAR and TN-MAR values are represent changes in primary organic productivity or changes in OM (Olsen et al. 2013). Lacustrine OM has two major sources of organic matter in lake sediments are autochthonous (aquatic plants living in the lake water column) and allochthonous (soil and terrestrial plants in the catchment) (Meyers and Teranes 2001; Meyers 1994). Values of C/N ratio and $\delta^{13}C_{org}$ of lacustrine OM may help distinguish between different sources of OM and related biogeochemical changes (Leng et al. 2006; Meyers and Teranes 2001). Due to low carbohydrate and high protein contents, C/N ratios of algae and phytoplankton are only about 5–12, generally less than 10. Submerged and floating aquatic macrophytes or organic matter of a mixed source have C/N ratios between 10 and 20 (Hedges et al. 2002; Meyers 1994). In contrast, C/N ratios in terrestrial vascular plants exhibit higher than 20 due to their low protein content and abundance of cellulose (Meyers 1994; Talbot and Lærdal 2000). The C/N ratios within core JP-C mostly less than 13 (ranges from 10.8 to 15.3 with a mean value of 11.9) are slightly higher than aquatic source (<10), which may be as the result of nitrogen availability deficiency (Talbot and Lærdal 2000). Lake-internal processes such as nitrogen limitation can result in elevated the C/N ratios (between 8 and 15 for algae) and is a common nutrient limiting element in lakes (Hecky and Kilham 1988; Olsen et al. 2013; Talbot and Lærdal 2000). This inference is further supported by the low $\delta^{15}N_{org}$ around ~2–3 ‰ suggesting atmospheric nitrogen ($\delta^{15}N \sim 0$–1 ‰) as a dominant nitrogen source (Chen R, unpublished data). Hence it is possible that despite the slightly elevated C/N ratios that the OM is predominantly of aquatic origin and actually represents nutrient poor conditions. C/N ratios in lacustrine sediments could also change due to anaerobic decomposition of organic matter, where organic carbon is remineralized to carbon dioxide while the NH_4^+ is adsorbed onto clay minerals (Schubert and Calvert 2001; Tareq et al. 2011). According to significant positive relationship between TOC-MAR and TN-MAR contents ($r^2 = 0.98$, $p < 0.001$; Fig. 6.6) was observed for Jingpo Lake sediments, suggested that inorganic nitrogen content in Jingpo Lake sediment was negligible (~0.05 %). Thus, the C/N ratios could be representative of the bulk organic matter (Talbot and Lærdal 2000). In summary, C/N ratios are mostly less than 13 in the Jingpo Lake, it is possible that despite the slightly elevated C/N ratios that the OM of the core JP-C is mainly from aquatic plants (e.g., phytoplankton) and contain little or no carbon-rich cellulose or lignin terrestrial vegetation (Leng et al. 2006; Meyers and Lallier-vergés 1999; Meyers 1997). Therefore, the TOC-MAR values reflect the primary productivity of lake algae and aquatic plants (Hodell and Schelske 1998; Hollander et al. 1993;

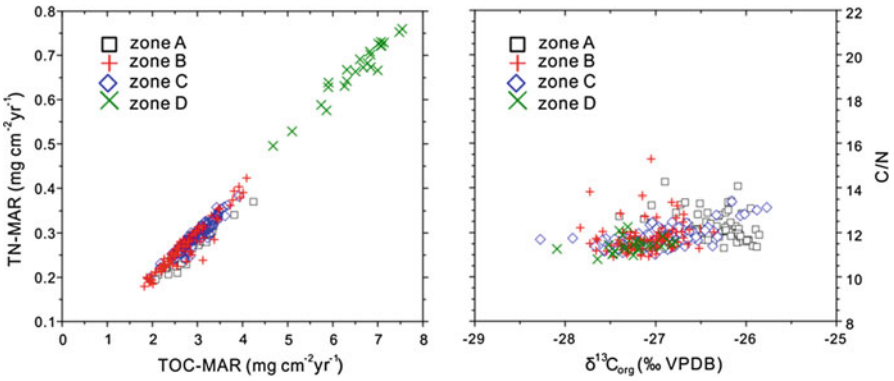

Fig. 6.6 Scatter plots of core JP-C TOC-MAR, TN-MAR, C/N and $\delta^{13}C_{org}$ data. TOC-MAR versus TN-MAR (*left*), C/N versus $\delta^{13}C_{org}$ (*right*)

Meyers and Teranes 2001). The higher values of TOC-MAR from autochthonous sources are considered as representative of higher primary production in the lake.

The $\delta^{13}C_{org}$ values of lacustrine sedimentary OM have frequently been used as environmental proxies because these changes are directly or indirectly linked to changes in the environment and climate of the lake catchments (Leng and Marshall 2004; Lücke et al. 2003). However, the $\delta^{13}C_{org}$ values of lake sediments is complex and influenced by many factors, such as the OM derived from allochthonous or autochthonous (Meyers 1994), the differential fractionation associated with the inorganic carbon source (CO_2, HCO_3^-) used for photosynthesis (Leng et al. 2006), variable productivity (Leng and Marshall 2004) and dissolved inorganic carbon (DIC) assimilation, as well as anthropogenic carbon released into the environment because of fossil fuel combustion (the Suess effect) (Wang et al. 2013b). C4 land plants use the Hatch-Slack pathway have $\delta^{13}C_{org}$ values that range from about $-9\,‰$ to $-17\,‰$ with an average value of $-13\,‰$ (Fry and Sherr 1984), whilst C3 land plants and lacustrine algae exhibit a range of $\delta^{13}C_{org}$ values between -22 and $-34\,‰$ with an average of $-27\,‰$ (O'Leary 1988). The C/N ratios of Jingpo Lake indicate that OM is primarily derived from algae and aquatic vegetation, the $\delta^{13}C_{org}$ record is likely an indicator of within-lake processes (i.e. aquatic plant types and / or abundances). Moreover, the $\delta^{13}C_{org}$ values are not correlated with C/N ratios (Fig. 6.6) suggesting that $\delta^{13}C_{org}$ is not controlled by changes in OM sources (i.e. from allochthonous to autochthonous sources). Primary production in lakes can influence the changes in OM $\delta^{13}C_{org}$ values. Algae and aquatic plants preferentially utilize ^{12}C to produce lacustrine OM (Hodell and Schelske 1998). However, increased primary productivity in lakes exhaustion of available light $\delta^{13}C$ within the lake carbon pool, resulting in dissolved atmospheric CO_2 becoming limited ($\delta^{13}C = -7\,‰$) and forcing algae and aquatic plants to utilize ^{13}C-enriched dissolved HCO_3^- ($\delta^{13}C = 1\,‰$) within the lake as their source of carbon (Meyers and Teranes 2001). In Jingpo Lake, the most of high/low $\delta^{13}C_{org}$ values coupled

with relatively high/low TOC-MAR from the core JP-C may be attributable to primary production in lakes predominantly controls the changes in $\delta^{13}C_{org}$ values (apart from ~1050 to 1250 cal. yr BP and from ~150 cal. yr BP to present, these two intervals may be seriously affected by human activities). Thus, $\delta^{13}C_{org}$ values variations of autochthonous sedimentary OM in Jingpo Lake can serve as a proxy of lacustrine palaeoproductivity, i.e., higher TOC-MAR and higher $\delta^{13}C_{org}$ values indicates higher temperature climate and stronger EASM, and vice versa.

6.4.3.2 Grain Size and Magnetic Susceptibility

The grain size composition variability in lacustrine sediment core can indicate the changes of the sedimentary environment (Lambiase 1980) related to hydrologic energy variations, such as transport capacity (Hakanson and Jansson 1983; Liu et al. 2008) and lake levels (An et al. 2012). The grain-size of core JP-C is dominated by clay and silt fraction with an average content of 40.6 and 56.2 %, respectively (Fig. 6.4). Grain-size analyses for the sediments in core JP-C displayed the frequency curve of grain size distribution are usually unimodal (Fig. 6.7), that due to single sedimentary or transportation process. As Jingpo Lake catchment is located in central part of NE China surrounded by Zhangguangcai mountain and Laoye mountain (belongs to Changbai Mountain System), and there is covered by flourishing vegetation and rarely aeolian activities in this area. In winter season the Jingpo Lake is frozen affected by Mongolia–Siberian high pressure system, ice surface lack of aeolian activities sediments indicates sediments in core JP-C are most likely transported by river discharge, not by aeolian activities. Thus, grain size results are used to describe changes of the sedimentary environment related to hydrologic energy variations. According to the principle of lake sediment sorting (Lerman 1978), the grain size of lacustrine sediments becomes finer and finer from the shore to the center, and sediment belts of different grain size fraction levels can be distinguished. Namely, in lacustrine environments grain size variations through time can indicate water level fluctuations. Hence, the Md distribution is believed to be an indicator for palaeoshoreline proximity. We assume that with a rising lake level the median particle diameter of the sediment in the centre of the lake (i.e., coring location) is getting smaller because of a greater distance of the shoreline (inflow) to the coring location itself. On the contrary, when the lake level is low, thus shortening of the distance between river mouth and coring site may be the main reason for the contribution of coarser grain-size fraction in the core site (An et al. 2012). In addition, in the past 5000 year, Jingpo Lake catchment area had high density of vegetation cover and did not change significantly (Fig. 6.5), stronger surface runoff (thus implying wetter climatic conditions) would favor high input of clastic materials to Jingpo Lake, however, weaker surface erosion due to high density of vegetation cover would result in less input of coarser materials thus lead to more fine grain size fraction in lacustrine sediments and vice versa. Therefore, in this study we interpret the grain size distribution of Jingpo Lake sediments probably reflects changes in the EAM precipitation, i.e., the finer grain size fraction and

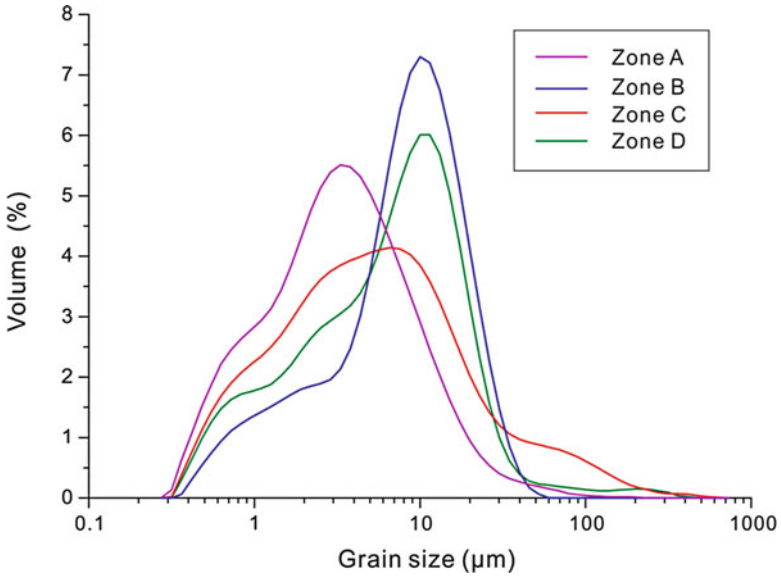

Fig. 6.7 Grain size distributions of different zones of sediment core JP-C. A, B, C and D represent the zone A, B, C and D respectively

lower Md might be explained by a higher laker levels reflect increased monsoonal precipitation rates over the lake region, and vice versa.

The magnetic susceptibility of sediments may indicate the relative proportion of magnetic minerals of the sediments. Since the development of environmental magnetism with the study of lake sediments in the 1970s (Thompson et al. 1980), it has been successfully adopted in reconstructing the climatic and environmental evolution of lacustrine sediments (Chen et al. 2013; Hodell et al. 1999). The bedrock surrounding the Jingpo Lake region consists mainly of granite, perlite and basalt, and the magnetic minerals in the Lake sediments derived from these volcanic rocks in the catchment exists in finer sediments. Therefore, variations of the χ_{lf} values are associated with catchment erosion, i.e., increase in χ_{lf} values indicated increasing erosive input synchronously with the stronger EASM climate conditions. Namely, during the rise in catchment soil erosion period have comparatively high χ_{lf} values are correlated to stronger EASM periods (apart from ~1050 to 1250 cal. yr BP and from ~150 cal. yr BP to present, these two intervals may be seriously affected by human activities) (Fig. 6.4).

6.4.3.3 Pollen Data

The pollen data presented here are complex and multivariate. Principal Components Analysis (PCA) was used to analyze the pollen assemblages in relationship to environmental factors by using inter-species correlations and no transformation of

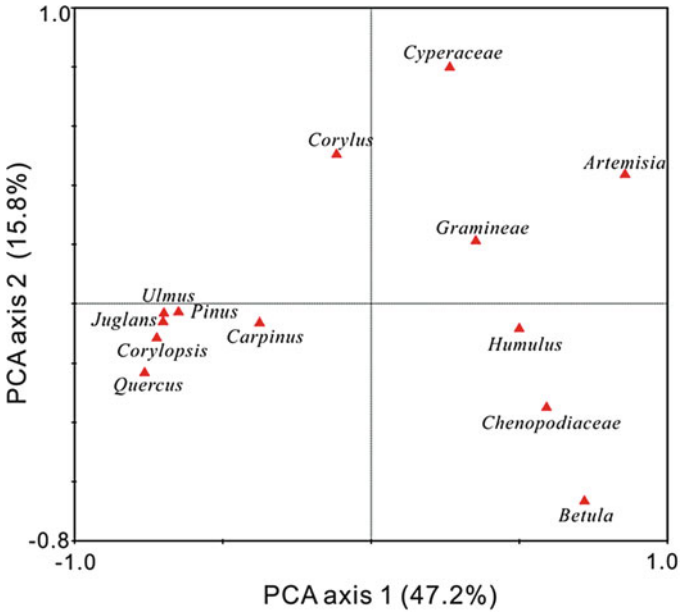

Fig. 6.8 Results of a principle components analysis of the Jingpo Lake pollen spectra (Chen et al. 2014)

pollen percentages. We used the percentages of 13 terrestrial pollen types with values greater than 1 % in at least two samples for numerical analyses using the CANOCO program version 4.5 (ter Braak and Smilauer 2002). The first and second principal components (PCA axis 1 and PCA axis 2) have eigenvalues of 0.472 and 0.158, explaining 47.2 and 15.8 % of total variance of pollen data respectively (Fig. 6.8). Broadleaved taxa (such as *Quercus*, *Ulmus*, *Juglans*, *Corylus* and *Carpinus*) and *Corylopsis* have negative loadings on PCA axis 1, whereas *Betula* and almost all herb taxa, such as *Artemisia*, *Chenopodiaceae*, *Gramineae*, *Cyperaceae* and *Humulus*, have positive side of PCA axis 1. The climate of the Jingpo Lake region is typically controlled by the temperate-humid oceanic monsoon climate. Meteorological data from northern China indicate that precipitation and temperature are key factors responsible for the spatial differentiation of modern vegetation (Gansert 2004; Xu et al. 2014). Because modern *Quercus*, *Carpinus*, *Corylus*, *Juglans* and *Ulmus* pollen frequencies are highly positively correlated with the mean annual temperature in NE China (Li et al. 2011). Several recent pollen record studies from Long Gang Volcanic Field maar and crater lakes (Lake Erlongwan, Lake Sihailongwan and Lake Xiaolongwan) in NE China indicate that broad-leaved trees (*Quercus*, *Ulmus*, *Juglanss* and *Carpinus*) and *Corylopsis* expanded corresponding to increase the intensity of the EASM (climate became warmer and wetter), however, increased the herbs (*Artemisia*, *Chenopodiaceae*, *Gramineae* and *Cyperaceae*) and *Betula* suggests that the climate became cooler and drier (Li et al. 2013; Stebich et al. 2009; Xu et al. 2014). Therefore, these implies

that the PCA axis 1 mainly represents intensity of the EASM with the sample scores on PCA axis 1 showing positive values related to cold and dry climate conditions and the negative values related to warm and wet climate conditions. In summary, the high abundance of *Quercus*, *Ulmus*, *Juglanss*, *Carpinus*, *Corylopsis* and low PCA axis 1 scores suggest warm and wet climatic conditions, whereas the high proportion of *Artemisia*, *Chenopodiaceae*, *Gramineae*, *Cyperaceae* and high PCA axis 1 indicate cool and dry conditions (Fig. 6.8) (Chen et al. 2014).

6.5 Discussion

6.5.1 Mid- to Late Holocene East Asian Monsoon Variations and Regional Comparisons

Based on high-resolution multi-proxy analyses of grain size, magnetic susceptibility, geochemistry and stable carbon isotope of sediments of core JP-C in Jingpo Lake, provides a detailed history of changes in the palaeoenvironment and palaeoclimate since ~5100 cal. yr BP. High $\delta^{13}C_{org}$ values coupled with relatively high TOC-MAR from ~5100 to 3600 cal. yr BP may be attributable to the exhaustion of available light $\delta^{13}C$ within the lake carbon pool, forcing aquatic plants to utilize ^{13}C-enriched dissolved carbon within the lake (Fig. 6.4). This may be attributed to the Jingpo Lake area experienced a relatively warm and humid period. The relatively high clay content and low Md value indicates that the lake level was high and the coring site was situated away from the lake shore. Moreover, the highest pollen percentages of *Ulmus*, *Juglans* and *Corylopsis* whereas the lowest pollen percentages of *Artemisia* and *Chenopodiaceae* from the core JP-C also indicating relatively strong EASM during this period (Fig. 6.5). This relatively strong EASM period has also been inferred from $\delta^{18}O$ record of Dongge Cave in eastern China (~5100–3500 year BP) (Dykoski et al. 2005) (Fig. 6.9c), the $\delta^{13}C$ record of Hani Peat in Northeastern China (~4700–3700 cal. yr BP) (Hong et al. 2005) (Fig. 6.9d), the redness record of Qinghai Lake close to the present East Asian summer monsoon limit in the northwest China (~5000–4000 cal. yr BP) (Ji et al. 2005) (Fig. 6.9e), the reconstruct Holocene sea surface temperatures in the western tropical Pacific Ocean (~5100–3600 cal. yr BP) (Stott et al. 2004) (Fig. 6.9f).

Around ~3600 cal. yr BP, rapidly decrease in the TOC-MAR, $\delta^{13}C_{org}$ values, clay content and χ_{lf} values suggest dry and cold climate conditions that may have been caused by a weakening of the EASM intensity until ~2100 cal. yr BP (Fig. 6.4). In addition, the rapidly increase in *Artemisia* and *Chenopodiaceae* pollen percentages and significantly reduced *Ulmus*, *Juglans* and *Corylopsis* pollen percentages from the core JP-C suggestive of the EASM circulation weakened (~3600–2100 cal. yr BP) (Fig. 6.5). Similar results have also been obtained from the stalagmite $\delta^{18}O$ record of Dongge Cave in eastern China (Dykoski et al. 2005), where climate changed to cool and dry during ~3500–2000 year BP (Fig. 6.9c).

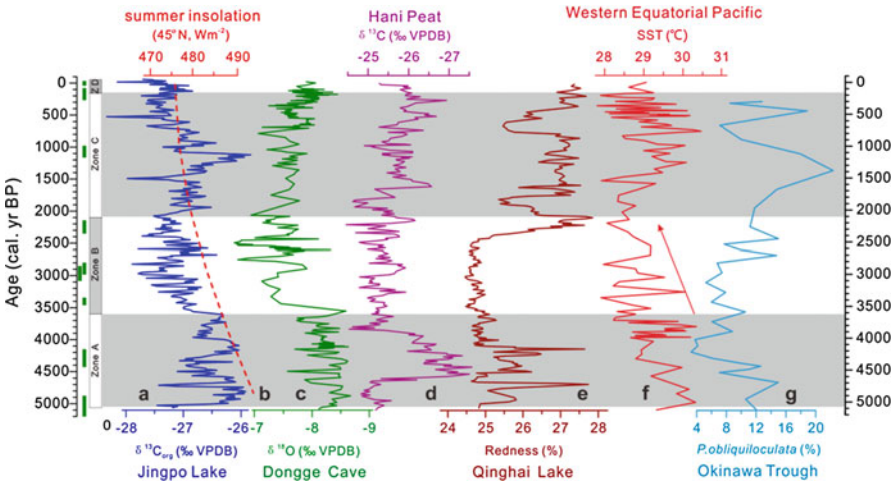

Fig. 6.9 Correlation of $\delta^{13}C_{org}$ values of total organic matter from Jingpo Lake (**a**) (*dark blue*, this study) with the NH summer solar insolation at 45°N (**b**) (*red dash line*, Laskar et al. 2004), a stalagmite$\delta^{18}O$ record from Dongge Cave (**c**) (*green*, Dykoski et al. 2005), cellulose $\delta^{13}C$ record from Hani peat (**d**) (*purple*, Hong et al. 2005), redness data from Qinghai Lake (**e**) (*brown*, Ji et al. 2005), sea-surface temperature reconstructed on the Mg/Ca ratio of *Globigerinoides rubber* from MD81 core in the western tropical Pacific (**f**) (*red*, Stott et al. 2004), and *Pulleniatina obliquiloculata* abundance represent the path and intensity of the warm Kuroshio Current in the northern Okinawa Trough (**g**) (*light blue*, Jian et al. 2000). *Green bars* indicate terrestrial plant fragments AMS ^{14}C dates of core JP-C with 2σ error

At Hani Peat in northeastern China, the gradually increase in $\delta^{13}C$ values of organic matter suggests an weakened EASM and wetter climate between ~3700 and 1700 cal. yr BP (Hong et al. 2005) (Fig. 6.9d). At Qinghai Lake close to the present EASM limit in the northwest China, decreased sediment redness indicates an decreased EASM rainfall (~4000–2200 cal. yr BP) (Ji et al. 2005) (Fig. 6.9e). In Taiwan, the desiccation of the subalpine Retreat Lake around ~4500–2100 cal. yr BP strongly indicates an decreased EASM rainfall (Selvaraj et al. 2011). Decreased the abundance of *P. obliquiloculata* in the northwestern Pacific Ocean also suggest a weakening of the EASM rainfall during ~4100–1900 cal. yr BP (Jian et al. 2000) (Fig. 6.9g). This cool and dry period has also been inferred from the reconstruct Holocene sea surface temperatures (SST) in the western tropical Pacific Ocean (~3700–1800 cal. yr BP) (Stott et al. 2004) (Fig. 6.9f).

During the period of ~2100–150 cal. yr BP, a gradual increase in $\delta^{13}C_{org}$ values, with large and frequent fluctuations, and an increase in the clay content and TOC-MAR values probably indicated the monsoonal circulation enhancement since ~2100 cal. yr BP (Fig. 6.4). In this period, the rapidly increase in *Carpinus*, *Juglans* and *Corylopsis* pollen percentages indicated warm and humid conditions caused by a strengthening of the EASM (Fig. 6.5). However, this period is characterized by the apparent increase in χ_{lf} values, sand content and a gradually increase in *Artemisia*,

Gramineae and *Chenopodiaceae* pollen percentages and a gradually decrease in *Pinus* pollen percentages values in this period (Figs. 6.4 and 6.5). These may be indicative of human activities most likely caused this change. In forest region, *Artemisia* and *Gramineae* pollen percentage increased to higher values generally indicates more open landscape and intensified human activities (Li et al. 2011; Sun et al. 1997), and the *Betula* is regarded as the pioneer species in the Changbai Mountains, because it colonizes the land rapidly after slash-and-burn activity (Jiang et al. 2008). Therefore, these pollen percentage changes may be indicative of human activity impact on the regional vegetation. Moreover, a sharply increase in χ_{lf} values in this period possible indicate increased human activity.

Numerous studies indicate that the Holocene climate change is characterized as generally cooling and drying in AM regions (Fleitmann et al. 2003, 2007; Wang et al. 2005), following the gradual decrease in northern hemisphere summer insolation during the last 11,500 years (Kutzbach and Street-Perrott 1985). Nevertheless, a recent review of some recent high-resolution, well-dated monsoon proxy records seems to suggest an abnormal increase in AM strength during the late Holocene, in contradiction with the generally weakening Holocene Asian summer monsoon trend (Zhao et al. 2013). In this study, we based on multi-proxy records of the core JP-C in Jingpo Lake suggest warm and humid conditions that may have been caused by a strengthening of the EASM intensity during ~2100–150 cal. yr BP. This strengthening of EASM during late Holocene has also been inferred from the stalagmite sediments $\delta^{18}O$ record of Dongge Cave in eastern China (~2000–150 year BP) (Dykoski et al. 2005) (Fig. 6.9c), the $\delta^{13}C$ record of Hani Peat in Northeastern China (since ~1700 cal. yr BP) (Hong et al. 2005) (Fig. 6.9d), the TOC record from the subalpine Retreat Lake in Taiwan (after ~1900 cal. yr BP) (Selvaraj et al. 2011), the increased sediment redness values in Qinghai Lake (since ~2200 cal. yr BP) (Ji et al. 2005) (Fig. 6.9e), the similar results have also been obtained from the reconstruct Holocene sea surface temperatures in the western tropical Pacific Ocean (after ~1800 cal. yr BP) (Stott et al. 2004) (Fig. 6.9f), and the abundance of *P. obliquiloculata* in the northwestern Pacific Ocean (since ~1900 cal. yr BP) (Jian et al. 2000) (Fig. 6.9g). Moreover, our $\delta^{13}C_{org}$ record provides several centennial-scale warm/cool phases in the Jingpo Lake may correspond to the late Holocene climate anomalies (Fig. 6.9a), including warm periods of ~700–1300 AD (Medieval Warm Period; MWP) and ~1850 AD–present (Current Warm Period; CWP), and cool periods of ~400–700 AD (Dark Age Cold Period; DACP) and ~1350–1850 AD (Little Ice Age; LIA) (Figs. 6.9 and 6.10).

It is worth noting that the sharply increase in χ_{lf}, C/N and $\delta^{13}C_{org}$ values, the notable decrease in *Pinus*, *Quercus*, *Ulmus* and *Juglans* pollen percentages and the rapidly increase in *Betula*, *Artemisia* and *Chenopodiaceae* pollen percentages during the period of (~1250–1050 cal. yr BP or ~700–900 AD) (Figs. 6.4 and 6.5), these changes may be indicative of open landscape and intensified human activities in this period. A number of historical files and archaeological documents show the human activities in the Jingpo Lake area during this period. The Yinggeling Phase I culture (Neolithic) occupied almost the entire area of the Changbai Mountains around ~4000 cal. yr BP (Jia 2005; Zhao 2011). After a short period

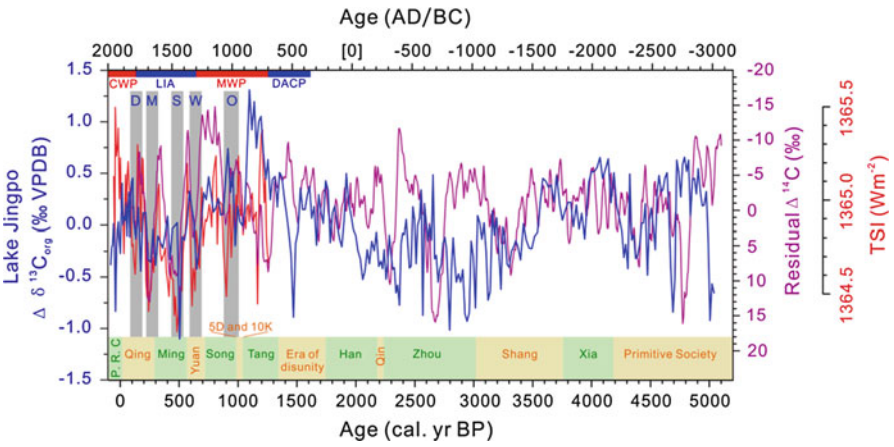

Fig. 6.10 Comparison of the detrended $\delta^{13}C_{org}$ record (*blue line*) with the residual $\Delta\ ^{14}C$ record (*purple line*) (Reimer et al. 2004) and Total Solar Irradiance reconstructions based on the smoothed ^{10}Be record from the South Pole for the last 1200 year (*red line*) (Bard et al. 2000). DACP, and MWP, LIA and CWP represent the Dark Age cold period, the Medieval Warm Period, Little Ice Age and Current Warm Period respectively. O, W, S, M, and D refer to Oort, Wolf, Spörer, Maunder and Dalton sunspot minima respectively

of cultural unification the Yinggeling Phase I culture was replaced by Yinggeling Phase II culture around 3500 cal. yr BP (Jia 2005; Zhao 2011), and it mainly distributed in the south of Changbai Mountains along the Mudanjiang River and Tumenjiang River areas (Jia 2005). These Neolithic archaeological sites in Jingpo Lake area excavated a number of stone tools (include hunting tools, gathering tools, woodcutting tools, and simple agricultural tools) reveal that the native people relied on collecting, hunting, and primitive agriculture (Jia 2005). Therefore, in the Neolithic Age, human activity that alters the original natural environment pattern is very limited. But during the early Tang Dynasty, the Sumo Mohe (or Sokmal Malgal) established an independent kingdom in 698 AD called Bohai, or Balhae Kingdom (1252–1024 cal. yr BP or 698–926 AD) in the northeast of ancient China. The historical existence of Bohai Kingdom roughly coincided with the Tang Dynasty. The Kingdom of Bohai existed for over 200 years and during most of that time it dominated the river basins of the Mudanjiang River, Songhuajiang River, and portions of the Heilongjiang (Amur) Rivers (Garcia 2012). The Kingdom of Bohai had five capital cities, and the supreme capital was named "Shangjing" was located in the northern margin of Jingpo Lake at Dongjingcheng Town, Mudanjiang City, Heilongjiang Province (Sun 2009). The Tang dynasty has been described as the summit of classical Chinese Civilization, a golden age of agriculture, literature and art. Bohai Kingdom actively imported aspects of the political and agriculture system of Tang Dynasty, many agricultural tools, irrigation facilities and crops such as foxtail millet, broomcorn millet, rice and soybean were found at Bohai Kingdom archaeological sites from this period (Lu 2009). These indicate that

human activities, especially the agricultural activities intensified. In Bohai Kingdom period, intensified human activities through the destruction of the native vegetation to expand cropland, and causes soil erosion. Thus, during the period of ~1250–1050 cal. yr BP (~700–900 AD), the rapidly increase in χ_{lf} values indicate the enhanced the soil erosion over the lake region. The highest C/N ratios in this period indicating greater contribution of terrestrial OM, that could be a result of intensified human activities destruction of native vegetation. Results from the $\delta^{13}C_{org}$ values of dominant plant species in communities on Changbai Mountains indicated that the dominance of C_3 plants in this region, the mean $\delta^{13}C$ values of shrubs and trees within <720 m a.s.l. are −27.36 ‰ and −25.94 ‰, respectively (Tan et al. 2009). Therefore, the most positive shifts in $\delta^{13}C_{org}$ values (between −25.77 and −26.36 ‰) occurred at ~1250–1050 cal. yr BP (~700–900 AD), which correspond to the period of greater contribution of terrestrial OM in Jingpo Lake sediment. Furthermore, our study also shows a rapidly decrease in *Pinus* and *Quercus* and a significant increase in *Betula*, *Artemisia* and *Chenopodiaceae* occurred at ~1250–1050 cal. yr BP (700–900 AD). This selective vegetation change based on pollen data indicates that intensified human activities could be a result of forested areas were cleared for agriculture and cities were developed (Li et al. 2011). *Pinus* and *Quercus* decrease in the Changbai Mountainous area maybe because its preferred use as major construction timber. *Betula* is regarded as the pioneer species in the Changbai Mountains, because it colonizes the land rapidly after slash-and-burn activity (Jiang et al. 2008). We infer that the successive rises of the Liao (907–1125 AD), Jin (1115–1234 AD) and Yuan (1206–1368 AD) Dynasties of nomadic people in NE China would be responsible for expansions of both *Artermisia* and *Chenopodiaceae* plants.

Since ~150 cal. yr BP, a rapidly increase in clay content indicate that lake level rose (Fig. 6.4). While the highest values of TOC-MAR/TN-MAR and χ_{lf}, and unprecedented low C/N ratios imply a significant enhancement of aquatic productivity. We hypothesize that this could be affected by intensified human activities as deforestation, agriculture, industry and soil erosion can lead to abruptly increase in magnetic susceptibility values and sharply increase in nutrients in lake sediments.

It should be noted that other studies have found evidence that climate change may have played a role in the collapse of historical cultures (Yancheva et al. 2007; Zhang et al. 2008). Our data also suggest that the dynastic transitions and the chaotically divided of some Chinese dynasties tended to occur when the EASM was weakening and precipitation was decreased (Fig. 6.10). Chinese dynastic transitions often resulted from peasant uprisings during phases of crop failure and famine, consistent with a weakening of the EASM intensity. For instance, the collapse of the Shang Dynasty and the Zhou Dynasty may well coincide with the EASM circulation weakened, the chaotically divided period of the Five Dynasties and Ten Kingdoms coincide with the climate was cold and dry. However, the Tang and Song Dynasty has been described as the summit of classical Chinese Civilization, a golden age of political, economy, agriculture, literature and art, in agreement with

humid and warm climate. Although we cannot directly relate these major Chinese societal events with our palaeoclimatic record, which will need further research on the relationship between climate and human cultural changes.

6.5.2 *Possible Forcing Mechanism for Mid- to Late Holocene East Asian Monsoon Variability*

The area of the Jingpo Lake is located in the region of the EAM, the moisture/rainfall brought by the monsoon circulation results from seasonal changes in land–sea atmospheric pressure distribution (Gao 1962; Wang 2006) which is triggered by variations in solar insolation and solar irradiance over decadal- to millennial time scales. In this study, multi-proxy results indicated a general weakening of the EASM intensity in Jingpo Lake region, following the gradual decrease in NH summer solar insolation at 45 °N over the last ~5,100 years (Fig. 6.9b). This synchronicity suggests that solar insolation may have influenced the climate of the study region on the orbital scale. However, our study result demonstrates an abnormal increase in EASM strength since ~2100 cal. yr BP. This phenomenon cannot be explained by long-term NH summer insolation change, because Holocene NH summer insolation show a continuously and gradually decreased trend without any reversal (Laskar et al. 2004). Moreover, the decadal to centennial variability of the EASM cannot be explained by changes in solar insolation. Previous palaeoclimate studies suggested a possible link between solar activity changes and EASM intensity (Liu et al. 2009; Selvaraj et al. 2007; Wang et al. 2005). Numerical simulations suggest that monsoon intensity could be sensitive to relatively small solar activity changes (Shindell et al. 2001). To test this link, we compared the detrended $\delta^{13}C_{org}$ values ($\delta^{13}C_{org\text{-}detrended}$) record from the Jingpo Lake with the residual atmospheric ^{14}C ($\Delta^{14}C$) and ^{10}Be records (Bard et al. 2000; Reimer et al. 2004), which can be used to represent solar activity (Fig. 6.10). We found that the variations in Asian monsoon intensity indicated by $\delta^{13}C_{org\text{-}detrended}$ are generally correspond to residual $\Delta^{14}C$ and Total Solar Irradiance (TSI) reconstructions based on the smoothed ^{10}Be record fluctuations on multi-decadal and centennial-scales. Generally, enhanced EASM (higher $\delta^{13}C_{org\text{-}detrended}$) generally corresponds to higher solar irradiance (smaller $\Delta^{14}C$), whereas weakened EASM (lower $\delta^{13}C_{org\text{-}detrended}$) correspond to lower solar irradiance (larger $\Delta^{14}C$). Moreover, within chronological uncertainty, the weakened EASM intensity could be identified for the Oort, Wolf, Spörer, Maunder and Dalton solar minima. These correlations suggest a possible link between solar activity and EASM variability on the NE China during the Mid- to Late Holocene.

To further confirm this correlation, we using the program REDFIT (Schulz and Mudelsee 2002), a spectral analysis of the $\delta^{13}C_{org\text{-}detrended}$ record in Jingpo Lake revealed six statistically significant cycles centered on 201, 81, 65, 56, 43 and 36 years (above the 90 % confidence level) (Fig. 6.11). The 201 year cycle and 65 years cycle are very similar to the well-known de Vries (Suess) solar activity

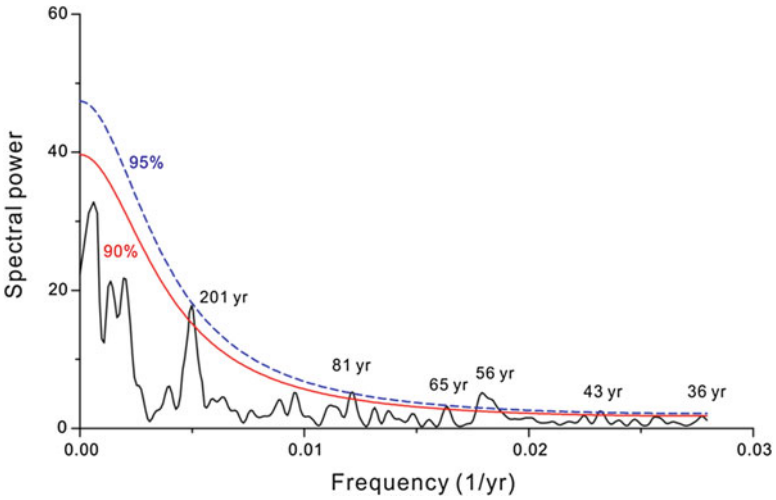

Fig. 6.11 Results of spectral analysis for the detrended $\delta^{13}C_{org}$ record from Jingpo Lake over the past 5100 year. Peaks are labeled with their period in years above 90 % (*solid line*) confidence level. *Dashed line* shows 95 % confidence levels

cycle of ~200 year (Usoskin and Mursula 2003) and Gleissberg solar activity cycle of ~70 year (Beer et al. 2000), respectively. This 200 year de Vries oscillation has been reported in monsoon controlled region, for example, $\delta^{18}O$ values from Dongge Cave (Dykoski et al. 2005; Wang et al. 2005) and Qunf Cave (Fleitmann et al. 2003), detrended TOC content in Kusai Lake (Liu et al. 2009) and the iron oxide content signal in Qinghai Lake (Ji et al. 2005). The records from monsoon controlled region such as $\delta^{18}O$ values from Dongge Cave (Dykoski et al. 2005) and Qunf Cave (Fleitmann et al. 2003) also show a significant ~70 year periodicity. Similar periodicities of 81, 56, 43 and 36 years were found in the residual $\Delta^{14}C$ record (Reimer et al. 2004) and other Asian monsoon region records (Dykoski et al. 2005; Fleitmann et al. 2003; Wang et al. 2005). These similar cycles demonstrate that solar irradiance may have played a role in the variation of EASM intensity.

Recent studies have demonstrated that Asian monsoon climate is sensitive to small changes in solar irradiance during the Holocene (He et al. 2013; Liu et al. 2009; Selvaraj et al. 2007), their results suggested that small variations in solar irradiance can lead to significant changes in the monsoon climate. Solar irradiance variations were considered to be responsible for decadal to centennial monsoon climate changes by affect the thermal contrast between the tropical Pacific Ocean and the Asian continent. Therefore, we suggest that the ocean–atmosphere interacting processes, particularly changes in the Western Pacific Warm Pool (WPWP) SST, in the tropical Pacific may play a significant role in driving the monsoon circulation variability. Namely, the SST of WPWP and the Kuroshio Current originating from the North Equatorial Current in the western Pacific can be considered as significant driving forces.

Prior to ~3600 cal. yr BP, the EASM intensity in the study region were strong. During the period between ~3600 and 2100 cal. yr BP, the drier and colder climate conditions in the Jingpo Lake region shows that the EASM weakened (Figs. 6.4 and 6.5). This remarkably weak EASM period has also been found from a number of palaeoclimate records from the East Asian monsoon region (Dykoski et al. 2005; Hong et al. 2005; Ji et al. 2005; Selvaraj et al. 2007; Wen et al. 2010) (Fig. 6.9). Since ~2100 cal. yr BP, we multi-proxy results indicated warm and humid conditions caused by a strengthening of the EASM (Figs. 6.4 and 6.5). Similar results have also been obtained from the East Asian monsoon region (Dykoski et al. 2005; Hong et al. 2005; Ji et al. 2005; Selvaraj et al. 2007, 2011) (Fig. 6.9). It is noticeable that the researchers combine oxygen isotope and Mg/Ca ratios of planktonic *Globigerinoides ruber* retrieved from sediment cores in the western tropical Pacific to reconstruct the Holocene SST of WPWP (Stott et al. 2004) (Fig. 6.9e). The SST of WPWP in the western tropical Pacific were mostly above 29 °C before ~3700 cal. yr BP, a notable decrease between ~3700 and 2000 cal. yr BP shows less than 29 °C, a remarkable increase since ~2000 cal. yr BP (Fig. 6.9e). This coincidence suggests that SST of WPWP in the western tropical Pacific may have influenced the EASM of the study region. The change in SST of WPWP in the western tropical Pacific is fundamentally linked to El Niño–Southern Oscillation (ENSO) variability. Strikingly, during the period between ~3600 and 2100 cal. yr BP, the decreased EASM as revealed by the Jingpo Lake record and other palaeoclimate records from the East Asian monsoon region (Fig. 6.9) correspond to a sharp decrease in reconstructed SST in the western tropical Pacific, which is an indication of intense El Niño phase. Previous studies demonstrated that the modern El Niño phase is associated with weakened EASM intensity (Selvaraj et al. 2007, 2011). Decreased SST in the western tropical Pacific could reduce the formation of water vapor over the source area of the EASM, thereby decreasing the moisture available for transport via the monsoon circulation from the western tropical Pacific onto the Asian inland and leading to a weakened summer monsoon. This seems to agrees well with the decrease in the moisture and heat transport from the western tropical Pacific to the northern North Pacific as inferred from a substantial decrease in abundance of warm-water planktonic foraminifera *Pulleniatina obliquiloculata*, an indicator species of the path and intensity of the warm Kuroshio Current, in the sediment cores of northern Okinawa Trough between ~4100 and 2100 cal. yr BP (Jian et al. 2000) (Fig. 6.9g). These data suggest that changes in the EASM precipitation on millennial to centennial scales could be related to ocean–atmosphere interactions in the tropical Pacific within age uncertainties. A weakened, eastward shifted Kuroshio Current and decreased SST of WPWP in the western tropical Pacific could remove warm tropical waters eastward, cause the convection in the North Pacific Ocean to occur further east and reduce the formation of water vapor over the source area of the EASM, thus decreasing the moisture available for transport via the monsoon circulation from the low-latitude western tropical Pacific onto the Asian inland and resulting in a weakened summer monsoon. In summary, this study indicates that changes in the East Asian monsoonal intensity on decadal to centennial scales at mid- to high latitudes in NE China during the Mid- to Late Holocene

might have been related to orbitally induced insolation changes, change in solar output, and changes in oceanic–atmospheric circulation. However, more well-dated, multi-proxy, and high-resolution palaeoclimatic records, as well as palaeoclimatic modeling are needed to confirm this possible solar-ocean–atmosphere interaction.

6.6 Conclusion

Palaeoclimatic reconstruction based on multi-proxy data (sedimentological, magnetic, geochemical, and stable carbon isotopic) from a well-dated lacustrine sediment core of Jingpo Lake in the northeastern China has provided a high-resolution record of EAM variability during the past ∼5100 cal. yr BP. The climate was relatively warm and humid during the period from ∼5100 to 3600 cal. yr BP. Since ∼3600 cal. yr BP, multi-proxy data suggest dry and cold conditions that may have been caused by a weakening of the EAM intensity until ∼2100 cal. yr BP. During the period of ∼2100 to 150 cal. yr BP, all proxies indicated warm and humid conditions caused by a strengthening of the EAM intensity. After ∼150 cal. yr BP, the Jingpo Lake affected by intensified human activities. The variability of EAM in northeastern China have a good correlation with other high-resolution East Asian Monsoon proxy records in China such as stalagmite, lake sediment and peat sediment, and reflecting similar multi-decadal to millennial monsoonal variation. This study demonstrates that solar irradiance may have played a role in the variation of EASM intensity on multi-decadal to centennial scale, i.e., intensified in the EASM intensity is generally correlated with increases in solar irradiance, whereas a weakened EASM corresponded to reductions in solar irradiance. Additionally, a spectral analysis of the $\delta^{13}C_{org\text{-}detrended}$ record reveals significant periodicities centered on 201 years, 81 years, 65 yearss, 56 years 43 years and 36 years. These periodicities were found in solar activity record and other EAM region palaeoclimatic records. Furthermore, the variation of EASM intensity coincidence with reconstructed SST in the western tropical Pacific and the path and intensity of Kuroshio Current. Therefore, this study indicates that both changes in solar output and changes in oceanic–atmospheric circulation have played a significant role in variability of the EAM at mid- to high latitudes in northeastern China during the Mid- to Late Holocene. Lastly, it should be noted that this study have found evidence that abrupt climate changes coincides with the collapse or the beginning and the chaotically divided of some Chinese dynasties, which will need further research on the relationship between climate and human cultural changes.

Acknowledgements We wish to thank Qingfeng Jiang and Hao Long for their help during field coring, and also thank Hao Long and Luo Wang for their helpful discussions and suggestions during the preparation of the manuscript. This study is supported by the National Basic Research Program of China (2012CB956100) and the CAS/SAFEA international partnership program for creative research teams (No. KZZD-EW-TZ-08).

References

An C-B, Tang L, Barton L, Chen F-H (2005) Climate change and cultural response around 4000 cal yr B.P. in the western part of Chinese Loess Plateau. Quat Res 63(3):347–352, http://dx.doi.org/10.1016/j.yqres.2005.02.004

An C-B, Lu Y, Zhao J, Tao S, Dong W, Li H, Jin M, Wang Z (2012) A high-resolution record of Holocene environmental and climatic changes from Lake Balikun (Xinjiang, China): implications for central Asia. The Holocene 22(1):43–52. doi:10.1177/0959683611405244

Bard E, Raisbeck G, Yiou F, Jouzel J (2000) Solar irradiance during the last 1200 years based on cosmogenic nuclides. Tellus B 52(3):985–992. doi:10.1034/j.1600-0889.2000.d01-7.x

Beer J, Mende W, Stellmacher R (2000) The role of the sun in climate forcing. Quat Sci Rev 19(1–5):403–415, http://dx.doi.org/10.1016/S0277-3791(99)00072-4

Bond G, Kromer B, Beer J, Muscheler R, Evans MN, Showers W, Hoffmann S, Lotti-Bond R, Hajdas I, Bonani G (2001) Persistent solar influence on North Atlantic climate during the holocene. Science 294(5549):2130–2136. doi:10.1126/science.1065680

Chen H, Fan Q, Gao F, Sun Q (2005) Summary of the studies on the Holocene volcanoes in Jingpohu. Recent Dev World Seismol 8:16–18 (in Chinese with English abstract)

Chen F, Yu Z, Yang M, Ito E, Wang S, Madsen DB, Huang X, Zhao Y, Sato T, John B, Birks H, Boomer I, Chen J, An C, Wünnemann B (2008) Holocene moisture evolution in arid central Asia and its out-of-phase relationship with Asian monsoon history. Quat Sci Rev 27(3–4):351–364, http://dx.doi.org/10.1016/j.quascirev.2007.10.017

Chen F, Liu J, Xu Q, Li Y, Chen J, Wei H, Liu Q, Wang Z, Cao X, Zhang S (2013) Environmental magnetic studies of sediment cores from Gonghai Lake: implications for monsoon evolution in North China during the late glacial and Holocene. J Paleolimnol 49(3):447–464. doi:10.1007/s10933-012-9677-3

Chen R, Shen J, Li C, Zhang E, Sun W, Ji M (2014) Mid- to late-Holocene East Asian summer monsoon variability recorded in lacustrine sediments from Jingpo Lake. Northeastern China The Holocene. doi:10.1177/0959683614561888

Chu G, Sun Q, Wang X, Li D, Rioual P, Qiang L, Han J, Liu J (2009) A 1600 year multiproxy record of paleoclimatic change from varved sediments in Lake Xiaolongwan, northeastern China. J Geophys Res Atmos 114(D22), D22108. doi:10.1029/2009JD012077

Cosford J, Qing H, Eglington B, Mattey D, Yuan D, Zhang M, Cheng H (2008) East Asian monsoon variability since the Mid-Holocene recorded in a high-resolution, absolute-dated aragonite speleothem from eastern China. Earth Planet Sci Lett 275(3–4):296–307. doi:10.1016/j.epsl.2008.08.018

Craig H (1957) Isotopic standards for carbon and oxygen and correction factors for mass-spectrometric analysis of carbon dioxide. Geochim Cosmochim Acta 12(1–2):133–149

Dearing J (1994) Environmental magnetic susceptibility, Using the Bartington MS2 system. Chi Publ., Kenilworth

Dykoski C, Edwards R, Cheng H, Yuan D, Cai Y, Zhang M, Lin Y, Qing J, An Z, Revenaugh J (2005) A high-resolution, absolute-dated Holocene and deglacial Asian monsoon record from Dongge Cave, China. Earth Planet Sci Lett 233(1–2):71–86. doi:10.1016/j.epsl.2005.01.036

Fan Q, Sun Q, Li N, Yin J, Chen H, Gao F, Zhang X (2003) The section of airfall clastic rock of Holocene volcano in Jinbo Lake and its eruptive history. Seismol Geol 25:3–11 (in Chinese with English abstract)

Fleitmann D, Burns SJ, Mudelsee M, Neff U, Kramers J, Mangini A, Matter A (2003) Holocene forcing of the Indian Monsoon recorded in a stalagmite from Southern Oman. Science 300(5626):1737–1739. doi:10.1126/science.1083130

Fleitmann D, Burns SJ, Mangini A, Mudelsee M, Kramers J, Villa I, Neff U, Al-Subbary AA, Buettner A, Hippler D, Matter A (2007) Holocene ITCZ and Indian monsoon dynamics recorded in stalagmites from Oman and Yemen (Socotra). Quat Sci Rev 26(1–2):170–188, http://dx.doi.org/10.1016/j.quascirev.2006.04.012

Fry B, Sherr EB (1984) delta super (13) C measurements as indicators of carbon flow in marine and freshwater ecosystems. Contrib Mar Sci 27:13–47

Gansert D (2004) Treelines of the Japanese Alps – altitudinal distribution and species composition under contrasting winter climates. Flora – Morphology, Distribution, Functional Ecology of Plants 199(2):143–156, http://dx.doi.org/10.1078/0367-2530-00143

Gao Y (1962) On some problems of Asian monsoon. In: Gao YX (ed) Some questions about the East Asian Monsoon. Science Press, Beijing

Garcia CD (2012) Horsemen from the edge of empire: the rise of the Jurchen Coalition (322 pp). Available at: https://dlib.lib.washington.edu/researchworks/bitstream/handle/1773/20679/Garcia_washington_0250E_10365.pdf?sequence=1&isAllowed=y

Ge QS, Zheng JY, Hao ZX, Shao XM, Wang W-C, Luterbacher J (2010) Temperature variation through 2000 years in China: an uncertainty analysis of reconstruction and regional difference. Geophys Res Lett 37(3), L03703. doi:10.1029/2009GL041281

Grimm EC (1987) CONISS: a FORTRAN 77 program for stratigraphically constrained cluster analysis by the method of incremental sum of squares. Comput Geosci 13(1):13–35, http://dx.doi.org/10.1016/0098-3004(87)90022-7

Guo L, Feng Z, Li X, Liu L, Wang L (2007) Holocene climatic and environmental changes recorded in Baahar Nuur Lake core in the Ordos Plateau, Inner Mongolia of China. Chin Sci Bull 52(7):959–966. doi:10.1007/s11434-007-0132-1

Hakanson L, Jansson M (1983) Principles of lake sedimentology. Springer, Berlin, 316

He Y, Zhao C, Wang Z, Wang H, Song M, Liu W, Liu Z (2013) Late Holocene coupled moisture and temperature changes on the northern Tibetan Plateau. Quat Sci Rev 80:47–57. doi:10.1016/j.quascirev.2013.08.017

Hecky R, Kilham P (1988) Nutrient limitation of phytoplankton in freshwater and marine environments: a review of recent evidence on the effects of enrichment. Limnol Oceanogr 33(4):796–822

Hedges JI, Baldock JA, Gélinas Y, Lee C, Peterson ML, Wakeham SG (2002) The biochemical and elemental compositions of marine plankton: a NMR perspective. Mar Chem 78(1):47–63, http://dx.doi.org/10.1016/S0304-4203(02)00009-9

Herzschuh U (2006) Palaeo-moisture evolution in monsoonal Central Asia during the last 50,000 years. Quat Sci Rev 25(1–2):163–178, http://dx.doi.org/10.1016/j.quascirev.2005.02.006

Herzschuh U, Winter K, Wünnemann B, Li S (2006) A general cooling trend on the central Tibetan Plateau throughout the Holocene recorded by the Lake Zigetang pollen spectra. Quat Int 154–155:113–121, http://dx.doi.org/10.1016/j.quaint.2006.02.005

Hodell DA, Schelske CL (1998) Production, sedimentation, and isotopic composition of organic matter in Lake Ontario. Limnol Oceanogr 43(2):200–214

Hodell DA, Brenner M, Kanfoush SL, Curtis JH, Stoner JS, Xueliang S, Yuan W, Whitmore TJ (1999) Paleoclimate of Southwestern China for the past 50,000 yr inferred from lake sediment records. Quat Res 52(3):369–380, http://dx.doi.org/10.1006/qres.1999.2072

Hollander DJ, McKenzie JA, Hsü KJ (1993) Carbon isotope evidence for unusual plankton blooms and fluctuations of surface water CO_2 in "Strangelove Ocean" after terminal Cretaceous event. Palaeogeogr Palaeoclimatol Palaeoecol 104(1):229–237

Hong YT, Wang ZG, Jiang HB, Lin QH, Hong B, Zhu YX, Wang Y, Xu LS, Leng XT, Li HD (2001) A 6000-year record of changes in drought and precipitation in northeastern China based on a δ13C time series from peat cellulose. Earth Planetary Sci Lett 185(1–2):111–119, http://dx.doi.org/10.1016/S0012-821X(00)00367-8

Hong YT, Hong B, Lin QH, Zhu YX, Shibata Y, Hirota M, Uchida M, Leng XT, Jiang HB, Xu H, Wang H, Yi L (2003) Correlation between Indian Ocean summer monsoon and North Atlantic climate during the Holocene. Earth Planetary Sci Lett 211(3–4):371–380, http://dx.doi.org/10.1016/S0012-821X(03)00207-3

Hong YT, Hong B, Lin QH, Shibata Y, Hirota M, Zhu YX, Leng XT, Wang Y, Wang H, Yi L (2005) Inverse phase oscillations between the East Asian and Indian Ocean summer monsoons during the last 12 000 years and paleo-El Niño. Earth Planetary Sci Lett 231(3–4):337–346, http://dx.doi.org/10.1016/j.epsl.2004.12.025

Hong YT, Hong B, Lin QH, Shibata Y, Zhu YX, Leng XT, Wang Y (2009) Synchronous climate anomalies in the western North Pacific and North Atlantic regions during the last 14,000 years. Quat Sci Rev 28(9–10):840–849, http://dx.doi.org/10.1016/j.quascirev.2008.11.011

Hou J, D'Andrea WJ, Liu Z (2012) The influence of 14C reservoir age on interpretation of paleolimnological records from the Tibetan Plateau. Quat Sci Rev 48:67–79, http://dx.doi.org/10.1016/j.quascirev.2012.06.008

Huang CC, Pang J, Zhou Q, Se C (2004) Holocene pedogenic change and the emergence and decline of rain-fed cereal agriculture on the Chinese Loess Plateau. Quat Sci Rev 23(23–24):2525–2535, http://dx.doi.org/10.1016/j.quascirev.2004.06.003

Huang XZ, Chen FH, Fan YX, Yang ML (2009) Dry late-glacial and early Holocene climate in arid central Asia indicated by lithological and palynological evidence from Bosten Lake, China. Quat Int 194(1–2):19–27, http://dx.doi.org/10.1016/j.quaint.2007.10.002

Ji J, Shen J, Balsam W, Chen J, Liu L, Liu X (2005) Asian monsoon oscillations in the northeastern Qinghai–Tibet Plateau since the late glacial as interpreted from visible reflectance of Qinghai Lake sediments. Earth Planet Sci Lett 233(1–2):61–70. doi:10.1016/j.epsl.2005.02.025

Jia PWM (2005) Transition from foraging to farming in Northeast China. Department of Archaeology, Faculty of Arts, University of Sydney

Jian Z, Wang P, Saito Y, Wang J, Pflaumann U, Oba T, Cheng X (2000) Holocene variability of the Kuroshio Current in the Okinawa Trough, northwestern Pacific Ocean. Earth Planetary Sci Lett 184(1):305–319, http://dx.doi.org/10.1016/S0012-821X(00)00321-6

Jiang W, Leroy SAG, Ogle N, Chu G, Wang L, Liu J (2008) Natural and anthropogenic forest fires recorded in the Holocene pollen record from a Jinchuan peat bog, northeastern China. Palaeogeogr Palaeoclimatol Palaeoecol 261(1–2):47–57, http://dx.doi.org/10.1016/j.palaeo.2008.01.007

Kutzbach JE, Street-Perrott FA (1985) Milankovitch forcing of fluctuations in the level of tropical lakes from 18 to 0 kyr BP. Nature 317(6033):130–134

Lamb HH (1985) Climatic history and the future. Princeton, NJ: Princeton University Press.

Lambiase JJ (1980) Hydraulic control of grain-size distributions in a macrotidal estuary. Sedimentology 27(4):433–446. doi:10.1111/j.1365-3091.1980.tb01192.x

Laskar J, Robutel P, Joutel F, Gastineau M, Correia A, Levrard B (2004) A long-term numerical solution for the insolation quantities of the Earth. Astronomy Astrophys 428(1):261–285

Leng MJ, Marshall JD (2004) Palaeoclimate interpretation of stable isotope data from lake sediment archives. Quat Sci Rev 23(7–8):811–831, http://dx.doi.org/10.1016/j.quascirev.2003.06.012

Leng M, Lamb A, Heaton TE, Marshall J, Wolfe B, Jones M, Holmes J, Arrowsmith C (2006) Isotopes in lake sediments. In: Leng M (ed) Isotopes in palaeoenvironmental research, vol 10, Developments in paleoenvironmental research. Springer, Dordrecht, pp 147–184. doi:10.1007/1-4020-2504-1_04

Lerman A (1978) Lakes: chemistry, geology, physics. Springer, New York

Li C, Wu Y, Hou X (2011) Holocene vegetation and climate in Northeast China revealed from Jingbo Lake sediment. Quat Int 229(1–2):67–73, http://dx.doi.org/10.1016/j.quaint.2009.12.015

Li J, Mackay AW, Zhang Y, Li J (2013) A 1000-year record of vegetation change and wildfire from maar lake Erlongwan in northeast China. Quat Int 290–291:313–321, http://dx.doi.org/10.1016/j.quaint.2012.08.2104

Liu X, Herzschuh U, Shen J, Jiang Q, Xiao X (2008) Holocene environmental and climatic changes inferred from Wulungu Lake in northern Xinjiang, China. Quat Res 70(3):412–425, http://dx.doi.org/10.1016/j.yqres.2008.06.005

Liu X, Dong H, Yang X, Herzschuh U, Zhang E, Stuut J-BW, Wang Y (2009) Late Holocene forcing of the Asian winter and summer monsoon as evidenced by proxy records from the northern Qinghai–Tibetan Plateau. Earth Planetary Sci Lett 280(1–4):276–284, http://dx.doi.org/10.1016/j.epsl.2009.01.041

Long H, Lai Z, Wang N, Li Y (2010) Holocene climate variations from Zhuyeze terminal lake records in East Asian monsoon margin in arid northern China. Quat Res 74(1):46–56, http://dx.doi.org/10.1016/j.yqres.2010.03.009

Long H, Lai Z, Fuchs M, Zhang J, Li Y (2012) Timing of Late Quaternary palaeolake evolution in Tengger Desert of northern China and its possible forcing mechanisms. Global Planetary Change 92–93:119–129, http://dx.doi.org/10.1016/j.gloplacha.2012.05.014

Lu W (2009) Research on the development of agriculture, forestation, herding and fishing in Bohai Kingdom. J Anhui Agric Sci 37(2):865–867 (in Chinese with English abstract)

Lücke A, Schleser GH, Zolitschka B, Negendank JFW (2003) A Lateglacial and Holocene organic carbon isotope record of lacustrine palaeoproductivity and climatic change derived from varved lake sediments of Lake Holzmaar, Germany. Quat Sci Rev 22(5–7):569–580. doi:10.1016/s0277-3791(02)00187-7

Maher BA, MengYu H, Roberts HM, Wintle AG (2003) Holocene loess accumulation and soil development at the western edge of the Chinese Loess Plateau: implications for magnetic proxies of palaeorainfall. Quat Sci Rev 22(5–7):445–451, http://dx.doi.org/10.1016/S0277-3791(02)00188-9

Mann ME, Jones PD (2003) Global surface temperatures over the past two millennia. Geophys Res Lett 30(15):1820. doi:10.1029/2003GL017814

Mann ME, Zhang Z, Rutherford S, Bradley RS, Hughes MK, Shindell D, Ammann C, Faluvegi G, Ni F (2009) Global signatures and dynamical origins of the little ice age and medieval climate anomaly. Science 326(5957):1256–1260. doi:10.1126/science.1177303

Meyers PA (1994) Preservation of elemental and isotopic source identification of sedimentary organic matter. Chem Geol 114(3–4):289–302, http://dx.doi.org/10.1016/0009-2541(94)90059-0

Meyers PA (1997) Organic geochemical proxies of paleoceanographic, paleolimnologic, and paleoclimatic processes. Org Geochem 27(5–6):213–250, http://dx.doi.org/10.1016/S0146-6380(97)00049-1

Meyers P, Lallier-vergés E (1999) Lacustrine sedimentary organic matter records of late quaternary paleoclimates. J Paleolimnol 21(3):345–372. doi:10.1023/A:1008073732192

Meyers PA, Lallier-Vergès E (1999) Lacustrine sedimentary organic matter records of Late Quaternary paleoclimates. J Paleolimnol 21:345–372

Meyers P, Teranes J (2001) Sediment organic matter. In: Last W, Smol J (eds) Tracking environmental change using lake sediments, vol 2, Developments in paleoenvironmental research. Springer, Dordrecht, pp 239–269. doi:10.1007/0-306-47670-3_9

O'Leary MH (1988) Carbon isotopes in photosynthesis. Bioscience 38(5):328–336

Olsen J, Anderson NJ, Leng MJ (2013) Limnological controls on stable isotope records of late-Holocene palaeoenvironment change in SW Greenland: a paired lake study. Quat Sci Rev 66:85–95, http://dx.doi.org/10.1016/j.quascirev.2012.10.043

Parplies J, Lücke A, Vos H, Mingram J, Stebich M, Radtke U, Han J, Schleser GH (2007) Late glacial environment and climate development in northeastern China derived from geochemical and isotopic investigations of the varved sediment record from Lake Sihailongwan (Jilin Province). J Paleolimnol 40(1):471–487. doi:10.1007/s10933-007-9176-0

Porter SC, An Z (1995) Correlation between climate events in the North Atlantic and China during the last glaciation. Nature 375(6529):305–308

Qian H, Yuan X-Y, Chou Y-L (2003) Forest vegetation of Northeast China. In: Kolbek J, Šrůtek M, Box E (eds) Forest vegetation of Northeast Asia, vol 28, Geobotany. Springer, Dordrecht, pp 181–230. doi:10.1007/978-94-017-0143-3_6

Reimer PJ, Baillie MGL, Bard E, Bayliss A, Beck JW, Bertrand CJH, Blackwell PG, Buck CE, Burr GS, Cutler KB, Damon PE, Edwards RL, Fairbanks RG, Friedrich M, Guilderson TP, Hogg AG, Hughen KA, Kromer B, McCormac G, Manning S, Ramsey CB, Reimer RW, Remmele S, Southon JR, Stuiver M, Talamo S, Taylor FW, van der Plicht J, Weyhenmeyer CE (2004) IntCal04 terrestrial radiocarbon age calibration, 0-26 cal kyr BP. Radiocarbon 46:1029–1058.

Reimer PJ, Baillie MGL, Bard E, Bayliss A, Beck JW, Blackwell PG, Ramsey CB, Buck CE, Burr GS, Edwards RL, Friedrich M, Grootes PM, Guilderson TP, Hajdas I, Heaton TJ, Hogg AG, Hughen KA, Kaiser KF, Kromer B, McCormac FG, Manning SW, Reimer RW, Richards DA, Southon JR, Talamo S, Turney CSM, Plicht J, Weyhenmeyer CE (2009) IntCal09 and Marine09 radiocarbon age calibration curves, 0-50,000 years cal BP. Radiocarbon 51:1111–1150

Schubert CJ, Calvert SE (2001) Nitrogen and carbon isotopic composition of marine and terrestrial organic matter in Arctic Ocean sediments: implications for nutrient utilization and organic matter composition. Deep Sea Res Part I: Oceanogr Res Papers 48(3):789–810, http://dx.doi.org/10.1016/S0967-0637(00)00069-8

Schulz M, Mudelsee M (2002) REDFIT: estimating red-noise spectra directly from unevenly spaced paleoclimatic time series. Comput Geosci 28(3):421–426, http://dx.doi.org/10.1016/S0098-3004(01)00044-9

Selvaraj K, Chen CTA, Lou J-Y (2007) Holocene East Asian monsoon variability: links to solar and tropical Pacific forcing. Geophys Res Lett 34(1), L01703. doi:10.1029/2006GL028155

Selvaraj K, Arthur Chen C-T, Lou J-Y, Kotlia BS (2011) Holocene weak summer East Asian monsoon intervals in Taiwan and plausible mechanisms. Quat Int 229(1–2):57–66, http://dx.doi.org/10.1016/j.quaint.2010.01.015

Shao X, Xu Y, Yin ZY, Liang E, Zhu H, Wang S (2010) Climatic implications of a 3585-year tree-ring width chronology from the northeastern Qinghai-Tibetan Plateau. Quat Sci Rev 29(17–18):2111–2122, http://dx.doi.org/10.1016/j.quascirev.2010.05.005

Shen J (2012) Spatiotemporal variations of Chinese lakes and their driving mechanisms since the Last Glacial Maximum: a review and synthesis of lacustrine sediment archives. Chin Sci Bull 58(1):17–31. doi:10.1007/s11434-012-5510-7

Shen J, Xingqi L, Sumin W, Matsumoto R (2005) Palaeoclimatic changes in the Qinghai Lake area during the last 18,000 years. Quat Int 136(1):131–140, http://dx.doi.org/10.1016/j.quaint.2004.11.014

Shen J, Wu X, Zhang Z, Gong W, He T, Xu X, Dong H (2013) Ti content in Huguangyan maar lake sediment as a proxy for monsoon-induced vegetation density in the Holocene. Geophys Res Lett 40(21):5757–5763. doi:10.1002/grl.50740

Shindell DT, Schmidt GA, Mann ME, Rind D, Waple A (2001) Solar forcing of regional climate change during the Maunder Minimum. Science 294(5549):2149–2152. doi:10.1126/science.1064363

Stebich M, Mingram J, Han J, Liu J (2009) Late Pleistocene spread of (cool-)temperate forests in Northeast China and climate changes synchronous with the North Atlantic region. Global Planetary Change 65(1–2):56–70, http://dx.doi.org/10.1016/j.gloplacha.2008.10.010

Stott L, Cannariato K, Thunell R, Haug GH, Koutavas A, Lund S (2004) Decline of surface temperature and salinity in the western tropical Pacific Ocean in the Holocene epoch. Nature 431(7004):56–59, http://www.nature.com/nature/journal/v431/n7004/suppinfo/nature02903_S1.html

Stuiver M, Reimer PJ (1993) Extended 14C data base and revised CALIB 3.0 14C age calibration program. Radiocarbon 35:215–230

Sun Q (2009) On the territory, natural environment and economic distribution of the Bohai State in Tang Dynasty. J Changchun Normal Univ (Human Soc Sci) 1:014

Sun X, Song C, Wang F, Sun M (1997) Vegetation history of the Loess Plateau of China during the last 100,000 years based on pollen data. Quat Int 37:25–36, http://dx.doi.org/10.1016/1040-6182(96)00008-0

Sun Q, Xie M, Shi L, Zhang Z, Lin Y, Shang W, Wang K, Li W, Liu J, Chu G (2013) Alkanes, compound-specific carbon isotope measures and climate variation during the last millennium from varved sediments of Lake Xiaolongwan, northeast China. J Paleolimnol 50(3):331–344. doi:10.1007/s10933-013-9728-4

Talbot M, Lærdal T (2000) The Late Pleistocene – Holocene palaeolimnology of Lake Victoria, East Africa, based upon elemental and isotopic analyses of sedimentary organic matter. J Paleolimnol 23(2):141–164. doi:10.1023/A:1008029400463

Tan W, Wang G, Han J, Liu M, Zhou L, Luo T, Cao Z, Cheng S (2009) δ 13C and water-use efficiency indicated by δ 13C of different plant functional groups on Changbai Mountains, Northeast China. Chin Sci Bull 54(10):1759–1764. doi:10.1007/s11434-009-0046-1

Tareq SM, Kitagawa H, Ohta K (2011) Lignin biomarker and isotopic records of paleovegetation and climate changes from Lake Erhai, southwest China, since 18.5 ka BP. Quat Int 229(1–2):47–56, http://dx.doi.org/10.1016/j.quaint.2010.04.014

ter Braak CJF, Smilauer P (2002) CANOCO reference manual and CanoDraw for Windows user's guide: software for canonical community ordination (version 4.5). Biometris, Wageningen [etc.]

Thompson R, Stober JC, Turner GM, Oldfield F, Bloemendal J, Dearing JA, Rummery TA (1980) Environmental applications of magnetic measurements. Science 207(4430):481–486. doi:10.1126/science.207.4430.481

Thompson LG, Mosley-Thompson E, Davis ME, Bolzan JF, Dai J, Klein L, Yao T, Wu X, Xie Z, Gundestrup N (1989) Holocene–late pleistocene climatic ice core records from qinghai-tibetan plateau. Science (New York, NY) 246(4929):474–477

Thompson LG, Yao T, Davis ME, Henderson KA, Mosley-Thompson E, Lin P-N, Beer J, Synal H-A, Cole-Dai J, Bolzan JF (1997) Tropical climate instability: the last glacial cycle from a Qinghai-Tibetan ice core. Science 276(5320):1821–1825. doi:10.1126/science.276.5320.1821

Thompson LG, Yao T, Mosley-Thompson E, Davis ME, Henderson KA, Lin P-N (2000) A high-resolution millennial record of the South Asian Monsoon from Himalayan ice cores. Science 289(5486):1916–1919. doi:10.1126/science.289.5486.1916

Usoskin IG, Mursula K (2003) Long-term solar cycle evolution: review of recent developments. Solar Phys 218(1–2):319–343. doi:10.1023/B:SOLA.0000013049.27106.07

Walker M (2005) Quaternary dating methods. Wiley, Hoboken

Wang B (2006) The Asian Monsoon. Springer, Berlin

Wang S, Dou H (1998) Lakes in China. Science Press, Beijing, pp 506–509 (in Chinese)

Wang YJ, Cheng H, Edwards RL, An ZS, Wu JY, Shen C-C, Dorale JA (2001) A high-resolution absolute-dated late Pleistocene Monsoon record from Hulu Cave, China. Science 294(5550):2345–2348. doi:10.1126/science.1064618

Wang Y, Cheng H, Edwards RL, He Y, Kong X, An Z, Wu J, Kelly MJ, Dykoski CA, Li X (2005) The Holocene Asian Monsoon: links to solar changes and North Atlantic climate. Science 308(5723):854–857. doi:10.1126/science.1106296

Wang Y, Liu X, Herzschuh U (2010) Asynchronous evolution of the Indian and East Asian Summer Monsoon indicated by Holocene moisture patterns in monsoonal central Asia. Earth-Sci Rev 103(3–4):135–153, http://dx.doi.org/10.1016/j.earscirev.2010.09.004

Wang L, Li J, Lu H, Gu Z, Rioual P, Hao Q, Mackay AW, Jiang W, Cai B, Xu B, Han J, Chu G (2012a) The East Asian winter monsoon over the last 15,000 years: its links to high-latitudes and tropical climate systems and complex correlation to the summer monsoon. Quat Sci Rev 32:131–142, http://dx.doi.org/10.1016/j.quascirev.2011.11.003

Wang L, Rioual P, Panizzo VN, Lu H, Gu Z, Chu G, Yang D, Han J, Liu J, Mackay AW (2012b) A 1000-yr record of environmental change in NE China indicated by diatom assemblages from maar lake Erlongwan. Quat Res 78(1):24–34, http://dx.doi.org/10.1016/j.yqres.2012.03.006

Wang G, Li J, Liu X, Li X (2013a) Variations in carbon isotope ratios of plants across a temperature gradient along the 400 mm isoline of mean annual precipitation in north China and their relevance to paleovegetation reconstruction. Quat Sci Rev 63:83–90, http://dx.doi.org/10.1016/j.quascirev.2012.12.004

Wang L, Mackay AW, Leng MJ, Rioual P, Panizzo VN, Lu H, Gu Z, Chu G, Han J, Kendrick CP (2013b) Influence of the ratio of planktonic to benthic diatoms on lacustrine organic matter δ13C from Erlongwan maar lake, northeast China. Org Geochem 54:62–68. doi:10.1016/j.orggeochem.2012.09.010

Wanner H, Beer J, Bütikofer J, Crowley TJ, Cubasch U, Flückiger J, Goosse H, Grosjean M, Joos F, Kaplan JO, Küttel M, Müller SA, Prentice IC, Solomina O, Stocker TF, Tarasov P, Wagner M, Widmann M (2008) Mid- to Late Holocene climate change: an overview. Quat Sci Re 27(19–20):1791–1828, http://dx.doi.org/10.1016/j.quascirev.2008.06.013

Wen R, Xiao J, Chang Z, Zhai D, Xu Q, Li Y, Itoh S, Lomtatidze Z (2010) Holocene climate changes in the mid-high-latitude-monsoon margin reflected by the pollen record from Hulun Lake, northeastern Inner Mongolia. Quat Res 73(2):293–303, http://dx.doi.org/10.1016/j.yqres.2009.10.006

Wischnewski J, Mischke S, Wang Y, Herzschuh U (2011) Reconstructing climate variability on the northeastern Tibetan Plateau since the last Lateglacial – a multi-proxy, dual-site approach comparing terrestrial and aquatic signals. Quat Sci Rev 30(1–2):82–97, http://dx.doi.org/10.1016/j.quascirev.2010.10.001

Wu W, Liu T (2004) Possible role of the "Holocene Event 3" on the collapse of Neolithic Cultures around the Central Plain of China. Quat Int 117(1):153–166, http://dx.doi.org/10.1016/S1040-6182(03)00125-3

Xiao J, Xu Q, Nakamura T, Yang X, Liang W, Inouchi Y (2004) Holocene vegetation variation in the Daihai Lake region of north-central China: a direct indication of the Asian monsoon climatic history. Quat Sci Rev 23(14–15):1669–1679, http://dx.doi.org/10.1016/j.quascirev.2004.01.005

Xu D, Lu H, Chu G, Wu N, Shen C, Wang C, Mao L (2014) 500-year climate cycles stacking of recent centennial warming documented in an East Asian pollen record. Sci Rep 4. doi:10.1038/srep03611, http://www.nature.com/srep/2014/140109/srep03611/abs/srep03611.html#supplementary-information

Yancheva G, Nowaczyk NR, Mingram J, Dulski P, Schettler G, Negendank JF, Liu J, Sigman DM, Peterson LC, Haug GH (2007) Influence of the intertropical convergence zone on the East Asian monsoon. Nature 445(7123):74–77. doi:10.1038/nature05431

You H, Liu J (2012) High-resolution climate evolution derived from the sediment records of Erlongwan Maar Lake since 14 ka BP. Chin Sci Bull 57(27):3610–3616. doi:10.1007/s11434-012-5244-6

Zhai D, Xiao J, Zhou L, Wen R, Chang Z, Wang X, Jin X, Pang Q, Itoh S (2011) Holocene East Asian monsoon variation inferred from species assemblage and shell chemistry of the ostracodes from Hulun Lake, Inner Mongolia. Quat Res 75(3):512–522, http://dx.doi.org/10.1016/j.yqres.2011.02.008

Zhang Q-B, Cheng G, Yao T, Kang X, Huang J (2003) A 2,326-year tree-ring record of climate variability on the northeastern Qinghai-Tibetan Plateau. Geophys Res Lett 30(14):1739. doi:10.1029/2003GL017425

Zhang P, Cheng H, Edwards RL, Chen F, Wang Y, Yang X, Liu J, Tan M, Wang X, Liu J, An C, Dai Z, Zhou J, Zhang D, Jia J, Jin L, Johnson KR (2008) A test of climate, sun, and culture relationships from an 1810-year Chinese Cave record. Science 322(5903):940–942. doi:10.1126/science.1163965

Zhang J, Chen F, Holmes JA, Li H, Guo X, Wang J, Li S, Lü Y, Zhao Y, Qiang M (2011) Holocene monsoon climate documented by oxygen and carbon isotopes from lake sediments and peat bogs in China: a review and synthesis. Quat Sci Rev 30(15–16):1973–1987, http://dx.doi.org/10.1016/j.quascirev.2011.04.023

Zhao B (2011) Sequence and chronology of the Neolithic culture in the Mudanjiang River Valley. Huaxia Archaeol 1:117–120 (in Chinese with English abstract)

Zhao C, Chang Y-P, Chen M-T, Liu Z (2013) Possible reverse trend in Asian summer monsoon strength during the late Holocene. J Asian Earth Sci 69:102–112, http://dx.doi.org/10.1016/j.jseaes.2012.09.028

Zhou Y (1997) Geography of the vegetation in Northeast China. Science Press, Beijing

Zhou W, Yu X, Jull AJT, Burr G, Xiao JY, Lu X, Xian F (2004) High-resolution evidence from southern China of an early Holocene optimum and a mid-Holocene dry event during the past 18,000 years. Quat Res 62(1):39–48, http://dx.doi.org/10.1016/j.yqres.2004.05.004

Zhou W, Xie S, Meyers PA, Zheng Y (2005) Reconstruction of late glacial and Holocene climate evolution in southern China from geolipids and pollen in the Dingnan peat sequence. Org Geochem 36(9):1272–1284, http://dx.doi.org/10.1016/j.orggeochem.2005.04.005

Zhu L, Zhen X, Wang J, Lü H, Xie M, Kitagawa H, Possnert G (2009) A ∼30,000-year record of environmental changes inferred from Lake Chen Co, Southern Tibet. J Paleolimnol 42(3):343–358. doi:10.1007/s10933-008-9280-9

Chapter 7
Rapid Environmental Change of Jingpo Lake in Mid-Holocene: Inferred from Fluvial/Lacustrine Sedimentary Facies Transition

Rong Chen and Ji Shen

Abstract The Jingpo Lake is the China's largest lava-dammed lake, however, the formation age of Jingpo Lake and associated volcanic eruption events are poorly understood and still under controversy. In this study, we obtained a 12.72-m-long sediment core (JP-C) from Jingpo Lake in south Heilongjiang Province, northeast China, and used AMS radiocarbon dating of terrestrial plant macrofossils to provide a robust chronology. This study will focus on the sediments below 954 cm depth. Lithology, multi-proxy analyses and microbiological fossils data reveal rapid transition from fluvial to lacustrine sedimentary environment related to volcanic eruption events. Three stages of sedimentary environment change are documented: (i) Unite 1, fluvial sedimentary facies (below 1,232 cm, prior to ~5,120 cal. yr BP); (ii) Unite 2, transition sedimentary facies (between 1,232 and 1,154 cm, from ~5,120 to 5,060 cal. yr BP); (iii) Unite 3, lacustrine sedimentary facies (above 1,154 cm, after ~5,060 cal. yr BP). Our results suggest that Unite 1 represents fluvial sedimentary facies, while the lacustrine sedimentary facies developed afterwards. Between 1,250 and 1,240 cm intervals, the highest MS values and high amounts of charcoal could be the result of the Jingpo volcanoes eruption at ~5,135 cal. yr BP. During and after the volcanic eruptions, the lava flows descending along lowland areas and valleys may block many river valleys and eventually dammed the Mudanjiang River and created Jingpo Lake. Therefore, the core JP-C provides clear evidence that the Jingpo Lake was gradually formed

R. Chen
State Key Laboratory of Lake and Environment, Nanjing Institute of Geography and Limnology, Chinese Academy of Sciences, 73 East Beijing Road, Nanjing 210008, P. R. China

University of Chinese Academy of Sciences, Beijing 100049, P. R. China

J. Shen (✉)
State Key Laboratory of Lake and Environment, Nanjing Institute of Geography and Limnology, Chinese Academy of Sciences, 73 East Beijing Road, Nanjing 210008, P. R. China
e-mail: jishen@niglas.ac.cn

K. Kashiwaya et al. (eds.), *Earth Surface Processes and Environmental Changes in East Asia*, DOI 10.1007/978-4-431-55540-7_7

after the Holocene volcanic eruption of Jingpo volcanoes (after ~5,135 cal. yr BP). The stabilization of the lacustrine sedimentary environment had formed after ~5,065 cal. yr BP.

Keywords Jingpo Lake • Lava-dammed lakes • Volcanic eruptions • Sedimentary facies transition

7.1 Introduction

Lakes are normally formed under various geological and geographical backgrounds. As an important component of the terrestrial hydrosphere, lakes have close links with the atmosphere, biosphere and lithosphere. Lake evolutional processes usually involve geological, physical, chemical and biological processes, and these processes are all documented by lacustrine sediment archives (Shen 2013). Therefore, lacustrine sediment generally possesses a continuous record with high-resolutions that provides abundant information can be used to track past climatic and environmental changes (Last and Smol 2001). Volcanic eruptions are among the most effective agents of geomorphic change on Earth in terms of geologically instantaneous debris production (Korup and Clague 2009). During and after the volcanic eruptions, magma can erupt to the surface and form lava flows. The lava flows rapidly descending along lowland areas and valleys may dammed the confluences of tributary streams, and form lava-dammed lakes (Rodolfo and Umbal 2008). The sudden drainage of naturally lava-dammed lakes has caused some of the largest floods on Earth, potentially resulting in severe loss of lives and property (O'Connor and Costa 2004). Therefore, systematic study of the lava-dammed lakes histories, particularly the formation age and evolutional processes, is essential to understanding the occurrence of natural disasters, and consequently, in developing and applying adequate strategies for prevention and mitigation of natural disasters and loss of life and property (Alcántara-Ayala 2002).

The Jingpo volcanoes (44°08′-44°14′N, 128°29′-128°34′E, ~1,000 m above sea level) is located in the Zhangguangcai Mountains, Southeastern Heilongjiang Province, NE China, which is an important component of the circum-Pacific volcanic belt. The Jingpo volcanoes is situated in the eastern part of the east-west trending Central Asian Orogenic Belt (CAOB) and in the western part of the Dunhua-Mishan Fault (Davis and Marc 2001; Buchan et al. 2002; Yan and Zhao 2008). The Jingpo volcanoes are in front of the currently active Pacific slab, which is subducted beneath Eurasia (Chuvashova et al. 2007). According to K-Ar analysis, ^{14}C dating and thermoluminescence dating results, volcanic activity in this area occurred in four stages: Paleocene-Eocene; Late Miocene; Pleistocene; and Holocene. More than ten craters were created during a series of fissure eruptions between 5,500 and 5,200 yr BP when basaltic glass was formed on the surface of the lava (Fan et al. 2003, 2005; Chuvashova et al. 2007; Jia et al. 2013). During this time lava flowed over 300 km^2 forming an extensive basaltic plain (Fig. 7.1) (Jia et al. 2013). This large amount of lava flows filled many small river valleys and

formed numerous long distance lava tubes. The lava flows eventually blocked the Mudanjiang River and created Jingpo Lake (Fan et al. 2003; Yan and Zhao 2008; Jia et al. 2013). However, the formation age of Jingpo Lake and associated volcanic eruption events are poorly understood and still under controversy, and clues regarding them are urgently needed. Based on volcanic activity, a number of studies have suggested that Jingpo Lake formed about 10 ka BP (Wang and Dou 1998; Li et al. 2011). According to ^{14}C dating of carbonized wood and charcoal samples, however, some other scholars suggested that Jingpo Lake formed about 5,500–4,400 yr BP (Zhang et al. 2002; Fan et al. 2003, 2005; Chuvashova et al. 2007; Jia et al. 2013). According to fluvial/lacustrine sedimentary facies transition, we can conclude that the formation age of Jingpo Lake. Therefore, in this study, we present a multi-proxy analyses results with robust chronologies (AMS ^{14}C ages obtained from terrestrial plant leaves and charcoal) of a sedimentary sequence derived from Jingpo Lake. Lithology, grain size, magnetic susceptibility, geochemistry, pollen concentration, and diatom concentration were studied for their ability to explore the formation age of Jingpo Lake and the directly related to the timing of volcanic events.

7.2 Regional Setting

The Jingpo Lake (43°46′-44°03′N, 128°27′-129°03′E, ~350 m above sea level) is located in Ning'an County, Southeastern Heilongjiang Province, NE China (Fig. 7.1). It is the China's largest lava-dammed lake and formed by lava damming of the Mudanjiang River. The lake has a surface area of ~92 km^2, with a maximum water depth of 48 m and an average depth of 12.9 m. The length of Jingpo Lake from north to south is ~45 km, and the widest distance from east to west is only ~6 km (Wang and Dou 1998). Jingpo Lake is mainly fed by surface run-off and precipitation. There are around 30 rivers flowing into the Jingpo Lake; most of these rivers drain into the south part of lake, and the lake water outflows from the northwest to the Mudanjiang River. The south part of the lake is shallow and the deepest part in the northern part of the lake. Jingpo Lake is surrounded by low mountains, topography of the catchment is dominated by hilly plains with a small relative elevation, and with the major rock types include granite, alkali olivine basalts, basanites and tephrites (Zhang et al. 2002).

This region is dominated by the East Asian Monsoon system which shows a strong seasonal variability. The mean annual precipitation (include snowfall) at nearby Ning'an meteorological station is ~545 mm for the period 1951–2012. Most of the precipitation falls as rain during the summer and autumn months (May–September), which supplies ~81 % of the annual precipitation, and with the peak precipitation of ~123 mm in August. The mean annual temperature is ~4.3 °C with a maximum monthly mean of ~22.1 °C in July and a minimum of −17.7 °C in January. The present-day terrestrial vegetation in the Jingpo Lake catchment belongs to the temperate mixed-forest flora of Changbai Mountain, comprised of evergreen conifers and deciduous broadleaved trees (Qian et al. 2003). The native vegetation is characterized by a *Pinus koraieusis* mixed conifer and broadleaved forest zone, which now deteriorates to secondary broadleaved forest (Li et al. 2011).

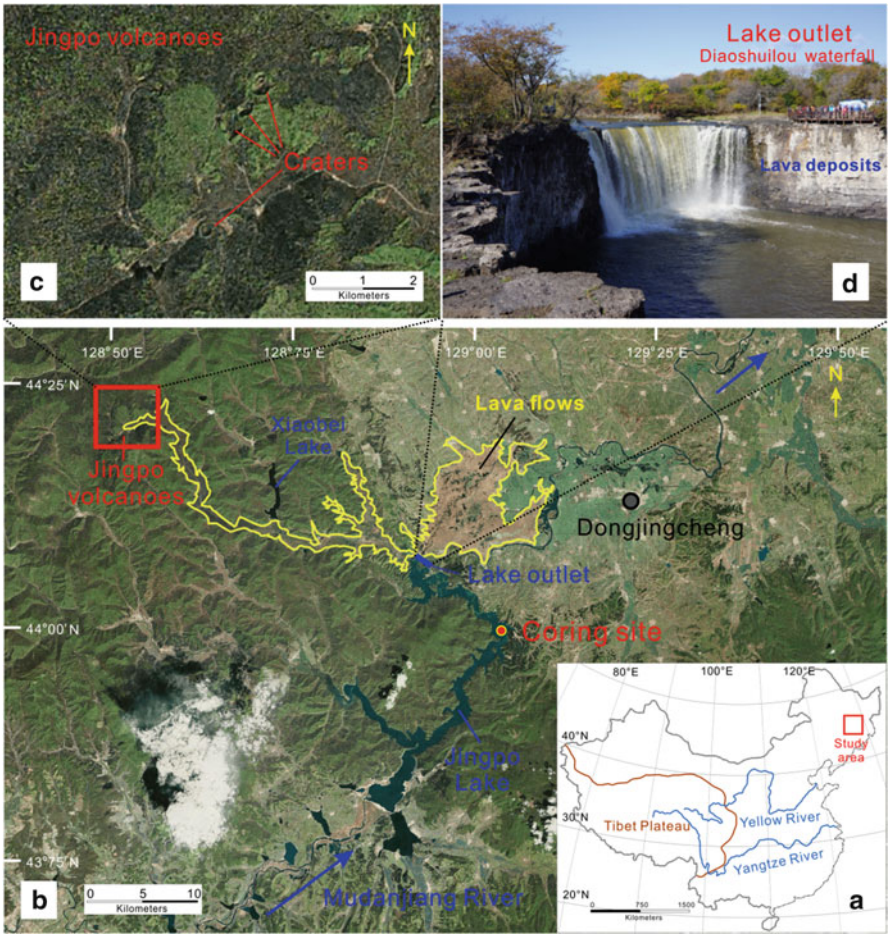

Fig. 7.1 (**a**) The location of Jingpo Lake within the Heilongjiang Province. The *red square* denotes the location of our study area. (**b**) Topographic map of Jingpo Lake catchment and the sediment core sampling sites. The *blue arrow* indicate the direction of the Mudanjiang River, the *red square* denotes the Jingpo volcanoes area. (**c**) Topographic map of Jingpo volcanoes area. (**d**) A photo of the Diaoshuilou waterfall, outlet of Jingpo Lake

7.3 Materials and Methods

7.3.1 Coring and Dating Methods

In August 2012, a 1,302-cm-long sediment core (JP-C) was recovered from a water depth of 30.9 m in the northeastern part of Jingpo Lake (43°59′N, 129°02′E) (Fig. 7.1b), using Austria UWITEC^{TM} piston coring system with PVC tubes in 2.0 m length and 60 mm diameter. The sediment cores were placed in polyvinyl

chloride tubes and transported to the Nanjing Institute of Geography and Limnology, Chinese Academy of Sciences. Overlaps between the core sections were identified using scanned magnetic susceptibility data, resulting in a 1,272 cm continuous sediment record. This study will focus on the sediments below 954 cm depth. Prior to laboratory analysis, the core was sub-sampled at 2 cm intervals, and the samples were freeze-dried and kept in cold storage at 4 °C.

Ten samples of terrestrial plant macrofossils were handpicked for accelerator mass spectrometry (AMS) ^{14}C dating, which can minimize the carbon reservoir effects (or old carbon effects) that commonly occur in lacustrine sediments. These samples were dated at the Laboratory of Beta Analytic Inc., Florida of the USA. All AMS ^{14}C dates were calibrated into calendar years before present (0 cal. yr BP = 1950 AD) using the program Calib 6.0 utilizing the IntCal 09 calibration dataset (Reimer et al. 2009).

7.3.2 Analytical Methods

For grain size analyses, 0.5 g wet sediment samples were pretreated with 10–20 ml of 30 % H_2O_2 to remove organic matter, washed with 10 % HCl to remove carbonate, rinsed with deionized water, and then treated with 20 ml of 0.05 M $(NaPO3)_6$ on an ultrasonic vibrator for 10 min to facilitate dispersion. Grain size distributions between 0.02 and 2,000 μm were determined using a Malvern Mastersizer 2000 analyzer. Magnetic susceptibility was analyzed using a Bartington Ltd MS2 Magnetic Susceptibility Meter linked to an MS2B Dual Frequency Sensor (470 and 4,700 Hz). Total organic carbon content (TOC) and total nitrogen content (TN) were measured using a CE Model 440 Elemental Analyzer after removing carbonates with 10 % HCl. Replicate analyses of well mixed samples showed that precision was ca. ± <0.1 % (1 SD). C/N values were derived from these data. All these methods were analyzed at 4-cm intervals.

Pollen samples were taken at 10–20 cm intervals. Each sample was treated with 10 % HCl, 10 % KOH, HF and a hot acetolysis mixture, in accordance with the standard methods (Faegri et al. 1989). Lycopodium spores with known numbers were added to each sample in order to facilitate the calculation of pollen concentrations before the chemical treatment. Diatom samples were analyzed at 4-cm intervals. 0.5 g wet sediment for each sample was treated using standard procedures with 10 % HCl and 30 % H_2O_2 (Battarbee et al. 2001). Four replicate subsamples are potentially available from each sample. Diatom valves were enumerated on each of two prepared slides from each sample, resulting in two replicate abundance estimates. At least 300 valves were counted per sample and taxon abundances expressed as percentage of total count. Counts were made using an Olympus microscope (BX 51) with oil immersion objective (magnification × 1,000).

All these multi-proxy analyses were performed in the State Key Laboratory of Lake Science and Environment, Nanjing Institute of Geography and Limnology, Chinese Academy of Sciences.

7.4 Results and Discussion

7.4.1 Lithology and Chronology

The lithology of the core JP-C is mainly composed of silty clay and/or clayey silt, except for the coarse sand and fluvial gravel emerging at the deepest part of the core (Fig. 7.2). The core can be subdivided into three major sedimentological units (Fig. 7.2): the lower unit (below 1,232 cm) consists of yellowish-brown coarse sand and fluvial gravel, the middle unit (1,232–1,154 cm) consists of gray brown sandy silt, and the upper unit (above 1,154 cm) consists of black brown silty clay and dark brown clayey silt.

The results of the ten AMS ^{14}C ages of the core JP-C are presented in Table. 7.1 and Fig. 7.2. Terrestrial plant macrofossils (such as leaves and charcoal) from lake sediments for AMS ^{14}C ages can yield reliable radiocarbon dates. Therefore, the age–depth model was established by linear interpolation between each pair of the mid-points of the 2-sigma calibrated age range. The basal age of the core is ~5,150 cal. yr BP, and the age-depth model shows a linear relationship ($R^2 = 0.994$). The sediment accumulation rate (SAR) of the 954–1,154 cm interval is 0.24 cm/year, below 1,154 cm depth the SAR is 1.32 cm/year.

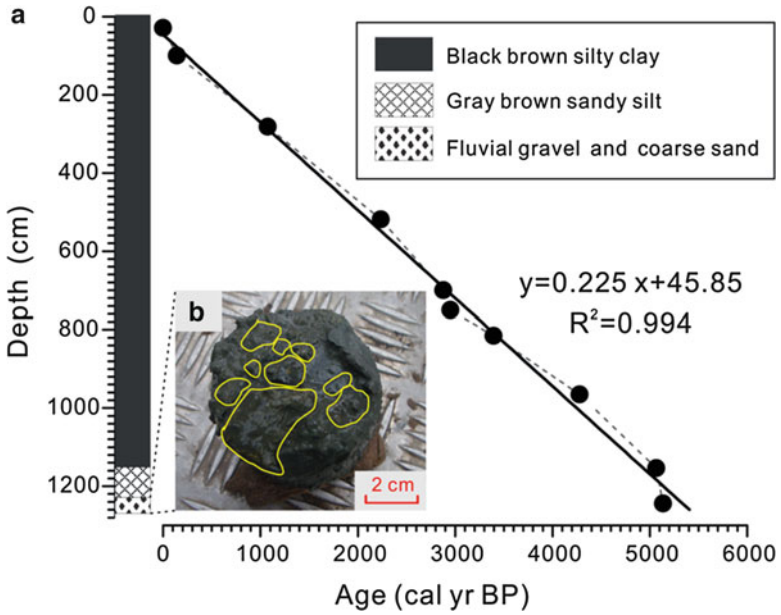

Fig. 7.2 (**a**) Sediment lithology and age–depth model of the sediment core JP-C from Jingpo Lake. (**b**) A fieldwork photo showing the sediment bottom of the JP-C core, *yellow line* indicates the fluvial gravel

Table 7.1 Conventional and calibrated AMS ^{14}C radiocarbon dates for JP-C core from Jingpo Lake, Heilongjiang Province, NE China

Lab number	Sample name	Core depth (cm)	Dated material	Age (^{14}C yr BP $\pm$ 1σ)	$^{13}C/^{12}C$ ‰	Calibrated age (cal. yr BP) 2σ ranges	Median age (cal. yr BP)
Beta-330281	JPP-1	28.5	Leaf fragment	Modern carbon	NA	Modern carbon	Modern
Beta-330291	JPP-11	100	Leaf fragment	110 $\pm$ 30	−29.8	10–270	140
Beta-330282	JPP-2	282	Leaf fragment	1,150 $\pm$ 30	−26.8	980–1,170	1,075
Beta-330283	JPP-3	519	Leaf fragment	2,210 $\pm$ 30	−27.0	2,140–2,330	2,235
Beta-330285	JPP-5	700	Leaf fragment	2,790 $\pm$ 30	−25.4	2,800–2,960	2,880
Beta-330286	JPP-6	750	Leaf fragment	2,830 $\pm$ 30	−27.2	2,860–3,040	2,950
Beta-330287	JPP-7	815	Leaf fragment	3,160 $\pm$ 30	−27.6	3,350–3,440	3,395
Beta-330289	JPP-9	965	Leaf fragment	3,850 $\pm$ 30	−27.1	4,150–4,410	4,280
Beta-330290	JPP-10	1,154	Leaf fragment	4,420 $\pm$ 30	−28.0	4,870–5,260	5,065
Beta-330295	JPP-12	1,244	Charcoal	4,470 $\pm$ 30	−25.8	4,970–5,300	5,135

7.4.2 Proxy Interpretations

The grain size composition variability in lacustrine sediment core can indicate the changes of the sedimentary environment (Lambiase 1980) related to hydrologic energy variations, such as transport capacity (Hakanson and Jansson 1983; Liu et al. 2008) and lake levels (An et al. 2012). But if the source of the sediments does significant change, the grain-size can give information about changes in the hydrodynamics of inflowing streams, changes in the internal hydrodynamics, and external factors affecting the catchment erosion (Sun et al. 2002). The magnetic susceptibility of sediments has been used as an indicator of the relative proportion of terrestrial magnetic minerals in the sediments (Thompson and Oldfield 1986).

The type and amount of lacustrine sedimentary organic matter (OM) reflects past fluctuations in lake productivity and terrestrial inputs linked to climate-induced environmental changes, catchment-related processes and lake internal changes (Meyers 1997; Meyers and Lallier-vergés 1999; Talbot and Lærdal 2000; Meyers and Teranes 2001; Leng and Marshall 2004; Leng et al. 2006; Cook et al. 2012). In general, the amount of organic matter in lake sediments is a function of changes in organic production in the lake, catchment vegetation changes and transfer of terrestrial particulate and dissolved organic matter to the lake, loss processes, and dilution effects (by varying inorganic inputs) (Meyers and Lallier-vergés 1999; Meyers and Teranes 2001; Cook et al. 2012). The two known major sources of organic matter (OM) in lake sediments are autochthonous, i.e. aquatic plants living in the lake water column, and allochthonous, i.e. terrestrial plants growing in the catchment (Meyers and Lallier-vergés 1999; Meyers and Teranes 2001). The C/N ratios has been used to distinguish these two source of sedimentary OM (i.e., whether primarily derived from terrestrial or aquatic sources), owing to the distinguishing characteristics of aquatic and vascular plants (Meyers and Lallier-vergés 1999; Talbot and Lærdal 2000; Meyers and Teranes 2001; Leng et al. 2006). Since aquatic OM is relatively enriched in nitrogen rich proteins, and vascular plant OM is relatively enriched in nitrogen depleted lignin and cellulose, the ratio of carbon to nitrogen is much lower in aquatic OM than in OM of terrestrial origin. Therefore, aquatic OM source has C/N ratios less than 10, while C/N ratios in terrestrial plants are commonly higher than 20 (Meyers and Lallier-vergés 1999; Talbot and Lærdal 2000; Meyers and Teranes 2001; Leng et al. 2006). C/N ratios between 10 and 20 typically indicate a mix of aquatic and terrestrial organic matter (Meyers 1997; Meyers and Lallier-vergés 1999; Talbot and Lærdal 2000; Meyers and Teranes 2001; Leng and Marshall 2004; Leng et al. 2006; Cook et al. 2012).

7.4.3 The Formation Age of the Jingpo Lake

The core JP-C was divided into three major sedimentary units according to multi-proxy analyses results of grain size (Fig. 7.3a-c), magnetic susceptibility (MS) (Fig. 7.3d), TOC (Fig. 7.3e), TN (Fig. 7.3f), C/N (Fig. 7.3g), pollen concentration (Fig. 7.3h) and diatom concentration (Fig. 7.3i).

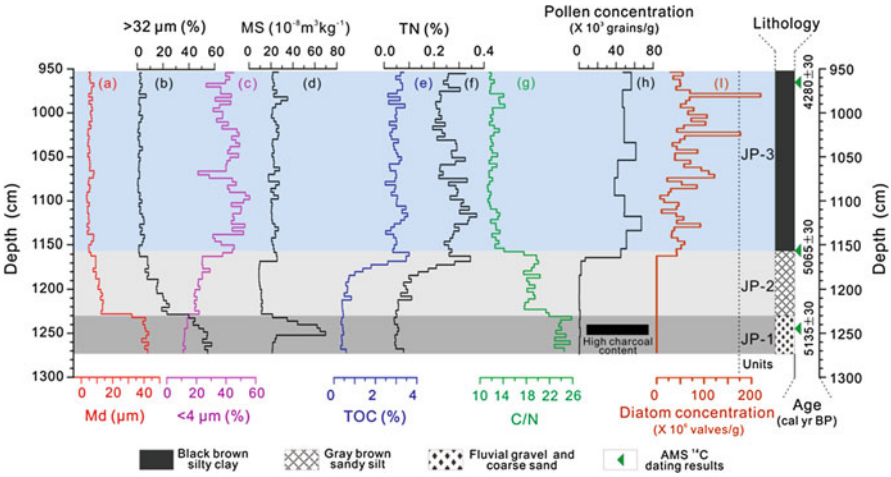

Fig. 7.3 Results of the core JP-C in Jingpo Lake: (**a**) median grain size, (**b**) the contents of grain size >32 μm, (**c**) the contents of grain size <4 μm, (**d**) magnetic susceptibility, (**e**) TOC content, (**f**) TN content, (**g**) C/N ratios, (**h**) pollen concentration, (**i**) diatom concentration. *Black bar* indicate high charcoal content layer, and *green solid triangles* represent terrestrial plant macrofossils AMS ^{14}C ages

7.4.3.1 Fluvial Sedimentary Facies (Unit JP-1, 1,272–1,232 cm)

Unit JP-1 (1,272–1,232 cm; ~5,150–5,120 cal. yr BP). This unit is characterized by the highest contents of grain size >32 μm (ranging from 40.0 to 57.6 %, mean of 50.0 %) and the median grain size (Md) values (ranging from 32.3 to 42.9 μm, mean of 40.2 μm) for the entire core, and the lowest contents of grain size <4 μm (ranging from 11.0 to 14.8 %, mean of 12.6 %). An important feature of this unit is the highest MS values with large fluctuations, and range from 21.2 to 69.7×10^{-8} m^3 kg^{-1}, with an average value of 37.3×10^{-8} m^3 kg^{-1}. TOC and TN results exhibit broadly similar changes for the entire core. In this unit, TOC and TN values vary between 0.86 and 1.64 % (mean of 1.04 %) and between 0.04 and 0.08 % (mean of 0.05 %), respectively. The C/N ratios range from 21.9 to 25.6 with a mean ratio of 23.9. Almost no pollen grains and diatom valves were found in this unit.

The base of the core JP-C (Unit JP-1) is distinctly different from the remainder of the sediment core. This unit is composed mostly of fluvial gravel and coarse sand. The coarse, angular and poorly sorted gravel and coarse sand at the very bottom of the core is of fluvial origin (Fig. 7.2b), that require a high energy transported by the Mudanjiang River to the coring site at Jingpo Lake formed before. The fluvial sedimentary environment is not conducive to the organic matter growth and accumulation and microbiological fossils sedimentation and preservation, therefore, the extremely low TOC, TN, pollen concentration, and diatom concentration observed in this unit (Fig. 7.3). The C/N ratios are greater than 21 in this unit

(Fig. 7.3g), indicate that the organic matter is derived from terrestrial plant sources. Altogether, we suggest that this unit represents fluvial sedimentary facies period.

Notably, a significant high MS values and charcoal contents were observed between 1,250 and 1,240 cm intervals (Fig. 7.3). When volcanic activity occurs, the physical and chemical characteristics of sediments will change significantly. During and after the Jingpo volcanoes eruption, large number of vegetation was burning by the blazing lava, which produces large amounts of charcoal. In the meantime, the fall tephra was contains large amounts of Fe and other metal elements (Zhang et al. 2002; Fan et al. 2003, 2005). Therefore, between 1,250 and 1,240 cm intervals, the highest MS values and high amounts of charcoal could be the result of the Jingpo volcanoes eruption at ~5,135 cal. yr BP (Fig. 7.3). Our result is consistent with the volcanic eruption of Jingpo volcanoes had been occurred between 5,500 and 5,200 cal. yr BP, based on measured section of air fall clastic rock and ^{14}C dating of carbonized wood and charcoal samples (Fan et al. 2003, 2005; Chuvashova et al. 2007; Jia et al. 2013).

7.4.3.2 Transition Sedimentary Facies (Unit JP-2, 1,232–1,154 cm)

Unit JP-2 (1,232–1,154 cm; ~5,120–5,060 cal. yr BP). This unit is characterized by an abrupt and simultaneous increase in TOC and TN values. TOC ranging from 0.87 to 5.85 % with an average value of 2.27 % and TN ranging from 0.05 to 0.35 % with an average value of 0.15 %, C/N ratios are stable at ~18 (ranging from 12.6 to 21.4, mean of 18.3). The MS values fluctuate between 9.1 and 25.0×10^{-8} m^3 kg^{-1} with a mean of 12.6×10^{-8} m^3 kg^{-1}. Md values (ranging from 4.7 to 14.0 μm, mean of 10.3 μm) and the contents of grain size >32 μm (ranging from 1.3 to 24.7 %, mean of 12.8 %) exhibited rapid decreasing trends in this unit, concurrently, the contents of grain size <4 μm increased significantly (ranging from 18.9 to 45.4 %, mean of 25.2 %). At the end of this unit, the concentration of pollen and diatom increase significantly.

During and after the Jingpo volcanoes eruption, the large amount of lava flows rapidly enter lowland areas and valleys beyond the volcanoes where they may temporarily or permanently alter the valley bottom topography and disrupt the hydrologic regime of streams and rivers, and eventually dammed the Mudanjiang River and created Jingpo Lake (Fig. 7.4). Then the Jingpo Lake formed, almost all proxies show strong fluctuations, indicating a high variability in the sedimentary environment in this stage. The grain size component of >32 μm is decreasing and that of <4 μm is increasing since the beginning of this unit, suggesting a decreasing transport capacity and a rising river or lake levels. In addition, the gradually increase in TOC and TN values and the rapid increase in concentration of pollen and diatom at the end of this unit indicate that intense to weaker water dynamic depositional environment conducive to the accumulation and preservation of organic matter and microbiological fossils (Fig. 7.3). The decreasing C/N ratios (Fig. 7.3g), showing an increasing fraction of autochthonous organic matter, suggest that the plant organic matter in this unit is derived from a mixture of sources, especially algae and aquatic

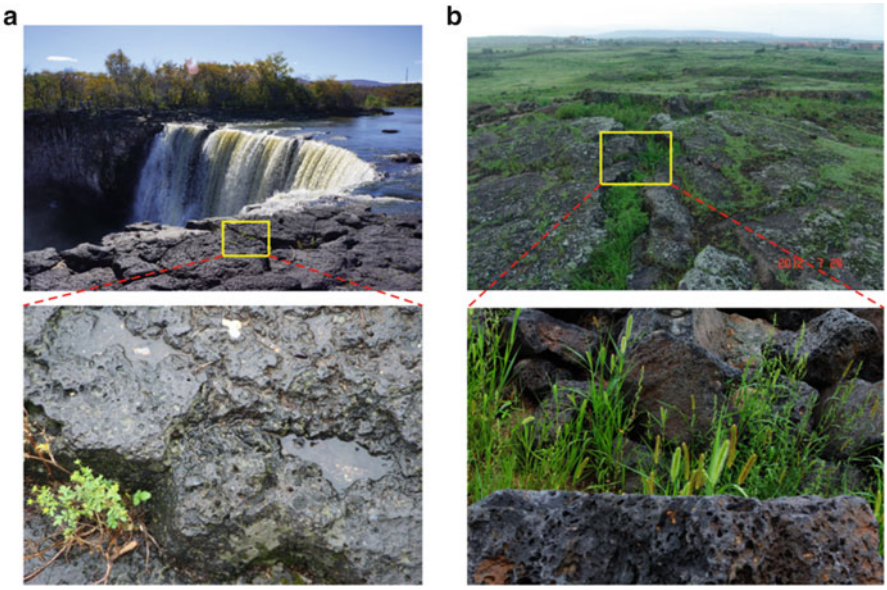

Fig. 7.4 (**a**) A photo of the Diaoshuilou waterfall, outlet of Jingpo Lake, the *yellow square* denotes the volcanic rock. (**b**) A fieldwork photo showing the basaltic plain formed by lava flows at ~1 km north of Jingpo Lake, the *yellow square* indicates the basalt

vegetation and only a small contribution from terrestrial vegetation. In summary, the onset of Jingpo Lake formation (as indicated by the rapid deposition of clays, decrease in sands, and increase in TOC, TN, pollen, and diatom concentrations) occurred soon after the Jingpo volcanoes eruption (~5,135 cal. yr BP).

7.4.3.3 Lacustrine Sedimentary Facies (Unit JP-3, 1,154–954 cm)

Unit JP-3 (1,154–954 cm; ~5,060–4,230 cal. yr BP). The characteristic feature of this unit is the lowest Md values (ranging from 3.4 to 8.1 μm, mean of 5.4 μm) and the contents of grain size >32 μm (ranging from 0.4 to 6.8 %, mean of 2.3 %), but the highest contents of grain size <4 μm (ranging from 21.0 to 55.9 %, mean of 47.1 %). TOC and TN increased to their highest values (ranging from 2.08 to 4.24 % and 0.20 to 0.37 %, mean of 2.80 and 0.27 %, respectively), while the C/N ratios decreased to their lowest values (ranging from 11.4 to 14.1, mean of 12.3). The MS values are relatively high, and ranging from 17.7 to 35.2×10^{-8} m^3 kg^{-1}, with an average value of 23.0×10^{-8} m^3 kg^{-1}. The most striking feature of this unit is that the both pollen concentration and diatom concentration increase significantly and reaches their maximum values, averaging up to 50.4×10^3 grains g^{-1} and 60.1×10^6 valves g^{-1}, respectively.

A stable lake system had formed during this unit, as indicated by the typical homogeneous lacustrine sediment characteristic. The highest contents of grain size <4 μm and the lowest contents of grain size >32 μm and Md values (Fig. 7.3) suggest the stable lake sedimentary environment in this period (low transport capacity). The relatively stable C/N ratios, less than 13 for most of the investigated period in JP-C (Fig. 7.3g), suggest that the organic matter is mainly from autochthonous sources. Moreover, the highest average values of TOC and TN indicate that lake sedimentary environment conducive to the organic matter growth, accumulation and preservation. In addition, the highest concentrations of pollen and diatom (Fig. 7.3) also suggest the stable lacustrine sedimentary environment (weaker water dynamic condition), because of lake environment conducive to the pollen preservation and algae (include diatom) accumulation and preservation. In general, the stabilization of the lacustrine sedimentary facies indicate that the Jingpo Lake eventually formed after ~5,065 cal. yr BP.

7.5 Conclusion

The Jingpo Lake is the China's largest lava-dammed lake and formed by lava damming of the Mudanjiang River, however, the formation age of Jingpo Lake and associated volcanic eruption events are poorly understood and still under controversy. In this study, we obtained a 12.72-m-long sediment core (JP-C) from Jingpo Lake (lava-dammed lake) in south Heilongjiang Province, northeast China, and used AMS radiocarbon dating of terrestrial plant macrofossils to provide a robust chronology. This study will focus on the sediments below 954 cm depth. Lithology and multi-proxy analyses results indicate that the core JP-C can be subdivided into three major sedimentological units: (i) Unite 1, fluvial sedimentary facies (below 1,232 cm, prior to ~5,120 cal. yr BP); (ii) Unite 2, transition sedimentary facies (between 1,232 and 1,154 cm, from ~5,120 to 5,060 cal. yr BP); (iii) Unite 3, lacustrine sedimentary facies (above 1,154 cm, after ~5,060 cal. yr BP). Therefore, the core will provide an opportunity to determine the formation age of Jingpo Lake and the directly related to the timing of volcanic eruption events. Lithology and analyses results suggest that Unite 1 represents fluvial sedimentary facies, while the lacustrine sedimentary facies developed afterwards. Between 1,250 and 1,240 cm intervals, the highest MS values and high amounts of charcoal could be the result of the Jingpo volcanoes eruption at ~5,135 cal. yr BP. This volcanic eruption is consistent with the Holocene volcanic eruption of Jingpo volcanoes had been occurred between 5,500 and 5,200 cal. yr BP. During and after the volcanic eruptions, the lava flows descending along lowland areas and valleys may block many river valleys and eventually dammed the Mudanjiang River and created Jingpo Lake. Therefore, the core JP-C provides clear evidence that the Jingpo Lake was gradually formed after the Holocene volcanic eruption of Jingpo volcanoes (after ~5,135 cal. yr BP). The stabilization of the lacustrine sedimentary facies had

formed after the beginning of the Unite 3 was reflected by the typical homogeneous lacustrine sediment characteristic and multi-proxy analyses data. Namely, our data indicate that the Jingpo Lake eventually formed after ~5,065 cal. yr BP.

Acknowledgements We wish to thank Qingfeng Jiang and Hao Long for their help during field coring. This study is supported by the National Basic Research Program of China (2012CB956100), and the CAS/SAFEA international partnership program for creative research teams (No. KZZD-EW-TZ-08).

References

Alcántara-Ayala I (2002) Geomorphology, natural hazards, vulnerability and prevention of natural disasters in developing countries. Geomorphology 47(2–4):107–124. doi:http://dx.doi.org/10.1016/S0169-555X(02)00083-1

An C-B, Lu Y, Zhao J, Tao S, Dong W, Li H, Jin M, Wang Z (2012) A high-resolution record of Holocene environmental and climatic changes from Lake Balikun (Xinjiang, China): implications for central Asia. Holocene 22(1):43–52. doi:10.1177/0959683611405244

Battarbee R, Jones V, Flower R, Cameron N, Bennion H, Carvalho L, Juggins S (2001) Diatoms. In: Smol J, Birks HJ, Last W, Bradley R, Alverson K (eds) Tracking environmental change using lake sediments, vol 3, Developments in paleoenvironmental research. Springer, Dordrecht, pp 155–202. doi:10.1007/0-306-47668-1_8

Buchan C, Pfänder J, Kröner A, Brewer TS, Tomurtogoo O, Tomurhuu D, Cunningham D, Windley BF (2002) Timing of accretion and collisional deformation in the Central Asian Orogenic Belt: implications of granite geochronology in the Bayankhongor Ophiolite Zone. Chem Geol 192(1–2):23–45. doi:http://dx.doi.org/10.1016/S0009-2541(02)00138-9

Chuvashova I, Rasskazov S, Yasnygina T, Saranina E, Fefelov N (2007) Holocene volcanism in central Mongolia and northeast China: asynchronous decompressional and fluid melting of the mantle. J Volcanol Seismol 1(6):372–396

Cook CG, Leng MJ, Jones RT, Langdon PG, Zhang E (2012) Lake ecosystem dynamics and links to climate change inferred from a stable isotope and organic palaeorecord from a mountain lake in southwestern China (ca. 22.6–10.5 cal ka BP). Quatern Res 77(1):132–137. doi:http://dx.doi.org/10.1016/j.yqres.2011.09.011

Davis GA, Marc S (2001) Paleozoic and Mesozoic tectonic evolution of central and eastern Asia, vol 194. Geological Society of America, Boulder

Faegri K, Kaland PE, Krzywinski K (1989) Textbook of pollen analysis, 4th edn. Wiley, Chichester

Fan Q, Sun Q, Li N, Yin J, Chen H, Gao F, Zhang X (2003) The section of airfall clastic rock of Holocene volcano in Jinbo Lake and its eruptive history. Seismol Geol 25:3–11 (in Chinese with English abstract)

Fan Q, Sun Q, Li N (2005) Variety of volcanic rocks at Jingpohu. Dev Nat Sci 8(15):943–950 (in Chinese with English abstract)

Hakanson L, Jansson M (1983) Principles of lake sedimentology. Springer, Berlin, 316

Jia PW, Doelman T, Torrence R, Glascock MD (2013) New pieces: the acquisition and distribution of volcanic glass sources in northeast China during the Holocene. J Archaeol Sci 40(2):971–982. doi:http://dx.doi.org/10.1016/j.jas.2012.09.001

Korup O, Clague JJ (2009) Natural hazards, extreme events, and mountain topography. Quatern Sci Rev 28(11–12):977–990. doi:http://dx.doi.org/10.1016/j.quascirev.2009.02.021

Lambiase JJ (1980) Hydraulic control of grain-size distributions in a macrotidal estuary. Sedimentology 27(4):433–446. doi:10.1111/j.1365-3091.1980.tb01192.x

Last WM, Smol J (2001) Tracking environmental change using lake sediments, vol 1, Basin analysis, coring, and chronological techniques. Kluwer Academic Publishers, Dordrecht

Leng MJ, Marshall JD (2004) Palaeoclimate interpretation of stable isotope data from lake sediment archives. Quatern Sci Rev 23(7–8):811–831. doi:http://dx.doi.org/10.1016/j.quascirev.2003.06.012

Leng M, Lamb A, Heaton TE, Marshall J, Wolfe B, Jones M, Holmes J, Arrowsmith C (2006) Isotopes in lake sediments. In: Leng M (ed) Isotopes in palaeoenvironmental research, vol 10, Developments in paleoenvironmental research. Springer, Dordrecht, pp 147–184. doi:10.1007/1-4020-2504-1_04

Li C, Wu Y, Hou X (2011) Holocene vegetation and climate in Northeast China revealed from Jingbo Lake sediment. Quatern Int 229(1–2):67–73. doi:http://dx.doi.org/10.1016/j.quaint.2009.12.015

Liu X, Herzschuh U, Shen J, Jiang Q, Xiao X (2008) Holocene environmental and climatic changes inferred from Wulungu Lake in northern Xinjiang, China. Quatern Res 70(3):412–425. doi:http://dx.doi.org/10.1016/j.yqres.2008.06.005

Meyers PA (1997) Organic geochemical proxies of paleoceanographic, paleolimnologic, and paleoclimatic processes. Org Geochem 27(5–6):213–250. doi:http://dx.doi.org/10.1016/S0146-6380(97)00049-1

Meyers P, Lallier-vergés E (1999) Lacustrine sedimentary organic matter records of late quaternary paleoclimates. J Paleolimnol 21(3):345–372. doi:10.1023/A:1008073732192

Meyers P, Teranes J (2001) Sediment organic matter. In: Last W, Smol J (eds) Tracking environmental change using lake sediments, vol 2, Developments in paleoenvironmental research. Springer, Dordrecht, pp 239–269. doi:10.1007/0-306-47670-3_9

O'Connor JE, Costa JE (2004) The world's largest floods, past and present: their causes and magnitudes, vol 1254. Geological Survey (USGS), Reston

Qian H, Yuan X-Y, Chou Y-L (2003) Forest vegetation of Northeast China. In: Kolbek J, Šrůtek M, Box E (eds) Forest vegetation of Northeast Asia, vol 28, Geobotany. Springer, Dordrecht, pp 181–230. doi:10.1007/978-94-017-0143-3_6

Reimer PJ, Baillie MGL, Bard E, Bayliss A, Beck JW, Blackwell PG, Ramsey CB, Buck CE, Burr GS, Edwards RL, Friedrich M, Grootes PM, Guilderson TP, Hajdas I, Heaton TJ, Hogg AG, Hughen KA, Kaiser KF, Kromer B, McCormac FG, Manning SW, Reimer RW, Richards DA, Southon JR, Talamo S, Turney CSM, van der Plicht J, Weyhenmeyer CE (2009) IntCal09 and Marine09 radiocarbon age calibration curves, 0-50,000 years cal BP. Radiocarbon 51:1111–1150

Rodolfo KS, Umbal JV (2008) A prehistoric lahar-dammed lake and eruption of Mount Pinatubo described in a Philippine aborigine legend. J Volcanol Geotherm Res 176(3):432–437. doi:http://dx.doi.org/10.1016/j.jvolgeores.2008.01.030

Shen J (2013) Spatiotemporal variations of Chinese lakes and their driving mechanisms since the Last Glacial Maximum: a review and synthesis of lacustrine sediment archives. Chin Sci Bull 58(1):17–31

Sun D, Bloemendal J, Rea DK, Vandenberghe J, Jiang F, An Z, Su R (2002) Grain-size distribution function of polymodal sediments in hydraulic and aeolian environments, and numerical partitioning of the sedimentary components. Sediment Geol 152(3–4):263–277. doi:http://dx.doi.org/10.1016/S0037-0738(02)00082-9

Talbot M, Lærdal T (2000) The Late Pleistocene - Holocene palaeolimnology of Lake Victoria, East Africa, based upon elemental and isotopic analyses of sedimentary organic matter. J Paleolimnol 23(2):141–164. doi:10.1023/A:1008029400463

Thompson R, Oldfield F (1986) Environmental magnetism. Springer, Dordrecht

Wang S, Dou H (1998) Lakes in China. Science Press, Beijing, pp 506–509 (in Chinese)

Yan J, Zhao J-X (2008) Cenozoic alkali basalts from Jingpohu, NE China: the role of lithosphere–asthenosphere interaction. J Asian Earth Sci 33(1–2):106–121. doi:http://dx.doi.org/10.1016/j.jseaes.2007.11.001

Zhang Z, Feng C, Li Z, Li S, Xin Y, Li Z, Wang X (2002) Petrochemical study of the Jingpohu Holocene alkali basaltic rocks, northeastern China. Geochem J 36(2):133–154

Chapter 8
Palaeohydrological and Palaeoenvironmental Fluctuations of the Historic Eurimji Lake

Ju Yong Kim, Wook-Hyun Nahm, Dong-Yoon Yang, Sei-Sun Hong, Sang-Heon Yi, Han-Woo Choi, Jaesoo Lim, Jin-Young Lee, Jin-Cheul Kim, Jin-Kwan Kim, Kyeong-Nam Jo, Kota Katsuki, Hyo-Seok Park, Kenji Kashiwaya, Noriko Hasebe, Keisuke Fukushi, Noritake Endo, Ji Shen, Yong Wang, and Keun-Chang Oh

Abstract Lake Eurimji is located in the northern part of Jaecheon, Chungbug Province, in South Korea. It is well known for its scenic beauty as a nationally registered landscape site (Yang GS, Jungwon Munhwa 14:1–38, 2010). Since the late Bronze Age, its water has been used for agricultural irrigation. The lake was initially formed at the mouth of a fanglomerate where Jurassic granites blocked

J.Y. Kim (✉) • W.-H. Nahm • D.-Y. Yang • S.-S. Hong • S.-H. Yi • H.-W. Choi • J. Lim • J.-Y. Lee J.-C. Kim • J.-K. Kim • K.-N. Jo • K. Katsuki • H.-S. Park
Department of Quaternary Geologic Research, Geologic Research Division, Korea Institute of Geoscience and Mineral Resources, 124 Gwahang-no, Yuseong-gu, Daejeon 305-350, Korea
e-mail: kjy@kigam.re.kr

K. Kashiwaya
Institute of Nature and Environmental Technology, Kanazawa University, Kakuma, Kanazawa 920-1192, Japan

Department of Geography, National Taiwan University, Daan District, Taipei 10617, Taiwan

N. Hasebe
Institute of Nature and Environmental Technology, Kanazawa University, Kakuma, Kanazawa 920-1192, Japan

Korea Institute of Geoscience and Mineral Resources, 124 Gwahang-no, Yuseong-gu Deajeon 305-350, South Korea

K. Fukushi
Institute of Nature and Environmental Technology, Kanazawa University, Kakuma, Kanazawa 920-1192, Japan

N. Endo
Department of Earth Sciences, Graduate School of Natural Science & Technology, Kanazawa University, Kanazawa, Ishikawa 920-1192, Japan

J. Shen • Y. Wang
State Key Laboratory of Lake Science and Environment, Nanjing Institute of Geography and Limnology, Chinese Academy of Sciences, 73 East Beijing Road, Nanjing 210008, P.R. China

K.-C. Oh
Quaternary Laboratory, Quaternary Environment Research, Daejeon 305-340, Korea

K. Kashiwaya et al. (eds.), *Earth Surface Processes and Environmental Changes in East Asia*, DOI 10.1007/978-4-431-55540-7_8

the main course of a stream channel at about 305 m above sea level (m.a.s.l.). Natural levees grew laterally near the main outlets of the fan-valley mouth up to about 307 m.a.s.l. The lake accumulated organic sandy mud on the sand-and-gravel streambeds extending toward the southern valley mouth near Yongdu Mt., the ages of which were dated as early as ca. 3,000 calibration years Before Present (cal-yr BP). The early evidence of lake deposits is supported by radiocarbon ages for organic muds below the lowermost artificial layers in Lake Eurimji, which vertically constitute the bottom of Eurimji bank or dyke at about 306.5 m.a.s.l. The height is about 15 m. The present study reconstructs the paleo-precipitation of Lake Eurimji by applying an age mode to core sediments in the ER3-1 borehole using the mean grain size of sediments trapped at the bottom of the lake. The results show that lake sediments accumulated at an extremely high rate, ca. 3.49 mm/year during the Early Three Kingdoms Period, around 2,120–1,340 cal-yr BP. The average grain size of the trapped sediments is proportional to the total amount of precipitation during the elapsed time of each monitoring session. Both the paleoclimatic cyclicity and historical documents indicate that droughts in the lake catchment areas prevailed at 80 AD, 120 AD, 160 AD, 310 AD, 350 AD, 460–500 AD, and 620 AD, while relatively wet conditions occurred at approximately 90 AD, 150 AD, 200 AD, 240 AD, 320 AD, 360 AD, 435 AD, and 530 AD. These drought records suggest a multi-decadal cyclicity, particularly during the Early Three Kingdoms Period. This may imply that multi-decadal to century scale fluctuations of winter and summer monsoons controlled the sedimentary regime of Lake Eurimji catchment areas during this period in South Korea.

Keywords Lake catchment • Sediment trap • Paleo-precipitation • Lake monitoring • Historical document • Drought frequency

8.1 Introduction

Lake Eurimji is the oldest historical human-made reservoir lake on the Korean peninsula; however, its exact age remains controversial. Lee (1959) suggested that the lake might have been constructed in the Iron Age, around 2,000 BP, whereas several other studies have argued that the lake was not built until the reign of King Jinheung of the Silla Dynasty (ca. 540–576 AD). The latter opinion is supported by legends related to several places named after Ureuk, a famous master of the Gayakeum, a musical instrument, in the Jecheon area during this king's reign. Lake Eurimji, located at the valley mouth of the Mt. Yongdu catchment area, is now famous for its scenic beauty. Its origin may be studied by dating the construction of its banks or based on the earliest accumulation of the bottom sediment (Kim et al. 2000a, b). It remains debatable as to whether or not the lake existed at approximately ca. 2,000 yr BP (Kim et al. 2009a, b, 2010). To better understand the establishment of Lake Eurimji, it is important to obtain as many radiocarbon ages as possible from the bottommost part of its banks (Kim et al. 2012). The aims of the present study were to reveal the ages of the oldest sediments in the lake, below the Eurimji bank; obtain undisturbed bottom sediment cores and trace changes in the lake environment;

and compare paleoclimatic signals of sediment cores to extreme drought periods recorded in historical documents. To date the initial construction of Lake Eurimji, and document the paleoenvironmental and paleohydrological changes in the lake, we obtained radiocarbon dates of lake bottom sediments, gathered multi-proxy data on sediment cores, and collected trap sediments from the bottom of the lake.

8.2 Background of Study Area

The Lake Eurimji reservoir (37°10′6.9″N, 128°12′38.0″E), located at approximately 300 m above sea level (m.a.s.l.; Fig. 8.1), has been used as a water reservoir for irrigation. The reservoir has a maximum depth of 7 m, a 2-km-long shoreline, a water surface area of 158,677 m^2, and a water storage capacity of 6,661,891 m^3 (Fig. 8.1). The height of the levee is about 11 m, and the total length is about 320 m (Jecheon City Office 2010). The Haso stream, which originates from Mt. Yongdu (871 m), brings freshwater into the lake. At the higher elevations around Mt. Yongdu (400–900 m), the main bedrock type is Precambrian granitic gneiss, and the slopes are generally steep and stepwise. Jurassic biotite granite is prevalent at lower elevations (270–400 m), where a valley plain with a relatively gentle slope once existed at the mouth of the reservoir (Kim et al. 2012). Due to differences in geological features and weathering rates, the slope of Haso stream changes at a knickpoint approximately 2.4 km upstream of the lake. The lake includes several alluvial cones (fans) consisting of sand and gravel, which were formed during the Last Glacial Period (Kim et al. 2012). The fan system exhibits three steps of incision, which are recognized as a low terrace system (Kim et al. 2012; Lee 2010). The terraces exhibit signs of frequent landslides, which are seen along the fore-edges and escarpments. Near the lake, the valley deepens as a result of strong differential erosion derived from faults after emplacement of Jurassic granite. The valley is topographically protected from severe winter monsoons, and therefore the downstream area of the Eurimji valley has favorable conditions for agriculture. It has been assumed that the construction of agricultural paddies started in the beginning of the late Bronze Age (close to 2,800 yr BP), based on the general occurrence of paddy remains in the middle part of South Korea (Lee 2006, 2010; Jang 2010; Seong 2010). The primary land use in this area has not changed in the last two millennia. At higher elevations in the Mt. Yongdu catchment, the land cover is mainly pine and broadleaf forest. The lower elevation areas are occupied mostly by agricultural lands where rice has been cultivated. The irrigation season extends from March to June, with the highest demand in April and May. The Eurimji reservoir is located in the mid-latitude temperate zone, which is characterized by seasonal winds and a continental climate. In recent decades, the seasonal mean temperatures have varied from −5.3 °C in January to 23.7 °C in August, with a yearly mean temperature of 10.2 °C. The annual mean rainfall in the area is 1,295 mm. This region receives 55 % of its precipitation during the summer monsoon season (Jecheon City Office 2010).

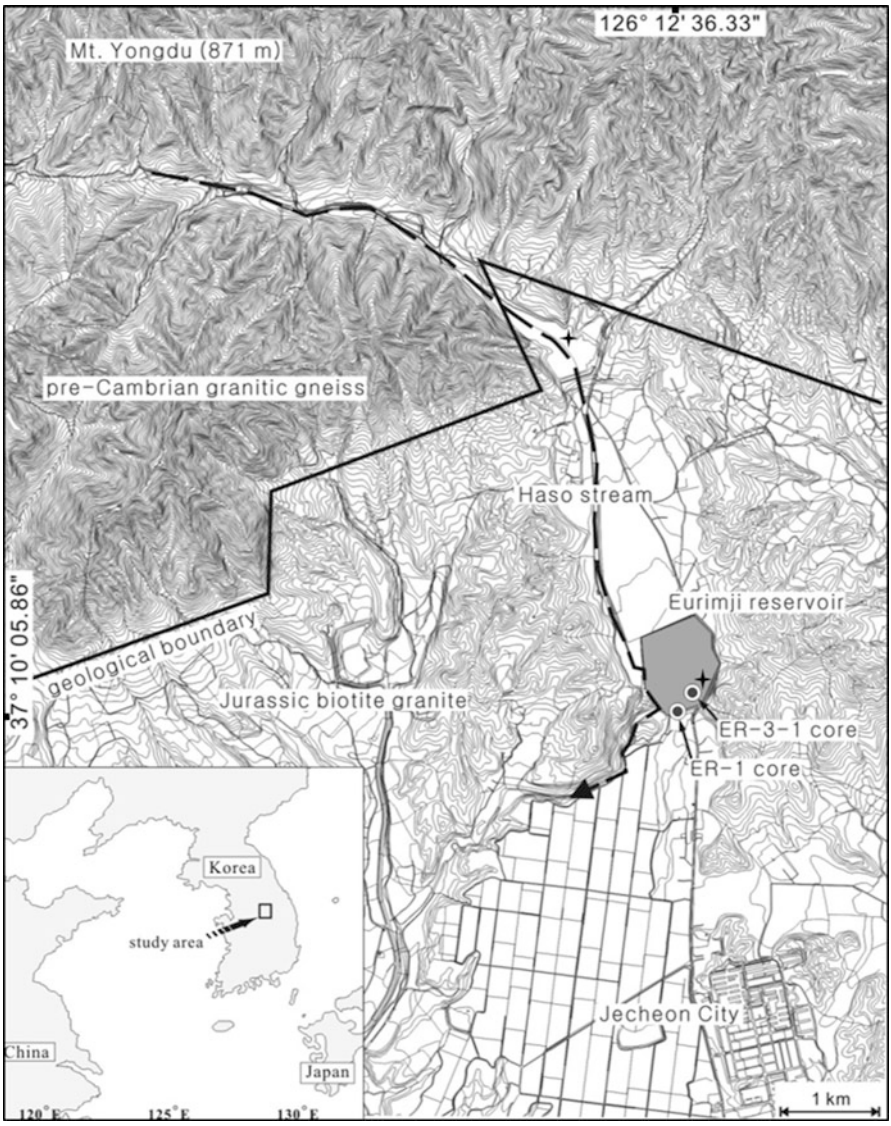

Fig. 8.1 Map of Lake Eurimji (Figure slightly modified from Nahm et al. 2012)

8.3 Materials and Methods

Echo-sounding and ground penetration radar surveys of Eurim Lake (Fig. 8.2a–d; Kim et al. 2000a, b) covered the general background of Lake Eurimji. We observed the boundaries between natural sandy gravels with organic-rich lake sediments and constructed anthropological layers in the outer Eurimji bank, where five trenches

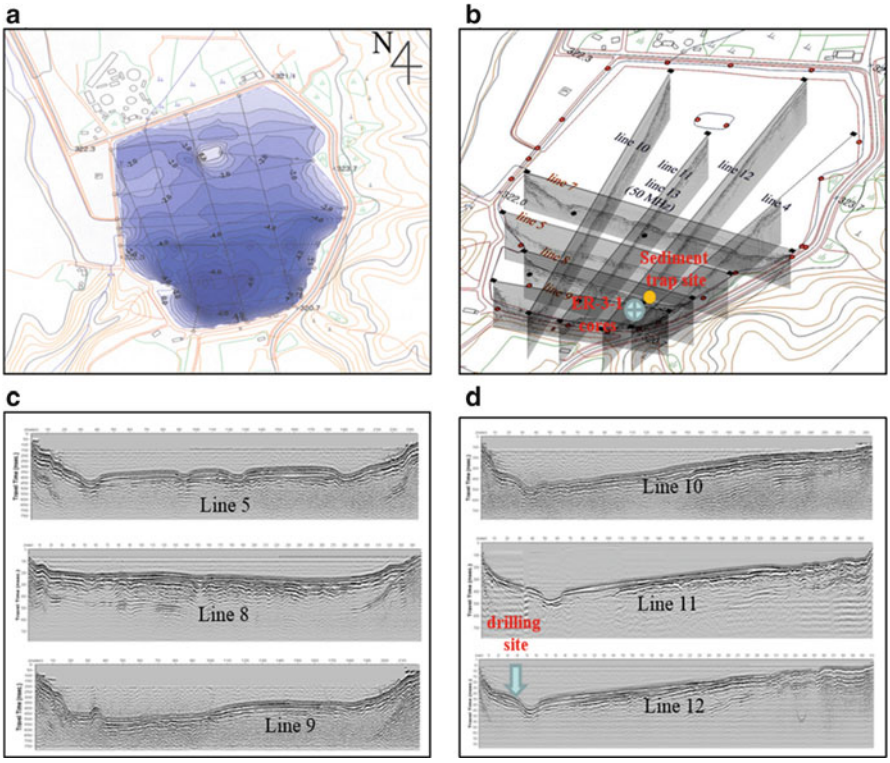

Fig. 8.2 Background information on Lake Eurimji: (**a**) bathymetric map, (**b**) GPR survey lines, (**c**) east–west bottom sediment profiles, and (**d**) north–south bottom sediment profiles

were dug by the Jungwon National Research Institute of Cultural Heritage in 2012–2013 (JNRICH 2014) (Fig. 8.3). Sediment traps were installed at the lake bottom to obtain bottom sediments, which was performed in late spring/summer/early autumn (April–September) and late autumn/winter/early spring (October–March) in two different years. Meteorological data were recorded at Jecheon Meteorological Post about 2 km from Lake Eurimji, and total precipitation was checked during each interval of lake sediment monitoring. In addition, extreme events documented in the Samguk-Sagi (Chronicles of the Three Kingdoms) were analyzed to determine every 10-year drought frequency during the Three Kingdom Period (50–650 AD). Sedimentological borehole logging was performed for the cores of the lake bottom (ER3-1, 37°10′06.97″N, 126°12′38.69E) (Fig. 8.1 and Table 8.1). ER-1 cores (Fig. 8.1) obtained from Eurimji bank in 2009 were used to reference artificial layers (Nahm et al. 2012; Kim et al. 2012). Cores (6.98 m long; ER3-1) were obtained from the reservoir bottom using a standard stationary piston sampler with an inner diameter of 74 mm. The core was cut and sliced at an interval of 0.5 m. The cores were sub-sampled in the laboratory at 1-cm intervals. After removing carbonates and organic matter using 10 % HCl and 30 % H_2O_2, respectively, a

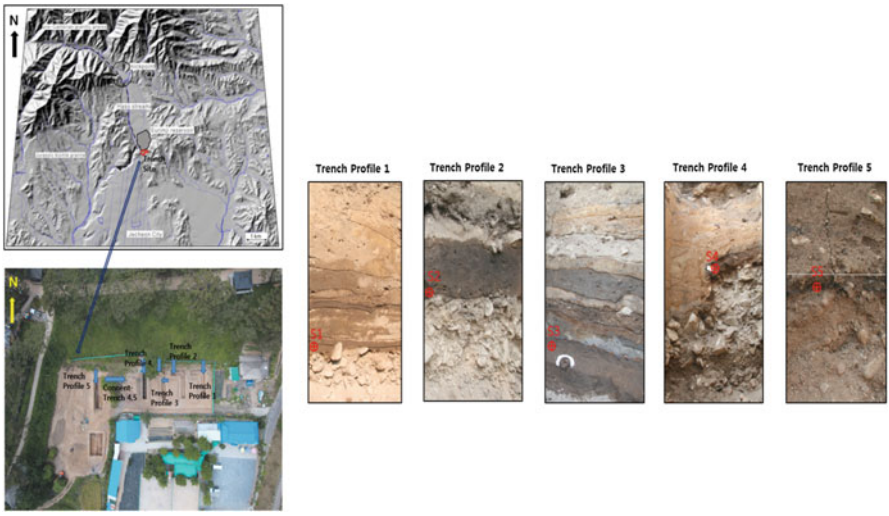

Fig. 8.3 Excavated trench sites in the outer bank of Lake Eurimji. Note: Radiocarbon ages of the bottom sediments are 1,740 ± 50 (*S1*) at trench profile 1, 1,740 ± 50 (*S2*) at trench profile 2, 1,740 ± 50 (*S3*) at trench profile 3, 1,740 ± 50 (*S4*) at trench profile 4, and 1,740 ± 50 (*S5*) at trench profile 5. The radiocarbon ages at the connected trenches 4 and 5 are listed in Table 8.1

Table 8.1 Geographical characteristics of the borehole drilled at the Lake Eurimji

Boreholes	Coordinates	Core length (m)	Altitude (m.a.s.l.)	Remarks
	Lat./Long.			
ER-3-1	N 37°10′06.97″	6.98	314.23-307.25	Lake Eurimji bottom
	E 126°12′38.69″			

grain-size analysis of the bulk sediment was performed using a Mastersizer 2000 laser particle analyzer (Malvern Instruments, Ltd., Worcestershire, UK) capable of detection in the 0.02–2,000-μm range, with sodium hexametaphosphate used as the dispersing agent. Eight samples for radiocarbon dating were obtained from the ER-3-1 sediment cores and organic muds with plant remains in bank bottoms. Radiocarbon ages were measured at the KIGAM AMS laboratory using an HVEE AMS/multipurpose beam line-MPS 4130-Tandetron device. The CalPal07 program (www.calpal-online.de) was used to convert radiocarbon ages (^{14}C yr BP) to calendar years (BC or AD) (Danzeglocke et al. 2008).

Low-frequency magnetic susceptibility was measured using an MS2 susceptibility meter (Bartington Instruments, Ltd., UK) with dual-frequency sensors. The averaged results were used to calculate the percent frequency-dependent susceptibility as defined by Thompson and Oldfield (1986). An aliquot of each of the sediment subsamples was dried to a constant weight at 60 °C, ground to a particle size of 0.063 mm, decalcified using 1N HCl, and then homogenized using an agate mortar and pestle. Aluminum capsules containing 2–3 mg of the processed

sediment samples were analyzed for total organic carbon (TOC) and total nitrogen (TN) concentrations were determined by combustion at 900 °C in a FlashEA-1112 (Thermo Finnigan S.p.A., Milan, Italy).

8.4 Results

8.4.1 Core Description

The core was subdivided into four sedimentary units (Fig. 8.4). From the bottom to the top, these were: unit 1 (307.25–308.02 m, 0.77-m thickness), unit 2 (308.02–310.55 m, 2.53-m thickness), unit 3 (310.55–311.90 m, 1.35-m thickness), and unit 4 (311.90–314.23 m, 2.33-m thickness). Figure 8.4 shows the profiles of several sedimentological and geochemical properties that were analyzed from core ER3-1. Table 8.2 summarizes the nine ^{14}C ages that were obtained from core ER3-1 and the profiles of excavated trenches (Nahm et al. 2012; JNRICH 2014).

– Unit 1 (307.25–308.02 m)

  The sediments in unit 1 were classified as S (sand) and zS (silty sand). The interval from 307.25 to 307.44 m included several sub-angular pebbles. One thin clay layer was intercalated from 307.48 to 307.53 m (5-cm thickness). An upward-fining trend was obvious from 307.56 to 307.98 m (Fig. 8.6).

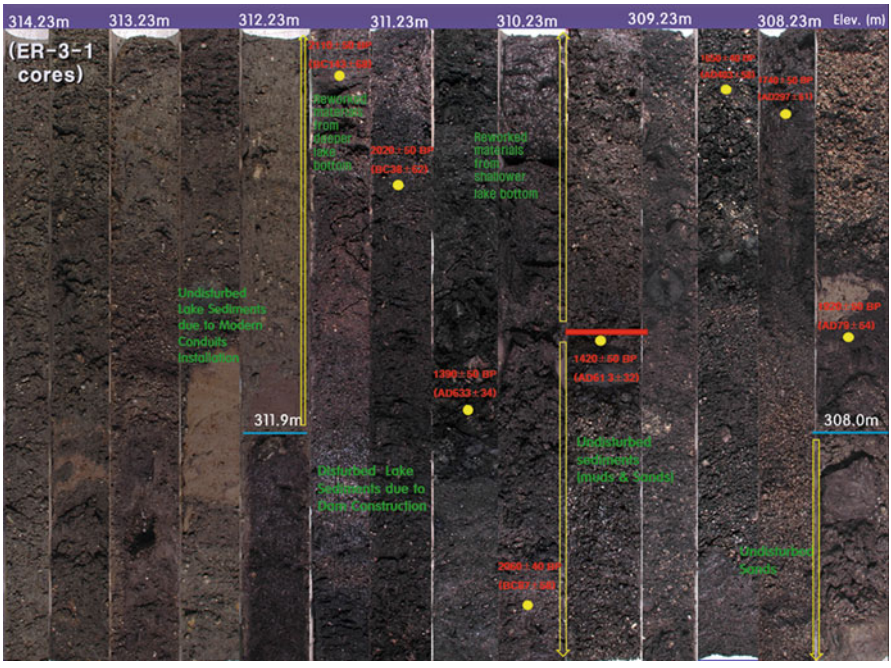

Fig. 8.4 Photographs of bottom sediment cores in Lake Eurimji

Table 8.2 Radiocarbon ages of core sediment ER3-1 taken from Lake Eurimji

Core	Sample ID	Material	Altitude (unit)	^{14}C yr BP	d^{13}C	Calendar year
ER-3-1	ISa090033	Bulk carbon	309.52 m (2)	1,420 ± 50	−26.0	AD 613 ± 32
ER-3-1	IWd090006	Plant fragment	309.45 m (2)	1,250 ± 50	−27.5	AD 768 ± 69
ER-3-1	ISa090102	Bulk carbon	308.81 m (2)	1,650 ± 40	−24.8	AD 403 ± 58
ER-3-1	ISa090034	Bulk carbon	308.05 m (2)	1,740 ± 50	−23.6	AD 297 ± 61
ER-3-1	ISa090035	Bulk carbon	307.51 m (1)	1,920 ± 50	−24.0	AD 79 ± 54
ER-B-1	KGM-Isa120028	Bulk carbon	306.40 m (0)	2,020 ± 30	−24.7	BC 24 ± 84
ER-B-3	KGM-Isa120029	Bulk carbon	304.90 m (0)	2,420 ± 40	−27.6	BC 497 ± 98
ER-B-3	KGM-Isa120030	Bulk carbon	305.10 m (0)	2,550 ± 30	−28.7	BC 772 ± 29
ER-B-3	KGM-Isa120031	Bulk carbon	306.20 m (0)	2,500 ± 30	−22.8	BC 650.5 ± 32.5

– Unit 2 (308.02–310.55 m)
  Silt and sand were dominant. The sediments in unit 2 were classified as zS and sZ (sandy silt). Unit 2 was characterized by four layers of plant matter (308.5, 309.0, 309.4, and 310.4 m) between sediments, and the spacing between layers varied from 50 to 90 cm. AMS ^{14}C dating of the bulk carbon in the sediments that were sandwiched between the plant layers indicated an age of about 2,000–1,600 ^{14}C yr BP, but the results from the plant materials indicated a range 1,300–1,200 ^{14}C yr BP. The upper part of unit 2 (−309.52 m.a.s.l.) was disturbed artificially after ca 1,200 yr BP.
– Unit 3 (310.55–311.90 m)
  Unit 3 was composed of dark gray to black zS and sZ. Some pebbles were observed around 311.56-m elevation. Unit 3 was also disturbed artificially after ca 1,200 yr BP.
– Unit 4 (311.90–314.23 m)
  This unit consisted primarily of yellowish-brown sZ, with some clay layers. This unit showed increased magnetic susceptibilities. Present-day garbage (styrofoam) was found at around 312.80 m. It was also disturbed by ancient agricultural activity.

To construct a meaningful age model based on radiocarbon ages, it may be important to confirm whether this core conforms to a linear age model. Only sediment cores below 309.5 m.a.s.l. were undisturbed, and thus we used sediment cores from between 309.5 and 307.25 m.a.s.l. to consider climate changes; we selected unit 1 (307.25–308.02 m) and the lower part of unit 2 (308.02–309.5 m) for further study of multi-proxy data.

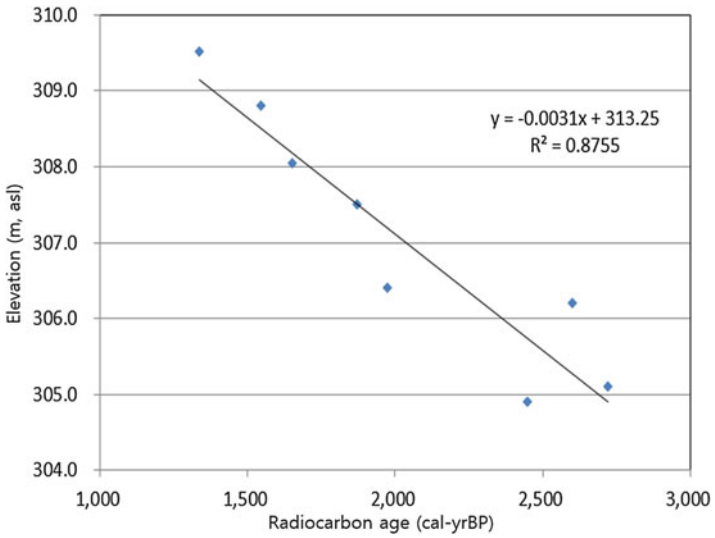

Fig. 8.5 Age model of bottom sediments in Lake Eurimji based on radiocarbon dating of an undisturbed core sediment (ER3-1)

8.4.2 AMS Dating

The results of the AMS dating are shown in Table 8.1. The oldest age of the bottom sediments was calculated to be ca. 1,920 yr BP from core ER3-1, but 2,500 yr BP based on the third, fourth, and fifth trenches of the outer bank. Above 309.5 m.a.s.l., the gray mud layer with plant fragments yielded an age of 1,200–1,300 yr BP from core ER3-1 (Nahm et al. 2012). However, the bulk sediment samples from the gray sandy mud layers obtained from the trench profiles at the outer bank revealed an older age than that reported in previous research (Nahm et al. 2012). Our data suggest that the oldest sediments date to the late Bronze Age. The accumulation rate of bottom sediments was calculated to be 3.49 mm/year (Fig. 8.5), an unusual and relatively high rate compared to a natural lake. This may have been caused by anthropological interference in the catchment area of this lake even below 309.5 m, while the upper elevations could have been heavily disturbed by the construction of the lake's banks at ca. 1,200 yr BP (Kim et al. 2012; Yang et al. 2009; Nahm et al. 2012).

8.4.3 Sediment Trap

Sediment traps were manufactured divided into four compartments on the bottom and installed oriented in a north and south direction at the southeastern corner of

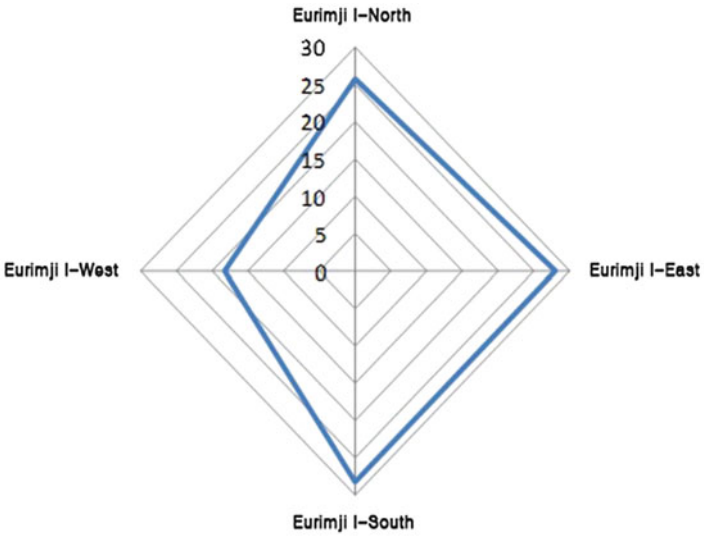

Fig. 8.6 Monitoring data obtained using an oriented sediment trap in Lake Eurimji

Lake Eurimji, where the ER-3-1 sediment cores were obtained, from October 2011 to April 2013. Bottom sediments were recovered biannually, and total weights and mean grain sizes were measured. We found that the total amounts of sediment derived from the north and east were higher than from the other two directions (Fig. 8.6).

The mean grain size was coarser in summer than in winter (Fig. 8.7). Accumulation of bottom sediment was indicative of a north- and east-direction anomaly of sediment inflow into the lake, depending on prevailing bottom currents. In the late spring and summer (April–September), both the amount of trap sediments and mean grain size increased, probably because of intense rainfall during the summer monsoon (Fig. 8.8).

8.4.4 Multi-proxy Data

Core ER3-1, taken between the elevations of 309.5 and 307.25 m.a.s.l., was used to determine environmental changes in the lake based on multi-proxy data (Fig. 8.9; Nahm et al. 2012). The bottom sediments were predominantly sands (~70 %) with some silts (~30 %) and clays (1–2 %). The mean grain size was 2.73–6.21 phi, with an average size of 3.52 phi (very fine sand) among 67 sub-samples analyzed below 309.5 m.a.s.l. The magnetic susceptibility (MS, Lf) was 704.3–3030.7 m-SI (mean, 704.3 m-SI). The mean TOC and TN values were 0.8 wt.% (0.28–1.71 wt.%) and 0.05 wt.% (0.02–0.11 wt.%), respectively. The mean TOC/TN ratios ranged

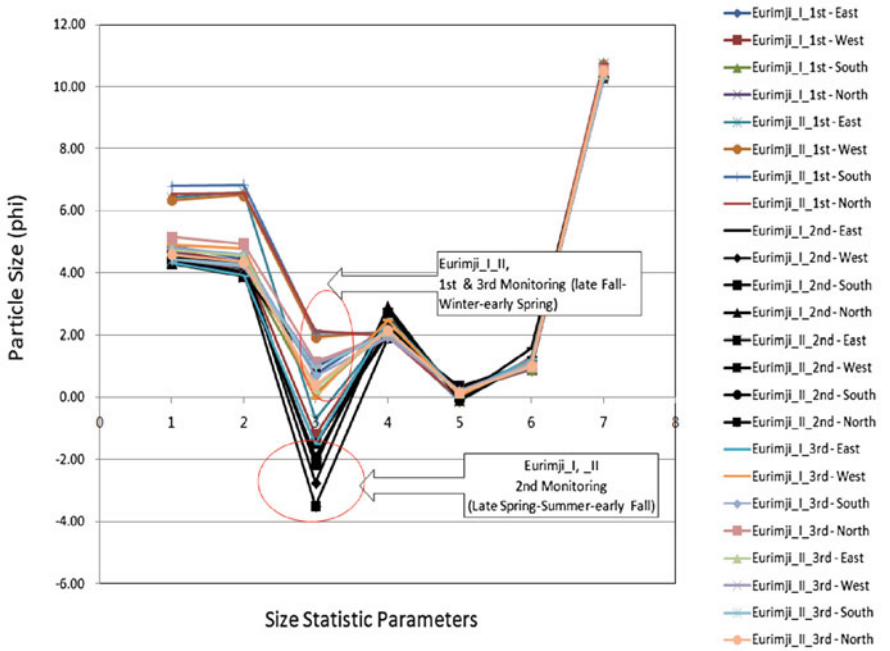

Fig. 8.7 Weight of bottom sediment obtained from Lake Eurimji

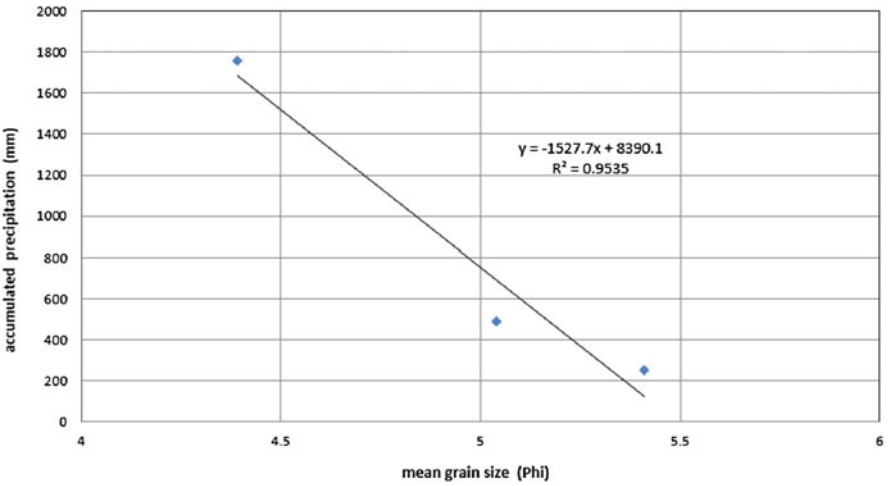

Fig. 8.8 Mean grain size versus rainfall during the monitoring period in Lake Eurimji

between 11.9 and 33.1, averaging 18.2. In unit 1 (N = 22) the mean grain size, MS, TOC, TN, and TOC/TN were 3.66 phi, 395.4 m-SI, 0.44 wt.%, 0.03 wt.%, and 14.0, respectively. In the lower part of unit 2 (N = 44) the values were 3.44 phi,

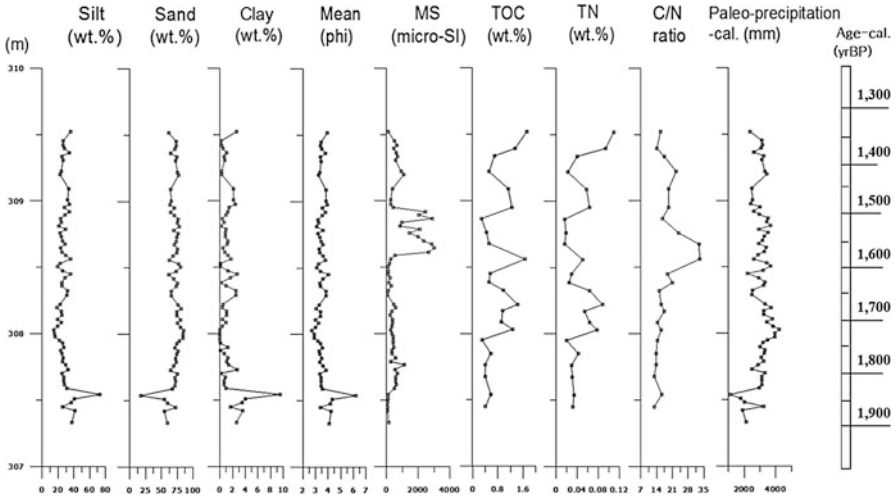

Fig. 8.9 Grain size, magnetic susceptibility, TOC, TN, T/C, and paleo-precipitation (calculated) between 1,400 and 1,900 cal-yr BP

858.8 m-SI, 0.95 wt.%, 0.05 wt.%, and 19.6, respectively. This implies that bottom sediments in unit 2 are coarser with a higher MS than those in unit 1; they also have more organic carbon and nitrogen (Nahm et al. 2012).

8.5 Documentary Records (Samguk-Sagi)

Written documents related to extreme climate events are available from Samguk-Sagi. Extreme drought signals were expressed as "no rain, dry, very or extremely dry." In particular, during the Silla Dynasty, drought frequency was very high during the periods 286–335 AD, 786–835 AD, and 886–935 AD (Table 8.3). In this study the raw data were compiled and re-arranged in 10 year-cycles to correlate with the bottom sediments of Lake Eurimji cores (ER3-1).

8.6 General Discussion

8.6.1 Age of Lake Eurimji Reservoir

Previously, the Eurimji reservoir was thought to have been constructed using stone dams during the late Iron Age, or 540–576 AD, during the reign of King Jinheung of the Silla Dynasty (Yang et al. 2009). However, some bank materials – including wood fragments, twigs, leaves, and seeds – may indicate a much younger date of

Table 8.3 Dryness frequency data based on the "Samguk-Sagi" (historical document of the Early Three Kingdoms Period) (KMI 2011)

Historical age (yr BP)	Number of dryness	Historical age (yr BP)	Number of dryness
1,340	1	1,620	0
1,350	1	1,630	3
1,360	1	1,640	1
1,370	2	1,650	1
1,380	1	1,660	1
1,390	0	1,670	2
1,400	0	1,680	0
1,410	1	1,690	2
1,420	1	1,700	2
1,430	0	1,710	0
1,440	1	1,720	1
1,450	5	1,730	0
1,460	0	1,740	3
1,470	2	1,750	1
1,480	0	1,760	2
1,490	1	1,770	1
1,500	1	1,780	0
1,510	0	1,790	0
1,520	0	1,800	1
1,530	2	1,810	1
1,540	3	1,820	0
1,550	1	1,830	1
1,560	1	1,840	1
1,570	2	1,850	1
1,580	0	1,860	1
1,590	0	1,870	2
1,600	0	1,890	1
1,610	1	1,990	0

construction (ninth century AD). These materials also suggest that ancient engineers constructed an earthen dam by mixing tree debris with tampered clays to prevent reservoir water seepage. Since the ninth century AD, the bottom sediments of the lake at ca. 310.4 m.a.s.l. have been repeatedly disturbed either due to bank repair or modern deliberate rupturing to avoid lake flooding during excessive rainfall. The age of the oldest lake sediments in the lake below Eurimji bank, however, has been controversial. The present study clarifies the age by dating sediments from the bottommost part of the Eurimji bank.

The bottom sediments contain four sedimentary layers, which formed in the following four stages: (1) the post-dam-construction upper mud layer; (2) the middle layer of the artificial fill related to the dam construction, (3) the lower lake layers, and (4) the lowermost alluvial layer of the initial valley (Kim et al. 2009a, b, 2010).

During the construction of the artificial bank at the southern end of the lake, many parts of the oldest bottom sediments above 309.5 m.a.s.l. were disturbed, and artificial bank materials were mixed with older bottom sediments of about 2,000 yr BP. Anthropogenetic mixing of layers is likely to be higher in sediment cores obtained from above 310.6 m.a.s.l., where disturbance from major bank construction carried out in the ninth century AD is evident (Nahm et al. 2012).

However, the lower layers of sediments were dated to ca. 1,920 yr BP (Table 8.2), and showed a linear pattern of sediment heights versus sediment ages to about 1,420 yr BP. In addition, they contained more muddy sands and gravels, as found in the excavation trenches at the outer wall of the Eurimji bank. The oldest sands and gravels below the bank materials are assumed to be derived from old valley-fills and fluvial deposits. This was also identified in core ER-1 (Fig. 8.1), particularly below 308.0 m (Nahm et al. 2012; Kim et al. 2012; Yang et al. 2009). This may suggest that the bottom sediments of the lake accumulated long before the construction of the major bank at ca. 1,200 yr BP. In fact, based on the ER3-1 core, the bottom sediments existed 1,920-2,550 yr BP. Our data suggest that ancient people could have built artificial levees using the gravel and sand material deposited at the bottom of the Eurimji Valley, particularly in a notched-shaped valley overlain by concavely fractured Jurassic basement rocks at the southwestern part of Lake Eurimji (Kim et al. 2000a, b). This concave part below the Eurimji bank was identified between trenches 4 and 5 during the excavation of the outer wall of the bank (Fig. 8.3).

8.6.2 Environmental Changes During the Early Three Kingdoms Period

Sediment cores taken from above 307.25 m up to the lower part of unit 2 in the ER3-1 borehole (309.5 m.a.s.l.) were relatively stable. As shown in Table 8.2, the oldest age was determined to be ca. 2,550 yr BP (−772 BC), which is considered the late Bronze Age on the Korean Peninsula. As shown in Fig. 8.9, the multi-proxy data indicate that the small mean grain size is related to the drought signals in general; therefore, relative drought periods may be inferred from the dominance of fine-grained sediments in Lake Eurimji. The drought periods included 80 AD, 120 AD, 160 AD, 310 AD, 350 AD, 460–500 AD, and 620 AD. Relative wet signals were found at 90 AD, 150 AD, 200 AD, 240 AD, 320 AD, 360 AD, 435 AD, and 530 AD (Fig. 8.10). In addition, five MS peaks were identified at approximately 160 AD (307.75 m), 275 AD (308.20 m), 390 AD (308.65 m), 440 AD (308.90 m), and 540 AD (309.25 m) (Fig. 8.9). These peaks were neither positively proportional to the TOC, TN, and C/N values nor related to grain size or size populations. This may reflect human interference since 2,000 yr BP. Considering both the stable bottom parts of the sediment cores and bottom sediments in the excavated trenches, we obtain a sedimentation rate as high as 3.49 mm/year (Fig. 8.5). This high rate of sedimentation may also reflect human interference in areas where vegetation was rather scarce (Kang et al. 2009). At about 308.2–308.6 m.a.s.l., palynological evidence is poor because of low palynological productivity between AD 380 and

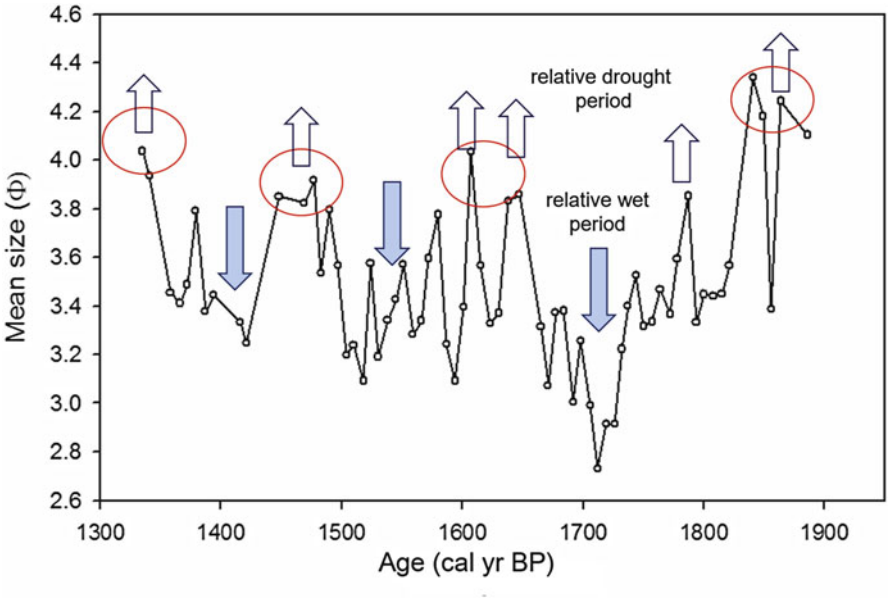

Fig. 8.10 Comparison of relative drought periods inferred from fine-grained sediments in Lake Eurimji during the Silla Dynasty (AD 50–650). Relative drought signals - 80 AD, 120 AD, 160 AD, 310 AD, 350 AD, 460–500 AD, and 620 AD; relative wet signals - 90 AD, 150 AD, 200 AD, 240 AD, 320 AD, 360 AD, 435 AD, and 530 AD

AD 285 (Kang et al. 2009). The low production might be influenced either by a dry climate in general or by human interference in or around Lake Eurimji catchment areas. Human influence may be more plausible because the sedimentation rate after 2,100–2,200 yr BP accelerated, as reported for the Paju Wetland, where since about the third century BC, the natural sedimentation rate has increased up to 0.16–0.29 mm/year (Nahm et al. 2012). However, this rate is far less than that seen in Lake Eurimji. This may be due in part to differences in prevailing agricultural activity between these sites.

Since the middle Bronze Age (ca. 3,500 yr BP) in Korea, agricultural activities have been widespread, and cultivation of rice, millet, barley, wheat, and soybean has been recorded at many archeological sites, including in association with Mumun pottery and Doldaemun, Gongyeolmun, and Ijungguyeon since ca. 1,500 BC (Lee 2006, 2010). Many small-scale agricultural paddy fields and agricultural tools have been documented at many excavation sites in Korea. Therefore, in Lake Eurimji catchment areas, the multi-proxy data may not represent pure natural signals of environmental change. However, sediment trap data from the monitoring site indicate that mean grain size increases with the total amount of precipitation, which applies in general to the ER-3-1 sediment cores, in which the mean grain size may be related to the total amounts of paleo-precipitation since 1,920 yr BP. This will elucidate possible changes in relative dryness and wetness in the Lake Eurimji catchment areas.

8.6.3 Historical Climatic Signals

Historical reservoirs have been excavated on the Korean peninsula. The Lake Eurimji reservoir bank was initially constructed from the late Bronze Age (ninth century BC) to the Iron Age (~first century AD), while the major construction was performed during the eighth century AD in the reign of King Wonseong of the Silla Dynasty. Baekgolje dam in Kimjye County was initially constructed in 330 AD, Sijye in Gyeonju City in 429 AD, Cheonjae in Youngcheon City in 531 AD, and Gonggeumji in Sangju City after 655 AD (Jang 2010; Seong 2010; Lee 2010; Yang et al. 2009). Construction of hydrological banks or dams suggests that ancient societies needed water reservoirs, as well as hydrological facilities, to enable agricultural activity during periods of drought. It is interesting that among the drought signals documented in Samguk-Sagi, the period between 286 AD and 335 AD is particularly conspicuous (Fig. 8.11). This may coincide with the construction age of Baekgolje dam in Kimjye County. Paleoclimatic signals based on sediment cores can also be compared to the drought signals recorded at Samguk-Sagi. In the present study on Lake Eurimji, we found that historical drought signs were associated with poor palynological productivity (Kang et al. 2009), small mean grain size (Fig. 8.10), and low MS (Fig. 8.9). Proxies (TOC, TN, C/N) related to biomass (Fig. 8.9), however, may not indicate any direct response to drought. In particular, the frequency of drought between 286 AD and 335 AD near Lake Eurimji may have been extremely high (Figs. 8.10 and 8.11), in line with Park and

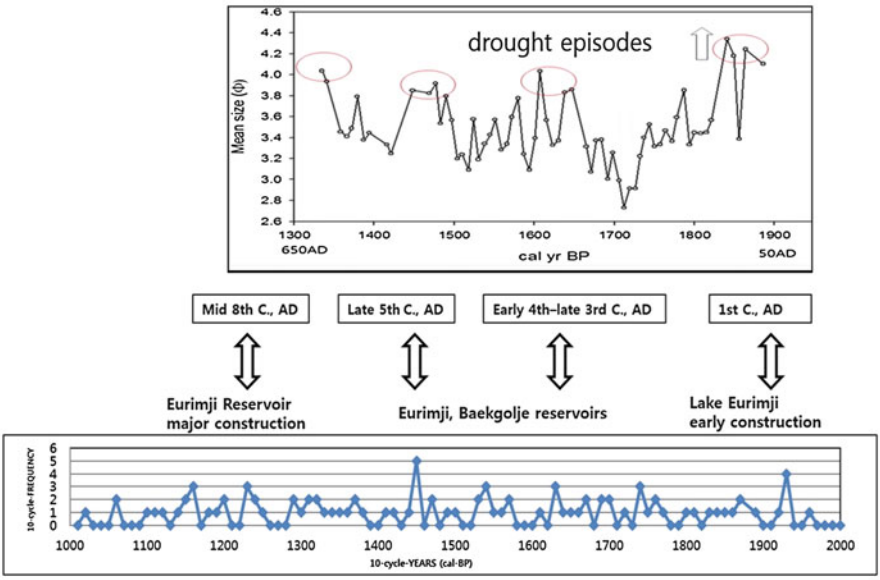

Fig. 8.11 Correlations of climatic changes between documentary records and bottom sediment cores

Rii (2007). Dry periods prevailed in the Korean Peninsula from 600 BC to about 800 AD, as is evidenced by data from the Yugu fluvial plain in the Keum River Basin and documented historical data from Samkuk-Sagi (Yoon and Hwang 2009; Lim et al. 2012).

8.7 Conclusion

The sediment layers of the Lake Eurmji reservoir consist of old alluvial (valley-fill) deposits in the lower part (<307 m.a.s.l.); pre-1,400 yr BP pre-damming natural lake deposits in the middle part (307–310.4 m.a.s.l.); and artificial material (310.4–315 m.a.s.l.) and heavily contaminated and disturbed post-damming lake deposits in the upper part (>315 m.a.s.l.). The earliest stone bank construction may have been initiated at ca. 2,000 yr BP during the late Iron Age. The major stage of construction took place during the time of the Unified Silla Dynasty, in the ninth century AD. The bottom sediments of the lowermost level of the reservoir were dated to the late Bronze Age to the early Iron Age based on the excavated trench profiles. The base of the Eurimji bank, composed of organic-rich sandy sediments and derived from natural processes, were dated to 2,550 yr BP (in excavated profiles) and 1,920 yr BP (in the reservoir).

A particularly severe drought period was found between 286 and 335 AD. This is consistent with a previous study by Park et al. (2007) that found drought signals in 311–320 AD. Historical extreme droughts may be associated with natural climatic changes that occurred in late 3rd and early fourth century AD in South Korea. The construction of an early Baekgolje dam (historically recorded in 330 AD, during the reign of King Biryu of the Baekje Dynasty) may also be associated with the prevalence of drought in the southern part of the Korean Peninsula. Radiocarbon ages of 2,550–1,920 yr BP in Lake Eurimji sediments and 2,020–1,720 yr BP in accumulated plant layers at the bottom of the Baekgolje dam both suggest that general dryness has prevailed since 2,000 yr BP in the southwestern part of Korea. In summary, it can be concluded that both Lake Eurimji reservoir sediments and Baekgolje dam sediments suggest that droughts in the Korean Peninsula induced nation-wide construction of hydrological banks or dams, particularly during the early Three Kingdoms Period (275–360 AD).

Acknowledgments This research was supported financially by the China-Japan-Korea international collaboration research project (2011–2013) funded by the National Research Foundation of Korea, and the Basic Research Project of the Korea Institute of Geoscience and Mineral Resources (KIGAM) funded by the Ministry of Knowledge Economy of Korea, and the Radioactive Waste Management of the Korea Institute of Energy Technology Evaluation and Planning (KETEP) grant funded by the Korea government Ministry of Knowledge Economy (2012171020001B).

References

Danzeglocke U, Joris O, Weninger B (2008) CalPal-2007. Available at: www.calpal-online.de
Jang HS (2010) Historical meaning and value of Lake Eurimji, Jecheon. J Jungwon Munhwa 14:163–184 (in Korean)
Jecheon City Office (2010) Unpublished data. Available at: www.okjc.net
JNRICH (Jungwon National Research Institute of Cultural Heritage) (2014) Report on the preliminary and site excavation in Lake Eurimji of Jecheon County. Jungwon National Research Institute of Cultural Heritage Academic Research Book 13:1–161
Kang S-J, Yi S, Kim JY (2009) Late Holocene environment and vegetation change of Eurimji Reservoir, Jecheon, Korea. Korean J Quatern Res 23(2):34–47
Kim JY, Yang DY, Lee J-Y, Yi S, Kim J-H (2000a) Preliminary geologic investigation of Lake Eurimji. Chungbuk National University Museum and Jaecheon City. Research Report 60:9–94 (in Korean)
Kim JY, Yang DY, Lee J-Y, Kim J-H, Yi S (2000b) Depositional environment and formation ages of Lake Eurimji. Korean J Quatern Res 14(1):7–32 (in Korean with English Abstract)
Kim JY, Yang DY, Nahm WH (2009a) Comparative research of bank materials and lake records of Lake Eurimji in Korea. Chungbuk Munwhaje Yeongu 3:5–22
Kim JY, Yang DY, Hong S-S, Yi S, Hwang S-H, Nahm WH, Lim J, Lee J-Y, Kim J-C, Kim J-K, Shin J-H, Yun H-S, Oh K-C (2009b) Quaternary geology and geoscientific analysis of Lake Eurimji, Jecheon County, Korea. KIGAM consulting report, pp 1–90 (in Korean)
Kim JY, Yang DY, Kang SJ, Yi SH, Nahm WH, Lim JS, Whang SH, Yun HS, Kim JK, Hong SS, Lee JY, Oh KC, Kim JC (2010) Process of Lake Eurimji formation and embankment construction Jecheon City, Korea. J Jungwon Munhwa 14:39–111 (in Korean)
Kim JY, Nahm WH, Yang DY, Shin J-H, Lee J-Y, Hong S-S, Kim J-K, Lee H-J, Krivonogov S, Safonova I (2012) The Eurim Lake and its hosting valley: a unique ancient reservoir with bank constructions in Korea. Trans Jpn Geomorphol Union 33(2):137–148
KMI (Korea Meteorological Institute) (2011) Meteorological records from ancient Korea including astronomical and seismological records from Samguk-Sagi (history of the three kingdoms) and Samguk-Yusa (memorabilia of the three kingdoms). KMA (Korea Meteorological Administration), Korea Meteorological Record Book 1:1–136
Lee BD (1959) History of Korea. Jindan Association, Eulyu Publishing Co., Seoul, pp 306–307 (in Korean)
Lee HJ (2006) Absolute dates of Mumun and Yayoi pottery. J Korea Archeol Soc 60:236–257 (in Korean with English Abstract)
Lee HJ (2010) Paleogeomological analysis of alluvial plain of Eurim Lake. In: Proceedings of the 2nd Eurimji symposium, Jecheon County Korea, pp 29–31
Lim J, Yi S, Nahm W-H, Kim J-Y (2012) Holocene millennial-scale vegetation changes in the Yugu floodplain, Kongju area, central South Korea. Quat Int 254:92–98
Nahm W-H, Kim J-Y, Lim J, Yu K-M (2011) Responses of the upriver valley sediment to Holocene environmental changes in the Paju area of Korea. Geomorphology 133:80–89
Nahm W-H, Kim JK, Kim J-Y, Lim J, Kim JC, Yu K-M (2012) Topographical evolution and 14C age dating of the construction of the Eurimji reservoir (Jecheon, Korea). J Archaeol Sci 39:3706–3713
Park C, Rii HU (2007) A study on drought and heavy rain in the period of three kingdoms of Korea. J Climat Res 2(2):94–104
Seong JY (2010) The feature and significance of Lake Eurimji through development of ancient irrigation facilities in Korea. J Jungwon Munhwa 14:103–126
Thompson R, Oldfield F (1986) Environmental magnetism. Allen and Unwin, London, 227pp
Yang GS (2010) Historicity and value of Jecheon Eurimji. J Jungwon Munhwa 14:1–38

Yang DY, Kim JY, Nahm WH, Yi S, Lim J, Kim JK, Yun HS (2009) Environmental change of Eurimji area before levee construction and source material of the levee analyzed by geochemistry. J Korean Geomorphol Assoc 16(4):101–107 (in Korean with English Abstract)

Yoon S-O, Hwang S (2009) The natural hazards and drought periodicity in Korea during the ancient times based on Samguksaki. J Korean Geogr 44(4):497–509

Chapter 9
Late Quaternary Environmental Changes of the Hwajinpo and Songjiho Lagoons on the Eastern Coast of Korea

Jong-Gwon Yum, Keiji Takemura, Kang-Min Yu, Wook-Hyun Nahm, Sei-Sun Hong, Dong-Yoon Yang, Kota Katsuki, and Ju Yong Kim

Abstract The Hwajinpo and Songjiho lagoons, located 25 km apart on the mid-eastern coast of Korea, are known tectonically stable. Two core sediments were obtained from the Hwajinpo lagoon (HJ99) and Songjiho lagoon (SJ99). Lithologic, geochemical and paleontological data include grain size, water content, magnetic susceptibility, soft X-ray of core samples, TOC, TN, C/N, TS, C/S, assemblages of mollusc and palynomorphs remains. Based on multi-proxy data, six main lithological units were identified in both lagoons, indicative of paleoenvironmental changes during the Holocene, as well as the evolutionary histories of each lagoons related to Holocene sea level changes of the East Sea (Japan Sea). The environmental changes of both lagoons are considered mainly due to the lake/sea level fluctuation during the Late Quaternary because the mineral composition analysis does not show any provenance changes. Although the lithologic changes in the both lagoons do not show any temporal similarity, T-R (transgression and regression) trends based on the grain size variation shows simultaneity. T-R diagram presents three cycles clearly since 7,800 ^{14}C yr BP. Highstand sea levels (transgressions) are appeared at about 7,400, 5,500, and 2,200 ^{14}C yr BP, while lowstand sea levels (regressions) at about 6,500, 4,100, and 1,800 ^{14}C yr BP during the Holocene. Especially, the anthropogenic deposits in both lagoons since about 300 cal-yr BP

J.-G. Yum
Exploration Department, Korea National Cooperation, 305 Jongga-ro, Jung-gu, Ulsan 681-816, Korea

K. Takemura
Beppu Geothermal Research Laboratory, Institute for Geothermal Sciences, Graduate School of Science, Kyoto University, Beppu 874-0903, Japan

K.-M. Yu
Department of Earth System Sciences, Graduate School of Sciences, Yonsei University, 134 Shinchon-dong, Sodaemun-ku, Seoul 120-749, Korea

W.-H. Nahm • S.-S. Hong • D.-Y. Yang • K. Katsuki • J.Y. Kim (✉)
Department of Quaternary Geologic Research, Geologic Research Division, Korea Institute of Geoscience and Mineral Resources, 124 Gwahang-no, Yuseong-gu, Daejeon 305-350, Korea
e-mail: ydy@kigam.re.kr; kjy@kigam.re.kr

K. Kashiwaya et al. (eds.), *Earth Surface Processes and Environmental Changes in East Asia*, DOI 10.1007/978-4-431-55540-7_9

show relatively very high sedimentation rate than previous depositional units. The rapid sedimentation was due to human activities, agricultural reclamation and/or deforestation in both lagoon-catchment areas.

Keywords Hwajinpo Lagoon • Songjiho Lagoon • Depositional environment • Late Quaternary • Holocene • Core sediments • Multi-proxy • East Sea (Sea of Japan) • T-R diagram • Sea level change

9.1 Introduction

Lagoons occupy 13 % of coastal areas worldwide, and are often impacted by both natural and anthropogenic influences (Mee 1978; Sikora and Kjerfve 1985; McRae et al. 2000). Present lagoons exhibit salinities that range from completely fresh to hypersaline, depending on local climatic conditions, (Kjerfve 1994; Moore and Slinn 1984; Sakaguchi et al. 1985; Kjerfve and Magill 1989; Knoppers et al. 1991; Nakata et al. 2000; Smith 2001). In other word, costal lagoonal sediment should be a sensitive recorder of influence on local climate change, as well as relationship between sea and land area including human activity.

Coastal lagoons formed as a result of rising sea level mostly during the Holocene and the building of coastal barriers by marine processes (Kjerfve 1994; Matsubara 2000). Many sedimentary researches on coastal lagoon system indicate that the origin and geological histories of coastal lagoon are associated with the sea level changes during late Quaternary (e.g. Dominguez et al. 1987; Kraft et al. 1981; Omoto 1979; Koba et al. 1982; Selivanov 1996; Morton et al. 2000). Lagoonal systems can provide understanding changes in sea level because even for a small variation of sea level, the lagoonal system responds sensitively (e.g. Endo et al. 1982, 1989; Jujii and Fuji 1982; Howell et al. 1988; Cater et al. 1989; Eitner 1996; Kirk and Lauder 2000; Li et al. 2001).

The Hwajinpo Lagoon (38°27′N, 128°28′E) located on the eastern coast of Korea is the largest coastal lake in South Korea and Songjiho which 25 km southward away from the Hwajinpo is the fifth one. Since they located near the DMZ (demilitarized zone) the border with North Korea, the lagoons preserved the sediment records without disturbing of the modern industrial developments (Yum 1996). This study area of Hwajinpo and Songjiho lagoons reported tectonically stables and it means that the study areas provide the record of the eustatic sea level fluctuation.

Bak et al. (2013) indicate rich diatom production at about 5,000 yr BP in Songjiho Lagoon. And it could be useful for comparing the sea level fluctuation of Japanese Islands side that is tectonically active area in the East Sea (Japan Sea). These lagoons of the study area have a potential of containing a continuous record of paleoclimate in the late Quaternary period. Otherwise, they are located on the boundary of the warm and cold current (Bukan cold current which are branch of Liman current and Dongan warmcurrent which are branch of Kuroshio warm current), and also provide the information of circulation history of East Sea. There are several previous researches like ecological and fishery studies (e.g. Uhm 1971,

1973), however a few have reported the geologic and environmental aspect of both lagoons. Jung and Park (1976) reported for bottom sediment distribution of the Hwajinpo, Park and Kim (1981) for sand barrier developments, and Yum et al. (2003, 2004) for recent depositional environment of the Hwajinpo Lagoon. Hwajinpo and Songjiho Lagoons have been interested target areas for many researcher for the sea level changes during the Holocene (Okada 1978; Korotkii 1985; Minoura et al. 1997). Up to now previous researches of coastal lagoons are mostly resulted from the western coast areas in Japanese Island Arc, which are known active tectonic block. Instead, in Korean peninsula lagoons are located in tectonically stable areas. Lithological and geochemical analysis to core samples from lagoons should provide information on reconstruction of the paleoenvironments during the Holocene, and ascertaining sea level fluctuation. In Korean peninsula we may also identify the sea level rising episodes, particularly thick massive muds in unit 5 of MW-1 cores, unit 2 in MW-2 cores, unit 3 in JD-1 cores, unit 5 in IL-3 cores (the Youngsan estuarine river mouth), as well as unit 1 in CL-4 cores and unit 2 of HY cores (Pyeongtaek wetland), which are all indicative of strong influence of brackish or marine environment (Nahm et al. 2008, 2013; Nahm and Hong 2014; Bloom and Park 1985).

The object of this research is to reveal the stages of depositional environments, trace trending of transgression and regression of lagoonal system, and improve the evolution model of Lagoons with sea level changes based on multi-proxy data, encompassing lithologic units, water contents, grain size, mineral composition, TOC-TN-C/N, TS-C/S, biogenic records, as well as age model.

9.2 Background of Study Area

The Hwajinpo Lagoon is composed of two small brackish water lakes (Inner Lake and Outer Lake of the Hwajinpo) connected to each other by a narrow and shallow channel (Fig. 9.1). It has the area of 2.4 Km^2 with a maximum depth of 3.7 m. Two mainstreams drain into the Inner Lake of Hwajinpo Lagoon. The drainage basin is distributed in limited small area, and the width of largest stream is about 5 m near the river mouth (Fig. 9.2). The Outer Lake of the Hwajinpo has a shallow inlet to the sea, which is connected only during rainy summer season (the monsoon season) or by seawater inflowing due to high waves. Halocline has developed in each lake and is controlled by the flux of fresh water during the summer. And for the last 200 years the Hwajinpo Lagoon has been brackish water condition (Yum et al. 2003).

The Songjiho Lagoon, the fifth largest natural lake in the South Korea, is brackish water coastal lagoon (Fig. 9.3). It has an area of 0.63 km^2 with a maximum depth of 2.6 m. It is composed of two different small lakes as the Hwajinpo Lagoon. However, the lakes are connected with deep channel that the different water bodies can move easily into each lake.

The tidal range is less than 50 cm on the both lagoons. Annual precipitation ranges from ca. 1,200 to 1,300 mm in the study area, and temperatures range from −4 to 26 °C, with the annual mean temperature at 11 °C. Ice-covering of both lagoon in winter is unusual as influence of the saline water body.

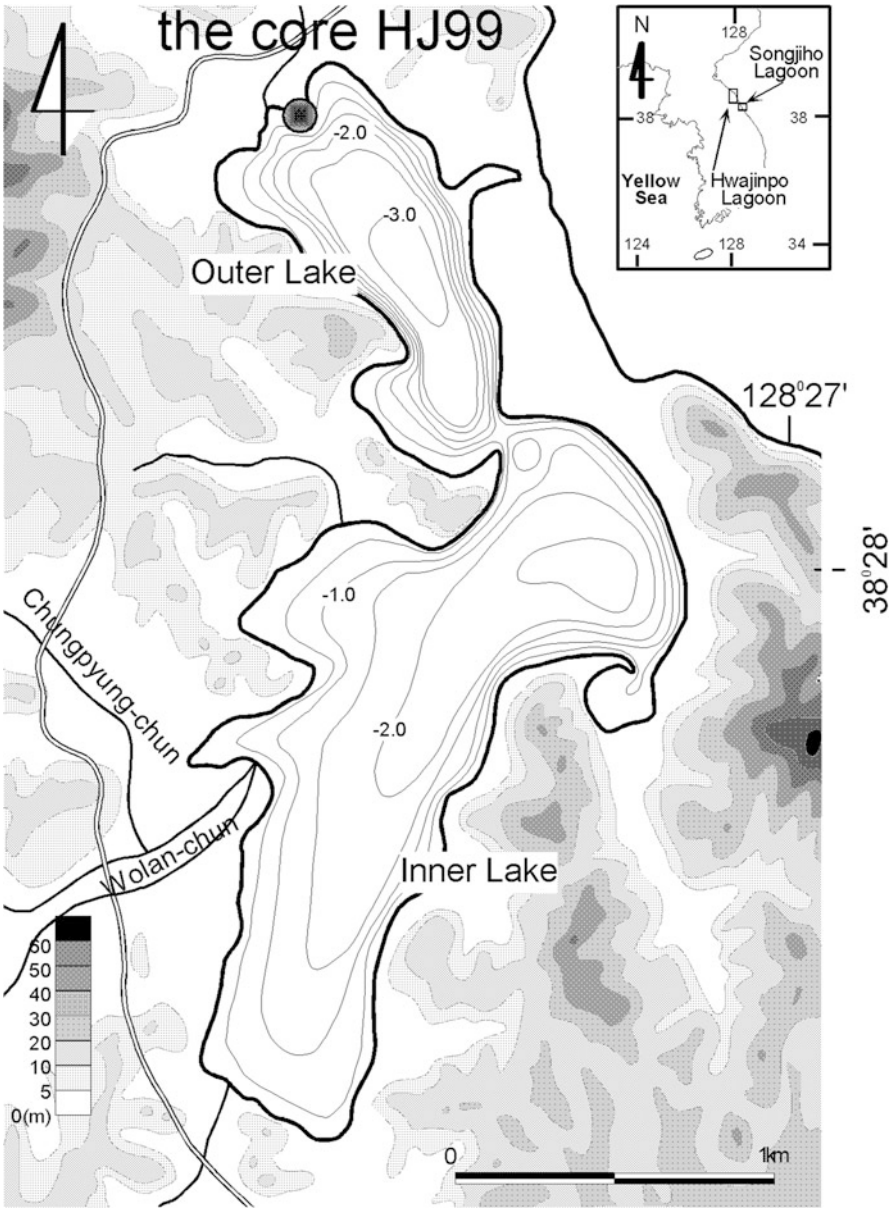

Fig. 9.1 The location of the Hwajinpo Lagoon on the eastern coast of Korea including the site of the HJ99 core and a bathymetry map of the lagoon. The narrow channel between the inner and outer lakes of Hwajinpo Lagoon originated from the morphology of the basement rock

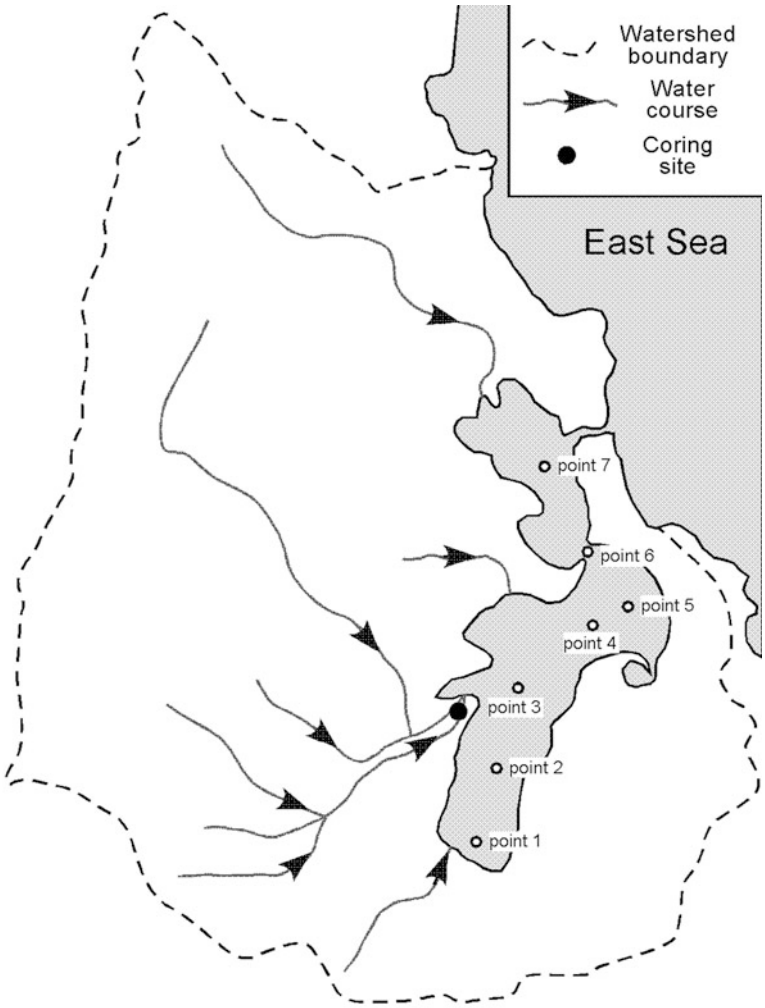

Fig. 9.2 The drainage basin of the Hwajinpo Lagoon. The largest stream (Chungpyong River) has a width of about 10 m near the river mouth

Rocks of basement around the both lagoons area consist mainly of metamorphic rocks of the Jurassic Daebo Granite, the Gyeonggi Gneiss Complex, and Cretaceous to Tertiary hypabyssal igneous and intrusive volcanic rocks. In the drainage basin of Hwajinpo, granite and gneiss complex rocks are dominant. While granite covered partially with Tertiary basalt is dominant in the Songjiho area.

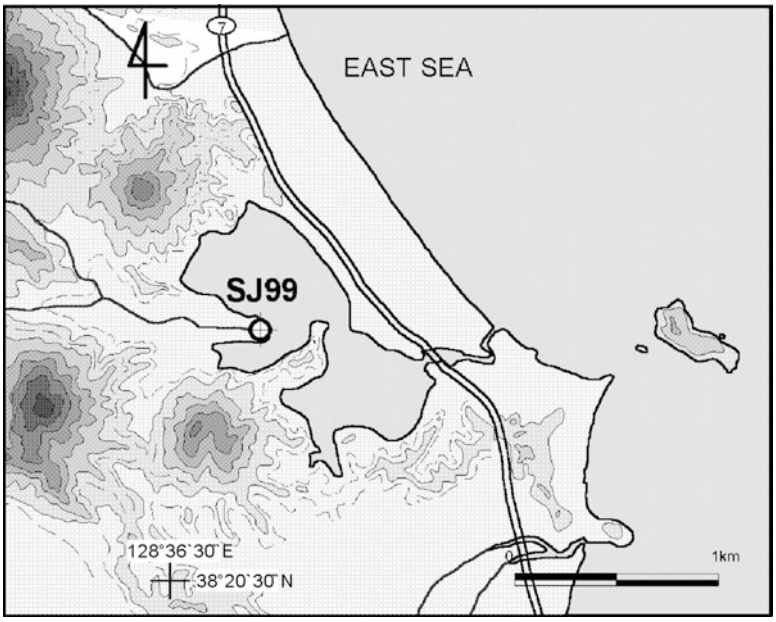

Fig. 9.3 The location of the Songjiho Lagoon and the site of the SJ99 core. The inlet to the sea closed in normal time. The northern and southern parts of the lagoon were connected by narrow and deep channels allowing water to move easily into each lagoon

9.3 Materials and Methods

Bathymetrical survey in the both lagoon was carried out by using echo-sounding equipment with DGPS (Differential Global Positioning System) (FEG-770, FUSO electronics Inc.). Geomorphologic and Geologic survey was achieved within drainage basin. To seek for evidence of sea level change, terraces and bench and notch were measured at coastal and fluvial plain areas. Terrace distribution was mapped from large-scale satellite image and field survey. Topographic profiles of the terrace, bench and notch sequences were measured of concern with local sea level, using a hand level and vertical scale.

A 10.4 m long and 5.5 cm diameter the boring core (HJ99; continued thin wall core method) was collected from the Hwajinpo Lagoon (Fig. 9.1) in the September of 1999. And also 13.5 m long and 5.5 cm diameter the boring core (SJ99) was collected from the Songjiho Lagoon in same season. The core was sealed in the field site and stored vertically in order to prevent water loss and disturbance. In the laboratory, it was described and photographed using 35 mm film after splitting into two vertical halves, and X-radiograph was carried out with the acryl slab ($1 \times 5 \times 30$ cm). We obtained continuous cubic samples (plastic boxes, 7 cm^3) at interval of 2.3 cm for magnetic susceptibility (Bartington MS2 and MS2B: Dearing 1999). Then they were subdivided into 2.5 cm slices. After remove the outer rim of

core sample to prevent from contaminates, one forth of remained slices was dried 48 h at 70 °C in order to calculate sediment water content and for chemical and grain size analyses, according to Folk and Ward (1957).

Total organic carbon (TOC), total sulfur (TS), and total nitrogen (TN) concentration were measured by a gas chromatography with a combustion method at about 1,800 °C (Carlo Erba elemental analyzer EA1108) after removal of carbonates with 1 M-HCL (Sampei et al. 1997). Grain size of sediment was analyzed by a laser-equipped diameter distributor (Mastersizer 2000, Malvern instruments). One gram of fresh sample was used after adding enough 10 % H_2O_2, and then left for 3 days at room temperature. Sand fraction was calculated by the wet sieving method. Each datum is from a 2.5 cm thickness layer of every 12.5 cm interval in the core.

For fine sand fraction, mineral composition was counted on the smear slide under the optical microscope (Microphoto-FXA, Nikon). They are divided into light mineral (except mica), heavy mineral, rock fragments, mica grain and volcanic glass, and also counted plant fragments and diatom abundance.

For description of lamina feature in cores, 5×6 cm sized thin section were made of method of resin-impregnation of dry sediment (Kemp 1990), and then observed under the microscope (Eclipse E400, Nikon). Molluscan shells were identified and counted by following collecting method. When the core subdivided, all mollusc individuals at every 12.5 cm interval along the horizontal plane of core were collected. All molluscs and their fragments that are bigger than sand size were collected. For analysis of dinoflagellate, sediment sample at every 20 cm were treated using the method suggested by Matsuoka et al. (1989). A 2 ml wet samples was placed into a polyethylene beaker and then treated to remove calcium carbonate and silicate minerals with HCl and HF, respectively. After sieving the samples with 125 and 20 mm metallic screens, the residues were mounted from a 2 ml volume. Observations were carried out under an interference optical microscope (Olympus BH 2) until more than 200 dinoflagellate cysts were identified.

We have obtained 13 radiocarbon (seven data from the Core HJ99 and six data from the Core SJ99) ages from wood and plant fragments. Radiocarbon ages were determined by AMS method described by Kitagawa et al. (1993). Single pieces of terrestrial macrofossil such as leaves and small branches were selected and washed repeatedly with distilled water and cleaned chemically by acid-alkali-acid (AAA) treatments to remove secondary contamination. For relatively large plant samples (>5 mg dry weight), holocellulose was also prepared from AAA-treated plant materials by benzene-ethanol extraction and delignification with sodium chloride (Table 9.1).

All processes were carried out in a dust-free room to reduce potential contamination during sample preparation. The Terrestrial macro fossils were sealed in an evacuated Vycor tube with CuO, and combusted at 850 °C in an electronic furnace. The resulting CO_2 was purified cryogenically in a high-vacuum preparation system and then converted to graphite by reducing the CO_2 on Fe-powder with hydrogen gas in a sealed Vycor tube at 650 °C. ^{14}C ages of samples were measured along with the standard (NIST HOxII) using the Tandetron AMS at the Dating and Materials Research Center, Nagoya University (Nakai et al. 1984; Nakamura et al. 1987).

Table 9.1 Carbon 14 age dating of the core HJ99 and SJ99 from Hwajinpo and Songjiho lagoons

Sample (The core HJ99)	Depth (cm)	Lab.no (HK)	Radiocarbon age (yr BP)
Terrestrial wood fragment	309	3129	60 ± 30
Terrestrial wood fragment	348	3130	115 ± 30
Terrestrial wood fragment	408	3132	1,450 ± 40
Terrestrial wood fragment	610	3135	2,910 ± 110
Terrestrial wood fragment (a leaf)	685	3137	4,050 ± 60
Terrestrial plant fragment	707	3138	4,240 ± 80
Terrestrial wood fragment	794	2965	5,580 ± 50

Sample (core SJ99)	Depth (cm)	Lab. ID no (HK)	Radiocarbon age (yr BP)
Terrestrial wood fragment	467	3119	190 ± 35
Terrestrial wood fragment	521	3120	130 ± 35
Terrestrial wood fragment	739	3121	2,460 ± 50
Peat	877	3122	3,620 ± 60
Terrestrial wood fragment	1,107	3125	7,420 ± 110
Terrestrial wood fragment	1,142	2964	7,760 ± 60

We corrected carbon isotope fractionation by $\delta^{13}C$, measured on a Finigan MAT 252 mass spectrometer. Conventional ^{14}C ages were calculated according to the procedure outlined by Stuiver and Polach (1977) and calibrated years by Stuiver et al. (1998).

9.4 Results

9.4.1 The Core HJ99 from Hwajinpo Lagoon

9.4.1.1 Core Description

The 10.4 m thick core HJ99 of the Hwajinpo Lagoonal sediment was divided into six major lithologic units based on grain size and sedimentary structure observed by logging and X-radiograph. These units have been named the H1, H2, H3, H4, H5, and H6 units from the top to the bottom (Fig. 9.4). They are subdivided into 11 subunits based on the chemical and biological variations.

The unit H1 is 4.034 m thick (0–4.034 m below ground level, mbgl) and is composed of granule bearing sand and very coarse sand intercalated thin silty mud layer. The unit H1 is subdivided into upper (H1-U), middle (H1-M), and lower (H1-L) subunits. The uppermost subunit H1-U consists of poorly sorted granule sand containing wood fragments and gastropods. The subunit H1-M consists of very coarse sand with gastropod fragments. The subunit H1-L consists of pebbly sand with silty mud intercalation.

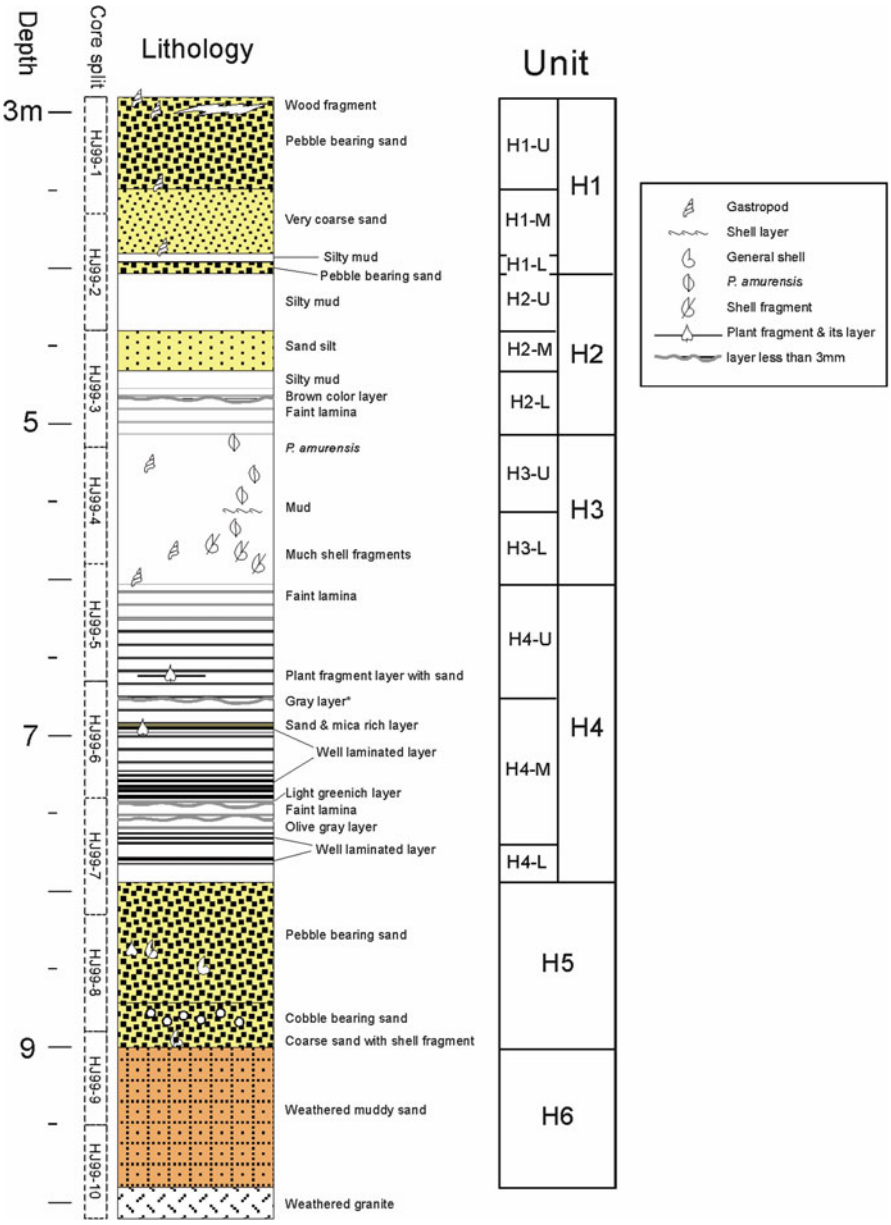

Fig. 9.4 Lithostratigraphic units of the HJ99 core from Hwajinpo Lagoon, The "gray layer" was determined by X-radiographs. The core split is the boundary of the thin wall tube of the corer. They were collected at 75-cm intervals

The unit H2 is 1.030 m thick (4.034–5.064 mgbl) and is continuous with the overlying the unit H1. It consists of thin alternations of silt and mud interspersed with sandy silt. The unit Hs is subdivided into upper (H2-U), middle (H2-M), and lower (H2-L) subunits. The subunit H2-U consists of mainly silty mud. The subunit H2-M consists of sandy silt containing small shell fragments and mica grain rarely. The subunit H2-L consists of silty mud with faint lamination. A 0.5 cm thick brown color layer appears in the lowermost of the subunit H2-L at about 5.06 m.

The unit H3 is 0.967 m thick (5.064–6.030 mgbl) and is considered to be continuous with the unit H2. It consists of brownish dark gray non-laminated mud with abundant shell (bivalve and gastropod) and its fragments in all part of this unit. A 1 cm thick shell and their fragments layer appear at 5.55 m. The unit H3 is divided into upper subunit H3-U and lower subunit H3-L on the boundary of this shell layer.

The unit H4 is a 1.908 m thick (6.030–7.938 mgbl) composed of alternating layer of well-laminated, faint laminated and non-laminated mud and clay. It is subdivided into three subunits namely upper (H4-U), middle (H4-M), and lower (H4-L) based upon the clarity of lamination. The subunit H4-U is defined by the faint lamination with plant fragment sporadically. The top of this unit is continuous with the bottom of the unit H3. The subunit H4-M consists mostly of thin well-laminated layers intercalated by moderate or faint laminated layers. Thin layers about 0.5 cm thick which show different color intercalated four times in this subunit at 6.767 m (bright gray), 7.222 m (gray), 7.426 m (light greenish) and 7.509 m (olive gray) respectively. The subunit H4-L consists mostly of non-laminated mud layer. The most well laminated layer (3.6 cm thick) in whole core appear at 7.788 ~ 7.824 mgbl (Fig. 9.5).

The unit H5 is 1.062 m thick (7.938–9.000 mgbl) and is considered to be diastemic with the unit H4. It consists of alternations of poorly sorted gravel sand and very coarse sand layer, and abundant shell and their fragments are present in all parts of this unit. The lower part of this unit is contains coarse material from granule to pebble sized embedded in bright gray silty mud matrix with shell and wood fragments.

The unit H6 is 0.900 m thick (9.000–9.900 mgbl) and contains very coarse materials from pebble to cobble sizes embedded in an olive-gray silty sand matrix. The materials in this unit are strongly weathered and poorly sorted. The contact between this unit and the overlying unit is considered to be unconformable.

The other physical records from the core HJ99 such as water content, susceptibility, sand percentage, mean grain size, and degree of sorting are summarized in Fig. 9.6. Mineral composition including the percentage of very fine sand ($3 \sim 4\varphi$) to other sand fraction ($-1 \sim 3\varphi$), percentage of light mineral, heavy mineral, rock fragments, and mica grain per very fine sand (Fig. 9.7).

9.4.1.2 Water Content

The variation of water content shows relevant to the lithologic changes. The upper part of the unit H5 displays low water content (average of 33.4 %). The unit H4

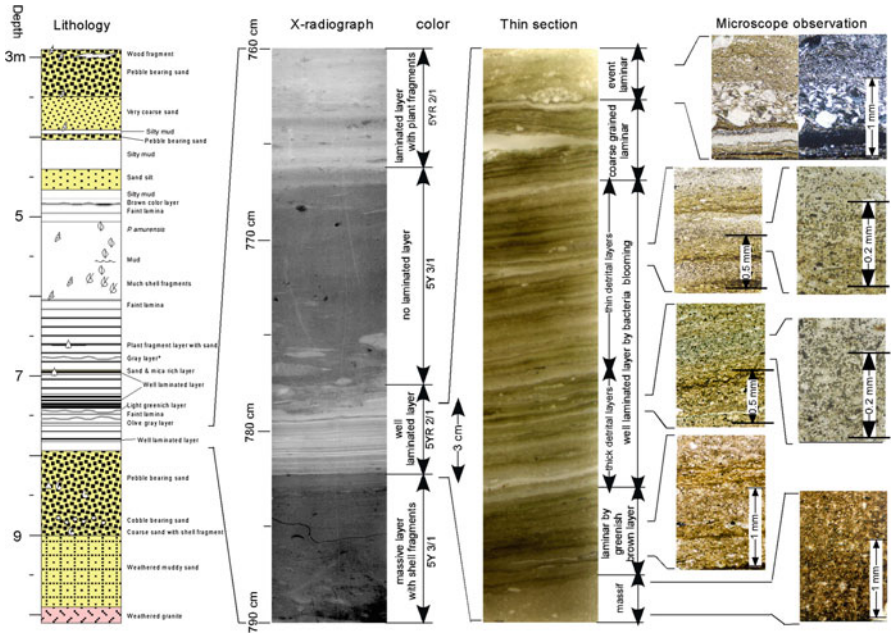

Fig. 9.5 Preliminary analysis of lamination in the HJ99 core from lithology, X-radiography, and thin sections with microscopic observation. The lamination in the middle part originated from bacteria (Cyanobacteria) blooms. From the sedimentation rate in this range, the lamination was considered to have an annual varve structure

shows relatively high water content values (average of 59.6 %) than previous unit H5. In the subunit H4-L the values are shown increasing trend from 33 to 60 %. The values of water content in subunit H4-M (average of 60.6 %) are shown slightly increasing trend, and slightly decreasing trend in the subunit H4-U (average of 62.9 %). The decreasing trend from 61 to 45 % are shown in lowermost part of subunit H3-L, then the water content show constant value in whole the unit H3 with an average of 44.7 %. In all part of the unit H2, water content show slightly decreasing trend from 44 to 31 % with an average of 33.6 %. Water content in unit H1, coarse sand layer, are relatively low with an average of 25 %.

9.4.1.3 Magnetic Susceptibility

From H2 to H1 units, the values are relatively higher than the lower part of core with an average of 2.24 and show the slightly decreasing trend in the range from 5.65 to 1.12. From the unit H4 to unit H3, the values of weight magnetic susceptibility are less than 0.77 with more or less fluctuation. The average value of this range is 0.32. Thus, weight magnetic susceptibility values (log scale of magnitude of susceptibility) of the core HJ99 show distinctive shifting on the boundary between H3 and H2 unit.

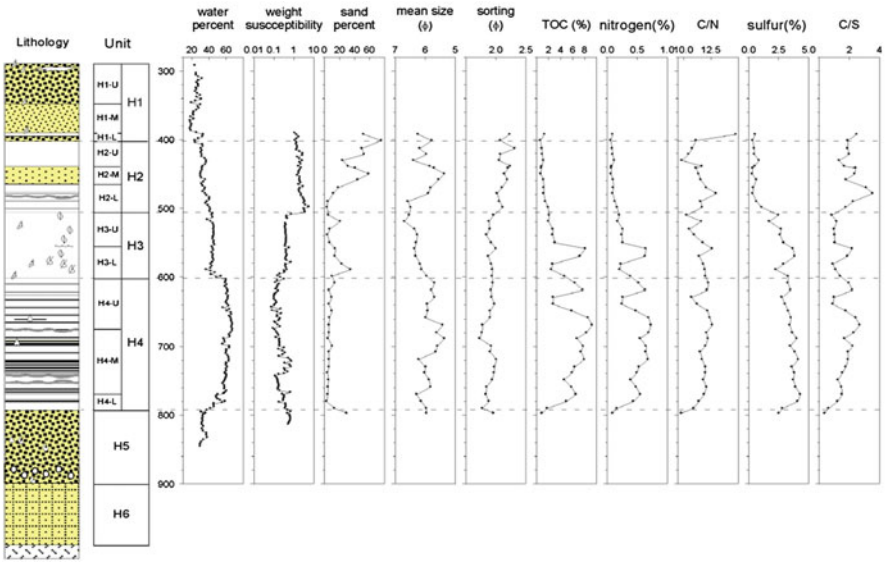

Fig. 9.6 Sedimentological and chemical data from the HJ99 core from the Hwajinpo Lagoon. Mean grain size was determined only for muddy units because the high sand content of unit H5 produced values beyond the limit of the analyzer. Sorting and mean grain size were calculated by Folk's method (Folk and Ward 1957); *TOC* total organic carbon, *C/N* ratio of total organic carbon and nitrogen, *TS* total sulfur, *C/S* ratio of total organic carbon and sulfur. The data from H5 could not be compared with other units because coarse grains dominated in this unit

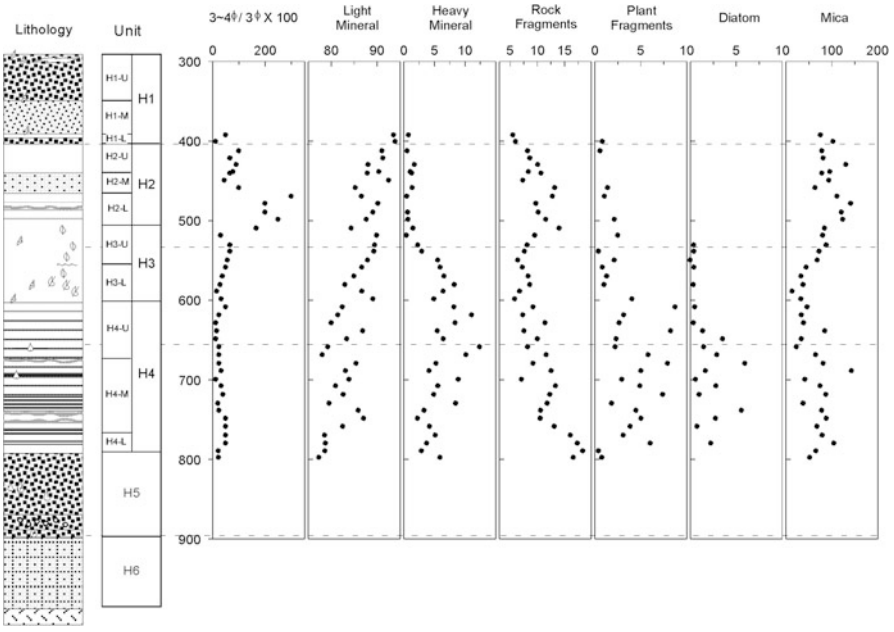

Fig. 9.7 The mineral composition of the HJ99 core including the percentage of very fine sand, light and, heavy minerals, rock fragments, and mica grains

9.4.1.4 Grain Size Analysis

Sand percentage, mean grain size and sorting results from the core are summarized in Fig. 9.6. Sand percentage in the subunit H4 are increased slightly from 2.8 to 6.6 % with an average of 6.0 %. The drastic increased value of sand percentage at the lower part of unit H3 shows the decreasing trend. In the unit H2, sand percentage increases from the 3.5 % up to 75 % except in the range of the subunit H2-M that show high sand contents related to sandy lithology. The value of VS % (very fine sand percentage: weight percentage of $3 \sim 4$ φ vs. $-1 \sim 3$ φ) indicate that the sand grains are mostly composed of very fine sand size in the subunits H2-M and H2-L.

The mean grain size from the bottom of subunit H4-L to subunit H4-M shows a slight increasing trend even with some fluctuation, which ranges from 5.4 to 6.3 φ. The trend of grain size changes to decreasing from the boundary between H4-M and H4-U to the topmost of subunit H4-U ranging from 5.4 to 6.7 φ. Then grain size becomes coarser in the unit H2. General trend of sorting shows increasing with more or less fluctuation in the whole core that ranges from 1.7 to 2.3 φ

9.4.1.5 Mineral Composition

Each mineral composition calculated by the percentage for the sum of light, heavy and rock fragment grain (Fig. 9.7). Mica was excluded from the counting as light mineral, because their attribute of floating in water body due to the planer mineral shape.

Most of grains are composed of mainly biotite, quartz and feldspars with some rock fragment and opaque minerals. Quartz and feldspar are dominant in light mineral with more than 80 %. Mica mineral, such biotite and muscovite, are contained very common through the core with an average value of 74.6 %.

Heavy mineral percentages in the units H4 and H3 are more than five times higher than those of the unit H2 and the subunit H1-L. Rock fragment was contained average 10.3 % in the core, ranging from 0.4 to 8.8 %. Plant fragments are contained very few in the upper units H3 and H2, while the unit H4 contained relatively much amount more than five times to H3 and H2 units. The contents of diatom are also much in the unit H4 than units H3 and H2.

9.4.1.6 TOC, TN and C/N

The TOC (total organic carbon), TN (total nitrogen), C/N (ratio of organic carbon and nitrogen), TS (total sulfur) and C/S (ratio of organic carbon and sulfur) results from the core are summarized in Fig. 9.6.

In the unit of H4-L, the TOC contents show steep increasing trend due to lithologic change from sand to mud. The laminated subunit H4-M shows a higher content of TOC (average of 6.7 %) with slight increasing trend. In subunits H4-U and H3-L (average of 5.5 %), the value of TOC shows a fluctuation pattern ranging

from 2.5 to 9.2 %. Subsequently, the value of TOC show less than 2.7 % with decreasing trend to 0.6 % from the subunits H3-U and the unit H2. The content of TN show a very similar trend to the TOC through the core ranged from 0.1 to 0.7 %. The C/N ratio does not show much variation (average value of 11.7) through the core ranged between 9.8 and 14.8 with fluctuation.

9.4.1.7 TS and C/S

On the steep TS increasing in the subunit H4-L due to change of grain size, TS from the subunit H4-M to the unit H3 shows deceasing trend ranging 4.1-2.5 % with an average value of 3.3 %. The unit H2 exhibits very low sulfur content of less than 0.8 % with an average value of 0.48 %. The C/S ratio through the core ranged from 0.8 to 2.7 with an average of 1.7 except the subunit H2-L showing a peak shape (maximum value of 3.6).

9.4.1.8 Biologic Records

The stratigraphic distributions and relative abundance of mollusan fossils are shown in Fig. 9.8. Nine species of molluscs are present in the core HJ99, including five unidentified species. All of them are shallow estuarine types of mollusc affected by seawater (Table 9.2). Especially, *Potamocorbula amurensis* is a typical brackish type mollusc in the coastal area of Korea (Kwon et al. 1993). Unit H5 contains estuarine type of molluscs while units H4 and H2 have no mollusc. Unit H3 contains plenty of mollusc and fragments including the specific species of brackish water type mollusc, *P. amurensis*. Unit H1 containing mainly *P. amurensis* presents in recent condition of Hwajinpo Lagoon (Yum et al. 2003, 2004, 2006)

9.4.1.9 Age Determination

An age-depth model was constructed from seven AMS radiocarbon dates (Fig. 9.9). The radiocarbon age dating ranged from 5,580 ^{14}C yr BP at the mid part of the unit H5 to 60 ^{14}C yr BP in top of the unit H1 (Table 9.1). A straight line was fit between sections of constant sedimentation to construct this age-depth model. According a radiocarbon datum from the corresponding unit of Yum et al. (2003, 2004, 2006), sedimentation rate is assumed 1.35 mm/year in this unit (dot line in Fig. 9.14). In the unit H4, sedimentation rate is calculated to 0.69 mm/year by linear interpolation. Units H3 and H2 has 1.38 mm/year of sedimentation rate. In the subunit H1-L, the sedimentation rate is 0.47 mm/year while in the subunit H1-U the rate indicate very fast depositional environment with 7.02 mm/year of sedimentation rate.

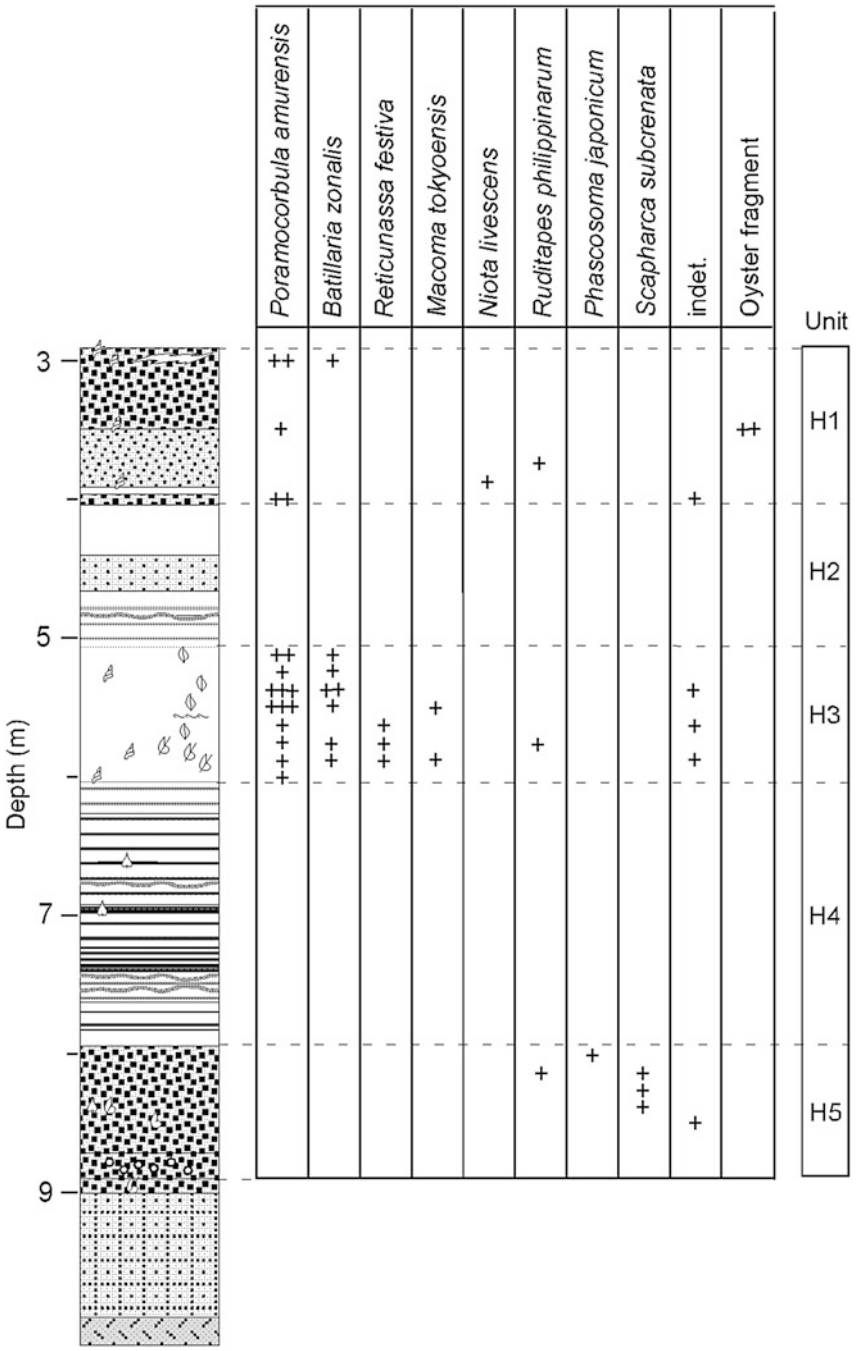

Fig. 9.8 Mollusk abundance in the HJ99 core from Hwajinpo Lagoon; +: 1; ++: 2 ~ 3; +++: more than 3 individuals

Table 9.2 Attribute and habitat of the molluscs from the cores HJ99 and SJ99

Species	Distribution	Inhabitation
Batillaria zonalis (Bruguiere)	To South Hokkaido	Estuarine, mud
Niotha livescens (Philippi)	All Japan except Hokkaido	Tidal zone ~20 m depth, fine sand
Reticunassa festiva (Powys)	To South Hokkaido	Tidal zone in estuarine, pebbly sand
Scapharca subcrenata (Lischke)	To Southwest Hokkaido, Honshu, Shikoku, Kyushu, Korean Peninsular	Tidal zone in estuarine ~ subtidal zone, fine sand
Macoma tokyoensis (Makiyama)	To South Hokkaido, Kyushu, Korean Peninsular	~20 m depth, estuarine, mud
Phascosoma japonicum (Reeve)	To south Kyushu	Tidal zone ~60 m depth, fine sand
Ruditapes philippinarum (A. Adams et Reeve)	Sahaline, Japan, Korean, China	Tidal zone ~10 m depth, muddy sand gravel, Estuarine effected by fresh water
Potamocorbula amurensis (Shrenck)		Brackish water condition

9.4.2 The Core SJ99 from Songjiho Lagoon

9.4.2.1 Lithologic Units

The 13.5 m thick section of the Songjiho Lagoonal sediment (the core SJ99) was divided into six major lithologic units based on grain size and sedimentary structure observed by logging and X-radiograph. These units have been named the units S1, S2, S3, S4, S5, and S6 from the top to bottom (Fig. 9.10). They are subdivided into 13 subunits based on the other chemical and biological variation.

The unit S1 is 5.514 m thick (0–5.514 mgbl) and is composed of sand and silt intercalated thin mud layers. The unit S1 is subdivided into upper (S1-U), middle (S1-M), and lower (H1-L). The subunit S1-M presents very low sulfur content and relatively high C/S ratio subunits S1-U and S1-L. It consists of plant layer interspersed plant fragments through the unit, and a 0.5 cm thick reddish brown sand layer appears in the subunit S1-M at 5.34 m depth.

The unit S2 is 0.710 m thick (5.514–6.224 mgbl) and is considered to be conformable with the unit S1. It consists of brownish dark gray non-laminated mud with bivalve shells and its fragments occurred all part of this unit. Subunits are divided into two subunit, the upper (S2-U) and lower (S2-L) subunits based on the change of TOC and TN contents.

The unit S3 is 2.901 m thick (6.224–9.125 mgbl) composed of alternating of well-laminated, faint laminated and non-laminated mud layers. The subunit S3-U (upper subunit of S3) is defined by the faint lamination with sporadic plant fragment. The middle part of subunit S3-U presents faint-lamination more or less clearly

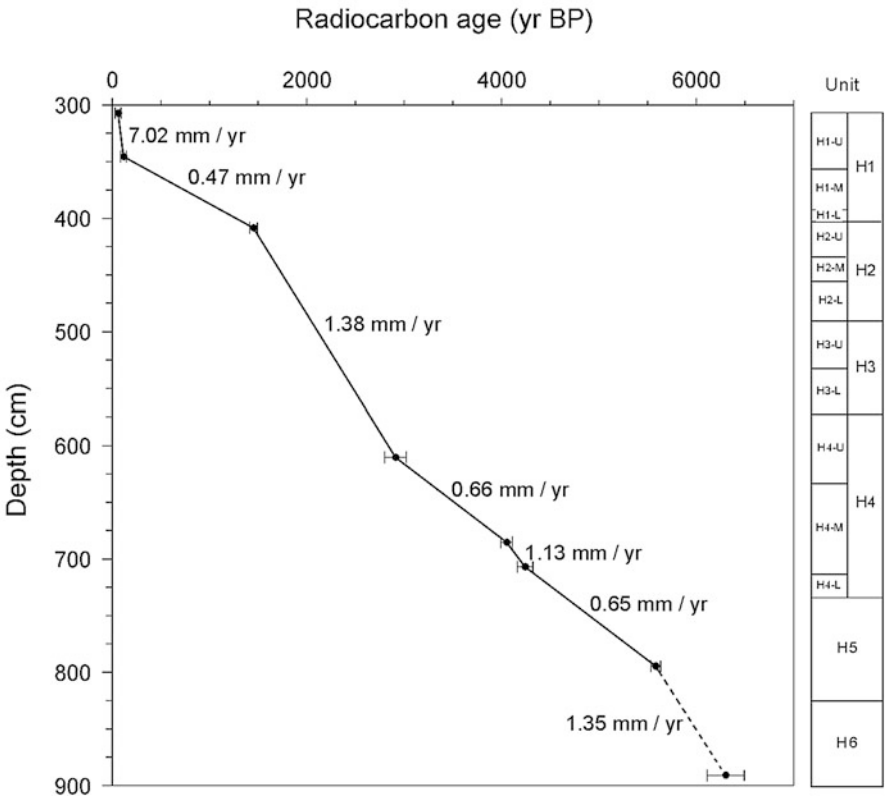

Fig. 9.9 Sedimentation rate in the HJ99 core calculated by radiocarbon dating

than upper and lower part of the subunit S3-U. The subunit S3-L (lower subunit of S3) consists mostly of thin well-laminated layers intercalated by moderate or faint laminated layers. Thin layers about 0.5 cm thick which show different color intercalated in the subunit S3-L at 8.33 m (gray) and at 8.65 m (bright gray) depth respectively.

The unit S4 is 1.356 m thick (9.125–10.481 mgbl) and it considered to be continuous with the unit S3. It consists of non-laminated mud layer with much plant fragment. In the subunit S4-U (upper subunit of S4) vertical wave shaped structure has been developed (Fig. 9.11). As the boundary of plant fragment with 2 cm thickness at 9.73 m depth, the subunits S4-M (middle subunit of S4) and S4-L (lower subunit of S4) consist of massive mud layer with much plant fragments. The subunit S4-M could be characterized by the very low sulfur content even there is no lithologic difference with the subunit S4-L.

The unit S5 is 0.659 m thick (10.481–11.140 mgbl) and it is considered to be continuous with the unit S4. It consists of mud with intercalated by plant rich thin layer. In the subunit S5-U (upper subunit of S5) the bedding boundaries of 3–4 cm

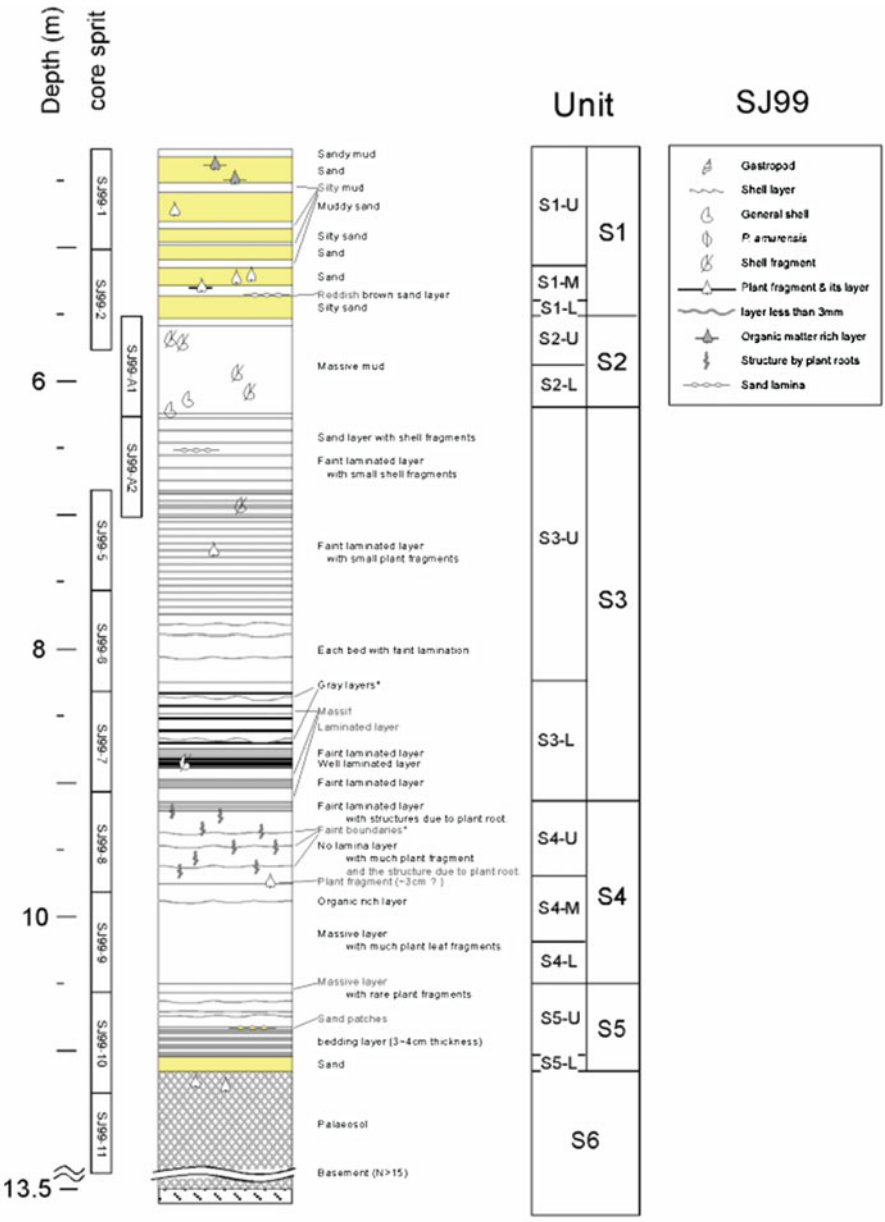

Fig. 9.10 Lithostratigraphic units of the SJ99 core from Songjiho Lagoon. The "gray layer" was determined by X-radiographs. The core split is the boundary of the thin wall tube of the corer. They were collected at 75-cm intervals

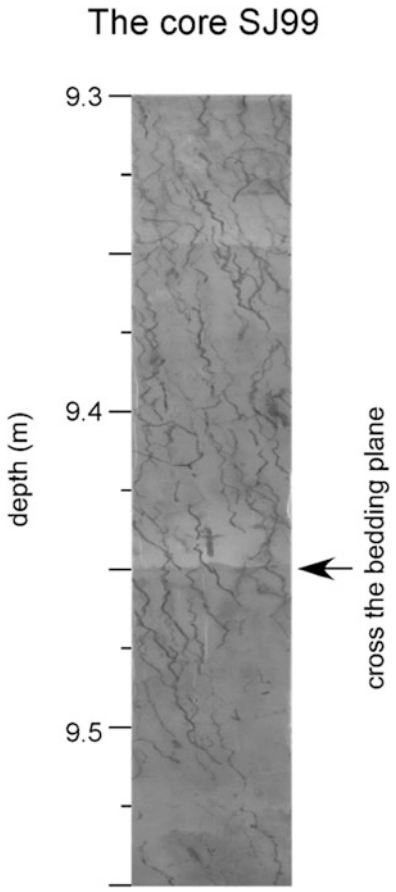

Fig. 9.11 A vertical wave-shaped structure (unknown structure) on the X-radiograph of the SJ99 core

interval were described on the X-radiograph. The subunit S5-L (lower subunit of S5) is defined as very coarse sand layer and is considered to be diastemic with the subunit S5-U. It is similar feature with the unit H5 of the core HJ99.

The unit S6 is 2.360 m thick (11.140–13.500 mgbl) and consists of clay with sporadic plant fragments such as root remains. The lowest part of the unit, the N value indicates basement rock (N > 15).

The physical records, such as water content, susceptibility, sand percentage, mean grain size, and degree of sorting are summarized in Fig. 9.12. Mineral composition including the percentage of VS%, percentage of light mineral, heavy mineral, rock fragments, and mica grain per very fine sand are illustrated in Fig. 9.13.

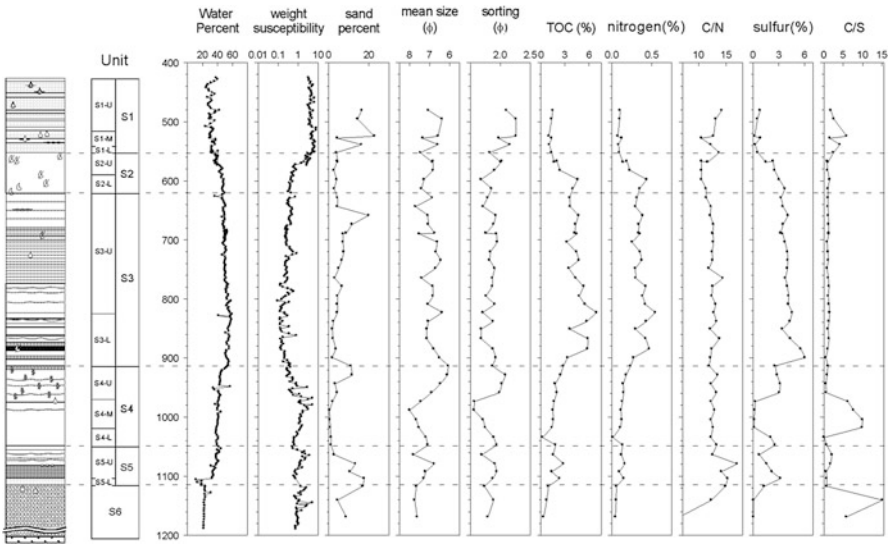

Fig. 9.12 Sedimentological and chemical data from the Songjiho Lagoon core. Mean grain size was determined only for muddy units because the high sand content of subunit S1-U produced values beyond the limit of the analyzer. Sorting and mean size were calculated by Folk's method (Folk and Ward 1957); *TOC* total organic carbon, *C/N* ratio of total organic carbon and nitrogen, *TS* total sulfur, *C/S* ratio of total organic carbon and sulfur. The data from S1-U could not be compared with the other units because coarse grains dominated in this unit

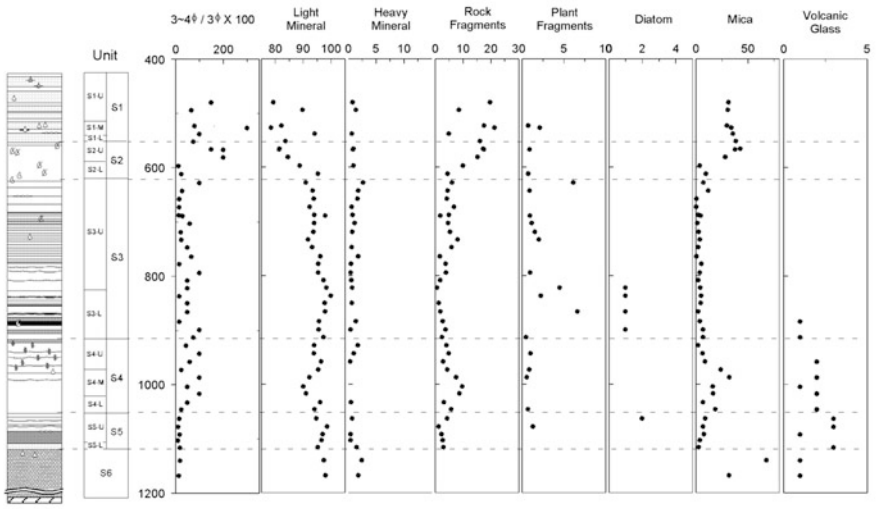

Fig. 9.13 Mineral composition of the SJ99 core including the percentage of very fine sand, light and heavy minerals, rock fragments, and mica grains as a proportion of very fine sand

9.4.2.2 Water Content

The variation of water content shows a relevance to the lithologic changes, especially with the grain size. The subunit S6-U display low and constant water content with an average value of 23.4 %. It shows slight increasing trend from 21.8 to 24.0 %. In the sand layer, the subunit S5-L, the value of water content are shown very low with an average of 15.9 % and subsequently in the subunit S5-U water content are relatively high (average of 38.1 %) with increasing trend. The unit S4 shows increasing trend continuously begun from previous unit from 38 to 54 %. After drastic increasing of about 1 % difference at the boundary between units S4 and S3, the subunit S3-L shows slightly increasing trend again with an average of 54.3 %. And the S3-U shows decreasing trend from 59.5 to 41.6 %. Subsequently, this decreasing trend is continuous in the unit S2 with an average value of 43.1 %. The water content shows more or less fluctuated values according to the grain size In the unit S1, even there is a continuous trend of decreasing.

9.4.2.3 Magnetic Susceptibility

Weight Magnetic susceptibility values (log scale of magnitude of susceptibility) of the core SJ99 show distinctiveness of variation on the boundary between units S1 and S2 likely clear boundary between units H1 and H2 of the core HJ99. The unit S6 shows an average value of 1.33 with several fluctuations. The increasing trend in range from 0.51 to 3.71 is clear in the subunit S5-U. The subunit S5-L did not be measured due to the coarse sand layer. After the drastic decreasing at the boundary between units S5 and S4, increasing trend is again shown clearly from subunits S4-L and S4-M in the range from 0.60 to 5.26. Subsequently, the decreasing trend began from the S4-U is continuous up to the S3-L in the range from 0.13 to 5.24, even though several peaks are presented in this range. In the subunit S3-U shows slightly increasing trend with an average value of 0.34. The increasing trend is continuous up to the subunit S2-U. At the boundary of units S1 and S2, the magnetic susceptibility increase drastically like the core HJ99 as mentioned above. The subunit S1-U shows relatively constant value (average of 4.91) with slight fluctuation.

9.4.2.4 Grain Size Analysis

Sand percentage, mean grain size and sorting results from the core SJ99 are summarized in Fig. 9.12. The drastic increasing of sand percentage in the subunit S5-L change to decreasing tendency in the subunit S5-U within the range from 17.7 to 2.7 %. The subunits S4-L and S4-M show lower sand percentage less than 2 % and the subunit S4-U show increasing trend up to 11 %. Except the range from the 5.50 to 5.80 m depth, sand fraction percentage are shown low value less than 8 % with an average of 4.4 % from the subunit S4-U to the subunit S1-U. In the subunits S1-M and S1-U, the sand fraction percentage is relatively high due to intercalated sand

layers. The mean grain size shows an increasing trend in the unit S5 and it shows a decreasing trend though subunits S4-L and S4-M. Again, showing an increasing trend in the unit S4-U, grain size show decreasing trend with some fluctuation from the unit S3 to the subunit S2-L. In the unit S1-M and the subunit S1-U, the mean grain size shows a slight increasing trend. The degree of sorting shows relatively constant from the bottom to the subunit S2-L, although they are fluctuated. In the subunit S2-L and the unit S1, they are shown increasing trend, ranging from 1.7 to 2.3 φ.

9.4.2.5 Mineral Composition

Each mineral composition calculated by the percentage for the sum of light, heavy and rock fragment grain (Fig. 9.13; Takemura and Yokoyama 1991). Most of grains are composed of mainly biotite, quartz, and feldspar with some rock fragment. The grains of more than 90 % are dominantly light minerals such as quartz and feldspar. Heavy mineral was contained average 0.7 % ranging from 0 to 8.8 % through the core. In the subunit S2-U and unit S1 rock fragment are more than three times higher than those of the other units below. Especially, the Refractive Index (R.I.) of volcanic glasses in the lower part of The core SJ99 show an average value of 1.4985 corresponding the R.I. of AT tephra (Table 9.3; Takemura and Danhara 1994).

9.4.2.6 TOC, TN and C/N

The TOC (total organic carbon), TN (total nitrogen), C/N (ratio of organic carbon and nitrogen), TS (total sulfur) and C/S (ratio of organic carbon and sulfur) results from the core SJ99 are summarized in Fig. 9.12.

The TOC contents show fluctuation pattern in the units S5 and subunit S4-L with an average value of 1.6 %. In the subunits S4-M and S4-U, the TOC content show slight increasing trend with the range from 1.4 to 2.5 %. This increasing trend continues in the subsequent subunit S3-L, and it is steeper than below units and fluctuated within range from 2.8 to 4.5 %. With the peak of TOC on the boundary between subunits S3-L and S3-U, the values of TOC decrease slightly from the subunit S3-U up to the subunit S2-L within range from 3.2 to 7.0 %. This decreasing

Table 9.3 Reflective index for glass grain in the SJ99 core

Depth (m)	Measuring refractive index[a]	Count no. of grains	Reference
10.05	1.4983, 1.4978	2	AT (1.498–1.501) by Matsumoto et al. (1987)
10.79	1.4978, 1.4992, 1.4985	3	”
11.17	1.4985, 1.4989, 1.4983, 1.4991	4	”

[a]Measured by RIMS2000

trend continues steeply in the subunits S2-U and S1-L. The subunits S1-U and S1-M show relatively low TOC content with an average value of 1.23 %. The content of TN shows a very similar trend to the TOC through the core. However, C/N ratio indicating effect of terrestrial origin matter shows more than two cycles of sinuous variation.

9.4.2.7 TS and C/S

The unit S6 shows nearly 0 % in sulfur content. The average value of TS from the unit S5 to the subunit S4-L is 1.9 %. However, the subunit S4-M shows very low sulfur content with an average of 0.19 % again. Subsequently the subunit S4-U shows higher average value (about 3.0 %) than previous subunit S4-L. After abrupt increasing at the boundary between subunits S4-U and S3-L, the TS show decrease trend through the range from subunit S3-L to subunit S2-U. In the unit S1, the TS show very lower values with an average of 0.52 %, especially in the subunit S1-M the value of TS shows less than 0.2 % indicating the fresh water condition. The C/S ration ranged from 0.1 to 2.1 with an average value of 1.1 except subunit S4-M, S4-L, and unit S1. From the subunits S4-L to S4-M the higher value of C/S indicate fresh water condition (average of 8.4). The unit S1 also show relatively high C/S value effected by fresh water with maximum value of 5.9.

9.4.2.8 Biologic Records

The stratigraphic distributions and relative abundance of molluscan fossils are shown in the Core SJ99 (Fig. 9.14). Three species of molluscs are present in the core, including two unidentified species. All of them are shallow estuarine types of mollusc affected by seawater (Table 9.2), even the number of individuals is too little. *P. amurensis* is a typical brackish type mollusc in Korea (Kwon et al. 1993). *R. festiva* inhabits in fine sand substratum near tidal zone. The present of *R. festiva* in the core SJ99 coincident the high sand content in the subunit S3-U though the muddy matrix is dominated in this subunit.

9.4.2.9 Age Determination

An age-depth model was constructed from six AMS radiocarbon dates (Fig. 9.15). A straight line was fit between sections of constant sedimentation to construct this age-depth model. The radiocarbon dates (Table 9.1) indicate that unit S6 formed before about 7,760 yr BP. In the lower part of unit S5 the sedimentation rate is 1.05 mm/year. The subunit S5-U and the unit S4 have 0.61 mm/year of sedimentation rate. Up to S1-L, the sedimentation rate is about 1 mm/year while the units of S1-M and S1-U has very high sedimentation rate similar to the subunit H1-U of the core HJ99.

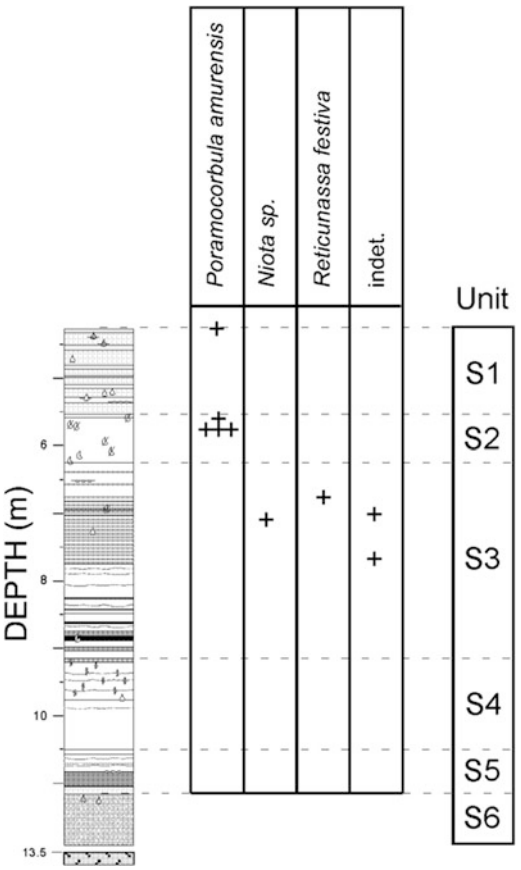

Fig. 9.14 Mollusk abundance in the SJ99 core from Songjiho Lagoon; +: 1–2; +++: more than 3 individuals

9.5 General Discussion

9.5.1 Stages of Depositional Environmental Changes

From the several proxy data of the cores, reconstructing of environmental condition during the Holocene can be possible with great clarity and in considerable detail. We applied these useful data as environmental record, in order to reconstruct the paleoenvironmental history based on stages of the Outer Lake of Hwajinpo Lagoon and Songjiho Lagoon

9.5.1.1 The Stages of the Outer Lake of Hwajinpo Lagoon

The six stages of depositional environments were identified in the outer Lake of Hwajinpo Lagoon as following.

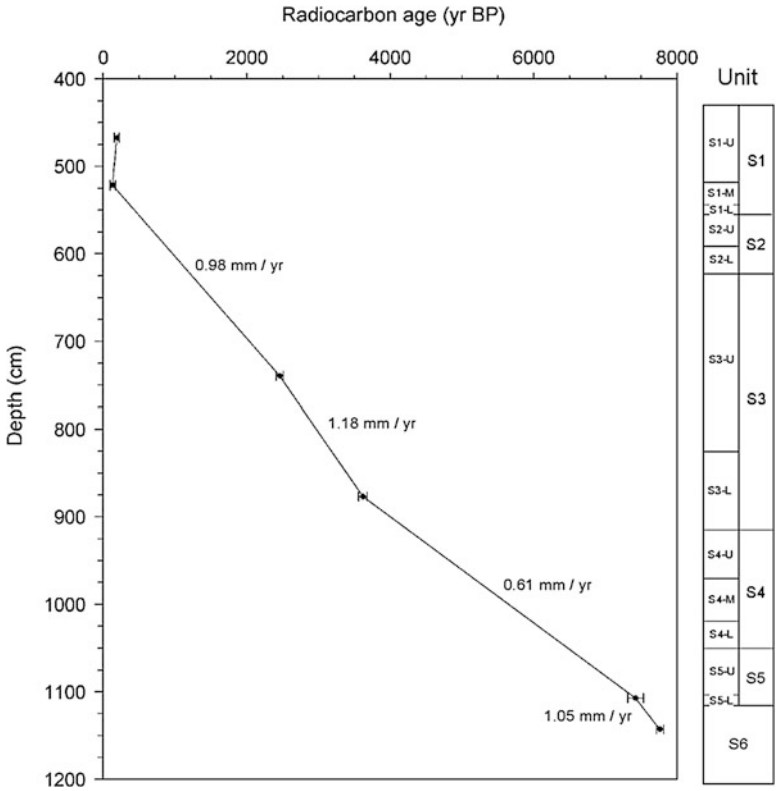

Fig. 9.15 Sedimentation rate in the SJ99 core calculated by radiocarbon dating

Unit H6 Weathered Deposit on the Exposed Basement (Before 6,800 ^{14}C yr BP) The basement rock of the Hwajinpo Lagoon area is Gyeonggi Gneiss Complex intruded by Daebo granites that have been the most clastic sources of depositional material to Hwajinpo lagoon. The time when unit H6 was exposed could be before last glacial maximum period, because the bottom of unit H5 started deposition after 6,800 ^{14}C yr BP (Yum et al. 2003, 2004, 2006).

Unit H5 Estuarine Deposit (About 6,000 ^{14}C yr BP) Unit H5 could be considered tidal inlet sand deposits of estuarine environments during a transgression starting before 5,600 ^{14}C yr BP. The gravel layer in the lower part of this unit was considered as lag deposit, which was deposited in the initial time of transgression. Unit H5 displays lower water content related to very poor sorting due to the mixing of sand and silt-size grains. The assemblage of estuarine type molluscs indicates the condition of the Hwajinpo as an open estuarine system when unit H5 was deposited.

Unit H4 Stagnant Brackish Lagoonal Deposit (5,500–2,800 ^{14}C yr BP) Yum et al. (2003, 2004) have suggested that the difference in bottom condition is a conse-

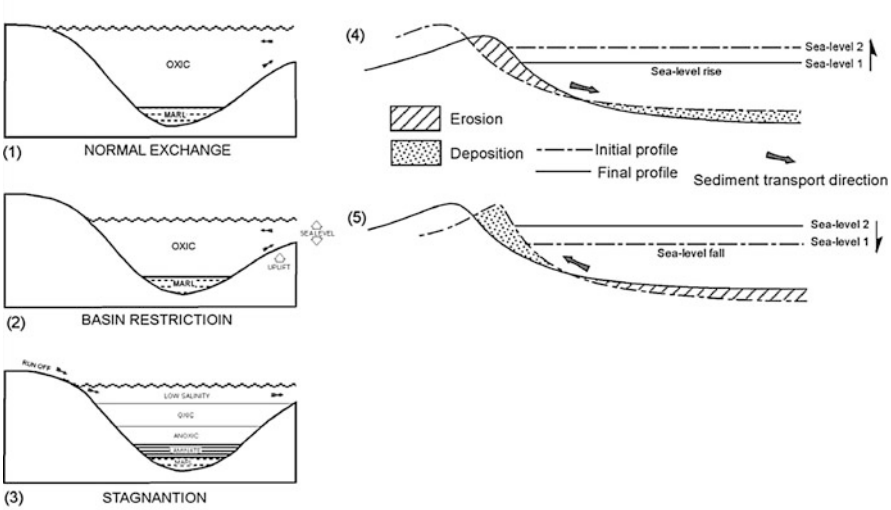

Fig. 9.16 Conceptual runoff-stagnation model for the formation of laminites at Virica and Gela. (*1*) Normal exchange between the oxic waters of the depositional basin and the adjacent ocean, followed by (*2*) subsequent restriction due to fluctuations in sea level and/or tectonic activity. Finally, (*3*) the development of low oxygen conditions and laminite formation. A reduction of surface water salinities (due to runoff) created a density gradient large enough to restrict vertical mixing and promote exchange between the surface and deeper waters of the basin. The runoff would bring in terrestrial organic matter and terrigenous sediments, the relative amounts of which determined if the laminite was organic-rich (Virica) or not (Gela) (Howell et al. 1988); (*4*) Brunn's rule of translation of the shoreface profile (Bruun 1962). During a rise in sea level, erosion prevails in the upper part of the profile causing the shoreline to recede. (*5*) During a fall in sea level, the inverse is true (Dominguez et al. 1987)

quence of monsoon, which may account for the annual variation of precipitation at Hwajinpo Lagoon area. However, well-laminated structure in the unit H4 could remain on the condition of stable bottom water and/or the absence of bioactivity even the monsoon affects strongly. The runoff-stagnation model of Howell et al. (1988) by sea level change explains the development of well laminated layer in brackish lagoonal system (Fig. 9.16). The isolated basin by development of sand spit of Hwajinpo Lagoon is suitable to apply this model.

Unit H4 show higher water content values than the previous units H5 and H6. It indicates well sorting and an accordingly stable condition as well. The sulfur contents are relatively high at the range of about 2.5 %, indicating a relatively oxygen poor condition on the bottom sediments. The change of grain size from sand to silt at the boundary between units H5 and H4, might be result from a rapid change in the depositional environment. From the result of depositional environment of unit H4 could be deduced to stagnant bottom and brackish water condition.

The corresponding layer (unit D) of the core HJ95 is deposited in the brackish environment on the bases of diatom assemblage (Yum et al. 2003, 2004). This unit D layer of HJ95 deposited on the estuarine sand layer aged about 6,000 ^{14}C yr BP and overlying layer is marl deposit with much shell and its fragments, same as the unit H4 of HJ99.

Unit H3 Oxic Condition Marl Deposit (2,200–2,800 ^{14}C yr BP) The fining upward trend of grain size begun from subunit H4-L by the rising the lake-level continues up to unit H3. The abundance of shells from unit H3 indicates that the condition of the lake was open and has sufficient oxygen and nutrients in contrast to the previous one as the oxic condition model of Howell et al. (1988). Mollusca, represented by *P. amurensis* indicates a brackish water condition. A constant value for the water content and susceptibility, and much shell with their fragments occurred in the same range of this unit H3. It should be the consequence of an active bioturbation could be a possible explanation for this feature. The decreasing of the shell fragment at the top of unit H3 indicates beginning of the environment change from enough oxygen to oxygen poor condition in the Hwajinpo lagoon. The decreasing trend of TS in the top of unit H3 supports this phenomenon, i.e. the sulfur supplied from sea water ready to diminish as similar as oxygen decreasing phenomena by the isolating the Hwajinpo lagoonal system.

Unit H2 Isolated Lake Deposit Influenced by Fresh Water (About 1,700 ^{14}C yr BP) The low sulfur content of Unit H2 with its higher value of C/S indicates a decrease of seawater influx. The faint lamination in the unit H2-L implies a stable and stagnant condition similar to the unit H4. This could be due to the falling down of sea level, i.e. sand barrier developed by sea level rising during the previous stage (unit H3) made the outer lagoon isolated from the sea. Human activity can also be considered for the development of sand spit when evaluating these phenomena. However, the general steady trend of grain size indicates that the barrier was not constructed due to sudden environmental change, such as a typhoon or flood event. The effect of sea level falling is a more reasonable way of explaining the isolation phenomenon.

The progressing the falling down of lake-level took place the progradation of river delta near the coring location, then the sandy silt layer (subunit H2-M) deposited when the minimum stage of lake-level. The land use by human being can be also inferred another explanation to the sand rich sedimentation. However, TOC and C/N ratio does not show the abrupt change induced by human activities. In the subunit H2-U, lake-level recovered and grain size also became fine than previous sandy silt layer.

Unit H1 Prograding River Delta (Since 1,200 ^{14}C yr BP) As final stage, river delta deposit consisting silt and sand was prograding upon the coring location. Presence of *P. amurensis* in this unit indicates brackish water condition. The value of C/N of subunit H1-L indicates high influx of terrestrial material. Sedimentation rate of the unit H1-U imply that the subunit H1-U deposited only during a couples of century (from 150 year before present). It is perhaps due to the human land use and subsequent weathering rate increasing.

9.5.1.2 The Stages of the Songjiho Lagoon

The six stages of depositional environments were identified in the Songjiho Lagoon as following.

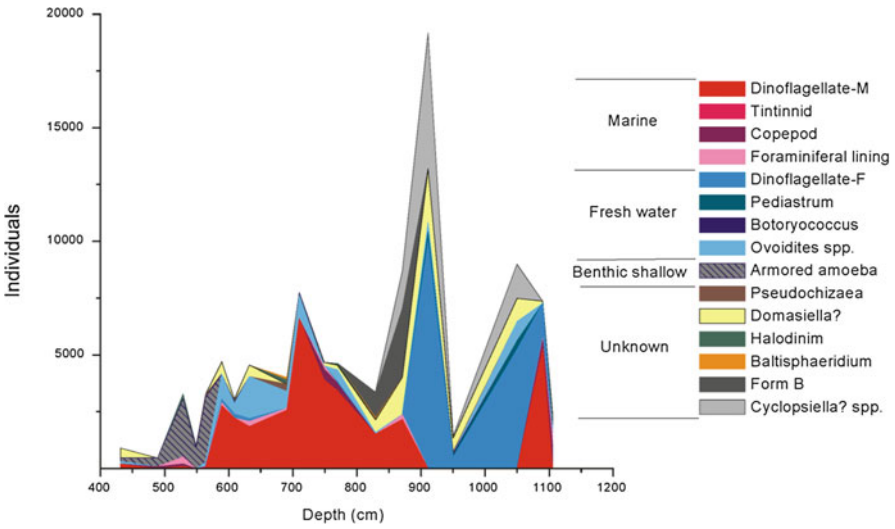

Fig. 9.17 Diagram showing the palynomorph analysis of the SJ99 core

Unit S6 Exposed Basement Rock and Soil Deposit (Before 7,800 ^{14}C yr BP) The basement rock of the Songjiho Lagoon area is Jurassic Daebo granite covered partially with Tertiary basal that has been the main clastic sources of depositional material to the Songjiho lagoon. The unit S6 could be exposed before the last glacial maximum, because the bottom of unit S5 begun deposition about 7,800 ^{14}C yr BP.

The constant low water contents in this unit imply the homogenous structure. X-radiograph also does not show any bedding plane or lamination. TOC content also shows the nearly zero percentage at the mid part of the unit S6, implying this layer is originated from pedogenesis. The much plant fragments at the top of unit S6 is also an evidence the pedogenesis of this unit. Matsuoka (Fig. 9.17) mentioned that this layer has no dinoflagellate as in soil environments. Glass grains from the top part of the unit S6 classified to AT tephra (Table 9.3). The pedogenesis of unit S6 formed at least before 22,000–23,000 ^{14}C yr BP.

Unit S5 Estuarine Deposits (~7,500 ^{14}C yr BP) The unit S5 could be considered estuarine deposit during the transgression starting before 7,800 ^{14}C yr BP (Table 9.1). The gravely sand layer in the lower part (subunit S5-L) considered as lag deposit that was originated in the initial time of transgression. High sulfur concentration indicates the influx of the marine water. Nevertheless the high C/N ratio shows the sedimentation materials are still originated from the land. This critical environment as illustrated by Howell's model (stagnant lagoon: Fig. 9.16) also supported by the coexistent of benthic foraminifera and fresh water dinoflagellate (Fig. 9.17).

Unit S4 Fresh Water Lake Deposit (~5,500 ^{14}C yr BP) Finer grain size from the boundary between units S5 and S4 continues up to mid part of the unit S4 without

fluctuation. This relatively stable and fine grain size variation may imply the basin was stagnant condition. Simultaneously, the very low sulfur content indicates fresh water condition during the subunit S4-M deposited. From the homogeneous lower and middle part of the S4(S4-L and S4-M), the isolated water lake is too shallow to form the anoxic laminated bed. The reason to become fresh water condition need further study. Damming effect such as development of sand barrier, human activity and/or volcanic lava flowing could be a possibility to understand this fresh water condition. If the falling of sea level is the cause of the fresh water condition, grain size must show coarsening upward in this range. However grain size display rather fining upward trend. And so the geomorphic change above mentioned should be the origin of this fresh water condition in this range.

The upward coarsening develops in the subunit S4-U. This variation of grain size indicates the change of distance from the provenance in isolated basin that influenced by falling of lake level changes. In the subunit S4-U vertical wave structure (VWS) is observed (Fig. 9.11). They are cut the horizontal plane vertically, and have variety of thinness, length and the waveform. Still we do not know the exact origin of VWS, the remains of plant root could be one of possibility to explain VWS. Perhaps the reed, which is spread out around lakeshore now on day, grew on the paleo lakeshore. And it might be that the remains of plant root were piled up like Fig. 9.11.

Unit S3 Stagnant Brackish Lagoonal System (4,000–2,500 year ^{14}C yr BP) The annual variation of lake creates laminated structure in bottom sediment from the absent condition of bioactivity. The faint and well-laminated layers in the unit S3 are consistent with the absence of molluscs indicating the oxygen poor condition. The runoff stagnation model of Howell et al. (1988) explains the origin of well-laminated layer in the brackish lagoonal system (Fig. 9.16). The isolation of Songjiho from development of sand barrier due to the rising of sea level (Brunn's rule, Fig. 9.10) is suitable for applying Howell's model.

The dinoflagellate also indicates that the surface water condition is brackish when the unit S3 was deposited. The slight decreasing of grain size and the diminishing of C/N ratio are clear criteria of the rising of sea level. The sea level rising make that the sea water influx enough to provide oxygen to the bottom of lagoon (Fig. 9.16). And the lamination became faint upward this unit due to increasing of oxygen supply according to sea level rising.

Unit S2 Oxic Condition Mark Deposit (About 1,000 ^{14}C yr BP) The fining upward of grain size from the unit S3 due to the rising the lake-level continues up to subunit S2-L. The abundance of shells from subunit S2-L indicates that the condition of the lake was open and has sufficient oxygen and nutrients in contrast to the previous environment (unit S3). Molluscs, represented by P. amurensis indicate a brackish water condition. A constant value of the water content and susceptibility, and much shell with their fragments occurred in this unit S2-L. It should be the consequence of an active bioturbation.

The decreasing of the shell fragment at the unit S2-U indicates that the environment of Songjiho Lagoon changed from enough oxygen to oxygen poor condition.

The decreasing trend of TS in the subunit S2-U supports this phenomenon, i.e. the sulfur supplied from sea water diminished as similar as oxygen decreasing phenomena by the isolating the Hwajinpo lagoonal system.

Unit S1 Isolated Lake/Lagoonal Deposit Influenced by Fresh Water (About 450 ^{14}C yr BP) The low sulfur content of the unit S1 with the relatively higher value of C/S indicates a diminishing of seawater influx condition. The high C/N ration in the subunit S1-M implies the much influx of terrestrial material. These could be due to the falling down of sea level, i.e. sand barrier that was developed by sea level rising during the previous stage (unit S2) formed the outer lagoon isolating from the sea by subsequent sea level falling. Human activity could be also considered as the origin of development of the intercalated layer with sand and mud because the age of layer is young enough to infer the historic event such as land use for farming.

9.5.2 The Trend of Transgression and Regression (T-R Diagram) of Lagoons

By the Howell's concept the relative sea level rise causes the lithologic change from laminated layer to marl deposit in a lagoonal basin (Fig. 9.9). For example, the transition from the unit H4 to unit H3 indicates the rising of sea level. As mention as before, grain size are variable with the sea level changes with lithologic change on the assumption of stable provenance condition. On the bases of this grain size variation concept, the distance from the provenance could be deduced and it should be related with sea level changes. And the sea level should be changed coincidently on the eastern coastal area including the Hwajinpo and Songjiho lagoons. Here, we describe the transgression and regression trend diagram (T-R diagram) indicate the transgression and regression trend deduced from the grain size change.

T-R diagram shows two and half cycles of sea level change in the Hwajinpo area (Fig. 9.18). In the Songjiho, three and half cycles of sea level changes could be inferred (Fig. 9.18). Standing water points (maximum rising and/or minimum falling) of study area shows almost coincident each other between Hwajinpo and Songjiho lagoons at 5,700 and 2,200 ^{14}C yr BP respectively. Although we could not describe the lithologic changes that indicate the low stand maximum trend in this range (about 660 ~ 690 cm depth), the sand percentage and the mean grain size show higher value and imply the higher energy condition when the layer deposited. It supposed that the location of the core SJ99 is far from the river mouth than that of the core HJ99. And the coarsening effect from the sea level falling is diminished in the Songjiho basin than that of the Hwajinpo. However the simultaneous falling sea level event at that moment is clear in both coastal lagoons.

T-R diagram shows more than three times transgression in the study area. Many sea level studies have been done around East Sea area, Jo (1980)'s Holocene sea level curves on the south-eastern coastal area is very similar trend with this study. The age of regression show reasonable comparison with the result of this study (Fig. 9.19).

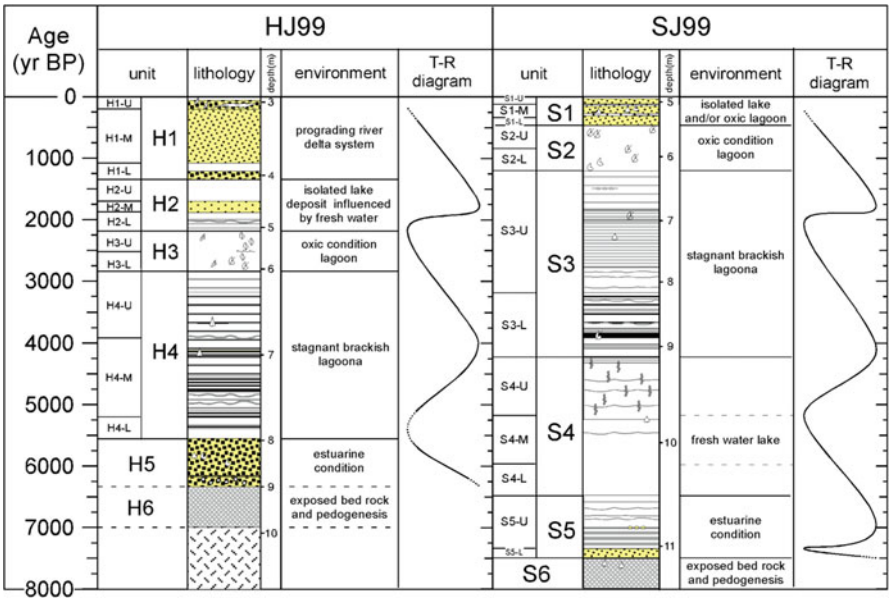

Fig. 9.18 Comparison of the HJ99 and SJ99 cores based on the chronology and environment. The conceptual evolutionary history of the outer lake of the Hwajinpo and the Songjiho lagoons. T-R diagram: Transgression Regression (*T-R*) trends in the Hwajinpo and Soongjiho lagoons

On the assumption that two major erosional landform in study area (about 80 and 160 cm amsl; Fig. 9.6) formed during the Holocene, the each erosional landform is related with high standing sea level span. The high standing about 7,500 ^{14}C yr BP reported at more 10 m below than present sea level in world wide area (Jo 1980; Pirazzoli 1991). And another high stand about 300 ^{14}C yr BP has too short period to form erosional landform period. Therefore, the high stands age on 5,700 and 2,200 ^{14}C yr BP supposed to form erosional landforms on the above sea level of the 160 and 80 cm respectively.

Lakes Shinji and Nakaumi are also costal lagoons in Japan located along the Sea of Japan. The origin and development of these lakes are related to post-glacial sea level changes. Moreover, the morphological setting that is composing of inner and outer lagoon is similar to that of the Hwajinpo Lagoon in Korea. Many studies on Lake Shinji and Nakaumi have been carried out the detail (e.g. Tokuoka et al. 1990; Sampei et al. 1994; Nakamura et al. 1996). Nakamura et al. (1996) complied the results from historic sites to establish sea level curve around the Lakes Shinji and Nakaumi. This trend also shows much similarity with the result of this study.

The trend of sea level changes from the Hwajinpo and Songjiho lagoons seems to be very similar with each other because they are situated in the same condition. Hence the trend of sea level fluctuation from the two lagoons shows similarities with that of Lake Shinji and Nakaumi (Nakamura et al. 1996; Fig. 9.24). The sea

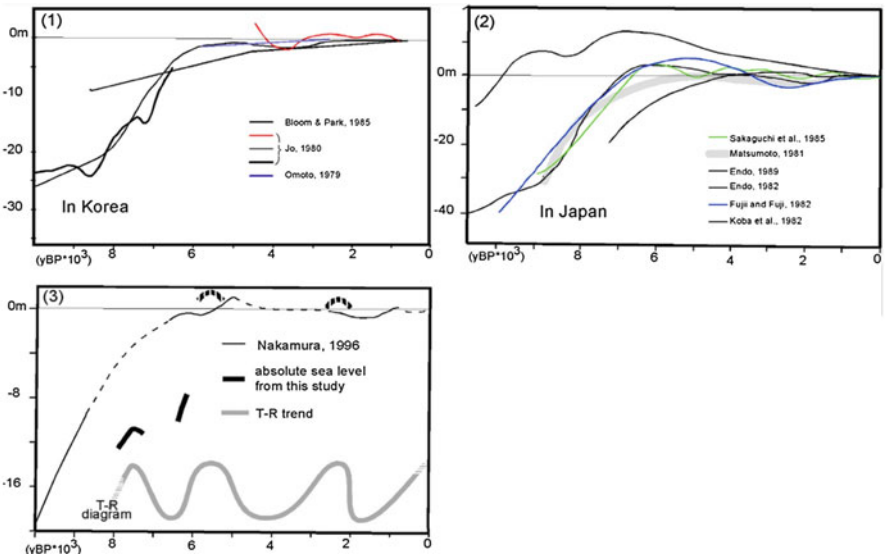

Fig. 9.19 Late Quaternary sea level records around Korea and Japan (*1*) Holocene sea level curves in Korea (Han 1994) (*2*) Relative sea level curves in Japan (Umitsu 1991) (*3*) Sea level changes in the eastern part of Shimane in Japan (Nakamura et al. 1996) and the absolute sea level records determined in this study

level changes of the Japan Sea from other reports (Okada 1978; Toyoshima 1978; Jo 1980) also supports T-R diagram inferred from the present study.

9.5.3 The Evolution Model of Lagoons with Sea Level Changes

On the basis of these results, we could describe the conceptual evolution model of the Hwajinpo Lagoon as shown in Fig. 9.18. The basement rock (Precambrian Gyeonggi Gneiss Complex) was exposed and its surface had been strongly weathered before 6,800 ^{14}C yr BP. Estuarine sediments deposits including bay types of shell with their fragments overlying on the basement rock. The estuarine deposit on the basement rock reported in other coastal areas of Korea. Jo (1980) thought the sandy deposits containing mollusc should be related to a rise in the sea level during the early Holocene. Therefore, it is certain that the Hwajinpo Lagoon became an estuarine system during same sea level rising. Subsequently, the falling sea level caused the Hwajinpo to be isolated in a brackish condition due to frequent influx of sea water. However, the bottom condition was anoxic and not enough for living organisms, and the lamination layer developed in the isolated environment (5,500–2,800 ^{14}C yr BP).

The increase of the sea level again allowed the lake bottom to get a sufficient influx of sea water containing enough oxygen, so that many molluscs could live in this higher lake level condition (2,800–2,200 ^{14}C yr BP). By subsequent slight falling sea level, the Hwajinpo Lagoon might be isolated easily to be a coastal lake influenced from fresh water influx (about 1,700 ^{14}C yr BP). It ought to be the roll of damming by development of barrier and/or inlet sand deposit during this high stand condition of water. After that, with the rising sea level, the Hwajinpo Lagoon has reached its present condition and the river delta was prograding upon the HJ99 coring location.

On the other hands, the conceptual evolution model of the Songjiho Lagoon could be described as follows. The basement rock (Daebo Granite) was exposed and its surface had been strongly weathered. And on that weathered surface the plants were grown and AT tephra glasses was deposited simultaneously by wind blows or ephemeral runoff during heavy rain. Then, during the sea level rising (Fig. 9.18), the estuarine sand deposits were formed on that subaerial weathered surface. At the same time, the sand barrier also developed with the sea level rising (Fig. 9.9). However, the sea level falling occurred during unit S4-L and S4-M, and it made the Songjiho basin isolated because the previous sand barrier role as a dam to the basin. Again, according to the rising the sea and/or lake level during S4-U unit, the reed had spread all shallow shoreline. Subsequently, the Songjiho Lagoon became brackish lagoon by the continuous sea level rising.

The sand rich layer at the depth of 6.5 m coincident with the sandy rich subunit H2-M of the HJ99 core and the age of two events occurred about 1,500 ^{14}C yr BP. These coarsening events imply simultaneous environmental changes. From grain size variation of HJ95 core and HJ99 core this trend in not indicates accident event but continuous environmental change although the time is not long period. On these base concepts, we deduce this coarsening size variation origin the short period sea level falling.

Subsequently, the increase of sea level again allowed the lake bottom to get a sufficient influx of sea water, so that many molluscs could live in this condition. And finally the Songjiho Lagoon has reached its present condition and human activity for land use supplied much sand deposition eventually to form the intercalating bedding.

9.6 Conclusion

The reconstruction of the paleoenvironment from this study allows the establishment of evolutionary models and sea level trends of the Hwajinpo and Songjiho lagoons. The stages of different depositional environment of the Outer Lake of Hwajinpo Lagoon can be divided into six units; (1) Exposed basement rock (unit H6; before 6,800 ^{14}C yr BP), (2) Estuarine deposit (unit H5; about 6,000 ^{14}C yr BP), (3) Stagnant brackish lagoonal deposit (unit H4: 5,500–2,800 ^{14}C yr BP), (4) Oxic condition marl deposit (unit H3; about 2,500 ^{14}C yr BP), (5) Isolated lake deposit

influenced by fresh water (unit H2; about 1,700 ^{14}C yr BP), (6) Prograding river delta deposit (unit H1; beginning about 1,000 ^{14}C yr BP).

The stages of different depositional environment of the Songjiho Lagoon can be divided into six units since the last 7,800 ^{14}C yr BP; (1) Exposed basement rock and soil (unit S6; before Holocene period), (2) Estuarine deposits (unit S5; about 7,500 ^{14}C yr BP), (3) Fresh water lake deposit (units S4; about 5,500 ^{14}C yr BP), (4) Stagnant brackish lagoonal system (unit S3; 4,000–2,500 ^{14}C yr BP), (5) Oxic condition marl deposit (unit S2; about 1,000 ^{14}C yr BP), (6) Isolated lake/lagoonal deposit influenced by fresh water (unit S1; beginning about 450 ^{14}C yr BP).

The environmental change should be related to sea level fluctuations during the Late Quaternary. The transgression and regression (T-R) trend deduced from grain size variation in the Hwajinpo and Songjiho lagoons show simultaneity. T-R trend present three and half cycles since 7,800 ^{14}C yr BP. High stand sea levels by transgression are appeared about at 7,400, 5,500, and 2,200 ^{14}C yr BP. And Low stand sea levels by regression are appeared about at 6,500, 4,100, and 1,800 ^{14}C yr BP.

Acknowledgements This research was partially supported by the China-Japan-Korea international collaboration research project (2011–2013) funded by the National Research Foundation of Korea, and the Basic Research Project of the Korea Institute of Geoscience and Mineral Resources (KIGAM) funded by the Ministry of Knowledge Economy of Korea.

References

Bak YS, Nahm WH, Lee SJ (2013) Holocene paleoenvironmental changes from diatom analysis of sediments from the Songjiho Lagoon on the eastern coast of Korea. J Geol Soc Korea 49(2):297–303

Bloom AL, Park YA (1985) Holocene sea-level history and tectonic movements. Republic of Korea. Quat Res Japan 24:77–83

Bruun P (1962) Sea level rise as a cause of shore erosion. Amer Soc Civil Eng Proc J Waterways Harbors Div 88:117–130

Cater RWG, Forbes DL, Jennings SC, Orford JD, Shaw J, Taylor RB (1989) Barrier and lagoon coast evolution under differing relative sea level regimes: examples from Ireland and Nova Scotia. Mar Geol 88:221–242

Dominguez JML, Martin L, Bittencourt ACSP (1987) Sea level history and quaternary evolution of river mouth-associated beach-ridge plain along the east-southeast Brazilian coast: a summary. In: Nummedal D, Pilkey OH, Howard JP (eds) Sea level fluctuation and coastal evolution, Society of Economic Paleontologists and Mineralogists, Special publication no.41. Society of Economic Paleontologists and Mineralogists, Tulsa, pp 115–128

Eitner V (1996) Geomorphological response of the East Frisian barrier islands to sea level, rise: an investigation of past and future evolution. Geomorphology 15:57–65

Endo K, Skimoto K, Takano T (1982) Holocene stratigraphy and paleoenvironments in the Kanto Plain, in relation to the Jomon transgression. In: Proceedings of the Institute of Natural Sciences. College of Humanities and Sciences, Nihon Univ 17:1–16

Endo K, Kosugi M, Matsushita M, Miyaji N, Hishida R, Takano T (1989) Holocene environmental history in and around the Paleo-Nagareyama Bay, central Kanto plain. Quat Res Japan 28:61–77

Folk RL, Ward WC (1957) Brazos River bar: a study in the significance of grain-size parameters. J Sediment Petrol 27:3–26

Han SJ (1994) Quaternary sea-level changes and their implication in the evolution of coastal, depositional environments (III). Report from Korea Ocean Research and Development Institute (KORDI, Ansan city, Korea)

Howell MW, Thunell RE, Tappa E, Rio D, Sprovieri R (1988) Late Neogene laminated and opal-rich facies from the Mediterranean region: geochemical evidence for mechanisms of formation. Palaeogeogr Palaeoclimatol Palaeoecol 64:265–286

Jo W (1980) Holocene sea level changes on the east coast of Korea Peninsula. Geogr Rev Jpn 53:317–328

Jujii S, Fuji N (1982) Postglacial sea-level changes in the Hokuriku region, central Japan. Quat Res Japan 21:183–193

Jung WY, Park YA (1976) Depositional environments of the recent sediments in the Hwajinpo Lake, Gangweondo, Korea. J Oceanol Soc Korea 11(2):64–70

Kemp AES (1990) Sedimentary fabrics and variation in lamination style in Peru continental margin upwelling sediments. In: Suess E, von Heune R et al (eds) Proceedings of ODP scientific results 112. Ocean Drilling Program, College Station, pp 43–58

Kirk RM, Lauder GA (2000) Significant coastal lagoon systems in the South Island, New Zealand - coastal, processes and lagoon mouth closure. Sci Conserv 146:5–47

Kitagawa H, Masuzawa T, Nakamura T, Matsumoto E (1993) A batch preparation method of graphite targets with low background for AMS ^{14}C measurements. Radiocarbon 35(2):295–300

Kjerfve B (1994) Coastal lagoons. In: Kjerfve B (ed) Coastal lagoon processes, Elsevier oceanography series, 60. Elsevier, Amsterdam, pp 1–8

Kjerfve B, Magill KE (1989) Geographic and hydrographic characteristics of shallow coastal lagoons. Mar Geol 88:187–199

Knoppers B, Kjerfve B, Carmouze JP (1991) Tropic state and water turn-over time in six choked coastal lagoons in Brazil. Biogeochemistry 14:149–166

Koba M, Nakata T, Takahashi T (1982) Late Holocene eustatic sea-level changes deduced from the geomorphological features and their ^{14}C dates in the Ryukyu Islands. Japan Palaeogeogr Palaeoclimatol Palaeoecol 39:231–260

Korotkii AM (1985) Quaternary sea-level fluctuations on the northwestern shelf on the Japan Sea. J Coast Res 1(3):293–298

Kraft JC, John CJ, Marx PR (1981) Clastic depositional strata in a transgressive coastal environment: Holocene epoch. Northeastern Geol 3(3–4):268–277

Kwon OK, Park SM, Lee JS (1993) Coloured shells of Korea. Academy Publishing Co, Seoul, 446p

Li CX, Zhang JQ, Fan DD, Deng B (2001) Holocene regression and the tidal radial sand ridge system formation in the Jiangsu coastal zone, east China. Mar Geol 173:97–120

Matsumoto E, Maeda Y, Takemura K, Nishida S (1987) New radiocarbon age of Aira-Tn Ash (AT). Quat Res Japan 26:79–83

Matsuoka K, Fukuyo Y, Anderson DM (1989) Method of modern dinoflagellate cyst studies. In: Okaichi T, Anderson DM, Nemoto T (eds) Red tides: biology, environmental science an toxicology. Elsevier Science Co., New York, pp 461–479

Matsubara A (2000) Holocene geomorphic development of coastal barriers in Japan. Geogr Rev Jpn Ser A 73(5):409–434

McRae C, Snape CE, Sun CG, Fabbri D, Tartari D, Trombini C, Fallick AE (2000) Use of compound-specific stable isotope analysis to source anthropogenic, aromatic hydrocarbons in a lagoon sediment. Environ Sci Technol 34(22):4684–4686

Mee LD (1978) Coastal lagoons. In: Riley J, Skirrow O (eds) Chemical oceanography, 2nd edn. Academic, New York, pp 441–490

Minoura K, Hoshino K, Nakamura T, Wada E (1997) Late Pleistocene-Holocene paleoproductivity circulation in the Japan Sea, sea-level control on δ^{13}C and δ^{15}N records of sediment organic material. Palaeogeogr Palaeoclim Palaeoecol 135:41–50

Moore NH, Slinn DJ (1984) The physical hydrology of a lagoon system on the Pacific coast of Mexico. Estuar Coast Shelf Sci 19:413–426

Morton RA, Ward GH, White WA (2000) Rates of sediment supply and sea-level rise in a large coastal lagoon. Mar Geol 167:261–284

Nahm WH, Hong SS (2014) Holocene environmental changes inferred from sedimentary records in the lower reach of the Yeongsan River, Korea. Holocene:1–12

Nahm WH, Kim JC, Bong PY, Kim JY, Yang DY, Yu KM (2008) Late quaternary stratigraphy of the Yeongsan Estuary, Southwestern Korea. Quatern Int 176–177:13–24

Nahm WH, Kim JK, Kim JY, Yi S, Lim J, Kim JC (2013) The Holocene climatic optimum in Korea: evidence from wetland records. Palaeogogr Palaeoclim Palaeoecol 376:163–171

Nakai N, Nakamura T, Kimura M, Sakase T, Sato S, Sakai A (1984) Accelerator mass spectrometry of ^{14}C at Nagoya University. In: Wolfli W, Polach HA, Anderson HH (eds) Proceedings of the 3rd international symposium on accelerator mass spectrometry. Nucl Instr Method Phys Res B29(B5):171–174

Nakamura T, Nakai N, Ohishi S (1987) Techniques of tandem accelerator mass spectrometry and their applications, to ^{14}C measurements. In: Gove HE, Litherland AE, Elmore D (eds) Proceedings of the 4th international symposium on accelerator mass spectrometry. Nucl Instr Method Phys Res B29(B5):355–360

Nakamura T, Tokuoka T, Onishi I, Sampei Y, Takayasu K, Takehiro F, Ege K, Nishio K, Watanabe M (1996) Holocene environmental changes and lowland historic sites in eastern part of the Shimane Prefecture. Laguna 3:9–11

Nakata K, Horiguchi F, Yamamuro M (2000) Model study of lakes Shinji and Nakaumi – a coupled coastal lagoon system. J Mar Syst 26:145–169

Okada A (1978) Sea-level change and geomorphic development since the last glacial age in the Wakasa Bay region central west of the Japan Sea coast. Geogr Rev Jpn 51(2):131–146

Omoto K (1979) Holocene sea-level changes: a critical review. Sci Rep Tohoku Univ 7th ser 29:205–222

Park BK, Kim WH (1981) The depositional environments of lagoons in the east coast of Korea. J Geol Soc Korea 17:241–249

Pirazzoli PA (1991) World atlas of Holocene sea level changes, Elsevier oceanography series, 58. Elsevier, Amsterdam, 300p

Sakaguchi Y, Kashima K, Matsubara A (1985) Holocene marine deposits in Hokkaido and their sedimentary environments. Bull Dep Geogr Univ Tokyo 17:1–17

Sampei Y, Matsumoto E, Tokuoka T, Inoue D (1997) Changes in accumulation rate of organic carbon during the last 8,000 years in sediments of Nakaumi Lagoon. Jpn Mar Chem 58:39–50

Sampei Y, Yomura H, Otsuka M, Yoshida K, Suzuki N (1994) Decomposition of organic matter and the organic carbon content of sediments, in Lake Shinji, southwest Japan. Earth Sci 48(4): 317–332

Selivanov AO (1996) Morphological changes on Russian coasts under rapid sea-level changes: examples from the Holocene history and implications for future. J Coast Res 12(4):823–830

Sikora WB, Kjerfve B (1985) Factors influencing the salinity of Lake Pontchartrain, Louisiana, a shallow, coastal lagoon: analysis of a long-term data set. Estuaties 8(2A):170–180

Smith NP (2001) Seasonal-scale transport patterns in a multi-inlet coastal lagoon. Estuar Coast Shelf Sci 52:15–28

Stuiver M, Polach HA (1977) Discussion: reporting of ^{14}C data. Radiocarbon 19(3):335–363

Stuiver M, Reimer PJ, Bard E, Beck JW, Burr GS, Hughen KA, Kromer B, McCormac G, van der Plicht J, Spurk M (1998) INTCAL98 radiocarbon age calibration, 24,000-0 cal BP. Radiocarbon 40:1041–1083

Takemura K, Danhara T (1994) A method for determination of volcanic glass concentrations in sedimentary, sequences and its application to quaternary studies. Geoarchaeology 9(4): 301–316

Takemura K, Yokoyama T (1991) Mineral composition of sand grains at the coast and rivers around Lake Biwa. In: Foundation of Nature Conservation in Shiga (ed) Landscape and environment of Shiga, scientific studies of Shiga Prefecture, Japan, Separate volume for geomorphology and geology. Foundation of Nature Conservation in Shiga, Otsu, pp 687–701

Tokuoka T, Onish I, Takayasu K, Mitunashi T (1990) Natural history and environmental changes of Lakes Nakaumi and Shinji. Mem Geol Soc Jpn 36:15–34

Toyoshima Y (1978) Postglacial sea level change along San'in District, Japan. Geogr Rev Jpn 51(2):147–157

Uhm KB (1971) Studies on the productive structure in some lakes in Korea. Korean J Bot 14:15–23

Uhm KB (1973) Ecological comparison of several lakes in summer stagnation period. Korean J Bot 16:17–34

Umitsu M (1991) Holocene sea-level changes and coastal evolution in Japan. Quatern Res (Tokyo) 30(3):187–196

Yum JG (1996) Characteristics of a coastal lagoon, Hwajinpo, in the eastern coast of Korea, and its comparison with coastal lagoons in Sanin region in Japan. M.Sc. thesis, Shimane University, Matsue, Japan, 72p

Yum JG, Takemura K, Tokuoka T, Yu KM (2003) Holocene environmental changes of the Hwajinpo Lagoon on the eastern coast of Korea. J Paleolimnol 29:155–166

Yum JG, Yu KM, Takemura K, Naruse T, Kitamura A, Kitagawa H, Kim JC (2004) Holocene evolution of the outer lake of Hwajinpo Lagoon on the eastern coast of Korea; environmental changes with Holocene sea-level fluctuation of the East Sea (Sea of Japan). Radiocarbon 46(2):797–808

Yum JG, Han MS, Yu KM (2006) Age calibration of environmental changes in the Inner Lake of Hawjinpo Lagoon by using AMS radiocarbon dating. Sae Mulli 53(2):114–124

Chapter 10
Multi-proxy Evidence for Late-Holocene Agricultural Activities from Coastal Lagoons on the East Coast of Korea

Jungjae Park and Mark Constantine

Abstract Multi-proxy records of chronologically well-defined sediments have been recently reported from four lagoons (Bongpo marsh, Lake Cheonjinho, Lake Ssangho, and Lake Soonpogaeho) in the Yeongdong region on the east coast of Korea. They deserve close examination as they clearly show the transition towards an agricultural society and local land-use changes during the late Holocene. Bongpo marsh began to develop ca. 650 BC as a coastal lagoon was rapidly filled with organic matter. Rice agriculture intensified sufficiently to cause a noticeable shift in the pollen record from ca. AD 600. An intensification in rice agriculture began from ca. AD 780 at Lake Cheonjinho and from ca. 100 BC at Lake Ssangho. Soonpogae lagoon was almost completely isolated from the sea by sand barriers when human impact intensified about AD 80. Rice agriculture was introduced into Sokcho/Gosung area (Lake Cheonjinho and Bongpo marsh) long after its arrival in the Gangneung/Yangyang area (Lakes Soonpogae and Ssangho), despite the absence of any geomorphic barrier to hinder the spread of rice cultivation along the coast. This finding indicates that it is difficult to identify the arrival date of rice agriculture in a specific area using pollen records since the pollen is generally a better indicator of the beginning of agricultural intensification. The multi-proxy data examined in this paper imply that in order to pinpoint dates of important agricultural events and reconstruct land-use history, it is essential to take a multidisciplinary approach using both palynological and archaeological evidence.

Keywords Rice agriculture • Land-use history • Lagoonal sediments • Pollen • Multi-proxy • East coast • Korea

J. Park (✉) • M. Constantine
Department of Geography, Seoul National University, Sillim-dong, Gwanak-gu, Seoul 151-742, Republic of Korea
e-mail: jungjaep@snu.ac.kr

K. Kashiwaya et al. (eds.), *Earth Surface Processes and Environmental Changes in East Asia*, DOI 10.1007/978-4-431-55540-7_10

10.1 Introduction

Not many paleoenvironmental studies have been carried out in Korea due to the small number of natural lakes, sediments of which are usually considered an ideal target for paleoenvironmental analyses. The east coast of Korea contains several coastal lagoons, however, where suitable bottom sediments are available. Japanese scientists performed pollen studies of lagoonal sediments in the late 1970s and presented crucial information on the paleoclimate and paleoecology of Korea (Yasuda et al. 1979). Subsequent studies on lagoonal sediments have produced several pollen records (Fujiki and Yasuda 2004; Yoon et al. 2008) and geochemical data (Yum et al. 2003).

Exact information on the history of rice agriculture in the east coast of Korea is essential to establish the routes and times of the diffusion of rice agriculture in the whole southern Korean peninsula because rice cultivation is believed to have been most recently disseminated into this area (Park 2007). Combined proxy data from coastal lagoons arrayed along the east coast would therefore be helpful for understanding the temporal and spatial nature of agricultural spread in Korea. However, most previous research from lagoons has focused on climate and environmental change rather than human activities, leading to controversy on the origins of rice agriculture in the area (Yoon et al. 2008; Kim and Park 2011).

Most importantly, due to the absence of dates for right depths where pollen indicators of agriculture steeply rose in frequencies, many previous works could not determine the exact time for the introduction of rice agriculture into the east coast, but merely estimated the age of its beginning through coarse interpolation of dates. Furthermore, being based only on pollen records, these studies determined the age for its beginning, which is obviously less reliable than one based on various proxy data altogether: accurate dating requires as many proxy as possible. The thick cultivated top layers and low resolutions of the terrestrial sedimentary sequence also prevented the tracking of paleoenvironmental change using sediments and weakened any detailed discussion of the land use history. Therefore, late Holocene agricultural activities across the Korean peninsula have been discussed mainly based on few archaeological remains (Choe 1982; Im 1992; Chon 1992; Crawford and Lee 2003; Ahn 2010).

To better understand the uncertainty in the introduction of rice agriculture into the east coast and postulate reliable hypotheses for its occurrence, more scientific evidence needs to be produced through interdisciplinary work. Recently, chronologically well-defined paleoenvironmental records were newly reported from several coastal lagoons in the Yeongdong region on the east coast (Park et al. 2012a, b; Park and Shin 2012). These new multi-proxy records deserve examination because they all clearly show the transition towards an agricultural society and illustrate local land-use changes during the late Holocene. Relatively intact lagoonal sediments with a high sedimentation rate provide a good opportunity to document the late Holocene anthropogenic environmental changes, to reveal when rice agriculture began in each study site, and to resolve the uncertainty about the times of the dissemination of rice cultivation practices. This paper evaluates the

paleoenvironmental and archaeological interpretation and chronology of several lagoonal sediments in which the beginning of rice cultivation is well exhibited – Bongpo marsh (Park et al. 2012a), and Lakes Cheonjinho, Ssangho (Park and Shin 2012), and Soonpogaeho (Park et al. 2012b).

10.2 Multi-proxy Evidence from Coastal Lagoons of the East Coast

10.2.1 Coastal Lagoons in Yeongdong Region

Bongpo lagoonal marsh (38°14′52″N 128°33′47″E) and Lake Cheonjinho (38°15′13″N 128°33′20″E) are located close to each other on the central east coast of Korea while Lakes Ssangho (38°05′06″N 128°33′47″E) and Soonpogaeho (37°49′10″N 128°53′16″E) are located further south (Fig. 10.1). A number of freshwater coastal lagoons were formed on the east coast during the late Holocene, probably due to agricultural disturbance on the upper western areas that led to a gradual rise in sediment influx, which closed the estuaries and river outlets, and eventually transformed them into lagoonal marshes (e.g. Bongpo marsh).

Korea's peninsular location on the eastern edge of the Eurasian continent affords it both continental and oceanic climates. The southeastern monsoon brings hot/humid summers and the northwest winter monsoons brings cold/dry winters to the region. On the eastern side of the Korean peninsula, the Taebaek mountains, rising to an altitude of over 1,500 m and standing only about 20 km west of the coastline, block the northwest monsoon and create a Foehn effect wind that moderates the temperature of the east coast, leaving the area relatively warm in winter. Compared to interior areas at similar latitudes, the winter is relatively warm while the summer is relatively cool due to the oceanic influence on the coast. Mean monthly temperatures around study sites range from −0.3 – 0.4 °C in January to 23.7–24.6 °C in August, and average annual rainfalls are between 1,402 and 1,464 mm (Korea Meteorological Administration n.d.).

The Korean vegetation map proposed by Yim (1977) assigned the vegetation around the study sites to the cool temperate forest zone consisting of *Quercus mongolica*, *Quercus serrata*, *Abies holophylla*, *Carpinus laxiflora* and *Styrax spp*. However, the anthropogenic disturbances to the natural vegetation of the area have led to the domination of Pinus densiflora in the uncultivated lands in the study area. In Mt. Odae, an adjacent mountain national park, *Pinus densiflora*, *Quercus serrata*, *Rhus trichocarpa*, and *Lindera obtusiloba* are important and common species below 700 m. Between 700 and 900 m, *Acer mono*, *Fraxinus rhynchophylla*, *Prunus sargentii*, *Fraxinus mandshurica*, *Euonymus oxyphyllus*, and *Carpinus laxiflora* are the main species. The high altitudinal zone (>1,000 m) is mainly dominated by cold-resistant tree species such as *Quercus mongolica*, *Acer pseudo-sieboldianum*, *Tilia amurensis*, *Abies holophylla*, *Carpinus cordata*, *Betula costata*, *Kalopanax pictus*, and *Pinus koraiensis* (Yu et al. 2003). Common aquatic species around

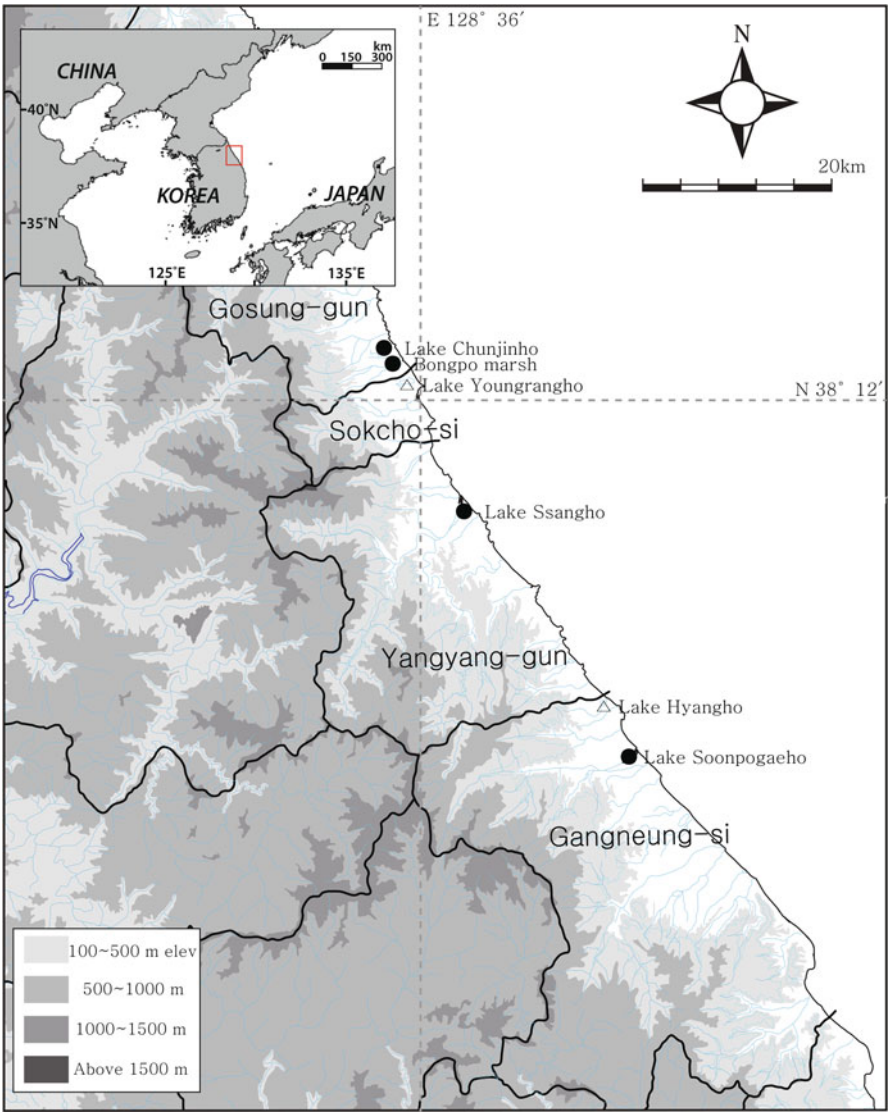

Fig. 10.1 Location map of the four Yeongdong coastal lagoons examined in this study. Pollen sites examined here are indicated by *solid black circles*

these lagoons include *Phragmites australis* and *P. japonica*, *Persicaria thunbergii*, *Juncus effuses*, *Bidens frondosa*, *Eleocharis mamillata*, *Anemone koraiensis*, *Scirpus maritimus*, *Persicaria sieboldii*, *Potamogeton crispus* and *P. distinctus*, *Lycopus lucidus*, *Typha angustifolia*, *Trapa japonica*, *Nymphaea tetragona*, *Zizania latifolia*, *Utricularia vulgaris*, *Miscanthus saccariflorus*, *Arthraxon hispidus*, and *Myriophyllum spicatum*.

The main crop in Kangwon Province, where studied lagoons are located, is rice. However, other crops such as corn (*Zea mays*) and white potatoes (*Solanum tuberosum*) are also important due to a lack of paddy land. Farmers in the region occasionally grow tobacco (*Nicotiana tabacum*), hops (*Humulus lupulus*) for beer, mulberry (*Morus alba*) for silk, hemp (*Cannabis sativa*) for fiber, ginseng (*Panax ginseng*) and various other highland vegetables. Compared to the other regions of Korea, the area around the study site is much less productive because of its mountainous nature.

The following discussion examines the implications of the proxy records from Bongpo marsh (Figs. 10.2 and 10.3), and Lakes Cheonjinho (Fig. 10.4), Ssangho (Fig. 10.5), and Soonpogae (Figs. 10.6 and 10.7) in the Yeongdong region and examines the extent to which they reflect the start of rice agriculture and the subsequent changes in agricultural land use. Radiocarbon dates for all the proxy records evaluated in this chapter were shown in Table 10.1.

10.2.2 Bongpo Marsh

10.2.2.1 Human-Induced Vegetation Change

Cyperaceae, which was almost absent in zone 1a (ca. 1,250–650 BC), became explicitly important from the beginning of zone 1b (ca. 650 BC – AD 600), indicating that a freshwater coastal marsh succeeded a coastal lagoon as the latter was no longer significantly affected by sea water because of an increased influx of clastics and organic matter from the adjacent land area. A radiocarbon date at 300 cm depth suggests that the conversion to a marsh probably took place around 650 BC. Unlike Zone 1a, Zone 1b exhibited a high variation in *Pinus* and *Quercus* frequencies. In general, changes in these two taxa were associated with environmental changes occurring in a relatively wide area since their pollen are produced in large quantities and could be dispersed over long distances. On the other hand, herb pollen related to agricultural disturbance was almost completely absent. The high variability in *Pinus* and *Quercus* frequencies and the relatively few anthropogenic herb pollens in zone 1b reflect the action of anthropogenic influences on the regional surroundings, although rice agriculture had not yet commenced in the local study area. This interpretation is supported by the rapid increase in microscopic charcoal frequencies from the middle of zone 1b.

Much of the evidence in zone 2 (ca. AD 600–1870) is indicative of full-scale rice agriculture in the area. The abrupt rise of wild Poaceae, cultivated Poaceae, and *Artemisia*, along with an increase in *Pinus* and decrease in *Quercus*, imply the expansion of agriculture in the area. An extensive work of land reclamation is reflected by peaks of Monolete spore frequencies and charcoal concentrations, and a complete absence of Cyperaceae at the lower boundary. Sedges may have been burned in the vicinity of the marsh and rice subsequently grown. Seriously disturbed areas around rice fields were presumably occupied first by ferns, which, however,

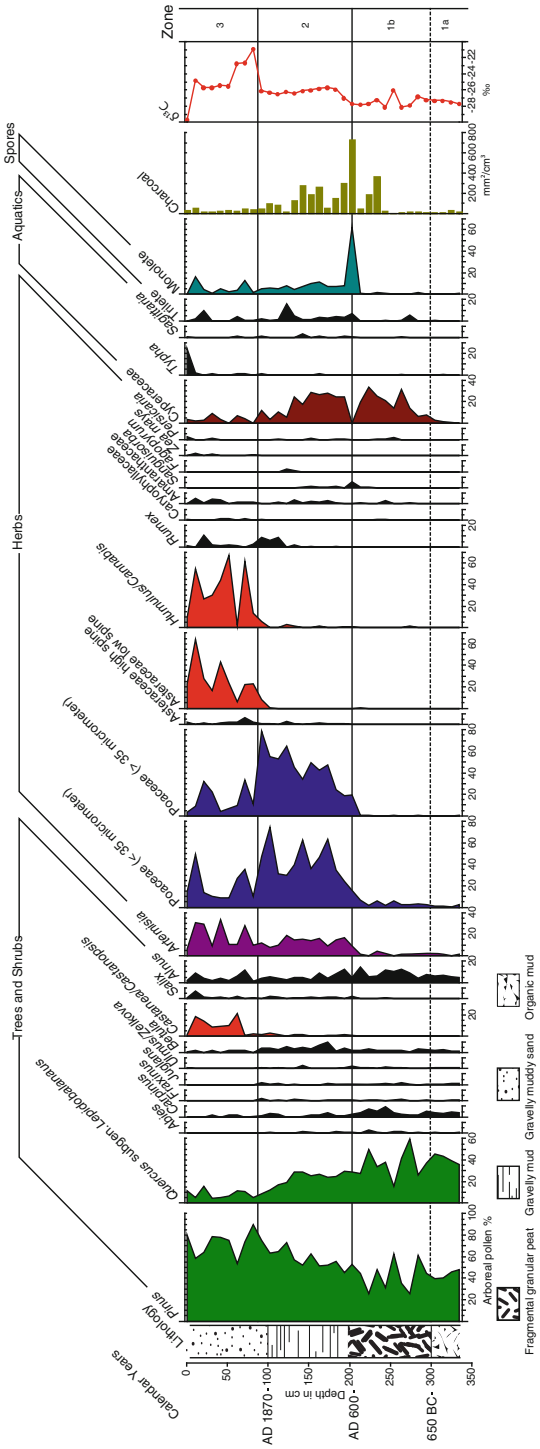

Fig. 10.2 Selected pollen and spore taxa, microscopic charcoal, and $\delta^{13}C$ values from the Bongpo sediment core (Redrawn from Park et al. 2012a)

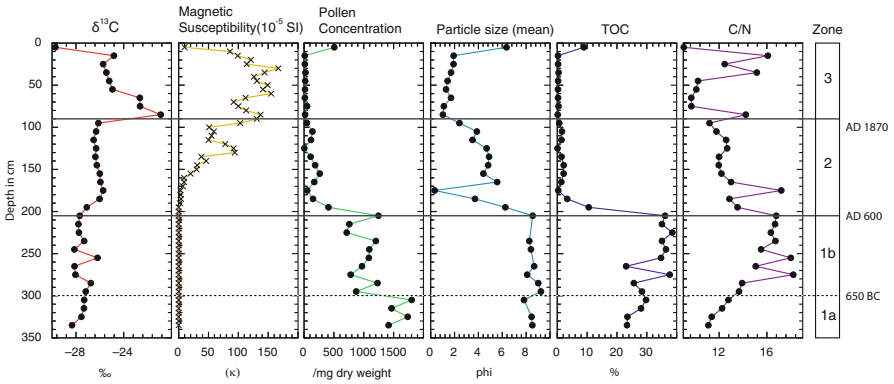

Fig. 10.3 $\delta^{13}C$, magnetic susceptibility, TOC, pollen concentration, C/N, and particle size (mean) from the Bongpo sediment core (Redrawn from Park et al. 2012a)

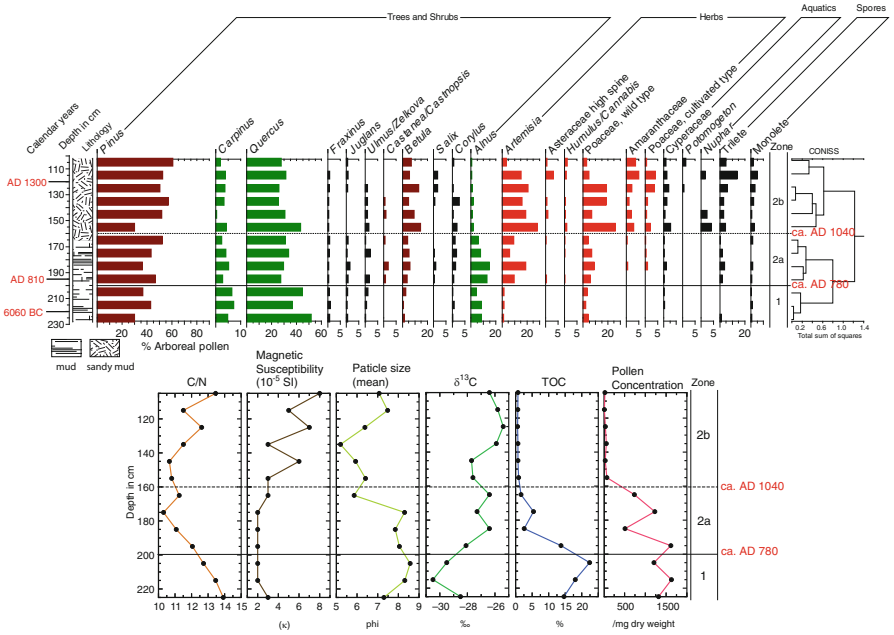

Fig. 10.4 Selected pollen and spore taxa, $\delta^{13}C$, magnetic susceptibility, TOC, pollen concentration, C/N, and particle size (mean) from the Chenonjinho sediment core (Redrawn from Park and Shin 2012)

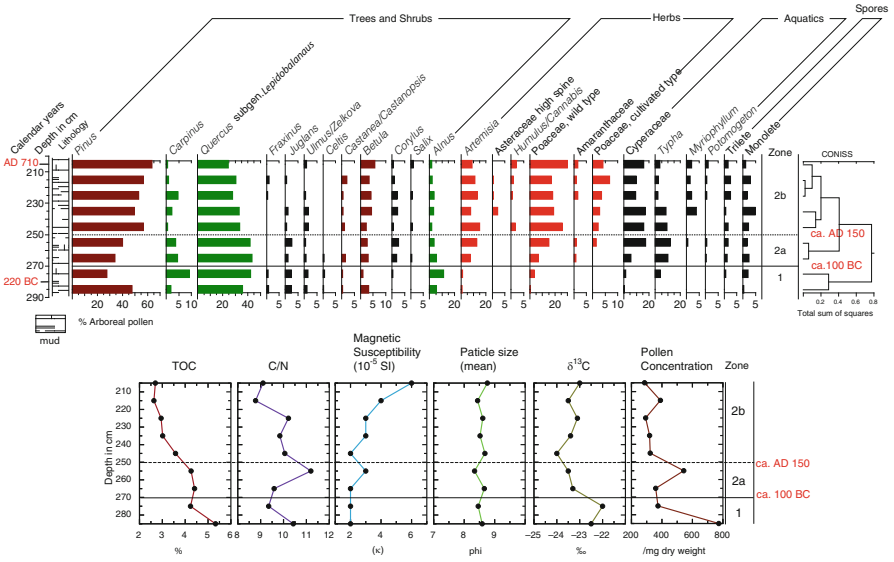

Fig. 10.5 Selected pollen and spore taxa, $\delta^{13}C$, magnetic susceptibility, TOC, pollen concentration, C/N, and particle size (mean) from the Ssangho sediment core (Redrawn from Park and Shin 2012)

seem to have been out-competed by sedges in a very short time. The gradual expansion of cultivated fields is implied by the steady rise in wild and cultivated Poaceae and a steady decline in Cyperaceae. Land clearance for agriculture would have created an open environment suitable for heliophyte trees such as *Betula* and *Salix* but unsuitable for sciophyte trees such as *Carpinus* and *Ulmus*. A decrease in *Alnus* indicates that the alder habitat around the marsh was also disturbed by agricultural activity.

Zone 3 (ca. AD 1870 – present) corresponds to the period of decreasing agricultural activities. Extremely high sedimentation rates imply that the marsh was rapidly filled by the deposition of a large amount of clastic sediment. This may have been associated with excessive logging and deforestation, which brought about heavy soil erosion in the catchment basin (Lee 2003). As described in "The Annals of the Joseon Dynasty", a record of national affairs and the activities of the state between AD 1413 and 1865, rampant deforestation occurred in Korea through the eighteenth and nineteenth centuries as uncontrolled logging became widespread (Lee and Park 1997; Lee 2003). Rice productivity thus may have significantly declined in this period due to the downstream effects of deforestation.

The Little Ice Age (LIA) on the Korean peninsula was divided into three sub-periods (AD 1551–1650, 1701–1750, and 1801–1900) by Kim (1984) based on the "Munhunbigo", a historical text from the Joseon Dynasty. She concluded that the Korean peninsula encountered relatively cool and humid climatic conditions during all the LIA sub-periods and stressed that the last sub-period (1801–1900) was

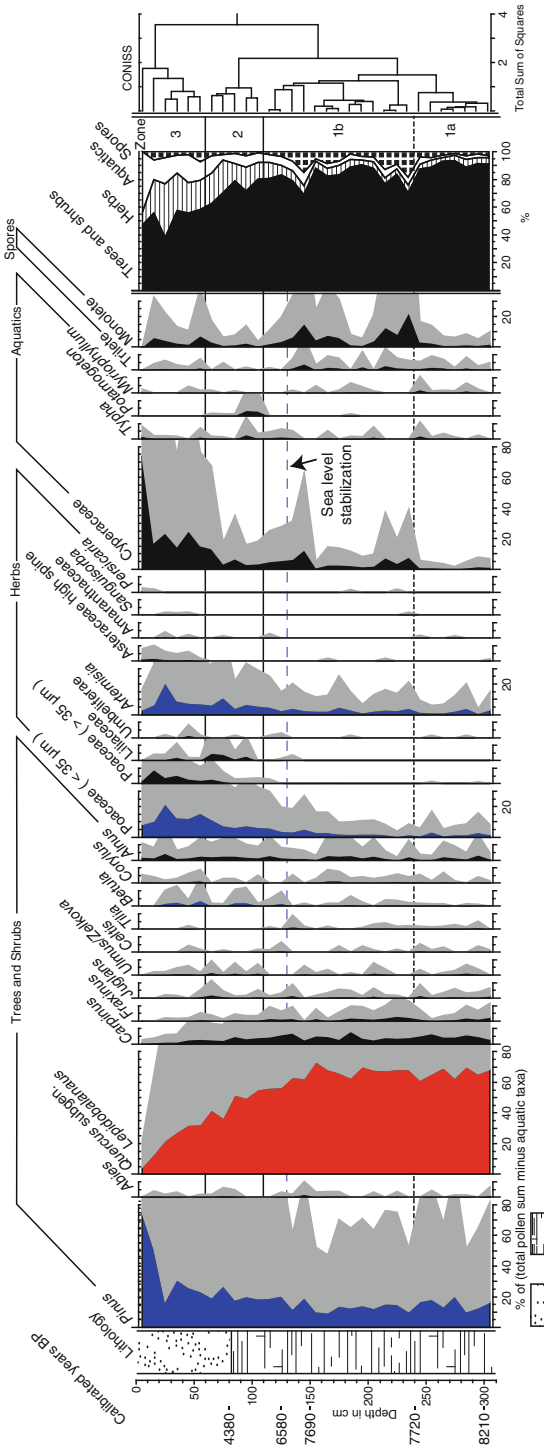

Fig. 10.6 Selected pollen and spore taxa from the Soonpogaeho sediment core (Redrawn from Park et al. 2012b)

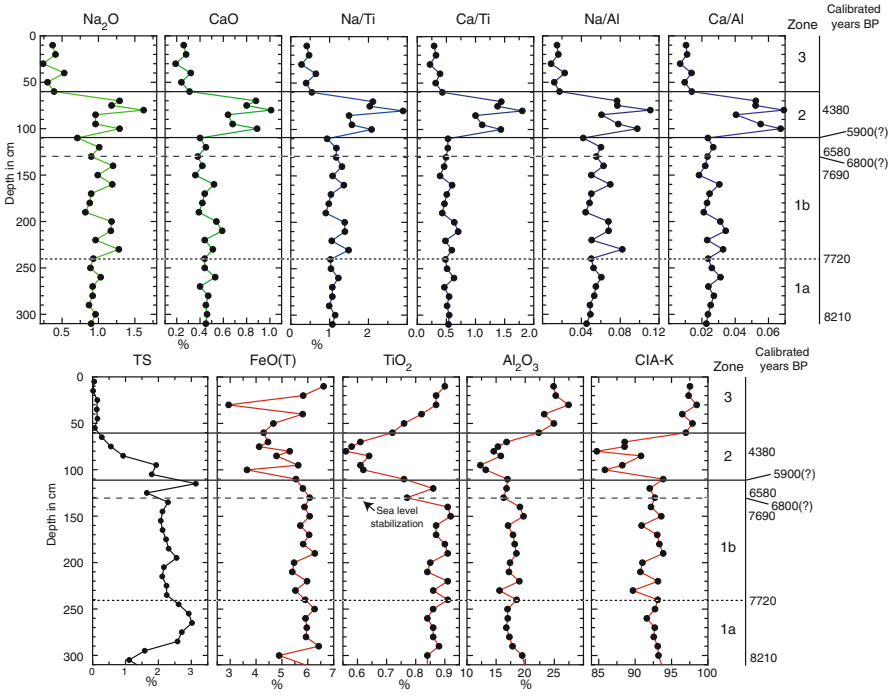

Fig. 10.7 TS, immobile elements ($Fe_2O_{3\,tot}$, TiO_2, and Al_2O_3), ratios of alkali and alkaline earth elements (Na_2O and CaO) to hydrolysates (TiO_2, and Al_2O_3), and CIA-K values from the soonpogaeho sediment core (Park et al. 2012b)

characterized by particularly high levels of rainfall. The 1770–1968 Seoul rainfall records showed that Seoul, the capital city of the Joseon dynasty, received relatively large precipitation between 1800 and 1870 (Kim 1970). Also, δ18O records from Chinese caves indicate an increase of precipitation in East Asia during 1850–1880 (Zhang et al. 2008). A dendroclimatological investigation suggested that 1660–1680 and 1830–1850 were the coolest periods over the past 350 years in central Korea (Choi et al. 1992). During the nineteenth century, low temperature may have directly hindered rice growth, causing pervasive destitution and disease outbreaks, and high precipitation may have exacerbated the problem of clastic influx to rice fields.

High frequencies of Pinus and a relative low abundance of *Quercus*, and especially a high abundance of *Castanea/Castanopsis* are indicative of widespread anthropogenic disturbance in the area. People may have cultivated chestnut trees and harvested nuts in the area as slash-and-burn cultivation must have naturally led to an increase in the number of chestnut trees. Chestnut trees and pines are typical sunlight-loving trees. The absence of *Abies*, *Fraxinus*, *Juglans*, and *Ulmus* may have been strongly associated with the high sedimentation rates but also to the impact of deforestation. In contrast, *Alnus* and *Salix* frequencies did not decrease despite continuous deforestation. Alders and willows presumably managed to occupy

Table 10.1 Radiocarbon dates for four lagoonal sediment cores from the east coast of Korea

Core	Sample depth (cm)	Material dated	Laboratory no.	Age (^{14}C year BP)	Two σ age range[a]	Median
Bongpo marsh	100	Plant remains	SNU11-R010	30 ± 40	AD1812-AD1919	AD1870
	140	Bulk sediment	SNU11-R191	420 ± 40	AD1420-AD1523	AD1470
	160	Bulk sediment	SNU11-R150	440 ± 40	AD1410-AD1519	AD1450
	205	Plant remains	SNU10-R217	1,450 ± 50	AD533-AD667	AD600
	270	Bulk sediment	SNU11-R151	2,340 ± 40	539BC-357BC	410BC
	300	Plant remains	SNU11-R192	2,530 ± 50	803BC-508BC	650BC
	320	Plant remains	SNU10-R202	2,080 ± 130	396BC-AD173	110BC
Lake Cheonjinho	120	Bulk sediment	SNU11-R137	690 ± 50	AD1238-AD1330	AD1300
	195	Plant remains	SNU10-R215	1,210 ± 50	AD679-AD899	AD810
	220	Bulk sediment	SNU10-R149	7,190 ± 60	6215BC-5983BC	6060BC
Lake Ssangho	210	Bulk sediment	SNU11-R138	1,310 ± 40	AD647-AD778	AD710
	280	Seed	SNU10-R147	2,160 ± 60	373BC-53BC	220BC
Lake Soonpogaeho	60	Bulk sediment	SNU14-R034	1,920 ± 40	AD17-AD213	AD80
	80	Bulk sediment	SNU11-R008	3,940 ± 50	2572BC-2289BC	2430BC
	125	Charcoal	SNU10-R204	5,780 ± 50	4766BC-4498BC	4630BC
	150	Bulk sediment	Beta-294013	6,860 ± 40	5836BC-5665BC	5740BC
	240	Bulk sediment	SNU10-R278	6,880 ± 60	5892BC-5645BC	5770BC
	300	Bulk sediment	Beta-294014	7,390 ± 40	6390BC-6104BC	6290BC

[a]All dates were calibrated with the intcal09 data set (Reimer et al. 2009)

agricultural fields that had been abandoned due to destructive effects of clastic influx. During this period, upland crop farming appears to have become significant with the declined rice production. The frequencies of low spine Asteraceae and *Humulus*/*Cannabis* evidently increased. The overall sizes and shapes of low spine Asteraceae pollen in this study suggested that *Aster* may have been the major crop genus of the family Asteraceae in the area. *Cannabis* was contemporaneously cultivated, probably for hemp clothing production, while *Zea mays* seems to have been newly diffused to the area. This increase in the importance of upland crops and the sudden drop of cultivated Poaceae frequencies indicate that the shifts in land-use patterns from lowland rice agriculture to upland cultivation could at least partially be attributed to the severe influx of clastics into rice fields.

10.2.2.2 Human-Induced Environmental Change of the Lagoon

The high C/N ratios in zone 1b imply that a marsh was finally formed due to the accumulation of much terrigenous plant debris as dead organic matter. The low C/N ratios in zone 1a may have been associated with algal organic matter deposited under lagoonal conditions. Marine algae usually have C/N ratios less than 10 (Meyers 1994), whereas terrestrial C3 vegetation commonly show C/N ratios of >12 (Prahl et al. 1980). The decline in pollen concentrations from zones 1a to 1b might have resulted from the larger sedimentation rates during the marsh formation after ca. AD 1. The high pollen concentrations and TOC values in zone 1 imply that humans had not yet started to disturb the local arboreal environment. Magnetic susceptibility values were very low throughout zone 1, suggesting that the Bongpo site was free from terrestrial clastics caused by deforestation in the corresponding period.

Conspicuously low pollen concentrations and TOC values in zone 2 indicate that natural forests surrounding the marsh were devastated or severely reduced. On the other hand, unlike pollen concentrations and TOC values, magnetic susceptibility values began to rise from the middle of the zone (160–170 cm), not from the lower boundary. This difference between the proxies was attributed to the creation of highly magnetic minerals such as maghemite in the soil by human activities (Blake et al. 2006; Clement et al. 2011). Slash-and-burn cultivation that significantly altered the magnetic properties of soils probably started a bit later than lowland rice agriculture. This interpretation is also supported by an apparent increase in the *Betula* frequencies at the depth of 175 cm.

An abrupt increase in $\delta^{13}C$ values in the lower part of zone 3 implies that upland C4 crops such as millet, sorghum and maize became more important as local food resources than in the previous zones. Plants that use the C4 pathway of photosynthesis usually produce organic matter with $\delta^{13}C$ values ranging from -14 to -10 ‰, whereas plants that use the C3 pathway of photosynthesis (e.g., rice) strongly discriminate against heavier isotope (^{13}C) and yield organic matter with $\delta^{13}C$ values ranging from -30 to -22 ‰ (Bender 1971; Farquhar et al. 1989). This proxy information is undoubtedly useful because rice pollen is indistinguishable from C4 Poaceae crop pollen. The increased importance of upland cultivation was

implied by high $\delta^{13}C$ values and the high percentages of low spine Asteraceae and *Humulus*/*Cannabis*. Lastly, the increased clastic influx and vegetation loss due to deforestation were further supported by the consistently high values of magnetic susceptibility and extremely low pollen concentrations and TOC values throughout the zone.

10.2.3 Lake Cheonjinho

Human impact was seemingly trivial during the period corresponding to zone 1 (? – ca. AD 780). Natural forests remained undisturbed as indicated by high percentages in *Quercus* and *Carpinus*, representative Holocene climax taxa in Korean peninsula, and by high values in TOC and pollen concentration. Insignificant human disturbance is implied by low percentages in herb taxa and spores and also by low MS values and fine grain sediments, associated with minimized soil erosion and sediment influx.

Environmental change caused by agricultural activities started to be clearly seen from zone 2a (ca. AD 780–1040). *Quercus* and *Carpinus* decreased while there was an increase in *Pinus*, *Betula*, *Castanea*, and *Corylus*, light-demanding trees preferring disturbed habitats. The beginning of agriculture is also clearly suggested by high frequencies in Poaceae and *Artemisia*, two major herb indicators of agricultural disturbance, the appearance of Amaranthaceae and Asteraceae, and the increased importance of spores. Rapidly decreasing TOC percentages and pollen concentration and diminished mean phi values and rebounding of C/N ratios in the upper part are indicative of deforestation, leading to consequent increase in soil erosion and terrestrial inputs of organic matter. However, it seems that deforestation induced by deliberate burning did not yet occur seriously given that MS values still remained low.

In zone 2b (ca. AD 1040 – ?), agricultural intensification and reclamation of wetlands are implied by a prominent increase in pollen indicators of agricultural disturbance such as Poaceae and *Artemisia* and by a decline in *Alnus*, respectively. The rapid but steady rise in MS values suggests that humans increasingly used fire as larger habitable areas became necessary due to the population growth associated with a rise in agricultural productivity. Rising human-induced fire frequencies probably led to increased number of pine and birch trees. Extremely low TOC % and pollen concentration seem to have arisen from dilution effects, related to tremendously increased sediment influx due to the deforestation. Steady increase in C/N ratios and coarse grain sediments imply an increase in the influx of terrestrial organic matter and clastic materials from upland areas.

10.2.4 Lake Ssangho

In zone 1 (? – ca. 100 BC), the presence of undisturbed natural forests is suggested by very low frequencies in wild Poaceae and *Artemisia*, absence of cultivated Poaceae, low MS values, high frequencies in *Carpinus*, *Quercus*, and *Juglans*, and high TOC percentages and pollen concentrations. Generally low and steady C/N ratios (∼10) indicate that high productivity was maintained by algae, probably in a relatively deep lake. High and nearly unvaried phi values (∼8.5 ϕ) throughout whole sediment profile also imply that the coring location remained continuously in a lacustrine environment under stable sedimentary condition.

In zone 2a (ca. 100 BC – AD 150), frequencies in *Quercus* did not change much from the previous zone despite an apparent increase in agricultural pollen indicators such as Artemisia and Poaceae. Nevertheless, the continued low MS values and only minute decrease in TOC percentages both indicate that forest disturbance was not substantial during this period because it was before the introduction of full-scale rice agriculture in this area. However, the reclamation of wetland and deforestation undoubtedly started from this period given the decrease in importance of *Alnus* on floodplains and the increase in light-demanding small trees such as *Corylus*.

Zone 2b (ca. AD 150 – ?) is characterized by an intensified agriculture, as implied by high frequencies in Poaceae, *Artemisia*, Asteraceae, and *Humulus*/*Cannabis*. Intensification of agriculture resulted in increasing percentages in light-loving trees such as *Pinus*, *Betula*, and *Castanea*, but decreasing percentages in climax trees such as *Carpinus*, *Quecus*, *Juglans*, and *Ulums. Alnus* percentages also declined due to escalated agricultural and reclaiming activities. Serious logging and deforestation occurred with population growth stimulated by increased agricultural productivity and subsequent settlement expansion. Such forest disturbance led to soil erosion, as indicated by increasing MS values. According to Ssangho results, agricultural intensification and population growth seem to have appeared ∼250 years after the early stage of rice agriculture, which is analogous to the case of Lake Cheonjinho, indicating that these two sites presumably experienced a similar process of agricultural development.

10.2.5 Lake Soonpogaeho

10.2.5.1 Mid-Holocene Environmental Change

In zone 1a (ca. 8,200 cal year BP – ca. 7,700 cal year BP), development of dense and stable forest is implied by high frequencies of pollen from trees and shrubs and high pollen concentrations. Important characteristics of zone 1b (ca. 7,700 cal year BP – ca. 5,900 cal year BP) are a drastic increase in sea level indicated by high sedimentation rates and apparent dominance of *Quercus*. Zone 2 (ca. 5,900 cal year BP – ca. 1,900 cal year BP) is characterized by conspicuous changes in pollen assemblages and relatively low sedimentation rates. The pollen evidence implies that the forest density was decreased and sunlight-loving trees such as pines and

birches subsequently expanded their habitat as climatic conditions became more disadvantageous to mesic hardwood species. The increasing importance of herbs such as *Artemisia* and Poaceae also reflects the development of drier conditions.

During the weathering process, base-forming mobile elements (Ca, Mg, K, Na) are leached and refractory immobile elements (Al, Ti, Fe) enriched relative to the composition of the original unweathered material (Mason and Moore 1982). The degree of chemical weathering is therefore implied by the relative proportion of the immobile oxide Al_2O_3 versus mobile oxides CaO and Na_2O (CIA-K index) (Maynard 1992; Sheldon et al. 2002). Change in the relative abundances of these oxides in lake sediments may indicate different degrees of the chemical weathering in source areas, enabling the reconstruction of past climate change (Lucchini et al. 2003; Selvaraj et al. 2007). Low CIA-K values and high ratios of alkalis/hydrolysates in zone 2 are most likely associated with the decreased rainfall and relatively low chemical weathering. In addition, the trough demonstrated by immobile elements TiO_2, Fe_2O_{3tot}, and Al_2O_3 indicates a possibly diminished erosional input of clastics to the core site, presumably as a consequence of decreasing precipitation.

The very low TS values at the 2/3 zone boundary all suggest that a nearly closed coastal water body had developed and that marine water had little effect on Soonpogae Lagoon. TS in sediments is a useful proxy to reconstruct shifts between oceanic and freshwater depositional conditions in estuarine environments. Concentrations of dissolved sulfate in most freshwaters are much lower than in seawater and the boundary of pyrite sulfur concentrations between marine and freshwater depositional conditions is about 0.2–0.3 % (Berner and Raiswell 1984).

10.2.5.2 Late-Holocene Human-Induced Environmental Change

The age of the zone 2/3 boundary was determined as 1,900 cal year BP using the newly obtained radiocarbon date at a depth of 60 cm, not included in Park et al. (2012b)'s list of radiocarbon dates. Soonpogae Lagoon was almost completely isolated from the sea and little influenced by seawater, as indicated by the low TS values around the zone 2/3 boundary. It is therefore possible that intensified agricultural activities and consequent clastic influx caused the present form of the Soonpogae Lagoon.

Clear evidence of late Holocene human impact is shown in zone 3. Human disturbance of forests is reflected by an abrupt increase in sunlight-loving trees and a corresponding drop of shade-tolerant mesic hardwoods. Cultivating activities intensified in this period, as suggested by the increasing percentages of agricultural plants such as Poaceae and of disturbance indicators such as *Artemisia* and fern spores.

The large influx of terrestrial clastics, probably due to agricultural disturbance, is implied by an increase in three erosional indicators (TiO_2, Fe_2O_{3tot}, and Al_2O_3). High CIA-K values and low ratios of alkalis/hydrolysates do not appear to have been associated with warm-humid climate but rather with large leaching losses of base cations in soil as a consequence of agricultural deforestation.

10.3 Overall Discussion and Implications on the Beginning of Rice Agriculture in Yeongdong Region

The Yeongdong region has been believed to be the last area in the southern Korean peninsula for the introduction of rice agriculture (Park 2007). The start of rice agriculture and its diffusion routes in this area have attracted research interest due to the reported large time difference in the beginning dates of rice agriculture between the Sokcho area and Gangneung area, despite the lack of any geomorphic barrier to hamper the diffusion of rice cultivation along the east coast (Yoon et al. 2008). This led to the suggestion of some possible errors and uncertainties in the chronology from Lake Youngrangho (Yasuda et al. 1979; Yoon 1998; Yoon et al. 2008).

However, the estimated age for the introduction of rice agriculture at the Youngrangho site is supported as the pollen records from adjacent Bongpo marsh and Lake Cheonjinho are similarly indicative of a late beginning of rice agriculture (Figs. 10.2 and 10.4). The start dates of rice agriculture suggested in Choenjinho and Bongpo studies would be much more accurate than those in previous studies since the former used radiocarbon dates obtained from the exact depths where rice agriculture was presumed to have started, whereas the latter roughly interpolated ages for those depths, as mentioned earlier. This supports the action of other causes, rather than dating errors, for the large time discrepancy (470–930 years) in the beginning of rice agriculture between the two areas on the east coast (Table 10.2).

In East Asia, the appearance of cultivated Poaceae and the rapid increase in wild Poaceae were considered the most reliable evidence for the beginning of rice agriculture. However, pollen records from east coast lagoons could not be used to accurately determine the initial arrival date of agricultural culture in the area. Intensification of rice agriculture on the contrary was relatively well demonstrated

Table 10.2 The start dates of rice cultivation in pollen sites on the east coast of Korea

Site	Longitude	Latitude	Estimated start time of agriculture (AD/BC)	Authors
Gosung	128°33′20″E	38°15′13″N	ca. AD 780	Park and Shin (2012)
Lake Cheonjinho				
Gosung	128°33′47″E	38°14′52″N	ca. AD 600	Park et al. (2012a)
Bongpo marsh				
Sokcho	128°35′03″E	38°12′55″N	ca. AD 550	Yasuda et al. (1979)
Lake Youngrangho				
Yangyang	128°39′39″E	38°05′06″N	ca. 100 BC	Park and Shin (2012)
Lake Ssangho				
Jumunjin	128°45′30″E	37°54′28″N	ca. 150 BC	Fujiki and Yasuda (2004)
Lake Hyangho				
Gangneung	128°53′16″E	37°49′10″N	ca. AD 80	Park et al. (2012b)
Lake Soonpogaeho				

by the dramatically increasing importance in pollen indicators of agricultural disturbance such as Poaceae, *Artemisia*, Amaranthaceae, and Asteraceae. It seems that agricultural disturbance is not clearly indicated in fossil pollen assemblages until agricultural activities are intensified to such an extent that anthropological herb pollen are not suppressed in relative percentages by abundant arboreal pollen. In Yeongdong pollen records, river-transported upland pollen possibly dampened the pollen signals of local agricultural disturbance in lowlands.

The archaeological evidence of carbonized cereals implies that the arrival of rice cultivation occurred as early as ca. 1,000 BC in the study area (Ahn 2002; Kim and Park 2011). Kim and Park (2011) explained the temporal discrepancy in the introduction of rice agriculture between the pollen records and the archaeological evidence (1,000–1,500 years) on the basis that the carbonized cereal grains directly indicated the earliest date of rice cultivation in the area whereas the pollen better reflected the start of agricultural intensification. In general, the pollen of cereal crops is poorly dispersed and not strongly represented in a pollen diagram. Thus, the seemingly late beginning of rice agriculture in pollen records may not mean that rice cultivation started later in the study area than in neighboring areas, but rather that rice agriculture only intensified sufficiently to become noticeable relatively late. Although we cannot exclude the possibility that these grains were imported from other areas, the presence of local crop production was strongly supported by the discovery of semilunar stone blades at the same place, which are generally believed to have been used for crop harvesting (Kim and Park 2011).

Kim and Park (2011) attributed this temporal difference to the role of rice as the major staple food, and not the luxury food in the area during the Bronze Age. Small-scale scattered agricultural activities may not have altered the surrounding environment sufficiently to be indicated in the pollen records. An inherently poor crop productivity in the Yeongdong region probably restricted rice to a luxury food even long after the arrival of rice agriculture. An old document "Taekriji", describing the geography of Korea, written in the mid-eighteenth century, stated that the crop production of the Yeongdong region was the lowest in the country because of arable land shortage, so many residents worked in producing salts and fishing for their living (National Geographic Information Institute 2006). Temporally uncorrelated change in agricultural pollen indicators between Sokcho/Gosung and Gangneung/Yangyang records could therefore also be attributed to the different start dates in the agricultural intensification, rather than the different arrival dates of rice cultivation. Less arable lands and consequent lower population density in the Sokcho/Gosung area may have resulted in the later agricultural intensification than the Gangneung/Yangyang area.

10.4 Conclusion

Multiproxy data from four coastal lagoons on the east coast of Korea provided valuable information about agricultural activities and related paleoenvironmental change during the late Holocene. Application of a multi-proxy approach in these

studies enabled several uncertainties to be resolved. Bongpo marsh began to develop ca. 650 BC as a coastal lagoon was rapidly filled with organic materials. Rice agriculture intensified sufficiently to be implied in pollen records and the area of deforestation increased from ca. AD 600. The land-use shifted from lowland rice agriculture to upland cultivation as agricultural production decreased after ca. AD 1870, presumably due to heavy deforestation, increased precipitation, and the consequent severe influx of clastic sediments on rice fields. Rice agriculture began to be intensified from ca. AD 780 at Lake Cheonjinho and from ca. 100 BC at Lake Ssangho. Soonpogae lagoon was almost completely isolated from the sea by sand barriers when human impact intensified about AD 80.

The introduction of rice cultivation into the Sokcho/Gosung area lagged well behind that in the Gangneung/Yangyang area, despite the lack of any geomorphic barrier to hamper the spread of rice agriculture along the coast. This finding indicates that it is difficult to identify the arrival date of rice agriculture in a specific area using pollen records since the pollen generally better represented the beginning of agricultural intensification. The low productivity of crop cultivation in the Yeongdong region seems to have caused this temporal discrepancy between initial arrival of rice cultivation and agricultural intensification. Thus, both micro and macrofossil data examined in this chapter imply that the dating of important agricultural events and the reconstructing of land use history necessitate a multidisciplinary approach, with a particular focus on palynological and archaeological evidence.

Acknowledgements This research was supported by the National Research Foundation of Korea Grant funded by the Korean Government (NRF-2013R1A1A2006864 and NRF2012S1A5A8022554).

References

Ahn SM (2002) Analysis of carbonized rice grains from Gyo-dong. In: Baek H, Ji H, Park Y (eds) Gyo-dong settlement in Gangneung. Gangneung University Museum, Gangneung, pp 115–126. (in Korean)

Ahn SM (2010) The emergence of rice agriculture in Korea: archaeobotanical perspectives. Archaeol Anthropol Sci 2(2):89–98

Bender MM (1971) Variations in the $^{13}C/^{12}C$ ratios of plants in relation to the pathway of photosynthetic carbon dioxide fixation. Phytochemistry 10(6):1239–1244

Berner RA, Raiswell R (1984) C/S method for distinguishing freshwater from marine sedimentary rocks. Geology 12(6):365–368

Blake W, Wallbrink P, Doerr S, Shakesby R, Humphreys G (2006) Magnetic enhancement in wildfire-affected soil and its potential for sediment-source ascription. Earth Surf Process Landforms 31(2):249–264

Choe CP (1982) The diffusion route and chronology of Korean plant domestication. J Asian Stud 41(3):519–529

Choi JN, Yu KB, Park WK (1992) Paleoclimate reconstruction for Chungbu mountainous region using tree-ring chronology. Korean J Quatern Res 6:21–32. (in Korean with English abstract)

Chon YN (1992) Introduction of rice agriculture into Korea and Japan: from the perspective of polished stone implements. In: Aikens CM, Rhee S-N (eds) Pacific northeast Asia in prehistory. Washington State University Press, Pullman, pp 161–169

Clement BM, Javier J, Sah JP, Ross MS (2011) The effects of wildfires on the magnetic properties of soils in the Everglades. Earth Surf Process Landforms 36(4):460–466

Crawford G, Lee G (2003) Agricultural origins in the Korean Peninsula. Antiquity 77(295):87–95

Farquhar GD, Ehleringer JR, Hubick KT (1989) Carbon isotope discrimination and photosynthesis. Annu Rev Plant Biol 40(1):503–537

Fujiki T, Yasuda Y (2004) Vegetation history during the Holocene from Lake Hyangho, northeastern Korea. Quatern Int 123:63–69

Im HJ (1992) Prehistoric rice agriculture in Korea. In: Aikens CM, Rhee SN (eds) Pacific northeast Asia in prehistory. Washington State University Press, Pullman, pp 157–160

Kim ST (1970) Secular precipitation variations in Seoul, 1770–1968. Geogr Naksan 1:27–34. (in Korean with English abstract)

Kim YO (1984) The little ice age in Korea: an approach to historical climatology. Geogr Educ 14:1–16. (in Korean with English abstract)

Kim M, Park J (2011) Prehistoric rice cultivation and agricultural intensification in the Yeongdong Regions, Gwangwon, South Korea. J Korean Archaeol Soc 79:67–88. (in Korean with English abstract)

Korea Meteorological Administration (n.d.) Domestic climate data. Web. 25 Apr 2014. http://www.kma.go.kr/weather/climate/average_30years.jsp

Lee U (2003) Deforestation and agricultural productivity in Korea during the eighteenth and nineteenth centuries. Rev Econ Hist 34:31–57. (in Korean with English abstract)

Lee H, Park K (1997) Climatic change and agricultural crisis in Choson Korea, 1799–1825. J Choson Dynasty Hist 2:123–191. (in Korean with English abstract)

Lucchini F, Dinelli E, Calanchi N (2003) Chemostratigraphy of Lago Albano sediments (Central Italy): geochemical evidence of palaeoenvironmental changes in lateQuaternary. J Paleolimnol 29(1):109–122

Mason B, Moore CB (1982) Principles of geochemistry. Wiley, New York

Maynard J (1992) Chemistry of modern soils as a guide to interpreting Precambrian paleosols. J Geol 100:279–289

Meyers PA (1994) Preservation of elemental and isotopic source identification of sedimentary organic matter. Chem Geol 114(3):289–302

National Geographic Information Institute (2006) The geography of Gangwon. Ministry of Land, Transport and Maritime Affairs, Gwacheon-si

Park J (2007) Prehistoric diffusion routes of rice from China to Korea and within Korea as shown in archeological and historical evidence and pollen records. Geogr J Korea 41:103–122

Park J, Shin YH (2012) Late-Holocene rice agriculture and paleoenvironmental change in the Yeongdong Region, Gangwon, South Korea. J Korean Geogr Soc 47:641–653

Park J, Yu KB, Lim HS, Shin YH (2012a) Multi-proxy evidence for late Holocene anthropogenic environmental changes at Bongpo marsh on the east coast of Korea. Quatern Res 78(2): 209–216

Park J, Yu KB, Lim HS, Shin YH (2012b) Holocene environmental changes on the east coast of Korea. J Paleolimnol 48(3):535–544

Prahl FG, Bennett JT, Carpenter R (1980) The early diagenesis of aliphatic hydrocarbons and organic matter in sedimentary particulates from Dabob Bay, Washington. Geochim Cosmochim Acta 44(12):1967–1976

Reimer P, Baillie M, Bard E, Bayliss A, Beck J, Blackwell P, Bronk Ramsey C, Buck C, Burr G, Edwards R (2009) IntCal09 and Marine09 radiocarbon age calibration curves, 0–50,000 years cal BP. Radiocarbon 51(4):1111–1150

Selvaraj K, Chen CTA, Lou JY (2007) Holocene East Asian monsoon variability: links to solar and tropical Pacific forcing. Geophys Res Lett 34, L01703

Sheldon ND, Retallack GJ, Tanaka S (2002) Geochemical climofunctions from North American soils and application to paleosols across the Eocene-Oligocene boundary in Oregon. J Geol 110(6):687–696

Yasuda Y, Kim CM, Lee ST, Yim YJ (1979) Environmental changes and agricultural origin in Korea. In: Overseas research report. Japanese Ministry of Education, Tokyo, pp 1–19. (in Japanese)

Yim YJ (1977) Distribution of forest vegetation and climate in the Korean peninsula: IV. Zonal distribution of forest vegetation in relation to thermal climate. Jpn J Ecol 27:269–278

Yoon SO (1998) The environmental change and geomorphic development of Unsan alluvial plain in Kangreung city during the late Holocene. J Korean Geogr Soc 33(2):127–142. (in Korean with English abstract)

Yoon SO, Moon YR, Hwang S (2008) Pollen analysis from the Holocene sediments of Lake Gyeongpo, Korea and its environmental implications. J Geol Soc Korea 44:781–794. (in Korean with English abstract)

Yu JE, Lee JH, Kwon KW (2003) An analysis of forest community and dynamics according to elevation in Mt. Sokri and Odae. Korean J Agric For Meteorol 5:238–246. (in Korean with English abstract)

Yum JG, Takemura K, Tokuoka T, Yu KM (2003) Holocene environmental changes of the Hwajinpo Lagoon on the eastern coast of Korea. J Paleolimnol 29(2):155–166

Zhang P, Cheng H, Edwards RL, Chen F, Wang Y, Yang X, Liu J, Tan M, Wang X, Liu J (2008) A test of climate, sun, and culture relationships from an 1810-year Chinese cave record. Science 322(5903):940–942

Chapter 11
Comparison of Luminescence Dating Methods on Lake Sediments from a Small Catchment: Example from Lake Yogo, Japan

Kazumi Ito, Toru Tamura, Noriko Hasebe, Toshio Nakamura, Shoji Arai, Manabu Ogata, Taeko Itono, and Kenji Kashiwaya

Abstract When applying luminescence dating to sediment deposited in aquatic environments, a key issue for accurate age determination is resetting of acquired luminescence in sediment by surface exposure (bleaching) before burial. The time

K. Ito (✉)
Geological Survey of Japan, AIST, Central 7, 1-1-1 Higashi, Tsukuba, Ibaraki 305-8567, Japan

Japan Society for the Promotion of Science, Tokyo, Japan

Institute of Nature and Environmental Technology, Kanazawa University, Kakuma, Kanazawa 920-1192, Japan
e-mail: kazumi-itou@aist.go.jp

T. Tamura
Geological Survey of Japan, AIST, Central 7, 1-1-1 Higashi, Tsukuba, Ibaraki 305-8567, Japan

N. Hasebe
Institute of Nature and Environmental Technology, Kanazawa University, Kakuma, Kanazawa 920-1192, Japan

Korea Institute of Geoscience and Mineral Resources, 124 Gwahang-no, Yuseong-gu Deajeon 305-350, South Korea

T. Itono
Institute of Nature and Environmental Technology, Kanazawa University, Kakuma, Kanazawa 920-1192, Japan

T. Nakamura
Center for Chronological Research, Nagoya University, Furo-cho, Chikusaku, Nagoya, Aichi 464-8602, Japan

S. Arai
Department of Earth Science, Kanazawa University, Kakuma, Kanazawa 920-1192, Japan

M. Ogata
Graduate School of Natural Science and Technology, Kanazawa University, Kakuma, Kanazawa 920-1192, Japan

K. Kashiwaya
Institute of Nature and Environmental Technology, Kanazawa University, Kakuma, Kanazawa 920-1192, Japan

Department of Geography, National Taiwan University, Daan District, Taipei 10617, Taiwan

K. Kashiwaya et al. (eds.), *Earth Surface Processes and Environmental Changes in East Asia*, DOI 10.1007/978-4-431-55540-7_11

needed for bleaching is known to vary among the signals used in three methods: optically stimulated luminescence (OSL), infrared stimulated luminescence (IRSL), and post-infrared IRSL (pIRIR). A comparison of luminescence ages from these different signals is therefore useful to assess whether a sample was fully bleached before burial. In a comparison of OSL, $IRSL_{50/225}$ and $pIRIR_{225}$ ages of eight samples of fine-grained sediment from a 294-cm-long sediment core from Lake Yogo, a small-catchment lake in central Japan, the $IRSL_{50/225}$ and $pIRIR_{225}$ ages were much older than the OSL ages. The $IRSL_{50/225}$ residual signals were close to zero, and the difference between $pIRIR_{225}$ and OSL signals was much larger than the $pIRIR_{225}$ residual signals. Thus, $IRSL_{50/225}$ and $pIRIR_{225}$ signals were not completely bleached, which we attribute to the short sediment transport distance in this small catchment. Five corrected bulk radiocarbon (^{14}C) ages agreed with the OSL ages, except for two intervals in which OSL ages were about 500 and 1,900 years older than the corrected ^{14}C ages. These discrepancies are attributable to incomplete bleaching related to sediment transport, whereas the rest of the OSL ages show no evidence of incomplete bleaching. This study shows that even in samples in which the $pIRIR_{225}$ and $IRSL_{50/225}$ signals are not well-bleached, OSL dating yields accurate age estimates because of the faster bleaching rate.

Keywords OSL dating • Post-IR IRSL dating • Bulk ^{14}C dating • Lake sediments • Incomplete bleaching

11.1 Introduction

Lake sediments contribute to our understanding of past climate change in terrestrial areas (e.g., Colman et al. 1995; Williams et al. 1997). Depth profiles of lake sediment can provide proxy records that represent paleoenvironments (e.g., BDP-98 Members 2001; BDP-99 Members 2005). The determination of sedimentation age is critical for converting depth profiles of proxies to age profiles for reconstruction of paleoclimatic fluctuations. Radiocarbon (^{14}C) dating is typically used for age determination of lake sediments for ages up to about 40 ka (e.g., Nara et al. 2005; Watanabe et al. 2007, 2009). Optically stimulated luminescence (OSL) and infrared stimulated luminescence (IRSL) dating methods also have the potential to date the depositional age of sediments when the acquired luminescence of sediment entering the lake is reset by sunlight (bleached) during its transport from the catchment area to the basin. The age range of OSL and IRSL dating is from the present to about 200 ka, and these methods have been successfully applied to lake sediments (e.g., Juschus et al. 2007; Zheng et al. 2010). Buylaert et al. (2013) successfully applied another luminescence method, post-IR infrared stimulated luminescence (pIRIR) dating, to K-feldspar in lake sediments older than about 70 ka. However, Zheng et al. (2010) showed that OSL ages of lake sediment younger than about 10 ka had been overestimated.

Murray et al. (2012) proposed an approach to assess the degree of bleaching based on the different bleaching rates for OSL and pIRIR signals: if feldspar pIRIR

ages are close to quartz OSL ages, then the quartz must be completely bleached because the bleaching rate of the pIRIR signal in feldspar is much slower than that of the OSL signal in quartz. Their approach identifies well-bleached quartz independently of other age controls.

Before AD 1604, Lake Yogo was a small enclosed lake with a catchment area of 7.97 km^2. At that time, it was artificially connected to the Yogo River and its catchment area expanded to 35.37 km^2. The original Lake Yogo catchment is underlain by alluvial sediment and rocks of a Jurassic accretionary wedge, and it contains no volcanic rocks (Wakita et al. 1992). In applying OSL dating to this sediment, incomplete bleaching during sediment transport presents a significant potential problem because the initial catchment area was very small and the sediment may have traveled short distances.

This study tests the proposed approach of Murray et al. (2012) on lake sediment from a small catchment by using samples from Lake Yogo. As was done by Murray et al. (2012), we determined IRSL and pIRIR ages in addition to OSL ages. We also determined ^{14}C ages from plant residue and the bulk sediment to provide independent age controls. We then compared luminescence and radiocarbon ages to assess the effectiveness of OSL dating of the Lake Yogo sediment core, and the validity of the approach of Murray et al. (2012) for dating lacustrine sediments from a small catchment.

11.2 Sample and Methods

Samples for luminescence and ^{14}C dating were taken from a 294-cm-long sediment core (YG11-3) from Lake Yogo. The core, which was obtained from the deepest part of the lake (12.5 m) by piston coring (Fig. 11.1), is composed of homogeneous brown silty clay without any distinctive features. Under subdued red light, samples were collected at 2-cm core intervals, and each sample was split in two. The first split was dried at 110 °C for 2 days and then used for measurement of water content and radioisotope concentration. The other split was not dried and was used for luminescence measurement. Plant residues were sampled from core depths of 182 and 278 cm.

11.2.1 Luminescence Dating

For luminescence measurement, wet samples were chemically treated at room temperature using 10 % hydrogen chloride to remove carbonate and then 10 % hydrogen peroxide to remove organic matter. Then, the 4–11 μm sediment size fractions were extracted by a method based on Stokes' law by suspending the samples in a sodium oxalate solution. Portions of thesepolymineral fractions

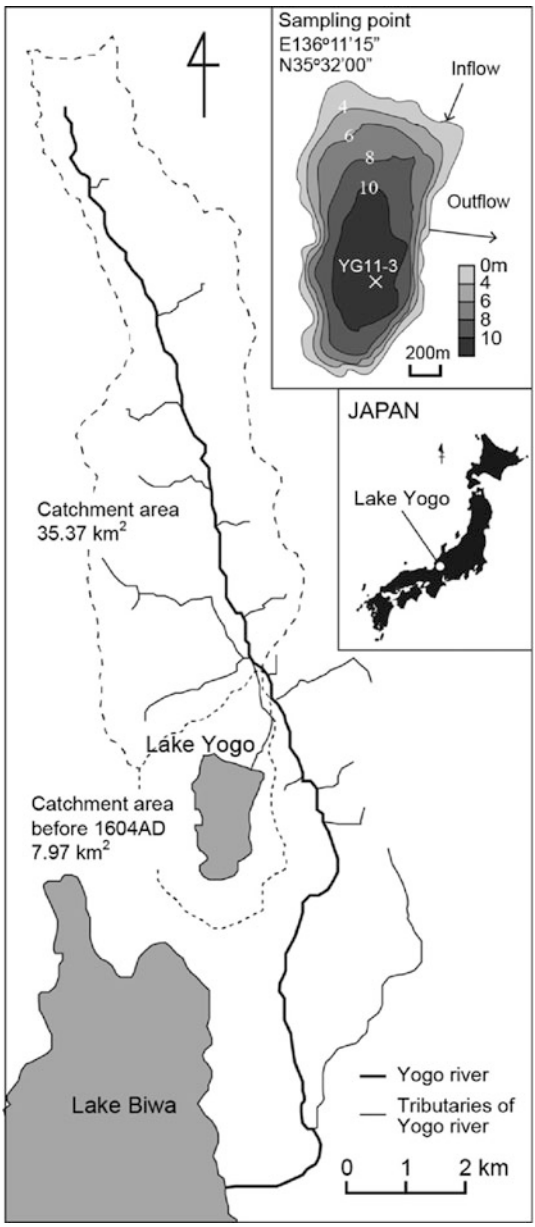

Fig. 11.1 Map showing the location of Lake Yogo and the sampling point. Inflow and outflow are through an artificial headrace

were used for IRSL and pIRIR dating, and the remaining fractions were further treated with 10 % hexafluorosilicic acid to remove feldspar and isolate the quartz fraction. The degree of contamination of the quartz fraction by feldspar, checked by observing IRSL emissions, was less than 1 % in all samples. Thequartz fraction was

Table 11.1 SAR protocols for D_e measurements

Step	OSL	$IRSL_{50/225}$ and $pIRIR_{225}$
1	Given dose	Given dose
2	Preheat for 10 s at 200 °C	Preheat for 60 s at 250 °C
3	OSL for 40 s at 125 °C (L_x)	IRSL for 200 s at 50 °C (L_x for $IRSL_{50/225}$)
4	–	IRSL for 200 s at 225 °C (L_x for $pIRIR_{225}$)
5	Given test dose	Given test dose
6	Preheat for 10 s at 160 °C	Preheat for 60 s at 250 °C
7	OSL for 40 s at 125 °C (T_x)	IRSL for 200 s at 50 °C (T_x for $IRSL_{50/225}$)
8	–	IRSL for 200 s at 225 °C (T_x for $pIRIR_{225}$)
9	Hot bleach for 40 s at 280 °C	Hot bleach for 200 s at 255 °C
10	Return to step 1	Return to step 1

then dated by OSL. The dried polymineral and quartz fractions (about 1.0 mg each) were suspended in acetone and placed on stainless steel disks 10 mm in diameter, after which the acetone was evaporated in an oven.

The luminescence signal was measured using a luminescence reader (DA-20, Risø) equipped with a $^{90}Sr/^{90}Y$ beta source at Geological Survey of Japan, AIST. Luminescence emissions in the ultraviolet region were measured through a Hoya U-340 filter for quartz OSL, and emissions in the blue-violet region were measured through Schott BG3, BG39, and GG400 filters, in ascending order, for polymineral IRSL and pIRIR. The single aliquot regenerative (SAR) protocol was applied to the determination of the equivalent dose D_e (Table 11.1; Murray and Wintle 2000). The OSL signal was measured for 40 s at 125 °C. The IRSL signal was measured for 200 s at 50 °C ($IRSL_{50/225}$), followed by pIRIR measurement for 200 s at 225 °C ($pIRIR_{225}$). The luminescence signal was sampled every 0.1 s. The luminescence intensities were derived from the integral of the first 0.5 s (5 channels) and 2.0 s (20 channels) after subtracting the last 5 s for the OSL decay curve and the last 10 s for the IRSL and pIRIR decay curves. Radioisotope concentrations of each sample were measured by laser-ablation inductively coupled plasma mass spectrometry and x-ray fluorescence (Ito et al. 2009, 2011) and converted into annual dose rates by the method of Adamiec and Aitken (1998). Cosmic dose rate was estimated following Prescott and Hutton (1994).

11.2.2 ^{14}C Dating

^{14}C dating of bulk sediment samples followed the protocol of Watanabe et al. (2009). Dried sediment was powdered, and then treated with 1.2 M HCl to remove carbonate. The sample was then combusted at 850 °C for 4 h with CuO wire, and the

resulting CO_2 was purified with ethanol, *n*-pentane, and liquid nitrogen in a vacuum line. The CO_2 was reduced to graphite by heating with iron and hydrogen at 650 °C for 6 h.

The procedure for ^{14}C dating of plant samples was after Nakamura et al. (2003). Small pieces of leaves were picked from the bulk sediment sample under the microscope and washed with distilled water to remove mineral grains. The leaves were treated with 1.2 M HCl and 1.2 M NaOH (acid-alkali-acid treatment), dried, and combusted. The resulting CO_2 was purified and reduced to graphite by the same procedure used for the bulk sediment sample.

The $^{14}C/^{12}C$ ratio of graphite was measured with a Tandetron accelerator mass spectrometer (Model-4130, HVEE) at the Center for Chronological Research, Nagoya University. The measured ratio was corrected by $\delta^{13}C$, which was measured with an isotope ratio mass spectrometer (MAT-252, Thermo Finnigan). All ^{14}C ages were converted to calendar years using the INTCAL09 data set (Reimer et al. 2009).

11.3 Results

11.3.1 OSL Dating

Quartz samples from Lake Yogo sediments exhibited OSL signals with a strong fast component (Fig. 11.2a), and the recycling ratio was close to unity. These samples thus differ from the volcanic quartz found elsewhere in Japan (e.g., Tsukamoto et al. 2003), which is characterized by anomalous fading and dominance of the slow component. Results of the preheat-plateau test, thermal transfer test, and dose recovery test for OSL analysis are presented in Fig. 11.3. The influence of hot bleaching was also investigated for these three tests, and the data with and without hot bleaching agreed within the standard error. The preheat-plateau test showed a plateau of D_e around 1.6 Gy over the preheat temperature range from 160 to 280 °C (Fig. 11.3a). The thermal transfer was almost negligible at all preheat temperatures except for 300 °C (Fig. 11.3b).

For the dose recovery test, the natural sample was initially bleached using a blue LED to reduce the natural OSL to almost the background level at room temperature. After bleaching, the sample was given a beta dose of approximately 2.0 Gy, which is close to the natural D_e, and then OSL was measured using preheat temperatures from 160 to 300 °C (Fig. 11.3c). The dose recovery ratio was close to unity at preheat temperatures from 160 to 280 °C. A preheat temperature of 200 °C for 10 s and a cut heat of 160 °C were chosen for all of our OSL measurements. Dose recovery tests were carried out on every sample at the preheat temperature of 200 °C, and the measured dose/given dose ratio was close to unity (1.01–1.03). The mean D_e values of repeated OSL measurements were determined by the central age model of Galbraith et al. (1999) and are shown in Table 11.3. Aliquots were accepted for mean D_e determination only if they yielded a recycling ratio within 1.0 ± 0.1.

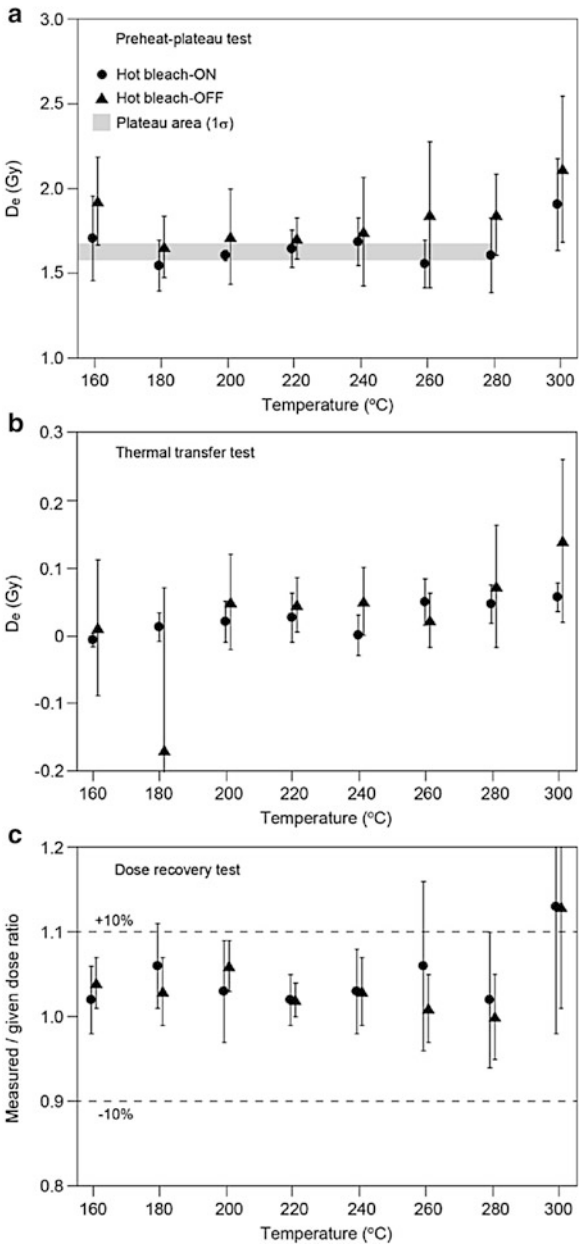

Fig. 11.2 Typical dose response curve for (**a**) OSL, (**b**) $IRSL_{50/225}$, and (**c**) $pIRIR_{225}$, together with decay curves (*inset*). A single exponential function was fitted to the dose–response curves

11.3.2 $IRSL_{50/225}$ and $pIRIR_{225}$ Dating

Examples of polymineral $IRSL_{50/225}$ and $pIRIR_{225}$ decay curves are shown in Fig. 11.2b, c. Unbleachable residual signals of $IRSL_{50/225}$ and $pIRIR_{225}$ were estimated in parallel with the D_e measurement and dose recovery test at a preheat

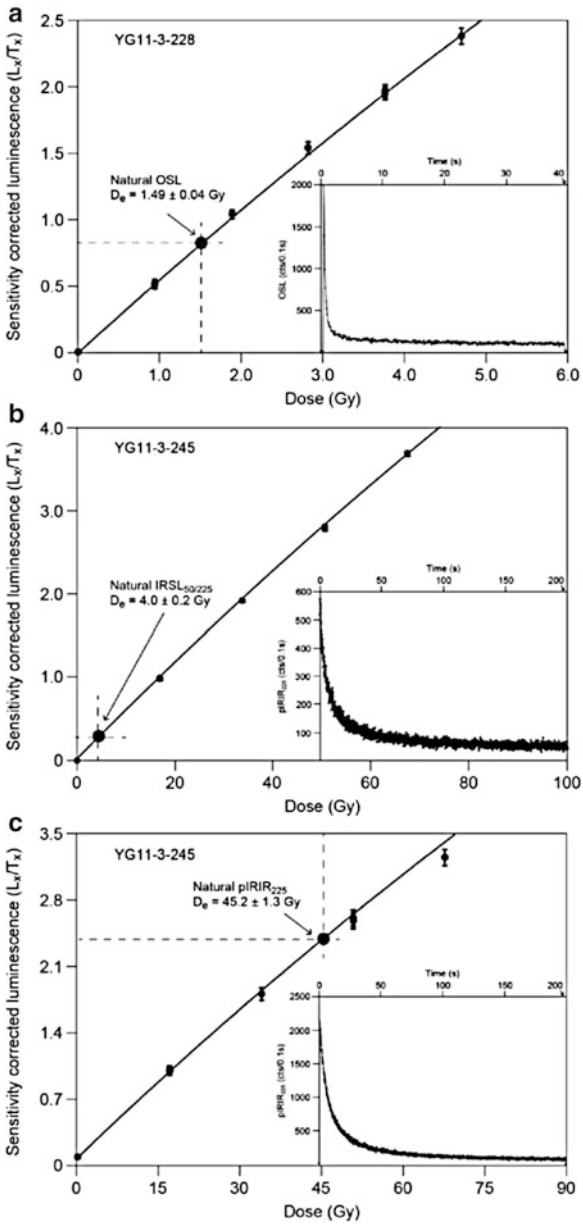

Fig. 11.3 Results of the (**a**) preheat-plateau test, (**b**) thermal transfer test, and (**c**) dose recovery test for OSL analysis on sample YG11-3-316. Each test was conducted with and without hot bleaches

temperature of 250 °C, following the protocol of Lowick et al. (2012). After the samples were exposed to natural sunlight for 2 days, the apparent residual doses were measured and plotted against the measured natural dose (Fig. 11.4). Although the residual dose of $IRSL_{50/225}$ was negligible, the $pIRIR_{225}$ signal contained a residual that was positively correlated with D_e. The residual dose was thus

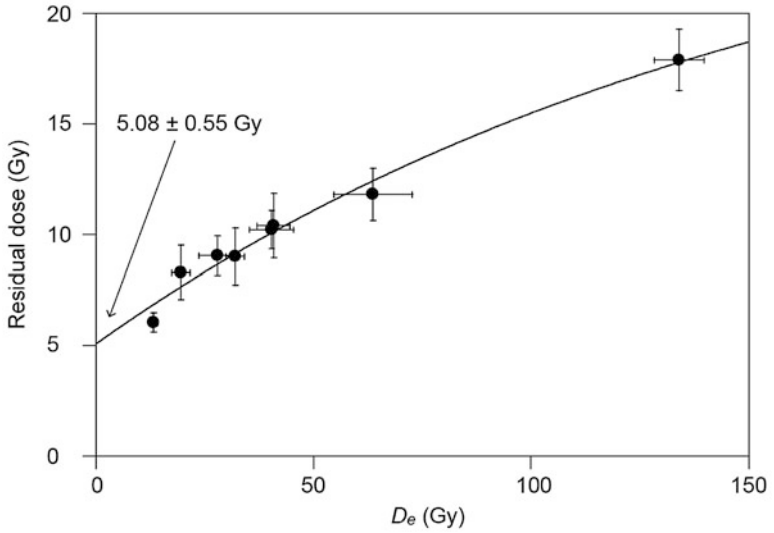

Fig. 11.4 The $pIRIR_{225}$ residual dose in the samples. The errors represent one standard error

calculated with an intercept value at $D_e = 0$ after the method proposed by Sohbati et al. (2011). The residual dose of 5.08 ± 0.55 Gy was subtracted from all D_e values of $pIRIR_{225}$. Dose recovery tests were carried out on three samples (YG11-3-124, −245, and −349) at the preheat temperature of 250 °C, and the dose recovery ratio was close to unity (1.03–1.10 for $IRSL_{50/225}$, 0.95–1.08 for $pIRIR_{225}$). D_e values of five aliquots were determined for both $IRSL_{50/225}$ and $pIRIR_{225}$, and their mean was used for final age determinations (Table 11.2).

The stability of the $pIRIR_{225}$ signal was checked by estimating the fading rate (g-value) on every aliquot, which was measured and calculated following the conventional procedure (Huntley and Lamothe 2001; Auclair et al. 2003) and expressed as the percentage of luminescence decay in a decade. Most g-values for $IRSL_{50/225}$ and $pIRIR_{225}$ were 2.5–3.4 %/decade and smaller than 1.5 %/decade, respectively (Table 11.2). These g-values are consistent with the understanding that $pIRIR_{225}$ signals are more stable than conventional IRSL signals (Thomsen et al. 2008; Buylaert et al. 2009; Thiel et al. 2010). A fading correction was not done for pIRIR signals, as Buylaert et al. (2012) suggested that samples with relatively low $pIRIR_{290}$ g_{2days} (1.44 %/decade) do not require the correction. To confirm that fading was negligible, it would be preferable to measure saturated samples (Buylaert et al. 2011). However, samples of that age were not available in the Lake Yogo sediment core. Therefore, we show pIRIR ages both uncorrected and corrected for fading. For $IRSL_{50/225}$ dating, we used a fading correction because of the higher g-values.

Radioisotope concentrations are shown in Table 11.3. The alpha dose rates for fine-grained quartz and fine-grained polymineral samples were calculated using a-values of 0.04 and 0.08, respectively (Rees-Jones 1995). The water content of the

Table 11.2 Values of D_e and fading rate (g-value) for fine-grained quartz OSL and for fine-grained polymineral $IRSL_{50/225}$ and $pIRIR_{225}$

Sample name	Depth (cm)	Lab. code	OSL					$IRSL_{50/225}$			$pIRIR_{225}$	
			n1[a]	n2[a]	D_e (Gy)	OD[b] (%)	n	D_e (Gy)	g_{2days}[c] (%/decade)	n	D_e[d] (Gy)	g_{2days}[c] (%/decade)
YG11-3-001	0	gsj13-98	23	21	0.30 ± 0.01	14	5	3.60 ± 0.21	2.62 ± 0.20	5	22.7 ± 4.1	0.88 ± 0.38
YG11-3-124	56	gsj13-99	25	21	0.42 ± 0.01	12	5	2.10 ± 0.16	2.53 ± 0.63	5	8.0 ± 0.8	0.77 ± 0.20
YG11-3-207	106	gsj13-100	21	20	0.55 ± 0.01	8	5	2.74 ± 0.16	2.87 ± 0.20	5	14.3 ± 2.6	0.67 ± 0.18
YG11-3-228	148	gsj13-101	22	21	1.51 ± 0.01	2	5	6.39 ± 0.37	3.31 ± 0.53	5	58.5 ± 10.2	1.03 ± 0.25
YG11-3-245	182	gsj13-102	21	19	1.18 ± 0.01	4	5	4.21 ± 0.13	3.17 ± 0.43	5	35.2 ± 5.3	1.25 ± 0.25
YG11-3-316	224	gsj13-103	38	28	1.61 ± 0.04	8	5	3.77 ± 0.12	3.11 ± 0.76	5	26.8 ± 4.3	0.96 ± 0.34
YG11-3-343	278	gsj13-104	25	21	3.50 ± 0.08	10	5	25.66 ± 3.46	3.14 ± 0.42	5	129.1 ± 11.4	1.37 ± 0.37
YG11-3-349	290	gsj13-105	22	20	2.78 ± 0.02	2	5	5.76 ± 0.27	3.35 ± 0.47	5	35.7 ± 6.0	1.16 ± 0.39

Note: Errors represent one standard error

[a] "n1" and "n2" represent number of measured and accepted aliquots, respectively

[b] *OD* over dispersion

[c] For each aliquot used for D_e measurement, fading test was also performed

[d] The D_e values of $pIRIR_{225}$ have a residual dose of 5.08 ± 0.55 Gy subtracted from the natural D_e values

Table 11.3 Concentration of radioisotopes from LA-ICP-MS analysis, water contents, cosmic ray and annual dose

Sample name	Depth (cm)	Lab. code	^{238}U (μg/g)	^{234}U (μg/g)	^{232}Th (μg/g)	^{87}Rb (μg/g)	Water content[a] (wt.%)	Cosmic ray (mGy/year)	Annual dose for quartz (mGy/year)	Annual dose for polymineral (mGy/year)
YG11-3-001	0	gsj13-98	2.05 ± 0.12	$(1.12 \pm 0.21) \times 10^{-4}$	7.98 ± 0.88	20.26 ± 0.23	423	0.1	0.59 ± 0.06	0.65 ± 0.07
YG11-3-124	56	gsj13-99	1.89 ± 0.14	$(1.56 \pm 0.15) \times 10^{-4}$	9.27 ± 1.94	21.74 ± 1.08	285	0.1	0.81 ± 0.10	0.92 ± 0.11
YG11-3-207	106	gsj13-100	1.59 ± 0.12	$(1.12 \pm 0.06) \times 10^{-4}$	6.42 ± 0.66	19.31 ± 0.64	342	0.1	0.57 ± 0.05	0.64 ± 0.05
YG11-3-228	148	gsj13-101	2.16 ± 0.18	$(1.41 \pm 0.39) \times 10^{-4}$	9.77 ± 1.50	28.01 ± 1.50	239	0.1	1.03 ± 0.13	1.15 ± 0.16
YG11-3-245	182	gsj13-102	1.46 ± 0.08	$(0.69 \pm 0.24) \times 10^{-4}$	5.65 ± 0.25	22.19 ± 1.00	369	0.1	0.49 ± 0.05	0.53 ± 0.06
YG11-3-316	224	gsj13-103	1.78 ± 0.15	$(1.35 \pm 0.29) \times 10^{-4}$	7.28 ± 0.29	22.37 ± 0.07	318	0.1	0.68 ± 0.06	0.76 ± 0.08
YG11-3-343	278	gsj13-104	1.91 ± 0.15	$(1.20 \pm 0.13) \times 10^{-4}$	8.03 ± 0.55	23.57 ± 0.20	299	0.1	0.75 ± 0.06	0.84 ± 0.07
YG11-3-349	290	gsj13-105	2.01 ± 0.26	$(1.34 \pm 0.10) \times 10^{-4}$	7.99 ± 1.23	28.36 ± 0.98	280	0.1	0.91 ± 0.10	1.00 ± 0.11

Note: The errors represent one standard error

[a]Water content is calculated by the model assuming the compaction

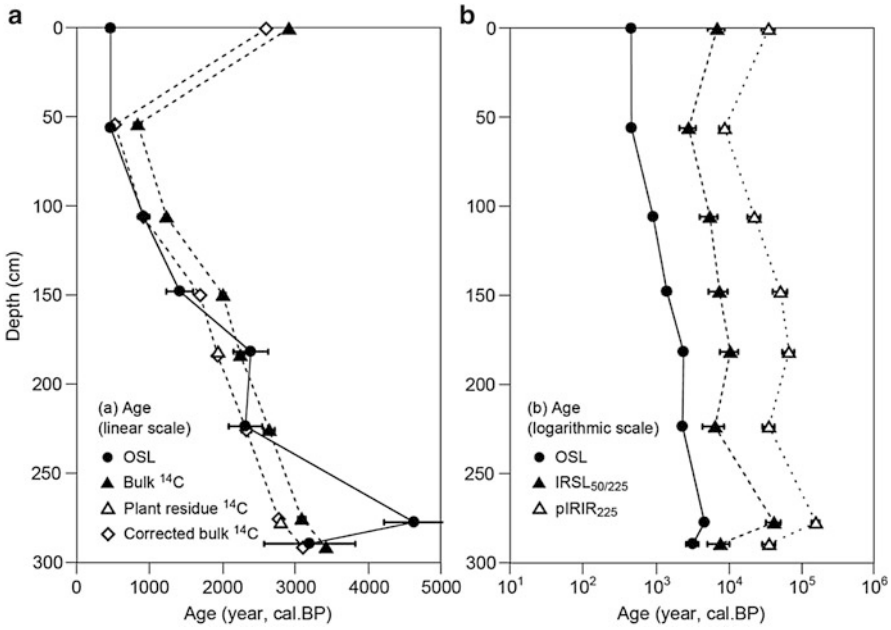

Fig. 11.5 Depth profiles of the Lake Yogo core showing (**a**) OSL, bulk ^{14}C, plant ^{14}C, and corrected bulk ^{14}C ages and (**b**) OSL, fading-corrected $IRSL_{50/225}$, and fading-uncorrected $pIRIR_{225}$ ages. The errors represent one standard error

samples decreased with increasing depth in the sediment core. We thus assumed an average water content for each sample as the mean between the water content of lake-floor sample YG11-3-001 and that of the sample. This modified water content (Table 11.3) was used for age determination. The calculated ages are shown in Table 11.4 and Fig. 11.5.

11.3.3 ^{14}C Dating

The bulk ^{14}C ages of samples YG11-3-246 and YG11-3-342 were generally about 300 years older than the plant residue ^{14}C ages of the adjoining samples YG11-3-245 and YG11-3-343 (Table 11.4). This overestimation is ascribed to the well-known old-carbon effect (e.g., Watanabe et al. 2009). We assumed that 300 years is the average overestimation of the bulk ^{14}C ages and subtracted it to yield the corrected bulk ^{14}C ages, which were compared with the OSL ages in this study.

Table 11.4 The $\delta^{13}C$ values and the ages for bulk ^{14}C, plant residue ^{14}C, quartz OSL, fading corrected $IRSL_{50/225}$, and uncorrected and corrected $pIRIR_{225}$ ages

								OSL	$IRSL_{50/225}$	$pIRIR_{225}$	
Sample name	Depth (cm)	Lab. code	Material for ^{14}C dating	$\delta^{13}C$ (‰)	^{14}C age (BP)	Calibrated ^{14}C age (cal.BP)	Lab. code	Age (y)	Corrected age (y)	Uncorrected age (y)	Corrected age (y)
YG11-3-001	0	NUTA2-19999	Sediment	−26.9	2,800 ± 20	2,900 ± 30	gsj13-98	520 ± 50	6,860 ± 1,760	378,000 ± 7,240	37,580 ± 7,930
YG11-3-123	54	NUTA2-20000	Sediment	−26.1	895 ± 20	830 ± 50					
YG11-3-124	56						gsj13-99	520 ± 60	2,790 ± 690	8,680 ± 1,400	9,250 ± 1,500
YG11-3-207	106	NUTA2-20001	Sediment	−28.2	1,270 ± 20	1,220 ± 30	gsj13-100	970 ± 80	5,440 ± 1,480	22,380 ± 4,520	23,700 ± 4,800
YG11-3-228	148						gsj13-101	1,470 ± 190	7,340 ± 2,130	50,850 ± 11,280	55,740 ± 12,440
YG11-3-229	150	NUTA2-21289	Sediment	−28.1	2,040 ± 20	2,000 ± 40					
YG11-3-245	182	NUTA2-20010	Plant residue	−32.8[a]	1,985 ± 25	1,930 ± 30	gsj13-102	2,440 ± 240	10,360 ± 2,900	65,960 ± 12,170	73,960 ± 13,780
YG11-3-246	184	NUTA2-20003	Sediment	−29.2	2,235 ± 20	2,235 ± 50					

(continued)

Table 11.4 (continued)

Sample name	Depth (cm)	Lab. code	Material for ^{14}C dating	$\delta^{13}C$ (‰)	^{14}C age (BP)	Calibrated ^{14}C age (cal.BP)	Lab. code	OSL	$IRSL_{50/225}$	$pIRIR_{225}$	
								Age (y)	Corrected age (y)	Uncorrected age (y)	Corrected age (y)
YG11-3-316	224						gsj13-103	2,370 ± 230	6,430 ± 2,110	35,240 ± 6,630	38,330 ± 7,310
YG11-3-317	226	NUTA2-20007	Sediment	−29.4	2,530 ± 20	2,630 ± 75					
YG11-3-342	276	NUTA2-20008	Sediment	−29.1	2,925 ± 20	3,075 ± 50					
YG11-3-343	278	NUTA2-20011	Plant residue	−30.5[a]	2,690 ± 20	2,790 ± 25	gsj13-104	4,680 ± 420	41,170 ± 9,330	154,500 ± 19,060	175,940 ± 22,740
YG11-3-349	290						gsj13-105	3,060 ± 330	7,610 ± 2,540	35,500 ± 7,080	39,340 ± 7,970
YG11-3-350	292	NUTA2-20009	Sediment	−28.7	3,185 ± 20	3,410 ± 25					

Note: The errors represent one standard error

[a]The $\delta^{13}C$ value of plant residue was measured by Tandetron Accelerator Mass Spectrometry

11.4 Discussion

The $IRSL_{50/225}$ and $pIRIR_{225}$ ages were much older than the OSL ages (Table 11.4), and the residual could not account for the excess. The slower bleaching rates for IRSL and pIRIR signals thus appear to have contributed to the excess in equivalent dose. Lake Yogo has a small catchment characterized by a short sediment transport distance, which would provide less opportunity for bleaching by sunlight and result in incomplete bleaching of IRSL and pIRIR signals. Nevertheless, except for samples YG11-3-001, YG11-3-245, and YG11-3-343, five OSL ages were concordant with corrected bulk ^{14}C ages, suggesting that there was generally enough sunlight exposure to reset the OSL signal. The IRSL signal also showed evidence of more complete bleaching than the pIRIR signal.

With regard to the three exceptional samples, there are two possible explanations for why the OSL ages were not concordant with the corrected bulk ^{14}C ages. First, for YG11-3-245 and YG11-3-343, the OSL ages were probably older than the corrected bulk ^{14}C ages because of incomplete bleaching. Mass movements such as river floods and landslides may lead to less exposure to sunlight and account for the poor bleaching of OSL. These two samples showed a larger difference between OSL and pIRIR ages than other samples, which is consistent with a short exposure to sunlight because the difference between the OSL and pIRIR residual signals is large for bleaching times of only a few seconds (Murray et al. 2012). In other samples, quartz was well bleached for OSL dating before deposition and gave reliable ages concordant with ^{14}C ages. Second, for sample YG11-3-001, from near the top of the core (8 cm depth), both OSL and corrected bulk ^{14}C ages may be overestimated. After 1960, the water balance of Lake Yogo came under artificial control for irrigation and flood-control purposes (Shimada et al. 2002); thus, changes in the organic carbon source and transport processes may have resulted in overestimated corrected bulk ^{14}C and OSL ages. The presence of radioactivity from ^{137}Cs (42.5 ± 5.7 Bq/kg) is evidence for the deposition of YG11-3-001 after 1960.

For coarse-grained sediments, the effects of bleaching on age determinations are best evaluated by the single-grain method and corresponding age models (such as MAM, Galbraith et al. 1999). However, for fine-grained sediments, the methods used in this study are most suitable. On the other hand, comparisons of quartz OSL and pIRIR ages (Murray et al. 2012) may be in effective in establishing the accuracy of OSL ages when the OSL signal is completely reset but IRSL and pIRIR signals are not fully reset, because of the difference in bleaching rates for the three signals. In that situation, one solution is to compare luminescence ages with an independent age control, and this study using sediment from Lake Yogo is an example of that approach's success. Laboratory studies suggest that sun exposure of no more than a few tens of seconds is enough to perturb OSL age estimates (Murray et al. 2012). If bleaching rates of OSL, IRSL, and pIRIR signals are accurately known, these may be used to constrain the approximate time of sediment's sunlight exposure before burial. Although OSL is the most reliable technique for age determination of

young sediment, the degree of sunlight exposure in a given sediment system may be important for estimating effects of incomplete bleaching when applying the pIRIR method to much older sediments.

11.5 Summary

1. The $IRSL_{50/225}$ and $pIRIR_{225}$ ages were much older than the OSL ages in samples from Lake Yogo, whereas the OSL ages were generally concordant with the corrected bulk ^{14}C ages. The difference in bleaching rates of these three luminescence signals appears to have contributed to these age differences. In the case of Lake Yogo, there was enough sunlight exposure to mainly reset the OSL signal but not enough to reset the IRSL and pIRIR signals. Therefore, the bleaching period and conditions are key issues for accurate age determination of samples from small catchment areas.
2. For incompletely bleached samples, comparisons between OSL and independent age controls may be more reliable than comparisons between different luminescence techniques. However, overestimated ages may be useful to constrain the approximate time of sunlight exposure before burial, based on the results of laboratory bleaching studies. For old samples, incomplete bleaching of the pIRIR signal is negligibly small compared to D_e and the pIRIR method may be used to determine the sedimentation age.

Acknowledgments We thank Akihiro Hasebe and Haruka Hayashi for their help with the LA-ICP-MS and XRF analyses, respectively. This work was supported by a JSPS Research Fellowship (24–810) for Young Scientists from the Japan Society for the Promotion of Science (Ito) and Grants-in-Aid for Scientific Research (A-23240120).

References

Adamiec G, Aitken M (1998) Dose-rate conversion factors: update. Ancient TL 16:37–50

Auclair M, Lamothe M, Huot S (2003) Measurement of anomalous fading for feldspar IRSL using SAR. Radiat Meas 37:487–492

BDP-98 Members (2001) The new BDP-98 600-m drill core from Lake Baikal: a key late Cenozoic sedimentary section in continental Asia. Quatern Int 80–81:19–36

BDP-99 Members (2005) A new Quaternary record of regional tectonic, sedimentation and paleoclimate changes from drill core BDP-99 at Posolskaya Bank, Lake Baikal. Quatern Int 136:105–121

Buylaert JP, Murray AS, Thomsen KJ, Jain M (2009) Testing the potential of an elevated temperature IRSL signal from K-feldspar. Radiat Meas 44:560–565

Buylaert JP, Thiel C, Murray AS, Vandenberghe DAG, Yi S, Lu H (2011) IRSL and post-IR residual doses recorded in modern dust samples from the Chinese Loess Plateau. Geochronometria 38:432–440

Buylaert JP, Jain M, Murray AS, Thomsen KJ, Thiel C, Sohbati R (2012) A robust feldspar luminescence dating method for Middle and Late Pleistocene sediments. Boreas 41:435–451

Buylaert JP, Murray AS, Gebhardt AC, Sohbati R, Ohlendorf C, Thiel C, Wastegard S, Zolitschka B, The PASADO, Team S (2013) Luminescence dating of the PASADO core 5022-1D from Laguna Potrok Aike (Argentina) using IRSL signals from feldspar. Quatern Sci Rev 71:70–80

Colman SM, Peck JA, Karabanov EB, Carter SJ, Bradbury JP, King JW, Williams DF (1995) Continental climate response to orbital forcing form biogenic silica records in Lake Baikal. Nature 378:21–28

Galbraith RF, Roberts RG, Laslett GM, Yoshida H, Olley JM (1999) Optical dating of single grains of quartz from Jinmium rock shelter, northern Australia: part 1, experimental design and statistical models. Archaeometry 41:339–364

Huntley DJ, Lamothe M (2001) Ubiquity of anomalous fading in K-feldspars and the measurement and correction for it in optical dating. Can J Earth Sci 38:1093–1106

Ito K, Hasebe N, Sumita R, Arai S, Yamamoto M, Kashiwaya K, Ganzawa Y (2009) LA-ICP-MS analysis of pressed powder pellets to luminescence geochronology. Chem Geol 262:131–137

Ito K, Hasebe N, Hasebe A, Arai S (2011) The matrix effect on 238U and 232Th measurements using pressed powder pellets by LA-ICP-MS. Geochem J 45:375–385

Juschus O, Preusser F, Melles M, Radtke U (2007) Applying SAR-IRSL methodology for dating fine-grained sediments from Lake El'gygytgyn, north-eastern Siberia. Quatern Geochronol 2:187–194

Lowick SE, Trauerstein M, Preusser F (2012) Testing the application of post IR-IRSL dating to fine grain waterlain sediments. Quatern Geochronol 8:33–40

Murray AS, Wintle AG (2000) Luminescence dating of quartz using an improved single-aliquot regenerative- dose protocol. Radiat Meas 32:57–73

Murray AS, Thomsen KJ, Masuda N, Buylaert JP, Jain M (2012) Identifying well-bleached quartz using the different bleaching rates of quartz and feldspar luminescence signals. Radiat Meas 47:688–695

Nakamura T, Oda T, Tanaka A, Horiuchi K (2003) High precision ^{14}C age estimation of bottom sediments of Lake Baikal and Lake Hovsgol by AMS. Gekkan Chikyu 42, Kaiyoushuppan, Tokyo, pp 20–31. (in Japanese)

Nara F, Tani Y, Soma Y, Soma M, Naraoka H, Watanabe T, Horiuchi K, Kawai T, Oda T, Nakamura T (2005) Response of phytoplankton productivity to climate change recorded by sedimentary photosynthetic pigments in Lake Hovsgol (Mongolia) for the last 23,000 years. Quatern Int 136:71–81

Prescott JR, Hutton JT (1994) Cosmic ray contributions to dose rates for luminescence and ESR dating: large depths and long-term time variations. Radiat Meas 23:497–500

Rees-Jones J (1995) Optical dating of young sediments using fine-grain quartz. Ancient TL 13:9–14

Reimer PJ, Baillie MGL, Bard E, Bayliss A, Beck JW, Blackwell PG, Bronk Ramsey C, Buck CE, Burr GS, Edwards RL, Friendrich M, Grootes PM, Guilderson TP, Hajdas I, Heaton TJ, Hogg AG, Hughen KA, Kaiser KF, Kromer B, McCormac FG, Manning SW, Reimer RW, Richards DA, Southon JR, Talamo S, Turney CSM, van der Plicht J, Weyhenmeyer CE (2009) IntCal09 and Marine09 radiocarbon age calibration curves, 0–50,000 years cal BP. Radiocarbon 51:1111–1150

Shimada T, Kashiwaya K, Hyodo M, Masuzawa T (2002) Hydro-environmental fluctuation in a lake-catchment system during the Late Holocene inferred from Lake Yogo sediments. Trans Jpn Geomorphol Union 23:415–431. (in Japanese with English abstract)

Sohbati R, Murray AS, Buylaert JP, Ortuño M, Cunha PP, Masana E (2011) Luminescence dating of Pleistocene alluvial sediments affected by the Alhama de Murcia fault (eastern Betics, Spain) – a comparison between OSL, IRSL and post-IR IRSL ages. Boreas 41:250–262

Thiel C, Coltorti M, Tsukamoto S, Frechen M (2010) Geochronology for some key sites along the coast of Sardinia (Italy). Quatern Int 222:36–47

Thomsen KJ, Murray AS, Jain M, Bøtter-Jensen L (2008) Laboratory fading rates of various luminescence signals from feldspar-rich sediment extracts. Radiat Meas 43:1474–1486

Tsukamoto S, Rink WJ, Watanuki T (2003) OSL of tephric loess and volcanic quartz in Japan and an alternative procedure for estimation D_e from a fast OSL component. Radiat Meas 37:459–465

Wakita K, Harayama S, Kano K, Mimura K, Sakamoto T, Hiroshima T, Komazawa M (1992) Geological map, 1: 200,000, Gifu. Geological Survey of Japan, Tsukuba

Watanabe T, Nakamura T, Kawai T (2007) Radiocarbon dating of sediments from large continental lakes (Lakes Baikal, Hovsgol and Erhel). Nucl Instrum Method Phys Res B 259:565–570

Watanabe T, Nakamura T, Watanabe Nara F, Kakegawa T, Horiuchi K, Senda R, Oda T, Nishimura M, Inoue Matsumoto G, Kawai T (2009) High-time resolution AMS ^{14}C data sets for Lake Baikal and Lake Hovsgol sediment cores: changes in radiocarbon age and sedimentation rates during the transition from the last glacial to the Holocene. Quatern Int 205:12–20

Williams DF, Peck J, Karabanov EB, Prokopenko AA, Kravchinsky V, King J, Kuzmin MI (1997) Lake Baikal record of continental climate response to orbital insolation during the past 5 million years. Science 278:1114–1117

Zheng YE, Zhou LP, Zhang JF (2010) Optical dating of the upper 22 m of cored sediments from Daihai Lake, northern China. Quatern Geochronol 5:228–232

Chapter 12
Possible Age Models for Lake Onuma Lacustrine Sediments Based on Tuffs Recovered in Three Cores

Noriko Hasebe, Taeko Itono, Kota Katsuki, Takuma Murakami, Shinya Ochiai, Nagayoshi Katsuta, Yong Wang, Jin-Young Lee, Keisuke Fukushi, Yoshihiro Ganzawa, Muneki Mitamura, Kuniaki Tanaka, Ju Yong Kim, Ji Shen, and Kenji Kashiwaya

Abstract Lake Onuma, Hokkaido, Japan, is located south of Hokkaido-Komagatake volcano. The present Lake Onuma was formed by an intensive eruption and partial collapse of the volcanic cone in 1640 AD, which caused a debris flow that

N. Hasebe (✉)
Institute of Nature and Environmental Technology, Kanazawa University, Kakuma, Kanazawa 920-1192, Japan

Korea Institute of Geoscience and Mineral Resources, 124 Gwahang-no, Yuseong-gu Deajeon 305-350, South Korea
e-mail: hasebe@staff.kanazawa-u.ac.jp

T. Itono • T. Murakami • S. Ochiai • K. Fukushi
Institute of Nature and Environmental Technology, Kanazawa University, Kakuma, Kanazawa 920-1192, Japan

K. Katsuki • J.Y. Lee • J.Y. Kim
Korea Institute of Geoscience and Mineral Resources, 124 Gwahang-no, Yuseong-gu Deajeon 305-350, South Korea

N. Katsuta
Faculty of Education, Gifu University, Yanagido 1-1, Gifu 510-1193, Japan

Y. Wang • J. Shen
State Key Laboratory of Lake Science and Environment, Nanjing Institute of Geography and Limnology, Chinese Academy of Sciences, 73 East Beijing Road, Nanjing 210008, P.R. China

Y. Ganzawa • K. Tanaka
Hokkaido University of Education, Hakodate Campus, Hachiman-cho 1-2, Hakodate, Hokkaido 040-8567, Japan

M. Mitamura
Department of Geosciences, Osaka City University, 3-3-138 Sugimoto Sumiyoshi, Osaka 558-8585, Japan

K. Kashiwaya
Institute of Nature and Environmental Technology, Kanazawa University, Kakuma, Kanazawa 920-1192, Japan

Department of Geography, National Taiwan University, Daan District, Taipei 10617, Taiwan

K. Kashiwaya et al. (eds.), *Earth Surface Processes and Environmental Changes in East Asia*, DOI 10.1007/978-4-431-55540-7_12

dammed the drainage. Three cores (ON12A, C, and D) were recovered from Lake Onuma to examine the environmental change in the region. These three cores are correlated based on lithological descriptions and water content fluctuation. Volcanic deposits Ko-a (1929 AD), Ko-c_1 (1856 AD), Ko-d (1640 AD), and possibly Ko-c_2 (1694 AD) were successfully identified with the help of radiocarbon age dating, ^{137}Cs radioactivity measurement, and chemical analyses, to construct an age model of these cores.

Keywords Hokkaido-Komagatake volcano • Lake Onuma • Geochronology • Historical eruption

12.1 Introduction

Lake Onuma, Hokkaido, Japan, is located south of Hokkaido-Komagatake volcano (hereafter HKV, Fig. 12.1). According to the historical record, the present Lake Onuma was formed in 1640 AD when an intensive eruption and partial cone collapse (the Kurumisaka debris avalanche) dammed the outflow of rivers (Yoshimoto and Ui 1998). Since then, several eruptions (1694, 1856, 1929, 1942) have deposited eruptive materials on land (Katsui et al. 1989), and materials from these events may have reached Lake Onuma, leaving some evidence in the lake sediments (Yoshimoto et al. 2007).

Lake sediments preserve a record of past environmental fluctuation and have frequently been studied to reconstruct palaeo-environment of regions (e.g., Takemura 1990; BDP98 Members 2001). In studying lake sediments, development of an age model plays a significant role in correlating the environmental events. Constructing an age model from sediments in Lake Onuma has the advantage of the known eruptive history of HKV. The Hokkaido area has been less influenced by human activity due to its low population, which is another advantage in studying Lake Onuma to understand naturally occurring environmental fluctuation.

Three cores (ON12A, C, and D) were recovered from Lake Onuma to reveal the environmental change of the region. The cores are here correlated to one another based on lithological descriptions and water content fluctuation. An age model of these cores was constructed using the identification of volcanic products, radiocarbon age dating, and ^{137}Cs radioactivity measurements.

12.2 Geologic Background

Lake Onuma consists of two basins, the eastern basin (called Onuma) and the western basin (called Konuma) (Fig. 12.1). Their surface areas are 5.12 and 3.80 km^2, respectively, and average water depths are 6.4 and 2.3 m, respectively. The maximum water depth is 13.6 m in Onuma and 5.5 m in Konuma. There are three inflow rivers, the Shukunobe, the Ikusa, and the Karima, and one outflow river, the Orito. An artificial channel and control dam were constructed in the southern side of Lake Konuma in 1961 and the outflow to the Orito river was blocked by the

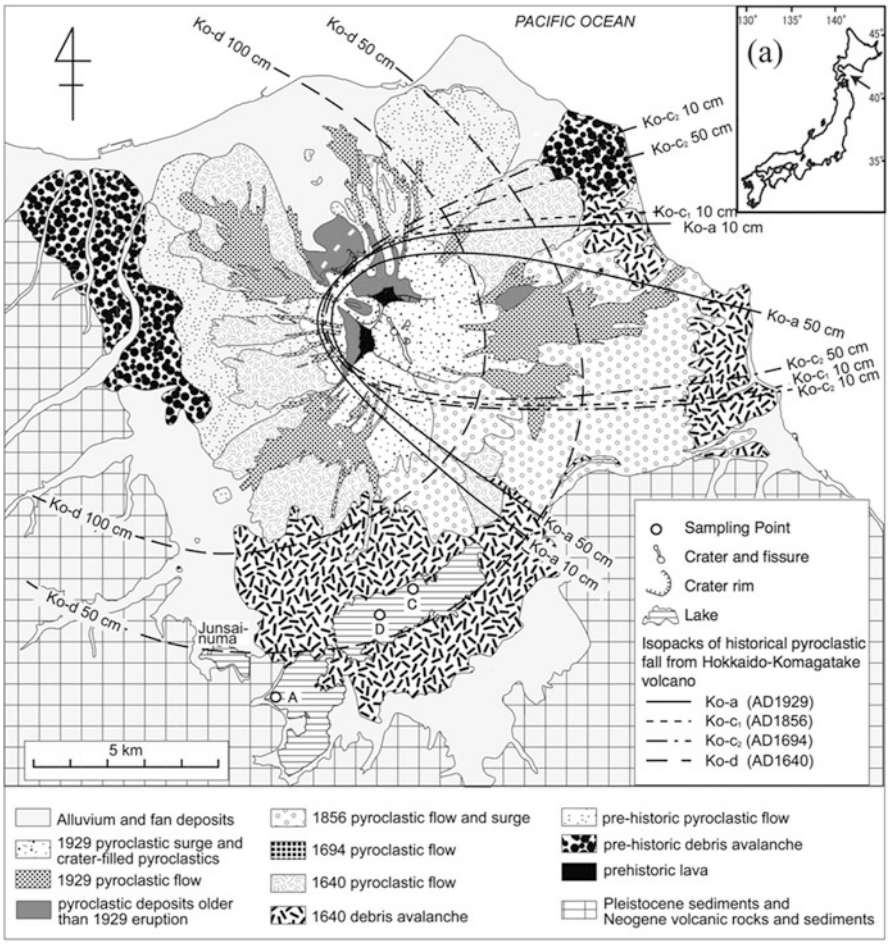

Fig. 12.1 Index map of Lake Onuma. Geological map of Hokkaido Komagatake Volcano (HKV) (Modified after Yoshimoto et al. 2007) and sampling points of this study. The *arrow* in the index map (**a**) indicates the location of Lake Onuma and HKV

sluice gate, resulting in a change of current direction within the lake. The lake water level is now controlled artificially (Tanaka 2005); detailed hydrologic information is found in the next chapters of this special issue (Itono et al. 2015; Ochiai et al. 2015).

The eruptive history of the HKV has been reconstructed based on detailed geological survey and examination of cores obtained from on-land locations (e.g., Katsui et al. 1989; Ganzawa et al. 2005; Yoshimoto et al. 2008). Since late Pleistocene the HKV has had four main active stages: > 39 ka, 20–12 ka, 6.8–6.3 ka, and <1640 AD, between which silences with few eruptions as long as >6 kyrs were found. Most HKV erupted materials have been andesite with average SiO_2 concentration of ~60 wt.% (Katsui et al. 1989) and show no significant variations in whole rock chemistry through the eruptive history. The eruptions were explosive, sometimes accompanied by collapses that created pyroclastic flows or debris avalanches.

Recent HKV eruptive activities were recorded in the historical literature. The eruption in 1640 produced the large debris avalanche (the Kurumisaka debris avalanche deposit) responsible for damming the rivers, and small mounds distributed in Lake Onuma were also formed by this catastrophic collapse. The 1640 eruption also produced several airfall pumice layers (Katsui et al. 1989), collectively named Ko-d, which accumulated a >50-cm-thick pyroclastic fall deposit in Lake Onuma. Yoshimoto and Ui (1998) deduced the following evolution of 1640 volcanic activity: initial land sliding, followed by collapse of an eruption column from a Plinian eruption (which produced the pyroclastic flow and airfall pumice), accompanied by further land sliding. The eruption in 1694 produced pumice airfall deposits on the east side of the volcano, that are collectively named Ko-c_2. The 1765 eruption was noted in the literature, though corresponding eruptive materials have not been reported on land. The 1856 eruption covered the southeast slope of the volcano (Fig. 12.1) with a pyroclastic flow that dammed the eastern outflow of Lake Onuma (Orito River), and produced an airfall pumice named Ko-c_1. The eruption in 1929 produced pumice airfall deposits (Ko-a) on the south-east slope of the volcano; the northern edge of present Lake Onuma is within the distribution area of the 1929 pumice fall (Katsui et al. 1989). The last major eruption of HKV was in 1942, when the main effect was localized around the top of the mountain. Thin volcanic ash (less than a few centimeters) is found in the east-south-east side of the volcano (Takahashi et al. 2004).

12.3 Sampling Methods

Two cores (ON12C, ON12D) were obtained from Lake Onuma and one (ON12A) from Lake Konuma in 2012 (Figs. 12.1, 12.2 and Table 12.1). Among them, ON12C is from the deepest part and is therefore expected to reflect stable and average hydro-environmental conditions in the lake. These core samples were obtained with an air pressure-type piston core sampler (maximum 4 m in length) with a polyvinyl chloride pipe of 8.3 cm in diameter. To obtain information from the top surface sediments, which are often lost by the piston core sampler, short core samples were also taken at the same sampling point as the long cores, using a gravity core sampler (1 m) with an acrylic tube of 5.2 cm in diameter. Information on collected cores is summarized in Table. 12.1. The results from the short, gravity cores will be published elsewhere.

12.4 Analysis

The core was cut to ∼1 m lengths at the sampling site. Back in the laboratory, Hokkaido University of Education, each ∼1 m length was opened, cut into halves lengthwise and subsampled for analyses mentioned below.

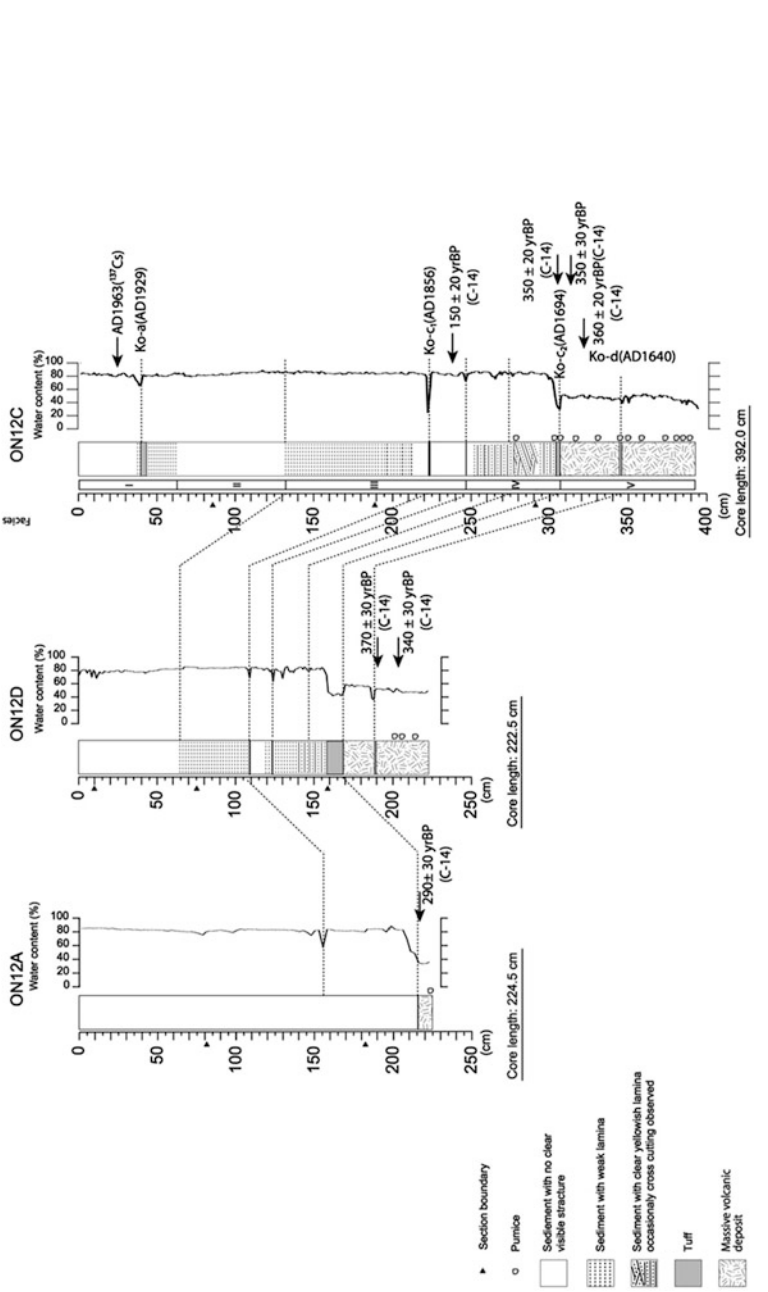

Fig. 12.2 Description and water content of three cores. Corresponding layers are connected with *dashed lines*. Layers where pumice fragments larger than a few centimetres in length were found are indicated. Layers with radiometric ages are indicated by *arrows*. Sedimentary facies (I to V) identified for ON12C core is indicated in the *box* next to the columnar section. Possible correlation to the HKV volcanic beds Ko-d, Ko-c_1, Ko-c_2, and Ko-a is also shown in the column. *Small black triangles* indicate the section boundary

Table 12.1 Information on collected core samples

Sampling point	Latitude	Longitude	Water depth (m)	Core ID	Length (cm)	Analytical interval (cm)
A	N41°58′34″.5	E140°38′45″.6	3.3	ON12A	223	2.5
				ON12AS02	76	1.0
C	N42°00′09″.3	E140°41′31″.7	11.7	ON12C	392	1.0/2.5
				ON12CS01	80	1.0
D	N41°59′50″.0	E140°40′57″.5	9.5	ON12D	223	1.0/2.5/3.0
				ON12DS01	66	1.0

Wood and plant fragments found at several depths in each core were sampled for radiocarbon dating. Radiocarbon ages were measured at the Institute of Accelerator Analysis Ltd or Korea Institute of Geoscience and Mineral Resources. After cleaning samples with tweezers, the plant samples were treated with HCl (1 M), NaOH (gradually raising the concentration level from 0.001 M to 1 M). Then a sample was combusted to produce CO_2 gas, which was then purified in a vacuum line and subsequently reduced to graphite by using hydrogen and an iron catalyst. The produced graphite was measured against a standard of oxalic acid (HOxII) provided by the National Institute of Standards and Technology (USA), using an accelerator mass spectrometry system. A blank was also measured for the background check. The obtained data were converted to calendar years by calibration with IntCal 09 (Institute of Accelerator Analysis Ltd) or OxCal (IntCal13: Korea Institute of Geoscience and Mineral Resources) (Reimer et al. 2013).

For all three cores, the water content was obtained for every 1 cm by measurement of wet mass and mass dried for 48 h in 110 °C. The whole particle size, mineral assemblage, and sediment density for all three cores were also analysed in Kanazawa University and will be reported elsewhere.

For the longest core, ON12C, portable XRF data was obtained using hand-held x-ray equipment (JEOL: handheld element analyser delta, Fig. 12.3) every 2.5 cm on the wet, flat surface of one split of the core. Then this half core with portable XRF data was cut every 2.5 cm for further analyses (e.g., palaeomagnetism, stable isotope, etc.), which will be reported elsewhere. Using the other half of core ON12C, U-channel sampling was carried out using a ∼40 cm long plastic U-channel, and the part of the half core remaining after U-channelling was cut every 1 cm for further analyses, including the water content and sedimentologic parameters mentioned above.

The ON12C core U-channel samples were first freeze-dried and then embedded in low viscosity resin (E205, Nichika Inc.) in a desiccator under low pressure. The samples were hardened at room temperature and further cut into ∼15-cm sections. After polishing the exposed surface, scanned XRF information was obtained with a Horiba XGT-2000 V X-ray analytical microscope (Katsuta et al. 2007). The scanned image was obtained as an average of 12 times-repeated scanning, and the resolution of the scanned image was 0.74 mm/pixel. A profile of relative concentration fluctuation along the core was created by calculating the average intensity for the

data from the same horizon (Fig. 12.3). The XRF results by portable detector versus scanning microscopy are compared in Fig. 12.3, and the effectiveness of on-site XRF analyses is examined for ON12C.

Selected ON12C core samples were also treated for the conventional bulk sample XRF measurement of the concentrations of the major elements (Si, Ti, Al, Fe, Mn, Mg, Ca, Na, K, P). First, each powdered bulk sample was heated for 2.5 h at 800 °C to remove sulfur, which would seriously damage the platinum crucible in the following procedure. Each sample was then mixed with $Li_2B_4O_7$ (the sample:$Li_2B_4O_7$ weight ratio was 1:10) in a platinum crucible and vitrified. The samples were finally analysed with a Rigaku System 3270 XRF spectrometer with a Rh tube (Ichiyama et al. 2006) to compare with the scanned and portable XRF results (Fig. 12.3). The analyses were carried out with a 50-kV accelerating voltage and 20-mA beam current.

Radioactivity from ^{137}Cs was also measured for the top part (~15–40 cm) of the ON12C core, to identify the time when the release of ^{137}Cs by nuclear tests into the atmosphere was maximum. Samples were dried and ground to homogeneity, then 1 g of each sample was packed in a plastic bag with a fixed volume. The radioactivity of each sample was measured with high performance Germanium semiconductor detectors (GEM-25-P4, ORTEC) at the Radioisotope Laboratory for Natural Science and Technology, Kanazawa University.

12.5 Results and Discussion

12.5.1 Portable XRF versus Scanning XRF

The portable XRF equipment used has several measurement modes with different sets of measured elements; two modes (ceramic mode and soil mode) were tested in this study. Numerous elements are measured by both modes, but some of these elements showed discordant results in this study, between the two measurement modes (e.g., P, Cl, S, Zr, Co, Ni, As, Cr, Cd, Zn, Pb, Sn, Sb, Pd, Ag). In most cases, one data set shows some fluctuation in concentration along the core depth, while the other data set shows more-or-less flat values. The flat values suggest this discrepancy may be caused by the different detection limits between the two modes. Some elements (K, Ca, Mn, Fe and Ti) show concordant fluctuation between the two measurement modes, and the data for these elements, together with Al and Si, which were only measured in the ceramic mode, are compared with the results of the scanning XRF (Fig. 12.3).

The lowest ~80 cm of the ON12C core and the horizon at the depth of ~220 cm are distinctive, with high Si, Ca, K, and Ti intensities. The conventional bulk sample XRF data (Table 12.2) suggests the major chemistry of this lowest ~80 cm corresponds to that of HKV products (Katsui et al. 1989), therefore these layers must mainly consist of volcanic products. Mn and Fe show fluctuation unrelated to volcanic products; they may be a proxy of some environmental condition of Lake Onuma.

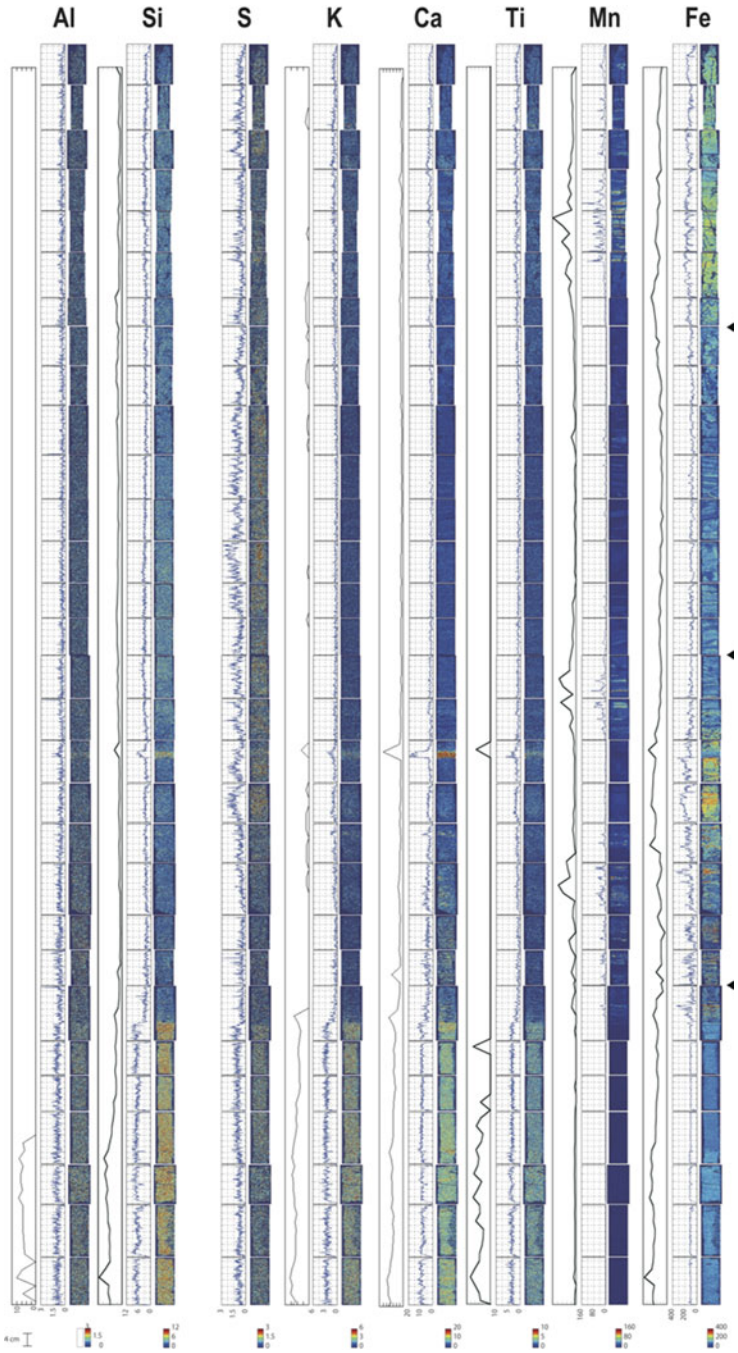

Fig. 12.3 (continued)

Table 12.2 XRF results (wt.%) by the conventional bulk method

Depth (cm)	281	296	297	321	359
SiO_2	38.6	46.0	37.0	66.2	65.4
TiO_2	0.2	0.2	0.2	0.5	0.6
Al_2O_3	37.9	33.2	29.1	17.1	18.1
FeO[a]	10.1	9.8	19.7	5.3	5.8
MnO	2.2	0.6	2.2	0.1	0.1
MgO	0.8	1.0	0.7	1.4	1.4
CaO	4.3	4.0	4.9	3.3	3.4
Na_2O	0.7	1.0	0.7	2.7	2.5
K_2O	0.4	0.6	0.4	1.4	1.3
P_2O_5	0.2	0.3	0.3	0.2	0.2
Total	95.2	96.6	95.0	98.2	98.8

12.5.2 ^{14}C Dating and ^{137}Cs Results

Dating results for ^{14}C, which gave the oldest limit of age of deposition, are summarized in Table 12.3 and representative values are plotted in Fig. 12.2. The deepest part of each core yielded more or less concordant ages older than ~300–400 yrBP and this result is consistent with their lithology being very similar (Fig. 12.2, see discussion below). For two horizons from ON12C (238 and 304 cm), two samples were analysed and they were concordant within a 2σ error range. There is a possibility that the slight difference may represent the different source of materials interbedded. The plant sample with younger ages must be close to the sedimentation age.

The results of radioactivity measurement of ^{137}Cs from the long, piston-cored ON12C samples at depths ~15–40 cm is shown in Fig. 12.4. The radioactivity profile shows peaks at ~26 and ~32 cm, among which the highest is at ~26 cm. Results from the short (~1 m), gravity-cored ON12C samples do not show such a disturbed profile (Ochiai et al. 2015). Currently, the reason why there is low radioactivity at the depth of ~29 cm (or high value at the depth of ~32 cm) is not certain. However, the issue may be analytical, and the depth with highest radioactivity corresponds most likely to the time when release of ^{137}Cs by nuclear tests into the atmosphere was maximum (1963 AD).

Fig. 12.3 Scanning and portable XRF results from core ON12C for Al, Si, S, K, Ca, Ti, Mn, and Fe, are plotted along the core length. Among the three columnar sections, on the *left* is the result of portable XRF measurement; horizontal scale is relative intensity and becomes high leftward. The *middle columnar* section is the average of scanning XRF data calculated for the same horizon; horizontal scale is relative intensity. The right columnar section is a scanning XRF map; the intensity is strong for *red* and becomes weak to *blue. Small black triangles* represent the section boundary. For scanning XRF measurement, a section is further cut into seven or eight pieces, and the boundaries are shown as *horizontal lines*. Due to this additional cutting for scanning XRF data, the vertical axis is not perfectly identical for the portable and scanning XRF data

Table 12.3 ^{14}C dating results

Sample number	Depth (cm)	Material	Age ± σ (yr BP)	$\delta^{13}C$ (‰)	pMC (%)	Calendar age (2σ range)
ON12C-239*	238	Plant fraction	150 ± 20	−25.51 ± 0.40	98.19 ± 0.27	1668–1706 calAD (15.9 %)
						1720–1782 calAD (32.8 %)
						1797–1820 calAD (11.2 %)
						1832–1882 calAD (17.9 %)
						1915–1946 calAD (17.6 %)
ON12C-239-2	238	Plant fraction	230 ± 40	−27.90 ± 0.90	97.19 ± 0.45	1520–1590 calAD (7.7 %)
						1620–1700 calAD (6.8 %)
						1720–1820 calAD (38.2 %)
						<1920 calAD (12.6 %)
ON12C-305-1*	304	Wood	350 ± 20	−28.75 ± 0.32	95.71 ± 0.26	1458–1529 calAD (44.1 %)
						1544–1634 calAD (51.3 %)
ON12C-305-2	304	Plant	400 ± 30	−33.20 ± 1.70	95.10 ± 0.41	1430–1530 calAD (76.4 %)
						1570–1630 calAD (19 %)
ON12C-125a	312	Plant	350 ± 30	−26.60 ± 0.20	95.79 ± 0.38	1450–1640 calAD (95.4 %)
ON12C-126a	314	Wood	350 ± 30	−25.30 ± 0.50	95.73 ± 0.39	1450–1640 calAD (95.4 %)
ON12C-321	320	Plant	360 ± 30	−25.60 ± 0.40	95.66 ± 0.38	1450–1530 calAD (47.7 %)
						1540–1640 calAD (47.7 %)

ON12D-193	192	Charcoal	370 ± 30	−27.20 ± 0.60	95.54 ± 0.38	1440–1530 calAD (55.0 %)
						1550–1640 calAD (40.4 %)
ON12D-68a	198	?	4070 ± 40	−37.80 ± 0.40	60.22 ± 0.33	2860calBC-2800calBC (13.7 %)
						2760calBC-2720calBC (4.6 %)
						2710calBC-2480calBC (77.2 %)
ON12D-70a	204	Fibrous root	340 ± 30	−31.60 ± 0.70	95.87 ± 0.38	1460–1640 calAD (95.4 %)
ON12A-85	208	Plant	690 ± 30	−20.70 ± 0.70	91.76 ± 0.37	1260–1320 calAD (68.9 %)
						1350–1390 calAD (26.5 %)
ON12A-88	216	Plant	290 ± 30	−26.60 ± 0.50	96.45 ± 0.38	1490–1670 calAD (95.4 %)

*Measured at Institute of Accelerator Analysis Ltd and calibrated by IntCal 09. Others were measured at the Korea Institute of Geoscience and Mineral Resources and calibrated by OxCal

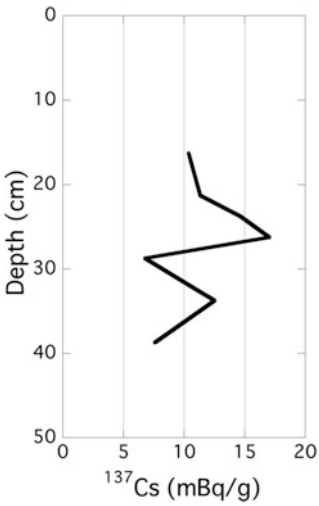

Fig. 12.4 ^{137}Cs activity profile measured for the top part of the ON12C core

12.5.3 Lithology

The lithologic description for all three cores is summarised in Fig. 12.2, together with the analysed water content. Five sedimentary facies were identified for the longest core, ON12C. From the top to the bottom, the identified facies in ON12C (detailed below) are: (I) black soft sediments (0 to ~63 cm), (II) dark olive green sediments (~63 to ~132 cm), (III) darker sediments with weak horizontal structures (~132 to 246 cm), (IV) clearly laminated yellowish layers (246 to 308 cm), and (V) massive brown sediments (308 to 392 cm).

(I) Black soft sediments (0 to ~63 cm): The peak radioactivity from ^{137}Cs was found in this facies. At the depth of ~40 cm, a grey tuff layer with a thickness of 4.6 cm is visible, and characterised by low water content. Weak lamination by intercalation of brown thin layers is visible from 3 cm above this grey tuff layer downward to ~63 cm. Scanned XRF Mn intensity showed fluctuation in this sediment by lamina.

(II) Dark olive green sediments (~63 to ~132 cm): The upper part of this facies is massive sediment with a mottled appearance, and the lower part shows a faint lamina. The boundary with the subjacent weakly laminated facies (III) is not clear.

(III) Darker sediments with weak horizontal lamination (~132 to 246 cm): This facies is characterized by the development of horizontal structures. Laminae consist of dark grey layers of 2 to 5 mm thickness interspersed in a matrix of black sediment. These laminae become faint and eventually disappear in the deeper part of the facies (~215 to 246 cm). A mottled appearance is dominant at depths ~195 to 215 cm.

A grey layer of ~2 cm thickness is clearly visible at the depth of 223 cm, and this layer is characterized by low water content. Beneath this grey layer,

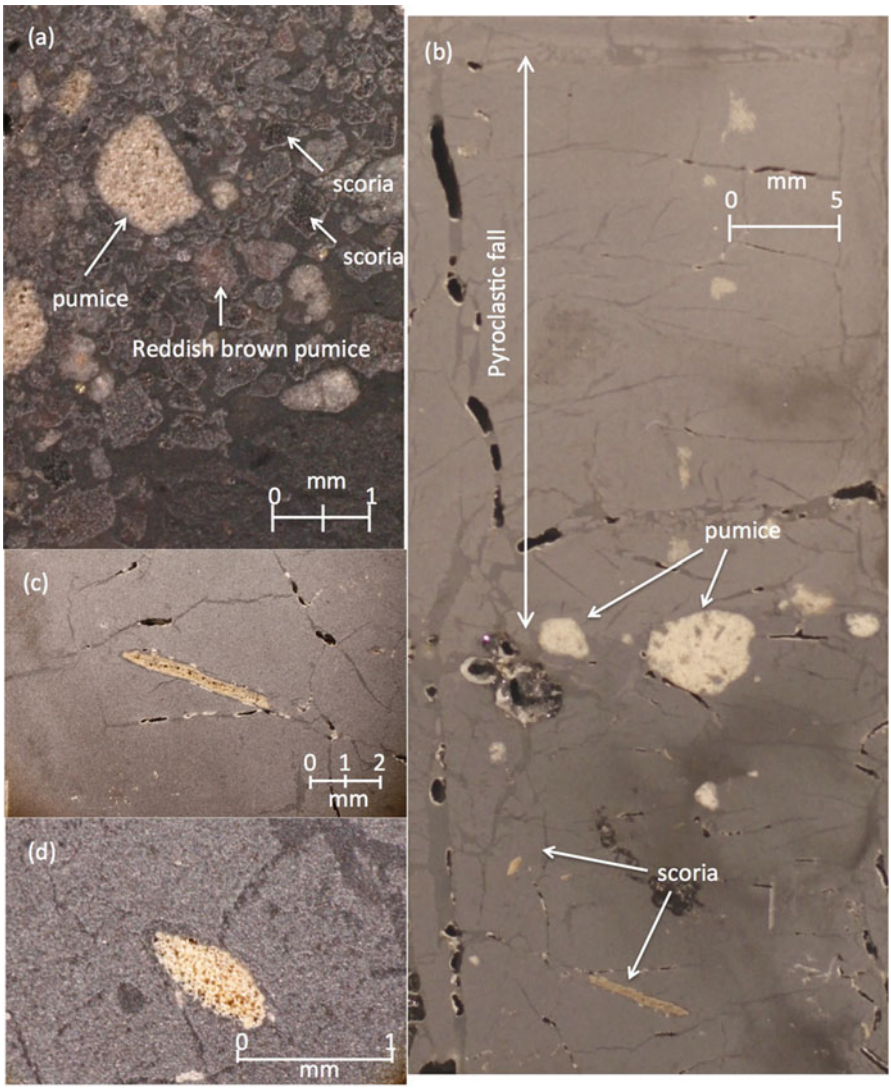

Fig. 12.5 Photographs of volcanic fragments found in core ON12C at the depths of (**a**) ~223 cm (possibly corresponding Ko-c_1 deposited in 1856) and (**b**) ~305 cm (possibly corresponding Ko-c_2 deposit in 1694 or Ko-d in 1640). Both (**c**) and (**d**) are enlarged photos of scoria fragments in photo (**b**); note that photo (**d**) is rotated for presentation

there is a layer < 1-cm thick of pumice, glassy scoria, and pale reddish volcanic fragments with the size of < 1 mm (Fig. 12.5a). A plant fragment was found at the depth of 238 cm, and the measured ^{14}C age for this fragment was 150 ± 20 yrBP (Table 12.3).

(IV) Clearly laminated yellowish layers (246 to 308 cm): This is a distinctive facies with obvious laminae of black, grey, and pale yellow sediment. In the upper part (246 to ~255 cm), black layers are dominant and the boundary with the overlying facies is not clear. The lower part is brighter in colour. The width of each layer varies, but the majority are less than ~5 mm. Black layers are thinner than the other two types (grey and pale yellow layers). Cross cutting structure is visible at the depth of ~280 to ~290 cm. The scanning XRF Mn intensities showed fluctuation in this facies. Near the top of this facies (at the depth of ~246 cm), a thin grey layer, which shows relatively low water content, is found. At the depth of ~280 cm, three very porous pumice pieces with the size of ~2 cm are included.

At the bottom of this facies, a grey layer with a thickness of ~3 cm is found (Fig. 12.5b), characterized by low water content, with many pumice fragments (<4 cm diameter) included in the lower half. Wood and plant fragments collected from this layer (depth 304 cm) yielded ^{14}C ages of about 350 yrBP (Table 12.3) and 400 yrBP. The discrepancy in ^{14}C age could be statistical, or could mean that an older plant was incorporated in the sediment. Glassy scoria (<1-mm diameter) was found ~4 cm above this grey layer. Beneath this grey layer, in sediments of the underlying facies (V), highly vesicular brown scoria (Fig. 12.5 b–d) fragments are found.

(V) Massive brown sediments (308 to 392 cm): Near the middle of this massive facies, at a depth of 345 cm, a greyish ash layer with a thickness of < 2 cm is found. Below this grey layer, blocks of pumice with diameters of a few centimetres to a maximum 6 cm (at the depth of 381 cm) are common. Above this grey layer, pumice fragments become rare and are found mainly at the top of the facies, and from a few horizons. This upper part of the facies contains highly vesicular brown scoria (Fig. 12.5b–d). Plant fragments are found in several horizons; ^{14}C ages from two samples showed concordant ages of ~350 yrBP. Conventional bulk XRF measurement (Table 12.2) indicates that the major element chemistry of this layer is consistent with chemical composition of HKV eruptive rocks.

12.5.4 Correlation of the Three Cores

Two cores, those from the main Lake Onuma (ON12C and ON12D) show similar lithology with correlatable water contents. The third core, ON12A from the western basin (Lake Konuma), did not show particular sedimentary structures except for the bottom brown massive sediment. It is not clear how the core ON12A from Lake Konuma can be correlated to the other cores except for the facies (V) found at the bottom and one layer with low water content that can be correlated to the corresponding horizon of the other two cores. Lake Konuma may be under a different sedimentation system than the main Lake Onuma.

The layer with low water content found just above facies (V) is very thick (∼10 cm) in the ON12D core compared to the ∼3 cm thickness in ON12C. This thickness is probably not representative of the actual *in situ* thickness, as the layer locates at the section boundary in ON12D and may have expanded during the core storage in the laboratory.

Due to the piston coring process, the top parts of these three long cores were not recovered. The length of the lost top part is probably longer for ON12D than for ON12C, because some of the structures found in the top of ON12C (e.g., pyroclastic fall layers and weak lamina found at a depth around 50 cm) are not found in the ON12D core.

12.5.5 Identification of Volcanic Products

Bulk XRF results show that the bulk chemistry of the massive sediment in facies (V) is similar to the volcanic products of the HKV (Katsui et al. 1989). Considering the ^{14}C age measured for the deepest sample from ON12D (340 ± 30 yrBP) and isopach maps of historical volcanic products (Fig. 12.1), the lowermost massive sediment would have been deposited from the volcanic activity in 1640. The grey tuff layer (fine ash) in the middle of facies (V) accompanies with thin pumice-rich part beneath it. This combination is similar to a fine ash layer (Ko-d_1) covering a lower pumice-rich layer (Ko-d_2) described by earlier works in 1970 (Katsui et al. 1989. Note that Katsui et al. 1989, renamed these volcanic units, d1 to d11 from lower to upper.) The fine ash layer is renamed as D5 in Yoshimoto and Ui (1998).

The upper part of facies (V) and overlying grey layer in facies (IV) needs some consideration to correlate to the volcanic activity. This upper layer in facies (V) may also be the product of the 1640 eruption, because there is no distinct sign of non-volcanic sedimentation in facies (V). Katsui et al. (1989) estimated the possible thickness of the 1640 pyroclastic fall in Lake Onuma to be 50–100 cm (Fig. 12.1). The facies (V) and overlying grey layer in core ON12C total about ∼90 cm in thickness; the lower limit of facies (V) is not recovered in the core, and therefore there is a possibility that the potential 1640 eruptive deposit thickness exceeds the estimate. Therefore , this upper part in facies (V) may be the result of secondary sedimentation of on-land volcanic product of 1640 eruption. Only the top part of facies (V) which still preserve scoria (Fig. 12.5b–d) may be related to direct supply of materials from the volcano. The youngest ^{14}C age for the uppermost part of facies (V) is 290 ± 30 (σ) yrBP, which is obtained from the ON12A core (Fig. 12.2 and Table 12.3); the calibrated calendar age covers the 1640 eruption event, yet the age is younger than most of the ^{14}C ages (∼350 yrBP) from facies (V). The volcanic activity in 1640 was so intense that plants had less bloom for a significant duration afterward, meaning that most plant residue in the lower part of the core would record the 1640 event. Assuming such circumstances, the grey layer at the bottom of facies

(IV) may be interpreted as corresponding to 1694 events (Ko-c2). Further detailed observation is needed to conclude whether this tuff layer corresponds to the 1640 or the 1694 volcanic activities.

At the depth of ∼224 cm in core ON12C, a distinct volcanic layer is visible (Fig. 12.5a), consisting of pumice, reddish brown pumice, and scoria. Beneath this layer, a ^{14}C age analysis yielded a result of 150 ± 20 (σ) yrBP, which corresponds to the Ko-c_1 pyroclastic fall of 1856. Between this layer and Ko-c_2 (or Ko-d), a thin ash layer was found at a depth of ∼245 cm with low water content. Volcanic activity in 1765 was recorded in historical literature, but the volcanic products have not been found on land (Katsui et al. 1989). There is a possibility that this layer corresponds to HKV events in 1765. The layer of low water content is found at the depth of ∼130 cm in ON12D and ∼265 cm in ON12C, though no clear tuff layer was visible. This layer may also be corresponding to the sedimentation of volcanic products.

The tuff layer found at a depth of ∼40 cm is below the ^{137}Cs peak (Figs. 12.2 and 12.4). The water content is low, as is found in other pyroclastic fall deposits. This layer is interpreted to correspond to Ko-a, marking volcanic activity in 1929.

12.6 Conclusions

Sedimentary cores recovered from Lake Onuma record pyroclastic fall deposits Ko-a (1929 AD), Ko-c_1 (1856 AD), Ko-d (1640 AD), and possibly Ko-c_2 (1694 AD). Core sample water content is a good indicator of volcanic products. The eruptions in 1795 might be represented in the cores, even though tuffs from these events have not been found on land. When eruptive history of the area has been well studied, these volcanic products become a good time marker. The sedimentation rate in Lake Onuma varies, based on these time markers. Sedimentary structures must reflect environmental changes in the area at the various scales. The geochronological framework proposed here would be helpful to understand the environmental fluctuation and its causation.

Acknowledgements Mr. Sadahito Kubo from JEOL assisted in acquiring measurements using the portable XRF. Mr. Yuichiro Nagamura assisted in ^{137}Cs measurement. The comments by Dr. Mistuhiro Yoshimoto helped improve the manuscript. This research was mainly supported by the Strategic International Research Cooperative Program among Japan, Korea and China (funding bodies: JST, DOIC & NRF). Noriko Hasebe's stay in KIGAM was supported by the KOFST. Carbon-14 dating at KIGAM was supported by the KIGAM project 14-3311-2 (Leader: Se-Song Hong).

References

BDP-98 Members (2001) The new BDP-98 600-m drill core from Lake Baikal: a key late Cenozoic sedimentary section in continental Asia. Quatern Int 80–81:19–36

Ganzawa Y, Kito N, Yanai S, Sadakata N (2005) Discovery of primary tephra layers and research of the early stage of the volcanic history of Hokkaido-Komagatake volcano, Japan. J Geol Soc Jpn 111:581–589

Ichiyama Y, Ishiwatari A, Hirahara Y, Shuto K (2006) Geochemical and isotopic constraints on the genesis of the Permian ferropicritic rocks from the Mino-Tamba belt, SW Japan. Lithos 89:47–65

Itono T, Kashiwaya K, Ochiai S (2015) Reconstructing modern hydro-environmental fluctuations inferred from lacustrine sediment in Lake Onuma, Hokkaido. In: Kashiwaya K, Shen J, Kim JY (eds) Earth surface processes and environmental changes in east Asia. Springer, Dordrecht, pp 269–285

Katsui Y, Suzuki T, Soya T, Yoshihisa Y (1989) Geological map of Hokkaido-Komagatake volcano. Geological Survey of Japan, Tsukuba

Katsuta N, Takano M, Kawakami S, Togami S, Fukusawa H, Kumazawa M, Yasuda Y (2007) Advanced micro-XRF method to separate sedimentary rhythms and event layers in sediments: its application to lacustrine sediment from Lake Suigetsu, Japan. J Paleolimnol 37:259–271

Ochiai S, Nagao S, Itono T, Suzuki T, Kashiwaya K, Yonebayashi K, Okazaki M, Kaeriyama M, Qin YX, Hasegawa T, Yamamoto M (2015) Recent Eutrophication and Environmental Changes in the Catchment Inferred from Geochemical Properties of Lake Onuma Sediments in Japan. In: Kashiwaya K et al (eds) Earth surface processes and environmental changes in East Asia. Springer, Dordrecht, pp 257–268

Reimer PJ, Bard E, Bayliss A, Beck JW, Blackwell PG, Ramsey CB, Buck CE, Cheng H, Edwards RL, Friedrich M, Grootes PM, Guilderson TP, Haflidason H, Hajdas I, Hatté C, Heaton TJ, Hoffmann DL, Hogg AG, Hughen KA, Kaiser KF, Kromer B, Manning SW, Niu M, Reimer RW, Richards DA, Scott EM, Southon JR, Staff RA, Turney CSM, van den Plicht J (2013) IntCal13 and Marine13 radiocarbon age calibration curves 0–50,000 years Cal BP. Radiocarbon 55:1869–1887

Takahashi R, Nakagawa M, Nakaniahi K, Yoshimoto M (2004) The 1942 Eruption of Hokkaido – Komagatake Volcano Was Phreatomagmatic. Jour Volcanological Soc Japan 49:1290142. (in Japanese with English abstract)

Takemura K (1990) Tectonic and climatic record of the Lake Biwa, Japan, region, provided by the sediments deposited since Pliocene times. Palaeogeogr Palaeoclimtol Palaeoecol 78:185–193

Tanaka T (2005) Water pollution factors of land use and river water quality in eutrophicated lake watersheds: Lake Oshima-Oonuma, Hokkaido, Japan. J Hum Environ Symbiosis 11:13–22. (in Japanese with English abstract)

Yoshimoto M, Ui T (1998) The 1640 sector collapse of Hokkaido Komagatake Volcano, Northern Japan. Bull Volcan Soc Jpn 43:137–148. (in Japanese with English abstract)

Yoshimoto M, Takarada S, Takahashi R (2007) Eruptive history of Hokkaido-Komagatake volcano, northern Japan. J Geol Soc Jpn 113(supplement):81–92. (in Japanese)

Yoshimoto M, Miyasaka M, Takahashi R, Nakagawa M, Yoshida K (2008) Reevaluation of the pre-1640 A.D. eruptive history of Hokkaido- Komagatake volcano, northern Japan. J Geol Soc Jpn 114:336–347

Chapter 13
Recent Eutrophication and Environmental Changes in the Catchment Inferred from Geochemical Properties of Lake Onuma Sediments in Japan

Shinya Ochiai, Seiya Nagao, Taeko Itono, Tomoyo Suzuki, Kenji Kashiwaya, Koyo Yonebayashi, Masanori Okazaki, Masahide Kaeriyama, Yu-Xue Qin, Takashi Hasegawa, and Masayoshi Yamamoto

Abstract This study investigated the continuous record of eutrophication in Lake Onuma based on the geochemical properties of two lake sediment cores obtained from the deepest part of the lake in 2011. Based on a tuff layer deposited during the eruption of Mt. Komagatake, and on the correlation between fluctuations in $\delta^{13}C$ and $\delta^{15}N$ values, two sediment cores, ON11-2-2 and ON11-6, were dated to the 1920s and 1890s, respectively. The $\delta^{13}C$ value and C/N ratio for the lake sediments show values within the ranges for planktonic material and river sediment, suggesting

S. Ochiai (✉) • S. Nagao • T. Suzuki • M. Yamamoto
Low Level Radioactivity Laboratory, Institute of Nature and Environmental Technology, Kanazawa University, O 24, Wake, Nomi, Ishikawa 923-1224, Japan
e-mail: sochiai@ies.or.jp

T. Itono
Institute of Nature and Environmental Technology, Kanazawa University, Kakuma, Kanazawa 920-1192, Japan

K. Kashiwaya
Institute of Nature and Environmental Technology, Kanazawa University, Kakuma, Kanazawa 920-1192, Japan

Department of Geography, National Taiwan University, Daan District, Taipei 10617, Taiwan

K. Yonebayashi • M. Okazaki
Faculty of Bioresources and Environmental Sciences, Ishikawa Prefectural University, 1-308, Suematsu, Nonoichi, Ishikawa 921-8836, Japan

M. Kaeriyama • Y.-X. Qin
School of Fisheries Sciences, Hokkaido University, 3-1-1, Minato-cho, Hakodate, Hokkaido 041-8611, Japan

T. Hasegawa
School of Natural System, College of Science and Engineering, Kanazawa University, Kakuma, Kanazawa 920-1192, Japan

K. Kashiwaya et al. (eds.), *Earth Surface Processes and Environmental Changes in East Asia*, DOI 10.1007/978-4-431-55540-7_13

that the lake sediment is a mixture of these sources and that their mixture ratio was almost constant since the 1920s. On the other hand, the $\delta^{15}N$ of two cores show a similar trend with increasing $\delta^{15}N$ from the 1950s–1960s to the present time. It is attributed to the increase in the $\delta^{15}N$ value of planktonic material reflecting anthropogenic nitrogen inflow to the lake.

Keywords Eutrophication • Lake sediment • Organic matter • $\delta^{13}C$ • $\delta^{15}N$

13.1 Introduction

Lakes are important resources for drinking water, irrigation, and hydroelectric power supply. Lake eutrophication is one of the serious environmental pollution problems (e.g., Smith et al. 1999) damaging to these lake water resources. Eutrophication has become a serious environmental problem in various lakes, such as Lake Nansihu, China (Liu et al. 2010), Lake Dianchi, China (Xiong et al. 2010), Myall Lake, Australia (Drew et al. 2008), and is sometimes caused by the inflow of anthropogenic nutrients.

Lake Onuma, a volcanic dammed lake on the southern Hokkaido Island in Japan, faces the progression of eutrophication resulting from water pollution during the past few decades. The chemical oxygen demand (COD), which reflects the concentration of dissolved organic matter, was relatively low (0.54–2.04 mg/L) during the 1930s in lake water (Yoshizumi et al. 1972). However, it increased to 2–4 mg/L in the 1970s (Yoshizumi et al. 1972; Imada et al. 1983) and remained stable at 3–5 mg/L in the 2000s, which is higher than the environmental quality standard for lake water (Hokkaido 2013). If eutrophication continues to progress, it may influence not only water quality but also fishery productivity, lake scenery, and tourism resources at the lake.

The cause of eutrophication in Lake Onuma is postulated to be anthropogenic nutrient inflow. The major nitrogen source may be livestock-derived nitrogen from the rivers (Tanaka 2005). To investigate the mechanism of eutrophication progression and to allow for accurate future predictions, reconstruction of the continuous record of past environmental change in lake-catchment is needed. The geochemical properties, total organic carbon (TOC), total nitrogen (TN), and carbon and nitrogen isotope ratios of lake sediments have been widely used to reconstruct long-term and recent environmental changes (e.g., Meyers and Ishiwatari 1993; Enters et al. 2006). The nitrogen isotope ratio, $\delta^{15}N$, can be used to evaluate eutrophication in rivers, lakes, and coastal areas (e.g., Valiela et al. 2000; Kohzu 2006; Liu et al. 2010). Therefore, this study aims to reveal the detailed continuous record of the progression of eutrophication based on the geochemical properties of Lake Onuma sediments.

13.2 Samples and Methods

Lake Onuma is located in the southern part of Hokkaido Island in Japan (Fig. 13.1). Lake Onuma is a dammed lake formed by the volcanic eruption of Mt. Komagatake in 1640 (Yoshimoto et al. 2007). This lake consists of the eastern basin (Onuma) and the western basin (Konuma) connected by a narrow channel. Water and catchment areas are about 8.9 km^2 and 173 km^2, respectively (Tanaka 2005). Average and maximum depths are 4.7 and 12.9 m. Three major rivers (Shukunobe, Ikusa, and Karima Rivers) flow into the Onuma basin. There was an outflow river in the eastern end of the Onuma basin before 1961. The outlet was closed and a waterway tunnel for a hydroelectric power plant was constructed in the southern part of the Konuma basin in 1961 (Fig. 13.1).

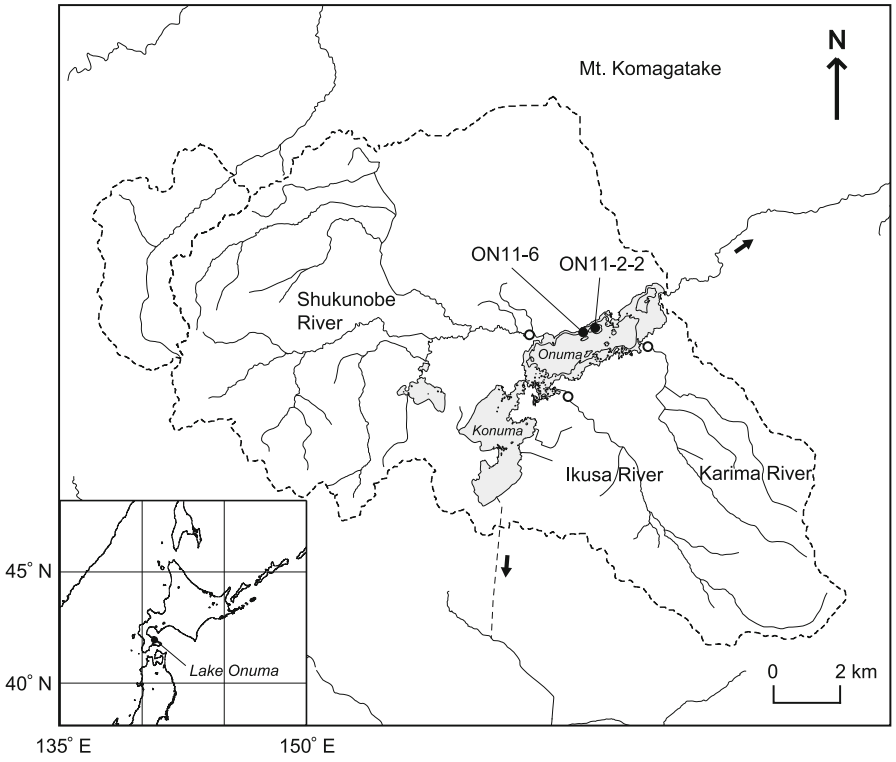

Fig. 13.1 Location and topographic maps of Lake Onuma. The *dashed line* indicates the catchment area of Lake Onuma. *Closed* and *open circles* show the sampling points of lake sediment cores and river sediments, respectively. The numerical map data were based on Fundamental Geospatial Data provided by the Geospatial Information Authority of Japan, and National Land Numerical Information provided by the Ministry of Land, Infrastructure, Transport and Tourism, Japan

Two sediment cores (ON11-2-2, 68 cm; ON11-6, 45 cm) were obtained around the deepest part of the Onuma basin with a gravity core sampler (Satake-type, RIGO, Japan) on September 20, 2011 (closed circles in Fig. 13.1). These sediment cores were sliced into 1-cm-interval subsamples. Planktonic material and lake water samples were collected from the sampling point of ON11-2-2 on June 5 and 6, 2012. Riverbed sediment and water samples were also collected at the main river mouths on June 6, 2012 (opened circles in Fig. 13.1). Water samples were filtered using a glass fiver filter for the dissolved organic carbon (DOC) and dissolved nitrogen (DN) measurements.

Freeze-dried sediment samples were grounded and treated with 1 M HCl to remove inorganic carbon for analyses of total organic carbon (TOC), total nitrogen (TN), and stable carbon and nitrogen isotope ratios. TOC and TN contents were measured with the elemental analyzer (2400 Series II, PerkinElmer, USA). The precision of TOC and TN analyses were ±0.009 % and ±0.003 %, respectively. The stable carbon and nitrogen isotope ratios were analyzed with three types of mass spectrometers (IsoPrime EA, GV Instruments, UK; DLTAplus and DELTA V Advantage, Thermo Fisher Scientific Inc., USA). Stable carbon and nitrogen isotope ratios are shown as $\delta^{13}C$ values relative to VPDB and $\delta^{15}N$ values relative to atmospheric N_2 as follows:

$$\delta^{13}C, \delta^{15}N = \left(R_{sample}/R_{standard} - 1\right) \times 1,000 \tag{13.1}$$

where R_{sample} and $R_{standard}$ are the $^{13}C/^{12}C$ or $^{15}N/^{14}N$ atomic ratios of the sample and international standard, respectively. The reference materials USGS40 ($\delta^{13}C_{VPDB} = -26.39$, $\delta^{15}N_{air} = -4.52$), L-Alanine ($\delta^{13}C_{VPDB} = -19.6$, $\delta^{15}N_{air} = 1.6$), ANU-sucrose ($\delta^{13}C_{VPDB} = -10.80$), IAEA-N1 ($\delta^{15}N_{air} = 0.4$), and IAEA-N2 ($\delta^{15}N_{air} = 20.3$) were used to calibrate the measurements. The precision of the $\delta^{13}C$ and $\delta^{15}N$ analyses were ±0.18 ‰ and ±0.31 ‰, respectively. The dissolved organic carbon (DOC) and dissolved nitrogen (DN) concentrations of lake and river water samples were analyzed with a TOC analyzer (TOC-V_{SCN}, Shimadzu, Japan).

The ^{210}Pb and ^{137}Cs concentrations were measured to estimate the age of the cores. The powdered samples were sealed into plastic bags (5.0 × 3.5 cm). After establishing the radioactive equilibrium between ^{222}Rn and ^{214}Pb (about 1 month), the activity concentration of ^{210}Pb (46.5 keV), ^{214}Pb (352 keV), and ^{137}Cs (661.6 keV) were determined by gamma-ray spectrometry using a Ge detector (LO-AX-51370-20, ORTEC, USA). The activity of excess ^{210}Pb ($^{210}Pb_{ex}$) was estimated by subtracting the activity of ^{214}Pb from that of ^{210}Pb.

The numerical map data were based on Fundamental Geospatial Data provided by the Geospatial Information Authority of Japan, and National Land Numerical Information provided by the Ministry of Land, Infrastructure, Transport and Tourism, Japan.

13.3 Results

13.3.1 Chemical Properties of Lake Sediments and Lake Water Samples

Figure 13.2a–d show the vertical changes in TOC and TN contents, C/N atomic ratio, $\delta^{13}C$ and $\delta^{15}N$ values of ON11-2-2. The C/N ratios, $\delta^{13}C$ and $\delta^{15}N$ values of the sediment samples represent the TOC/TN ratio, $\delta^{13}C$ value of organic matter, and $\delta^{15}N$ value of total nitrogen in the following discussion. The TOC and TN contents of sediment decrease with depth from 9 % to 3 %, and from 0.9 % to 0.4 %, respectively. The C/N ratio of sediment ranges from 9 to 11 and this range corresponds to the value of algae (Meyers 1994), suggesting that the sediment of Lake Onuma is largely influenced by autochthonous organic matter. The $\delta^{13}C$ value exhibits a relatively small variation around $-38‰$. On the other hand, the $\delta^{15}N$ value continuously increases upward through the core, from 2 to 7 ‰.

Figure 13.2e, f show the vertical changes in $\delta^{13}C$ and $\delta^{15}N$ values through ON11-6. The $\delta^{13}C$ and $\delta^{15}N$ values of the upper 30 cm show a similar trend to that of ON11-2-2, with $\delta^{15}N$ values increasing upward through the core. This result suggests that the bottom of ON11-2-2 corresponds to the ~30-cm-deep layer of ON11-6. On the other hand, the lower 30 cm section exhibits a different trend. The $\delta^{13}C$ and $\delta^{15}N$ values synchronously decrease upward through the core.

Table 13.1 shows the C/N ratio, $\delta^{13}C$ and $\delta^{15}N$ values of planktonic material and river sediment. The $\delta^{13}C$ and $\delta^{15}N$ values of river sediment range from −26.3 to −28.3 and from 3.1 to 3.9, respectively, which represent the organic matter from the catchment. On the other hand, the $\delta^{15}N$ value of planktonic material in Lake

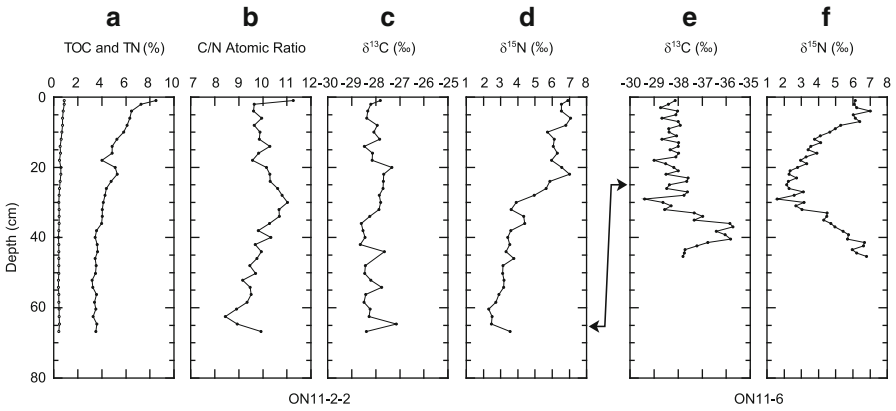

Fig. 13.2 Vertical changes in (**a**) TOC and TN contents, (**b**) C/N atomic ratio, (**c**) carbon isotope ratio $\delta^{13}C$, (**d**) nitrogen isotope ratio $\delta^{15}N$ for the ON11-2-2 core. Vertical changes in (**e**) carbon isotope ratio $\delta^{13}C$, and (**f**) nitrogen isotope ratio $\delta^{15}N$ for the ON11-6 core

Table 13.1 C/N ratio, $\delta^{13}C$, and $\delta^{15}N$ of planktonic material and river sediment

Sample	C/N atomic ratio	$\delta^{13}C$ (‰)	$\delta^{15}N$ (‰)	DOC (mgC/L)	DN (mgN/L)
ON11-2-2					
Plankton	6.12	−31.72	7.53		
Lake water				1.0240	0.4435
Ikusa River					
Sediment	11.48	−26.32	3.85		
River water				1.6780	0.6720
Karima River					
Sediment	15.35	−26.40	3.28		
River water				0.8875	1.4070
Shukunobe River					
Sediment	13.58	−28.27	3.09		
River water				1.1835	0.6270

Onuma is higher (7.5‰) than that of river sediment. The $\delta^{13}C$ and $\delta^{15}N$ values of the lake sediments are within the range for planktonic material and river sediment, suggesting that the sediment is a mixture of these sources. The DOC concentrations of river and lake water exhibit the same range (0.8875–1.6780 mgC/L). The DN concentration of river water ranges between 0.6720 and 1.4070 mgN/L, and is higher than that of lake water (0.4435 mgN/L), suggesting that the river is one of the major sources of dissolved nitrogen in Lake Onuma.

13.3.2 Age of the Sediment Cores

Figure 13.3 shows the vertical changes in water content of ON11-2-2 and ON11-6. Water content of the ON11-6 core was analyzed by Itono et al. (2015, this volume). A layer with low water content, corresponding to the tuff layer, is observed at a depth of 28–30 cm in ON11-6. This tuff layer can be correlated to the 1929 volcanic deposit (Ko-a) of Mt. Komagatake (Yoshimoto et al. 2007). On the other hand, the tuff layer could not be found in ON11-2-2, based on water content fluctuation and observation, implying that the bottom of the core is younger than 1929.

The age of the cores were also estimated based on the ^{210}Pb (Krishnaswamy et al. 1971; Appleby and Oldfield 1978) and ^{137}Cs methods (Ritchie and McHenry 1990). Figure 13.4a, b indicate the vertical changes in the activity concentrations of $^{210}Pb_{ex}$ and ^{137}Cs for ON11-2-2 and ON11-6, shown as a function of mass depth. The regression curves show the fitting results of the constant initial concentration (CIC) model (Pennington et al. 1973; Appleby and Oldfield 1983) as a first estimation.

The sedimentation rate of ON11-2-2 was estimated at 0.0924 g/cm^2/year. Based on this sedimentation rate, the bottom of ON11-2-2 was dated to 1908. However, this result does not correspond to the ages of the tuff layer and to those estimated using the ^{137}Cs method. The ^{137}Cs fluctuation first appears and peaks at 30 cm

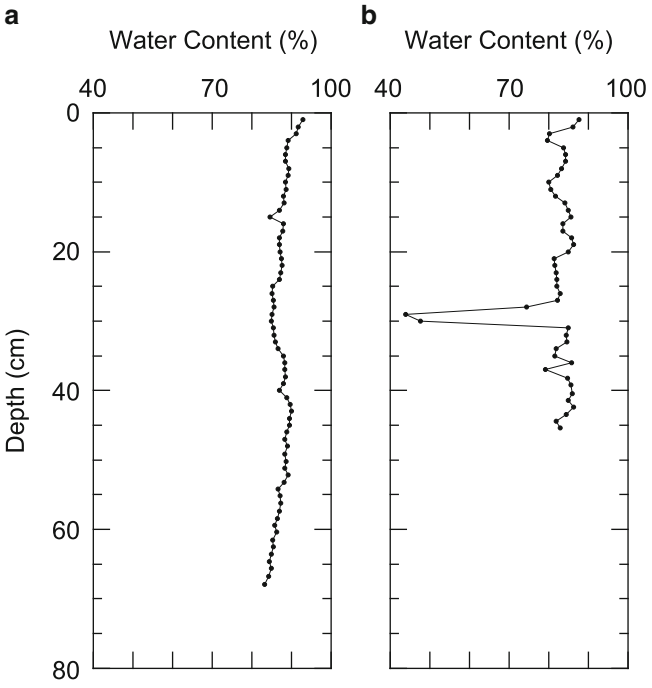

Fig. 13.3 Vertical changes in water content for the (**a**) ON11-2-2 and (**b**) ON11-6 cores

(4.1 g/cm^2) and 26 cm (3.4 g/cm^2), corresponding to the beginning of the ^{137}Cs global fallout in 1954 (Ritchie and McHenry 1990), and to the fallout peak of ^{137}Cs in 1963 in Japan (Katsuragi 1983; Katsuragi and Aoyama 1986; Igarashi et al. 1996). However, the ^{210}Pb ages for these depths are younger than those of ^{137}Cs (1963 and 1974, respectively). These discrepancies may result from artificial disturbance of sediment layer and/or dilution effect of $^{210}Pb_{ex}$ by biogenic silica. Fishery operations (smelt fishing using dragnets) were performed around the deepest area of the lake every year (Onuma Fisheries Cooperative Association, personal communication), possibly disturbing the surface sediment layer and causing the mismatches between tuff layer, ^{137}Cs and ^{210}Pb ages. Additionally, the dilution of catchment-derived $^{210}Pb_{ex}$ by autochthonous materials such as biogenic silica may affect the ^{210}Pb age. Mineral content from the catchment of the ON11-2-1 core, which was obtained at the same location as ON11-2-2, exhibit a significant variation from 20 to 60 % (Itono et al. 2015, this volume), reflecting the change in biogenic silica content. Therefore, the CIC model, assuming a constant initial $^{210}Pb_{ex}$ concentration on the sediment surface, may be influenced by a change in biogenic silica productivity. Because of this problem, the ^{210}Pb dating result was not used to establish the age model of the core.

For ON11-6, the sedimentation rate was estimated at 0.0782 g/cm^2/year. The age of the middle section of the tuff layer (29 cm deep) was estimated to 1926.

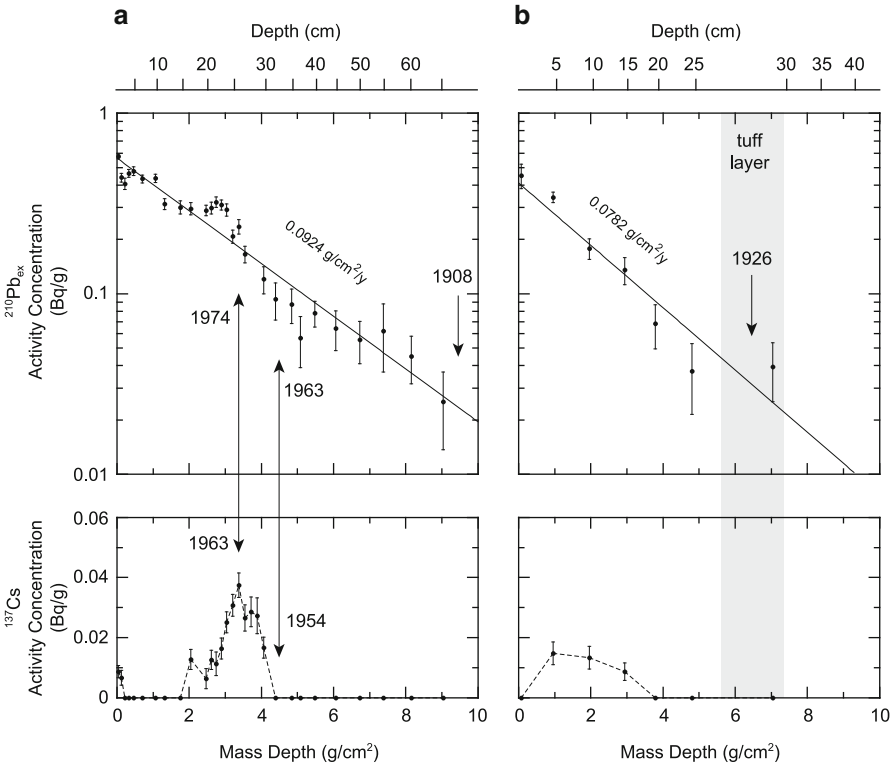

Fig. 13.4 Vertical changes in activity concentrations of excess $^{210}Pb_{ex}$ and ^{137}Cs for the (**a**) ON11-2-2 and (**b**) ON11-6 cores

This result supports the hypothesis that the tuff layer in ON11-6 corresponds to Ko-a deposit and that the disturbance by fishery operation and the dilution effect of autochthonous materials are negligible in this point. Assuming that the sedimentation rate of the section below the tuff layer is similar as that of the upper layer, the bottom of ON11-6 was dated to the 1890s.

The correlation between fluctuations in $\delta^{13}C$ and $\delta^{15}N$ values of ON11-2-2 and ON11-6 suggest that the bottom of ON11-2-2 can be correlated to the section just above the tuff layer (about 25 cm deep) of ON11-6. The bottom of ON11-2-2 was dated to the 1920s.

13.4 Discussion

Figure 13.5a shows the $\delta^{13}C$–C/N plot of lake sediment of ON11-2-2 and expected organic matter sources (autochthonous planktonic material and river sediment from catchment) in Lake Onuma. The values for the lake sediments are within the range for planktonic material and river sediment, suggesting that the organic matter

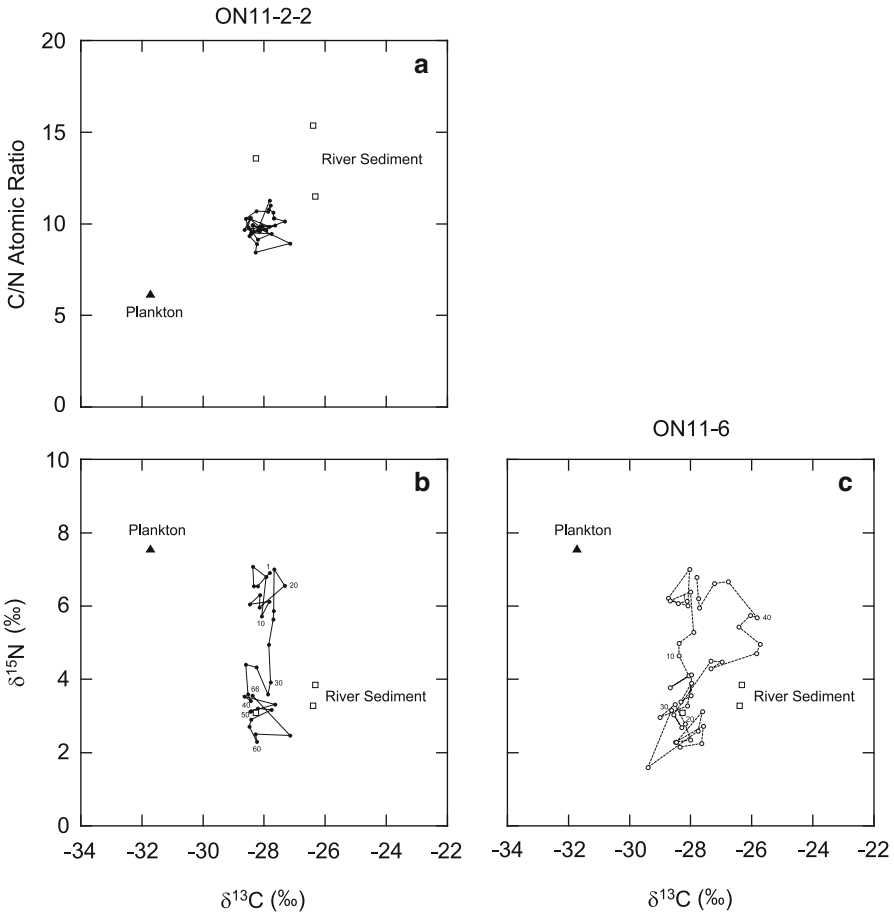

Fig. 13.5 (**a**) $\delta^{13}C$–C/N ratio and (**b**) $\delta^{13}C$– $\delta^{15}N$ plots of ON11-2-2 sediment, planktonic material, and river sediment. (**c**) The $\delta^{13}C$– $\delta^{15}N$ plots of ON11-6 sediment. *Circles* indicate sediment samples. *Triangle* and *square* indicate planktonic material and river sediment, respectively

contained within the lake sediment is a mixture of these organic matter sources, and that their mixture ratio has been almost constant since the 1920s.

On the other hand, the $\delta^{15}N$ value of the sediment has increased, although the organic sources are almost constant (Fig. 13.5b, c). Additionally, the $\delta^{15}N$ value of planktonic material is higher than that of river sediment. These results indicate that the increase of the sediment $\delta^{15}N$ value is attributed to the increase of the $\delta^{15}N$ value of plankton. Because the $\delta^{15}N$ value of phytoplankton is mainly determined by the isotopic composition of inorganic nutrients (e.g., Fogel et al. 1992), the $\delta^{15}N$ value of plankton reflects that of dissolved inorganic nitrogen (DIN) in the lake.

The $\delta^{15}N$ value of DIN derived from livestock and sewage water is larger than that of natural sources such as precipitation (Heaton 1986; Fogg et al. 1998).

It has been reported that the $\delta^{15}N$ value of organic matter becomes larger in watersheds with significant anthropogenic nitrogen loading (e.g., Valiela et al. 2000; Carmichael et al. 2004). Therefore, increasing anthropogenic nitrogen inflow has promoted the eutrophication of Lake Onuma and its influence has been recorded in the $\delta^{15}N$ fluctuation of the lake sediment. The dissolved nitrogen concentration of river water is higher than that of lake water (Table 13.1). These results also support the hypothesis that nitrogen loading from the river is the primary cause of eutrophication. The major nitrogen source may be the livestock-derived nitrogen, which is estimated at 50 % of nitrogen discharge from the main three rivers in 2000 (Tanaka 2005). The sediment records indicate that the contribution of livestock waste water to the lake has rapidly increased since the 1950s–1960s, and its influence still continues in present time.

In the section below the tuff layer in ON11-6 (Figs. 13.2e, f and 13.5c), $\delta^{15}N$ and $\delta^{13}C$ values synchronously increased downward through the core. This variation seems to differ from that of the post-tuff section where only the $\delta^{15}N$ value changed. This change in the isotopic composition of the sediment may be attributed to the shift of organic matter source and/or post-deposition diagenesis. Volcanic eruption and wildfire cause the clearance and the shift in the composition of vegetation in the catchment. Catchment vegetation disturbance affects the transport of soil and particulate organic matter (Beschta 1978; Bormann et al. 1974; Miller 1984), and their influences are recorded in the $\delta^{13}C$ and $\delta^{15}N$ values of the lake sediments (Lane et al. 2004; Routh et al. 2007). The post-deposition diagenesis also changes the isotopic composition of the sediment. The synchronous increase in $\delta^{15}N$ and $\delta^{13}C$ values can be interpreted as the result of diagenesis effect. Longer sediment record may provide more detailed information on vegetation changes and/or geochemical conditions in the lake.

13.5 Conclusions

This study aims to reconstruct the continuous record of lake-catchment environmental changes to evaluate the progression of eutrophication in Lake Onuma. The study of the sediment record of lake sediment geochemical properties leads to the following conclusions.

The ages estimated with the ^{210}Pb method does not correspond to the ages of the tuff layer and ^{137}Cs fallout peak in the ON11-2-2 core. These results may be attributed to the artificial disturbance of the sediment layer and/or to the dilution effect of $^{210}Pb_{ex}$ by biogenic silica. ON11-6 exhibits a tuff layer corresponding to the 1929 volcanic eruption. Correlation between fluctuations in $\delta^{13}C$ and $\delta^{15}N$ values of the ON11-2-2 and ON11-6 cores suggest that the bottom of ON11-2-2 is dated to the 1920s.

The $\delta^{13}C$ value and C/N ratio for lake sediments are within the ranges indicative of planktonic material and river sediment, suggesting that organic matter of lake

sediment is a mixture of these sources and that their mixture ratio has been almost constant since the 1920s. The $\delta^{15}N$ values of two cores show a similar trend of increasing $\delta^{15}N$ values since the 1950s–1960s. It indicates that the contribution of livestock waste water to the lake has rapidly increased since the 1950s–1960s, and that its influence continues in present time. In the section below the tuff layer, $\delta^{15}N$ and $\delta^{13}C$ values synchronously increased downward through the core. This fluctuation may be attributed to the shift of organic matter sources and/or to post-deposition diagenesis.

Acknowledgments We would like to thank Prof. K. Tanaka, Prof. Y. Ganzawa at Hokkaido University of Education, Prof. I. Imai at Hokkaido University, and the Onuma Fisheries Cooperative Association for their support in obtaining samples. We also thank Dr. T. Murakami, Dr. S. Nishimura, and Ms. Y. Kawano in the Low Level Radioactivity Laboratory at Kanazawa University, as well as Dr. A. Goto, Dr. T. Nemoto, Dr. K. Fukushi, and Dr. N. Hasebe at Kanazawa University for their support of this study.

References

Appleby PG, Oldfield F (1978) The calculation of lead-210 dates assuming a constant rate of supply of unsupported ^{210}Pb to the sediment. Catena 5:1–8

Appleby PG, Oldfield F (1983) The assessment of ^{210}Pb data from sites with varying sediment accumulation rates. Hydrobiologia 103:29–35

Beschta RL (1978) Long-term patterns of sediment production following road construction and logging in the Oregon Coast Range. Water Resour Res 14:1011–1016

Bormann FH, Likens GE, Siccama TG, Pierce RS, Eaton JS (1974) The export of nutrients and recovery of stable conditions following deforestation at Hubbard Brook. Ecol Monogr 44:255–277

Carmichael RH, Annett B, Valiela I (2004) Nitrogen loading to Pleasant Bay, Cape Cod: application of models and stable isotopes to detect incipient nutrient enrichment of estuaries. Mar Pollut Bull 48:137–143

Drew S, Flett I, Wilson J, Heijnis H, Skilbeck CG (2008) The trophic history of Myall Lakes, New South Wales, Australia: interpretations using $\delta^{13}C$ and $\delta^{15}N$ of the sedimentary record. Hydrobiologia 608:35–47

Enters D, Lücke A, Zolitschka B (2006) Effects of land-use change on deposition and composition of organic matter in Frickenhauser See, northern Bavaria, Germany. Sci Total Environ 369:178–187

Fogel ML, Cifuentes LA, Velinsky DJ, Sharp JH (1992) Relationship of carbon availability in estuarine phytoplankton to isotopic composition. Mar Ecol Prog Ser 82:291–300

Fogg GE, Rolston DE, Decker DL, Louie DT, Grismer ME (1998) Spatial variation in nitrogen isotope values beneath nitrate contamination sources. Ground Water 36:418–426

Heaton THE (1986) Isotopic studies of nitrogen pollution in the hydrosphere and atmosphere: a review. Chem Geol 59:87–102

Hokkaido (2013) Water quality of public water bodies in 2012 (in Japanese). Hokkaido, Sapporo

Igarashi Y, Otsuji-Hattori M, Hirose K (1996) Recent deposition of ^{90}Sr and ^{137}Cs observed in Tsukuba. J Environ Radioact 31:157–169

Imada K, Ito T, Yoshizumi K, Awakura T (1983) Transparency, COD and several dissolved ions of Lake Onuma in 1974 to 1980 (in Japanese). Rep Hokkaido Fish Hatchery 38:57–74

Itono K, Kashiwaya K, Ochiai S (2015) Reconstructing modern hydro-environmental fluctuations inferred from lacustrine sediment in Lake Onuma, Hokkaido. In: Kashiwaya K, Shen J, Kim JY (eds) Earth surface processes and environmental changes in east Asia. Springer, Dordrecht, pp 269–285

Katsuragi Y (1983) A study of ^{90}Sr fallout in Japan. Pap Meteorol Geophys 33:277–291

Katsuragi Y, Aoyama M (1986) Seasonal variation of Sr-90 fallout in Japan through the end of 1983. Pap Meteorol Geophys 37:15–36

Kohzu A (2006) Estimation of river eutrophication by using nitrogen isotope ratios (in Japanese). J Jpn Soc Hydrol Water Resour 19:413–419

Krishnaswamy S, Lal D, Martin JM, Meybeck M (1971) Geochronology of lake sediments. Earth Planet Sci Lett 11:407–414

Lane CS, Horn SP, Mora CI (2004) Stable carbon isotope ratios in lake and swamp sediments as a proxy for prehistoric forest clearance and crop cultivation in the Neotropics. J Paleolimnol 32:375–381

Liu E, Shen J, Zhang E, Wu Y, Yang L (2010) A geochemical record of recent anthropogenic nutrient loading and enhanced productivity in Lake Nansihu, China. J Paleolimnol 44:15–24

Meyers PA (1994) Preservation of elemental and isotopic source identification of sedimentary organic matter. Chem Geol 114:289–302

Meyers PA, Ishiwatari R (1993) Lacustrine organic geochemistry - an overview of indicators of organic matter sources and diagenesis in lake sediments. Org Geochem 20:867–900

Miller EL (1984) Sediment yield and storm flow response to clear-cut harvest and site preparation in the Ouachita Mountains. Water Resour Res 20:471–475

Pennington W, Cambray RS, Fisher EM (1973) Observations on lake sediments using fallout ^{137}Cs as a tracer. Nature 242:324–326

Ritchie JC, McHenry JR (1990) Application of radioactive fallout cesium-137 for measuring soil-erosion and sediment accumulation rates and patterns – a review. J Environ Qual 19:215–233

Routh J, Meyers PA, Hjorth T, Baskaran M, Hallberg R (2007) Sedimentary geochemical record of recent environmental changes around Lake Middle Marviken, Sweden. J Paleolimnol 37:529–545

Smith VH, Tilman GD, Nekola JC (1999) Eutrophication: impacts of excess nutrient inputs on freshwater, marine, and terrestrial ecosystems. Environ Pollut 100:179–196

Tanaka T (2005) Water pollution factors of land use and river water quality in eutrophicated lake watersheds: Lake Oshima-Onuma, Hokkaido, Japan (in Japanese). JAHES 11:13–22

Valiela I, Geist M, McClelland J, Tomasky G (2000) Nitrogen loading from watersheds to estuaries: verification of the Waquoit Bay Nitrogen Loading Model. Biogeochemistry 49:277–293

Xiong Y, Wu F, Fang J, Wang L, Yun L, Liao H (2010) Organic geochemical record of environmental changes in Lake Dianchi, China. J Paleolimnol 44:217–231

Yoshimoto M, Takarada S, Takahashi R (2007) Eruptive history of the Hokkaido-Komagatake volcano, northern Japan (in Japanese). J Geol Soc Jpn 113:81–92

Yoshizumi K, Atoda M, Ito T, Yonekawa T (1972) The recent states of the water quality on Lakes Onuma, Konuma and Junsainuma (in Japanese). Rep Hokkaido Fish Hatchery 27:43–58

Chapter 14
Reconstructing Modern Hydro-Environmental Fluctuations Inferred from Lacustrine Sediment in Lake Onuma, Hokkaido

Taeko Itono, Kenji Kashiwaya, and Shinya Ochiai

Abstract Surface core sediments obtained from Lake Onuma, Hokkaido, were used to reconstruct hydro-environmental changes during the past 100 years. The physical properties of lacustrine sediments record both physical environmental and artificial changes in the lake-catchment system.

Fluctuations in the mineral content and density of the core sediment indicate an increase of sediment discharge from 1950 to 1970. This may be related to land transformations such as land reclamation for agricultural use and the construction of resort areas in the catchment. The relationship between observed river discharge and precipitation near the Lake Onuma system is different in summer and winter. This indicates that the earth-surface processes in snowfall areas are different for the summer period (rainfall) and winter period (snow accumulation/snowmelt).

Keywords Lacustrine sediment • Earth-surface process • Lake-catchment system • Snowfall area • Artificial change

14.1 Introduction

Lacustrine sediments include information both on high-resolution regional changes and long global hydro-environmental ones. Therefore, they can be used for reconstructing past hydro-environmental changes and/or considering earth-surface processes (erosion, transportation and sedimentation) in lake-catchment systems. Changes in hydrological conditions in the systems are also recorded in the sediments. Modern hydrological conditions have been mainly observed with

T. Itono (✉) • S. Ochiai
Institute of Nature and Environmental Technology, Kanazawa University, Kakuma, Kanazawa 920-1192, Japan
e-mail: taeko.itono@staff.kanazawa-u.ac.jp

K. Kashiwaya
Institute of Nature and Environmental Technology, Kanazawa University, Kakuma, Kanazawa 920-1192, Japan

Department of Geography, National Taiwan University, Daan District, Taipei 10617, Taiwan

K. Kashiwaya et al. (eds.), *Earth Surface Processes and Environmental Changes in East Asia*, DOI 10.1007/978-4-431-55540-7_14

instrumental methods in many meteorological observatories established in various areas. However, data in pre-instrumental observation must be inferred using proxy ones. Physical property of lacustrine sediment is one of most convenient proxies for reconstructing past hydrological conditions at various time and space scales. Many tectonic, climatic and anthropogenic activities on the earth surface have been also recorded in the lacustrine sediments through hydrological processes in lake-catchment systems (Kashiwaya et al. 2012). Then, the sediments can be used to reconstruct environmental changes in areas without direct observational data as well as in past. Several such studies, in which physical properties of sediments such as grain size, density, etc. are used for proxies of physical environmental factors (hydrological factor, hydro-geomorphological factor, climatic factor, etc.), have already been conducted. In Lake Biwa, Japan, for example, mineral grain size and grain density are used for reconstructing past disastrous flood and typhoon (Itono et al. 2012). Mineral grain size in Lake Yogo sediments also provided a good indicator of precipitation (Shimada et al. 2002). In the study of a reservoir, Jinheung Pond in Korea, several peaks in grain-size fluctuation of pond sediments corresponded to peaks in precipitation detected by an instrumental observation (Nahm et al. 2010). Grain size is often used for hydro-meteorological factors, while combinations of physical properties can also be used for hydro-geomorphological factors as shown in the case of Lake Biwa (Itono et al. 2012).

In this chapter, we will discuss comparatively short-term environmental changes, considering hydro-geomorphological processes in the lake-catchment system of Lake Onuma (Hokkaido, northern Japan), where instrumental observation data are limited, in relation to volcanic, climatic and anthropogenic activities.

14.2 Area Studied and Core Sampling

Lake Onuma, located in the south of Hokkaido-Komagatake Volcano (hereafter HKV) (Fig. 14.1a), is a dammed lake formed by a volcanic-debris avalanche during the eruption of HKV in AD 1640 (Kurumisaka debris-avalanche: Yoshimoto et al. 2007). In the historical period, four Plinian eruptions of HKV (Ko-d, Ko-c2, Ko-c1 and Ko-a) have occurred—in AD 1640, 1694, 1856 and 1929, respectively (Yoshimoto et al. 2007).

Lake Onuma consists of two basins, the eastern basin (Onuma basin) and the western basin (Konuma basin) (Fig. 14.1c). The water area for the two basins is 5.12 km^2 and 3.80 km^2, and the average water depth for the two basins is 6.4 m and 2.3 m, respectively; the average for the whole of the two basins is 4.7 m. The maximum water depth is 13.6 m, in Onuma basin. The average residence time is 2.9 months. The catchment area of Lake Onuma is 173 km^2 (Tanaka 2005), which includes a small part of the Himekawa catchment because of the construction of an artificial flume (Fig. 14.1a, dashed line). There are three inflow rivers—the Shukunobe, the Ikusa, and the Karima—and one outflow river, the Orito. An artificial channel was constructed south of Konuma basin in 1961 for an electric power plant and irrigation. After that, outflow via the Orito was blocked by the sluice gate.

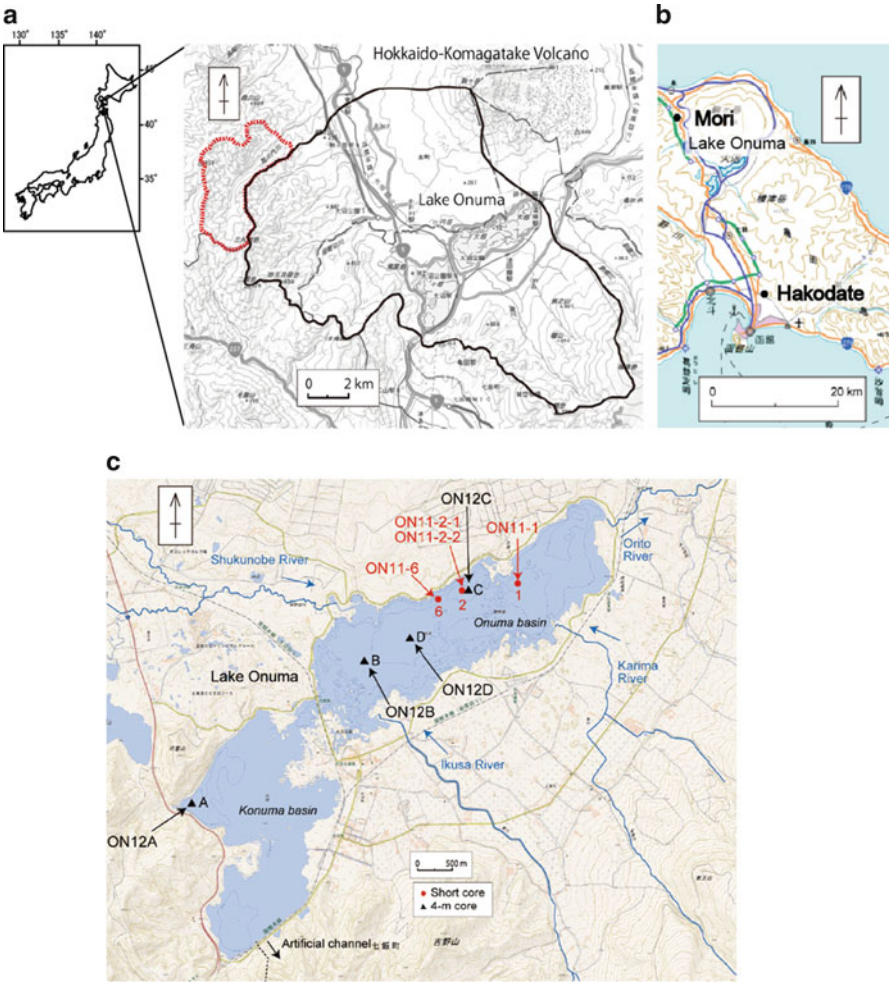

Fig. 14.1 Index map of Lake Onuma. (**a**) Catchment of Lake Onuma. Initial catchment area (*solid line*) and enlarged catchment area in 1978 (*red*, *dashed line*), (**b**) map of meteorological observatories around the catchment and (**c**) sampling points in Lake Onuma; short sediment cores (*closed circle*) and 4-m sediment cores (*closed triangle*). These maps are modified after GSI Maps (Geospatial Information Authority of Japan)

To obtain comparatively short-term environmental information, several short sediment cores were taken in Lake Onuma (Fig. 14.1c) with boats from the Fisheries Cooperative Association of Lake Onuma on September 20 in 2011 (Table 14.1). Sampling point 2 (core numbers ON11-2-1 and ON11-2-2) is the deepest point of the lake. Two other sampling points (1 and 6) (core number: ON11-1 and ON11-6) were also found useful to discuss hydro-environmental changes in the lake-catchment system. A gravity core sampler (1-m) with a polyvinyl chloride tube (a diameter of 5.2 cm) was used for the short-core sampling (ON11-2-1, ON11-2-2,

Table 14.1 Information of sediment cores obtained from Lake Onuma

Core number	Latitude	Longitude	Depth (m)	Point	Length (cm)	Slicing interval (cm)
ON11-1	N42°00′12″.0	E140°42′04″.5	6.4	1	72	1.0
ON11-2-1	N42°00′09″.4	E140°41′28″.7	11	2	96	1.0
ON11-2-2	N42°00′09″.4	E140°41′28″.7	11	2	68	1.0
ON11-6	N42°00′05″.3	E140°41′13″.7	8.3	6	45	1.0

ON11-1 and ON11-6). The modern catchment environmental changes in this lake have also been discussed with some of the same surface core samples from the viewpoint of chemical analysis (Ochiai et al. 2015, this volume).

In 2012, a piston core sampler (maximum 4 m in length) with an 8.3-cm-diameter polyvinyl chloride pipe was used for the long-core sampling. Three 4-m cores (ON12B, ON12C and ON12D) from the Onuma basin (B, C and D in Fig. 14.1c) and one 4-m core (ON12A) from the Konuma basin (A in Fig. 14.1c) were obtained for comparatively long-term examination (Hasebe et al. 2015, this volume); the core sample ON12C represented the deepest point in the basin. In addition, a gravity core sampler (1-m) was used to obtain short-core samples because the top parts of long cores are often lost when using the piston core sampler.

14.3 Analytical Items and Method

Core sediments were prepared by slicing at 1.0-cm intervals for various analyses. We analyzed mineral content, biogenic silica content, grain density, mineral grain size and radioactive concentrations of Cs-137 and excess Pb-210 (hereafter Pb-210ex). Mineral content in this paper is equivalent to the component that remains after the removal of organic content, HCl-solvable content and biogenic silica content from a sample.

The mineral content and biogenic silica content were determined by the method of Mortolock and Froelich (1989). The mineral grain size was determined using a laser diffraction particle size analyzer (SHIMADZU SALD-2000J). The density was measured with an auto-pycnometer using helium gas (Micrometerics Accypic 1330).

The radioactive concentrations of Cs-137 and Pb-210ex in ON11-1 were measured with high-performance Germanium semiconductor detectors (GEM-25-P4; ORTEC) and low-energy Germanium detectors (LO-AX-51370; ORTEC) at the Radioisotope Laboratory for Natural Science and Technology, Kanazawa University. The analytical program used here was PKview, developed by the Radiochemistry Laboratory, Kanazawa University. The radioactive concentration of ON11-2-2 and ON11-6 were measured at the Low Level Radioactivity Laboratory, Kanazawa University.

14.4 Hydrological Data Around the System

Physical properties of lacustrine sediments reflect hydrological conditions in the lake-catchment system as shown above (precipitation in the catchment, river discharge, water level change, etc.).

Data on precipitation around Lake Onuma system was obtained from two meteorological observatories located at Mori and Hakodate (Fig. 14.1b). Precipitation has been measured much longer at Hakodate Marine Observatory (ca. 140 years) than at the Mori Observatory (ca. 70 years). The data from Mori are mainly used for the discussion, which are supported by the data at Hakodate. The average monthly precipitations for Mori and Hakodate are shown Fig. 14.2a. The annual precipitation values for Mori and Hakodate are shown in Fig. 14.2c. There is a good relationship between annual precipitation in Mori and Hakodate during 1981–2010 as shown by the correlation coefficient ($R = 0.83$) (Fig. 14.2b). This good R value shows that the data from Hakodate can be used to estimate precipitation around the Onuma system.

In addition to annual precipitation, values for annual excess precipitation were determined. It is reported that mass-transport events are closely related to annual excess rainfall (Kashiwaya et al. 1986). Annual excess rainfall is an annual summation of the amount in excess of a given limit. Because the excess rainfall applies to areas without snow cover, it cannot be simply extended to snow-cover areas. Generally rainfall-related processes are different from snowfall-related (snowmelt-related) processes. In the studied area, the times of large mass transport are considered to be the spring melting season (Fig. 14.3a) and summer-fall (including typhoon) season (Fig. 14.2a). Here, we will examine two excess rainfall figures, that for the summer half-year, or summer season, from June through November, and that for the whole year, in order to clarify the rainfall-related processes. A 30-mm excess rainfall is employed as the daily limit for "excess" because were such a rainfall includes criterial value of heavy rainfall alarming in this district (>30 mm/h). It is expressed as follows:

$$R_{30} = \sum_i (R_i - 30), \tag{14.1}$$

where R_{30} is the annual summation of daily rainfall in excess of 30 mm. R_i is a daily rainfall ($R_i > 30$ mm). Results for the whole year and summer half-year for Mori and Hakodate are shown in Figs. 14.2d and 14.2e, respectively.

Secondly, precipitation and river discharge around Lake Onuma were checked. The catchment of Lake Onuma was enlarged for additional water supply in 1978. Both the total discharge (additional discharge and original discharge) and original discharge show nearly the same fluctuation (Hokkaido Electric Power Company, personal communication). Therefore, the original discharge (hereafter, "river discharge") is used here for discussion. During the interval of 1981 to 2010, the months of the largest average precipitation and largest river discharge were August and April, respectively (Figs. 14.2a and 14.3a). This may be reflected in large-rainfall-intensity events (floods, typhoons, heavy rainfalls, etc.) in the summer

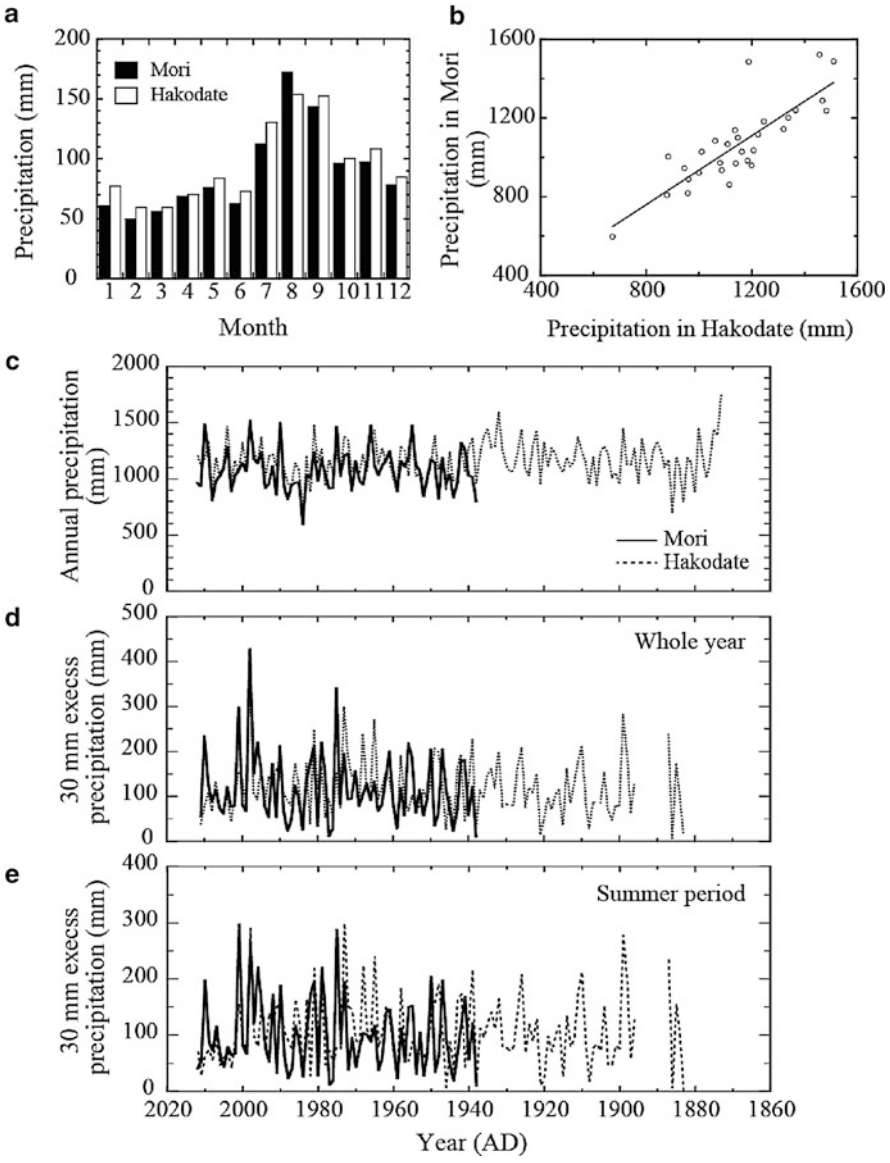

Fig. 14.2 Meteorological data around the Lake Onuma catchment. (**a**) Average monthly precipitation from 1981 to 2010 in Mori (*black*) and Hakodate (*white*), (**b**) comparison of annual precipitation between Mori and Hakodate. The regression curve is expressed as follows: $Y = 59.0 + 0.876X$, $R = 0.833$. Y precipitation in Mori, X precipitation in Hakodate, R correlation coefficient. Observational data in Mori (*solid line*) and Hakodate (*dashed line*); (**c**) annual precipitation, and 30-mm excess precipitation; (**d**) whole year and (**e**) summer period (from June to November)

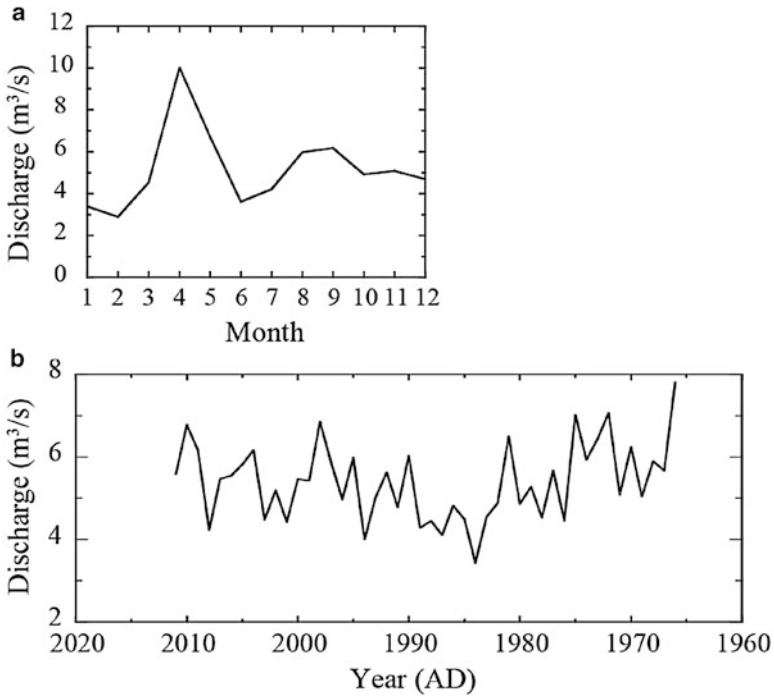

Fig. 14.3 Monthly and annual river discharge in Lake Onuma. (**a**) Average monthly river discharge in Lake Onuma from 1981 to 2010, and (**b**) annual river discharge in Lake Onuma

and snowmelt inflow in the spring. Indeed, it has been reported by Kashiwaya et al. (2012) that surface water discharge due to snow and/or ice melting as well as rainfall is a dominant external force for sedimentation rate in snowfall areas in Japan and Korea.

Annual precipitation in Mori and river discharge in Lake Onuma are shown in Figs. 14.2c and 14.3b. The relationship between them from 1981 to 2010 is shown in Fig. 14.4, and the correlation coefficient (R) is 0.88. The relationships between monthly precipitation and river discharge during the same interval were also checked. They are fairly good for summer season, but not so good in the winter and spring (Fig. 14.5). This may be related to snowfall (the reservoir effect with snow accumulation). From 1938 to 2012 the ratio of days in which the average monthly temperature fell below zero in December was about 68 % in Mori. It seems that December is the start of snowfall in Mori district. Part of the precipitation in winter is stored in the catchment as snow accumulation. As mentioned above, earth surface processes related to snowfall are somewhat different from those related to rainfall. It seems that direct erosional force is weaker in the period with snow cover than in the period without snow cover. It is reported that the correlation between seasonal sedimentation rate and seasonal rainfall without a snow cover period is much better than that with a snow cover period (Kashiwaya et al. 2012). River

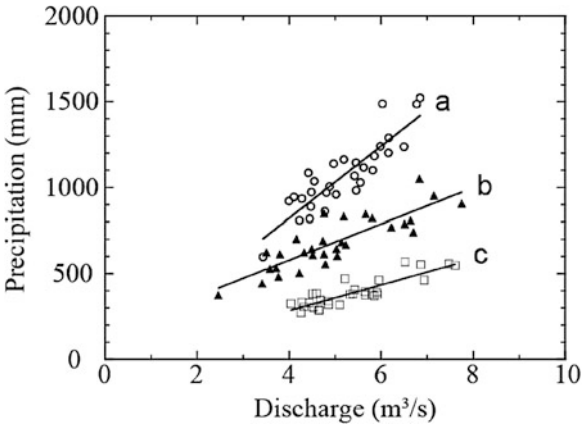

Fig. 14.4 The relationship between precipitation in Mori and river discharge in Lake Onuma from 1981 to 2010. Annual precipitation and river discharge (*open circle*), seasonal precipitation and river discharge in summer (*closed triangle*, from June to November) and that in the winter period (*open square*, from November to May). Regression curves are expressed as follows: (**a**) $Y = -16.0 + 209X$, $R = 0.88$ for annual, (**b**) $Y = 156 + 105X$, $R = 0.85$ for summer period, (**c**) $Y = -15.1 + 74.8X$, $R = 0.86$ for winter period. Y precipitation, X river discharge, R correlation coefficient

discharge in snowmelt season shows the largest value in the year (Fig. 14.3a). This may be related to the large sediment transportation from the catchment in the snowmelt period. As a convenient classification for discussions of earth-surface processes, the year can be divided into two periods (seasons): summer period (June to November) and winter period (December to May). There are good relationships between seasonal precipitation and river discharge in both the summer and winter periods (Fig. 14.4), indicating that lake-catchment processes are not the same in the two periods. This may be linked to varve formation in the past detected in the 4-m core: generally, fine sediments in winter and coarse sediments in summer. The correlation coefficients of the seasonal precipitation and river discharge in the summer and winter period are 0.85 and 0.86, respectively.

14.5 Radioactive Concentration and Sedimentation Rate

Fluctuations in radioactive concentrations are shown in Fig. 14.6. The layers of the largest Cs-137 radioactive concentration are located at a depth of 26 cm (3.37 g/cm^2; mass depth) and 16 cm (2.70 g/cm^2) for ON11-2-2 and ON11-1, respectively, while no Cs-137 peak layer could be detected in ON11-6 owing to the rough analytical interval of 5.0 cm. The layers indicating the largest peak in Cs-137 concentration must be related with the radioactive fallout centered around 1963 (Shimada et al. 2002; Katsuragi 1983). The sedimentation rates between 1963 and 2011 (sampling year) and the average sedimentation rates of the whole core are given in Table 14.2 on the basis of regression curves for Pb-210ex in Fig. 14.6.

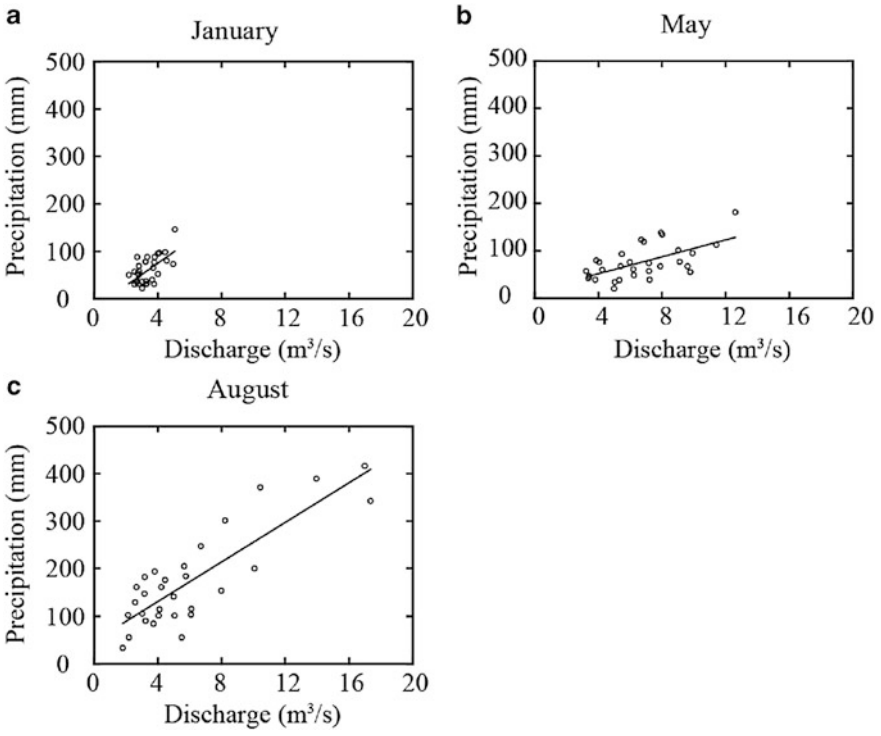

Fig. 14.5 Three types of trend of precipitation in Mori and river discharge in Lake Onuma from 1981 to 2010, in (**a**) January, (**b**) May and (**c**) August. Regression curves are expressed as follows: (**a**) $Y = -19.4 + 23.6X$, $R = 0.62$ for January, (**b**) $Y = 15.7 + 8.96X$, $R = 0.61$ for May, (**c**) $Y = 47.5 + 20.8X$, $R = 0.85$ for August. Y precipitation, X river discharge, R correlation coefficient

Table 14.2 Average sedimentation rate of sediment cores

Core number		ON11-6	ON11-2-2	ON11-2-1	ON11-1
Average sedimentation rate (g/cm^2/year)	1963–2011	–	0.070	0.086	0.056
	Whole period	0.078	0.092	0.113	0.064

The Cs-137 peak of ON11-2-1 at a depth of 33 cm (4.14 g/cm^2) was estimated, comparing fluctuation in ON11-2-2 whole grain size with that in ON11-2-1 (arrow-B in Fig. 14.7). The sedimentation rate of the ON11-2-1 for the upper part from the peak layer of Cs-137 concentration is given with this depth. The average sedimentation rate of ON11-2-1 for the whole core was estimated, multiplying the Pb-210ex-based sedimentation rate for the ON11-2-2 core by the ratio of the Cs-137-based rate for the ON11-2-1 to the ON11-2-2. The sedimentation rates of the cores are shown in Table 14.2.

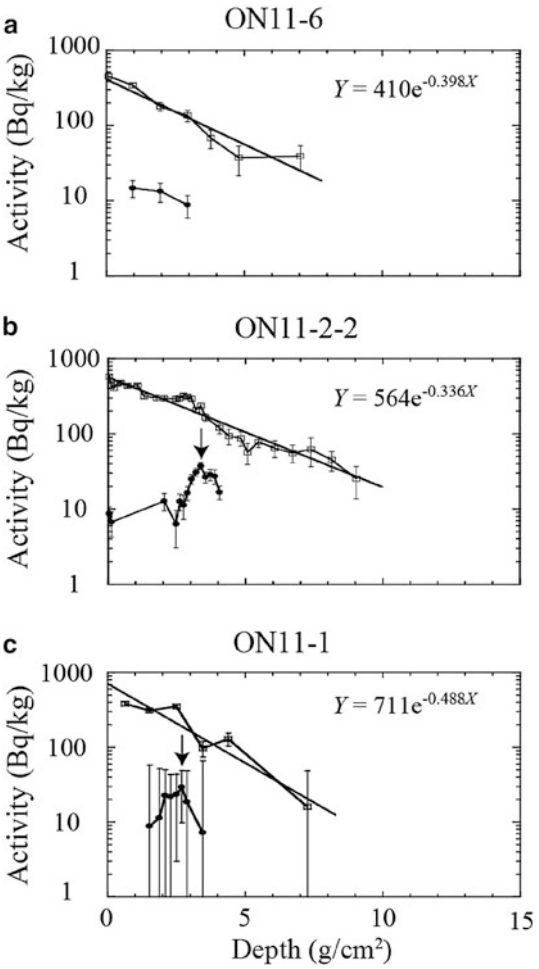

Fig. 14.6 Changes in excess Pb-210 activities (*square*) and Cs-137 activities (*circle*). The largest value in Cs-137 activity is shown by an arrow corresponding to the layer deposited around 1963. The equation in each figure shows the trend between excess Pb-210 activity and depth (g/cm^2). (**a**) ON11-6, (**b**) ON11-2-2 and (**c**) ON11-1

14.6 Discussion

We discuss here the changes of physical properties (water content, mineral content, density and mineral grain size), considering the ages.

Significant changes in physical properties could be found at 30 cm (7.04 g/cm^2; mass depth), 70 cm (9.20 g/cm^2) and 31 cm (6.00 g/cm^2) in the cores of ON11-6, ON11-2-1 and ON11-1, respectively (arrow-A in Fig. 14.8). Clear positive and negative peaks can be observed in this figure; the former peaks of mineral content, density, and mineral grain size and the latter one of water content in ON11-6 and ON11-1. On the other hand, these properties in ON11-2-1 show minor peaks. In the 4-m core obtained from Lake Onuma, the layer with low water content consists of volcanic products (Hasebe et al. 2015).

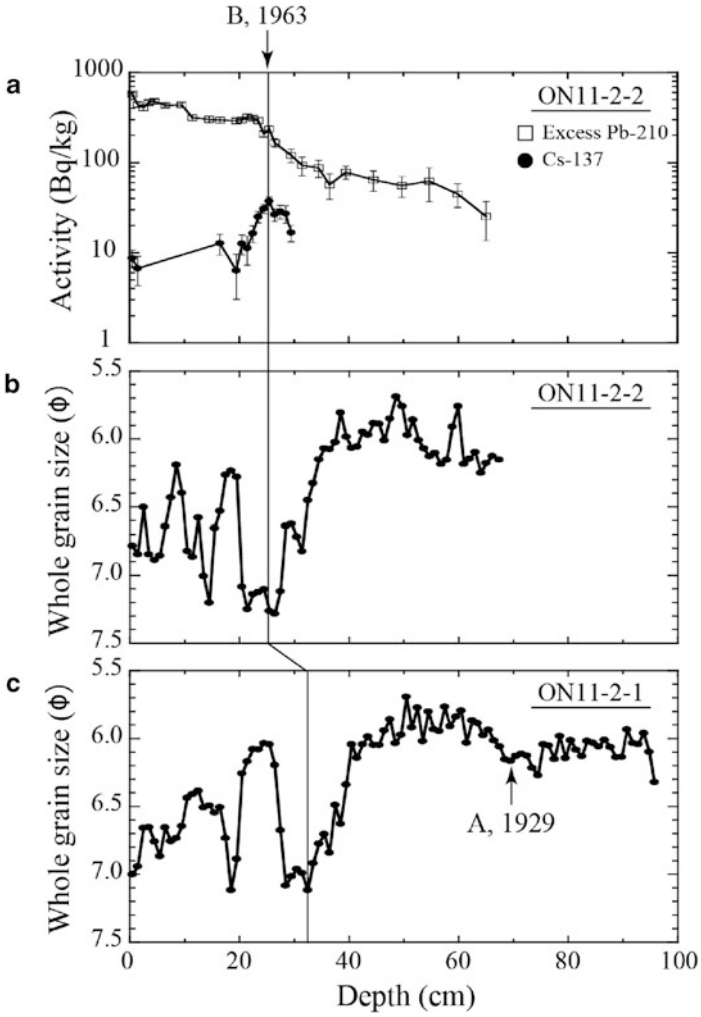

Fig. 14.7 Estimation of Cs-137 peak for ON11-2-1. (**a**) Change in excess Pb-210 (*square*) and Cs-137 (*circle*) activity of ON11-2-2, whole grain size variation of (**b**) ON11-2-2 and (**c**) ON11-2-1. *Arrow-A* shows estimated the eruption of HKV in 1929. *Arrow-B* indicates the layer deposited at around 1963 based on Cs-137 activity

Using the values of Cs-137 and Pb-210ex concentrations, the age of the layer shown by arrow-A (A-layer) is estimated by the following equation:

$$T(A) = 1963 - \{D(A) - D(1963)\} / SR(Pb), \tag{14.2}$$

where *T(A)* is the estimated age (year) of the A-layer, and *D(A)* and *D(1963)* are the mass depths of the A-layer and 1963-layer, respectively. *SR(Pb)* is the sedimentation

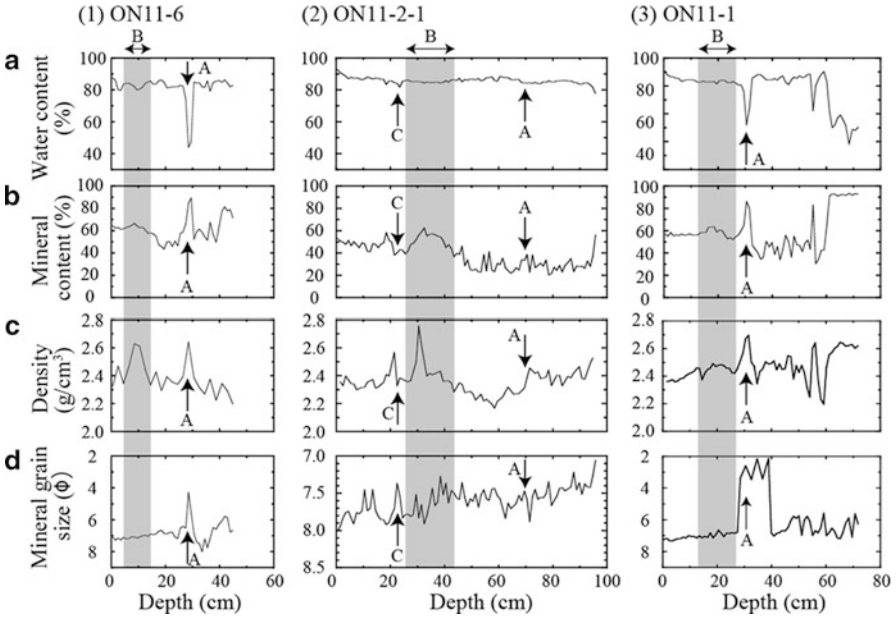

Fig. 14.8 Physical properties of short-core sediments from Lake Onuma. (1) ON11-6, (2) ON11-2-1 and (3) ON11-1. (**a**) Water content (%), (**b**) mineral content (%), (**c**) density (g/cm^3) and (**d**) mineral grain size (ϕ). *Arrow-A* shows estimated the eruption of HKV in 1929. B range shows the layer of peak in mineral content and density. Arrow-C shows estimated typhoon in 1975

rate given by Pb-210 dating. Average sedimentation rates with Pb-210ex were used to estimate the age of the lower-part sediments located below the 1963-layer. Using Eq. 14.2, the age of the A-layer in ON11-2-1 and ON11-1 were evaluated as 1918 and 1911, respectively. The age of the A-layer in ON11-6 was determined to be 1921 using only the Pb-210ex-based sedimentation rate.

Then we consider that the A-layer may correspond to the 1929 eruption of HKV (Fig. 14.8).

Here we infer the hydro-environmental fluctuations in the lake-catchment system over the past 100 years from the physical properties of the ON11-2-1 core, which was obtained from deepest part of Lake Onuma, possibly having much information. Three reliable time points, the 1929 eruption of HKV (A-layer in Fig. 14.8), 1963 (estimated Cs-137 peak) and 2011 (sampling date), were used to construct a tentative age model of the ON11-2-1 core (Fig. 14.9). The solid line connecting each point in Fig. 14.9 shows a linear age model of the core. The same method was applied to the other cores (for ON11-6 with two dates). Changes in the physical properties of the three cores are shown in Fig. 14.8. Convex peaks in density and mineral content variations can be detected in the B range in ON11-2-1 accompanied with a sharp peak of the density variation. Clear peaks are seen in the mineral grain size of ON11-2-1 and ON11-1. The B range includes the period of 1950–1970.

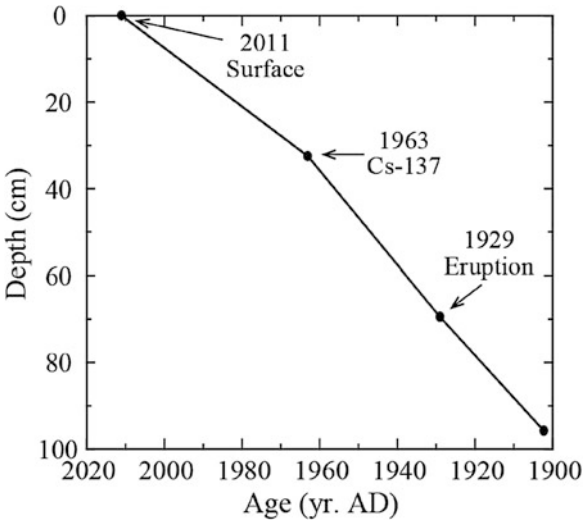

Fig. 14.9 Age model for ON11-2-1 core constructed by Cs-137 peak and the eruption of HKV in 1929

After the end of the World War II, land reclamation mainly for agricultural land use was rapidly promoted, followed by the acceleration of resort area construction in this district during the rapid economic growth from 1954 to 1973. The Shukunobe-river area and north catchment were notable zones influenced rapidly by land reclamation during this period. According to Kashiwaya et al. (1997), the grain density increased with the progress of land reclamation and decreased with the complement of the reclamation in the land transformation area. From checking air photographs (Geospatial Information Authority of Japan) taken from 1944 to 1976 in this area, the B range indeed corresponds to the time period around 1950 to 1970 (Fig. 14.10). The photos and documentary records in this area will be properly and quantitatively evaluated in the next stage of our study.

The C-layer was detected only in the ON11-2-1 core; this core enabled us to analyze events with high resolution due to its rapid sedimentation rate. We compared the data from this core with directly observed hydrological data to clarify the past detailed hydro-environmental conditions. Figure 14.11 shows the fluctuations in 30-mm excess daily rainfall (whole year and summer period) in Mori, and three physical properties of ON11-2-1. A numerical filter (Ormsby 1961) is used for the 30-mm excess daily rainfall in Mori to clarify the trends. Three peaks in the fluctuation of 30-mm excess rainfall (arrows 1, 2, and 3 in Fig. 14.11a, b) may correspond to those in grain size fluctuation (arrows 1, 2 and 3 in Fig. 14.11c).

Heavy rainfall disasters are recorded in the local history of this district (Mori Town 1980; Nanae Town 2001). Those in the recent period (1945–1980) occurred in 1955, 1961 and 1975, in which heavy rainfall in 1955 (July) and Typhoon No. 6 in 1975 (August) hit this district and induced many landslides. In the 1955 heavy rainfall disaster, floods and landslides occurred in the catchment of the Shukunobe, which is the main stream flowing into Lake Onuma (Mori town Library, Per. Com.). In the 1975 typhoon, there were many landslides and flooding in the district

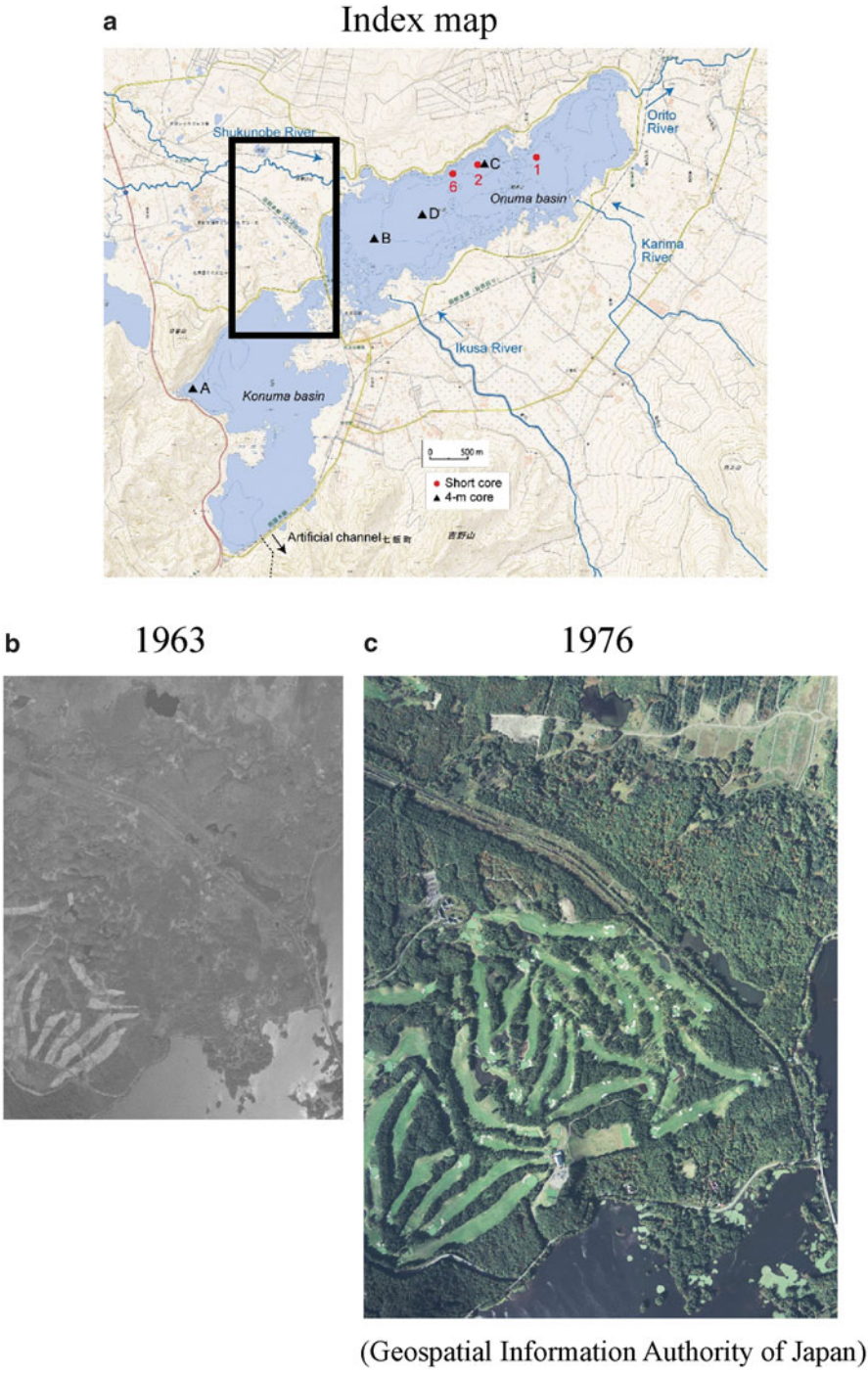

Fig. 14.10 Air photographs taken around the Lake Onuma. This figure is modified after the map and air photos (Geospatial Information Authority of Japan). (**a**) Index map of Lake Onuma. *Square* shows location of the photos. These photos were taken in (**b**) 1963 (MHO637X-C6-3; reference number) and (**c**) 1976 (CHO7618-C1C-7)

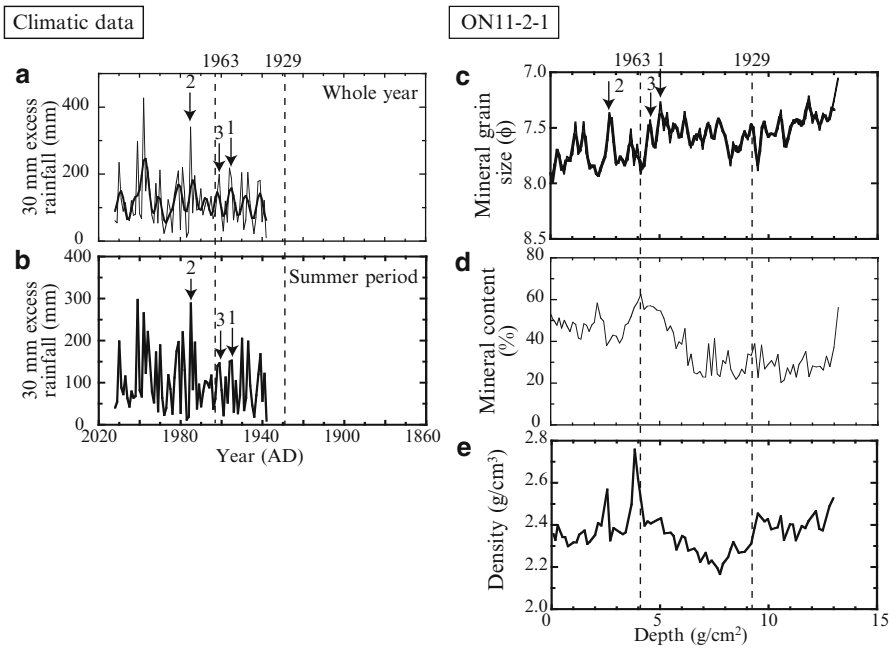

Fig. 14.11 Comparison of climatic data with physical properties of ON11-2-1. 30 mm excess rainfall in Mori; (**a**) whole year and (**b**) summer period (June – November). Physical properties of ON11-2-1; (**c**) mineral grain size (ϕ), (**d**) mineral content (%) and (**e**) density (g/cm^3). Each *arrow* shows the age of 1 (1955), 2 (1975) and 3 (1961), respectively. A numerical filter (Ormsby 1961) was used for the mineral grain size to minimize the effect of disturbance at the lake bottom caused by trawl fishery

(Mori town Library, Per. Com.). The evidence of the typhoon was recorded in the suspended sediment (SS) measured in Lake Onuma showing the average SS value of 22 mg/l (Fig. 14.12). The two largest peaks in mineral grain size shown by arrows 1 and 2 in Fig. 14.11 correspond to the years of 1955 and 1975. Another peak shown by arrow 3 can be attributed to the year 1961. The discussion of peak-matching is limited to these three points because of limited information, although there is a possibility that peaks around 1.1 g/cm^2 and 0.39 g/cm^2 also corresponded to years (1998 and 2010) with excess rainfall.

14.7 Conclusion

Analytical results of the physical properties of Lake Onuma sediments and hydrological observation data around the Lake Onuma (lake-catchment) system suggest that: (i) earth-surface processes in summer and winter periods differ in the snowfall area due to the following nature conditions: snowfall, snow accumulation, and

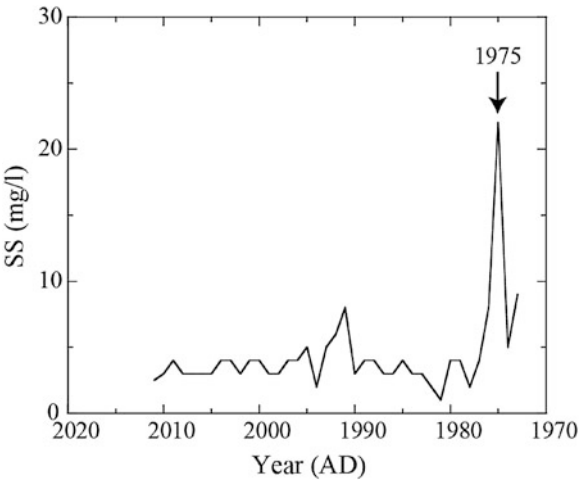

Fig. 14.12 Fluctuation of the average suspended sediment (SS) in Lake Onuma (Hokkaido Government 2012)

snowmelt; (ii) the eruption in 1929 HKV is clearly evidenced in various physical properties; (iii) the mineral grain size correlates highly with precipitation, such as typhoon and heavy rainfall; and (iv) fluctuations in mineral content and density indicate an increase of sediment discharge in the interval of 1950–1970, and may be related to land transformations in the catchment during that time.

Acknowledgement We thank Prof. Y. Ganzawa, Prof. K. Tanaka, Hokkaido University of Education, and Dr. K. Fukushi, Kanazawa University, for helping us obtain the core samples, Mr. B. Enkbayar, Mongolian Academy of Sciences, for assistance in the experiment concerning the density for the ON11-2-1 core, Hakodate Observatory for providing us with the meteorological data from Mori Observatory, Hakodate Marine Observatory and Onuma Observatory, Hokkaido Electric Power Company for providing us with the data on discharge in Lake Onuma, and Mori Town and Mori Library for providing us a history book and information about Mori Town. We also thank Dr. N. Hasebe and our colleagues in the limno-geomorphological laboratory at Kanazawa University for their support of this study. I thank the Japan Society for the Promotion of Science for Young Scientists for support of my study.

References

Geospatial Information Authority of Japan: Information of maps and Aerial photos. http://mapps.gsi.go.jp/

Hasebe N, Itono T, Katsuki K, Murakami T, Ochiai S, Katsuta N, Wang Y, Lee JY, Fukushi K, Ganzawa Y, Mitamura M, Tanaka K, Kim JY, Shen J, Kashiwaya K (2015) Possible age models for Lake Onuma lacustrine sediments based on tuffs recovered in three cores. In: Kashiwaya K (ed) Earth surface processes and environmental changes in east Asia. Springer, Tokyo

Hokkaido Government (2012) Hokkaido no Mizukankyou (Hydro-environment in Hokkaido): http://envgis.hokkaido-ies.go.jp/mizu_index.html. Accessed 13 June 2013

Itono T, Kashiwaya K, Sakaguchi A (2012) Disastrous flood events found in lacustrine sediments from Lake Biwa. Trans Jpn Geomorphol Union 33:453–468

Kashiwaya K, Okimura T, Kawatani T (1986) Dendrochronological information and hydrological conditions for landslides in Mt. Futatabisan Area of Rokko Mountains. Trans Jpn Geomorphol Union 7:281–290 (in Japanese with English abstract)

Kashiwaya K, Okimura T, Harada T (1997) Land transformation and pond sediment information. Earth Surf Process Landf 22:913–922

Kashiwaya K, Ochiai S, Okimura T, Nahm WH, Yang DY, Kim JY (2012) Erosion and sedimentation in Lake-catchment systems in Japan and Korea on the basis of an elementary process model. Trans Jpn Geomorphol Union 33:219–236

Katsuragi Y (1983) A study of ^{90}Sr fallout in Japan. Pap Meteorol Geophys 33:277–291

Mortlock RA, Froelich PN (1989) A simple method for the rapid determination of biogenic opal in pelagic marine sediments. Deep-Sea Res 36:1415–1426

Nahm WH, Lee GH, Yang DY, Kim JY, Kashiwaya K, Yamamoto M, Sakaguchi A (2010) A 60-year record of rainfall from the sediments of Jinheung Pond, Jeongeup, Korea. J Paleolimnol 43:489–498

Ochiai S, Nagao S, Itono T, Suzuki T, Kashiwaya K, Yonebayashi K, Okazaki M, Kaeriyama M, Qin YX, Hasegawa T, Yamamoto M (2015) Recent eutrophication and environmental changes in the catchment inferred from geochemical properties of Lake Onuma sediments in Japan. In: Kashiwaya K et al (eds) Earth surface processes and environmental changes in east Asia. Springer, Tokyo, pp 209–220

Ormsby JFA (1961) Design of numerical filters with applications to missile data processing. J Assoc Comput Mach 8:440–466

Shimada T, Kashiwaya K, Hyodo M, Masuzawa T (2002) Hydro-environmental fluctuation in a lake-catchment system during the late Holocene inferred from Lake Yogo sediments. Trans Jpn Geomorphol Union 23:415–431 (in Japanese with English abstract)

Tanaka T (2005) Water pollution factors of land use and river water quality in eutrophicated lake watersheds: Lake Oshima-Oonuma, Hokkaido, Japan. J Human Environ Symbiosis 11:13–22 (in Japanese with English abstract)

Town M (ed) (1980) Mori Choushi (History of Mori Town). Mori Town, Sapporo, 1279 p. (in Japanese)

Town N (ed) (2001) Nanae Choushi Zokkan (History of Nanae Town follow-up report). Nanae Town, Hakodate, 934 p. (in Japanese)

Yoshimoto M, Takarada S, Takahashi R (2007) Eruptive history of Hokkaido-Komagatake volcano, northern Japan. J Geol Soc Jpn 113(Suppl):81–92 (in Japanese)

Chapter 15
Sedimentation Processes Following the Construction of Waterway Tunnels in Sun Moon Lake, Taiwan

Shinya Ochiai, Jiun-Chuan Lin, Jian-Wei Lin, Chia-Hung Jen, Wen-Hu Chen, and Kenji Kashiwaya

Abstract Lake bottom topography and sedimentation rate measurements were used to study sedimentation processes following construction of artificial waterway tunnels in Sun Moon Lake, a natural lake that was transformed into a reservoir for a hydroelectric power plant. The sediment inflow rate from the waterway tunnels is influenced by the artificially controlled water inflow rate, and the sediment concentration associated with precipitation in the Zhuoshui River. Low sediment inflow rates were observed during winter and spring, and large rates were observed during the East Asian rainy season and typhoon season. Low sedimentation rates were observed during winter/ spring, and high sedimentation rates were observed during summer and autumn corresponding to the changes in the rate of sediment inflow. Results from a 1-dimensional sedimentation model suggest that the sediment deposition rate in Sun Moon Lake decreases exponentially with distance from the tunnels and erosion in shallow areas near the tunnels.

S. Ochiai (✉)
Department of Geography, National Taiwan University, No. 1, Sec. 4, Roosevelt Road, Taipei 106, Taiwan

Institute of Nature and Environmental Technology, Kanazawa University, Kakuma, Kanazawa 920-1192, Japan
e-mail: sochiai@ies.or.jp

J.-C. Lin • J.-W. Lin • W.-H. Chen
Department of Geography, National Taiwan University, No. 1, Sec. 4, Roosevelt Road, Taipei 106, Taiwan

C.-H. Jen
Center of Environment Education and Safety Health, National Kaohsiung Normal University, No. 116, Heping 1st Road, Kaohsiung 802, Taiwan

K. Kashiwaya
Institute of Nature and Environmental Technology, Kanazawa University, Kakuma, Kanazawa 920-1192, Japan

Department of Geography, National Taiwan University, Daan District, Taipei 10617, Taiwan

K. Kashiwaya et al. (eds.), *Earth Surface Processes and Environmental Changes in East Asia*, DOI 10.1007/978-4-431-55540-7_15

Keywords Lake sedimentation process • Sediment trap • Sedimentation rate • Grain size

15.1 Introduction

Siltation of reservoirs is one of the most serious problems for sustainable water use because it reduces water storage capacity, electricity production, and reservoir lifespan. It is estimated that the total water-storage capacity of the world's reservoirs is lost at a rate of 0.5–1 % per year because of sedimentation (World Commission on Dams 2000). As sediment yield and transport are high in Taiwan (Dadson et al. 2003; Lin et al. 2006), sedimentation is reducing about 0.4–0.7 % of the total storage volume of the major reservoirs every year (Su et al. 2006), suggesting that the lifespan of these reservoirs is approximately 140–250 years. Thus, sedimentation will have large influence on Taiwan's environment and economy in near future. This problem is important for not only artificial reservoirs but also natural lakes. Natural and human-induced land transformation (earthquake, dam construction, etc.) in lake-catchment systems has a large influence on the sedimentation processes in the lake (Page et al. 1994; Shimada et al. 2002; Kashiwaya et al. 2004).

Sun Moon Lake is located in the central part of Taiwan and confronted with a siltation problem caused by human activities. This lake has been used as a reservoir for hydroelectric power, irrigation, and water supply since the construction of an artificial dam in the beginning of the twentieth century. Ochiai et al. (2012) indicate that artificial sediment inflow has contributed greatly to the change in the lake basin based on the bathymetric map surveys. On the basis of this past sedimentation records, the lifespan of Sun Moon Lake may be 500 years. The eastern part of the lake may disappear within 100 years, resulting in large changes in the lake topography and scenery.

For sustainable water-resource use, an appropriate assessment of sedimentation processes is needed. Information on artificial impacts to a natural lake may provide clues on how to manage a reservoir properly. In this study, we examine the sedimentation processes after the construction of artificial waterway tunnels on the basis of field observations of the sedimentation rate and bottom topography during the rainy season.

15.2 Study Area

Sun Moon Lake is located in the central part of Taiwan (Fig. 15.1). This lake was formed by tectonic movements in the Pleistocene (Huang et al. 2000), and can be roughly separated into an eastern basin (Sun Lake) and a southwestern basin (Moon Lake) by a lake bottom saddle. The present Sun Moon Lake is a reservoir for hydroelectric production, irrigation, and water supply. The first construction on the lake was performed in 1934 to develop a hydroelectric power plant. At that time, two

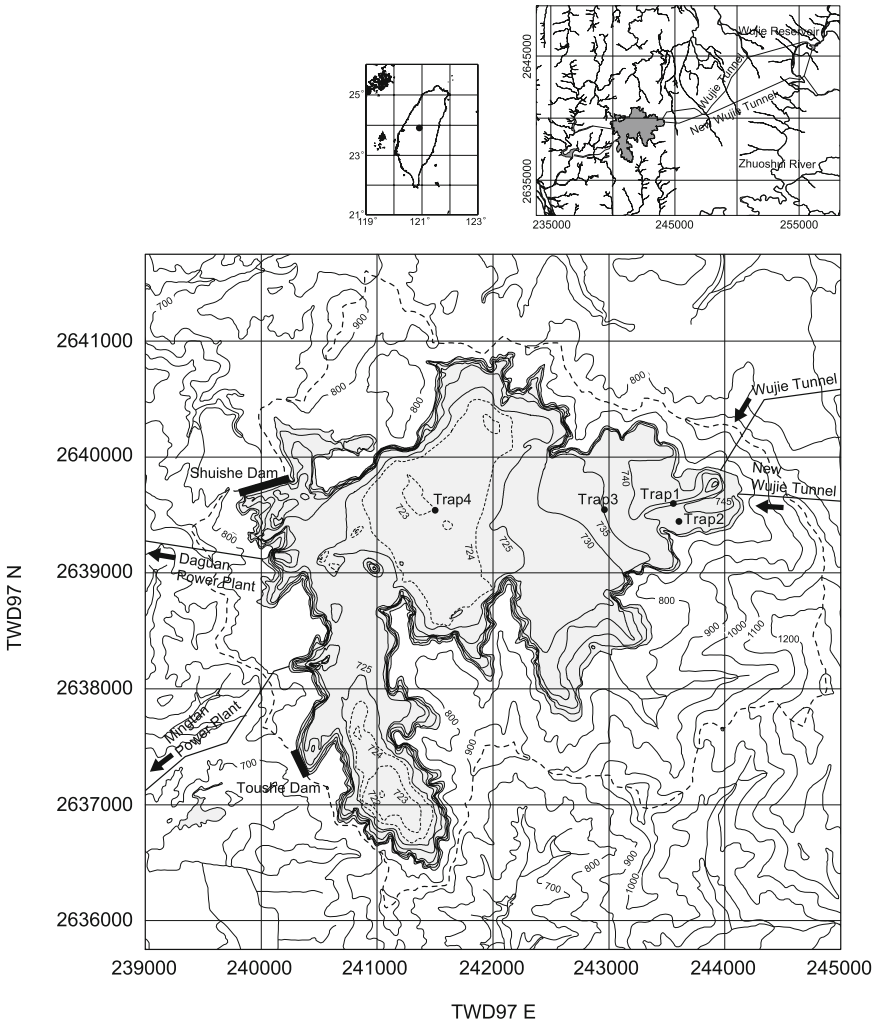

Fig. 15.1 Map of Sun Moon Lake. *Solid circles* indicate the observation points of the sediment traps. The bathymetric map of Sun Moon Lake is based on data from the Taiwan Power Company (2000)

dams (the Shuishe and Toushe Dams) were built to close the original outflow in the northwest section of the lake. There are two power plants called the Daguan (built in 1934) and Mingtan power plants (built in 1995). The water intakes of these power plants in the western part of the lake and the spillway near the Suishe dam are the only outflows of the lake. Upstream along the Zhuoshui River, the Wujie reservoir and two waterway tunnels (Wujie and New Wujie tunnels) were also constructed to supply water to Sun Moon Lake. The length and diameter of these tunnels are about 15 km and 5 m, respectively. The water inlets of these tunnels are located on the eastern shore of the lake. The water inflow and outflow of the present Sun Moon Lake are artificially controlled by the power plant operation. The highest

water level is limited by the spillway to 748.5 m a.s.l. The average water depth at the highest water level is 18 m. The maximum water depth is 33.5 m near the water intake of the Mingtan power plant in Moon Lake. Except for this artificial structure, the maximum depth is 25.5 m for Sun Lake and 26.5 m for Moon Lake. The water surface area and original (natural) catchment area are 8.4 km^2 and 8.6 km^2, respectively. The catchment of Sun Moon Lake is relatively small (the catchment to lake area ratio is about 1), suggesting that the sediment contribution from the original catchment is low. However, sedimentation has progressed because of the sediment from the Wujie and New Wujie waterway tunnels since the beginning of power plant operation.

15.3 Methods

To understand the sedimentation processes in Sun Moon Lake, we observed the sedimentation rate and measured grain size for approximately every month. We also measured the bottom topography and sediment inflow at the same time. The dates of these observations are shown in Table 15.1.

Four sediment traps were installed on the lake bottom (Fig. 15.1). Trap 1 and Trap 2 were installed near the water inlets of the Wujie tunnel and the New Wujie tunnel on October 25, 2007. Trap 3 was installed 500 m offshore from Trap 1 on December 27, 2007, and Trap 4 was installed in the center of Sun Lake on July 3, 2008. Each trap was a cylinder made of steel, initially with a diameter and height of 40 cm and 10 cm, respectively. On December 27, 2007, we changed the size, installing traps with a 30 cm diameter and 20 cm height, due to the large sedimentation rate. Sediment samples were collected monthly and were oven dried at 110 °C to obtain their dry weight. The grain sizes of the trap samples were measured with a laser diffraction particle size analyzer (SALD-2200, Shimadzu, Japan). The density of sediment particles was measured by a gas displacement pycnometer (AccuPyc 1330, Micromeritics, USA).

The sediment concentration of the inflowing water was measured at the water inlets of the Wujie and New Wujie tunnels. Water samples were taken at the same time as the trap sampling. In this study, the sediment concentration was defined as the evaporation residue obtained using a 110 °C drying oven.

At the same time as the trap sampling, the temporal change in the lake bottom height (elevation) around the trap-sampling point was measured using sonar (LMS-332C, LOWRANCE, USA), beginning on December 7, 2007. The sonar recorded the depth and position every 0.4 s along the ship's route. The position of a sonar observation was determined with the satellite-based differential GPS (D-GPS) included with the sonar equipment. The positioning error was determined to be less than 3 m by checking with the control point. The maps in this paper are based on a TWD97 2-degree Transverse Mercator coordinate system. The water level of Sun Moon Lake changes frequently because of the water consumption for the power plants and the inflow from the waterway tunnels. Therefore, the lake bottom

Table 15.1 Items and date of the observations

Date	Trap 1	Trap 2	Trap 3	Trap 4	Sediment concentration	Bottom elevation	Bathymetric survey
Oct. 20, 2007					+		
Oct. 25, 2007	+	+			+		
Nov. 1, 2007	+	+			+		
Nov. 15, 2007	N/A	N/A			+		
Dec. 7, 2007	N/A	+			+	+	
Dec. 14, 2007	N/A	N/A				+	
Dec. 27, 2007	+	N/A	N/A		+	+	
Jan. 11, 2008	N/A	N/A	N/A		+	+	
Jan. 26, 2008	+	+	+		+	+	
Feb. 22, 2008	+	N/A	+		+	+	
Mar. 9, 2008	+	+	+		+	+	
Mar. 28, 2008	+	N/A	+		+	+	
Apr. 21, 2008	+	+	+		+	+	+
May 12, 2008	+	+	+		+	+	
Jun. 3, 2008	+	N/A	+		+	+	
Jul. 3, 2008	+	+	+	+	+	+	
Jul. 17, 2008	+	N/A	+	+	+	+	
Aug. 2, 2008	+	+	+	+	+		
Aug. 16, 2008	+	+	+	+	+	+	
Sep. 1, 2008	+	+	+	+	+	+	
Sep. 25, 2008	N/A	N/A	+	+	+	+	
Nov. 11, 2008	N/A	+	+	+	+	+	+
Dec. 26, 2008					+	+	
Feb. 14, 2009	+	+	+	+	+		

topography is shown as lake-bottom elevations. The lake level, water inflow, and water outflow records are based on data from the Taiwan Power Company and Water Resource Agency, Taiwan. Meteorological data were provided by the Central Weather Bureau, Taiwan.

15.4 Results

15.4.1 Sediment Inflow from the Artificial Waterway Tunnels

Figure 15.2a shows the daily water inflow rate from the Wujie and New Wujie tunnels, and the outflow rate to the power plants. The water inflow and outflow, which are artificially controlled by the power plant operation, were relatively low during the winter and spring and high during the summer and autumn. Hydroelectric production consumed 99 % of the outflow water (Water Resources Agency 2007)

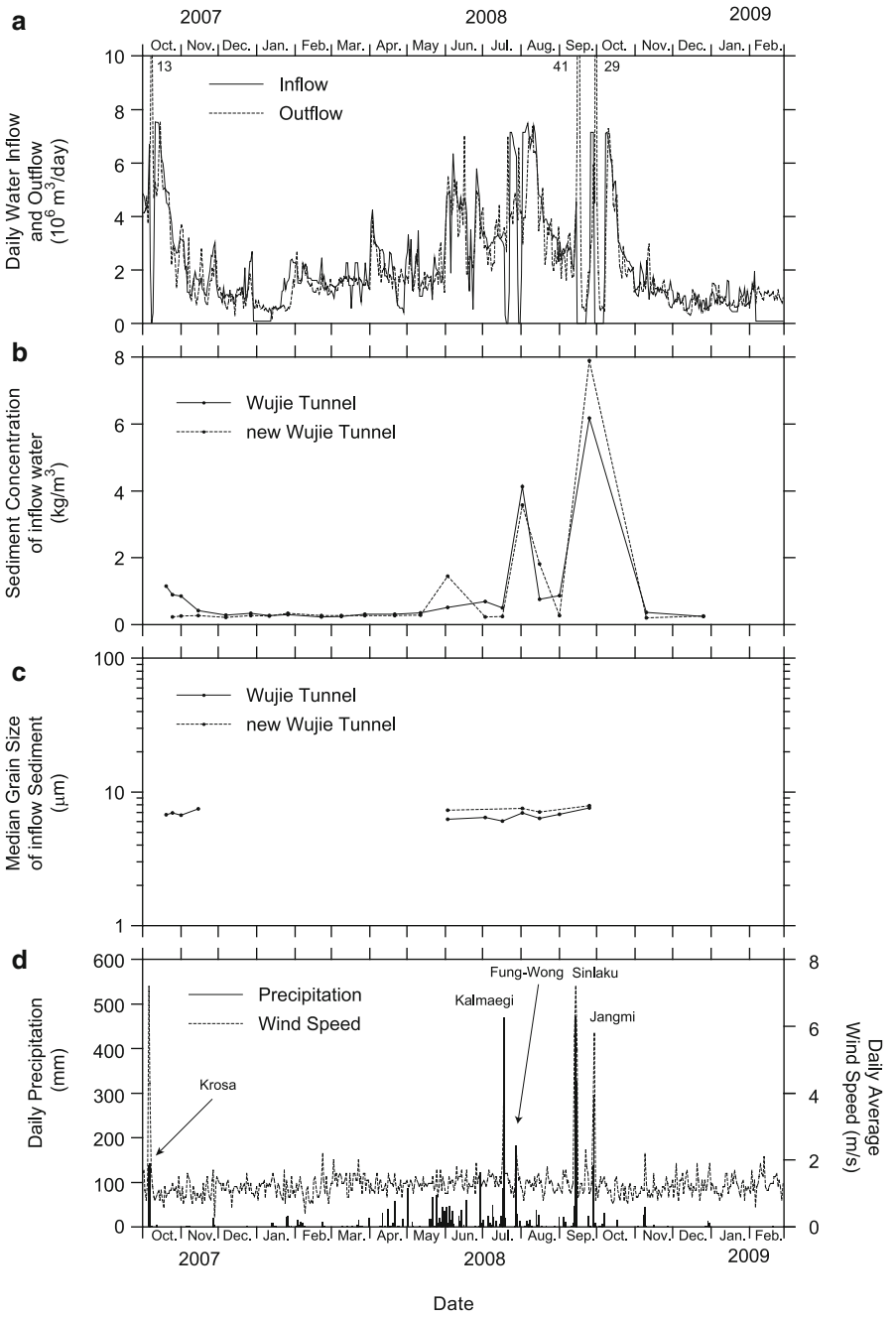

Fig. 15.2 Temporal changes in (**a**) daily water inflow rate from the Wujie and New Wujie tunnels and outflow rate to the power plants, (**b**) sediment concentration of inflow water from the Wujie and New Wujie tunnels, (**c**) median grain size of the sediment from the tunnels, and (**d**) daily precipitation and daily average wind speed at Sun Moon Lake. Typhoons are named by Asian nomenclature

and the water inflow rate almost corresponded to the outflow rate. This indicates that the water inflow reflects the water consumption of the electric power plants.

On the other hand, the sediment concentrations (Fig. 15.2b) from the Wujie and New Wujie tunnels seem to be related to natural factors. Figure 15.2d shows the changes in the daily precipitation in Sun Moon Lake and past typhoons labeled with Asian typhoon names. The precipitation was relatively low during the winter and spring and high during the subsequent summer and autumn. Heavy rainfalls occurred during the five typhoons that approached Taiwan in 2007 and 2008. After a typhoon, the sediment concentration greatly increased, up to 8 kg/m^3, suggesting that the sediment concentration of the inflow water entering the lake is influenced by sediment discharge in the Zhuoshui River, a water source of the Wujie tunnels.

Figure 15.2c shows the changes in the median grain size of the sediment from the tunnels. Although data were available only for high concentration periods because of a measurement limit in the grain size analysis, the grain size of the inflow sediment was almost constant (about 7 μm). The sediment consists almost exclusively of silt, with little sand content. This may result from the removal of coarse grains in the Wujie reservoir. This is a special characteristic of Sun Moon Lake that makes it different from normal reservoirs built along rivers.

The sediment inflow rate, Q_s, from the waterway tunnels was calculated from the mean water inflow rate, Q, and the mean sediment concentration, c_m, for each sampling interval with the following equation:

$$Q_s = c_m \cdot Q = \frac{c_1 + c_2}{2} \cdot \frac{V}{T} \tag{15.1}$$

where Q_s (kg/day) is the mean sediment inflow rate for a sampling interval; c_m (kg/m^3) and Q (m^3/day) are the mean sediment concentration and mean water inflow rate, respectively. The mean sediment concentration, c_m, is the average of the beginning value, c_1, and end value, c_2, of the interval. The average concentration at the Wujie tunnel and New Wujie tunnel is used for this calculation. The mean water inflow rate, Q, is calculated from the volume of the total water inflow, V (m^3), and the time length, T (day), of the interval. Figure 15.3 shows the calculated mean water inflow rate, Q, mean sediment concentration, c_m, and sediment inflow rate, Q_s, for each sampling interval. The sediment inflow rate was small in the winter and spring and large in the summer and autumn (Fig. 15.3b), reflecting interference between the artificial water inflow rate and precipitation-related sediment concentration. Five typhoons, Krosa in October of 2007, Kalmaegi and Fung-Wong in July of 2008, and Sinlaku and Jangmi in September of 2008, caused large amounts of precipitation and then extremely large sediment inflows (hereafter called sediment inflow events A, B, C, and D).

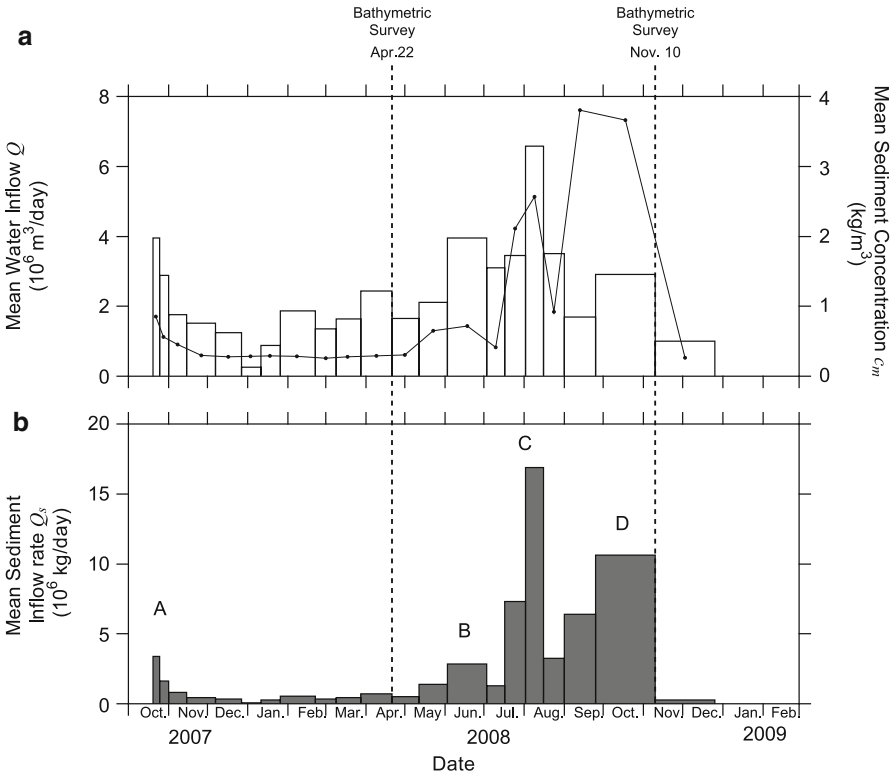

Fig. 15.3 (**a**) Mean water inflow rate Q (*white bar*) and mean sediment concentration c_m (*line*) for each sampling interval. (**b**) Sediment inflow rate Q_s for each sampling interval

15.4.2 Temporal Changes in Sedimentation Rate

Figure 15.4 shows changes in the sedimentation rate and grain size of the trap samples from October 25, 2007 to February 14, 2009 (some data are unavailable due to technical problems and are shown by hatched bars). The character "F" (full) on the bars indicates that the sediment traps overflowed due to high sedimentation events and the sedimentation rates during these events were thus underestimated. The average sedimentation rates of Traps 1, 2, 3, and 4 were 5.2, 3.0, 3.6, and 0.15 kg/m^2/day, respectively. Assuming water content and sediment density values of 50 % and 2.76 g/cm^3 (equivalent to values the obtained for surface sediment in Sun Moon Lake), sedimentation rates were equivalent to 7.2, 4.1, 4.9, and 0.21 mm/day, respectively. Rates for Traps 1, 2, and 3 were underestimated due to the overflowing of the sediment traps, as discussed above. Sedimentation rates were higher near the waterway tunnels and lower in the central part of the lake, which indicates that a large amount of sediment in the lake is sourced from the artificial

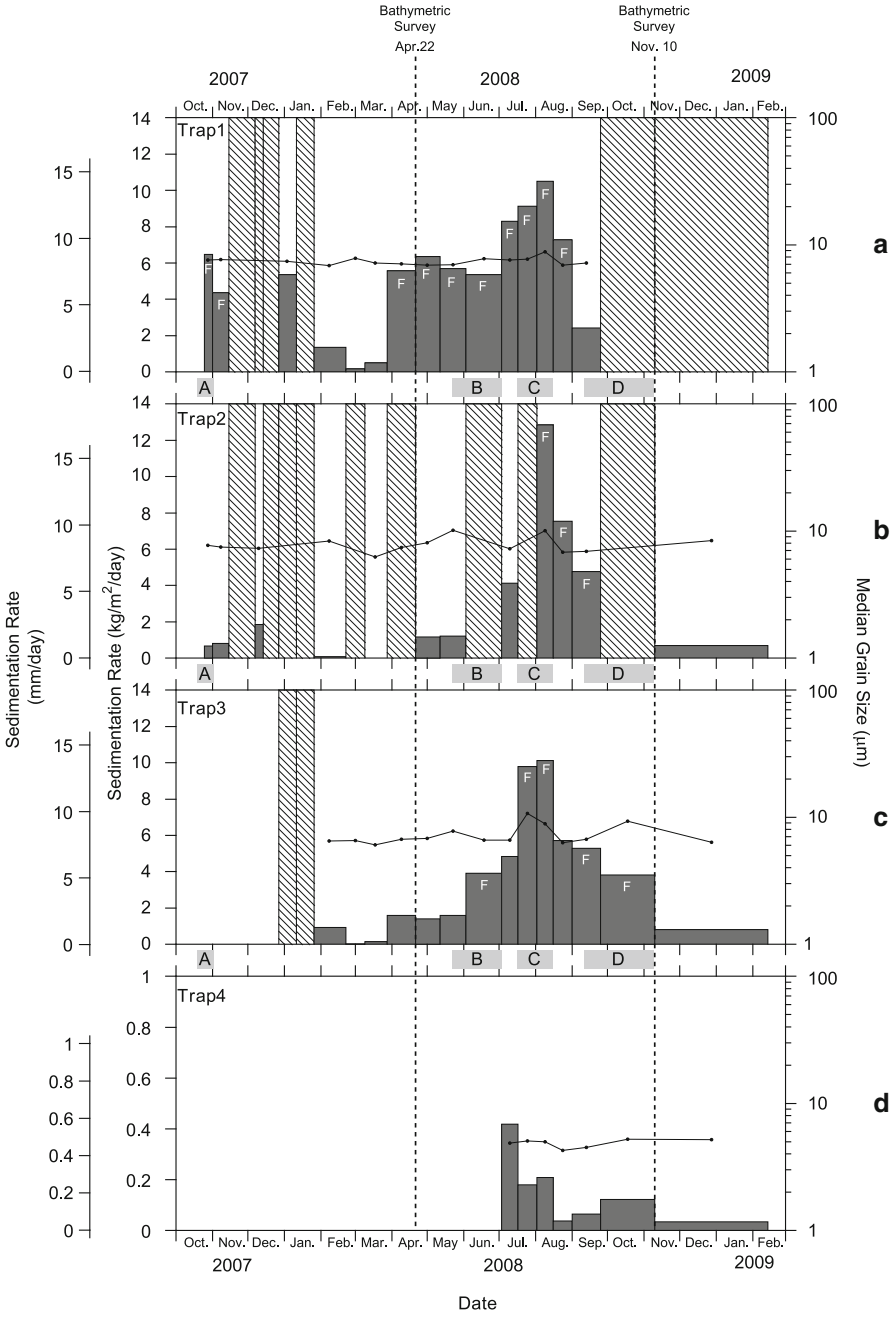

Fig. 15.4 Temporal changes in sedimentation rate measured with sediment traps (*bar graph*) and median grain size of trap samples (*line graph*) for (**a**) Trap 1, (**b**) Trap 2, (**c**) Trap 3, and (**d**) Trap 4

waterway tunnels. Sedimentation rates were relatively low during winter/spring and high during summer/autumn. Extremely high sedimentation events, in which the sediment traps overflowed, correspond to sediment inflow events B, C, and D (Fig. 15.5).

The median grain sizes of Trap 1, Trap 2, Trap 3, and Trap 4 for all of the intervals were 7.4, 7.8, 7.3, and 4.9 μm, respectively. The grain sizes of Trap 1, Trap 2, and Trap 3 were approximately uniform and slightly larger than that of the inflow sediment (6.9 μm). The smallest grain size was found in Trap 4, which is attributed to hydrological sorting effects in the lake. Larger grain sizes were observed during sediment inflow events C and D are attributed to typhoons activity; in addition, this is accompanied by a change in the sedimentation rates, particularly in Trap 3 and 4. Although, a change in the grain size of sediment in the traps was observed, the grain size of the inflow sediment remained constant. This suggests that the grain size fluctuation results from internal lake conditions such as water flow in the lake.

As sediment traps are unable to detect large changes in the sedimentation rate and also erosion, changes in the bottom elevation of the lake were measured by sonar-scanning. Figure 15.5 shows changes in the lake-bottom elevation (thin line with error bar) at the trap sampling points from December 7, 2007 to February 14, 2009. Elevation values for each trap were determined using the nearest sonar measurement points because it was impossible to reoccupy exactly the same subsurface point for every observation, especially in the offshore zone. Errors in elevation measurements were estimated from the relationship between the horizontal distance and vertical dispersion of the bottom topography. This relationship was estimated by calculating the standard deviation in the elevation of a sonar data point including various sizes of reference radii. Elevation errors >0.3 m were discarded and thus no data are available for these intervals. The gray band in Fig. 15.5 represents the sedimentation rate calculated from the change in elevation and the height of the band indicates the sedimentation rate error. The sedimentation rate measured by the trap is represented by the thick line. Sedimentation rates estimated from the sonar data are within error of the rate determined by the sediment traps at low sedimentation rates; however, the traps appear to underestimate high sedimentation rates, and furthermore, are unable to detect erosion.

The change in the lake-bottom elevation is below the limit of detection using sonar methods in the offshore region of the lake (Trap 4) and sedimentation rates are low. The elevation of the shore area near Trap 1, 2, and 3 changed in response to the sediment influx. The elevation remained constant during the winter 2007 and spring 2008, and then increased approximately 3 m from April to November 2008. Sediment inflow events (B, C, and D) were clearly represented in Trap 1, 2, and 3 (Fig. 15.5). Erosion of the bottom sediment occurred at Trap 1, 2, and 3 in winter 2008 and between the sediment inflow events; this is attributed to the changes in hydrological conditions of the lake and the sediment inflow rate.

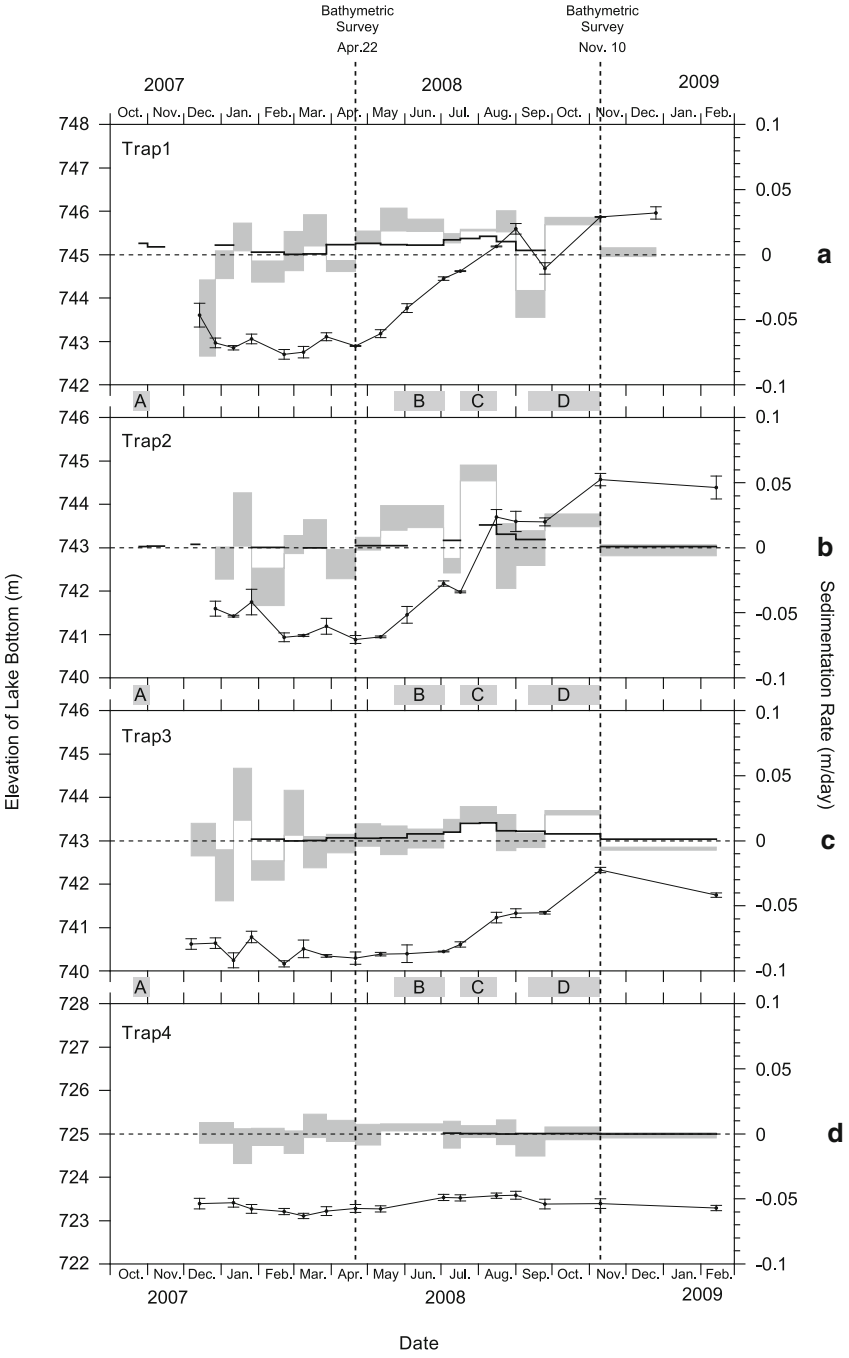

Fig. 15.5 Temporal change in lake-bottom elevation for trap sampling points (*thin line* with error bar). The *gray band* indicates sedimentation rate calculated from change in elevation. The width of the band represents the sedimentation rate error. The *thick line* indicates the sedimentation rate measured by the trap

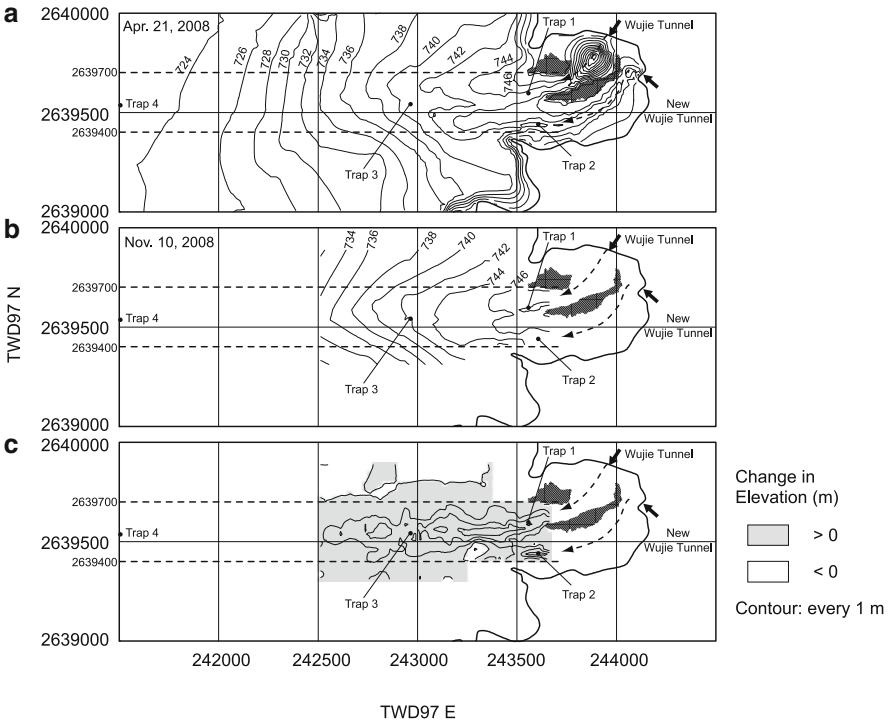

Fig. 15.6 Lake-bottom topography of the eastern area of Sun Moon Lake: (**a**) April 21, 2008 and (**b**) November 10, 2008. (**c**) Sediment thickness deposited from April 21, 2008 to November 10, 2008. The *gray area* indicates the sedimentation area. The *hatched areas* indicate the islands in the lake. An *arrow* indicates the water flow direction from the waterway tunnels to offshore

15.4.3 Sedimentation Pattern During Sediment Inflow Events

A bathymetric survey was performed in the eastern part of Sun Moon Lake to examine the changes in the lake-bottom topography corresponding to sediment inflow events B, C and D. Figure 15.6a, b show the lake bottom topography before (April 21, 2008) and after (November 10, 2008) the sediment inflow events. The bathymetric map of April 21, 2008 was compiled from ten surveys from December 7, 2007 to April 21, 2008. The lake is shallow near the waterway tunnels and becomes deeper with increasing distance from the tunnels, with the lake delta lying offshore from the tunnels. There is a lake bottom channel (sublacustrine channel) on the lake delta, which extends from the Wujie waterway tunnel to the offshore zone. Figure 15.6c shows the sediment thickness deposited during sediment inflow events and the gray area indicates a region in which sedimentation occurred. A large change occurred within the lake bottom channel in a 300 m wide area (dashed line, Fig. 15.6c), in which up to 3 m of sediment was deposited during the sediment inflow events.

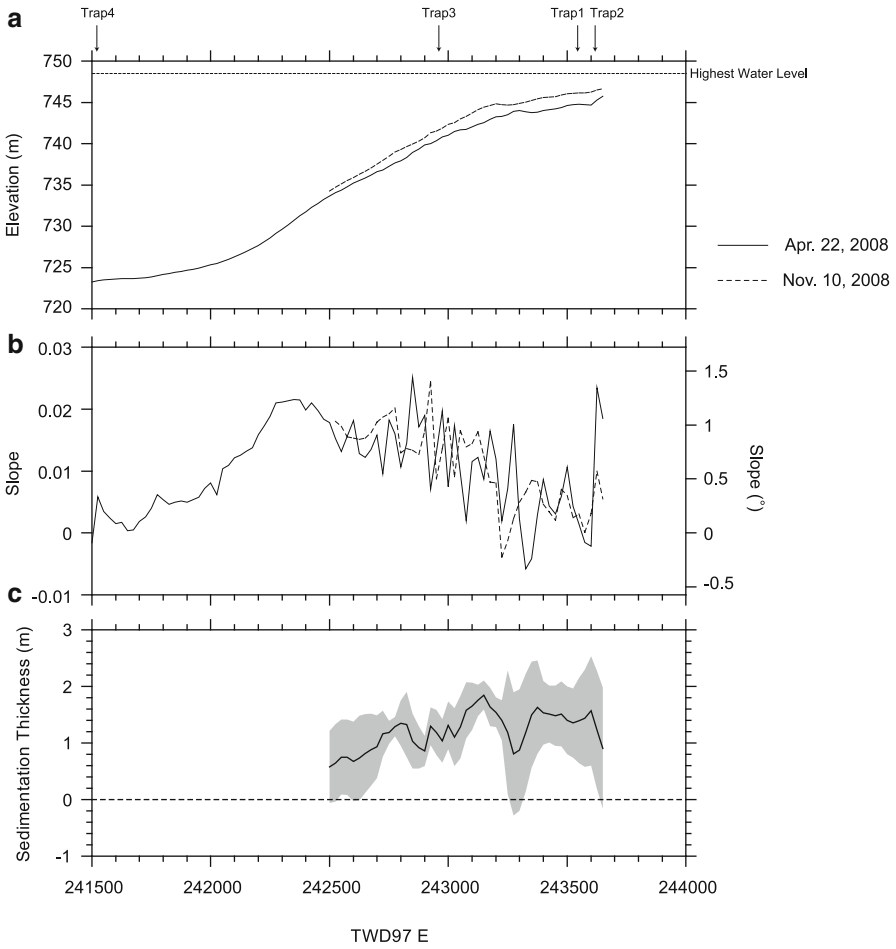

Fig. 15.7 (**a**) Cross section of the lake delta along the band area in Fig. 15.6. (**b**) Slope angle of the delta. (**c**) Sediment thickness during the sediment inflow events. The *thick solid line* indicates the sedimentation thickness and the *gray band* represents its error

Figure 15.7a indicates the average cross section of the lake delta along the band area shown in Fig. 15.6c. The elevation shown in Fig. 15.7a was averaged with respect to the N-axis within the band area. The topography of the delta in Sun Moon Lake is different from a typical coarse-grained delta in a reservoir, where a steep foreset bed is often formed. The slope angle of the delta is low, $<1°$ (Fig. 15.7b), and this may be attributed to the relatively fine grain size of inflow sediment from the waterway tunnels (Kostic et al. 2002). Adams and Schlager (2000) and Adams et al. (2001) proposed that lake delta slope and submarine slope profiles can be classified into three types of curvatures: linear, exponential, and Gaussian. A Gaussian profile is produced when an exponential slope is modified by wave-dominated transport,

gravity-driven transport, and erosion by currents at the upper section of the delta. The slope profile of Sun Moon Lake appears to fit a Gaussian curvature suggesting that the upper part of the slope has been disturbed by erosional processes.

Figure 15.7c shows the profile of the sediment thickness during the sediment inflow events where the thick solid line represents the observed sedimentation thickness and error is shown by the gray band. Sedimentation thickness reaches a maximum value offshore of the tunnel (TWD97 E = 243300) and decreases with the distance from this point on both sides. The bathymetric map survey drawn from the past 30 years of data also indicates that the longitudinal distribution of the sedimentation rate is approximated by a Gaussian distribution (Ochiai et al. 2012). These results imply that sediment is eroded and re-deposited near the tunnels due to water flow.

15.5 Discussion

15.5.1 Sedimentation Model

To discuss the sedimentation pattern during sediment inflow events, we use a simple 1-dimensional model (Fig. 15.8) where the x-axis is defined as the east-west direction and the origin of the x-axis is set in TWD97, E = 243650 m (Fig. 15.7). We assume that horizontal water flow is induced only by water discharge from the tunnel along the x-axis, and that there are no vertical flows in the lake. Thus, sediment is transported only by horizontal flow and settling. The spatial distributions of the sedimentation thickness during sediment inflow events are discussed below. If sedimentation and erosion occur at the lake bottom simultaneously, the net sedimentation rate, r_s, is expressed as:

$$r_s = r_d - r_e, \tag{15.2}$$

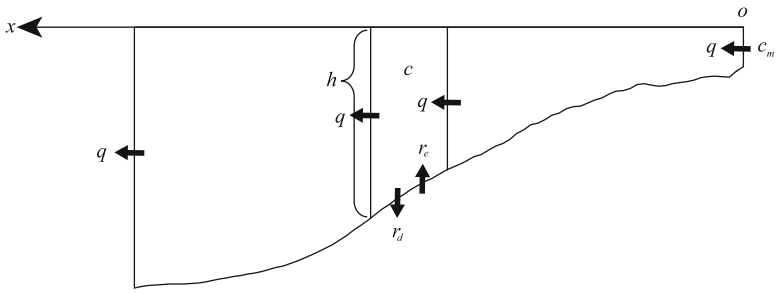

Fig. 15.8 Illustration of 1-dimensional sedimentation model

where r_d is the sediment deposition rate and r_e is the erosion rate. If vertical flow velocity is ignored, the deposition rate, r_d, is expressed as:

$$r_d(x) = w_s c(x), \tag{15.3}$$

where w_s is the settling velocity of the sediment and c is the volumetric sediment concentration in the water. We use the erosion rate from Sekine et al. (2003) where the erosion rate on a lake bottom is related to the shear stress (i.e. friction velocity) and water content, as expressed here:

$$r_e = \alpha R_{wc}^{2.5} u_*^3 \tag{15.4}$$

where α is a constant, R_{wc} is the water content of the bottom sediment, and u_* is the friction velocity. Friction velocity is assumed to be proportional to the mean velocity, u_m, of water through the cross section, and is thus given as:

$$u_* = \beta u_m = \beta \left(\frac{q}{h}\right), \tag{15.5}$$

where q is the water discharge for unit width, h is the water depth, and β is a constant. If the water content, R_{wc}, is constant, Eq. 15.4 is rewritten using Eq. 15.5 to produce Eq. 15.6:

$$r_e(x) = \alpha R_{wc}^{2.5} \left(\beta \left(\frac{q}{h(x)}\right)\right)^3 = K\left(\frac{q}{h(x)}\right)^3 \tag{15.6}$$

where K is a constant. Equation 15.2 can then be rewritten using Eqs. 15.3 and 15.6 to produce Eq. 15.7:

$$r_s(x) = w_s c(x) - K\left(\frac{q}{h(x)}\right)^3. \tag{15.7}$$

If the spatial distribution of sediment concentration c and depth h are given, the sedimentation rate is calculated using Eq. 15.7. Thus, spatial distribution of the sediment concentration in the lake is obtained by solving the following under steady state assumptions, as expressed by:

$$\frac{dc(x)}{dx} = -\frac{w_s}{q} c(x) + \frac{1}{q} K\left(\frac{q}{h(x)}\right)^3. \tag{15.8}$$

The terms on the right side of Eq. 15.8 express the settling and erosion of sediment on the lake bottom. Equation 15.8 was solved numerically using the Runge-Kutta method for nine sampling intervals from April 21, 2008 to November 10, 2008. The boundary condition for the concentration was given as $c = c_m$ at $x = 0$, where c_m represents the mean sediment concentration of the inflow sediment shown in

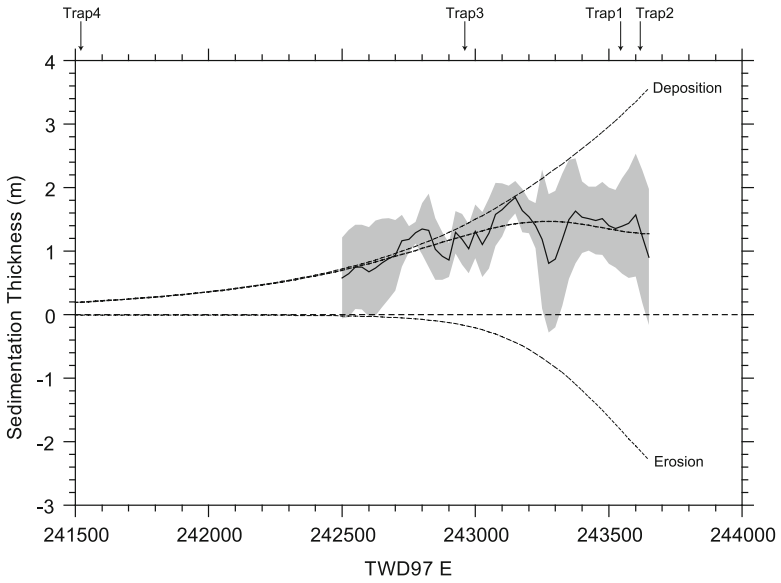

Fig. 15.9 Spatial distribution of calculated sedimentation thickness S_{total} (*thick dashed line*), deposition and erosion thickness (*thin dashed line*), and observed sedimentation thickness (*solid line*)

Fig. 15.3a. The water discharge, q, was calculated from the mean water inflow rate Q. Values of q and c_m were adjusted for nine intervals according to observation results shown in Fig. 15.3a. The water depth, h, was given by the constant vertical profile of elevation observed on April 22, 2008 (Fig. 15.7a). The total sedimentation during the nine intervals was calculated as:

$$S_{total}(x) = \sum r_{si}(x) \cdot \Delta t_i, \tag{15.9}$$

where r_{si} and Δt_i are the sedimentation rate and time length of the i-th sampling interval, respectively. In Eq. 15.8, constants w_s and K are unknown and optimum values for these parameters are determine parameter optimization (Nelder-Mead method; Nelder and Mead 1965) in order to minimize the error between the calculated total sedimentation, S_{total}, and the observed sedimentation thickness during the sediment inflow events (Fig. 15.7c).

15.5.2 Sedimentation Processes in Sun Moon Lake

The calculated total sedimentation thickness, S_{total}, is represented by a thick dashed line in Fig. 15.9. The sedimentation thickness distribution is in good agreement with observed values, which suggests that sedimentation during sediment inflow

events is adequately explained by this model. In Fig. 15.9, depositional and erosional thicknesses are indicated by thin, dashed lines. Depositional thickness decreases exponentially with distance from the tunnel, due to an exponential decrease in the sediment concentration. If erosion is ignored (second term in Eq. 15.8), the solution shows an exponential distribution of sediment concentration:

$$c(x) = c_m e^{-\frac{w_s}{q}x}. \tag{15.10}$$

The erosion of bottom sediment in the shallow area between the tunnel and Trap 3 (Fig. 15.9) is attributed to a large frictional velocity. Frictional velocity increases at shallower water depths (Eq. 15.5) and thus explains the low rates of sedimentation observed near the tunnel. In this region, sediment is temporarily deposited and subsequently re-deposited offshore.

On the basis of these results, sedimentation processes near the waterway tunnel is estimated as follows: (1) sediment concentrations and deposition rates decrease exponentially with distance from the tunnel at low erosion rates; (2) during high water inflow events, sediment is eroded from the shallow area, and re-deposited offshore from the tunnel. We infer that the profile of the delta reflects these processes; if the erosion is not significant, the profile of a delta acquires an exponential shape. Here, erosion has modified the slope profile of the Sun Moon Lake delta to represent a Gaussian curvature. These findings are in agreement with Adams and Schlager (2000) who proposed that a Gaussian profile is produced when an exponential slope is modified by wave-dominated transport, gravity-driven transport, and erosion by a current at the upper part.

Optimized parameters w_s and K were 2.13×10^{-4} m/s and 1.06×10^{-3}, respectively. The settling velocity of the inflow sediment from the tunnel (6.9 μm diameter) is calculated at 4.55×10^{-5} m/s with Stokes' low assuming the sediment density and water temperature are 2.76 g/cm^3 and 20 °C, respectively. Settling velocity estimated from the model fitting is an order of magnitude greater than measured values. Increased settling velocity is likely due to processes such as flocculation of particles and turbidity currents, which result from high sediment concentrations in the lake. Turbidity currents are known to be an important process in reservoir sedimentation (Fan and Morris 1992; De Cesare et al. 2001; Toniolo et al. 2007), and in the formation of submarine and sublacustrine channels. The critical sediment concentration to produce a turbidity current in a freshwater lake is low (<1 kg/m^3), and considerably higher in marine water (35–45 kg/m^3), which is due to the water salinity (Mulder and Syvitski 1995). Sediment concentrations in the Wujie tunnels are up to 8 kg/m^3, and therefore, turbidity current can theoretically occur in Sun Moon Lake and can be expected to contribute to the development of the lake bottom channel.

Wind-induced water currents and internal waves can also contribute to sediment re-suspension in a lake (e.g., Bailey and Hamilton 1997; Aota et al. 2006; Lee et al. 2007). Figure 15.2d shows the daily average wind speed at Sun Moon Lake. Large wind speeds are observed during the approach of a typhoon, which correspond with

high sedimentation rates in the traps and changes in the lake-bottom topography. The sedimentation model of representing the area near the tunnels during sediment inflow events can only take into account sediment supplied from the tunnels; however, measurements of the lake currents are necessary for a comprehensive discussion on the relationship between wind-induced currents and sedimentation processes for the entire lake.

15.6 Conclusions

1. The sediment inflow rate for waterway tunnels in Sun-Moon Lake, Taiwan is influenced by interactions between the artificially controlled water inflow rate, and sediment concentration in the Zhuoshui River, which is controlled by precipitation. Low sediment inflow rates were observed during winter and spring, whereas high rates were observed during the East Asian rainy season and typhoon season.
2. Relatively low sedimentation rates were observed by sediment traps and sonar methods during winter/ spring and increased during summer/ autumn, which correspond to sediment inflow events.
3. On the basis of a sedimentation model, sedimentation processes near the waterway tunnel is estimated as follows: (1) sediment deposition rates decrease exponentially with distance from the tunnel; (2) during high water inflow events, sediment is eroded from the shallow area and re-deposited offshore from the tunnel.

In summary, these results suggest that reducing the sediment inflow rate and proper control on erosion pattern near the tunnels are essential for the sustainable use of water resources in Sun Moon Lake.

Acknowledgements We thank Mr. Yeuan-Chang Cheng, Mr. Shih-Hung Liu, Mr. Tsu-Ta Chang, Mr. Jhih-Cheng Chen, and colleagues at the Taiwan geomorphological research laboratory of National Taiwan University. We also thank Mr. Han-Zhang Su, Mr. Yi-Qian Chen, and Mr. Wan-Qian Shi of the Sun Moon Lake National Scenic Area Administration for their support. Dr. Noritaka Endo at Kanazawa University is thanked for providing constructive feedback on this study, and Mr. Kuan-Pei Lin and Mr. Jian-Hong Zheng of the Taiwan Power Company for providing information on Sun Moon Lake. This study was supported by the National Science Council, Taiwan.

References

Adams EW, Schlager W (2000) Basic types of submarine slope curvature. J Sediment Res 70:814–828

Adams EW, Schlager W, Anselmetti FS (2001) Morphology and curvature of delta slopes in Swiss lakes: lessons for the interpretation of clinoforms in seismic data. Sedimentology 48:661–679

Aota Y, Kumagai M, Kashiwaya K (2006) Estimation of vertical mixing based on water current monitoring in the hypolimnion of Lake Biwa. JSME Int J 49:621–625

Bailey MC, Hamilton DP (1997) Wind induced sediment resuspension: a lake-wide model. Ecol Model 99:217–228

Dadson SJ, Hovius N, Chen H, Dade WB, Hsieh M, Willett SD, Hu J, Horng M, Chen M, Stark CP, Lague D, Lin J (2003) Links between erosion, runoff variability, and seismicity in the Taiwan orogen. Nature 426:648–651

De Cesare G, Schleiss A, Hermann F (2001) Impact of turbidity currents on reservoir sedimentation. J Hydraul Eng 127:6–16

Fan J, Morris GL (1992) Reservoir sedimentation. I: Delta and density current deposits. J Hydraul Eng 118:354–369

Huang C, Shea K, Chen M (2000) Explanatory text of the geologic map of Taiwan: Puli (in Chinese). Central geological survey, Taiwan

Kashiwaya K, Tsuya Y, Okimura T (2004) Earthquake-related geomorphic environment and pond sediment information. Earth Surf Proc Land 29:785–793

Kostic S, Parker G, Marr JG (2002) Role of turbidity currents in setting the foreset slope of clinoforms prograding into standing fresh water. J Sediment Res 72:353–362

Lee C, Schwab DJ, Beletsky D, Stroud J, Lesht B (2007) Numerical modeling of mixed sediment resuspension, transport, and deposition during the March 1998 episodic events in southern Lake Michigan. J Geophys Res 112, C02018

Lin J, Petley D, Jen C, Koh A, Hsu M (2006) Slope movements in a dynamic environment – a case study of Tacha River, Central Taiwan. Quat Int 147:103–112

Mulder T, Syvitski JPM (1995) Turbidity currents generated at River Mouths during exceptional discharges to the world oceans. J Geol 103:285–299

Nelder JA, Mead R (1965) A simplex method for function minimization. Comput J 7:308–313

Ochiai S, Lin JC, Kashiwaya K, Jen CH (2012) Influence of construction of dams and waterway tunnels on sedimentation rate and bottom topography in Sun Moon Lake, Taiwan. Trans Jpn Geomorphol Union 33:149–170

Page MJ, Trustrum NA, DeRose RC (1994) A high resolution record of storm-induced erosion from lake sediments, New Zealand. J Paleolimnol 11:333–348

Sekine M, Nisimori K, Fujio K, Katagiri Y (2003) Consideration on erosion process of cohesive sediment and erosion rate formula (in Japanese). Ann J Hydraul Eng JSCE 47:541–546

Shimada T, Kashiwaya K, Hyodo M, Masuzawa M (2002) Hydro-environmental fluctuation in a lake-catchment system during the late Holocene inferred from Lake Yogo sediments (in Japanese). Trans Jpn Geomorphol Union 23:415–431

Su HC, Jen KY, Luo JJ, Chen CS (2006) Analysis of reservoirs sedimentation potential in Taiwan (in Chinese). J Build Constr Technol 3:27–36

Taiwan Power Company (2000) Report of the measurement of sediment deposition in Sun Moon Lake (in Chinese). Taiwan Power Company, Taiwan

Toniolo H, Parker G, Voller V (2007) Role of ponded turbidity currents in reservoir trap efficiency. J Hydraul Eng 133:579–595

Water Resources Agency (2007) Statistic of water resources 2006 (in Chinese). Water Resource Agency, Taiwan

World Commission on Dams (2000) Dams and development. A new framework for decision-making. Earthscan Publications Ltd, London

Chapter 16
Response of Channels to Tectonic Activities: Flume Experiments for Bedrock Rivers Affected by Localized Uplift

Noritaka Endo and Takuya Nakauchi

Abstract Response of river channels to localized uplift was investigated using flume experiments where the base level was kept constant by a weir at the river mouth. We found three kinds of channel pattern responses; (1) channels that passed through the localized uplift area (generation of a water gap), (2) channels that avoided the uplift area, and (3) formation of a new river with the origin inside the uplift area. It is difficult to predict which type of response will happen in advance because localized uplift causes complicated changes in the channel network pattern, which results in variation of stream power due to interactions between several channels through confluence, avulsion, etc. In terms of the longitudinal profile of the channels, two types of responses were observed: (1) keeping a straight profile in the case of rivers flowing from much higher areas than the uplift area and (2) having a concave-up profile in the case of a newly formed channel running from the uplift area. A straight type of profile was also typical in the case of no uplift, so the concave-up profile is considered to be a "dynamic" equilibrium state that is realized between the descent due to fluvial erosion and the ascent due to uplift.

Keywords Flume experiment • Localized uplift • River channel change • Graded river

16.1 Background and Purpose of This Study

Rainfall and running water on the surface of the earth are main factors that influence the development of the landscape. River flows, especially flooding streams, have enormous powers that can change topographies and sometime result in disasters. Although such natural power can seem very drastic from the human perspective, development of regional-scale topographies takes a long time, i.e., on geologic time

N. Endo (✉) • T. Nakauchi
Department of Earth Sciences, Graduate School of Natural Science & Technology, Kanazawa University, Kakuma, Kanazawa 920-1192, Japan
e-mail: wisteria@staff.kanazawa-u.ac.jp

K. Kashiwaya et al. (eds.), *Earth Surface Processes and Environmental Changes in East Asia*, DOI 10.1007/978-4-431-55540-7_16

scales of tens of thousands of years or more. Flume experiments (physical model studies) are useful to understand drainage development in that both time and space scales can be downsized, which overcomes some of the practical problems that are typically encountered when collecting field observations of fluvial processes.

In general, drainage pattern of rivers change their shapes in response to tectonic activities and climate change. Climate change involves variation of the precipitation rate (which is related to the incision rate) and modification of temperature (resulting in sea level fluctuations, thus base levels). Experiments using artificial rainfall are one of the basic techniques that one can use to investigate the development of drainage basins (e.g., Flint 1973; Phillips and Schumm 1987; Pelletier 2003; Raff et al. 2004; Ouchi 2011). Besides, for specific purposes, various types of flume experiments have been conducted by many researchers, e.g., to study the relation to tectonic activities or sea level change (Ouchi 1985; Hasbargen and Paola 2000; Van Heijst and Postma 2001; Cazanacli et al. 2002; Muto and Steel 2004), self altering processes (spontaneous change) of channels (Bryant et al. 1995; Smith 1998; Sapozhnikov and Foufoula-Georgiou 1999; Ashworth et al. 2004), and pattern formation of channels (Phillips and Schumm 1987; Rosatti 2002; Murray and Paola 2003; Tal and Paola 2007). Some of the previous experiments evaluated alluvial rivers, while others examined bedrock rivers; a few studies investigated both types. Understanding of bedrock rivers, however, is still not well developed, especially in regards to their developmental processes, in comparison to alluvial rivers.

Here, we introduce the results of our preliminary experiments that were aimed at understanding the response of mountainous rivers (generally bedrock rivers) to localized uplift, in which rivers are affected by tectonic activity only in a part of the river network that is well developed on sloped substrate.

16.2 Methods

The observation area in the flume was 90 cm long and 90 m wide (Fig. 16.1). A weir of the full width of the flume was set up at the downstream end of the observation area. The weir was 4 cm high from the bottom of the flume and had a slit (ca. 1 cm wide and 2 cm deep) at the top center. The installation of the weir was to prevent change in the base level at the river mouth due to deposition of eroded sediments which could lead to delta development and/or progradation of the delta. The initial state was a flat slope with 7° slanting towards the downstream weir. The substrate was totally made up of a uniform mixture of sand (200 μm of diameter on average) and kaolinite at a ratio of 10:1., which was the proper hardness to reproduce drainage incision well in the model experiments (Ouchi 2011).

The precipitation was realized by 10 sprinklers set up 90 cm above the flume (Fig. 16.1). The sprinklers can supply fine mists that will not destroy the topography by making craters. The average precipitation rate was 52 mm/h.

The localized uplift area was 30 cm wide and 12 cm long, and it was located 25 cm away from the downstream weir. The apparatus used for the localized uplift

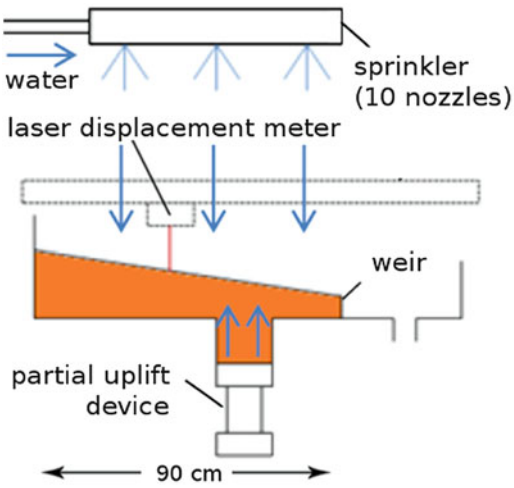

Fig. 16.1 Schematic diagram of the experimental setting

consists of a motor to jack up the bottom of a box filled with 15 cm deep sand; the walls of the box were fixed (Fig. 16.1). The uplifted substrate was composed of the same material as the initial slope. The uplift rate was 1 cm/h. The total time of an experimental run was 20 h, during which the uplift was realized within a limited period from 5 to 15 h. The comparison run of no uplift was performed for 15 h.

Each experimental run was performed by repeating cycles that included 2.5 h of precipitation and the measurement of the landform during a pause in the precipitation. The developed landform was digitalized using a laser displacement meter with grids of 5 mm intervals along the horizontal. A camera was also set up above the flume to take photos every 30 min. Outflows of sediments from the slit of the weir were collected every 30 min, and these were measured in terms of dry weight.

16.3 Results

16.3.1 Channel Course

16.3.1.1 No Uplift

Channels were developed via the action of surface water supplied by rainfall (Figs. 16.2 and 16.3). In the early stage, the growth of basins was driven mainly by valley head erosion of the main stream and large tributaries. Then, the rate of valley head erosion of the large streams decreased, while the lateral erosion of larger channels and the development of small tributaries became active. In the case of no uplift, the development of relatively large channels was almost finished by 5 h from the beginning of the run. Figure 16.3 displays the transition of three selected

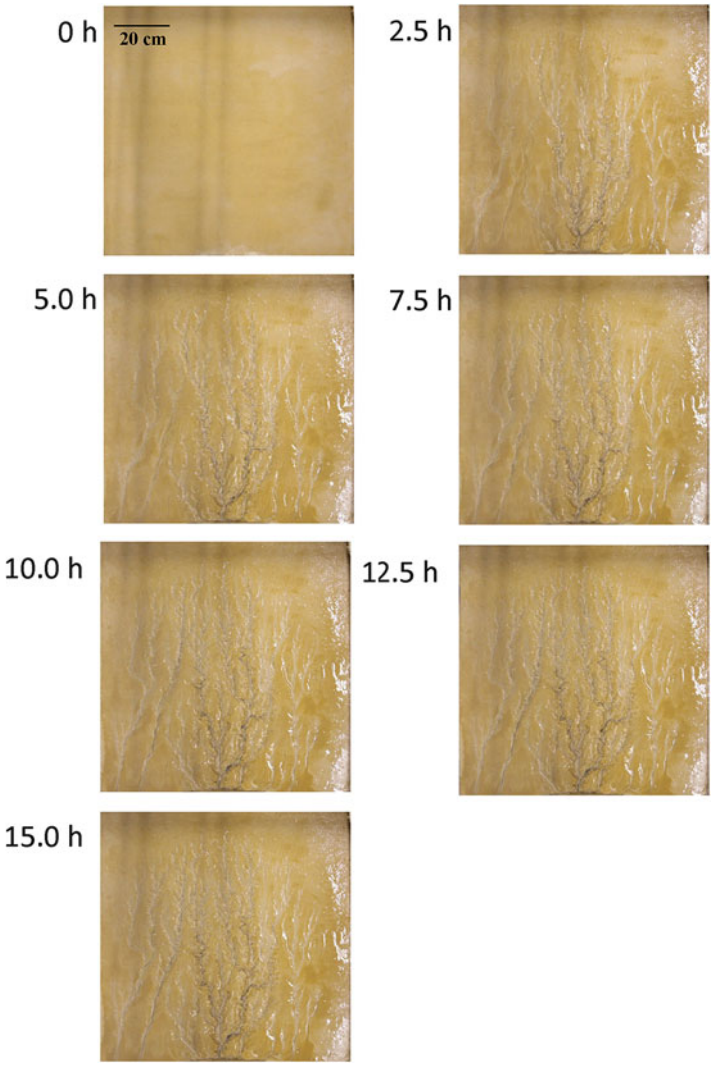

Fig. 16.2 Temporal change of the drainage by only precipitation with no uplift. Scale of all insets is the same

channels (Channels A, B, and C), and it shows that Channel A became the longest and the main stream at 5 h. After that time, the origin of each channel hardly moved, but the channel lengths changed somewhat owing to lateral erosion (meandering) of midway segments, especially in the case of Channels A and C.

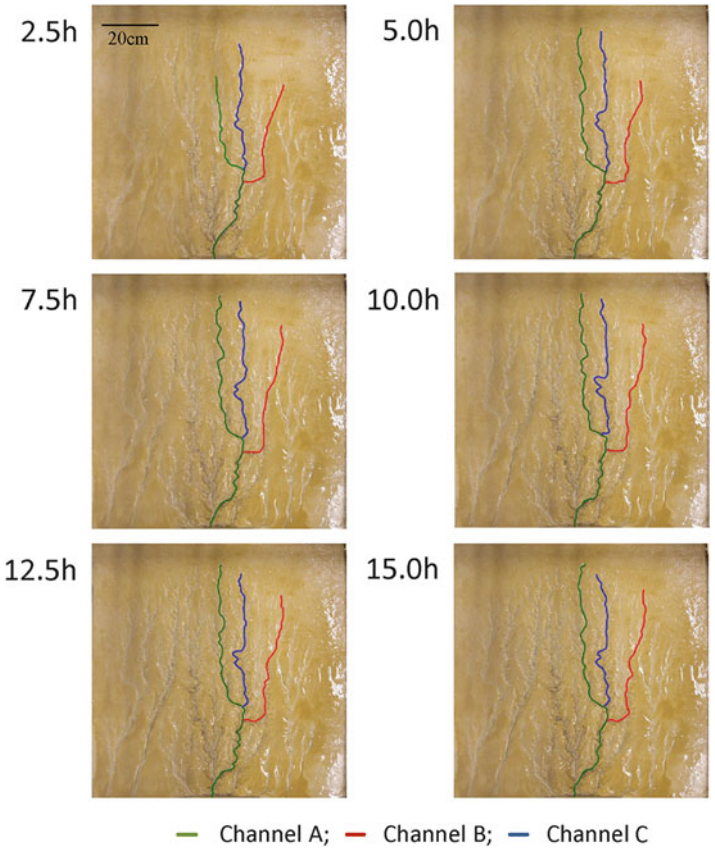

Fig. 16.3 The selected three channels in the case of no uplift are traced by *colored lines*. These three were analyzed to determine the longitudinal profile

16.3.1.2 Localized Uplift

In this study, the uplift was realized from 5 to 15 h during a run. Before uplift, the development of channels was similar to the case of no uplift. After the start of the localized uplift, in the area higher than (upstream of) the uplift area, the flow was disturbed by the uplift. Therefore, streams somewhat stagnated, the channels widened, and sediments partially settled there (Figs. 16.4 and 16.5). Figure 16.6 displays the transition of three selected channels (Channels D, E, and F). Channel D continued to run through the uplift area before and after the uplift started. Several streams joined upstream of the uplift area and became tributaries of Channel D, which resulted in a large discharge for Channel D. Conversely, some other channels shifted their courses from the uplift area to other places of no uplift (River E in Fig. 16.6), which resulted in new confluences outside of the uplift area. In contrast to relatively long channels, a short river originating from a place near and upstream

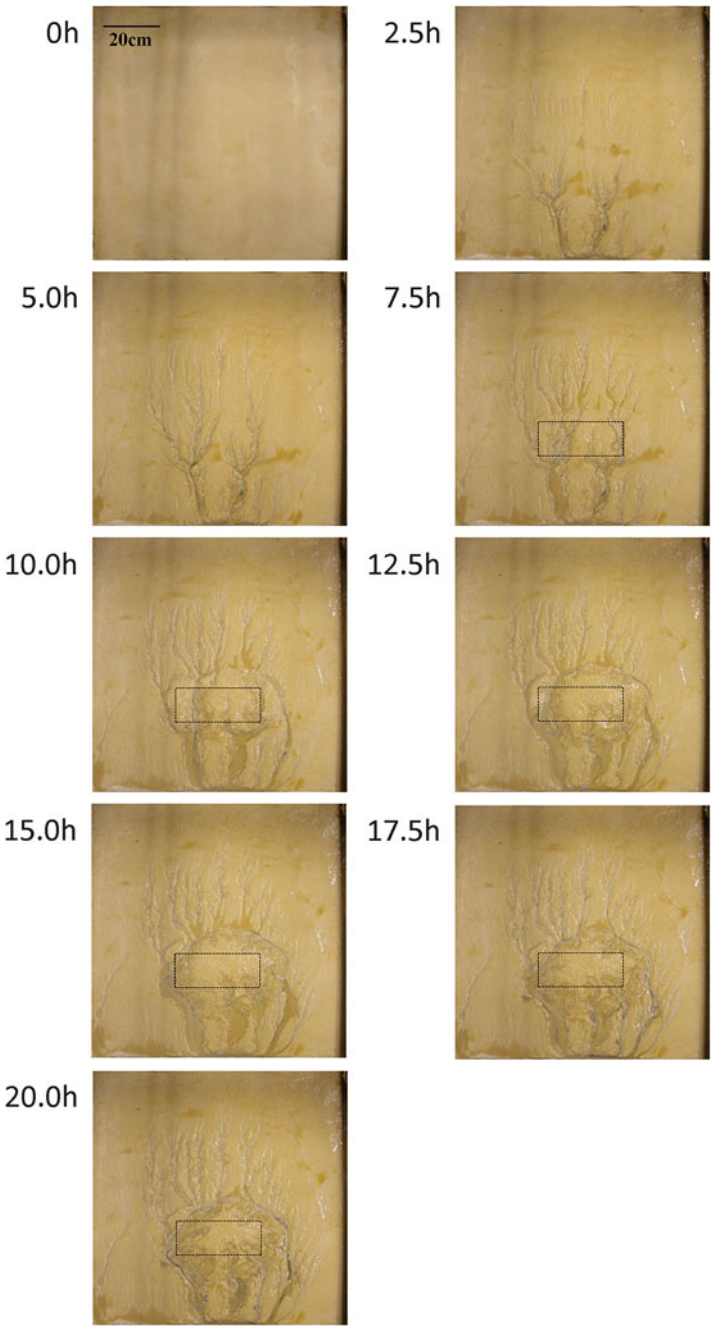

Fig. 16.4 Temporal change of the drainages by precipitation and localized uplift. The uplift area is shown by a *rectangle* with a *broken line*. Scale of all insets is the same

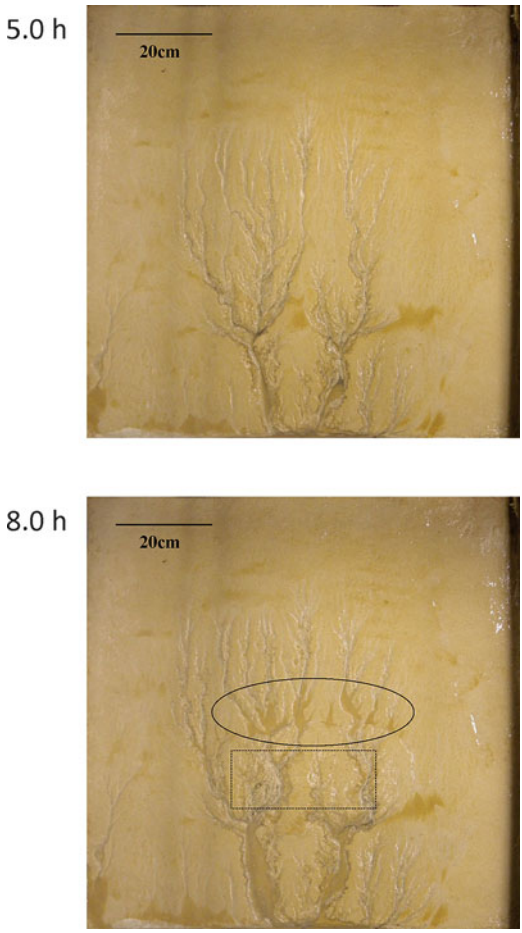

Fig. 16.5 Widening of channels upstream of the uplift area (an *oval* in the *bottom inset*) at 8 h (3 h after the localized uplift started) compared with conditions at 5 h (just before the uplift) (*top inset*). Dark *brown* parts inside the channels (within the *oval*) show sedimentary deposits. A *rectangle* with a *broken line* indicates the uplift area

of the uplift area shortened (River F in Fig. 16.6). The upstream part of the river disappeared during the uplift because mass wasting buried the channel; therefore, the origin moved into inside of the uplift area. Such rivers, in some cases, flowed partially within a part of preexisting channels.

After the uplift period ended, some new origins appeared inside the "previous uplift area" from which water flowed as rivers. Slope failures happened frequently inside the uplifted area even after the end of the uplift because the area became a local mound. Even so, the large channel that formed before the end of the uplift, which originated far upstream of the previous uplift, was not affected by slope failures and maintained the stream (Channel D).

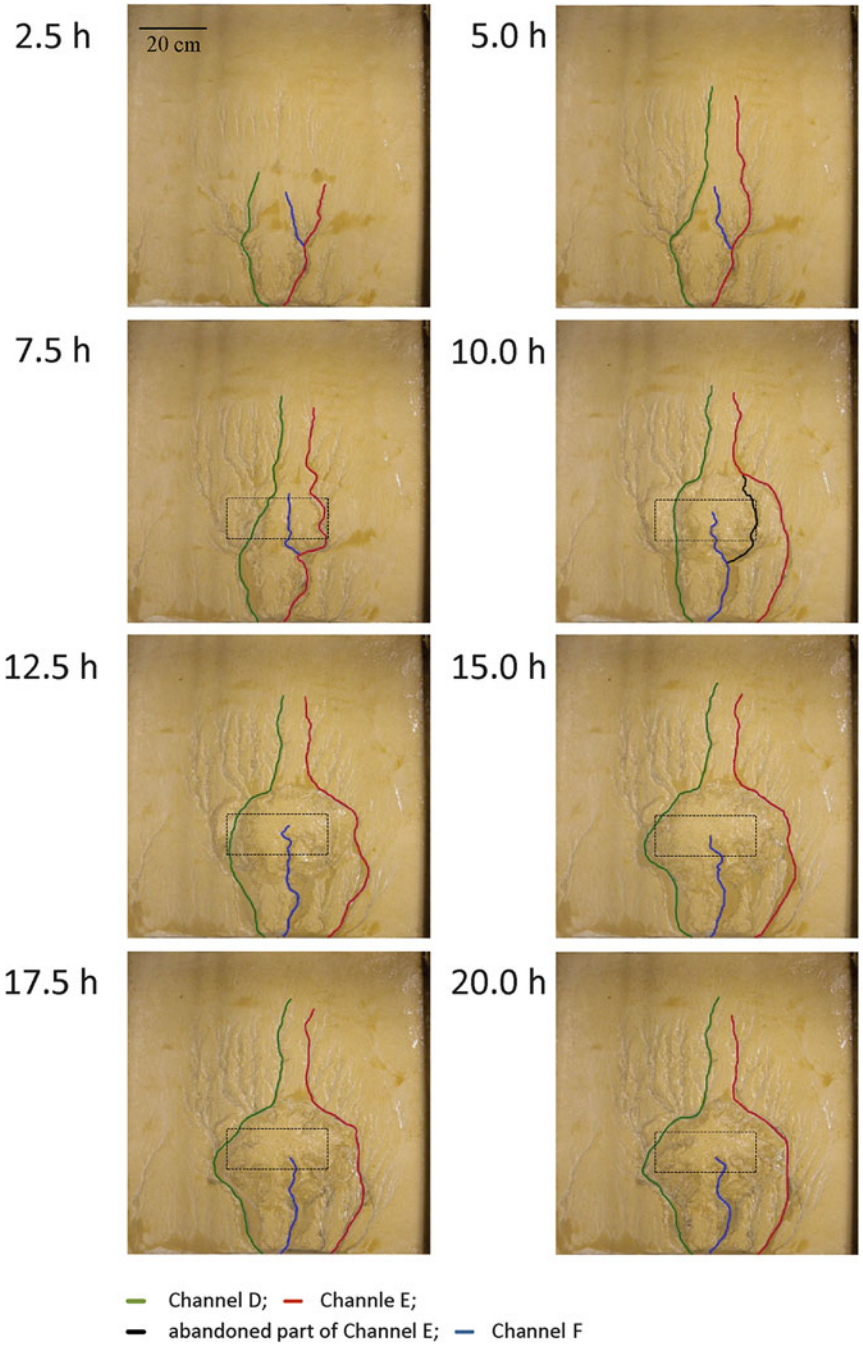

Fig. 16.6 The selected three channels in the case of localized uplift are traced by *colored lines*. These three were analyzed to determine the longitudinal profile. A *rectangle* with a *broken line* indicates the uplift area

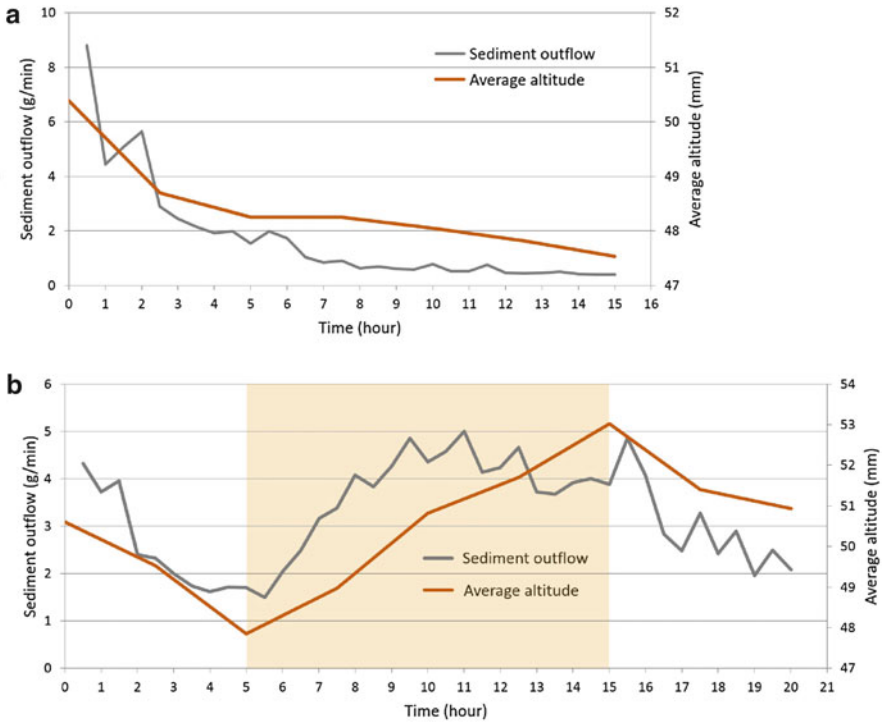

Fig. 16.7 Temporal change of sediment outflow and average elevation. (**a**) No uplift and (**b**) localized uplift. The halftone colored band indicates the period of localized uplift (from 5 to 15 h). The relatively large difference of sediment outflow between the two runs at very early stages before the uplift (within 1 h from the beginning of a run) is considered to have been caused by uncertain factors involving the bed surface in preparation for the initial slope, such as initial moisture of the sand material

16.3.2 Sediment Outflow and Average Elevation

16.3.2.1 No Uplift

Sediment outflow (initially about 9 g/min) basically decreased except for some temporary increases, and kept the low values (around 1 g/min after 6.5 h from the beginning of the run) (Fig. 16.7). The average elevation decreased fast during the first 5 h, but subsequently, the value decreased gradually.

16.3.2.2 Localized Uplift

Before the beginning of uplift, both sediment outflow and average elevation decreased, which was similar to the run with no uplift (Fig. 16.7). After the uplift

began, the sediment outflow increased until about 4 h had passed (9 h from the beginning of the run), and then the values stayed high (Fig. 16.7). The average elevation increased through the uplift period, although its increase rate was about half of the uplift rate owing to erosion. After the uplift ended, both sediment outflow and average elevation decreased again, although the sediment outflow still exhibited some fluctuations.

16.3.3 Longitudinal Profile

16.3.3.1 No Uplift

Figure 16.8 shows the temporal change in the longitudinal (streamwise) profiles of the three channels (Channels A, B, and C) that were featured in Fig. 16.3. At 2.5 h, the three channels were almost straight except for a part of Channel A near the confluence point. The three channels flowed along paths of almost the same

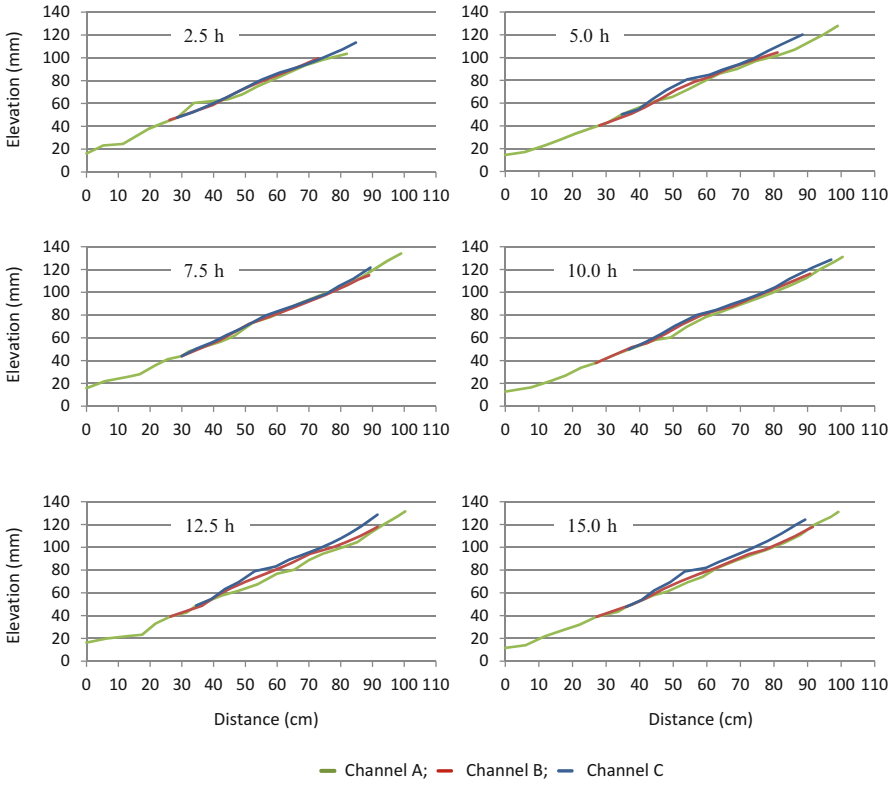

Fig. 16.8 Longitudinal profiles of the three channels shown in Fig. 16.3

elevation. At 5 h, in comparison with the state at 2.5 h, the three profiles shifted to lower elevations because of downward erosion; the profiles also became more linear. At 7.5 h, the three channels had very similar profiles in terms of both shape and elevation. After 10 h, however, the three channels deviated from each other again, and especially after 12.5 h, the profiles changed in terms of their lengths and shapes owing to lateral erosion of channels; downward erosion did not occur readily during this time. The length of all three channels shortened after attaining the maxima, but the time of the maximum length was different for the different channels—Channel A: maximum at 10 h; Channel B: maximum at 12.5 h; Channel C: maximum at 10 h (see Sect. 16.3.1.1 for the discussion about channel course changes). Although there were small irregularities, the three longitudinal profiles were basically straight.

16.3.3.2 Localized Uplift

Figure 16.9 shows the temporal change of longitudinal profiles in the case of localized uplift; the three analyzed rivers correspond to those in Fig. 16.6 (Channels D, E, and F). Just before uplift (5 h), the three profiles became similar to each other in comparison with those at 2.5 h. At 7.5 h (2.5 h after the start of uplift) in the uplift area and its surrounding region, the elevation of the channels increased owing to the uplift and the profiles became convex-up, although the extent of this change was different and seemed to be larger for the shorter channel (Channel F). The convex-up shape at the early stage of uplift directly reflects the raised ground.

At 15 h (10 h after the start of uplift), the profile of Channel D became more straight (more linear and smooth) than that at 7.5 h (Fig. 16.9). Additionally, Channel E changed into a straight profile, but Channel E (unlike Channel D) changed its channel course greatly (Fig. 16.6). Specifically, Channel E abandoned about two-thirds of its previous channel course and created a new course that detoured the uplift area. The abandoned part became a wind gap temporarily. Along with the large change of Channel E, Channel F became an independent channel from Channel E. Channel F had an origin upstream of the uplift area at 7.5 h, but the origin moved into the uplift area at 10 h because the drainage divide shifted owing to the uplift (Fig. 16.6). Although the longitudinal profile of Channel F was convex-up at 7.5 h, at 10 h the profile changed into concave-up, which was in contrast to the straight profiles of Channel D and Channel E. From 10 to 15 h, profiles of both Channels D and E became more straight. Channel D became longer because of lateral erosion of the channel (meandering) in the middle reach, so its river bed gradient along the channel became gentle. In contrast, Channel E shortened at 15 h because the channel course of the middle reach became more straight.

After the uplift ended, the shape of each profile did not change very much. Channel F stayed concave-up and Channels D and E remained straight in profile, although Channel D showed faster downward erosion than Channel E.

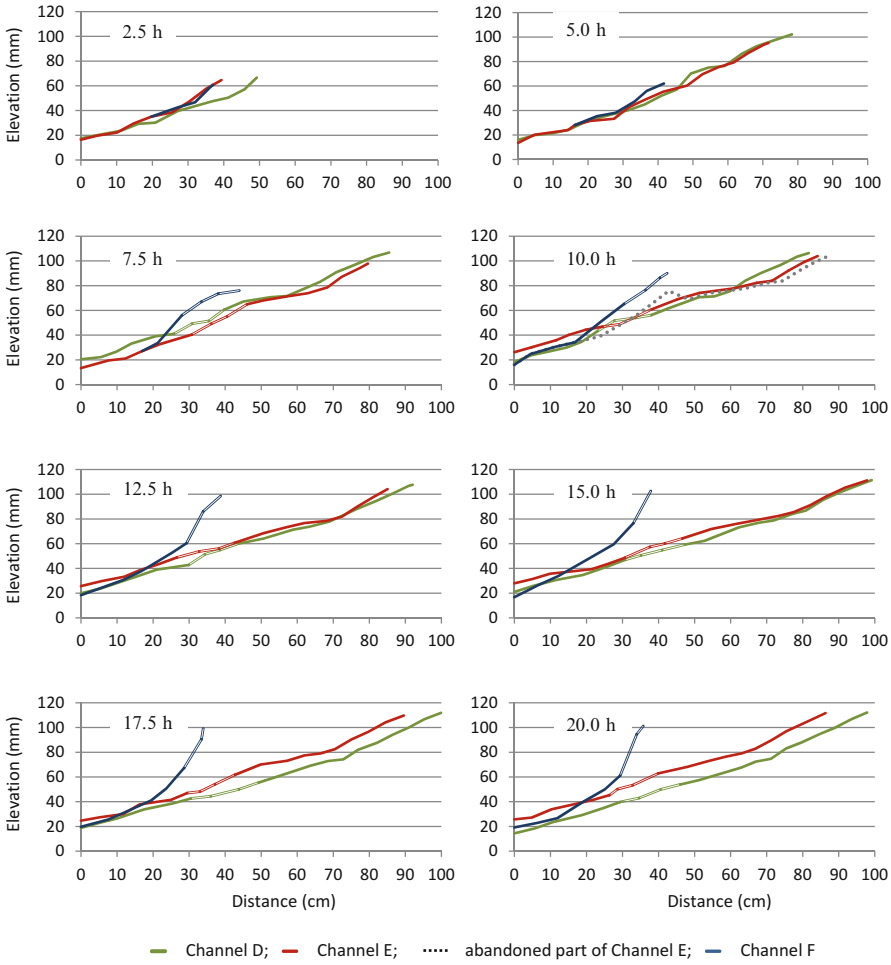

Fig. 16.9 Longitudinal profiles of three channels shown in Fig. 16.4. Segments of the *double line* indicate parts of channels overlapping the area of localized uplift. The period of uplift was from 5 to 15 h. To be exact, because the flume has only one outlet (a slit of the weir), downstream ends of all rivers should overlap, but actually there was a gap between divides forming a step-like topography in immediate proximity to the outlet (not appearing in the graph)

16.4 Discussion and Summary

The change of form of a single channel caused by localized uplift in the present study was in accordance with that observed in the previous experimental study (Ouchi 1985). Ouchi (1985) showed that if a single thread channel (not a braided river) was affected by localized uplift, the downstream side of the uplift area will maintain a single thread, whereas the upstream side will change into a braided

pattern. The braided pattern is a result of aggradation, which means that the upstream side of the uplift area tends to cause sedimentation. In the present study, during the relatively early time of the uplift period (within 2.5 h after the beginning of uplift), the downstream side of the uplift area remained in a single thread channel-form and the upstream side of the uplift area showed sedimentation (Fig. 16.5), although a braided pattern did not appear, but instead, a flat deposit area formed in the widened channel. The present study, however, revealed different responses at later times; in addition to the river maintaining its course in the uplift area, other rivers altered the channel path and avoided the uplift area (Fig. 16.6). The different responses in the present study compared to those from Ouchi (1985) probably result from the relatively faster uplift rate used here. Whether a channel flows through the uplift area or shifts to other places seems to be determined by chance, i.e., stochastic phenomena such as lateral migration and avulsion. The conventional understanding should hold true that water gap channels are generated if the local downward erosion rate overcomes the uplift rate. The downward erosion rate, which depends on stream power, however, is difficult to forecast over a relatively large time scale because it is difficult to predict how stream will join or recede owing to disturbances of the uplift area. Therefore, it is difficult to know in advance whether a water gap channel will form or not.

Longitudinal profiles in the no uplift case were typically of the straight type and were established within the first 2.5 h and maintained afterward (Fig. 16.8). In the present study, the base level stayed almost constant owing to the weir. The previous experimental studies (Ikeda et al 1986; Muto and Swenson 2005) showed that graded rivers took on a straight profile especially when a weir was settled at the downstream end, in which input sediments into the flume only bypassed the channel and therefore neither erosion nor sedimentation occurred, namely, the system was at equilibrium. In the present study, sediments were not supplied from outside of the flume, but they were spontaneously supplied into channels with materials eroded by incision; thus, the drainage was an erosional system on the whole and fundamentally could not achieve balance between erosion and sedimentation. Nevertheless, river profiles became straight similar to the graded rivers of previous studies, which is considered to have been because the total water inflow into the whole drainage by precipitation was constant and the topography adjusted for an efficient drain, and thus, the erosion rate decreased (Fig. 16.7a) and approached to a static stable state.

In the uplift case, even during and after the uplift period, some rivers maintained straight profiles, including both cases where a water gap was formed and the rivers detoured the lifted area (Channels D and E in Fig. 16.9). Such rivers flowed from a point far upstream of the uplift area (Fig. 16.6) and they had relatively large water discharges that caused fast downward erosion in comparison with uplift. In contrast, equilibrium (graded) rivers in natural fields tend to conserve concave-up profiles (approximated by the exponential function) (Zaprowski et al. 2005; Sougnez and Vanacker 2011). In the present study, the river flowing from inside the uplift area had a convex-up profile in the early stage, but later on it changed into a concave-up profile (Channel F in Fig. 16.9). The concave-up shape is considered to be a more stable state than the convex-up shape. Although discussions about each single

channel are difficult at present, the level-off of the sediment outflow around 9 h from the beginning of the run (Fig. 16.7) suggests that there was balance in the rates of erosion and uplift, i.e., proceeding to a dynamic equilibrium. According to the idea of dynamic equilibrium, a concave-up river profile suggests that the upstream area (a mountain containing the river origin) is still orogenetically active or that a river has a remnant shape of previously active periods. Actually, rivers with concave-up longitudinal profiles are generally located in zones with low uplift rates (Sougnez and Vanacker 2011).

A summary of the findings is as follows. Three kinds of river channel responses to localized uplift were observed: (1) channels passing through the uplift area (generation of a water gap), (2) channels detouring the uplift area, and (3) formation of a channel originating in the uplift area. It is difficult to predict which type of response will occur, because localized uplift affects stream power due to interactions of several channels through confluence, avulsion, etc. Longitudinal profiles of channels were observed to have two types: (a) straight and (b) concave-up. Relatively long rivers were not affected by localized uplift in terms of their longitudinal profile and they stayed straight, whereas rivers originating in a locally uplifted area changed their profile from convex-up to concave-up. It is considered that concave-up profiles are the stable state to be attained during orogenic activity as a dynamic equilibrium.

Acknowledgement This work was supported by JSPS KAKENHI Grant Number 25350424.

References

Ashworth PJ, Best JL, Jones M (2004) Relationship between sediment supply and avulsion frequency in braided rivers. Geology 32(1):21–24

Bryant M, Falk P, Paola C (1995) Experimental study of avulsion frequency and rate of deposition. Geology 23(4):365–368

Cazanacli D, Paola C, Parker G (2002) Experimental steep, braided flow: application to flooding risk on fans. J Hydraul Eng 128(3):322–330

Flint JJ (1973) Experimental development of headward growth of channel networks. Geol Soc Am Bull 84:1087–1094

Hasbargen LE, Paola C (2000) Landscape instability in an experimental drainage basin. Geology 28(12):1067–1070

Ikeda H, Iseya F, Iijima H (1986) On the formation of longitudinal stream profiles in a large flume. Bull Environ Res Center Univ Tsukuba 10:115–123 (in Japanese)

Murray AB, Paola C (2003) Modeling the effect of vegetation on channel pattern in bedload rivers. Earth Surf Process Landf 28:131–143

Muto T, Steel R (2004) Autogenic response of fluvial deltas to steady sea-level fall: implications from flume-tank experiments. Geology 32(5):401–404

Muto T, Swenson JB (2005) Large-scale fluvial grade as a non-equilibrium state in linked depositional systems: theory and experiment. J Geophys Res Earth Surf 77(1):2–12

Ouchi S (1985) Response of alluvial rivers to slow active tectonic movement. Geol Soc Am Bull 96:504–515

Ouchi S (2011) Effects of uplift on the development of experimental erosion landform generated by artificial rainfall. Geomorphology 127:88–98
Pelletier JD (2003) Drainage basin evolution in the rainfall erosion facility: dependence on initial conditions. Geomorphology 53:183–196
Phillips LF, Schumm SA (1987) Effect of regional slope on drainage networks. Geology 15:813–816
Raff DA, Ramîrez JA, Smith JL (2004) Hillslope drainage development with time: a physical experiment. Geomorphology 62:169–180
Rosatti G (2002) Validation of the physical modeling approach for braided rivers. Water Resour Res 38(12):1295
Sapozhnikov VB, Foufoula-Georgiou E (1999) Horizontal and vertical self-organization of braided rivers toward a critical state. Water Resour Res 35(3):843–851
Smith CE (1998) Modeling high sinuosity meanders in a small flume. Geomorphology 25:19–30
Sougnez N, Vanacker V (2011) The topographic signature of quaternary tectonic uplift in the Ardennes massif (Western Europe). Hydrol Earth Syst Sci 15:1095–1107
Tal M, Paola C (2007) Dynamic single-thread channels maintained by the interaction of flow and vegetation. Geology 35(4):347–350
Van Heijst MWIM, Postma G (2001) Fluvial response to sea-level changes: a quantitative analogue, experimental approach. Basin Res 13:269–292
Zaprowski BJ, Pazzaglia FJ, Evenson EB (2005) Climatic influences on profile concavity and river incision. J Geophys Res 110, F03004